

SYMPOSIUM ON COMPUTER SIMULATION OF PLASMA AND MANY-BODY PROBLEMS

GPO PRICE \$ _____

CFSTI PRICE(S) \$ 3.00

Hard copy (HC) _____

Microfiche (MF) 165

ff 653 July 65

FACILITY FORM 802

N67-37737

(ACCESSION NUMBER)

465

(PAGES)

(NASA CR OR TMX OR AD NUMBER)

N67-37761

(THRU)

1

(CODE)

25

(CATEGORY)

Williamsburg, Virginia

April 19-21, 1967



NATIONAL AERONAUTICS AND SPACE ADMINISTRATION

3
SYMPOSIUM ON
COMPUTER SIMULATION OF PLASMA
AND MANY-BODY PROBLEMS

*Cosponsored by
NASA Langley Research Center and
The College of William and Mary
held April 19-21, 1967, at
The College of William and Mary
Williamsburg, Virginia*



Scientific and Technical Information Division
OFFICE OF TECHNOLOGY UTILIZATION
NATIONAL AERONAUTICS AND SPACE ADMINISTRATION
1967
Washington, D.C.

This document is available from the Clearinghouse for Federal Scientific
and Technical Information (CFSTI), Springfield, Virginia, 22151, for \$3.00.

FOREWORD

Over the past 10 years, the rapidly growing capabilities of digital computers have made it possible to treat classical many-body problems in increasingly realistic ways. This capability has encouraged the development of a large number of specialized techniques for both direct simulation and more conventional solutions of such systems.

The purpose of this symposium is to provide a summary of past and present results, to provide a forum for exchanging current techniques and philosophies, and to assess future possibilities. It is believed that these proceedings will also serve as an introduction for those scientists newly interested in the field. Most of the papers included here deal with long-range forces and collective effects, such as those that occur in plasmas and astrophysical systems, although several neutral-gas problems are also included.

The panel discussions and audience comments were transcribed and edited for relevance and continuity; they have been approved in this form by the members of the panels. The papers and abstracts are presented as received from the authors. The views, comments, opinions, and findings expressed herein are not to be construed as an official position of either the National Aeronautics and Space Administration or the College of William and Mary.

PRECEDING PAGE BLANK NOT FILMED.

ACKNOWLEDGEMENTS

The Organizing Committee for the symposium wishes to acknowledge its indebtedness to The College of William and Mary and to the Langley Research Center of the National Aeronautics and Space Administration for their sponsorship. Their joint cooperation turned the conception of this symposium into reality.

The assistance and guidance of the Scientific Advisory Committee is also acknowledged as having played a significant role in providing the guidelines which made the program so successful. The members of this Committee were:

Charles K. Birdsall, Department of Electrical Engineering, University of California, Berkeley, California

Oscar Buneman, Institute for Plasma Research, Stanford University, Stanford, California

John M. Dawson, Plasma Physics Laboratory, Princeton University, Princeton, New Jersey

Marc R. Feix, Physics Department, College of William and Mary, Williamsburg, Virginia, and NASA Langley Research Center, Hampton, Virginia

The Organizing Committee:

Fred R. Crownfield
College of William and Mary, Williamsburg, Virginia

Marc R. Feix
College of William and Mary and NASA Langley Research Center, Hampton, Virginia

Frank Hohl
NASA Langley Research Center, Hampton, Virginia

Gary A. Massel
NASA Langley Research Center, Hampton, Virginia

CONTENTS

FOREWORD	iii
ACKNOWLEDGMENTS	iv

INTRODUCTORY ADDRESS

THE SYMBIOSIS OF COMPUTERS AND THEORETICIANS IN PLASMA PHYSICS	1
By O. Buneman, Stanford University	

PLASMA PHYSICS

COMPUTER EXPERIMENTS ON THE MICROSCOPIC THEORY OF PLASMAS	3	✓
By Marc R. Feix, Gary A. Massel, and Richard H. Weinstein, NASA Langley Research Center (Invited)		
INVESTIGATIONS OF NONLINEAR BEHAVIOR IN ONE-DIMENSIONAL PLASMA MODEL . . .	25	✓
By J. M. Dawson, Princeton University (Invited)		
SHOT NOISE IN THE LAGRANGIAN ONE-DIMENSIONAL MODEL	31	✓
By Christopher W. Barnes and D. A. Dunn, Stanford University		
INVESTIGATIONS OF A SHEET MODEL FOR A BOUNDED PLASMA WITH MAGNETIC FIELD AND RADIATION	39	✓
By Bruce Langdon and John Dawson, Princeton University		
NONLAMINAR EFFECTS IN PLASMA SLAB OSCILLATIONS	41	✓
By H. M. Schneider and A. Bers, Massachusetts Institute of Technology		
PRELIMINARY MEASUREMENTS OF NOISE IN A TWO-DIMENSIONAL ROD MODEL OF A PLASMA	57	✓
By R. W. Hockney, Stanford University		
MICRO-REVERSIBILITY IN COMPUTER SIMULATION	61	
By O. Buneman, Stanford University		
ON THE NUMERICAL SOLUTION OF POISSON'S EQUATION	63	✓
By Craig G. Smith, Princeton University		
DRIVEN OSCILLATIONS AND NORMAL MODES OF A NONUNIFORM PLASMA	73	
By William M. Leavens, Environmental Science Services Administration		
NUMERICAL STUDIES OF THE STEADY-STATE PLASMA SHEATH PROBLEM	75	✓
By Lee W. Parker, Mount Auburn Research Associates, Inc. (Cambridge, Mass.) and Edward C. Sullivan, NASA Goddard Space Flight Center		

NUMERICAL SOLUTION OF THE FOKKER-PLANCK EQUATIONS FOR A HYDROGEN PLASMA FORMED BY NEUTRAL INJECTION	85	✓
By John Killeen and Archer H. Futch, Lawrence Radiation Laboratory, University of California (Livermore)		

VLASOV THEORY

NONLINEAR STUDY OF VLASOV'S EQUATION FOR A SPECIAL CLASS OF DISTRIBUTION FUNCTIONS	91	✓
By K. V. Roberts and H. L. Berk, University of California (San Diego)		
NONLINEAR SOLUTIONS OF THE VLASOV EQUATION BY VELOCITY SPACE EXPANSION IN LAGUERRE POLYNOMIALS	137	✓
By R. J. Lomax, University of Michigan		
ASYMPTOTIC STATE OF THE TWO-STREAM INSTABILITY	145	
By Thomas P. Armstrong, University of Iowa		
ON SOME ASPECTS OF THE EIGENFUNCTION EXPANSION OF THE SOLUTION OF THE NONLINEAR VLASOV EQUATION	149	
By W. L. Sadowski, National Bureau of Standards (see also p. 433)		
FOURIER-HERMITE EXPANSION OF THE VLASOV EQUATION	151	
By Marc R. Feix and Frederick C. Grant, NASA Langley Research Center		
NUMERICAL SOLUTION OF THE VLASOV EQUATION IN A FOUR-DIMENSIONAL PHASE SPACE	155	
By John Killeen, Lawrence Radiation Laboratory, University of California (Livermore)		

MAGNETOHYDRODYNAMICS AND PLASMA DEVICES

MAGNETOHYDRODYNAMIC PLASMA CALCULATIONS	163	✓
By K. V. Roberts, University of California (San Diego)		
COMPUTER SIMULATION OF THE THETA PINCH	191	✓
By Thomas A. Oliphant, Los Alamos Scientific Laboratory		
COMPUTER SIMULATION OF BEAM BUNCHING	197	
By K. R. Crandall, Los Alamos Scientific Laboratory		
NONLINEAR HIGH FREQUENCY-PLASMA INTERACTION IN A MAGNETIC MIRROR	199	✓
By E. Canobbio and R. Collet, Centre d'Etudes Nucléaires de Saclay		
COMPUTER SIMULATION OF THE BEAM-PLASMA INTERACTION	217	✓
By J. A. Davis and A. Bers, Massachusetts Institute of Technology		

NUMERICAL SOLUTION FOR 1.5-DIMENSIONAL, TIME-DEPENDENT MAGNETOHYDRODYNAMIC PROBLEMS	237 ✓
By Klaus Hain, NASA Goddard Space Flight Center	
CALCULATION OF HIGHLY DISTORTED PLASMA INTERCHANGE MOTIONS WITH A NONLINEAR TWO-DIMENSIONAL TWO-FLUID COMPUTER MODEL	265
By J. A. Byers, Lawrence Radiation Laboratory, University of California (Livermore)	
THETA-PINCH SHOCK IMPLOSION CALCULATIONS BY MODEL SIMULATION OF COLLISIONLESS ION VLASOV EQUATION	269 ✓
By R. W. Kilb, General Electric Research and Development Center (Schenectady, N.Y.)	
ASTROPHYSICS	
MONTE CARLO METHODS IN STELLAR DYNAMICS	295
By Michel Hénon, Institut d'Astrophysique (Paris)	
RELAXATION OF A ONE-DIMENSIONAL SELF-GRAVITATING GAS	299 ✓
By Myron Lecar, Smithsonian Astrophysical Observatory and Harvard College Observatory and Leon Cohen, Hunter College and Smithsonian Astrophysical Observatory	
RELAXATION OF A TWO-COMPONENT SELF-GRAVITATING GAS	309 ✓
By Leon Cohen, Hunter College and Smithsonian Astrophysical Observatory and Myron Lecar, Smithsonian Astrophysical Observatory and Harvard College Observatory	
THE N-BODY GRAVITATIONAL PROBLEM AND THE SIMULATION OF GALACTIC CLUSTERS	315 ✓
By A. Hayli, Institut d'Astrophysique and Faculté des Sciences (Paris)	
ONE- AND TWO-DIMENSIONAL MODELS TO STUDY THE EVOLUTION OF STELLAR SYSTEMS	323 ✓
By Frank Hohl, NASA Langley Research Center	
GRAVITATIONAL EXPERIMENTS WITH A CYLINDRICAL GALAXY	337 ✓
By R. W. Hockney, Stanford University	
COLLECTIVE MOTIONS IN A SPHERICAL STAR CLUSTER	349 ✓
By Michel Hénon, Institut d'Astrophysique (Paris)	
STABILITY OF NUMERICAL INTEGRATION AND REGULARIZATION IN THE N-BODY PROBLEM	365
By V. G. Szebehely, E. M. Standish, and C. Frederick Peters, Yale University	

NEUTRAL GASES

VELOCITY AUTOCORRELATIONS FOR HARD SPHERES	367
By B. J. Alder and T. E. Wainwright, Lawrence Radiation Laboratory, University of California (Livermore)	

NUMERICAL EXPERIMENTS ON THE NONLINEAR KROOK MODEL OF THE BOLTZMANN EQUATION	369 ✓
By C. K. Chu, Columbia University	

THE NUMERICAL SIMULATION OF THE ATMOSPHERE (Presented orally only, not for publication)	
By Cecil E. Leith, Lawrence Radiation Laboratory, University of California (Livermore)	

BIBLIOGRAPHY AND CLASSIFICATION

COMPUTER EXPERIMENTS WITH CHARGED PARTICLES, CHARGED FLUIDS AND PLASMAS: A CLASSIFICATION AND BIBLIOGRAPHY	375 ✓
By Charles K. Birdsall, University of California (Berkeley)	

PANEL DISCUSSIONS AND CONCLUSIONS

METHODOLOGY IN THE N-BODY PROBLEM: LAGRANGE VERSUS EULER APPROACH - FIRST PANEL	407 ✓
APPLICATIONS AND ORGANIZATION OF THE NEW FIELD OF COMPUTATIONAL PHYSICS - SECOND PANEL	417

REGISTRATION

LIST OF ATTENDEES	429
-----------------------------	-----

INTRODUCTORY ADDRESS

Introductory Address

by

O. Buneman, Stanford University

The Symbiosis of Computers and Theoreticians in Plasma Physics*

Ideally, plasma theory should make precise predictions on the basis of precisely stated initial- and boundary-conditions, and the precisely known laws of interaction. Failures of the theory, or its slowness of progress, cannot be excused by lack of input data or by natural mysteries. Extreme complication, and our limited mathematical ability are to blame.

Our mathematical training and language are heavily biased toward linearity and our attempts to grapple with non-linearities employ such linearized language as "wave-wave interaction". The philosophy of developing in ascending powers of a "small" quantity has led to misleading answers in several areas of plasma theory (moment expansions, adiabaticity, interaction expansions) and an expansion in wave amplitudes has little chance of accounting properly for plasma turbulence.

Even in the linear domain the simple wave dispersion picture has delayed progress by decades as a result of its non-causal nature, and urgent linear problems have still remained unsolved for this very reason. Computer simulation scores over conventional theory because (1) it does not rely on linearity and (2) it operates causally, sequentially.

It is suggested that in future we retain the mathematical apparatus of conventional theory, in particular transforms, for those portions of our problems which are linear and have closed boundaries, and for the critical analysis of computer accuracy, stability, resolution, economy. For an understanding of the evolutionary and non-linear processes we let the computer show us the way. Simply watching the movies has already provided much insight and qualitative explanation of phenomena. In due course it will lead to the birth of a new mathematical language with which we can then operate quantitatively.

*Supported by NONR 225(83).

PLASMA PHYSICS

N67-37738

3 COMPUTER EXPERIMENTS ON THE MICROSCOPIC

THEORY OF PLASMAS

6 Marc R. Feix,*

NASA, Langley Research Center, and
The College of William and Mary6 Gary A. Massel, and Richard H. Weinstein
NASA, Langley Research Center

The kinetic theory of homogeneous stable plasmas was developed around 1960 by Lenard, Balescu, Rostoker and Rosenbluth. This theory gives the fluctuations, the correlations and some of the irreversible coefficients such as the drag and the diffusion for a plasma at thermal equilibrium. These results are also applicable outside thermal equilibrium provided one can define a stationary or "metastable" distribution $F(v)$. In both cases, the theory is completely described by a dielectric constant $\epsilon(k, \omega)$ given by the well-known relation

$$\epsilon(k, \omega) = 1 + \frac{\omega_p^2}{k} p \int_{-\infty}^{+\infty} \frac{\frac{dF(v)}{dv}}{\omega - kv} dv + i\pi \frac{\omega_p^2}{k|k|} \left(\frac{dF(v)}{dv} \right)_{v=\frac{\omega}{k}} \quad (1)$$

Computer experiments have been performed previously by J. Dawson,^{1,2} and O. Eldridge and M. Feix.^{3,4} In references 1, 3 and 4 the plasma was in thermal equilibrium and the agreement was good. In reference 2 a first step

* NRC-NAS Senior Postdoctoral Resident Research Associate

was taken to check the theory outside thermal equilibrium, with special emphasis on checking a prediction concerning the time of Maxwellianization.

It is the purpose of this paper to briefly sketch some recent results concerning both Maxwellian and non-Maxwellian plasmas. The experiments have given qualitative and quantitative checks with both Vlasov theory and some aspects of first-order theory.

I. COMPUTER PROGRAMS

The one-dimensional N-body problem with electrostatic interactions can be solved exactly as described in reference 3. However, it is necessary to stop at each crossing in order to recalculate the self-consistent electric fields. The computer time needed to treat a plasma of length L with a Debye distance D and for a time T is

$$\text{Computer time} = (nD)^2 \frac{L}{D} \omega_p T \theta \quad (2)$$

where θ is the machine time per crossing.

In order to study a plasma outside of thermal equilibrium, nD must be large enough so that the different order time scales are widely separated and one can define a metaequilibrium. In order to get reasonable statistical accuracy, it is usually necessary to take long time averages and require that during this time the physical quantity of interest should not change. As a consequence, nD should be large - certainly 20 or greater - and consequently, the time for the exact program will be very long. Thus an approximate program in which the system is advanced by fixed time increments has been used. The equations of motion for the plasma particles are

$$\begin{aligned}
 x &= x_0 + v_0 \Delta t + \frac{1}{2} \gamma_0 (\Delta t)^2 \\
 v &= v_0 + \gamma_0 \Delta t + \frac{1}{2} \dot{\gamma}_0 (\Delta t)^2
 \end{aligned}
 \tag{3}$$

where $\gamma_0 = \frac{q}{m} E_0$ and $\dot{\gamma}_0 = \frac{q}{m} \dot{E}_0 - \dot{E}_{-1}$. Use of the approximate program results in an enormous time saving because it scales as nD rather than $(nD)^2$. The conservation of energy in the approximate program, given as the fractional energy increase per ω_p^{-1} , is shown in figure 1. The necessity of including the \dot{E} term is evident from the figure. An important general feature of the approximate program is the increasing accuracy with increasing nD and decreasing ΔT allowing one to provide a good approximation to a Vlasov (large nD) plasma with reasonable computation times.

II. THE FOURIER CHARGE DENSITY SPECTRUM

The first series of experiments to be considered concerns the microscopic electric field, derived from the Fourier charge density

$$\rho(k, t) = \sum_j \sigma_j \exp[-ikx_j(t)] . \tag{4}$$

The autocorrelation of this quantity, i. e.,

$$C(k, \tau) = \langle \rho^*(k, t) \rho(k, t + \tau) \rangle_t , \tag{5}$$

is directly connected to the plasma dielectric constant $\epsilon(k, \omega)$. By calculating $\epsilon(k, \omega)$, one can check not only the linearized Vlasov equation (the Landau theory) but also fluctuating quantities to first order in the plasma parameter $(nD)^{-1}$ through the use of $\epsilon(k, \omega)$ in the dressed particle picture. The connection between $\epsilon(k, \omega)$ and plasma fluctuations and correlations has

been the object of many theoretical papers^{6,7,8} and represents a generalization of the Nyquist fluctuation-dissipation for collisionless plasmas.

The potential energy of the plasma per degree of freedom (i. e. for each wave number, in the Fourier representation) is calculated from the Poisson law and $C(k, \tau = 0)$. This has been checked previously by Dawson¹ and Eldridge and Feix³ for a Maxwellian plasma; with $F(v) = Ae^{-\beta v^2}$ the potential energy, normalized to units of kinetic energy is

$$W(k) = \left(\frac{1}{8\pi}\right) \langle |E(k, t)|^2 \rangle_t = \left(\frac{1}{2}\right) \frac{1}{1 + k^2 D^2} . \quad (6)$$

The experimental data given in figure 2 agrees fairly well with the theory except for the long wavelengths, where the fluctuations are large.

Unless instabilities are present, any one-dimensional distribution function should be stationary in time to first order in $g = \frac{1}{nD}$ (as shown later) and one may also calculate the potential energy harmonics for a nonequilibrium plasma; for example, the square distribution

$$F(v) = \frac{1}{2a} \quad \text{for } |v| \leq a$$

$$F(v) = 0 \quad \text{for } |v| > a$$

for which Dawson studied the relaxation. Because there is no high energy tail to this distribution there should be no excitation of long wavelengths; i. e. $\langle |E(k = 0, t)|^2 \rangle_t = 0$ instead of $1/2$ as for the Maxwellian.

The experimental results for the square distribution are shown in figure 3. The long wavelengths are found to be excited contrary to the prediction of the collisionless theory. It is necessary to take long time

averages in order to obtain any type of a steady result and even then large excursions are noted. The reason for this lack of agreement is found both in the limitations of the theory and the practicalities of the experiment.

In particular:

(a) The zero-order kinetic theory is valid at long wavelengths only for nD very large; mathematically speaking, the limits $g = \frac{1}{nD} \rightarrow 0$ and $k \rightarrow 0$ do not commute. For the case shown, the collisionless theory would not be applicable below $kD = 0.6$. Kaufman⁹ has shown that as $k \rightarrow 0$, $W(k)$ should go to a finite limit.

(b) Once excited, the long wavelengths experience little damping and the averaging times necessary for their equilibrium in the system are long enough to strain the overall accuracy of the problem - both from an error standpoint and also the eventual thermalization of nonequilibrium plasmas.

(c) The statistical accuracy of the long wavelength representation depends on the total number of particles considered both through the $\frac{L}{D}$ ratio ($L = N$ for $n = 1$) and the number of particles in the tail of the distribution function. As the $\frac{L}{D}$ ratio is increased, the number of wavelengths in the system for each mode grows, thereby improving the representation of each mode; this problem is critical for the $kD < 1$ range. Also, since the excitation and damping of long wavelengths is intimately tied to the superthermal particles, increasing the total number of particles (and thereby the numbers in the high velocity tail) should also help to improve the long wavelength energy balance, again from a statistical point of view. Increasing the number of particles we can treat is therefore a top priority goal.

III. FLUCTUATIONS ACROSS A PAIR OF GRIDS

To study the microscopic behavior of the plasma, one of the most useful approaches is to immerse a pair of idealized grids into the plasma and either launch a c. w. signal at a known frequency or to record the fluctuation across the grids. Theoretically, the two problems are very closely related because the solution of each requires obtaining the resultant signal of the entire k-spectrum. Thus the result is only frequency dependent.

Derfler and Simonen¹⁰ have recently launched signals into a plasma with an externally driven pair of grids and their data shows excellent agreement with the Landau dispersion relation. This represents one contribution to the dynamics of the plasma. Another is the contribution of the continuous distribution of eigenvalues^{11,12} or the branchline integral.¹³

In the computer experiments it is easier to use the grid pair as a passive probe with which to observe the potential fluctuations. The periodic boundary conditions which are necessary in computer simulation of an infinite plasma introduce unrealistic feedback (in the computer model) which makes it difficult to simulate launching a signal in an infinite plasma. In addition, the fluctuations are an inherently linear phenomenon.

The relation of the plasma dynamics to the fluctuation is made through an analogue of Nyquist's "Fluctuation-Dissipation Theorem."⁶ For the case of the finite sensing device - a grid pair - the analogous relation can be derived directly from Vlasov theory to give

$$S(\omega) = \frac{1}{4\pi} \frac{1}{\omega_p^2} \frac{1}{nD} \left(\frac{\Delta}{D} \right) \text{Re } z_g(\omega) \quad (7)$$

where $S(\omega)$ is the spectral function defined by

$$S'(\omega) = \frac{1}{2\pi} \int_{-\infty}^{+\infty} \langle \Phi^*(t) \Phi(t + \tau) \rangle \exp\{-i\omega\tau\} d\tau \quad (8)$$

and $z_g(\omega)$ is the impedance of the grid pair of separation:

$$z_g(\omega) = \frac{2\Delta}{i\omega} \int_{-\infty}^{+\infty} \left[\frac{\sin \frac{k\Delta}{2}}{\frac{k\Delta}{2}} \right]^2 \frac{1}{\epsilon(k, i\omega)} dk . \quad (9)$$

The properties of the plasma are manifested in the autocorrelation function

$$B(\Delta, \tau) = \langle \Phi(t) \Phi^*(t + \tau) \rangle \quad (10)$$

of the potential fluctuations. The steady-state plasma properties are given by $\tau = 0$ (i. e. $B(\Delta, 0) = \langle |\Phi(t)|^2 \rangle$). From equation (8) this is found to be the area under the $S(\omega)$ curve. For the Maxwellian plasma, $B(\Delta, 0)$ is shown to possess two distinct regions:

$$(a) \quad \frac{\Delta}{D} < 1$$

$$B(\Delta, 0) = \frac{1}{2nD} \left(\frac{\Delta}{D} \right)^2 \quad (11)$$

$$(b) \quad \frac{\Delta}{D} > 1$$

$$B(\Delta, 0) = \frac{1}{nD} \left(\frac{\Delta}{D} \right) . \quad (12)$$

These two regions correspond to the dominance of the individual particle behavior for $\frac{\Delta}{D} < 1$ and of the collective effects for $\frac{\Delta}{D} > 1$. Figure 4 shows very good agreement between the experiment and theory in both regions for several values of nD . The potential Φ is the actual potential normalized to kT/e and thus $B(\Delta, 0)$ scales as kT .

Turning attention to the non-Maxwellian distribution, one expects the k -integration to improve the accuracy of the quantities which are observed. This is indeed the case. As has been shown by Rostoker⁶ and Feix and Von Hagenow,⁷ the theory for an equilibrium plasma carries over to a non-equilibrium case if a metastable state exists. This occurs for one-dimensional plasmas as will be shown in the next section. Thus for a Druyvesteyn distribution, the theory again defines two regions:

$$(a) \quad \frac{\Delta}{D} < 1$$

$$B(\Delta, 0) = \frac{\alpha}{4nD} \left(\frac{\Delta}{D} \right)^2 \quad (13)$$

$$(b) \quad \frac{\Delta}{D} > 1$$

$$B(\Delta, 0) = \frac{3}{2nD} \quad (14)$$

where $\alpha = 1.48$ and where the mean energy of distribution is normalized to that of a Maxwellian. The experimental data is shown in figure 5. Here a distinct leveling is seen which was predicted by the theory and arises as a manifestation of the antishielding property of the Druyvesteyn and the square distributions. The quantitative discrepancy with the theory is due to the over-excitation of the long wavelengths described in section 2.

To study the dynamic behavior of the plasma, one can observe the autocorrelation function defined in equation (10). Figures 6 and 7 show the results for $\frac{\Delta}{D} = 2$ and $\frac{\Delta}{D} = 10$. For $\tau \approx 0$, the continuous spectrum, which is heavily damped, plays a role. For $\frac{\Delta}{D} = 10$, the initial damping is seen to be less than for $\frac{\Delta}{D} = 2$ because the long wavelengths are more strongly excited.

The behavior for large τ is dominated by the least damped portion of the spectrum which is the discrete pole, i. e. the Landau pole. Thus, asymptotically

$$B(\Delta, \tau) = \frac{1}{\sqrt{6\pi}} \frac{1}{nD} \left(\frac{\Delta}{D} \right)^2 \tau^{-1/2} \cos \omega_p \tau .$$

This same behavior has been predicted by Engelmann and Feix¹⁴ for the propagation of a pulse in a plasma. The $\tau^{-1/2}$ damping is due to the phase-mixing of many different modes. The agreement between experimental and theoretical results is shown in figures 6 and 7. It was only possible to obtain meaningful results up to $\tau \omega_p \approx 40$ since beyond there the accumulation of computer error began to destroy the correlations.

By taking the spectrum of $B(\Delta, \tau)$, it is possible to observe both the resonance of $\omega = \omega_p$ and the continuous distribution of eigenvalues. Thereby, the existence of this contribution is explicitly demonstrated.

IV. META-EQUILIBRIUM AND TEST PARTICLE BEHAVIOR

In calculations involving the nonequilibrium plasmas, the existence of stationary velocity distribution function was taken for granted. The time-dependent behavior of both the overall velocity distribution and test particle distribution can, however, be useful in checking the kinetic theory - especially for nonequilibrium plasmas. Test particle experiments, impossible to perform in a real experiment, are of particular interest in one-dimensional plasmas for which the test particle and overall distribution functions behave differently.

The Balescu-Lenard equation, i. e.

$$\frac{\partial F(\vec{v}_\alpha)}{\partial t} = 16\pi^3 e^4 n \int d\vec{k} \int d\vec{v}_1 \vec{k} \cdot \frac{\partial}{\partial \vec{v}_\alpha} \frac{\delta \vec{k} \cdot [\vec{v}_\alpha - \vec{v}_1]}{|\epsilon(\vec{k}, \vec{k} \cdot [\vec{v}_\alpha - \vec{v}_1])|^2 k^4} \left(\frac{\partial}{\partial \vec{v}_\alpha} - \frac{\partial}{\partial \vec{v}_1} \right) F(\vec{v}_\alpha) F(\vec{v}_1), \quad (16)$$

describes the thermalization of the one-particle distribution function (for particle α) in terms of interactions with field particles (denoted 1); the time scale of this relaxation is $\tau_1 = \frac{nD}{\omega_p}$ - first order in the graininess parameter. Because the Fourier transform of the electrostatic potential (i. e. $\vec{V}(k)$) has the same $\frac{1}{k^2}$ dependence in one and three dimensions, one may obtain a one-dimensional analog of equation (16) which may be obtained simply by removing the vector signs and changing the multiplicative constant from $16\pi^3$ to 4π . The Dirac δ -function $\delta(\vec{k} \cdot [\vec{v}_\alpha - \vec{v}_1])$ is nonzero only for

$$\left. \begin{array}{l} \vec{k} = 0 \\ \vec{v}_\alpha = \vec{v}_1 \\ \vec{k}_\perp \cdot \vec{v}_\alpha - \vec{v}_1 \end{array} \right\} \text{ in three dimensions and } \left\{ \begin{array}{l} k = 0 \\ \vec{v}_\alpha = v_1 \end{array} \right\} \text{ in one dimension.}$$

Thermalization in three dimension comes from waves normal to $[\vec{v}_\alpha - \vec{v}_1]$, but there is no thermalization on the scale of τ_1 in one dimension if $F(\vec{v}_\alpha) = F(v_1)$, the total distribution function. The existence of this meta-equilibrium was pointed out for the first time by Eldridge and Feix⁴ and checked by Dawson² with a one-species plasma model having an initially square velocity distribution. Dawson found thermalization to occur on a second-order time scale $\tau_2 \approx 10 \frac{(nD)^2}{\omega_p}$. Figure 8 shows a calculation similar to

that of Dawson's mode with a two-species model also using a square velocity distribution. The distribution function is shown for four plasmas with $nD = 10, 20, 40, 60$ at a scaled time $T = 4\tau_1$. As the separation of first and second order time scales increases (with increasing nD), second order effects become negligible and the original shape (indicated by the outline corners at $V = \pm 1.7$) is closely maintained; the only prominent change is the development of a small, high-velocity tail.

The absence of thermalization, while expected for a one-dimensional system having only short range, binary interactions, is at first surprising for a plasma, where the interactions are collective. The explanation is to be found in the test particle picture, in which individual particles emit waves (plasmons) which are resonantly absorbed by other particles. This process is analogous to a binary encounter, even though the propagation and damping of the waves is described by the collective properties of the plasma.

Relaxation effects are found to first order if we distinguish between a test particle distribution and the overall distribution function. Thus, if $F(V_\alpha) \rightarrow \phi(V_\alpha)$ and $V_\alpha = V_1$ then $\frac{\partial \phi(V_\alpha)}{\partial t} \neq 0$. Equation (16) may then be viewed as a Fokker-Planck equation with a time scale $\tau_1 = \frac{nD}{\omega_p}$, from which the drag and diffusion (in velocity space) of test particles can be calculated. A typical drag calculation for a Maxwellian plasma is shown in figure 9 giving the average velocity of groups of test particles as a function of the first-order time. All test particles initially have velocities within $\pm 10\%$ of the thermal velocity and the four sets of data represent $nD = 10, 20, 40, 60$. The overlap of the data clearly verifies the time scaling concept, because the fundamental plasma time (in units of ω_p^{-1}) over which the measurements extend changes by a factor of six as nD goes from 10 to 60.

The initial slope of the data gives a drag coefficient of within 10% of the theoretical value.

In general, the velocity diffusion coefficient can be shown to be¹⁵

$$\frac{d}{dt} [\langle v^2 \rangle - \langle v \rangle^2] = \left(\frac{\sigma}{m}\right)^2 \frac{1}{2\pi} \int_{-\infty}^{+\infty} d\omega \int_{-\infty}^{+\infty} dk \langle |E(k, \omega)|^2 \rangle \delta(\omega - kv) . \quad (17)$$

It is most convenient to examine the diffusion at zero velocity, for which the drag is zero and changes in the distribution function are entirely due to diffusion. Expressing the diffusion in terms of normalized velocity $V = \frac{v}{v_T}$ and first-order scaling time τ_1 , then the normalized diffusion coefficient at $V = 0$ is

$$\psi(V = 0) = \frac{d}{d\tau_1} [\langle V^2 \rangle - \langle V \rangle^2] = \begin{cases} 0.40 & \text{for } F(V) \text{ Maxwellian} \\ 0.86 & \text{for } F(V) \text{ square} \end{cases}$$

To obtain a valid measurement for a nonequilibrium plasma, nD must be large enough so that the metaequilibrium is maintained. Figure 10 shows experimental data for Maxwellian and square velocity distributions with $nD = 60$, and the diffusion coefficients given by the slopes of the data are .41 and .90 for the Maxwellian and square distributions respectively. This agreement is quantitatively good and re-enforces both the metaequilibrium and the applicability of the kinetic theory out of equilibrium.

V. CONCLUSIONS

Three kinds of problems have been treated: (1) the Fourier density function; (2) potential fluctuations; and (3) relaxation effects. For non-equilibrium plasmas, all three problems are intimately related to the prediction of a metaequilibrium in one dimension, i. e. the persistence of any stable distribution for times $T \ll \frac{(nD)^2}{\omega_p}$. This point was well established by the third problem, showing not only the existence of a metaequilibrium but giving good agreement for first-order scaling and measurements of the diffusion coefficient.

In the first type of problem, experimentally observed Fourier density functions for infinite plasmas at thermal equilibrium were well described by the usual linearized theory. For nonequilibrium plasmas, only qualitative agreement was found because of long wavelength difficulties. Large fluctuations in slowly damped, long wavelength modes are tied to the scarcity of high-velocity particles and would also require averaging times long enough to strain the metaequilibrium limitation and computer accuracy for the size of present problems. Computer accuracy in an approximate program includes both general cumulative errors and errors due to the larger number of crossings made by high-velocity particles.

The use of the grid pair as a probe to study plasma fluctuations introduces an interesting possibility for plasma diagnostics. Good agreement was obtained for both the static and the time-dependent analyses. The diffusional damping proportional to $\tau^{-1/2}$ was observed to dominate and would thus be expected to determine the propagation of a pulse in the plasma. Only alluded to in this paper was the existence of the contribution of the continuous

distribution of eigenvalue to the spectrum. This contribution has been explicitly observed in these computer experiments.

The experiments also showed the limited range of validity of the theory for finite nD . The relative success of equilibrium measurements comes from the fact that the ratio of each order of excitation and damping mechanisms, which determines the potential energy is $\frac{kT}{2}$ at equilibrium; i. e.

$$E_k = \frac{e_0 + ge_1 + g^2 e_2 + \dots}{\gamma_0 + g\gamma_1 + g^2 \gamma_2 + \dots}$$

where $\frac{e_0}{\gamma_0} = \frac{e_1}{\gamma_1} = \frac{e_2}{\gamma_2} \dots = \frac{kT}{2}$. Introduction of first-order effects would not, therefore, change the character of the small k result for equilibrium; for the square distribution, the vanishing zero-order result (for $k \rightarrow 0$) is easily swamped by nonzero higher order effects for finite nD .

Decisive results for long wavelength phenomena in nonequilibrium plasmas can be obtained only for much larger values of nD and $\frac{L}{D}$. The need for perhaps 10,000 particles and $nD > 100$ should prove to be a formidable test of the new generation of computers.

REFERENCES

1. Dawson, J.: One-Dimensional Plasma Model. Phys. Fluids, vol. 5, p. 445, 1962.
2. Dawson, J.: Thermal Relaxation in a One-Species One-Dimensional Plasma. Phys. Fluids, vol. 7, p. 419, 1964.
3. Eldridge, O. C. and Feix, M. R.: One-Dimensional Plasma Model at Equilibrium. Phys. Fluids, vol. 5, p. 1076, 1962.
4. Eldridge, O. C. and Feix, M. R.: Numerical Experiments with a Plasma Model. Phys. Fluids, vol. 6, p. 398, 1963.
5. Weinstein, R. H.: Computer Experiments on the Microscopic Behavior of One-Dimensional Plasmas. M. S. Thesis, Virginia Polytechnic Institute, 1967. To be proposed for NASA TN.
6. Rostoker, N.: Fluctuations of a Plasma (I). Nuclear Fusion, vol. 1, p. 101, 1961.
7. Dupree, T. H.: Dynamics of Ionized Gases. Phys. Fluids, vol. 4, p. 696, 1961.
8. Feix, M. R. and von Hagenow, K.: Connection Between Correlations and Fluctuations in a Plasma. Phys. Fluids, vol. 8, p. 1565, 1965.
9. Kaufman, A. N.: Extension of the Plasma Kinetic Equation to Small Wave Numbers. Phys. Rev. Letters, vol. 17, p. 1127, 1966.
10. Derfler, H. and Simonen, T. C.: Landau Waves. An Experimental Fact. Phys. Rev. Letters, vol. 17, p. 172, 1966.
11. Van Kampen, N. G.: On the Theory of Stationary Waves in Plasmas. Physica, vol. 21, p. 949, 1955.

12. Shure, F. C.: Boundary Value Problems in Plasma Oscillations, The Plasma Capacitor. Journal Nucl. Eng., Part G, vol. 6, p. 1, 1964.
13. Massel, G. A.: Kinetic Theory of Forced Oscillations in Plasmas. Ph. D. dissertation, North Carolina State University, 1967.
14. Engelmann, F., Feix, M., Minardi, E. and Oxenius, J.: On the Diffusion of an Electric Field in a Collisionless Plasma. Nuovo Cimento, vol. 22, p. 1012, 1966.
15. Hubbard, J.: The Friction and Diffusion Coefficients of the Fokker-Planck Equation in a Plasma. Proc. Royal Soc. of London, Part A, vol. 260, p. 114, 1961.

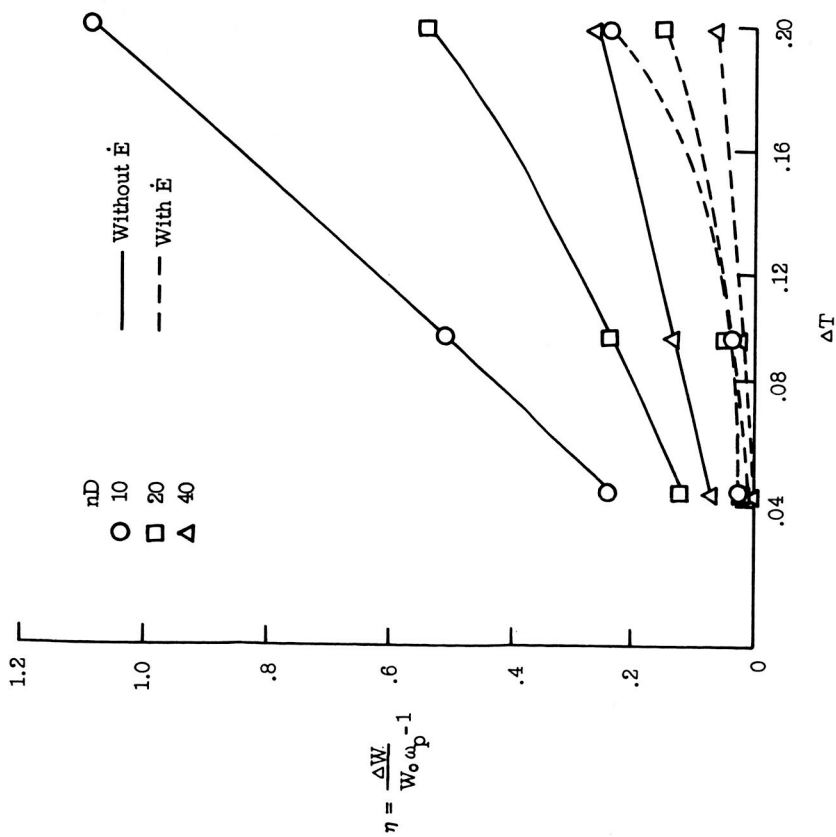


Figure 1.- Conservation of energy in the approximate program.

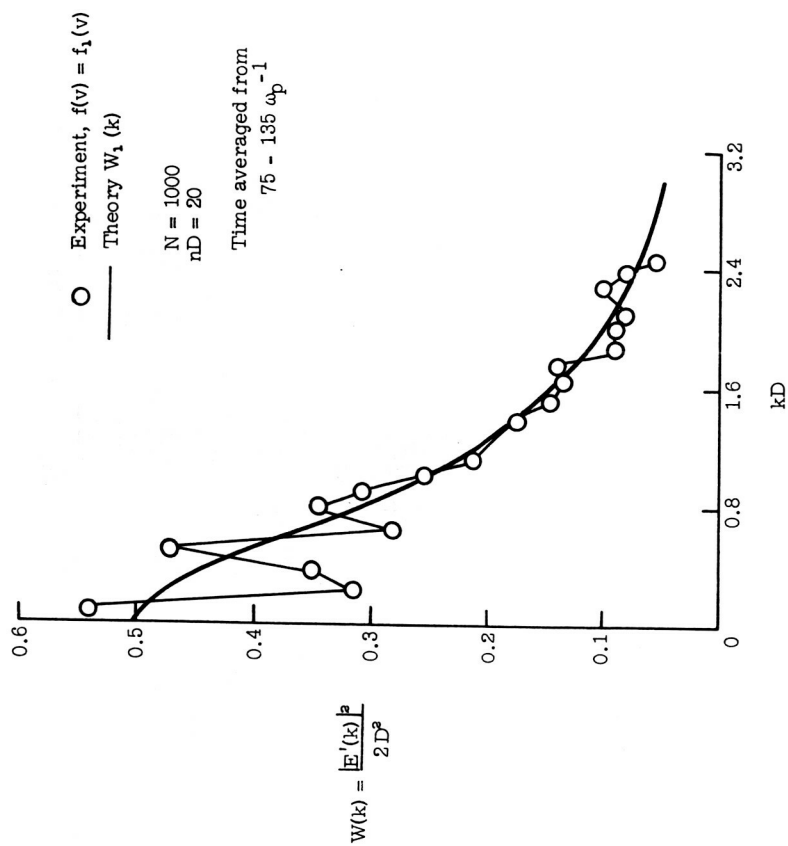


Figure 2.- Potential energy modes for a Maxwellian plasma.

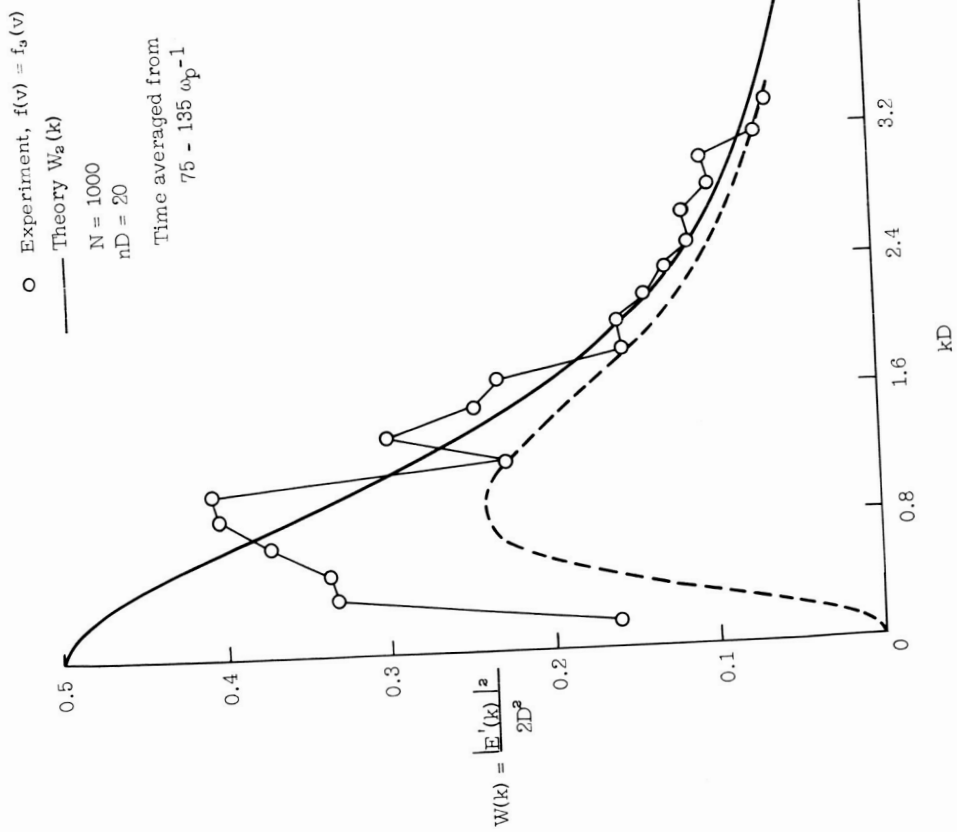


Figure 3.- Potential energy modes for a nonequilibrium plasma.

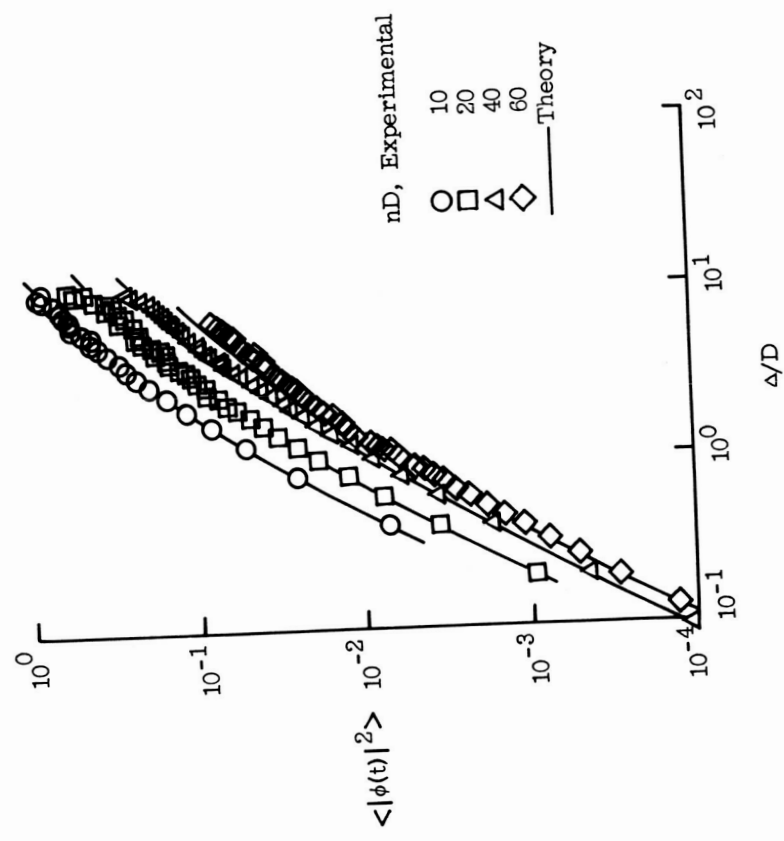


Figure 4.- Correlation function for $\tau = 0$ for a Maxwellian distribution.

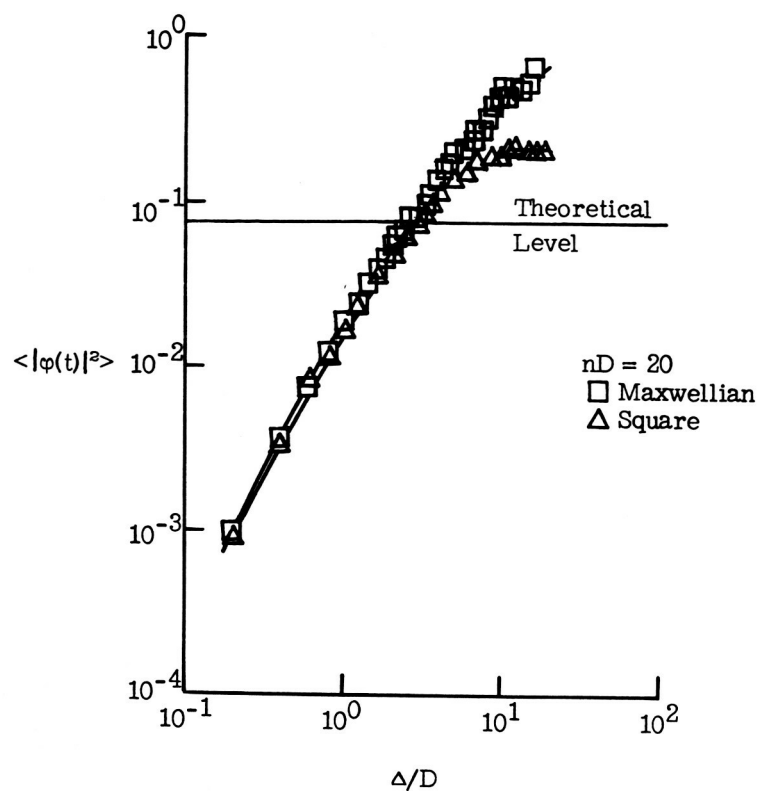


Figure 5.- Correlation function for $\tau = 0$ for a Druyvesteyn distribution.

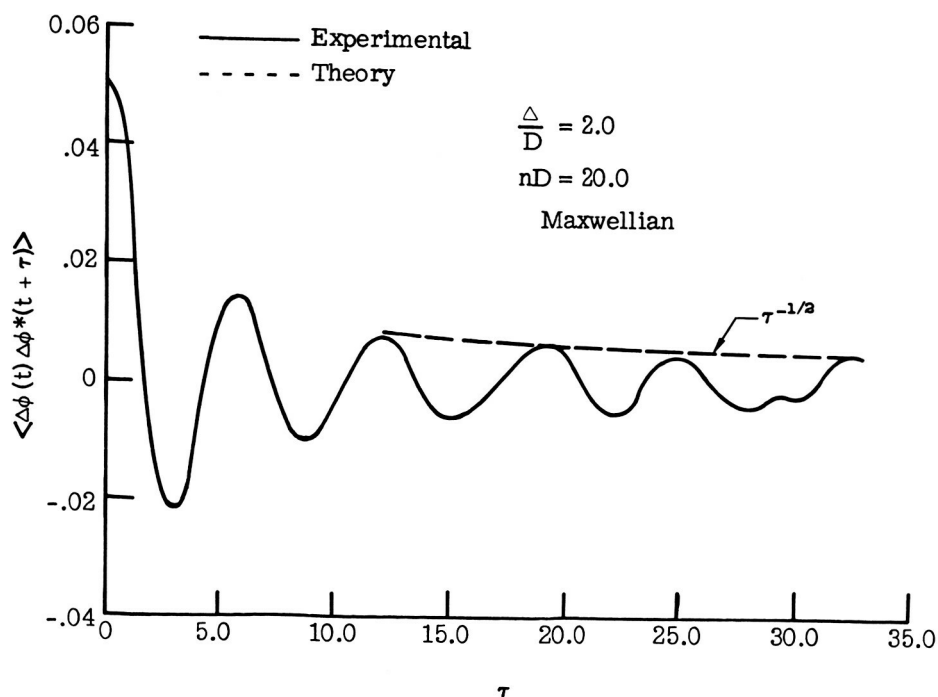


Figure 6.- Autocorrelation function for a Maxwellian distribution for $\frac{\Delta}{D} = 2$.

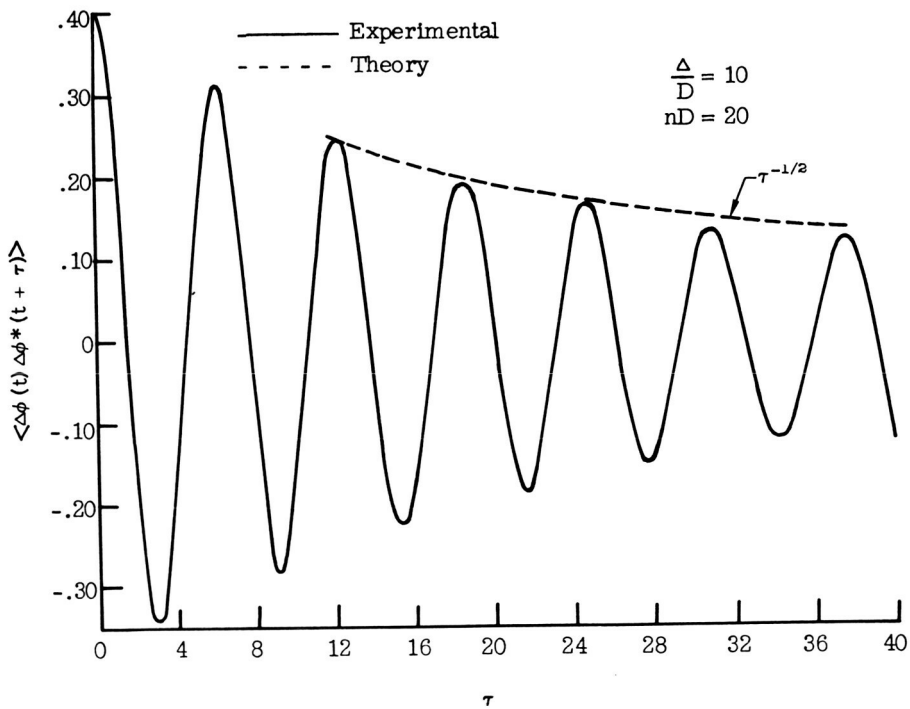


Figure 7.- Autocorrelation function for a Maxwellian distribution for $\frac{\Delta}{D} = 10$.

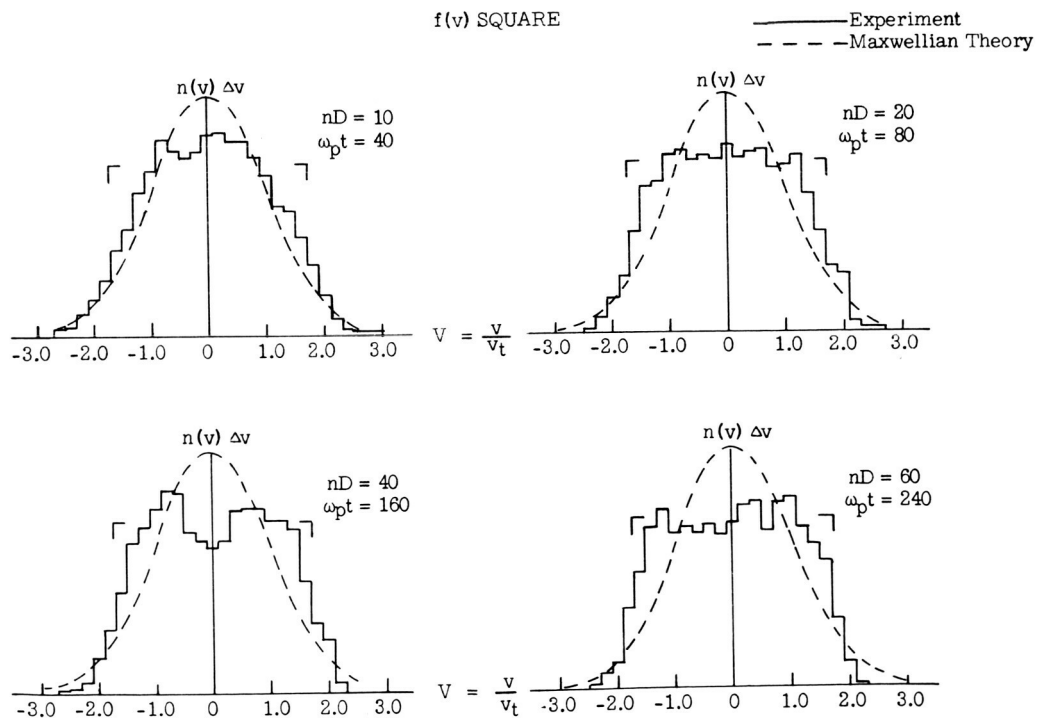


Figure 8.- Metaequilibrium velocity distribution.

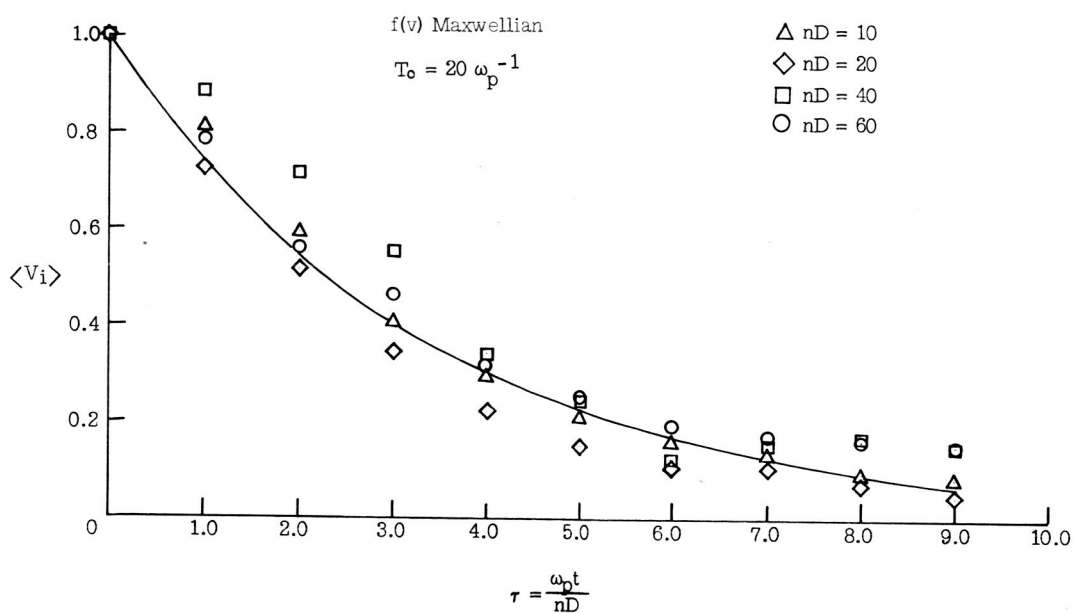


Figure 9.- Test particle drag - $f(v)$ Maxwellian.

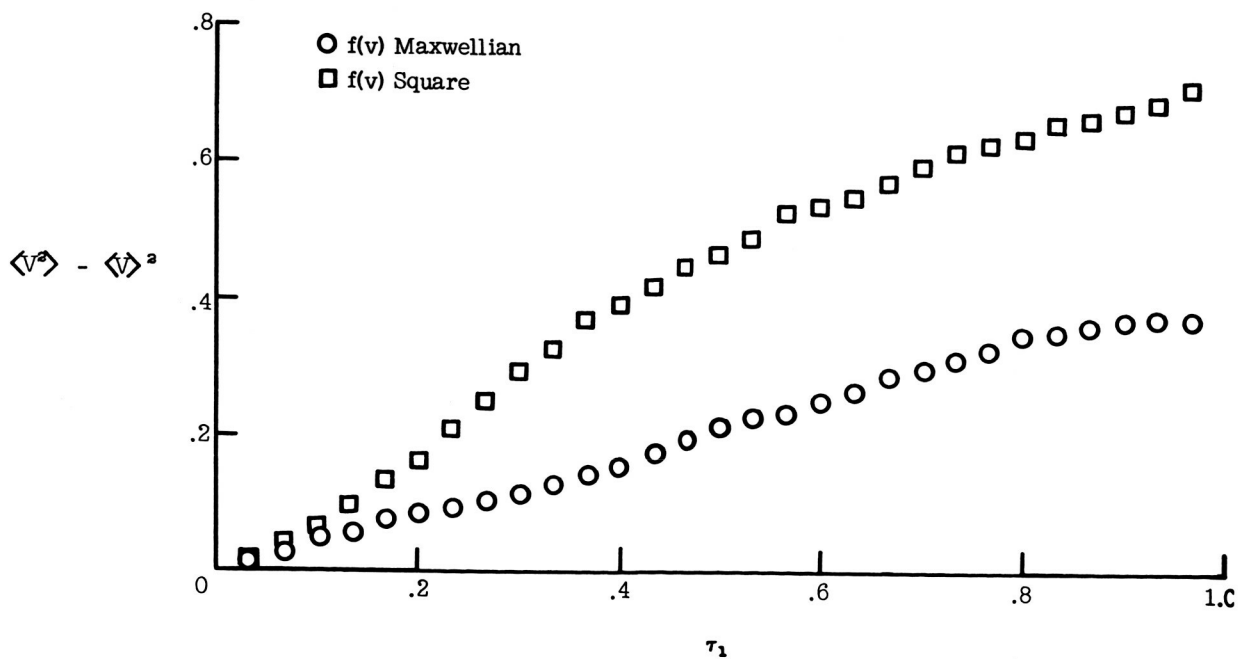


Figure 10.- Test particle diffusion at metaequilibrium.

N67-37739

3
INVESTIGATIONS OF NONLINEAR BEHAVIOR
IN ONE-DIMENSIONAL PLASMA MODEL*

J. M. Dawson 8/10/68

2
1 Plasma Physics Laboratory 3
Princeton University 11-1-68 2

The results of three experiments on the nonlinear behavior of one-dimensional plasmas are presented. The calculations were carried out in conjunction with Ramy Shanny of the General Electric Company, Space Sciences Laboratory, King of Prussia, Pennsylvania. The three experiments were the Landau damping of the large-amplitude plasma oscillation, mode coupling between two strongly excited plasma oscillations, and the turbulence generated by the passage of a weak beam through a plasma. A short summary of the results follows.

I. LANDAU DAMPING OF A LARGE-AMPLITUDE
PLASMA OSCILLATION

The Landau damping of a large-amplitude plasma oscillation was investigated. The wave had a phase velocity such that it fell in the tail of the velocity distribution where very few electrons appear. It was found that the damping was much stronger than was predicted by linear theory and that the damping increased rapidly with increasing amplitude of the wave. An explanation of these results is that the wave accelerates particles with velocities considerably less than its phase velocity up to velocities equal to or in excess of its phase velocity. The Landau damping of such a

wave is nonlocal, that is, it does not depend simply on the derivative of the distribution function at the phase velocity, but rather depends on the mean slope of the distribution function over a range of velocities that is roughly equal to that for which particles would be trapped if the wave were not damped.

II. INVESTIGATIONS OF MODE COUPLING ON A ONE-DIMENSIONAL PLASMA MODEL

This experiment sought to verify the theory of mode coupling through the mechanism of nonlinear Landau damping. The results are in agreement with the theory within the accuracy of the experiment as long as quasi-trapped particles (particles that would be trapped if one of the waves existed by itself) are avoided. These quasi-trapped particles, if they exist, give rise to a strong damping like that observed in the first experiment.

According to theory, two longitudinal modes with frequencies and wave numbers ω_1 , k_1 , ω_2 , k_2 should be coupled by the particles traveling at velocity v , $v = (\omega_1 - \omega_2)/(k_1 - k_2)$, where v is roughly the group velocity. The primary effect is to transfer energy from the short-wavelength, high-frequency mode to the long-wavelength, low-frequency mode. (The dispersion relation is $\omega^2 = \omega_p^2 + 3k^2 V_T^2$, where V_T is the thermal velocity of the particles.) The particles carry off a small amount of the wave energy. Figure 1 shows the result of one such experiment. Two modes were strongly excited with $(k\lambda_D)^{-1} = 3.5$ and 4.4 . The long-wavelength mode grows and the growth is almost exactly what is

predicted by theory. The short-wavelength mode decays somewhat more rapidly than theory would predict. It appears that some of the damping of the short-wavelength mode is due to collisions, i.e., because of the discrete nature of the model, the collisions between particles result in the absorption of some of the wave energy. Although this effect is small it is of significance in this experiment. By going to a very large system with a very hot plasma and very long wavelengths, it was possible to reduce this effect to about 10 percent of the mode coupling effect.

In order to obtain the results shown, it was found necessary to eliminate particles that could be accelerated into resonance with a shorter-wavelength mode. Therefore, the tail of the Maxwellian velocity distribution was truncated at 1.6 times the thermal velocity. Also, the amplitudes of all other wavelength modes, except the two that were specifically excited, were suppressed. This was done to prevent the diffusion of particles to the higher velocities that these modes caused. It was found that with these precautions the agreement with theory shown in Fig. 1 could be obtained.

III. TURBULENCE PRODUCED BY THE TWO-STREAM INSTABILITY IN A ONE-DIMENSIONAL PLASMA

Some numerical experiments have been carried out to investigate the turbulence produced in a one-species, one-dimensional plasma by a bump in the tail of the Maxwellian distribution. The purpose of the experiments was to see if the results could be explained by means of quasilinear theory.

Some aspects appear to agree with this theory but many do not. The initial velocity distribution consisted of two components--the main plasma and the beam plasma. The main plasma contained 95 percent of the particles and had a Maxwellian distribution. The beam contained 5 percent of the particles, it had a Maxwellian distribution whose width was equal to the thermal velocity of the main plasma, and it had a mean velocity which was 3.5 times the thermal velocity. The plasma contained 2,000 particles in all, and there were 10 sheets per Debye length. There were roughly 10 unstable modes.

The unstable modes grew and saturated after a few e-folding times. At the same time, the bump in the tail flattened out as predicted by theory. After the initial growth, the unstable modes remained at a relatively high level of excitation; however, their amplitudes showed relatively rapid time fluctuations, growing and dying in times of the order of one plasma period. This is contrary to the assumptions of quasilinear theory, which assumes that the amplitudes change only slowly in time. After the tail flattened out, there was a gradual diffusion of particles to higher velocities with particles ultimately reaching more than 7 times the thermal velocity (and roughly 3 times the maximum energy of any particle at time $t = 0$). The tail develops into a Maxwellian shape with a temperature of roughly 10 times the temperature of the main plasma. This temperature is roughly what one would get if one equated the beam energy to KT . The energy of the initially unstable waves is on the average equal to the energy of a particle

in the tail (KT for the tail). Thus, there appears to be a rapid thermalization of the tail particles among themselves and with the waves they interact with. None of this would be predicted by quasilinear theory. It appears that many of these effects may be due to the discrete nature or graininess inherent in the model. If one computes Cherenkov radiation of longitudinal waves by the particles in the tail, one finds that they emit as much energy as is contained in the waves in a time of the order of a few plasma oscillations. Thus, it appears that this is a very important effect. The waves appear to cause a rapid thermalization of the particles. This thermalization is much faster than one would predict from simple collisional calculations. Estimates of the importance of such interactions for energetic particles embedded in a cold plasma indicate that these effects can also be important in three dimensions.

* This work was performed under the auspices of the U. S. Atomic Energy Commission, Contract No. AT(30-1)-1238 and the Internal Research Program of the General Electric Company, Space Sciences Laboratory, King of Prussia, Pennsylvania. Use was made of computer facilities supported in part by National Science Foundation Grant NSF-GP579.

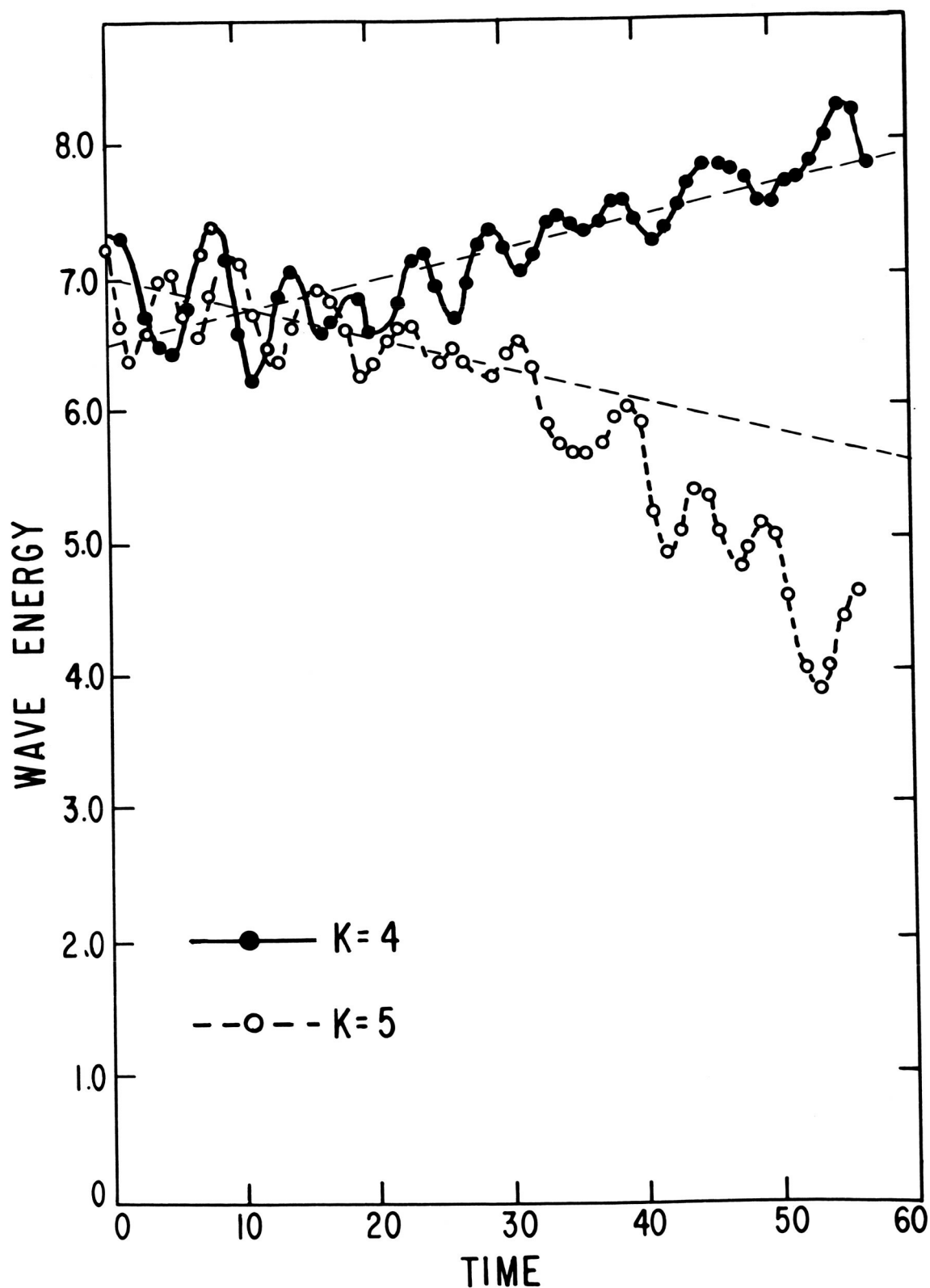


Figure 1.- Wave energy vs time for mode coupling between modes 4 and 5.

SHOT NOISE IN THE LAGRANGIAN ONE-DIMENSIONAL MODEL[†]

by

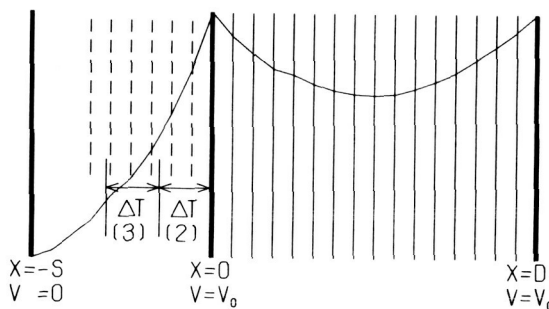
Christopher Barnes and D. A. Dunn
 Institute for Plasma Research,
 Stanford University
 Stanford, California

SUMMARY

Presented here are results of computer experiments designed to test the effects of coarse graining in the one-dimensional planar Lagrangian computer simulation of a one dimensional electron diode.

In recent years many researchers have made use of the one-dimensional charge sheet model in computer simulations of electron and plasma diodes, sometimes referred to as a Lagrangian or super-particle model¹⁻⁶. It is well known that the use of many sheets and small time steps in a simulation is desirable, although expense and computer size limitation place practical limits on the ultimate graininess of the model. This paper examines some of the effects of time and space coarse graining on a computer simulation of an electron diode using the Lagrangian model.

Fig. 1. One-dimensional planar model



The model is, as shown in Fig. 1, a planar, one-dimensional geometry. Electron sheets are injected at $x = 0$ as if they had been accelerated from a space-charge limited cathode at $x = -S$. The anode is placed at $x = D$. The

[†]This work was supported by the U.S. Army Electronics Laboratories under Contract DA-28-043 AMC-00482(E).

ratio D/S then specifies the relationship between diode spacing, injected current and DC injection potential. The injection mechanism can be understood by imagining all the sheets to be injected in the future as being lined up behind $x = 0$ with constant spacing between them (Fig. 1, dashed lines). Each time step the sheets lying in the next $\Delta x = V_o \Delta T$ are placed inside the diode ($x > 0$) with the same spacing. Thus it is possible to inject effectively a noninteger number of sheets per time step. This allows us to induce artificially some of the "noise" generated by the discrete nature of the computer model. The electric field in the diode is approximated by calculating the field at a discrete number of points at uniform intervals across the diode.

The physical parameters of the model are D/S and V_{th} , the ratio of cathode temperature in volts to mean DC potential V_o . The computer parameters are N_o = the number of sheets injected in one transit time, Δt = length of time step in transit times, $N_o \Delta t$ = the number of sheets injected each time step, and N_{cell} , the number of cells used in the field calculation. We measure the value of potential minimum and total diode current, from which is derived the RMS fluctuation current.

Consider first the simulation of a diode below limiting perveance ($D/S < 2.8$). The potential minimum and current in such a system are non-time-varying. A non-time-varying result is always found from the computer model provided that an integer number of sheets are injected each time step. However, if a non-integer number of sheets is injected each time step, the currents and potentials will fluctuate with amplitudes that are a function of the number of sheets in the diode and the number injected per time step. Figure 2 illustrates this for three different cases, with various N_o , $N_o \Delta t$. Each plot has several values of $N_o \Delta t$ with the first and last segments of each an integer $N_o \Delta t$. Two

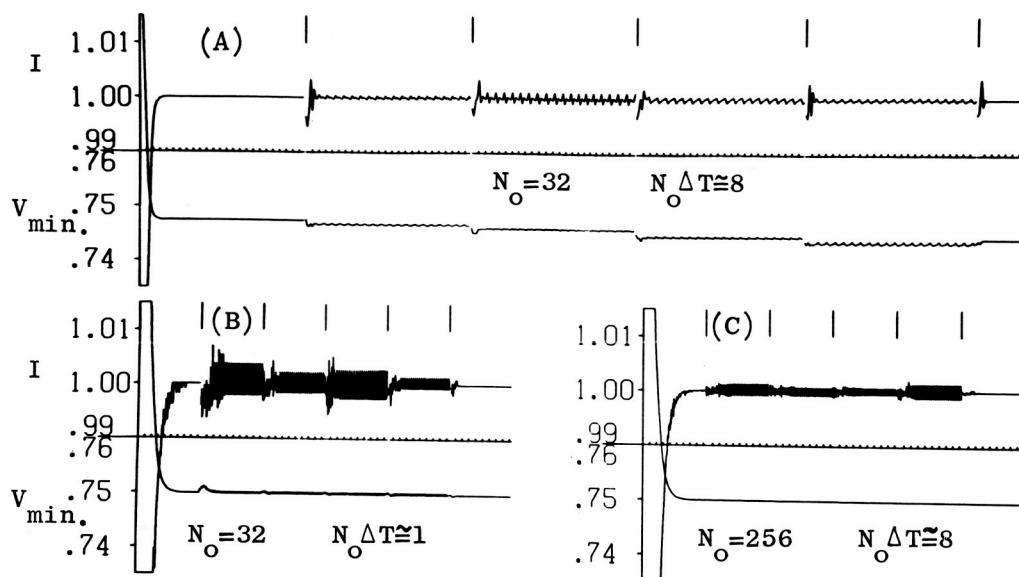


Fig. 2. Time variation of potential minimum (V_{\min}) and total diode current. Each tic on the horizontal axis corresponds to one transit time. For all three cases, $D/S = 2.0$, $V_{th} = 0.0$. Each case has six slightly different values of $N_O \Delta t$ with the first and last an integer. The points at which $N_O \Delta t$ was changed slightly are denoted by vertical dashes. (A) $N_O = 32$, $N_O \Delta t = 8.0, 8.8, 9.6, 10.4, 11.2, 12.0$. (B) $N_O = 32$, $N_O \Delta t = 1.0, 1.2, 1.4, 1.6, 1.8, 2.0$. (C) $N_O = 256$, $N_O \Delta t = 8.0, 8.2, 8.4, 8.6, 8.8, 9.0$.

effects can be seen. The current fluctuations seem to be a function of $N_O \Delta t$. Although $N_O \Delta t$ is noninteger, the number of sheets injected for any one time step of course is integral; thus if $N_O \Delta t = 8.5$, the model injects alternately 8 sheets and 9 sheets. The magnitude of the current fluctuation is then related to the fractional change in $N_O \Delta t$ from one time step to another. The second effect is that potential minimum fluctuations are related to N_O , i.e., the potential profile is smoother for large N_O . This noise is present in all models of this kind although not explicitly evident because of the presence of other effects.

Now suppose a beam with a finite temperature (half Maxwellian plus DC component) is injected into the diode. The potential minimum and current in the

diode will fluctuate due to shot noise. For Lagrangian super particle models the amplitude of the shot noise is very much greater than in real diodes because the charge per particle is much greater (by many orders of magnitude). This noise can mask collective effects if too few particles are used in a simulation. We present results of computer experiments designed to measure shot noise under varying conditions in a model of an electron diode in which both random velocity and current fluctuations can be introduced into the injected stream. Figure 3 shows three waveforms corresponding to three values of N_o , each case with four different Δt ranging from $1/4$ to $1/32$. Also shown are curves giving the dependence of the RMS current fluctuations on $1/\sqrt{N_o}$ and the number of field cells used.

It is well known that in an electron diode past limiting perveance, large oscillations are present in the potential minimum and current. We present the results of computer experiments in which a beam is injected with a perveance beyond limiting perveance with a finite temperature. Figure 4 shows results of four cases, for two different N_o and two different temperatures. Again several values of Δt are chosen for each run. It can be seen that with a thermal spread on the beam velocities, the oscillations are present with greatly reduced amplitude. Note that the number of sheets required to measure accurately this effect is an order of magnitude higher than is needed in the cold case, 32 being sufficient with $V_{th} = 0.0$ but at least 256 needed for $V_{th} = 0.1$. If V_{th} is made smaller the required N_o is even further increased. Figure 5 shows results obtained with $V_{th}=0.03$. With as many as $N_o = 2800$, it is not clear that the solution is constant with N_o .

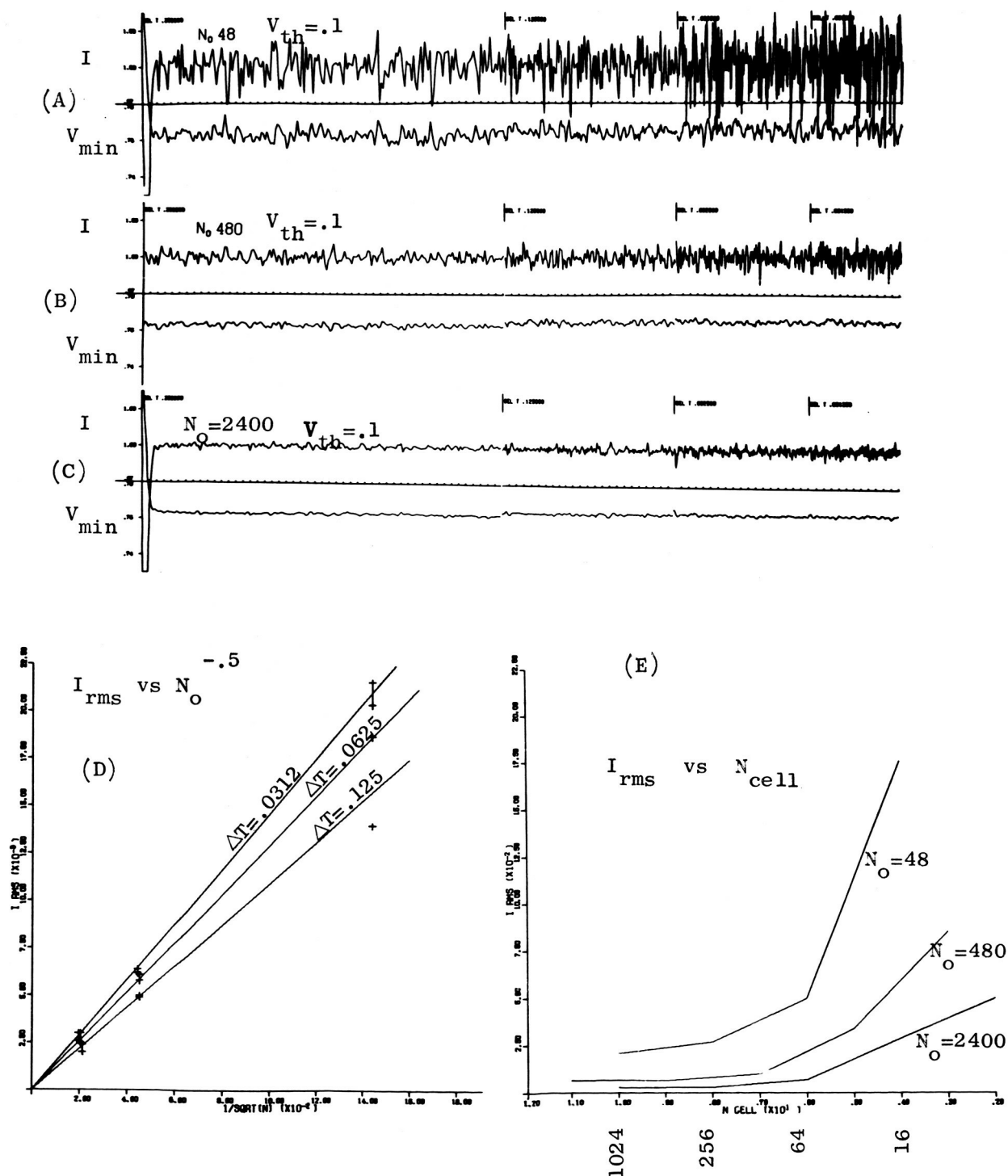


Fig. 3. $D/S = 2.0$, $V_{th} = 0.1$. (A) $N_O = 48$, (B) $N_O = 480$, (C) $N_O = 2400$. For each curve there are four different Δt : $1/4$, $1/8$, $1/16$, $1/32$, reading from left to right. (D) Plot of I_{rms} vs $1/\sqrt{N_O}$ for data shown in (A), (B), (C). The three curves show results for three values of Δt : $1/32$, $1/16$, $1/8$. (E) Plot of the effect of changing the number of field points (N_{cell}) on the fluctuation current. $\Delta t = 1/32$.

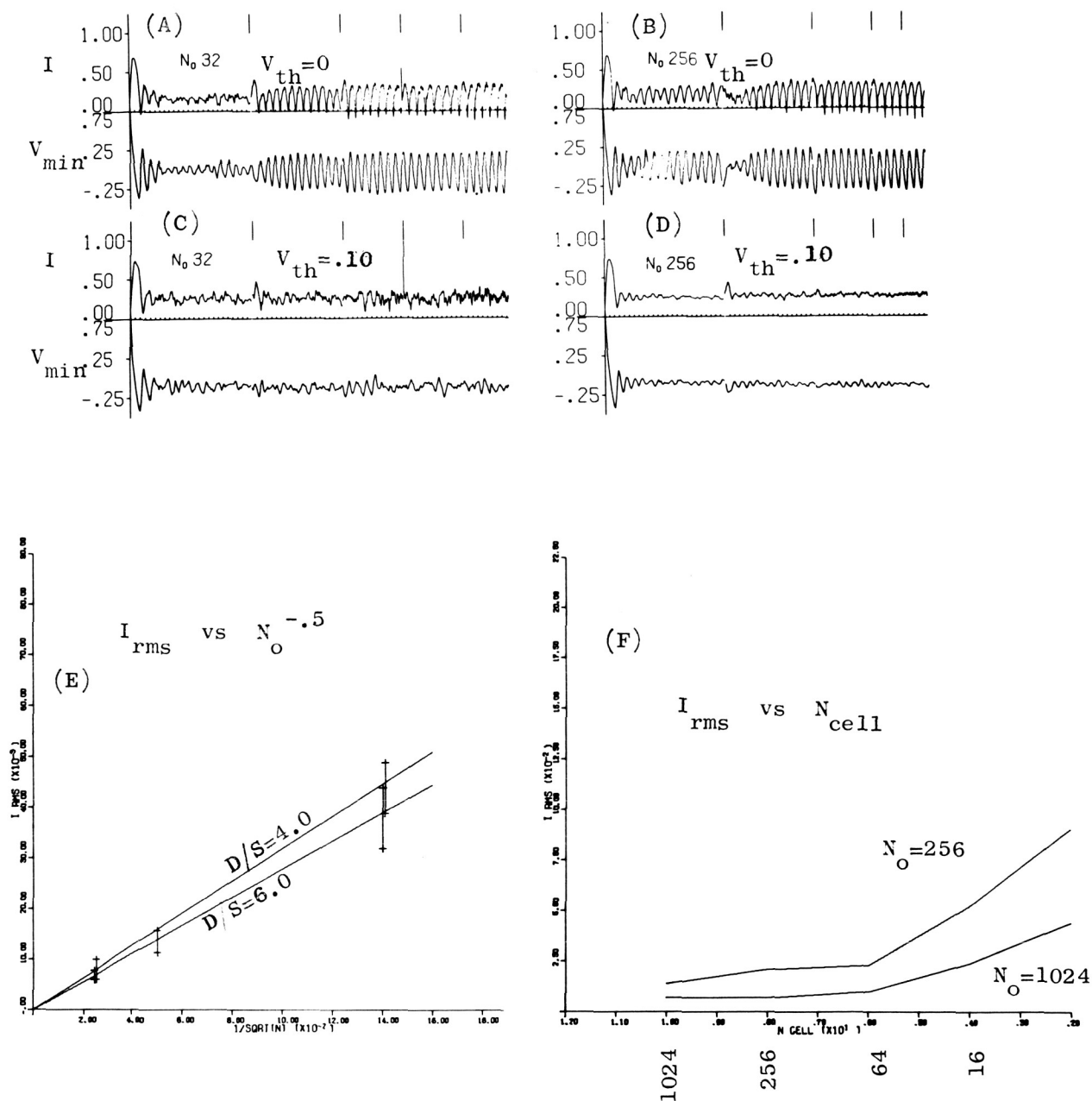


Fig. 4. $D/S = 4.0$, (A) $N_o = 32$, $V_{th} = 0$, (B) $N_o = 256$, $V_{th} = 0$, (C) $N_o = 32$, $V_{th} = 0.1$, (D) $N_o = 256$, $V_{th} = 0.1$. Again Δt varies between $1/4$ and $1/32$.
 (E) Plot of I_{rms} vs $1/\sqrt{N_o}$ for $D/S = 4.0$ and $D/S = 6.0$, $V_{th} = 0.1$.
 (F) Plot of I_{rms} vs N_{cell} for $D/S = 6.0$, $V_{th} = 0.1$ and two values of N_o , 256 and 1024.

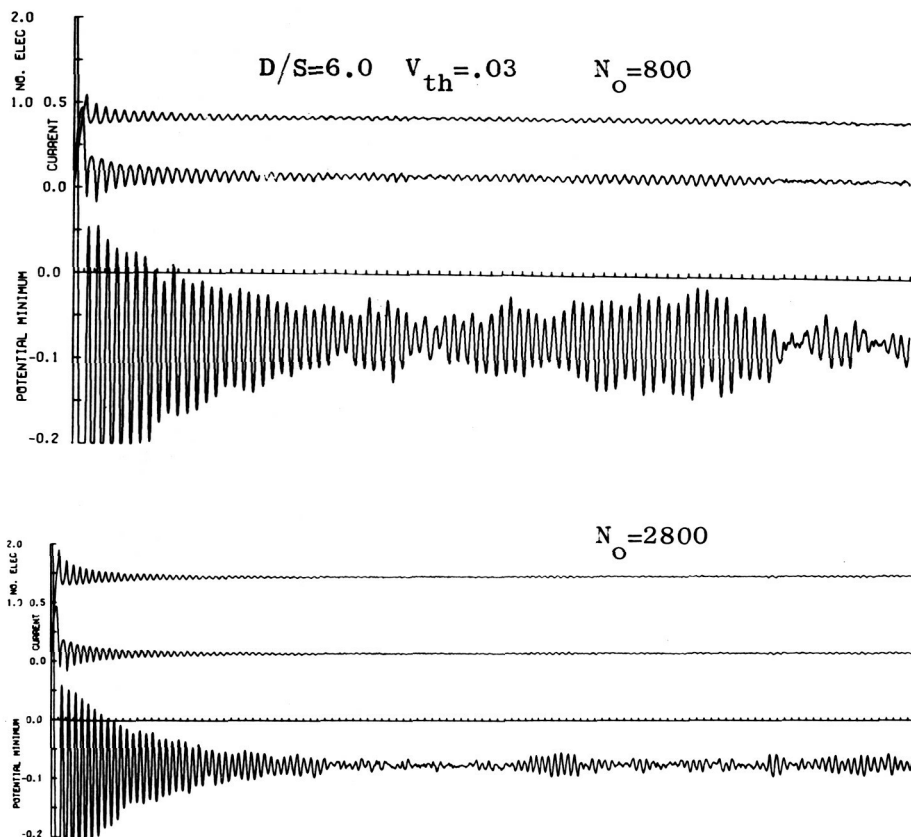


Fig. 5. Time variation of I and V_{min} for $D/S = 6.0$, $V_{th} = 0.03$, $N_O = 800$ and $N_O = 2800$. A curve showing the variations in time of the number of sheets in the diode is also plotted.

REFERENCES

1. C. K. Birdsall and W. B. Bridges, "Space-Charge Instabilities in Electron Diodes and Plasma Converters," Journal of Applied Physics, 32, No. 12, Dec. 1961.
2. W. B. Bridges and C. K. Birdsall, "Space-Charge Instabilities in Electron Diodes II," Journal of Applied Physics, 34, No. 10, Oct. 1963.
3. R. J. Lomax, J. Electron. Control, 9, 127 (1960).
4. P. Burger, "Theory of Large-Amplitude Oscillations in the One-Dimensional Low-Pressure Cesium Thermionic Converter," Journal of Applied Physics, 36, No. 6, June 1965.
5. C. K. Birdsall and W. B. Bridges, Electron Dynamics of Diode Regions, Academic Press (New York), 1966.
6. P. K. Tien and J. Moshman, J. Appl. Phys. 27, 1067 (1956).

INVESTIGATIONS OF A SHEET MODEL FOR A BOUNDED PLASMA WITH MAGNETIC FIELD AND RADIATION*

Bruce Langdon and John Dawson

Plasma Physics Laboratory
Princeton University

ABSTRACT

A number of extensions have been made to the usual one-dimensional sheet model for a plasma. The sheets, which lie in the y - z plane, are allowed to move in the x - y directions, passing freely through one another. The motion in the x direction produces the usual electrostatic field E_x , while the motion in the y direction produces radiation fields E_y and B_z , which are included in the calculation. A static external magnetic field in the z direction is included, and the smoothed-out neutralizing background charge density $n_0(x)$ varies with x . All quantities vary only in the x direction. The relevant Maxwell's and Newton's equations are

$$\frac{dp_x}{dt} = e E_x + \omega_c p_y$$

$$\frac{dp_y}{dt} = e E_y - \omega_c p_x$$

$$\omega_c = \frac{e}{m(v)c} (B_z + B_0)$$

$$\frac{\partial E_x}{\partial x} = 4\pi e [n(x, t) - n_0(x)] \quad n(x, t) = \sum_s \delta[x - x_s(t)]$$

$$\frac{\partial B_z}{\partial x} + \frac{1}{c} \frac{\partial E_y}{\partial t} = -\frac{4\pi}{c} J_y(x, t) \quad J_y(x, t) = e \sum_s v_{ys}(t) \delta[x - x_s(t)]$$

$$\frac{\partial E_y}{\partial x} + \frac{1}{c} \frac{\partial B_z}{\partial t} = 0$$

Since v_z , E_z , and B_y are all initially zero, they remain so.

Some things which can be done with the model are:

The spectrum of the Poynting flux as a function of x may be measured, and indicates where in the plasma emission originates. Under some conditions strong harmonic emission occurs.

The drag and diffusion of sheet velocities due to crossings may be measured.

By reflecting the radiation leaving the system back into it, one can watch the radiation field approach thermal equilibrium with the plasma.

If radiation with a flat spectrum is directed into the plasma, the reflective and transmissive properties of the plasma may be separated from the plasma's spontaneous emission. The cross-covariances of the inputs and outputs give the reflective and transmissive impulse responses; the cross-power spectra give the usual reflective and transmissive cross sections as functions of frequency.

Results of such experiments will be presented.

* This work was performed under the auspices of the Air Force Office of Scientific Research, Contract No. AF49(638)-1555. Use was made of computer facilities supported in part by National Science Foundation Grant NSF-GP579.

3 Nonlaminar Effects in Plasma Slab Oscillations*

6 H.M. Schneider and A. Bers 810

2 Research Laboratory of Electronics and
Department of Electrical Engineering,
Massachusetts Institute of Technology
Cambridge, Massachusetts 2

ABSTRACT

The dynamics of electrons which follow an initial displacement of the electron cloud in a cold plasma slab with tapered boundaries are presented. The behavior is quite different from the case where the slab has sharp boundaries. For a tapered slab, the time of first crossing depends on the amplitude of the initial displacement and the overtaking occurs for particles in the tapered region. If the initial displacement is small, overtaking takes place where ω_p' is a maximum and the time at which it occurs is inversely proportional to the initial displacement.

* This work was supported by the National Science Foundation (Grant GK-1165).

Introduction

The oscillations which result from an initial displacement perturbation of a one dimensional slab of cold electrons neutralized by a fixed background of ions have been known for some time⁽¹⁾. Recently, it was suggested that if the unperturbed electron and ion distributions have a sharp boundary with vacuum, the electrons which were originally displaced outside the ion background by the perturbation would not move synchronously and an overtaking or "scrambling" of electron trajectories would take place^(2,3). The time at which the first overtaking would occur was calculated for a sharply bounded plasma slab^(4,5). The result was that the first crossing always takes place in less than one plasma period, independent of the amplitude of the initial displacement. Computer experiments with a charge sheet model for the slab with a sharp boundary were in good agreement with this analytical result⁽⁶⁾. In addition, the computer experiments gave the dynamics of the electrons after the first overtaking, showing that the coherent oscillations of the slab were destroyed by a layer of electrons having random motions which spread to the center of the slab at a rate which was proportional to the amplitude of the initial perturbation^(6,7,8). The details of these results are given in Appendix I.

It is of interest to gain an understanding of just how important the assumption of a sharply bounded plasma is to the results obtained in those calculations. We wish to present some aspects of the oscillations of a cold plasma slab which has a gradual boundary with vacuum.

Charge Sheet Model Calculations for a Tapered Boundary

Consider a slab of plasma which is cold and which in equilibrium has electrons and ions distributed with the number

density $n(x)$ over a thickness d as is shown in Fig. 1. The ion and electron distributions are represented by a discrete number of charge sheets with the same charge per unit area on each sheet and the nonuniformity in the tapered regions ($0 < x < t$ and $(d-t) < x < d$) is modeled by a variable sheet spacing. The electron sheets were given a uniform displacement δ in the x -direction and their trajectories were computed, assuming that the ions are immobile (see Appendix II). In Fig. 2 we show the electron sheet trajectories for the case $t/d = \frac{1}{4}$ and $\delta/d = .04$ with the slab modeled by 50 sheets. Note that the first crossing of electron trajectories occurs in less than one plasma period of the central electrons. The new aspect of these results is that the overtaking particles are in the tapered region and were not originally displaced outside the ion background ($x > d$). In Fig. 3 we give electron sheet trajectories for the case $t/d = \frac{1}{4}$ and $\delta/d = .12$, a larger displacement than that in Fig. 2. Here we find the first overtaking occurring in less than half of a plasma period of the central electrons. This is a shorter time than in the case of a sharply bounded slab. From Figs. 2 and 3 we conclude that for a tapered slab the overtaking time depends on the amplitude of initial displacement, whereas in the sharply bounded case the overtaking time was independent of initial displacement. In Fig. 3 we note that the particles which first overtake are located in the tapered region at the bottom of the slab (having been displaced into the ion background) in contrast with the results for sharp boundaries where the initial scrambling always occurs near the top (particles displaced outside the boundary). In both Figs. 2 and 3 the overtaking eventually penetrates to the center of the slab in a manner which is similar

to the results obtained for sharply bounded slabs. The coherent oscillations of the central electrons are destroyed more rapidly as the amplitude of the initial perturbation is increased.

We will now give a theory based on a fluid description of the ions and electrons which shows that overtakings will occur in the bulk of an inhomogeneous cold plasma slab.

Overtakings in a slab with Tapered Boundaries

Assume that the electrons and ions in a one dimensional plasma slab of thickness d are cold and in equilibrium have equal number density distributions $n(x)$ where $0 < x < d$. If the ions are immobile, we can easily calculate the equation of motion for the electrons⁽⁵⁾. The electric field acting on an electron whose instantaneous position is x and unperturbed position is x_0 is given in the absence of overtakings by

$$E = \frac{e}{\epsilon_0} \left[\int_0^x n(x') dx' - \int_0^{x_0} n(x'_0) dx'_0 \right] \quad 0 < x < d \quad (1)$$

Here e is the magnitude of the charge on an electron. (Equation (1) applies to electrons which remain inside the ion background, which is the group of electrons whose motion we wish to find). The integrals over x' represent the contributions to the field due to the fixed ions, while those over x'_0 give the field due to the electron density. We note that the equation of motion of an electron may be written as

$$m \frac{d^2 x}{dt^2} = - \frac{e^2}{\epsilon_0} \int_{x_0}^x n(x') dx' \quad (2)$$

Here m is the mass of an electron. For a nonuniform plasma slab, equation (2) is a nonlinear differential equation. If the displacement from equilibrium x_0 is small, we may linearize this equation and obtain

$$\frac{d^2 x}{dt^2} = - \omega_p^2 (x_0) (x - x_0) \quad (3)$$

where

$$\omega_p^2 (x_0) = \frac{e^2 n(x_0)}{\epsilon_0 m} \quad (4)$$

is the local plasma frequency. We wish to solve equation (3) subject to the initial conditions that at $t = 0$, $x = x_0 + \delta$ and $\frac{dx}{dt} = 0$ (the initial displacement perturbation). The solution of (3) is

$$x = x_0 + \delta \cos \omega_p (x_0) t \quad (5)$$

This equation is valid for particles which remain inside the ion background. Let us apply the overtaking condition (4) $\frac{\partial x}{\partial x_0} = 0$ to equation (5) and call the time of overtaking t_0 . Then we have

$$\omega_p (x_0) t_0 \sin \omega_p (x_0) t_0 = \frac{\omega_p}{\delta \omega_p'} \quad (6)$$

where the prime indicates differentiation with respect to x_0 . This equation gives the overtaking times t_0 for a given displacement δ as a function of x_0 . To find the particles that

overtake the earliest we set $\frac{\partial t_o}{\partial x_o} = 0$. Then from eq. (6) we find

$$\left[\omega_p(x_o) t_o \right]^2 \cos \omega_p(x_o) t_o = - \frac{\omega_p'' \omega_p^2}{\delta (\omega_p')^3} \quad (7)$$

In Fig. 4, we show a graphical solution to equation (6) if x_o and δ are known. We have assumed $\omega_p(x_o)$ is symmetrical about the center of the slab. In this case there are two places in the slab where $|\omega_p'(x_o)| = \text{const.}$; only their signs will be different. For large initial displacements, an overtaking will first occur where ω_p' is positive ($x_o < d/2$) and then within one plasma period (measured at the local plasma frequency) where ω_p' is negative ($x_o > d/2$). As the displacement δ decreases, an overtaking occurs first for $x_o > d/2$ and then $x_o < d/2$. The overtakings are still within one period (at the local plasma frequency) of each other and the location of the first one jumps back and forth as δ decreases. This explains the change in location of the first crossings as a function of initial amplitude indicated in the charge sheet model calculations given in Figs. 2 and 3.

More general conclusions about the time of first overtaking in a tapered slab can be obtained if it is assumed that the initial displacement is very small. Then the solution to equation (6) is approximately

$$t_o \approx \frac{1}{\delta \omega_p}, \quad (8)$$

Applying the condition for first overtaking $\frac{\partial t_o}{\partial x_o} = 0$ to equation (8) we find that

$$\omega_p''(x_o) = 0 \quad (9)$$

The first overtaking occurs at the point where ω_p' is a maximum. The time of overtaking is inversely proportional to the amplitude of initial displacement.

An Example

We wish to show that a slab with smooth boundaries has overtakings in the region where ω_p' is a maximum as discussed in the previous section by integrating equation 2 for a simple density distribution.

Suppose the equilibrium density distribution in the slab is given by

$$n(x) = \frac{n_0}{4} \left(1 - \cos \frac{2\pi x}{d}\right)^2 \quad 0 < x < d \quad (10)$$

so that

$$\omega_p(x_0) = \omega_{po} \frac{1}{2} \left(1 - \cos \frac{2\pi x_0}{d}\right) \quad 0 < x_0 < d \quad (11)$$

where ω_{po} is the plasma frequency in the center of the slab (see Fig.6) The equation of motion (eq. 2) for electrons inside the slab is

$$\begin{aligned} \frac{d^2 x}{dt^2} = & - \frac{1}{4} \omega_{po}^2 \left[\frac{3}{2} (x - x_0) + \frac{d}{\pi} \left(\sin \frac{2\pi x_0}{d} - \sin \frac{2\pi x}{d} \right) \right. \\ & \left. + \frac{d}{8\pi} \left(\sin \frac{4\pi x}{d} - \sin \frac{4\pi x_0}{d} \right) \right] \end{aligned} \quad (12)$$

This equation was integrated numerically.

The results are shown in Fig. 7 for the case where the slab was given an initial displacement $\delta/d = 0.1$. The lines drawn in Fig. 7 are the integrated trajectories $x = x(x_0, t)$ for

values of x_0/d between 0.0 and 1.0 in steps of $\frac{1}{10}d$. The first overtaking occurs at the bottom of the slab for the particles whose unperturbed positions were between $(4/10)d$ and $(2/10)d$. (the linearized equations predict overtaking when $\omega_p'' = 0$ which for this density distribution (eq. 11) is $x_0 = d/4$ or $x_0 = 3d/4$).

Summary and Conclusions

The dynamics of electrons which result from an initial displacement perturbation of a slab with a tapered edge are fundamentally different from the case of a sharp boundary.

For a sharp boundary, the time of overtaking is independent of the amplitude of initial displacement and occurs for particles which were displaced outside the sharp ion background.

In a slab with a tapered boundary, the time of first overtaking depends on the amplitude of the initial displacement perturbation. For small initial displacements, the overtaking occurs for electrons in the tapered region where ω_p' is a maximum, and the time of overtaking is inversely proportional to the initial displacement.

It has been noted that linearized hydrodynamic equations for a cold inhomogeneous plasma have solutions (for similar initial value problems to those given here) in the first order electron density which are secular (of the form $t \sin \omega_p t$).⁽⁹⁾ These solutions may be related to the bunching and consequent crossing of trajectories illustrated by the Lagrangian analysis of a nonuniform slab such as is shown in Fig. 7. These difficulties with the Lagrangian and hydrodynamic descriptions indicate that a model in which nonlaminar effects are included in a self consistent manner (namely temperature) may be required when the plasma is inhomogeneous.

ACKNOWLEDGEMENT

This work was done in part at the M.I.T. Computation Center and in part using the facilities of Project MAC, at M.I.T. The assistance of the Computation Group of the Research Laboratory of Electronics at M.I.T. is also gratefully acknowledged.

Appendix I - Results for a Sharp Boundary

It has been shown from computer experiments that the oscillations of a plasma slab with sharp boundaries are destroyed by a scrambling which originally occurs near the surface.⁽⁶⁾ For small initial displacements, a layer of electrons with random motions spreads to the center of the slab at a constant rate R_s which is directly proportional to the amplitude of the displacement δ and given by the equation

$$R_s = 1.33 f_p \delta \quad 13$$

where f_p is the plasma frequency in cycles per second.⁽⁸⁾ The numerical factor in eq. 13 was found from the results of the computer experiments. If the plasma slab has thickness d , eq. 13 implies that the coherent oscillations are completely destroyed in a time T_d which is approximately

$$T_d \approx 0.38 (d/f_p \delta) \quad 14$$

The velocity distribution of the electron sheets has also been investigated. After the scrambling has made its way to the center of the slab, a Maxwellian was fitted to the velocity distribution of the electron sheets and a temperature of the slab was found. For example, with an initial displacement $\delta/d = .018$ we found a temperature which could be expressed by

$$\lambda_D = .007d \quad 15$$

where λ_D is the Debye length,

$$\lambda_D^2 = kT/m\omega_p^2 \quad 16$$

From conservation of energy, an upper bound on the Debye length can be found. If all the initial energy given to the slab by the displacement perturbation appears after a long time as thermal energy, the Debye length will be just equal to the amplitude of the initial displacement,

$$\lambda_D \approx \delta \quad \delta \ll d \quad 17$$

Appendix II - Calculation of Sheet Trajectories

The continuous electron and ion density distributions were both modeled by charge sheets.^(10,11) Since the ions were taken as having infinite mass, the ion sheets remained fixed in position. The motion of the electron sheets was obtained by the so called "exact" method which is described below.

An electron sheet experiences a constant force as long as it moves in the space between two other sheets. The electric field which acts on the sheet is the average of the electric fields on either side of it. When an electron sheet approaches another electron sheet or an ion sheet, it is allowed to pass freely through the other sheet. At this time of crossing, the electric field acting on the electron sheet changes and it obeys a new equation of motion. Thus crossing times play an important role if the exact electron trajectories are desired.

Initially, all the electron sheets are given a uniform displacement and their velocities are zero. The crossing times of all the electron sheets are calculated and the smallest one is found. The motion of all the sheets is updated to this first crossing time. The field acting on the crossing sheet is corrected to its new value (after crossing) and the next crossing time is again calculated.

The accuracy of the computations was checked by monitoring the total energy of the system (the kinetic energy of motion of the electron sheets plus the energy in the electric field) which should be conserved.

REFERENCES

1. L. Tonks, Phys. Rev. 37, 1458 (1931).
2. D.L. Bobroff, H.A. Haus, and J.W. Kluver, J. Appl. Phys. 33, 2932 (1962).
3. W.P. Allis, S.J. Buchsbaum, and A. Bers, Waves in Anisotropic Plasmas, Technology Press, Cambridge, Massachusetts, (1962), p. 152.
4. W.M. Leavens and I.B. Leavens, Bull. Am. Phys. Soc. I, 480, (1962).
5. W.M. Leavens and I.B. Leavens, Radio Science, I, 789 (1966).
6. H.M. Schneider, Phys. Fluids 9, 2299 (1966).
7. H.M. Schneider, Eighth Annual Meeting of the Division of Plasma Physics, American Physical Society, Boston, Nov. 1966.
8. H.M. Schneider, Quarterly Progress Report No. 84, Research Laboratory of Electronics, M.I.T., p. 149, Jan. 15, 1967.
9. E.M. Barston, Annals of Phys., 29, 282 (1964).
10. P.K. Tien, Proc. IRE, 44, 938 (1956).
11. J.M. Dawson, Phys. Fluids 5, 445 (1962).

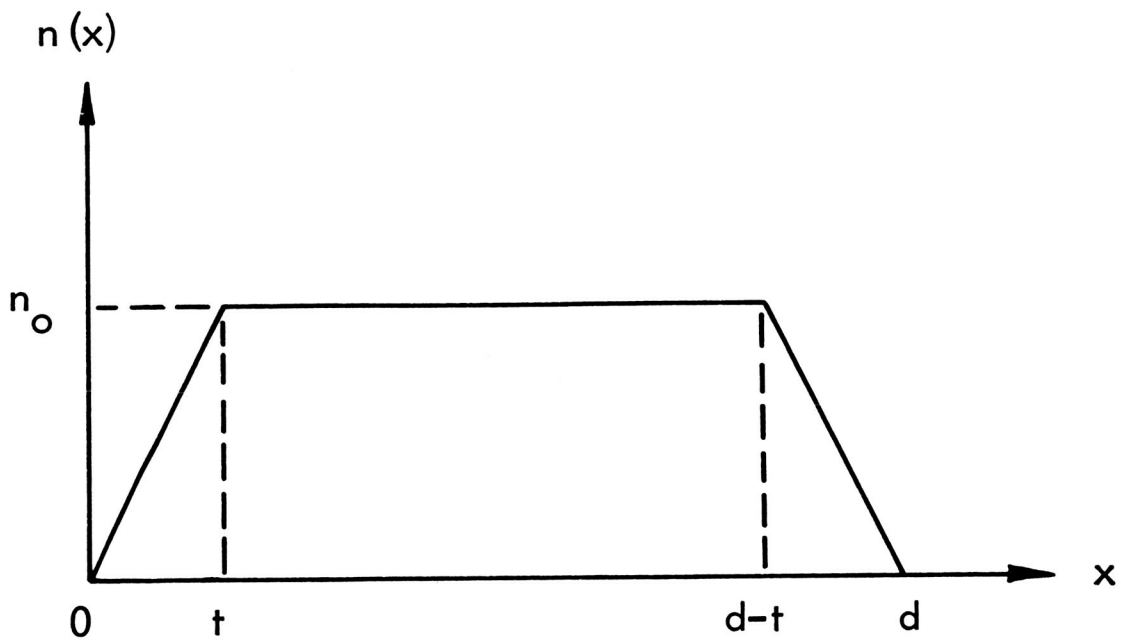


Figure 1.- Density in a tapered slab.

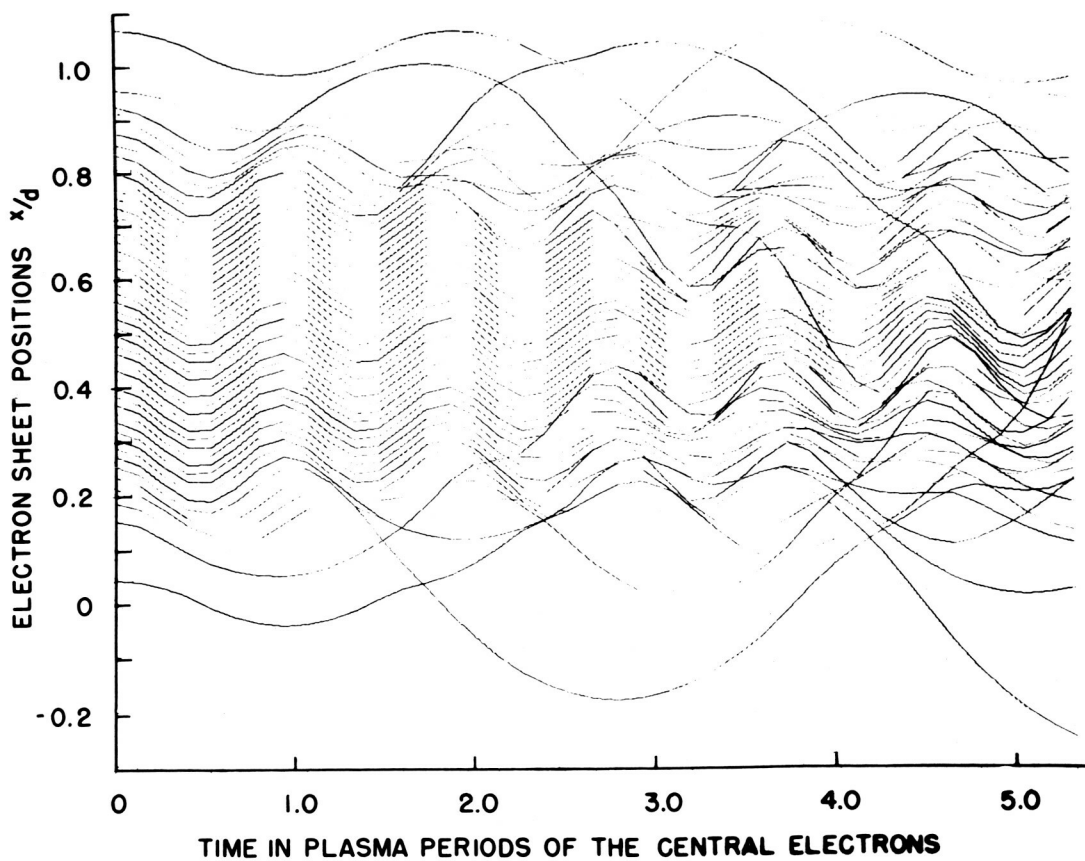


Figure 2.- Electron sheet trajectories in a tapered slab with tapered region of thickness $t/d = \frac{1}{4}$. Initial displacement $\delta/d = .04$.

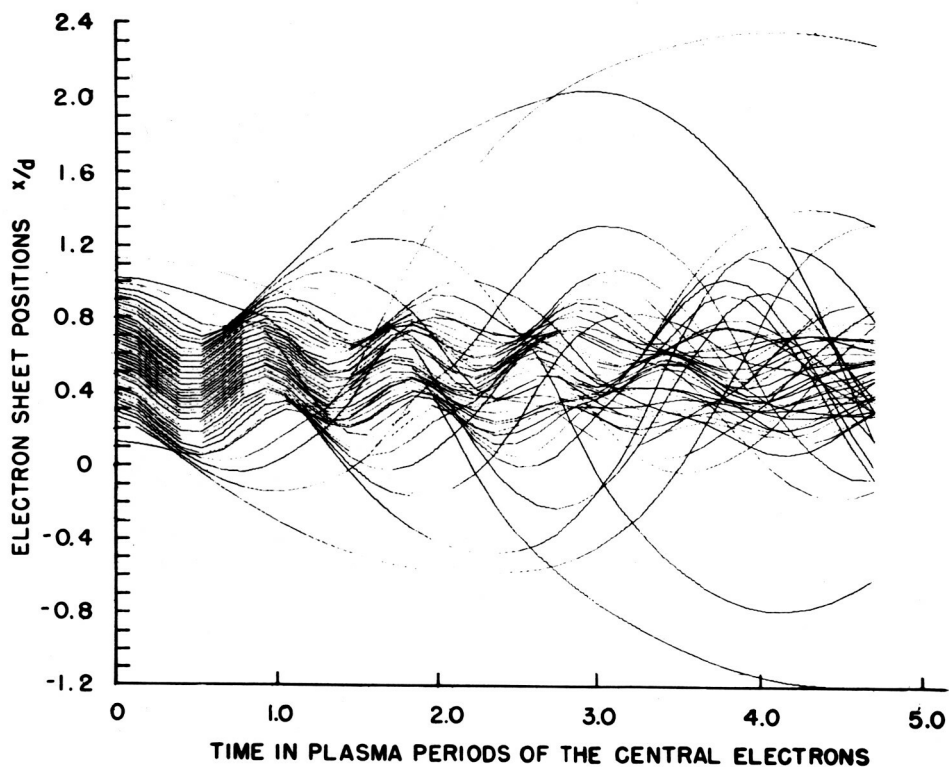


Figure 3.- Electron sheet trajectories in a tapered slab with tapered region of thickness $t/d = \frac{1}{4}$. Initial displacement $\delta/d = .12$.

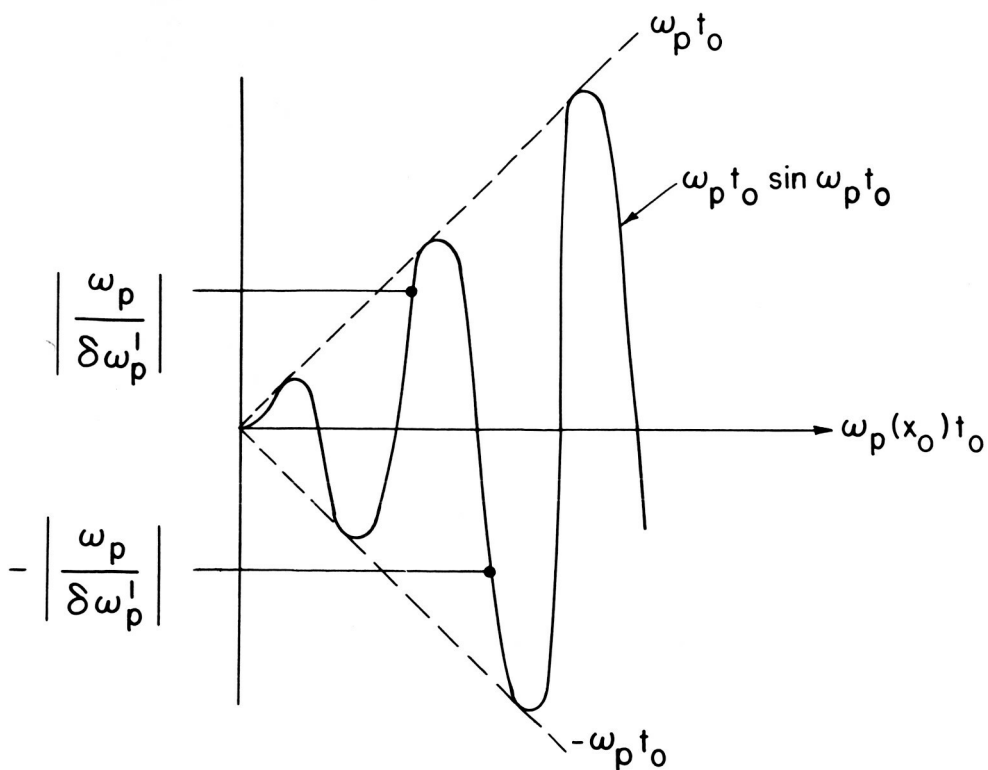
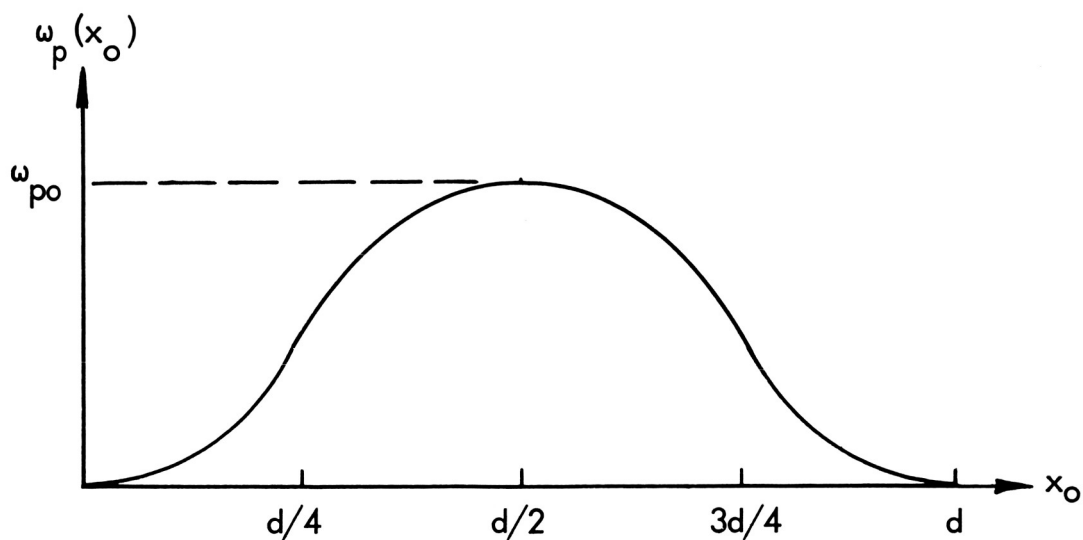


Figure 4.- Graphical solution of equation (6) for overtaking time t_0 .



$$\omega_p(x_o) = \frac{\omega_{po}}{2} \left(1 - \cos \frac{2\pi x_o}{d} \right)$$

Figure 5.- Density function for a slab with smooth boundaries.

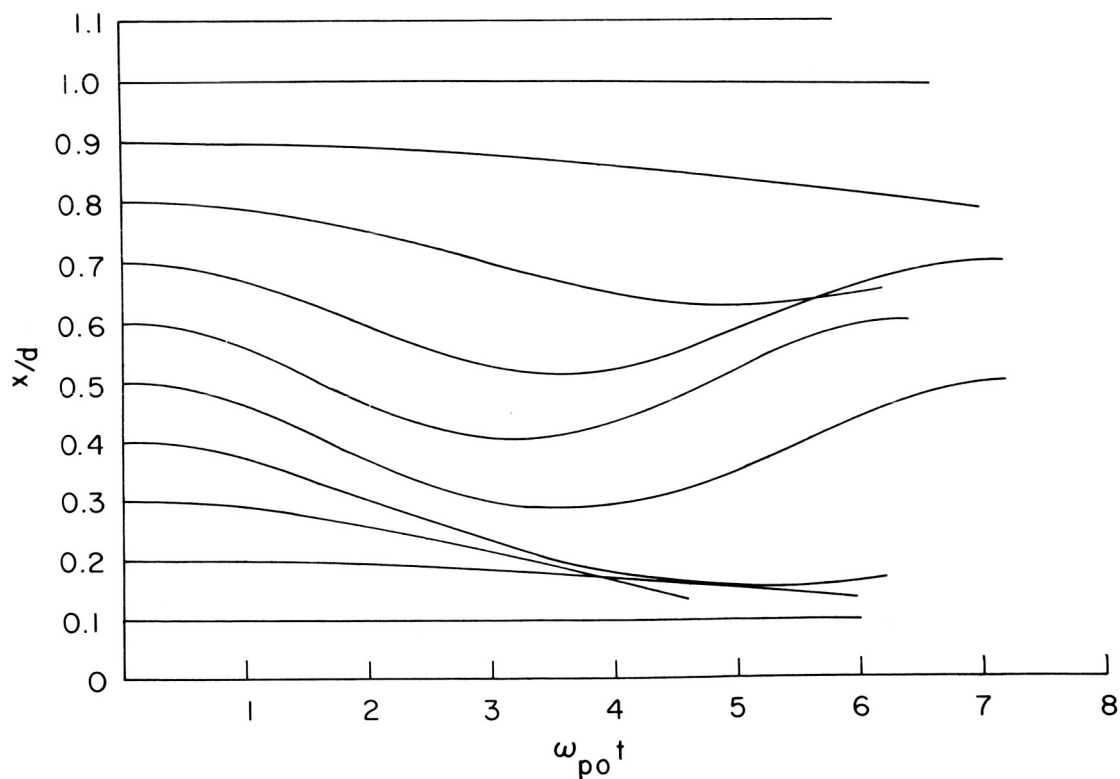


Figure 6.- Solution of equation (12) for an initial displacement $\delta/d = .1$. Trajectories for values of x_o between 0 and d .

3 Preliminary Measurements of Noise
in a Two-dimensional Rod Model of a Plasma

N67-37742

by

R. W. Hockney

2 Institute for Plasma Research, Stanford University

Computer models of the superparticle type grossly exaggerate the fluctuations (or noise) in a real plasma because, of necessity, each superparticle carries the charge of 10^6 or more electrons. It is important, therefore, to be able to estimate this "computer" noise in order to be sure that it does not cover-up the real physical phenomena that the computer model is attempting to simulate.

A formula has previously been derived for the mean square fluctuating field appropriate to a particular type of computer model.¹ We present here an alternative derivation of this formula and compare it with the measured values of the fluctuations.

In the model, space is divided into a square array of cells of side H . In the centre of each there is a mesh point which is used in the finite difference solution of Poisson's equation. In order to obtain the potential, a charge distribution over these mesh points is found by associating the charge of all the rods in a given cell with the mesh point at the center of the cell. The effect of this coarse-graining in space is to eliminate the force of interaction between rods when they are in the same cell, or separated by less than the mesh distance H .

Let there be N ion rods and N electron rods per square centimeter of the model each with a charge per unit length Q . Let us consider the fluctuating field on a test charge to be due to the statistical fluctuations of the charge density in each of the cells. This charge fluctuation being estimated simply as the square root of the number of rods in a cell.

Then the mean square charge fluctuation in a cell is

$$(\delta q)^2 = 2NH^2Q^2$$

The contribution of this fluctuation to the mean square fluctuating field on the test charge is

$$(\delta E)^2 = \left(2 \frac{(\delta q)}{r} \right)^2 = 4 \frac{(\delta q)^2}{r^2}$$

where r is the distance of the cell from the test charge. Assuming that these fluctuations are random the total mean square fluctuating field is

$$\langle E^2 \rangle = \sum_{\text{cells}} (\delta E)^2 \cong \int_H^{r_{\max}} \frac{4(\delta q)^2}{r^2} \cdot \frac{2\pi r dr}{H^2} = 16\pi N Q^2 \log_e \left(\frac{r_{\max}}{H} \right)$$

where r_{\max} is the maximum distance at which the effect of a charge is felt. The lower limit of the integration recognizes the absence of interaction at distances less than H .

In the case of a plasma, Debye shielding makes $r_{\max} = \lambda_D$. If we take the correlation time to be the time taken for a "thermal" particle to travel a Debye length, then the collision time can be derived and one obtains:

$$\frac{\tau_{pe}}{\tau_{coll}} = \frac{1}{N \lambda_D^2} \log_e \left(\frac{\lambda_D}{H} \right)$$

where

- τ_{pe} is the electron plasma period
- τ_{coll} is the collision time for electrons
- $N \lambda_D^2$ is the number of rods in a Debye square
- τ_c is the correlation time

In the case of a gravitational problem where there is no screening $r_{\max} = L$ the total dimension of the star system. The plasma period is replaced by the dynamic time scale. In galactic applications this is the rotation period of a galaxy in which centrifugal force balances gravitational attraction. Thus

$$\frac{\tau_{\text{rot}}}{\tau_{\text{coll}}} = \frac{1}{N_{\text{tot}}} \log_e \left(\frac{L}{H} \right)$$

where

N_{tot} is the total number of stars in the system

τ_{rot} the rotation period of the galaxy

A further refinement to the above formula is necessary to take into account the fact that, since the force on a rod is only computed every time step DT , a rod has a mean free path of $V_{\text{th}} DT$, where V_{th} is the characteristic thermal velocity. Hence the shielding distance cannot be less than this distance. To allow for this effect we replace the physical Debye length λ_D , by an effective Debye length in the computer model of $(\lambda_D + V_{\text{th}} DT)$. Hence

$$\langle E^2 \rangle = 16\pi N Q^2 \log_e \left(\frac{\lambda_D + V_{\text{th}} DT}{H} \right) \quad (1)$$

An alternative expression for the noise may be obtained from the thermal fluctuation theory expression:

$$\frac{\langle E^2 \rangle}{8\pi} = \frac{1}{2} kT \iint \frac{dk_x dk_y}{(1 + \lambda_D^2 k^2)}$$

integrating we obtain

$$\langle E^2 \rangle = 4\pi N Q^2 \log_e (1 + \lambda_D^2 k_{\max}^2) \quad (2)$$

Because of the finite mesh used in the solution of Poisson's equation

$k_{\max} = \pi/H$ in the computer model.

In the following table we compare the measured values of the RMS E-field fluctuations $\sigma = \sqrt{\langle E^2 \rangle}$ with formulas (1) and (2). The Datum case refers to the scaling used in the anomalous diffusion experiment in Reference 1, for which $N = 16,000 \text{ rods cm}^{-2}$, $Q = 2.4 \times 10^3 \text{ esu}$, $V_{\text{th}} = 3.9 \times 10^8 \text{ cm sec}^{-1}$, and $DT = 4 \times 10^{-11} \text{ sec}$. The other cases are the same except for the change in the variable shown. We see that both noise estimates give very similar results and that both agree very well with the measured values.

Case	Measured	Formula (1)	Formula (2)
DATUM	3.32	3.08	2.46
$Q \times 4; DT \times 1/4$	10.5	7.0	9.84
$Q \times 1/4$	0.88	0.93	0.61
$N \times 1/4$	1.64	1.33	1.23
$DT \times 1/4$	3.20	2.80	2.46
$V_{\text{th}} \times 1/4$	2.45	1.75	2.46
$V_{\text{th}} \times 1/16$	2.34	1.36	2.46

Measured and Calculated Values of RMS
E-field Fluctuations in a Rod-model of
a Plasma. Units esu of field.

Reference

1. R. W. Hockney, "Computer Experiment of Anomalous Diffusion", Phys. Fluids 9, 1826 (1966).

Micro-reversibility in Computer Simulation*

by

O. Buneman, Stanford University

The computer simulation of micro-dynamical processes often demands that the principle of reversibility be observed strictly. Five examples are presented to show how such reversibility can be achieved in fast integrations, in spite of the presence of first-order time-derivatives. The examples are: the Lorentz equation, relativistic orbits, orbits in central coordinates, gyro-center motion and continuity equations.

*Supported by NSF Grant GK-625.

N67-37743

3 On the Numerical Solution of Poisson's Equation

2 Craig G. Smith
Plasma Physics Laboratory, Princeton University, N.J. 2

A recurring problem in the computer simulation of plasma is the need to repeatedly integrate Poisson's equation numerically. Having thus obtained the potential, the solution must then be differentiated to calculate the electric field, which in turn is squared and integrated for the calculation of the energy. As this must be repeated hundreds of times in the course of an "experiment," some premium is attached to having a fast—even if at the expense of high accuracy—method for performing this computation.

The purpose of this note is to point out an appealing approach for the two-dimensional integration of Poisson's equation in a finite circular domain. The method is most appropriate for fluid or guiding-center simulations of plasma, for which the potential may be expected to be a reasonably smooth function of the spatial coordinates. It is not suitable for the exact treatment of dynamical systems for which close encounters are important.

Following Hockney,¹ Poisson's equation is first Fourier analyzed with respect to the azimuthal coordinate. But rather than numerically integrate the resulting system of ordinary differential equations in the radial coordinate, the solution is expressed in terms of integrals of the charge density with kernels which are simple powers of r . If the charge density is given a representation (such as by a finite power series in r), then the expressions for potential, electric field, and energy are immediately obtained

(and would likewise be finite power series). Furthermore, the electric field is given as a continuous function of r , which may be of use for the integration of the equation of evolution of the simulation.

The idea thus is to numerically fit the data (charge density) globally to a function and then to analytically integrate Poisson's equation and perform the subsequent differentiations and integrations to obtain the related quantities. The numerical approximation may be accomplished by the least-squares technique. If the coefficients describing the fit appear linearly in the representation, then solving for these unknowns need, in effect, be done only once; the coefficients are then repeatedly obtained by only matrix multiplication.

The crux lies in selecting the form for the approximation, and here a vast number of variations are possible. In order to place this discussion in definite context, the following describes an example which, in fact, has been tried successfully in one application.²

The problem then is to solve Poisson's equation,

$$\frac{1}{r} \frac{\partial}{\partial r} \left(r \frac{\partial \Phi}{\partial r} \right) + \frac{1}{r^2} \frac{\partial^2 \Phi}{\partial \phi^2} = - \frac{KT}{e} \left(\frac{R}{R_D} \right)^2 \delta$$

where r is the dimensionless radial coordinate measured in units of R ,

$\delta = (n_+ - n_-)/n_0$ is the dimension less charge density and R_D is the Debye length. Fourier analysis with respect to the azimuthal variable,

$$\Phi = \Phi_0 + \sum_{\ell=1}^{\infty} \left(\Phi_{\ell}^c \cos \ell \phi + \Phi_{\ell}^s \sin \ell \phi \right),$$

reduces the partial differential equation to a system of ordinary differential equations, whose solutions for either amplitude are (aside from the constant factor of the right hand side)

$$\Phi_0 = C_1 + \int \frac{dr}{r} \left(C_2 + \int r \delta_0 dr \right)$$

$$I_{\ell} = \left(C_1 + \frac{1}{2\ell} \int r^{-\ell+1} \delta_{\ell} dr \right) r^{\ell} + \left(C_2 - \frac{1}{2\ell} \int r^{\ell+1} \delta_{\ell} dr \right) r^{-\ell}.$$

The constants of integration, C_1 and C_2 , may be used to make the integrals definite. Typically, the potential would be approximated by the first L modes.

It is now supposed that δ is given as a set of values on a discrete grid in coordinate space. Since for cylindrical coordinates the elemental area is given by

$$r dr d\phi = \frac{1}{2} dr^2 d\phi$$

it is most appropriate to use r^2 as the variable measuring radial position. This results in a nonuniform grid in (r, ϕ) space, but the cells are then of equal weight. Thus δ_{ℓ} is assumed to be a function of r^2 and in particular a power series with a finite number of terms

$$\delta_{\ell} = r^{\ell} \sum_{m=1}^M a_{\ell, m} r^{2(m-1)}$$

where the r^{ℓ} factor is added to insure regularity of the solution at the origin.

With the boundary condition, $\Phi(1, \phi) = 0$, corresponding to a perfect conductor at R , the expressions for the Fourier amplitudes of the potential, electric field component, and energy (integral $\epsilon_0/2 \underline{E} \cdot \underline{E}$ over the entire domain) are simply

$$\Phi_{\ell} = - \frac{KT}{e} \left(\frac{R}{R_D} \right)^2 r^{\ell} \sum_{m=1}^{M+1} b_{\ell, m} r^{2(m-1)}$$

$$(E_r)_{\ell} = \frac{KT/e}{R} \left(\frac{R}{R_D} \right)^2 r^{\ell-1} \sum_{m=1}^{M+1} c_{\ell, m} r^{2(m-1)}$$

$$(E_{\phi})_{\ell}^{c, s} = \pm \frac{KT/e}{R} \left(\frac{R}{R_D} \right)^2 r^{\ell-1} \ell \sum_{m=1}^{M+1} b_{\ell, m}^{s, c} r^{2(m-1)}$$

$$\mathcal{E}_{\ell} = 1.09 \cdot 10^5 (KT)^2 \left(\frac{R}{R_D} \right)^4 \sum_{c, s} \sum_{m=1}^M \sum_{m'=1}^M [(\ell+m+m')(\ell+m)(\ell+m')]^{-1} a_{\ell, m}^c a_{\ell, m'}^s$$

with the following definitions

$$b_{\ell, m+1} = \frac{a_{\ell, m}}{4(\ell+m)m} \quad , \quad b_{\ell, 1} = - \sum_{m=2}^{M+1} b_{\ell, m}$$

$$c_{\ell, m+1} = (\ell+2m) b_{\ell, m+1} \quad .$$

The plus or minus sign applies, respectively, to the cosine or sine amplitude of E_{ϕ} . The coefficient of \mathcal{E} has the units $(eV \cdot cm)^{-1}$, and the

expression for \mathcal{E}_0 should contain an additional factor of two.

The above expressions are quite easily evaluated, and the numerical problem is that of determining the a 's. That is, we must fit the function

$$\delta(r) = r^\ell \sum_{m=1}^M a_m r^{2(m-1)}$$

(subscript ℓ now dropped) to the N data points δ_n given on the grid

$r_n^2 = (n - 1/2)/N$. The least squares technique chooses the a 's so as to minimize the expression

$$S \equiv \sum_{n=1}^N [\delta(r_n) - \delta_n]^2 .$$

Experimentally, however, it has been found useful to add side conditions to the fit. The first is a normalization requirement insuring that there is not created more electric field than what the total charge density can account for,

$$\int_0^1 \delta(r) r dr = \sum_{m=1}^M \frac{a_m}{2m + \ell} = \frac{1}{2N} \sum_{n=1}^N \delta_n .$$

Also, it has been found important to make some specification at the edge of the fit, $r = 0$ and 1 , since the least squares fit is unreliable for extrapolating data. For a perfectly absorbing boundary, since δ must go to zero, another condition imposed is

$$\delta(1) = \sum_{m=1}^M a_m = 0 .$$

At the origin $\delta(0) \equiv 0$ for $\ell \neq 0$. For $\ell = 0$, an extra data point is created

by extrapolating the data at the first two points back to the origin,

$$\delta_{N+1} = \frac{r_2^2}{r_2^2 - r_1^2} \delta_1 - \frac{r_1^2}{r_2^2 - r_1^2} \delta_2, \quad r_{N+1} = 0.$$

Confining ourselves to the case $\ell \neq 0$, the two side conditions determine two of the coefficients, say a_{M-1} and a_M , in terms of the others, and thus the fit is to the function

$$\delta(r) = g(r) \frac{1}{N} \sum_{n=1}^N \delta_n + \sum_{m=1}^{M-2} a_m h_m(r)$$

where

$$g(r) \equiv \frac{1}{4} (2(M-1) + \ell)(2M + \ell)(1 - r^2) r^{\ell + 2(M-2)}$$

$$h_m(r) \equiv r^{\ell + 2(m-1)} + \frac{1}{2} (2(M-1) + \ell - (2M + \ell) r^2) r^{\ell + 2(M-2)} - \frac{2}{\ell + 2m} g(r).$$

The effect of imposing side conditions is to complicate the functional dependence of the fit on r . Minimization of S with respect to the a 's results in a set of simultaneous equations determining the first $M-2$ coefficients

$$\sum_{m'=1}^{M-2} \sum_{n=1}^N h_{m,n} h_{m',n} a_{m'} = \sum_{n=1}^N \left\{ h_{m,n} - \frac{1}{N} \sum_{n'=1}^N h_{m,n'} g_{n'} \right\} \delta_n$$

where $g_n \equiv g(r_n)$ and $h_{m,n} \equiv h_m(r_n)$. As the equations are linear, the solution may readily be obtained; then a_{M-1} and a_M are given by a linear combination of the other a 's. Let H be the $M-2$ by N matrix $h_{m,n}$, and further let $B \equiv (H \cdot H^T)^{-1}$. Then the coefficients are given by the expression

$$a_m = \sum_{n=1}^N c_{m,n} \delta_n$$

where for $m = 1, \dots, M-2$,

$$c_{m,n} = \sum_{m'=1}^{M-2} b_{m,m'} \{ h_{m',n} - \frac{1}{N} \sum_{n'=1}^N h_{m',n'} g_{n'} \}$$

and for $m = M-1, M$,

$$c_{m,n} = \pm \frac{2m+\ell}{2} \left\{ \frac{2(2M-1-m)+\ell}{2N} + \sum_{m'=1}^{M-2} \left(1 - \frac{2(2M-1-m)+\ell}{2m'+\ell} \right) c_{m',n} \right\}.$$

The plus or minus sign applies, respectively, to the $M-1$ or M equation.

The treatment of the $\ell = 0$ case, for which a fictitious $N+1$ data point was added, proceeds in a similar fashion, and the above formulas may be taken over with ℓ set to zero. The exceptions are that H is now an $M-2$ by $N+1$ matrix, where $h_{m,N+1} = 1$ for $m = 1$ and is zero otherwise, and $g_{N+1} = 0$. Furthermore, to the expressions for $c_{m,1}$ and $c_{m,2}$ must be added, respectively, $\frac{3}{2} b_{m,1}$ and $-\frac{1}{2} b_{m,1}$.

The important point to note is that the inversion of the matrix, and hence the subsequent calculation of $c_{m,n}$, need be done only once. Then at each time step in the integration of the equation of evolution of the simulation, when the electric field must be updated, the a 's are obtained by simple matrix multiplication.

The choice for the representation in this example, a polynomial in r^2 , is the least sophisticated one from the standpoint of approximation theory,

but it is the most efficient scheme for machine computations. The sort of ($\ell = 0$) data to which it has been applied is shown in Fig. 1; a fifth-degree polynomial in r^2 ($M = 6$, $N = 10$) is adequate to describe the formation of the charge sheath near the boundary. The corresponding solution is shown in Fig. 2. In the interest of high accuracy, one can compromise with the execution speed and introduce more complex functions of r , but it should be obvious that it is highly desirable to have the parameters describing the fit appear linearly in the representation. Imposing side conditions is an extremely useful technique for "doctoring" the fit to the application.

This work was performed under the auspices of the U. S. Atomic Energy Commission, Contract No. AT(30-1)-1238, and made use of computer facilities supported in part by National Science Foundation Grant NSF-GP579.

¹R. W. Hockney, J. Assoc. Computing Mach. 12, 95 (1965).

²A. S. Bishop and C. G. Smith, Princeton Plasma Physics Laboratory Annual Report MATT-Q-23, p. 314 (1966).

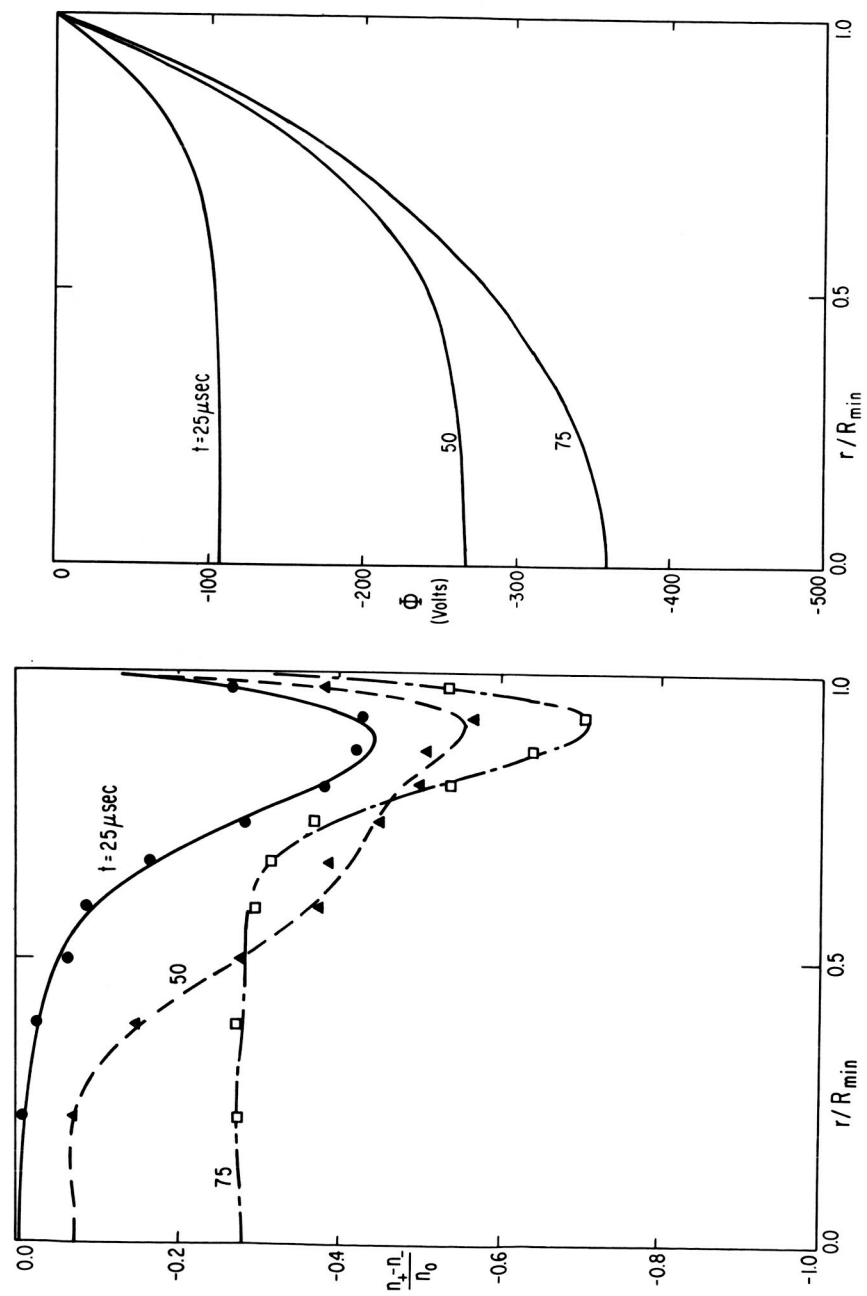


Figure 1.- Typical data approximated by a fit to a fifth-degree polynomial in r^2 .
Figure 2.- Potential corresponding to figure 1.

DRIVEN OSCILLATIONS AND NORMAL MODES OF A NONUNIFORM PLASMA

by

William M. Leavens

Environmental Science Services Administration
 Institute for Telecommunication Sciences and Aeronomy
 Boulder, Colorado

ABSTRACT

Over the past several years we have accumulated numerical solutions of the linearized Vlasov equation, obtained by the conductivity kernel method, for the driven oscillations of a realistic plasma model with a sheath. Most of the results are well described by a driven normal mode model, with a discrete spectrum of normal modes.

The conductivity kernel equation is:

$$E_p(x) = \int_0^L K_\omega(x; x') (E_p(x') + E_d(x')) dx' \quad (1)$$

where E_p is the oscillating electric field due to sources in the plasma and E_d is an externally supplied driving field. The conductivity kernel, $K_\omega(x; x')$, is a nonlinear function of ω , obtained by a formal solution of the Vlasov equation in terms of integrals over unperturbed orbits. For nonzero driving field, Eq. (1) has solutions for any real ω , the only difficulty being the numerical computation of K_ω at reasonable cost. The technique we have used to compute K_ω is described. For zero driving field, Eq. (1) has solutions only for certain values of ω . Thus far our only successful approach to the free oscillation problem has been to assume a normal mode representation of the solutions of the driven mode problem,

$$E_p(x) = \sum_{n=1}^N \frac{E_n(x)}{\omega^2 - \omega_n^2} + \text{a slowly varying part} \quad (2)$$

and to identify ω_n , $E_n(x)$ with the free oscillations, or "normal modes". The location of the ω_n 's in the ω -plane were first found by searching for the set of ω_n 's, with N as small as possible, which would give a good least square fit to the ω -dependence of E_p . This was an especially successful procedure for analyzing the ω -dependence of

$$V_\omega = \int_0^L E_p(x) dx.$$

Five distinct poles were able to completely describe V_ω over the frequency range studied. The slowly varying part does not contribute to V_ω

Having found the ω_n 's, the "eigenfunction" $E_n(x)$ can be determined by successfully subtracting out the poles from Eq. (2), in such a way as to maximize the "smoothness" of the remainder. This procedure has been carried out for $E_1(x)$, but it is not yet complete for the higher E_n 's.

The discrete spectrum is an inherent property of the nonuniform plasma; it is not introduced by boundary conditions. The existence of a few normal modes which dominate the plasma response opens the possibility of quite another kind of plasma simulation, in which the plasma is represented entirely by the normal modes.

REFERENCES

Drummond, J. E., R. A. Gerwin, and G. B. Springer, J. Nucl. Energy, Part C: Plasma Phys. 2 (1961). Formulation.

Leavens, W. M., dissertation, University of California at San Diego (1964), also J. Res. N.B.S., Part D, Radio Science 69D, 1321 (1965). Formulation and solution of the Tonks-Dattner problem. For application to other problems see Phys. Letter 19, 118 (1965), and Meeting of the Division of Plasma Physics, American Physical Society, Boston (1966).

Pavkovich, J., Meeting of the Division of Plasma Physics, American Physical Society, San Diego (1963), also dissertation, Stanford University (1963). Formulation and calculation of sheath oscillations.

N67-37744

NUMERICAL STUDIES OF THE STEADY-STATE PLASMA SHEATH PROBLEM

By

Lee W. Parker

Mt. Auburn Research Associates, Incorporated
Cambridge, Massachusetts

and

Edward C. Sullivan

Goddard Space Flight Center, National Aeronautics and Space Administration
Greenbelt, Maryland

A number of plasma sheath problems where collisions may be neglected¹ (e.g., electrostatic plasma probes²⁻⁷, vehicles moving in the ionosphere⁷⁻¹⁰, plasma diodes¹¹, and ion engines¹²) may be described theoretically in terms of solutions of a particular form of the Poisson equation, in which the right-hand side (charge density) involves integrals over velocity space, where each integrand is in turn a solution of the associated Vlasov equation. This Poisson equation is usually a non-linear partial differential equation, and, in general, numerical methods are required to obtain solutions. Such solutions are beset by two principal difficulties.

One difficulty is connected with the fact that the charged particle density at a point is a functional of the potential distribution; that is, it depends not only on the local electrostatic potential, but also on the potential distribution elsewhere in space.

The other difficulty arises in problems comprising a large class important in practice where the potential vanishes at infinity. In the process of obtaining a solution by numerical means to such a problem, an inherent instability appears which prevents the solution from being carried to indefinitely large distances. If the asymptotic behavior (at large distances) of the solution were known, as in the case of a spherical probe²⁻⁶, it would be necessary only to carry the solution to a finite distance where the asymptotic condition could be invoked, such that the instability is not manifested. Since the asymptotic behavior of the solution is not generally known for the Poisson equation, as distinguished from the Laplace equation, a common procedure is to invoke an artificial condition (e.g., vanishing potential or potential gradient) at a finite boundary⁷⁻¹⁰. The boundary must then be taken sufficiently far out that the solution in the region of interest is

unaffected by the nature of the assumed boundary condition¹³. If the boundary is taken too far out, then, as will be shown, instability sets in and a solution cannot be obtained. If the boundary is taken too near, the solution is easily obtained but does not resemble the solution to the infinite-boundary problem.

These numerical aspects have been discussed in regard to special cases by Laframboise⁴, Parker⁷, Maslennikov and Sigov⁹, and Taylor¹⁰, who developed their own methods to apply to these cases. In the recent studies by Taylor¹⁰ on solutions to a moving cylinder problem, comparisons were made between various artificial boundary conditions, but the instability problem was not explored. On the other hand, Maslennikov and Sigov⁹ were concerned with the stability problem, but not generally with its relationship to the boundary. Thus, scattered information exists, but such information is not yet sufficient to enable a worker, without a great deal of preliminary development, to choose an appropriate method for solving a new problem when it involves an infinite boundary condition (or a large electrode separation). The investigation reported here is intended to clarify the numerical aspects of infinite-boundary problems, so that systematic methods may be developed. The previously-mentioned numerical difficulty associated with the non-local character of the charge density calculation^{2-7,10,11} will not be treated here.

In one-dimensional problems, the solution of the associated ordinary differential equation may be computed either by a "marching" (step-by-step) method in which the solution is propagated from one point to another²⁻⁶, or by a "grid" method in which the solution is determined simultaneously at a number of points. The marching method has the advantage of affording control over error propagation. However, in multi-dimensional problems leading to

non-linear partial differential equations, the grid method appears to be the only recourse^{7-10,12}, but little information exists regarding this method. A possible additional advantage of the grid method (even over the marching method in one-dimensional problems) is that it is unnecessary to establish in advance a catalogue of analytic properties for solutions, as must be done in the marching method. It is therefore desirable to study grid methods with regard to accuracy and economy of computing time. The grid method may be described as follows.

Let a finite region of interest in configurational space be overlaid by a grid of spatial points. If the values of the potential at the grid points are considered to be the components of a vector $\vec{\phi}$, the solution of the Poisson problem is the solution of a set of simultaneous equations of the form:

$$L \vec{\phi} = - \vec{\rho}(\vec{\phi}) \quad (1)$$

where L is a Laplacian matrix operator based on a difference approximation, and $\vec{\rho}$ is a charge density vector whose component ρ_k at the k -th grid point depends on the components of $\vec{\phi}$ at all of the grid points. (Numerical factors have been absorbed and it is assumed that an algorithm based on trajectory calculations is available for computing $\vec{\rho}$ from a given $\vec{\phi}$.) A general iteration procedure for solving (1) may be defined by:

$$L \vec{\phi}^{n+1} = - \sum_{m=0}^n b_m \vec{\rho}(\vec{\phi}^m) \quad (2)$$

where ϕ^n denotes the n-th iterate for ϕ , and the empirical set of coefficients (b_0, b_1, \dots, b_n) implies that successive density iterates are coupled in order to promote convergence. In direct iteration without coupling, one has $b_n = 1$ and $b_m = 0$ for $m \neq n$.

The instability referred to above manifests itself as a divergence in the iterative sequence defined by (2), and depends on the position of the grid boundary (for a given coupling scheme). Since the instability phenomenon occurs both in one-dimensional⁴ problems and in multi-dimensional⁷⁻⁹ problems, we decided to restrict our study to one-dimensional problems. This would afford not only a saving in computer time, but also a comparison with accurate solutions obtainable in other ways. To illustrate the nature of the phenomenon, calculations were performed on a spherical problem in which the sphere radius and potential were chosen to be 150 Debye lengths and 10 kT/e, respectively. The charge density was represented by a reasonable model function to save computer time. The potential was set equal to zero on the grid boundary, and the problem was solved for successive boundary positions at intervals of one Debye length. The iteration scheme chosen was such that two successive density iterates were coupled, in accord with the experience reported in References 4, 7, 8, 9, 11, and 12, where the coupling was found to yield an improvement over direct iteration. When the boundary was at 152, 153, or 154 (in Debye lengths), the values of the potential at points near the sphere changed noticeably with boundary position. When the boundary was at 155 or 156, the values of the potential at points near the sphere became stationary. (That is, the infinite boundary condition was well represented as far as these points were concerned.) However, the number of iterations required for convergence increased as the boundary was moved out. When the boundary was at

158, the successive iterates diverged¹⁴.

The instability represents the growth of errors from iteration to iteration. More analysis is required to clarify this phenomenon, but it is similar to the growth of the unwanted positive exponential solution which occurs when the marching method is applied to the equation $y''=y$. Numerical experiments run by Prince and Jeffries¹¹ on a plasma diode problem suggest that the instability is associated with the occurrence of an appreciable region of nearly-vanishing net charge density. In the plasma diode, the net charge density changes sign in the space between the two electrodes, and the region of nearly-vanishing net charge density spreads as the electrode spacing increases. By using a marching integration method with which error propagation could be carefully controlled, Prince and Jeffries obtained solutions for electrode spacings up to 100 Debye lengths. By using a grid method and coupling of two successive iterates, solutions were found to be limited to electrode spacings of about 20 Debye lengths.

We have run numerical experiments on a plasma diode problem using a grid method. The goal of these calculations is to develop methods for obtaining solutions in the limit of very large electrode separation, which should shed light on the infinite-boundary problem. Our results to date have tended to corroborate the above limitation of 20 Debye lengths. Experience gained in refinements of the iteration procedure and in the role played by significant figure accuracy will be reported. Work is in progress to determine the effects of further refinements, such as the use of an appropriately non-uniform distribution of grid points.

Further assessments on the efficacy of the grid method are afforded by application of this method to the perennially interesting spherical probe problem. Comparisons will be made with existing accurate ambi-monoenergetic solutions⁵⁻⁶.

REFERENCES AND FOOTNOTES

1. The references cited below are specifically concerned with the numerical aspects of the sheath problem.
2. I.B. Bernstein and I.N. Rabinowitz, "Theory of electrostatic probes in a low-density plasma," *Phys. Fluids* 2, 112-21 (1959).
3. L.S. Hall and R.P. Freis, "Theory of the electrostatic probe and its improved use as a diagnostic tool," University of California Lawrence Radiation Laboratory Report UCRL-12480, July 1965.
4. J. Laframboise, "Theory of spherical and cylindrical Langmuir probes in a collisionless Maxwellian plasma at rest," University of Toronto Institute for Aerospace Studies report UTIAS No. 100, June 1966.
5. K.G. Guderley and E.M. Valentine, "Theory of spherical probes in monoenergetic plasmas," Wright-Patterson Air Force Base Aerospace Research Laboratories Report ARL 66-0024, February 1966.
6. G.K. Medicus, "The carrier-attracting region of the spherical probe curve in the ambi-monoenergetic case," (to be published).
7. L.W. Parker, "A computer program for calculating the charge distribution about a space vehicle," American Astronautical Society Second Symposium on Interaction of Space Vehicles with an Ionized Atmosphere, Miami Beach, November 1965 (NASA report CR-401, March 1966); "Theory of electrostatic planar and spherical probes," NASA report CR-704, January 1967; "Theory of a satellite electrostatic probe," with E.C. Whipple, Jr. (to be published).
8. A.H. Davis and I. Harris, "Interaction of a charged satellite with the ionosphere," in Rarefied Gas Dynamics, L. Talbot, Ed. (Academic Press, New York, 1961).
9. M.V. Maslennikov and Yu.S. Sigov, "A discrete model for the study of the flow of a rarefied plasma about a body," *Soviet Physics-Doklady*, 9(12), 1063-5 (June 1965).

10. J.C. Taylor, "Disturbance of a rarefied plasma by a supersonic body on the basis of the Poisson-Vlasov equations - I," Planet. Space Sci. 15, 155-87 (1967).
11. D.C. Prince, Jr., and N.P. Jeffries, "Computer solutions of the Vlasov equations," General Electric Co. Final Report Contract No. NAS 8-5214, December 1964.
12. V. Hamza and E.A. Richley, "Numerical evaluation of ion-thruster optics," Lewis Research Center NASA TN D-1665, May 1963.
13. Assuming that this property is possessed by the solution.
14. At 157, a stationary oscillation occurred between successive iterates.

NUMERICAL SOLUTION OF THE FOKKER-PLANCK
EQUATIONS FOR A HYDROGEN PLASMA FORMED
BY NEUTRAL INJECTION*

John Killeen and Archer H. Futch

Lawrence Radiation Laboratory, University of California
Livermore, California

ABSTRACT

In those experiments in controlled-fusion research that employ the injection of energetic neutral atoms, a plasma is formed of initially hot ions and cold electrons. It is of interest to know the velocity-distribution functions of the electrons and ions as a function of time during the buildup of the plasma. The mathematical model for this problem is the Fokker-Planck equation. We use the form of the equation where the two-body force is an inverse square law as derived by Rosenbluth, MacDonald, and Judd.¹ In this work we have assumed that the velocity distributions are isotropic. We include a source of electrons and ions with a given velocity spread. Both species can be lost by

*Work performed under the auspices of the U.S. Atomic Energy Commission.

¹M. N. Rosenbluth, W. M. MacDonald, and D. L. Judd, Phys. Rev. 107, 1 (1957). Presented at the Symposium on Computer Simulation of Plasmas and Many-Body Problems, College of William and Mary, Williamsburg, Virginia, April 19-21, 1967.

Coulomb scattering into the loss cone, and the ions can be lost by charge exchange. The equation for each species is

$$\begin{aligned}
 (4\pi\Gamma_a)^{-1} \frac{\partial f_a}{\partial t} = & \frac{\partial^2 f_a}{\partial v^2} \left\{ \sum_b \left[\frac{1}{3v^3} \int_0^v f_b(v', t) v'^4 dv' + \frac{1}{3} \int_v^\infty f_b(v', t) v' dv' \right] \right\} \\
 & + \frac{\partial f_a}{\partial v} \left\{ \frac{1}{v} \sum_b \left[\frac{m_a}{m_b} \frac{1}{v} \int_0^v f_b(v', t) v'^2 dv' - \frac{1}{3v^3} \int_0^v f_b(v', t) v'^4 dv' \right. \right. \\
 & \left. \left. + \frac{2}{3} \int_v^\infty f_b(v', t) v' dv' \right] \right\} + f_a \left(\sum_b \frac{m_a}{m_b} f_b \right) \\
 & - f_a \left\{ \frac{p_a(v)}{v^3} \sum_b \left[\left(1 + \frac{m_a}{m_b} \right) \int_0^v f_b(v', t) v'^2 dv' \right. \right. \\
 & \left. \left. - \frac{1}{3v^2} \int_0^v f_b(v', t) v'^4 dv' + \frac{2v}{3} \int_v^\infty f_b(v', t) v' dv' \right] \right\} + s_a(v, t).
 \end{aligned}$$

The summations are taken over all the species being considered, including type a, and $p_a(v)$ is the probability that particles of type a and velocity v will be lost. The term for charge-exchange loss must be added to the above equation for ions. The term $s_a(v, t)$ represents the source of injected particles.

We consider electrons and ions of $Z = 1$. We introduce the dimensionless variable $x = v/v_0$, where v_0 is a constant and is a characteristic velocity. Let $f = (4\pi v_0/K_e)f_e$, where K_e is determined from the equation

$$n_e(0) = K_e \int_0^\infty f(x, 0) x^2 dx;$$

i. e., the constant is determined by the initial conditions with $n_e(0)$ equal to the initial electron density. Similarly, we let $g = (4\pi v_0/K_i)f_i$, where

$$n_i(0) = K_i \int_0^\infty g(x, 0)x^2 dx.$$

We introduce the dimensionless variable τ where $\tau = \left(\frac{1}{2} \Gamma_e K_e / v_0^3\right)t$. Let $\mu = m_e/m_i$ and $K = K_i/K_e$. Defining the functionals gives us

$$M(f) = \int_x^\infty f(y, \tau)y dy,$$

$$N(f) = \int_0^x f(y, \tau)y^2 dy,$$

and

$$E(f) = \int_0^x f(y, \tau)y^4 dy.$$

In terms of these new variables, the equation for the electron-distribution function becomes

$$\frac{\partial f}{\partial \tau} = A \frac{\partial^2 f}{\partial x^2} + B \frac{\partial f}{\partial x} + Cf + D, \quad (1)$$

where

$$A = \frac{2}{3} \left\{ \left[\frac{1}{3} E(f) + M(f) \right] + K \left[\frac{1}{3} E(g) + M(g) \right] \right\},$$

$$B = \frac{4}{3x} \left\{ \left[\frac{3}{2x} N(f) - \frac{1}{3} E(f) + M(f) \right] + K \left[\mu \frac{3}{2x} N(g) - \frac{1}{3} E(g) + M(g) \right] \right\},$$

and

$$C = 2(f + K\mu g) - p_e(x) \frac{4}{3x^2} \left\{ 2 \left[\frac{3}{2x} N(f) - \frac{1}{2x^3} E(f) + M(f) \right] \right. \\ \left. + K(1 + \mu) \left[\frac{3}{2x} N(g) - \frac{1}{2x^3} E(g) + M(g) \right] \right\}.$$

The term $D(x, \tau)$ describes the time-dependent source of electrons.

The equation for the ion-distribution function becomes

$$\frac{\partial g}{\partial \tau} = F \frac{\partial^2 g}{\partial x^2} + G \frac{\partial g}{\partial x} + Hg + L, \quad (2)$$

where

$$F = \frac{2}{3} \mu^2 \left\{ \left[\frac{1}{x^3} E(f) + M(f) \right] + K \left[\frac{1}{x^3} E(g) + M(g) \right] \right\},$$

$$G = \frac{4}{3x} \mu^2 \left\{ \left[\frac{1}{\mu} \frac{3}{2x} N(f) - \frac{1}{2x^3} E(f) + M(f) \right] + K \left[\frac{3}{2x} N(g) - \frac{1}{2x^3} E(g) + M(g) \right] \right\},$$

and

$$H = 2\mu^2 \left(\frac{1}{\mu} f + Kg \right) - H_1(x, \tau) - \mu^2 p_i(x) \frac{4}{3x^2} \left\{ \frac{1}{2} \left(1 + \frac{1}{\mu} \right) \left[\frac{3}{2x} N(f) - \frac{1}{2x^3} E(f) + M(f) \right] \right. \\ \left. + K \left[\frac{3}{2x} N(g) - \frac{1}{2x^3} E(g) + M(g) \right] \right\}.$$

The term $H_1(x, \tau)$ contains the charge-exchange-loss term, and $L(x, \tau)$ describes the time-dependent source of ions.

We wish to solve nonlinear differential Eqs. (1) and (2) on the domain $0 \leq x < \infty$, $\tau \geq 0$, with the boundary conditions $f \rightarrow 0$, $g \rightarrow 0$ as $x \rightarrow \infty$, and $\partial f / \partial x = \partial g / \partial x = 0$ at $x = 0$ for $\tau > 0$. The initial distributions $f(x, 0)$ and $g(x, 0)$ are given.

For the numerical solution we choose the domain $0 \leq x \leq x_J$, where x_J is specified for each problem and is taken large enough to include the high-velocity tail of the electron distribution. As the electrons increase in temperature, the distribution spreads out; thus, the choice of x_J determines when the calculation must be stopped in order to preserve accuracy. At $x = x_J$, we take the boundary condition $f = g = 0$.

In the domain $0 \leq x \leq x_J$, $\tau \geq 0$, consider the finite-difference mesh defined by $x_j = j\Delta x$, $j = 0, 1, 2, \dots, J$, and by $\tau^n = n\Delta\tau$, $n = 0, 1, 2, \dots$. Let $f_j^n = f(x_j, \tau^n)$, $g_j^n = g(x_j, \tau^n)$, $A_j^n = A(f_j^n, g_j^n, x_j, \tau^n)$, $B_j^n = B(f_j^n, g_j^n, x_j, \tau^n)$, etc. We define the first and second difference approximations by

$$(\delta f)_j^n = \frac{f_{j+1}^n - f_{j-1}^n}{2\Delta x}$$

and

$$(\delta^2 f)_j^n = \frac{f_{j+1}^n - 2f_j^n + f_{j-1}^n}{(\Delta x)^2}.$$

We approximate Eqs. (1) and (2) by the following implicit difference equations:

$$\frac{f_j^{n+1} - f_j^n}{\Delta\tau} = \left[A_j^{n+1} (\delta^2 f)_j^{n+1} + B_j^{n+1} (\delta f)_j^{n+1} + C_j^{n+1} f_j^{n+1} + D_j^{n+1} \right]$$

and

$$\frac{g_j^{n+1} - g_j^n}{\Delta\tau} = \left[F_j^{n+1} (\delta^2 g)_j^{n+1} + G_j^{n+1} (\delta g)_j^{n+1} + H_j^{n+1} g_j^{n+1} + L_j^{n+1} \right].$$

The terms A_j^{n+1} , etc., are computed from f_j^n and g_j^n and are extrapolated.

The above equations are solved by the algorithm described by Richtmyer.² The scheme is numerically stable in practice, and there is no restriction on the time step. This is an essential part of the calculations because as the electron temperature increases, the transfer rate decreases and the time step, Δt , must be continually increased during the calculation in order to progress toward equilibrium in a sensible manner.

A plasma potential is computed at each time step of the calculation by requiring charge neutrality. A critical velocity, $v_c(t)$, is determined such that electrons with $v < v_c$ are not lost and that those with $v > v_c$ can be lost by scattering into the loss cone. At each time step, the electron density is compared to the ion density and v_c is modified accordingly. The plasma potential is obtained from $e\phi = 1/2 (mv_c^2)$.

Numerical results are presented for a case with a source of 15-keV protons and 10-eV electrons. In this case, the particle densities increase from 10^5 to 10^{10} and the electron temperature from 10 eV to 200 eV.

²R. D. Richtmyer, Difference Methods for Initial Value Problems (John Wiley & Sons, New York, 1956), p. 101.

VLASOV THEORY

N67-37745

NONLINEAR STUDY OF VLASOV'S EQUATION FOR A
SPECIAL CLASS OF DISTRIBUTION FUNCTIONS

K. V. Roberts*

and

H. L. Berk

University of California, San Diego

*On leave of absence from Culham Laboratory, Abingdon, England.

ABSTRACT

Calculations on the "water bag model" of a two stream instability have been made by following the motion of the phase space boundaries. Although the distribution function is locally randomized, a large scale non-linear wave is observed. This wave is due to the condensation of holes in phase space which formally act as negative mass particles in that like charges attract one another. The subsequent development of the system depends on the dynamical interaction of the holes with each other and the plasma background. This evolution should be studied statistically, and to begin with, computer calculations have been made for a two hole collision. Statistically, the most probable final state of the simple water bag model is a Fermi distribution and it is important to determine to what extent the actual dynamics allows the system to relax to this state.

NONLINEAR STUDY OF VLASOV'S EQUATION FOR A
SPECIAL CLASS OF DISTRIBUTION FUNCTIONS

K. V. Roberts and H. L. Berk

I. Introduction

The evolution of a collisionless 1-dimensional plasma or gravitational system is described by Vlasov's equation

$$\frac{\partial f}{\partial t} + v \frac{\partial f}{\partial x} - \frac{\partial \phi}{\partial x} \frac{\partial f}{\partial v} = 0 \quad (1)$$

together with Poisson's equation for the potential energy function ϕ . Although the linear^{1,2} and quasi-linear^{3,4} solutions of the coupled Vlasov-Poisson equations have been extensively analyzed, there is still the need to gain some further physical understanding of their non-linear solutions.⁵

The distribution function $f(x, v, t)$ can be pictured as the density of an incompressible "phase fluid" which moves in two-dimensional (x, v) -space. The hydrodynamics, statistical mechanics⁶ and thermodynamics^{7,8} of this model fluid are intrinsically well worth studying, and as we shall show, the detailed analysis of fluid motion in phase space emphasizes nonlinear features which have not been stressed in previous numerical⁹⁻¹² or theoretical¹⁻⁴ work on the Vlasov equation, or on the exact dynamics of an N-particle system. Many of these features are intuitively quite straightforward, and there is a useful analogy between a phase fluid and an ordinary incompressible liquid such as water, although in fact it often turns out that numerical or analytic calculations on phase fluid are simpler to perform.

The density of the fluid in (\mathbf{x}, \mathbf{v}) -space will usually be inhomogeneous, although it follows from Liouville's theorem that the density of each individual moving element must remain constant in time. However, in ordinary hydrodynamics it is convenient and physically obvious to work with a liquid of constant density wherever possible, since this greatly simplifies the equations. Such a liquid may be bounded by a free surface on which waves can propagate, and may also contain cavities of various shapes. In a similar way, to study nonlinear phenomena in phase space in their simplest form one can assume that $f = 1$ in certain regions, and $f = 0$ elsewhere.

This "water-bag model" was introduced by de Packh¹³, and has since been employed by a number of workers for analytic and numerical calculations¹⁴⁻¹⁶. The state of the system at time t is completely defined by specifying the boundary curves $C_j(t)$ between the $f = 0$ and $f = 1$ regions, so that its evolution can readily be followed. The curves C_j can support stable or unstable waves, depending on their orientation, and these are analogous in some respects to gravitational waves or Rayleigh-Taylor instabilities on liquid surfaces, with the added advantage that they can be followed quite accurately into the far nonlinear regime.

For both the hydrodynamic and the Vlasov systems, there is a natural generalization to the case of several fluids of different constant densities, (a typical example would be oil floating on water), and here again the interfaces can support stable or unstable waves. We have therefore developed a computer program, outlined in Section III, which follows the time evolution of a waterbag system with any number of closed or open boundary curves C_j , separating regions R_i in which the distribution function takes arbitrary

constant values f_i . It can be used for a variety of plasma and gravitational problems.

One of the examples to be discussed here is a two-stream instability, in which an electron plasma is slightly perturbed at $t = 0$ from an equilibrium characterized by four equally-spaced horizontal straight lines:

$$f(v) = \begin{cases} 1, & \frac{v_0}{2} < |v| < v_0, \\ 0, & (\text{otherwise}). \end{cases} \quad (2)$$

There is a uniform positive neutralizing background, and periodic boundary conditions are imposed at $(x=0, L)$. The most striking feature of the calculation, illustrated in Fig. (2) is the behavior of the $f=0$ 'cavity' which initially occupies the strip $(|v| < v_0/2)$ between the two plasma layers. This must preserve constant area as it deforms, and it is seen to coalesce into holes of roughly elliptical shape so that a stable large amplitude electrostatic wave is set up. Superimposed on this wave are coherent oscillations and random fluctuations.

These holes in phase space behave in a way which at first sight may be rather surprising since although they are positively charged they are evidently attracted to one another and thus behave like particles of negative mass. Several equivalent explanations of this phenomenon can be given.

We may note that the boundaries of the holes are determined by the motion of negatively charged electrons, which are indeed attracted towards a neighboring positively charged region. Alternatively, the situation is perhaps easier to envisage if we invoke a formal duality between the two-stream plasma problem and an equivalent gravitational problem (Sections VI and

IX) in which the law of force is attractive and the $f = 0$ and $f = 1$ regions are interchanged. In the transformed system the holes become globular masses which attract each other in the usual way.

In a similar vein, Dory¹⁷ has observed the formation of holes in phase space in his numerical calculations on the negative mass instability of circular accelerators, and has demonstrated a duality with the two-stream instability which he calls "mass conjugation".

The two outer curves can be seen to play only a limited role in the two-stream solution. To a good approximation, we show in Section VI that they merely exert a screening effect on the Coulomb fields of the holes, modifying the attraction by a factor $\exp(-\kappa x)$. The nonlinear behavior of the unstable distribution (2) can therefore be rather accurately related to that of a single gravitating strip ($0 < |v| < \frac{v_s}{2}$), with Poisson's equation replaced by

$$\frac{d^2 \phi}{dx^2} - \kappa^2 \phi = \rho \quad (3)$$

The roughly elliptical cavities correspond to the gravitational equilibria found by Hohl, Feix and Staton¹⁶, and a theoretical discussion is given in Section VI. We have carried out some numerical experiments on the dynamical interaction between holes, and these are described in Section VIII. If the interaction between two colliding holes is weak, they excite waves on each other but survive the collision essentially unscathed. If it is strong enough, the two holes coalesce into one highly excited region. In each case, a hole gets rid of excess energy by evaporating off layers from its boundary. This evaporated material becomes more and more randomized as time goes on, so that

the system appears to exhibit a two-phase thermodynamic equilibrium.

This picture certainly suggests that a new statistical formalism should be developed, to describe the evolution of the background plasma and also of the holes. An appropriate form of statistical mechanics has recently been worked out by Lynden-Bell⁶, and one of the most interesting features is that individual fluid elements obey a classical 'exclusion principle', since no two elements can occupy the same region of phase space. If there are only two types of region, $f = 0$ and $f = 1$, the Lynden-Bell distribution is identical to that of Fermi

Our numerical results show however that a further extension of the theory is required, since in many cases it is the holes that set up a Lynden-Bell distribution, with the plasma merely acting as a background medium that determines the law of force between them. We expect this distribution to be metastable, and to relax to the most probable state as time goes on.

II. Evolution of the System

The instantaneous state of a system described by the Vlasov equation may be represented by a set of contours

$$f(x, v, t) = \text{constant} \quad (4)$$

in phase space. Both closed and open curves are allowed, and the contour belonging to a given value f_i may consist of any number of disconnected portions. The evolution of the system is represented by the motion of these contours, and exhibits a number of simplifying features.

In the absence of velocity dependent forces, each point on a contour moves according to the characteristic equations

$$\frac{dx}{dt} = v \quad (\text{independent of } x, t), \quad (5)$$

$$\frac{dv}{dt} = -\frac{\partial \phi}{\partial x} \quad (\text{independent of } v), \quad (6)$$

so that the motion combines a uniform horizontal shear, constant in time, with a non-uniform and variable vertical shear. According to Liouville's theorem the overall system preserves topology, area, energy and momentum. Thus contours retain their relative ordering and do not appear or disappear; they cannot cross, cut or rejoin, and the number of separate pieces of any contour $f(x, v) = f_i$ remains the same. An invariant area function $A(f)$, is defined by the condition that

$$\int_{f_1}^{f_2} A(f) df \quad (7)$$

is the total area of the region enclosed by all branches of the contours f_1 and f_2 .

At each instant of time the potential function required in (6) is to be calculated from Poisson's equation, which we take as

$$\frac{d^2 \phi}{dx^2} = -\lambda \left[\int f(x, v) dv - B \right] \quad (8)$$

It may be generalized to include the effect of screening if required. The constant λ is negative for a gravitational system and positive for a plasma, and the uniform background charge is adjusted so that

$$\frac{1}{L} \int_0^L dx \int dv f(x, v) = B \quad (9)$$

The system possesses an energy integral

$$\mathcal{E} = \frac{1}{2} \iint f(x, v) v^2 dx dv + \frac{1}{2\lambda} \int \left(\frac{\partial \phi}{\partial x} \right)^2 dx \quad (10)$$

and a momentum integral

$$P = \iint f(x, v) v dx dv \quad (11)$$

The field energy is negative for a gravitational system.

Using this formulation of the Vlasov equation, we obtain a model that is readily treated numerically by taking only a finite number of contours. Thus phase space consists of a number of non-overlapping regions; for each

the distribution function takes a constant value f_i , and only the motion of the bounding curves C_j need be computed according to equations (5) and (6). It follows from Liouville's theorem that the number of regions, their areas and the values f_i are all invariant with time, together with the number and topology of the curves. The equilibria, stability and linear oscillations of the curves C_j have been studied analytically for a number of plasma, stellar and electron-beam problems.^{13,14,16}

Each C_j may be represented either parametrically by a pair of functions $(x_j(s, t), y_j(s, t))$ where s labels the points on a directed curve and t is the time, or by a single function $v_j(x, t)$ which in general will be multi-valued, since each C_j may cross a vertical line $x = \text{constant}$ an arbitrary number of times.

The solution of equations (5) and (6) is straightforward, and the central problem is to compute the charge distribution to be inserted in (8). Let the vertical through point x be intersected by curves at points

$$v_1 > v_2 > \dots > v_n \quad (12)$$

which divide it into segments with f -values

$$f_{1/2}, f_{3/2}, \dots, f_{n+1/2} \quad (13)$$

Then apart from a possible constant charge density which may be included in the background charge B , we find

$$\int f(x, v) dv = \sum_{\alpha=1}^n v_{\alpha} (f_{\alpha+1/2} - f_{\alpha-1/2}) \quad (14)$$

This may be evaluated by a method to be discussed in Section III. The motion of a C_j is therefore completely determined by its instantaneous geometry.

For the waterbag model, the area-function becomes a sum of δ - functions

$$A(f) = \sum a_i \delta(f - f_i) \quad (15)$$

Each distinct f_i corresponds to a different "fluid". It should be noticed that the topology of the curves really exerts no constraint on the motion of these fluids. For example, one region can separate into two, joined by an arbitrarily thin "umbilical cord". Similarly, two regions can coalesce to form one, provided that this is threaded by one or more thin slivers which formally preserve the topology. This situation is illustrated, for example, in the numerical results of Fig. 2. Therefore it is permissible to allow arbitrary distributions of fluid in working out the statistical mechanics, provided that area conservation and the exclusion principle are satisfied.

III. Computer Program

Computers have already been extensively used to study collisionless systems described by the Vlasov-Poisson equations, either by following the motion of a large number of 'particles'^{9,10}, or by solving the partial differential equation itself^{11,12}. The particle method is widely applicable and fast, but it leads to statistical fluctuations in the charge density which have a purely numerical origin, and these give rise to fluctuating electric fields and anomalous diffusion effects that are absent from the exact mathematical solution. Whether or not these matter in practice will depend on the parameters of the problem. On the other hand the direct solution of (1) by treating it as a partial differential equation leads to a two-dimensional computation in general, since motion in an (x,v) phase space must be described. Because of the "free streaming" of particles the solutions become more and more contorted as time goes on, so that both Eulerian and Lagrangian mesh techniques give trouble, and methods depending on Fourier expansion and orthogonal functions are often used^{11, 12}.

The main problem is to calculate the charge density, and since the waterbag model gives the simple representation (14) it seems worthwhile to develop a computational method based on direct integration of the area between the curves. Calculations using the particle technique have already been made by Hohl, Feix, and Staton¹⁶.

We place enough points on each curve to describe it as accurately as required, and since in general each curve becomes longer and more contorted as time goes on we arrange to add new points automatically wherever necessary. Together with the coordinates x_i , v_i of the i^{th} point we store the memory

location of the next point i' on the curve. If it becomes necessary to add a new point i'' between them, we place this at the center of the straight segment (i, i') and adjust the chaining so that $(i \rightarrow i'')$, $(i'' \rightarrow i')$. At present a new point is added whenever a segment becomes too long, but it would be preferable to make the addition of points depend on the curvature.

Points are moved according to the leap-frog scheme

$$x_i(t + 2\Delta t) = x_i(t) + v_i(t + \Delta t) \Delta t \quad (16)$$

$$v_i(t + 2\Delta t) = v_i(t) + a_i(t + \Delta t) \Delta t \quad (17)$$

where $a = -\frac{\partial \phi}{\partial x}$ is the acceleration. Two complete sets of curves are therefore required, defined at even and odd parity times

$$\begin{aligned} t &= 2n \Delta t & (\text{even}), \\ t &= (2n+1) \Delta t & (\text{odd}). \end{aligned} \quad (18)$$

Each set of curves defines the charge distribution and velocity which govern the motion of the other. This scheme works very well in practice, although there is a weak computational instability which is inhibited by bringing the two sets of curves into agreement at intervals, (currently every 20 timesteps).

To calculate the charge density, we divide the x -axis into fixed 'Eulerian' intervals of equal length Δx . Since each region R_i is represented by a polygon, the problem is to calculate the area of the intersection of a general polygonal region with the strip $x_m < x < x_m + \Delta x$. To do this, introduce an extra temporary point wherever a segment is crossed by an interval

boundary, and consider the set of sub-segments so formed. Each directed sub-segment (i, i') lies entirely within some interval m , and separates two regions with f -values f_1, f_2 say. Then the total charge within the interval is

$$\lambda \sum \frac{1}{2} (x_{i'} - x_i) (v_{i'} + v_i) (f_2 - f_1) \quad (19)$$

summed over all sub-segments belonging to m .

The program is written in Fortran IV, but uses fixed-point arithmetic in critical sections in order to minimize machine time. These could be converted to machine code to produce a further increase in speed, but a typical run only occupies about 5 minutes on a CDC 3600. The program can be adapted for a variety of problems; periodic, reflecting or open systems, electric or gravitational fields, an arbitrary number of regions R_i with different f -values, a screened or unscreened Coulomb law of force, and plane, cylindrical or spherical one-dimensional geometry.

IV. Linear Theory of the Two Stream Instability

The linear theory of the two stream instability is now a classic problem², but we briefly review it here to illustrate applications of the water-bag model. For the equilibrium we choose the distribution function shown in Fig. (1) with $V_3 = -V_2$ and $V_4 = -V_1$.

The linearized equation of motion of a point on a curve C_i , for a perturbation proportional to $\exp(-i\omega t + ikx)$ is

$$(-i\omega + ikv_i) \delta v_i = -ik \phi_k \quad (20)$$

The normalized potential ϕ_k satisfies Poisson's equation which is given by

$$k^2 \phi_k = \frac{\omega_p^2}{2(V_1 - \beta V_2)} \left[(\delta v_1 - \delta v_4) - \beta (\delta v_2 - \delta v_3) \right] \quad (21)$$

where $\omega_p^2 = \frac{4\pi n_0 e^2}{m}$ and n_0 is the mean electron density. Equation (21) gives

$$\delta v_i = \frac{k \phi_k}{\omega - kv_i} \quad (22)$$

and substituting this into (21) and factoring ϕ_k , we obtain the dispersion relation,

$$\epsilon(\omega, k) \equiv 1 - \frac{\omega_p^2}{(V_1 - \beta V_2)} \left[\frac{V_1}{\omega^2 - k^2 V_1^2} - \frac{\beta V_2}{\omega^2 - k^2 V_2^2} \right] \quad (23)$$

Since the dispersion relation can be rewritten in the following quadratic form,

$$\omega^4 - a\omega^2 + b = 0 \quad (24)$$

where

$$a = \left[k^2 (V_1^2 + V_2^2) + \frac{\omega_p^2 V_1}{(V_1 - \beta V_2)} \right]$$

$$b = k^4 V_1^2 V_2^2 + \frac{\omega_p^2 k^2 V_1 V_2}{(V_1 - \beta V_2)} (V_2 - \beta V_1)$$

the solution is

$$\omega^2 = \frac{1}{2} \left[a \pm (a^2 - 4b)^{1/2} \right] \quad (25)$$

For $b < 0$, this can be negative and the system is unstable. If there is no lower bound for k , the instability condition is

$$\beta > V_2/V_1 \quad (26)$$

The choice of a plus sign in equation (25) yields the mode $\omega \sim \omega_p$, which is the rapidly oscillating wave that is present even in the absence of a depression in phase space. The choice of the lower sign gives rise to the low frequency mode that is primarily driven by the depressed phase space region. If $kV_1 \ll \omega_p$, the dispersion relation for this mode is approximately

$$\omega^2 = \frac{k^2 V_2 (V_1 - \beta V_2)}{\omega_p^2} \left[-\frac{\omega_p^2 (\beta V_1 - V_2)}{(V_1 - \beta V_2)} + k^2 V_1 V_2 \right] \quad (27)$$

This mode is excited by the modulation of the inner surfaces which causes the high velocity streams to lose kinetic energy. The mode is unstable if the electric field is able to absorb enough potential energy to balance this kinetic energy and then continue to modulate the streams. It is stable if the electric field energy cannot absorb all the kinetic energy, so that the system

has to oscillate in a negative energy mode (one can easily verify that the negative energy criterion $\omega \frac{\partial \epsilon}{\partial \omega} < 0$ is fulfilled in this case).

If $v_2 \ll v_1$, an interesting gravitational analogy results. In this limit, the dispersion relation for the low frequency mode is found from Eq. (25) to be

$$\omega^2 = -\frac{k^2 v_2^2}{(\omega_p^2 + k^2 v_1^2)} \left[\frac{(\rho v_1 - v_2) \omega_p^2}{v_2} - k^2 v_1^2 \right] \quad (28)$$

This result can be derived directly from the equations of motion, if we assume $\omega L \ll v_1$, where L is the characteristic length of variation of an excitation. In this case we can neglect the term $\frac{\partial v}{\partial t}$ in the equation of motion for the outer curves. We then find that the bounding curves obey the relation

$$\frac{1}{2} v_{1,4}^2(x) + \phi(x) = \frac{1}{2} v_1^2 \quad (29)$$

After linearizing this solution we find

$$\delta v_{1,4} = -\phi(x) / v_{1,4} \quad (30)$$

and substituting this into Poisson's equation and neglecting ρv_2 compared with v_1 , we find

$$\frac{\partial^2 \phi}{\partial x^2} - \frac{\omega_p^2}{v_1^2} \phi = \frac{\rho (\delta v_2 - \delta v_3)}{2 v_1} \equiv \rho(x) \quad (31)$$

The left hand side is Poisson's equation with a shielding term, and the right hand side is equivalent to the charge density of a gravitational fluid of density $\rho(x)$ in the inner region of phase space. Since a gravitational

fluid is self-attracting we expect the system to condense to a blob. The outer curves shield the strength of the gravitational interaction, and if ϵ is small enough, the condensation is prevented. One can easily establish that the linear dispersion relation derived from (31) is identical to (28).

V. Numerical Experiment on the Two Stream Instability

Figure 2 shows some results of a nonlinear calculation on the two-stream problem, in which the plasma is slightly perturbed at $t=0$ from an equilibrium characterized by Equation (2). The $f=1$ regions have been shaded in, so that the motion of the plasma is emphasized. We employ periodic boundary conditions over a length L , and perturb the initial equilibrium with 16 randomly-chosen amplitudes and phases, i.e. the 4 longest waves on each curve. The parameters of the problem are

$$\frac{V_0 \Delta t}{\Delta x} = .25 \quad \omega_p \Delta t = 1/20 \quad , \quad \Delta x = L/64 \quad (32)$$

where Δx is the grid used for evaluating Poisson's equation, and ω_p is the radian plasma frequency. The unstable modes are $n = 1, 2$ where the wave-number is $k = 2n\pi/L$, and the linear growth rates are $\gamma/\omega_p = 0.30, 0.315$.

Each of the four curves is originally determined by 64 equally-spaced Lagrangian points, joined by straight-line segments in phase space. Because a new point is added at the center of a line segment whenever it becomes too long, many more points may be needed to describe the system at later times, and 1734 points have been used in Fig. 2c (with an equal number for the curves of opposite parity). This contortion of the curves represents an increase in the complexity of the distribution function $f(x, v)$, but not necessarily of the electric field. The energy in the electrostatic modes drops off rapidly as n increases and therefore the number of Eulerian points needed to represent the electric field is quite small and does not increase with time. A calculation with $\Delta x = L/32$ gave phase diagrams almost identical

to those of Fig. 2.

The distribution function is shown at timesteps 250, 350, and 600. Initially the 16 modes proceed to develop according to linear theory. At step 250 significant nonlinear effects have taken place and some of the particles have been turned around by the field. At step 350 the electric field has almost reached its maximum (Fig. 3), and constructive interference between the $n = 1$ and $n = 2$ modes causes significant particle trapping. At step 450 the electric field has decreased somewhat, due to the increased flux of negatively charged fluid incident on the next positively charged region. The decrease in field enables some of the trapped particles to escape, and to cause further 'thermalization' of the distribution function.

The calculation cannot as yet be continued much beyond step 600 since too many points have to be added to the system. It is still reasonably accurate at this stage; there has been negligible crossing of the lines, and area and energy have been conserved to within 1.25% and 0.5%, respectively. We are attempting to make the program capable of longer runs by treating the thin 'slivers' and 'sandwiches' of fluid and vacuum that continually form by alternate methods.

The solution is dominated by a large amplitude standing wave, on which are superimposed coherent oscillations and random fluctuations. The formation of this wave is most apparent from Fig. 4, which emphasizes the motion of the cavity rather than that of the plasma. It is seen that by step 250 the cavity has developed into two holes of roughly elliptical shape, which resemble gravitational equilibria. These then attract one another, and coalesce into one large hole which subsequently oscillates. Some portion of the $\vec{h} = 0$

region is dispersed into smaller holes and fine-scale slivers, which become more and more randomized as time proceeds.

VI. Hole Equilibria

Since the two stream instability evolves into a state containing a standing electrostatic wave, produced by a hole in phase space, we now examine the standing wave equilibrium of the water-bag model in which, for simplicity, we choose $f = 0$ inside the hole. In order for the distribution function to be independent of time, each contour must be a constant energy curve. The outer curves, C_1 and C_4 have energies $\frac{1}{2}V_1^2$ and $\frac{1}{2}V_4^2$, while the inner curves C_2 and C_3 being trapped trajectories, have an energy $-V_2^2/2$. Curves (2) and (3), which are both on the energy contour $E = -\frac{V_2^2}{2}$, have been artificially distinguished so that each curve is a single-valued function of x . We solve this system for a single pulse but the method can also be used to find the solution for a periodic train of pulses. Poisson's equation is

$$\frac{\partial^2 \Phi}{\partial x^2} \equiv \frac{1}{2} \frac{\partial}{\partial \Phi} \left(\frac{\partial \Phi}{\partial x} \right)^2 = -\frac{\omega_p^2}{2\bar{V}} \left[\sqrt{V_1^2 - 2\Phi(x)} + \sqrt{V_4^2 - 2\Phi(x)} - 2\bar{V} - 2\sqrt{-V_2^2 - 2\Phi(x)} \theta(-V_2^2 - 2\Phi(x)) \right] \quad (33)$$

where $\bar{V} = \frac{1}{2}(V_1 + V_4)$ is the condition necessary for overall charge neutrality and $\theta(x) = \begin{cases} 1, & x > 0 \\ 0, & x < 0 \end{cases}$.

This equation is easily solved by quadrature. The first integral is

$$\left(\frac{\partial \Phi}{\partial x} \right)^2 = \frac{\omega_p^2}{3\bar{V}} \left[(V_1^2 - 2\Phi)^{3/2} + (V_4^2 - 2\Phi)^{3/2} + 6\bar{V}(\Phi - \Phi_0) - (V_1^2 - 2\Phi_0)^{3/2} - (V_4^2 - 2\Phi_0)^{3/2} - 2(-V_2^2 - 2\Phi)^{3/2} \theta(-V_2^2 - 2\Phi) + 2(V_2^2 - 2\Phi_0)^{3/2} \right] \quad (34)$$

where $\Phi_0 = \Phi(x=0)$. We solve for V_3 from the condition that at infinity

$\Phi = 0$ and $\frac{\partial \Phi}{\partial x} = 0$, and find

$$(-V_2^2 - 2\Phi_0)^{3/2} = \frac{1}{2} \left[(V_1^2 - 2\Phi_0)^{3/2} + (V_4^2 - 2\Phi_0)^{3/2} - V_1^3 - V_4^3 + 6\bar{V}\Phi_0 \right] \quad (35)$$

Consistency requires that $\Phi_0 < 0$, $-2\Phi_0 > v_2^2$, and $(-v_2^2 - 2\Phi_0)^{3/2} > 0$

An examination of (35) establishes these points. In the limits $\Phi_0 \ll v_1^2, v_4^2$ or $\Phi_0 \gg v_1^2, v_4^2$ we find

$$(-v_2^2 - 2\Phi_0)^{3/2} = \frac{3\sqrt{\Phi_0}}{2v_1v_4} \Phi_0^2 \quad (\Phi_0 \ll v_1^2, v_4^2) \quad (36a)$$

$$(-v_2^2 - 2\Phi_0)^{3/2} = (-2\Phi_0)^{3/2} + 3\sqrt{\Phi_0} \Phi_0 \quad (\Phi_0 \gg v_1^2, v_4^2) \quad (36b)$$

Having established the consistency of our solution we now integrate

(34) again, so that $\Phi(x)$ is determined by the following quadrature,

$$x = - \int_{\Phi_0}^{\Phi} \frac{d\Phi}{|d\Phi/dx(\Phi)|} \quad (37)$$

where $\frac{d\Phi}{dx}$ is obtained from (34).

The solution may be interpreted qualitatively as follows. An incompressible hole in phase space dilutes the electron fluid density and hence a positively charged region is formed. Electrons cannot neutralize this region, since as they are attracted towards the center they accelerate, and thus spend less time in the center than at the end of the hole. Thus a solution in which the electron density is less at the center is self-consistent. Away from the center, the potential $-2\Phi_0$ decreases since the electron density increases. Outside the hole the electron fluid shields the positive charge accumulation in the usual way and from (37) we can show that $\Phi \propto \exp\left(-\frac{\omega_p |x|}{\sqrt{v_1 v_4}}\right)$ if $\Phi \ll v_1^2, v_4^2$.

In the limit $\Phi_0 \ll v_1^2, v_4^2$ we again see that our problem is equivalent to the screened gravitational problem. In order to gain a feel for

the equilibrium, we establish some scaling relationships for this case. It follows from (29) and (31) that the outer strings behave as instantaneous equipotentials, which shield the holes even if the latter are not in a stationary state. For the stationary problem the potential outside the hole is given by

$$\Phi \doteq \Phi_0 \exp(-\chi|x|) \quad (38)$$

where $\chi = \frac{\omega_p}{\sqrt{v_i v_e}}$. Thus the electric field $E = -\frac{\partial \Phi}{\partial x}$ near the edge of the hole is

$$E = -\chi \Phi_0 \quad (39)$$

and it decays according to the exponential shielding law outside the hole.

We estimate the size of the hole by first noticing that the potential difference $\Delta \Phi$ between its end and its center is found from Eq. (36a), to be

$$\Delta \Phi = \left(\frac{3}{2} \frac{\bar{v}}{v_i v_e} \Phi_0 \right)^{2/3} \quad (40)$$

A lower limit to the spatial extent of the hole is obtained if we determine the length L , which the bulk of the plasma needs to shield a potential drop $\Delta \Phi$, from the relation $\Phi_0 (1 - e^{-\chi L})$. Hence, $L \sim (\Phi_0 \bar{v})^{1/3} / \omega_p$ where we have taken $v_i \sim v_e \sim \bar{v}$.

Equation (36a) shows that a typical velocity of a point on the boundary of the hole scales as $\bar{v}_h \sim \left(\frac{\Phi}{v_i} \right)^{1/3}$ and thus the area of a hole $A \sim \bar{v} L$ scales as $A \sim \frac{\Phi}{\omega_p}$.

We do not as yet have a rigorous theory for the stability of these holes, but semi-quantitative analysis indicates that a single hole is a stable structure. On the other hand it is clear that a periodic set of

pulses is unstable in the strict sense. This is because adjacent holes being attracted towards each other will continue to drift towards one another once an initial displacement has been made.

We can examine the stability of a single pulse in two limits, when the potential is either large or small compared with the square of the thermal velocity. In the first case, the results must be identical with those of the gravitational dual problem. Since Feix, Hohl and Staton¹⁶ have found that the gravitational equilibrium blob is stable, it follows that in the plasma problem a small hole in phase space is also stable.

In the opposite limit, $-2\Phi_0 \gg v_1^2, v_4^2$ the distribution function inside a hole resembles two counter-streaming beams and we therefore investigate whether the two stream instability can occur. If the wavelength of the instability is much less than the hole size, then the configuration is certainly unstable. On the other hand, if the shortest unstable wavelength is much greater than the hole size, the two stream instability cannot occur and the configuration should be stable. For simplicity we shall take $v_1 = v_4$.

Since $-2\Phi_0 \gg v_1^2$ inside the hole, the two streams are very thin and widely separated from each other. Each stream's flux is determined by its value at the point where the hole pinches, i.e. where $-2\Phi = v_2^2$. From (36b) we find that $v_2^2 = (-2\Phi_0)^{1/2} v_1$ and hence the flux, F , of each stream is

$$F = \frac{n_0}{2} \left[v_1 (-2\Phi_0)^{1/2} \right]^{1/2} \quad (41)$$

where n_0 is the mean charge density over all space.

Inside the hole the potential governing the motion of the electrons can be approximately calculated by neglecting the electron density. Hence,

since $\frac{\partial^2 \Phi}{\partial x^2} \doteq \omega_p^2$,

$$\Phi = \frac{1}{2} \omega_p^2 (x^2 - L^2) \quad (42)$$

where $\omega_p^2 L^2 \doteq -2\Phi_0$. Since $-2\Phi_0 \gg v_i^2$, the velocity $v(L)$ of the stream near the hole center is $v(L) \simeq \omega_p L$ and L is also the approximate size of the hole. From flux conservation, we find that the electron density, $n(L)$ near the center of the hole is $n(L) \simeq \frac{n_0}{2} \left(\frac{v_i}{\omega_p L} \right)^{1/2}$.

Now the unstable mode with the largest wavenumber, k_c , for two thin counterstreaming beams is $k_c \simeq \frac{\omega_p(L)}{v(L)}$ and therefore,

$$k_c L \simeq \left(\frac{v_i}{\omega_p L} \right)^{1/2} \ll 1 \quad (43)$$

Thus an unstable wavelength cannot fit inside the hole and therefore a hole appears to be stable.

VII. Interaction between Holes

The next important step is to understand how holes interact with one another. The theory of hole-hole collisions is a complicated nonlinear mechanism for which we are currently seeking a theoretical description.

We can describe part of the motion of a two hole interaction precisely in one limiting case. If two holes are small compared to a Debye length, but do not overlap, then until the moment of overlap, the shape of each hole remains invariant as they are attracted toward one another. This is because the electric field produced by one hole is essentially constant over the region occupied by the other. Thus each hole lies in a uniform field and is consequently displaced as a rigid body, whose effective mass is the negative of the total mass of the displaced fluid. This simple description breaks down at the moment of overlap of the holes.

In the next section, two numerical experiments are described. In the first experiment, two large holes collide, and the resulting accumulation of positive charge produces a surge of electron flux which causes the two holes to coalesce and to throw off a significant fraction of their total area, which subsequently becomes randomized. In the other experiment, two smaller holes move rapidly through each other. In this case the holes remain coherent entities but there are severe tidal distortions that cause rapid pulsations of the holes. With a continuous distribution function, it is probable that the electrostatic fields produced by these pulsations would undergo Landau damping.

VIII. Numerical Experiments on Hole-Hole Collisions

We now discuss some numerical experiments on the interaction of two holes in the water-bag model. Two identical holes are assumed to approach each other with equal and opposite velocities. The velocity parameters are chosen so that v is the minimum separation of the upper and lower strings in the initial state and ΔV is the mean hole speed. The normalized speed is denoted by $u = \frac{\Delta v}{v}$. Φ_0 is the potential at the hole center and the normalized potential at that point is denoted by $\psi = -\frac{2\Phi_0}{v^2}$. Initially the holes are sufficiently separated so that the shielding clouds do not interact.

The parameters of the first run are,

$$u = .2, \quad \psi = .5, \quad \frac{v(1-u)}{2\Delta x} = 1/4$$

$$\omega_p \Delta t = .04213, \quad \Delta x = L/64 \quad (44)$$

The resulting evolution of the phase space fluid is shown in Fig. (6) and the electric field fluctuations are tabulated in Table 1.

From steps 0 to 300 the holes move freely towards one another with negligible interaction. The fluctuations which can be seen in the electric field are due to an initial mismatch of our initial conditions to the exact equilibrium. From steps 350 to 450 the shielding clouds interact and reduce the electric field somewhat as the negative charge clouds partially neutralize the positively charged region. However, from steps 500 to 550, we see that the two holes coincide in space, thus producing a large positively charged region and a significant increase in the electric field. This field sucks the electron fluid into the region, as seen from steps 650-750. The fluid attempts to neutralize the positively charged region but overshoots significantly. This

surge of electron flux destroys the distinctness of the two holes. However, the neutralizing flux ultimately saturates, and there is still enough positive charge present to maintain a hole structure. From steps 800-1000 we see that the system successfully reforms a solitary hole. The hole continues to pulsate, and the electric field energy is on the average less than the original field energy. However, most of the hole area is still trapped and only a small fraction of the area is lost as thermal agitation.

In the second run, illustrated in Fig. (7) and tabulated in Table 1, we consider two holes that have a weaker potential and approach each other faster. The parameters defining this run are,

$$u = .4, \quad \psi = .1, \quad \frac{V(1-u)}{2\Delta x} = 1/4, \quad \omega_p \Delta t = .0533, \quad \Delta x = L/64 \quad (45)$$

In this case the potentials associated with the holes are too weak and pass each other too quickly to produce a violent nonlinear interaction. One can see that as a result of three successive collisions, the holes undergo severe tidal distortions, but are still able to keep their identity and pulsate about their equilibrium shape. Some evaporation occurs after step 450, but the hole area lost over the entire run is very small. In the electric field data, we are unable to detect any systematic damping. However, it is possible that with a continuous distribution function, the pulsation energy would be removed by Landau damping which could perhaps cause a depression in phase space to thermalize completely.

IX. Energy and Duality

To get a further understanding of the solution described in Section V, we must develop some of the concepts mentioned in Section I. The total energy consists of two parts, kinetic and potential as indicated in Equation (10). The kinetic energy is always positive (if $f \geq 0$), while the field energy is positive for a plasma and negative for a gravitational system. In the case of a periodic plasma with momentum $P = 0$ and uniform background charge density B , there is a unique state of minimum energy \mathcal{E}_0 , symmetrical about the x -axis in phase space, in which the "fluid" regions are ordered in such a way that the more dense fluids is always nearer to the axis and all electric fields are zero. If $A(f)df$ is the area per unit length between $f, f+df$ then

$$v(f) = \frac{1}{2L} \int_f^{f_{\max}} A(f') df' \quad (46)$$

Any other state must have energy $\mathcal{E} > \mathcal{E}_0$, and in principle each initial state \mathcal{E}_i has a "free energy" $\mathcal{E}_F = \mathcal{E}_i - \mathcal{E}_0$ which is available to drive instabilities. This point has been emphasized by Gardner⁵ and Fowler⁶. Dense fluid can "fall" towards the x -axis, reducing its kinetic energy $\frac{1}{2} f v^2$ while displacing light fluid which "rises". Such a process releases energy which can either go into the electric field, or can be used to raise other portions of the fluid to higher velocities. Fig. 2a shows tongues of heavy fluid falling and bubbles rising just as in a Rayleigh-Taylor instability.

There are three constraints on the system, namely that \mathcal{E} , P and the function $A(f)$ remain invariant. The Lynden-Bell distribution is obtained⁶

by considering all possible re-arrangements of the fluid, subject to these constraints. However, it turns out that the statistically most favorable state that satisfies the constraints does not necessarily evolve and three examples may be given.

(a) Free streaming. In the limit of low density, as $\lambda \rightarrow 0$, there can be no electric fields and hence no acceleration, and each fluid element moves with uniform velocity ($x = vt$, $v = \text{constant}$). The averaged distribution function

$$\tilde{f}(v) = \frac{1}{L} \int f(x, v) dx \quad (47)$$

remains constant.

(b) Isotropic 3-dimensional distribution. It is known that the 3-dimensional analogue of the distribution (2) is linearly stable, and in fact any isotropic distribution $f(v_x^2 + v_y^2 + v_z^2)$ has this property¹⁸.

(c) Three stream distribution. If (2) is modified to

$$f = \begin{cases} 1, & (\frac{v_0}{2} < |v| < v_0) \\ 1-\theta & (|v| < v_0/2) \\ 0 & (\text{otherwise}) \end{cases} \quad (48)$$

the system is linearly stable if $\theta < \frac{1}{2}$.

Since the total energy is constant, the system will only be unstable if there is some specific coupling mechanism by which kinetic energy released by "dense fluid falling toward the x-axis" can either be given to the electric field, or can be used to "raise the height" of other fluid elsewhere. In the case of our numerical experiment with the two stream instability by the time

that Fig. 2c has been reached the electric field has already absorbed about as much energy as it can, and further rapid degeneration of the initial state can only take place if large amplitude waves can be excited on the two outer surfaces. However, these waves have a dispersion relation

$$\omega^2 = \omega_p^2 + k^2 v_0^2 \quad (49)$$

and therefore a minimum phase velocity $\frac{\omega}{k} = v_0$, and hence cannot readily be excited by disturbances in the fluid which move more slowly. The system has therefore reached a metastable state.

To make the correspondence between plasma and gravitational problems more formal we introduce two invariance principles. The computer solution depends only on the time evolution of the contours C_j , and this remains unchanged under two elementary transformations:

$$I. \quad f^* = -f, \quad \lambda^* = -\lambda, \quad B^* = -B, \quad \phi^* = -\phi, \quad \epsilon^* = -\epsilon \quad (50)$$

$$II. \quad f^* = f + C, \quad \lambda^* = \lambda \quad (51)$$

Here C is an absolute constant, independent of (x, v, t) . The transformation II must be supplemented by the addition of an infinite constant to the background charge density B , and also to the energy and momentum integrals.

These transformations are unphysical as they stand, but they may be combined together to give physical results. For example, it is meaningful to discuss the interaction of a finite number of holes $f = 0$ in an infinite electron sea $f = 1$. Making the transformation I, followed by II with $C = 1$, we obtain the equivalent gravitational dual problem of the interaction of a

finite number of $f = 1$ regions in a vacuum ($f = 0$). This has already been studied by Hohl, Feix, and Staton¹⁶, who demonstrate that an isolated $f = 1$ region takes up a stable equilibrium, roughly elliptical in shape. The excitation of small amplitude waves on such an equilibrium has been discussed by Ehrman¹⁴. A similar stability must therefore be shown by holes in an electron sea.

The gravitational dual of the two stream problem has

$$f = \begin{cases} 1, & (|v| < \frac{v_0}{2} \text{ and } |v| > v_0) \\ 0, & (\frac{v_0}{2} < |v| < v_0) \end{cases} \quad (52)$$

By arguments equivalent to those of Section V, it may be shown that the main influence of the two semi-infinite regions with $|v| > v_0$ is to screen the effect of disturbances on the inner strip, so that the problem is similar to that of a single gravitating strip $|v| < v_0/2$, with Poisson's equation modified to

$$\frac{d^2 \phi}{dx^2} - \chi^2 \phi = \rho(x) \quad (53)$$

X. Statistics

It is interesting to make some conjectures about the final state of the system. The statistical mechanics of collisionless phase fluid has been studied by D. Lynden-Bell and R.M. Lynden-Bell⁶ and applied to a gravitational problem. They show that such a fluid ought to obey a fourth type of statistics, which in general is different from those of Boltzmann, Fermi or Bose. The Lynden-Bell distribution function is obtained by evaluating the most probable partition of energy between the gravitational or electrostatic field, and a large number of incompressible elements of phase fluid with different densities f_i which all exclude one another. In the special case when f has only two values (0, 1), the distribution reduces to that of Fermi:

$$f_i(E) = \frac{f_0}{1 + \exp[(E - E_F)/Y]} \quad (54)$$

where the parameters E_F and Y are determined by the total energy and area, and $E = \phi + \frac{v^2}{2}$ is the sum of the potential and kinetic energies per unit mass.

In the more general problem, where f_i can take on several values, a correspondingly more general expression for f_i exists⁶. The parameter Y plays the part of a "temperature" and measures the random excitation of the system above the minimum energy state $Y = 0$. The zero temperature equilibrium is the one in which each region has a specified area and the total energy of the system is assigned its least possible value. The finite temperature equilibrium represents a system with more energy but with the integral of

$f_i(\gamma)$ equal to the integral of $f_i(\gamma=0)$. Note that γ is not immediately related to the temperature of the particles, and would be zero for any unperturbed stable state with $\frac{\partial f}{\partial E} < 0$, such as a Maxwellian. For the two stream problem calculated in Section V, the zero temperature state would be $f = 1$ for $|v| < \frac{v_0}{2}$ and zero elsewhere.

Near zero temperature we can explicitly relate v_F and γ to the total energy and density of a system described by (54) if no electrostatic potentials are present. At zero temperature the phase fluid is uniformly distributed in velocity space in the region $-v_{F_0} < v_F < v_{F_0}$ and $\frac{1}{2} v_{F_0} = E_F(\gamma=0)$. The total energy, W , of this system is then

$$W = \frac{1}{2} \int f v^2 dv = \frac{v_{F_0}^3}{3}$$

where in the normalization we set $f_0 = 1$.

We now imagine that we excite electric field oscillations in this system which causes the total energy to increase by δW where $\delta W \ll E_{F_0}$. After a sufficiently long time the distribution function will relax to a Lynden-Bell distribution, given by (54). From the normalization and the conservation of energy, we find the following relations by using the standard methods of integrating degenerate Fermi distributions¹⁹.

$$\delta v_F = v_F - v_{F_0} = -\frac{\pi^2 \gamma}{12 v_{F_0}} \quad (55a)$$

$$\delta W = \frac{\pi^2 \gamma}{12} \quad (55b)$$

We have attempted to attain these parameters numerically by perturbing a stable plasma defined by two horizontal curves. However, since the water-bag model does not contain any linear damping mechanism, the electric field oscillation persisted over the length of the calculations and we were unable to filter the equilibrium distribution function from the oscillatory motion.

Returning to our consideration of the two stream problem, we find that on a shorter timescale, an entirely different type of distribution is observed. Because the problem is equivalent to that of a gravitational strip, we first get an initial metastable distribution (54) for the holes, in which potential energy must be taken into account. At this stage the plasma acts only as a background medium, which governs the law of force by determining the screening length κ .

The stable large-amplitude wave that dominates our numerical solution corresponds to a "degenerate" Fermi-like distribution for the holes, and is a particular case of a Bernstein, Greene, Kruskal mode.⁵ Superimposed on this basic wave are regular oscillations and random small-scale fluctuations, and these arise from the energy difference between the basic equilibrium and the initial state (2). They approximate a finite temperature Fermi distribution in which part of the hole fluid has "evaporated".

If the distribution function (54) is to be set up in reality, it is necessary for sufficient stirring to take place so that the phase fluid becomes broken up into a large number of small elements which diffuse about at random and gradually accommodate themselves to the most probable distribution. How far and how quickly this happens in practice is a matter for further investi-

gation which we are now currently undertaking.

ACKNOWLEDGMENTS

We would like to thank the computer center of the University of California, San Diego for its excellent service. This work was supported jointly by the U. S. Atomic Energy Commission and the U. K. Atomic Energy Authority.

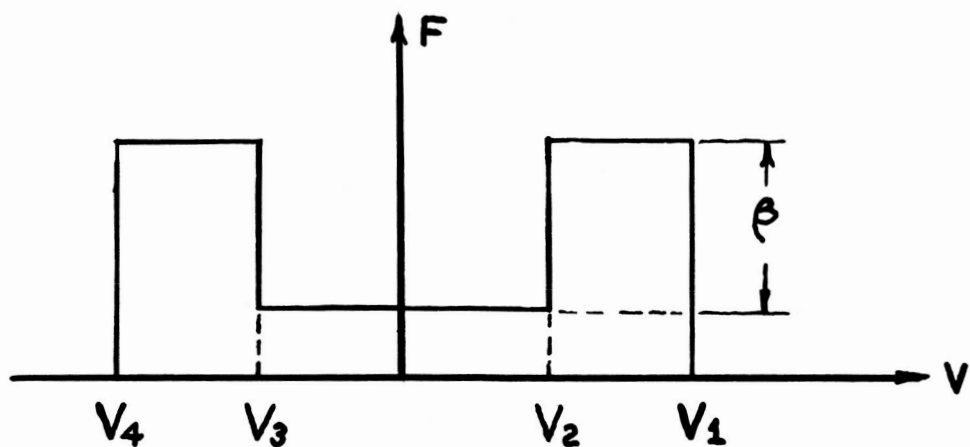
REFERENCES

1. L. D. Landau, J. Phys. (U.S.S.R.) 10, 25 (1940).
2. T. H. Stix, The Theory of Plasma Waves, McGraw Hill Company, New York, 1962.
3. W. E. Drummond, D. Pines, Nucl. Fusion Suppl., Pt. 3, 1049, (1962).
4. A. A. Vedenov, E. P. Velikov, R. Z. Sagdeev, Nucl. Fusion 1, 82 (1961).
5. I. B. Bernstein, J. M. Greene, M. D. Kruskal, Phys. Rev. 108, 546 (1957).
6. D. Lynden-Bell, Monthly Notices, Roy. Astron. Soc., 136, 101 (1967).
7. C. S. Gardner, Phys. Fluids 6, 839 (1963).
8. T. K. Fowler, Phys. Fluids 7, 249 (1964).
9. O. Buneman, Phys. Rev. 115, 503 (1959); J. Nucl. Energy, Pt. C, 2, 119 (1961).
10. J. M. Dawson, Phys. Fluids 5, 445 (1962); Nucl. Fusion, Suppl., Pt. 3, 1033, (1960).
11. G. Knorr, Zeits fur Naturf. 18a, 1304 (1963).
12. T. P. Armstrong, Thesis, University of Iowa (1966).
13. D. C. dePackh, J. Electron Contr. 10, 13a (1962).
14. J. B. Ehrman, J. Nucl. Energy, Pt. C, 8, 377 (1966).
15. H. L. Berk, et al. preprint IC/66/93, International Centre for Theoretical Physics, Trieste, Italy (1966).
16. F. Hohl, M. R. Feix, Phys. Letters 22, 432 (1966); M. R. Feix, F. Hohl, and L. Staton, Proc. 1966 Orsay Summer Institute (to be published).
17. R. A. Dory, J. Nucl. Energy, Pt. C, 6, 511 (1964).
18. G. Backus, J. Math. Phys., 1, 178 (1960).
19. C. Kittel, Elementary Statistical Physics, John Wiley and Sons, Inc., New York p. 92 (1958).

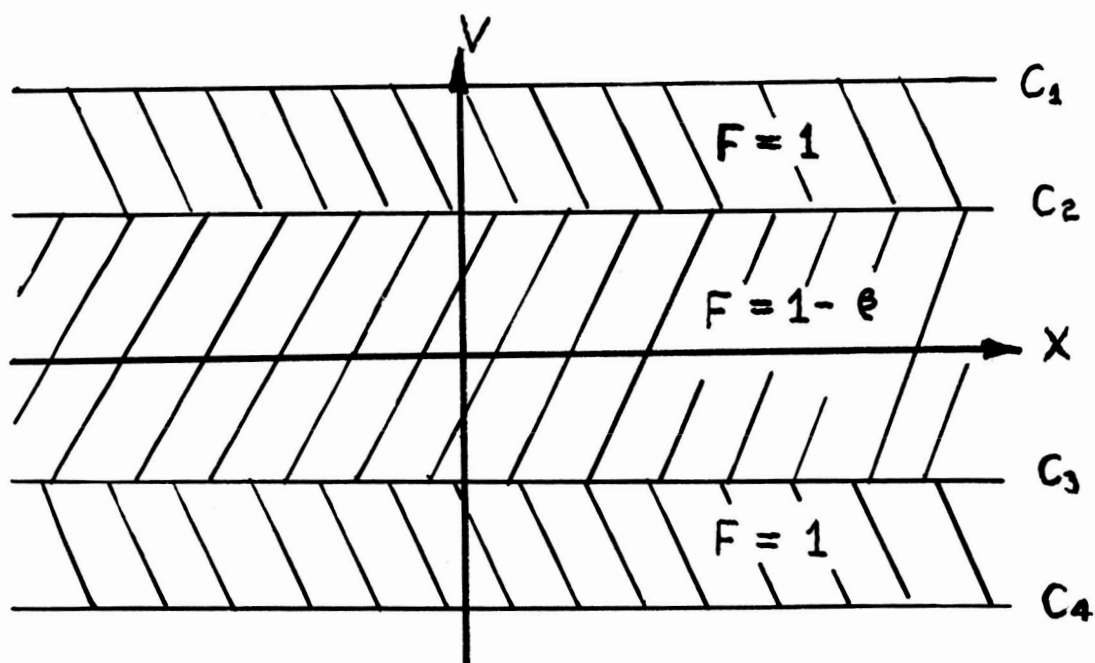
EVOLUTION OF TOTAL FIELD ENERGY
(UNITS ARBITRARY)

TIME STEP	FIRST RUN	SECOND RUN
0	.0648	.0913
50	.0799	.0636
100	.0654	.0555
150	.0686	.0403
200	.0818	.0594
250	.0665	.0588
300	.0724	.0493
350	.0547	.0652
400	.0613	.0607
450	.0460	.0364
500	.0621	.0527
550	.1098	.0446
600	.0533	.0493
650	.0463	.0331
700	.0204	.0771
750	.0157	.0514
800	.0339	.0298
850	.0633	.0329
900	.0692	.1298
950	.0609	.0717
1000	.0389	

TABLE I



(a)



(b)

Figure 1.- Equilibrium distribution function for two stream instability. Figure (a) shows F as a function of V and (b) shows the occupied regions of phase space.

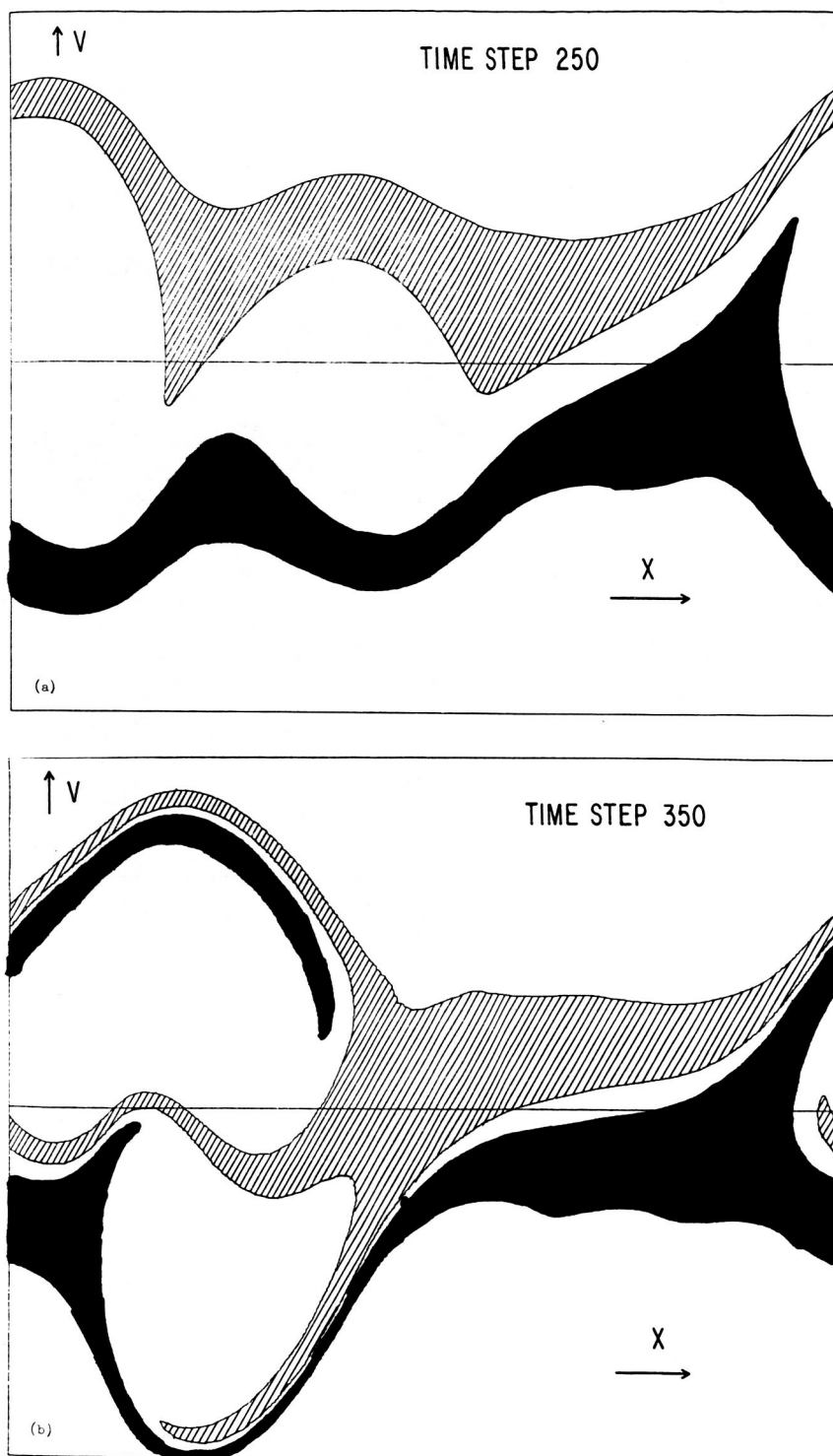


Figure 2.- Development of two stream instability in phase space. The horizontal and vertical coordinates are x , v , respectively. Regions occupied by the upper and lower streams are indicated by the shading.

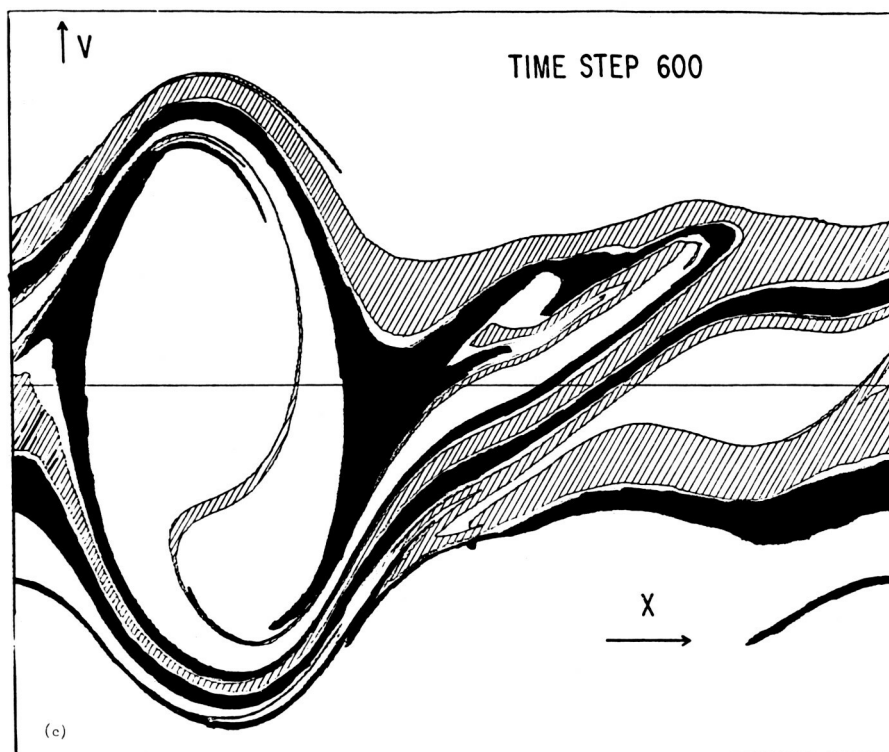


Figure 2.- Concluded.

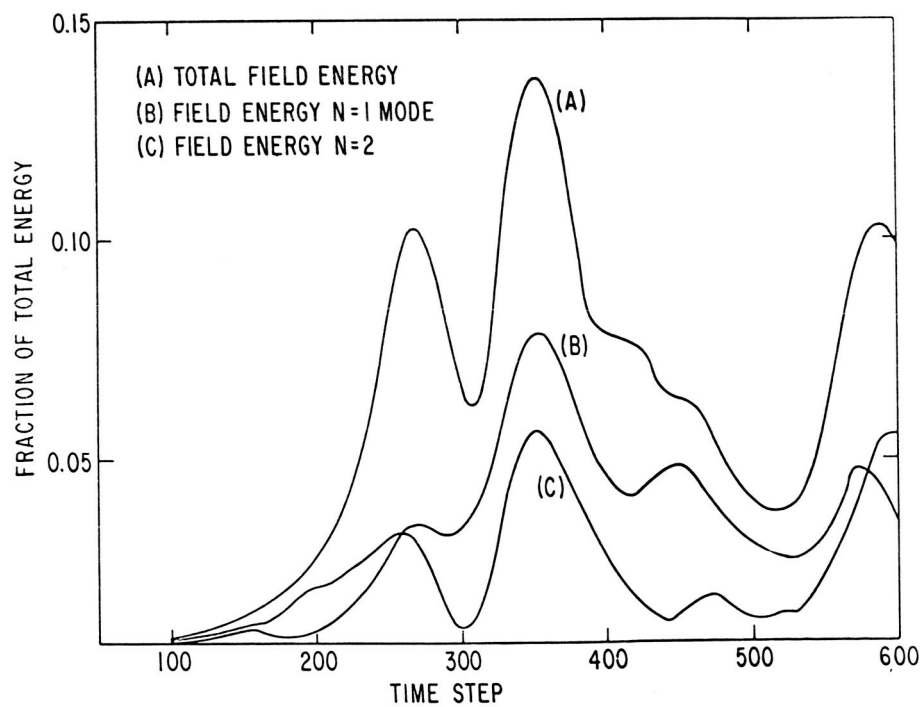


Figure 3.- Fraction of total energy in electric field as a function of time.

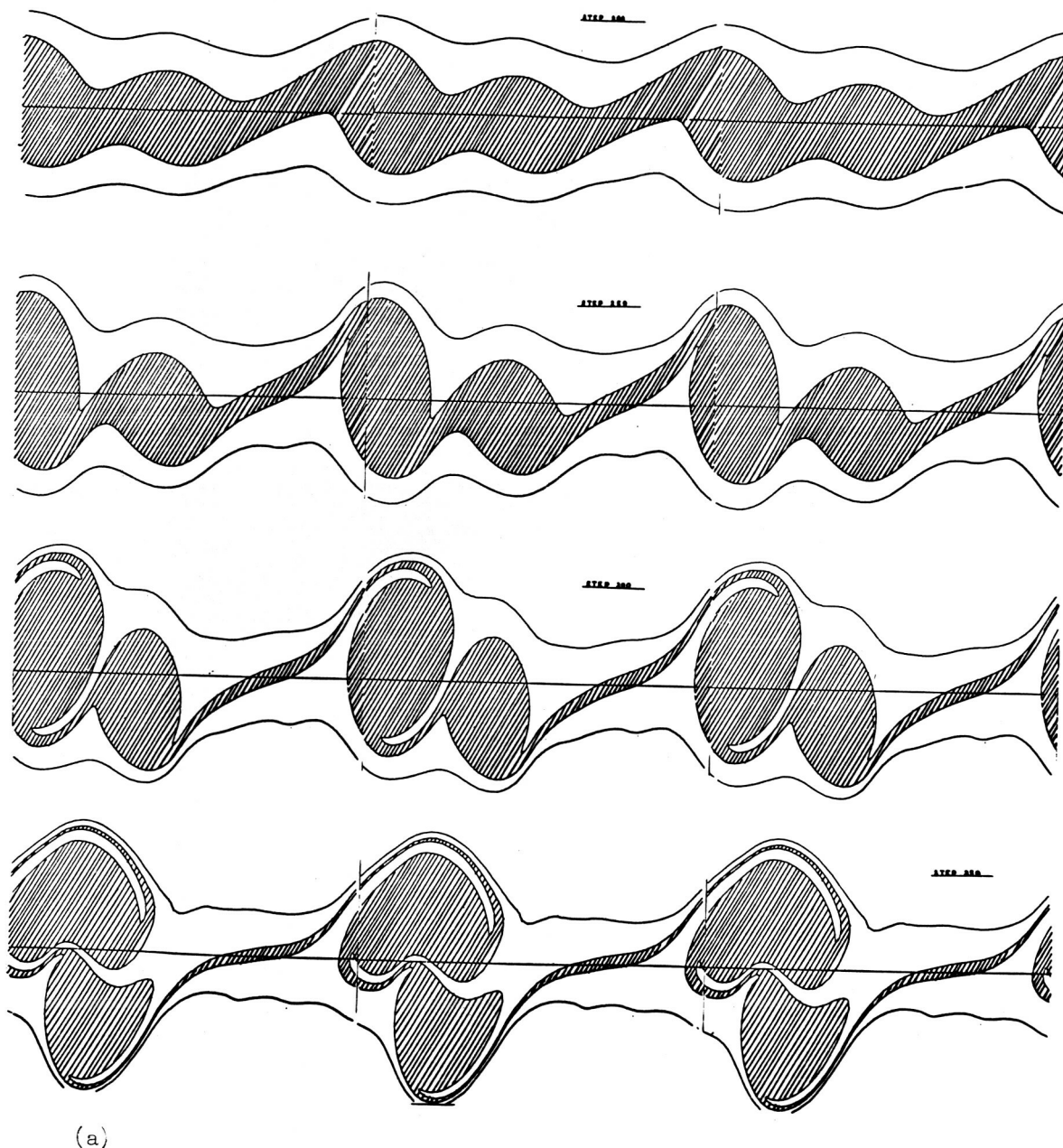


Figure 4.- Time evolution of the phase space holes from the original two stream distribution.

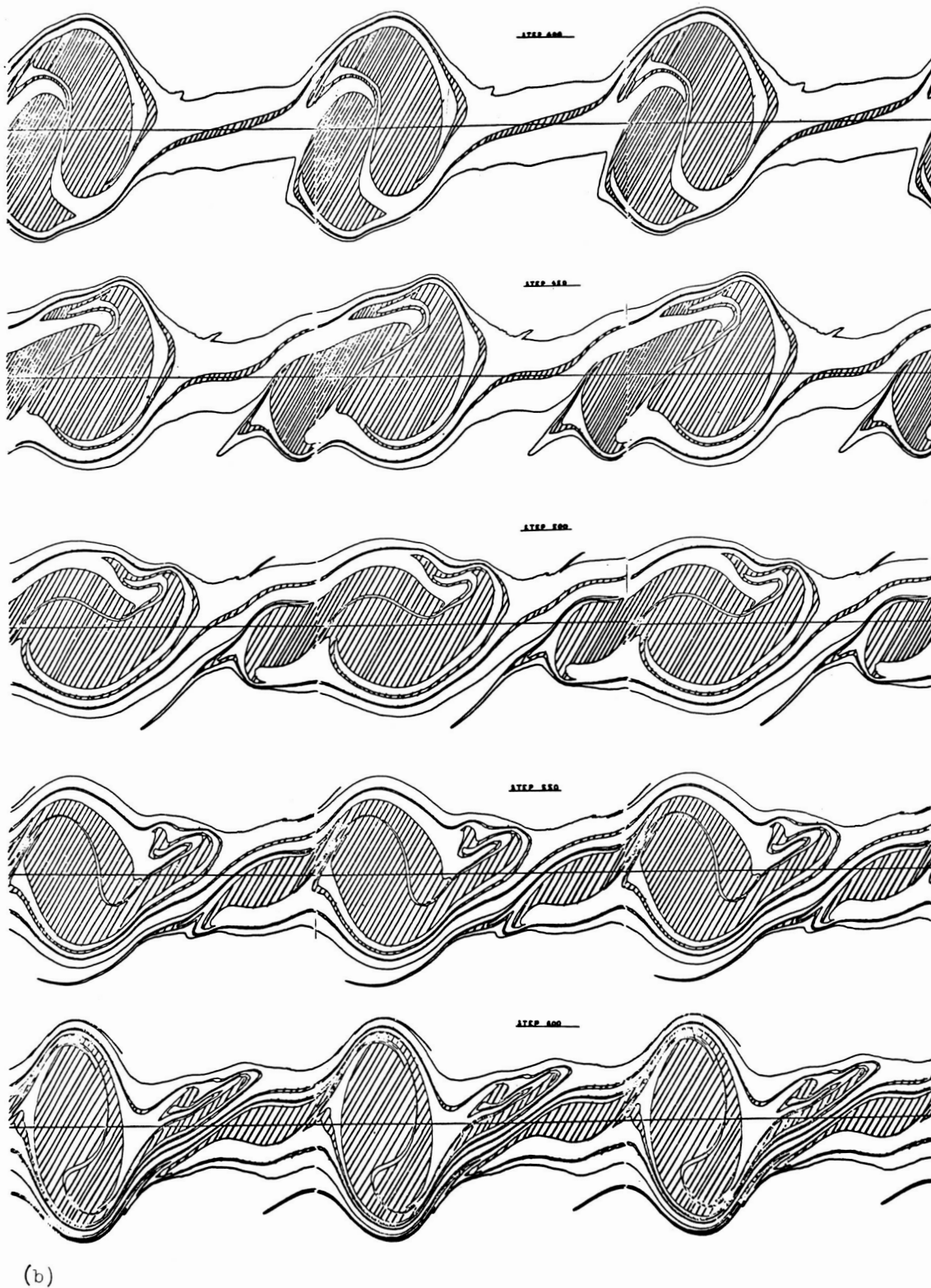


Figure 4.- Concluded.

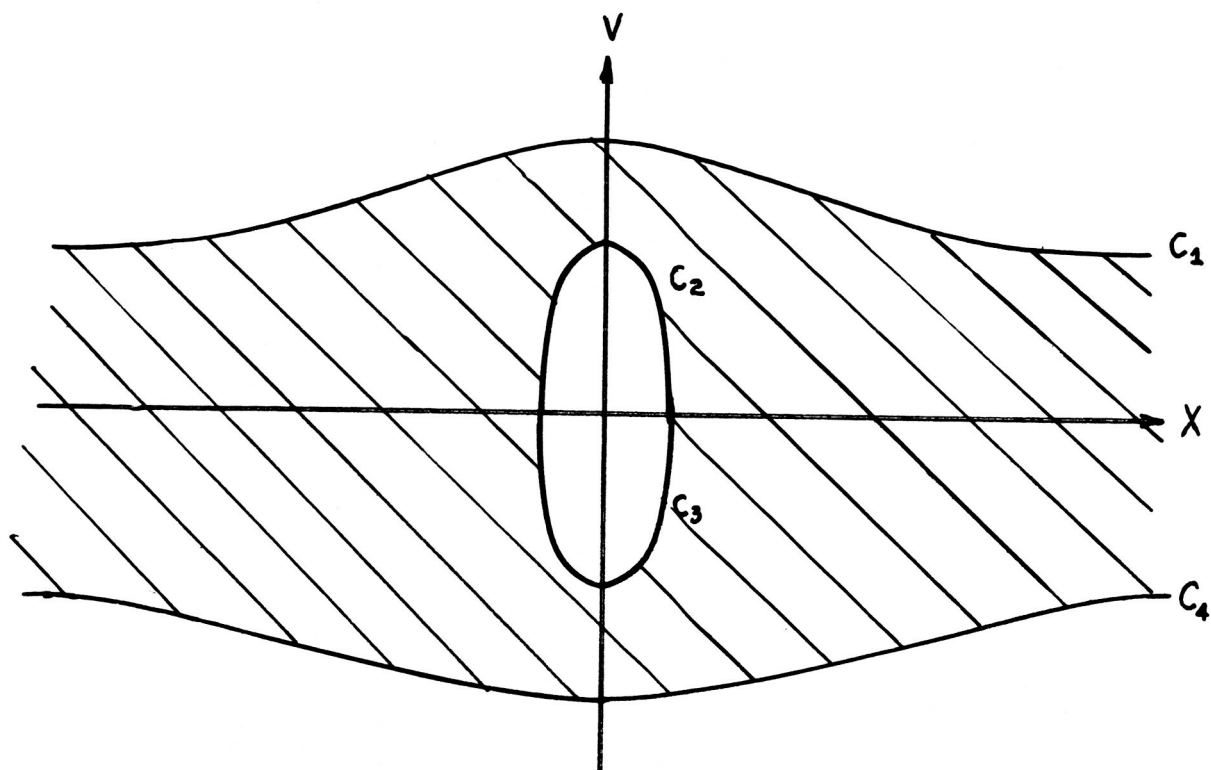


Figure 5.- Schematic picture of equilibrium hole derived from simplest water-bag model.

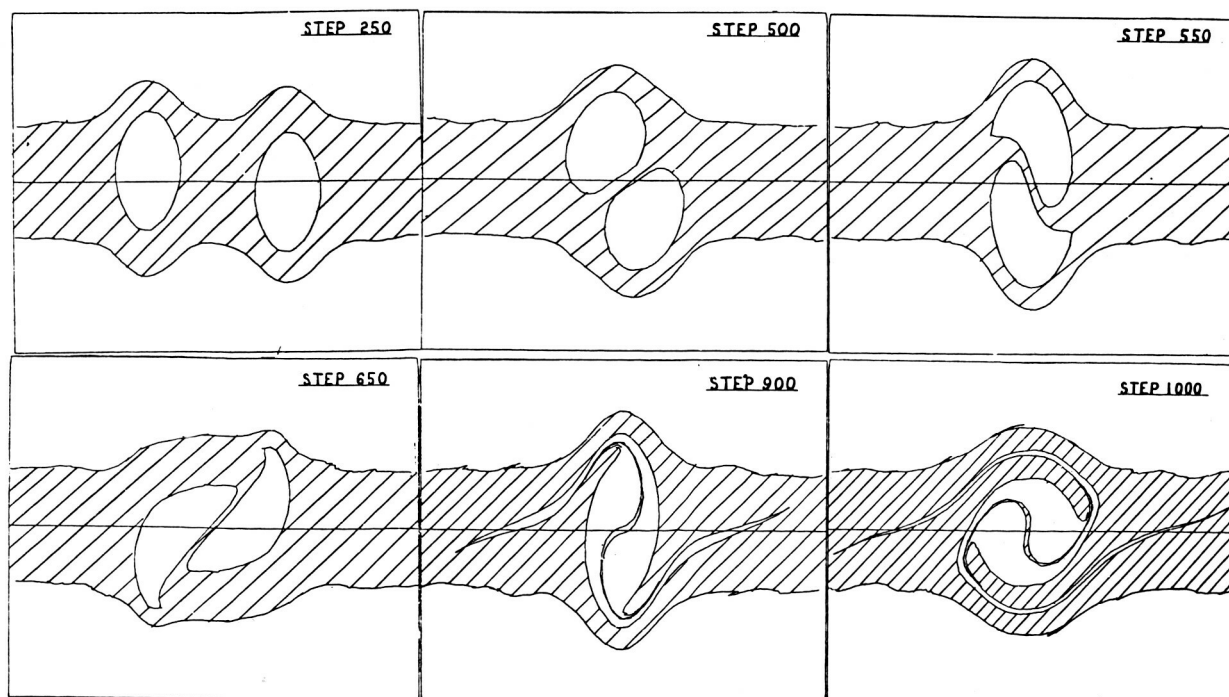


Figure 6.- Collision of two slow phase space holes.

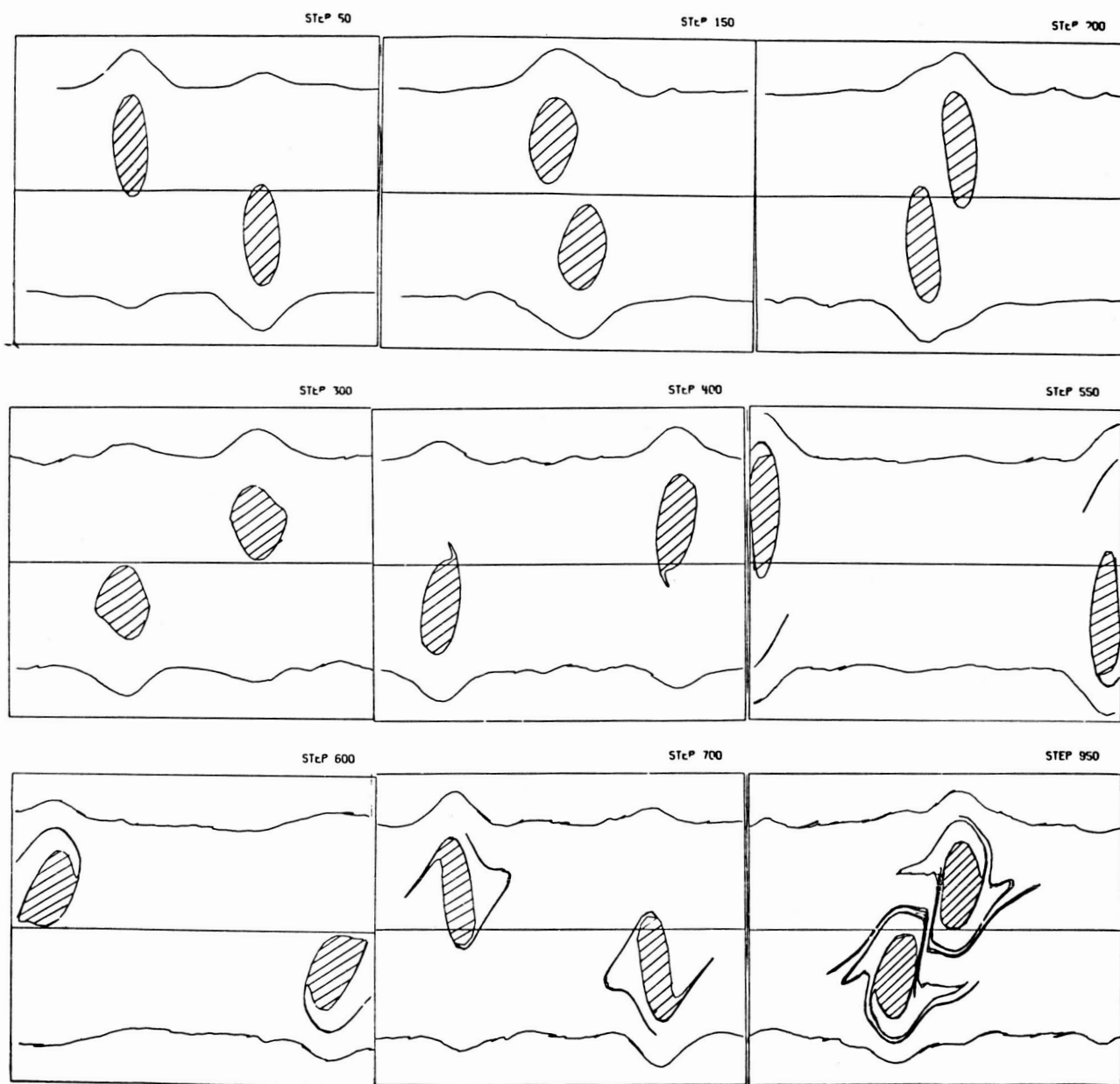


Figure 7.- Collision of two fast phase space holes.

NONLINEAR SOLUTIONS OF THE VLASOV EQUATION BY VELOCITY

SPACE EXPANSION IN LAGUERRE POLYNOMIALS*

R. J. Lomax

Electron Physics Laboratory, The University of Michigan

Ann Arbor, Michigan

If convective instabilities in a plasma are of interest and a closed system is being considered it is not possible to impose spatially periodic boundary conditions. It therefore becomes of interest to attempt to solve the Vlasov equation without this restriction.

When there is no static magnetic field and longitudinal waves in a one-dimensional system are considered, the Vlasov equation for the electrons and ions respectively is

$$\frac{\partial f_{e,i}}{\partial t} + v \frac{\partial f_{e,i}}{\partial x} + a_{e,i} \frac{\partial f_{e,i}}{\partial v} = 0, \quad (1)$$

where

$$a_e = -\frac{e}{m_e} E, \quad a_i = \frac{e}{m_i} E. \quad (2)$$

The electric field E is derived from Poisson's equation

$$\frac{\partial E}{\partial x} = \frac{e}{\epsilon_0} \int_{-\infty}^{\infty} (f_i - f_e) dv, \quad (3)$$

which, on integrating, gives

* This work was supported by USAEC, Fort Monmouth, N. J. on Contract No. DA-36-039 AMC-02269(E) and RADC, Griffiss Air Force Base, N. Y. on Contract No. AF30(602)-3569.

$$E(x,t) = \frac{e}{\epsilon_0} \int_0^x \int_{-\infty}^{\infty} (f_i - f_e) dv dx' - \frac{e}{\epsilon_0} \int_0^d \int_0^{x''} \int_{-\infty}^{\infty} (f_i - f_e) dv dx dx'' - \frac{V_d}{d} . \quad (4)$$

It is assumed that the plasma occupies the region $0 \leq x \leq d$ and that there is a potential V_d between $x = 0$ and $x = d$. It will be assumed here that V_d is maintained at a constant value (a-c short circuit) but an external circuit could easily be taken into account.

Because of the assumption of a diode-like region, the boundary conditions are

$$f_{e,i}(x,v,t) = \text{a given function for } \begin{cases} v > 0 & , \text{ at } x = 0 \\ v < 0 & , \text{ at } x = d \end{cases} , \quad (5)$$

and, since the distribution functions are specified only over half the velocity range, it is convenient to introduce half-range velocity moments defined by:

$$M_k^+ = \int_0^{\infty} v^k f(x,v,t) dv , \quad M_k^- = \int_{-\infty}^0 v^k f(x,v,t) dv . \quad (6)$$

It can be seen by taking corresponding moments of the Vlasov equation, Eq. 1, that the moments satisfy

$$\frac{\partial M_k^+}{\partial t} + \frac{\partial M_{k+1}^+}{\partial x} - k a M_{k-1}^+ = \pm a \delta_{0k} f(x,0,t) , \quad (7)$$

where δ_{ik} is the Kronecker delta.

In order to solve Eq. 7 it will be assumed that a finite n th order polynomial expansion in velocity space can be made (the effect of this on Landau damping will not be discussed here):

$$f_n^{\pm}(x,v,t) = w^{\pm}(v) \sum_{k=0}^{n-1} b_k^{\pm}(x,t) p_k^{\pm}(v) , \quad (8)$$

where the polynomials p_k^\pm are orthonormal with respect to the weighting function $w^\pm(v)$, i.e.,

$$\pm \int_0^{\pm\infty} w^\pm(v) p_i^\pm(v) p_j^\pm(v) dv = \delta_{ij} \quad (9)$$

and

$$p_k^\pm(v) = \sum_{m=0}^k c_{km}^\pm v^m. \quad (10)$$

It follows immediately from Eq. 8^{1,2,3} that

$$\sum_{m=0}^n c_{km}^\pm M_{km}^\pm = 0 \quad (11)$$

and

$$f_n^\pm(x, 0, t) = \left[\frac{c_{n-1, n-1}}{c_{n, n}} \sum_{k=0}^{n-1} (c_{n, k+1} c_{n-1, 0} - c_{n-1, k+1} c_{n, 0}) M_k^\pm \right]^\pm. \quad (12)$$

Equations 10 and 11 allow the set of moment equations, Eq. 7, to be closed at any order. By considering the subsequent motion of particles having almost zero velocity, it can be seen¹ that the choice of sign in Eq. 12 is $\text{sgn}(-a)$. This introduces coupling between the positive and negative moment equations (Eq. 7).

A linear transformation¹ can be made of the form

$$m_i^\pm = \sum_{j=0}^{n-1} \alpha_{ij}^\pm M_j^\pm \quad (13)$$

which reduces Eqs. 7, 11 and 12 to

$$\frac{\partial m_k^\pm}{\partial t} \pm \lambda_k \frac{\partial m_k^\pm}{\partial x} = \pm a \left[\frac{p_n''(\lambda_k)}{2p_n'(\lambda_n)} m_k^\pm - \sum_{\substack{j=0 \\ j \neq k}}^{n-1} \frac{m_j^\pm}{\lambda_k - \lambda_j} \right] - \frac{|a| c_{no}^2 c_{n-1}}{\lambda_k c_{nn}} \sum_{j=0}^{n-1} \frac{p_{n-1}(\lambda_j)}{\lambda_j p_n'(\lambda_j)} m_j^\pm \operatorname{sgn}(-a) ,$$

$$k = 0, 1, 2, \dots, n-1 , \quad (14)$$

where $\lambda_0, \lambda_1, \dots, \lambda_{n-1}$ are the zeros of $p_n(v)$.

For simplicity Laguerre polynomials have been used in actual numerical calculation⁴. Plots of the current density as a function of time in an electron-ion diode are shown in Figs. 1 to 3. In these figures, the electrons are emitted from $x = 0$ and the ions are emitted from $x = d$ with Maxwellian distributions at temperature T_e, T_i respectively. The time is normalized essentially to the transit time of an electron having the average thermal velocity, and the current density is normalized to the current which would flow in a single-species Child diode under otherwise identical conditions. Figure 1 shows the electron current density and Fig. 2 the ion current density at various planes when $m_i/m_e = 1000$, $T_e/T_i = 3$, $J_e/J_{ed} = J_i/J_{id} = 0.3536$ and $eV_d/kT_e = 2$. Figure 3 shows the electron current density for $m_i = m_e$, $T_e = T_i$, $J_e/J_{ed} = J_i/J_{ed} = 4\sqrt{2}$ and $eV_d/kT_e = 20$. Ions and electrons behave symmetrically.

When the particles have a streaming or drift velocity v_0 superimposed on their velocity distribution, it is convenient to modify the equations to prevent the velocity-distribution effects from being swamped⁵. This is done by redefining the velocity moments as

$$M_k^\pm = \int_{v_0}^{\pm\infty} (v - v_0)^k f(x, v, t) dv , \quad (15)$$

which leads only to a modification of the left-hand side of Eq. 14 to

$$\frac{\partial m_k^{\pm}}{\partial t} + (v_0 \pm \lambda_k) \frac{\partial m_k^{\pm}}{\partial x} . \quad (16)$$

The periodic situation can be treated by making a (finite) harmonic expansion in time. The nonlinear term involving the acceleration is handled by retaining only the same number of harmonics as appear in the original expansion of the moments.

REFERENCES

1. Dolph, C. L. and Lomax, R. J., "The Solution of Nonlinear Boundary-Value Transport Problems in Electron and Plasma Devices", Jour. Math. Anal. Appl., vol. 13, p. 391; March, 1966.
2. Krook, M., "On the Solution of Equations of Transfer. I", Astrophys. Jour., vol. 122, p. 488; 1955.
3. Zabusky, N. J., "The Nonlinear Vlasov Equation, Its Moment Description, and their Corresponding Linear Forms", Proc. 6th Internat. Conf. on Ionization Phenomena in Gases, vol. 1, p. 281, Paris; 1963.
4. Lomax, R. J., "Time Dependent Nonlinear Solution of the Landau-Vlasov Equations for an Electron-Ion Diode", Technical Report No. 92, Electron Physics Laboratory, The University of Michigan, Ann Arbor, Michigan; August, 1966.
5. Lomax, R. J., in Konrad, G. T., et al., "Investigation of Large-Signal Traveling-Wave Tubes", Technical Documentary Report No. RADC-TDR-64-231, p. 18, Electron Physics Laboratory, The University of Michigan, Ann Arbor, Michigan; July, 1964.
6. Lomax, R. J., in Rowe, J. E., "Semiconductor and O-Type Amplifier Investigations", Technical Report No. RADC-TR-66-513, p. 8, Electron Physics Laboratory, The University of Michigan, Ann Arbor, Michigan; October, 1966.

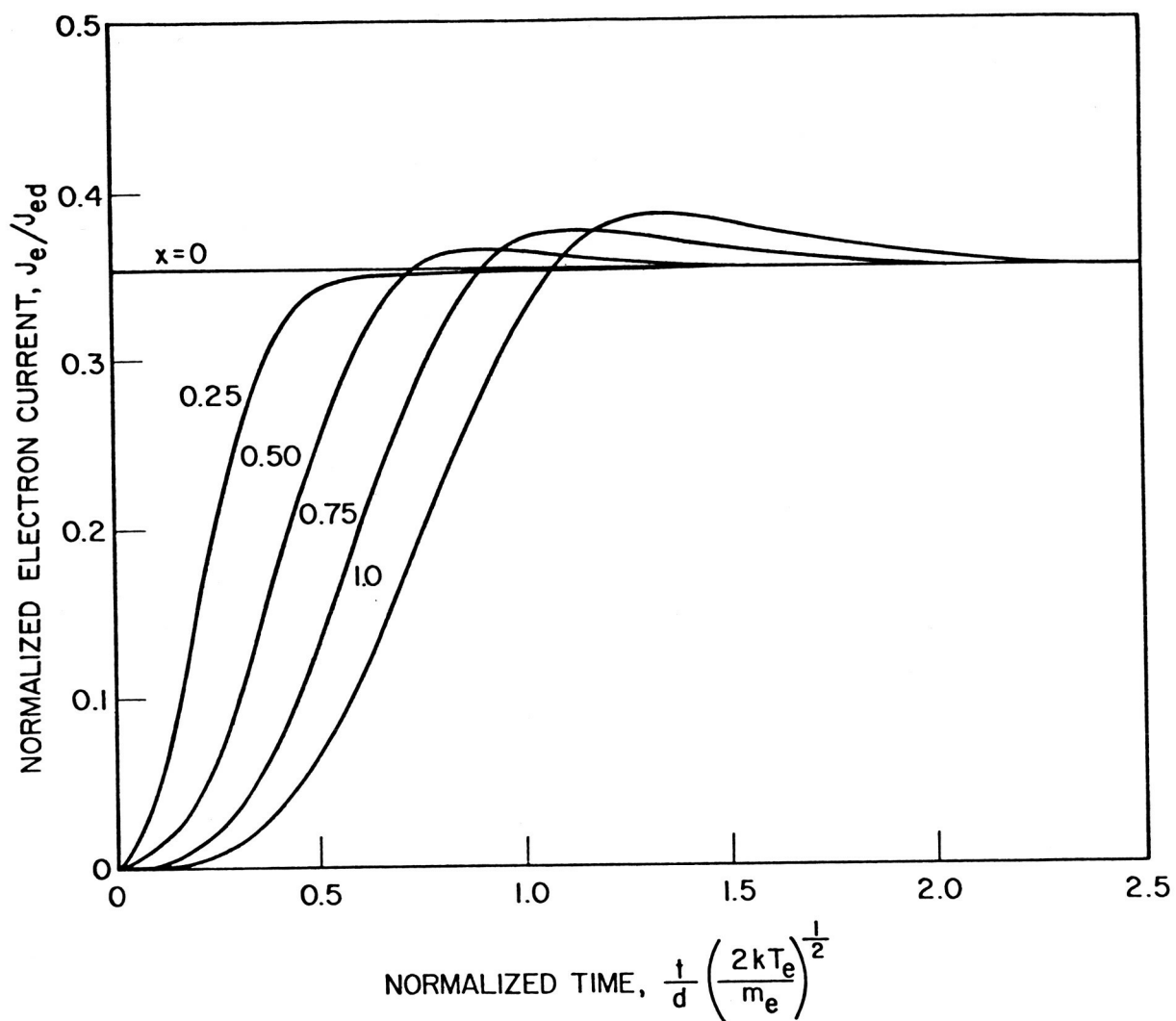


Figure 1.- Two-stream diode. Plot of the electron current density at various planes across the diode.

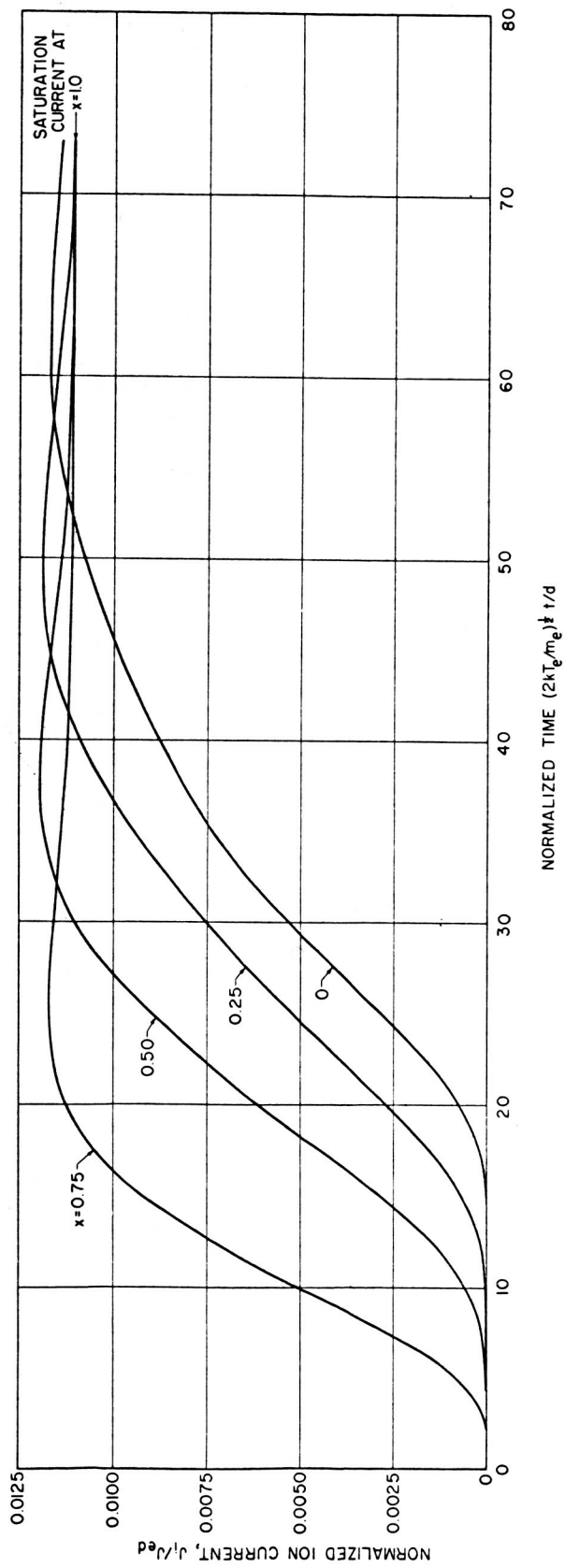


Figure 2.- Two-stream diode. Plot of the ion current density at various planes across the diode.

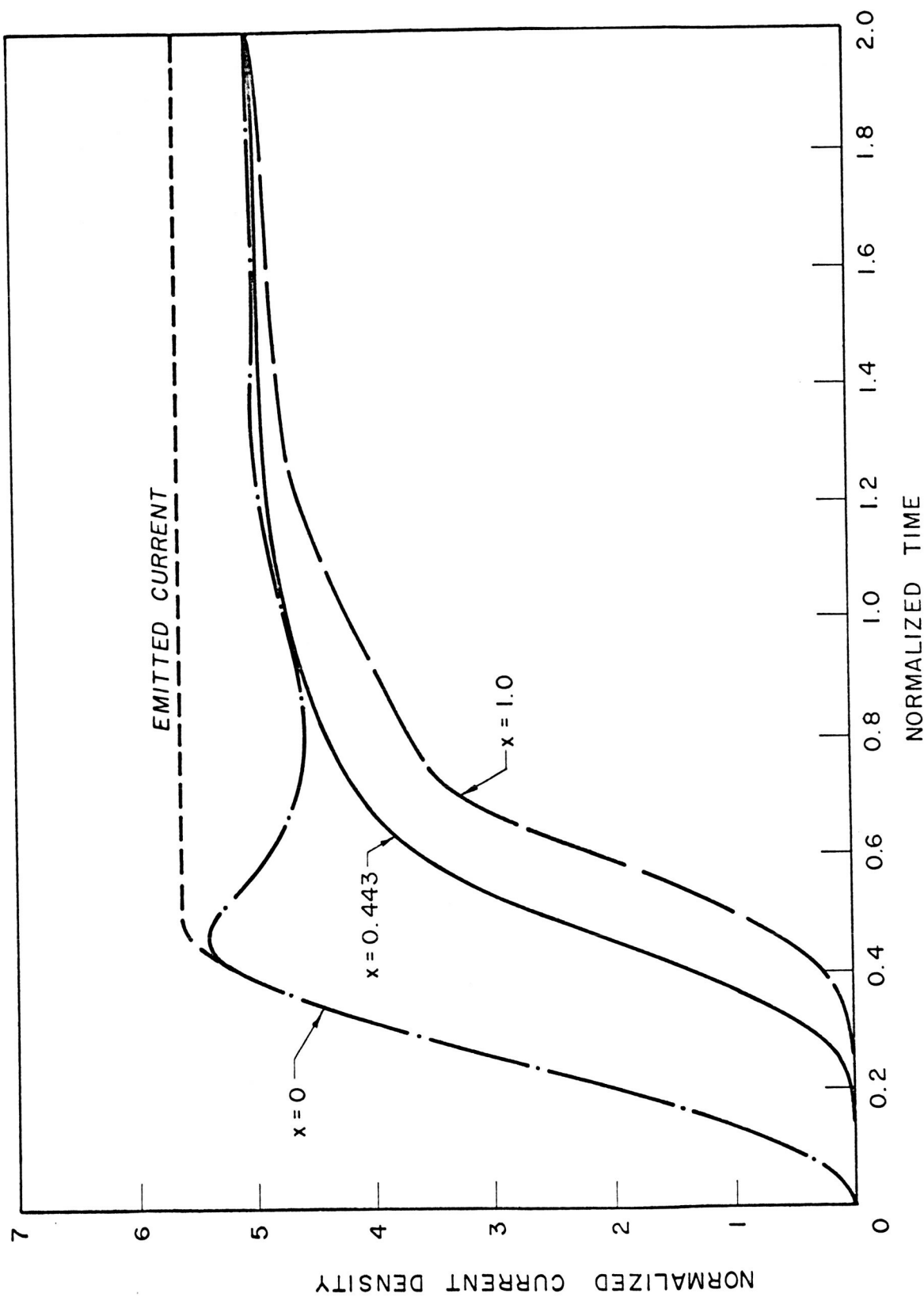


Figure 3.- The electron current density as a function of time at three planes in the discharge region. The ion current is identical except that the curves refer to $x = 1$, $x = 0.557$, and $x = 0$, respectively.

ASYMPTOTIC STATE OF THE TWO-STREAM INSTABILITY*

By Thomas P. Armstrong

University of Iowa

ABSTRACT

The nonlinear Vlasov equation for a one-dimensional electron plasma with periodic initial conditions is integrated numerically. Initial conditions of the form $f(x,v,0) = v^2 \exp(-v^2/2)(1 + \epsilon \cos kx)/(2\pi)^{1/2}$, $\epsilon \ll 1$, which are unstable to growing electrostatic waves^(1,2), are used. The resulting motion of the plasma is computed using a doubly expanded representation of $f(x,v,t)$ of the form:

$$f(x,v,t) = \sum_{n=-\infty}^{\infty} e^{inkx} \sum_{m=0}^{\infty} e^{-v^2/2} h_m(v) Z_{mn}(t)$$

The spatial dependence is represented as a Fourier series and the velocity dependence as a Gram-Charlier series similar to that used previously by Weisglas⁽³⁾, Engleman et al.⁽⁴⁾, and Grant and Feix^(5,6). Details of the expansion and numerical integration of the Vlasov and Poisson equations in this representation are given elsewhere^(7,8) and will not be discussed here.

The difficulty of secularly increasing velocity derivatives of $f(x,v,t)$ ^(9,10,11) is avoided by introducing a small collision term of the form

$$\frac{\partial f}{\partial t} = v_c \left[\frac{\partial(vf)}{\partial v} + \frac{\partial^2 f}{\partial v^2} \right] \text{ (dimensionless units)}$$

which bounds the velocity derivatives, as discussed by Grant and Feix⁽⁴⁾. The thermalization time due to the collision term used is ten times longer than

*University of Iowa Preprint 67-11.

the maximum times of interest here in the development of the two stream instability (collision frequency/growth rate = 0.01), so the numerical results obtained effectively apply to collisionless plasma. Thus the collision term is regarded only as a numerical convenience and is not thought to play any significant part in limiting the growth of the electrostatic field. The maximum field amplitude is shown numerically to be independent of the presence of a small collision term.

The solution of the nonlinear Vlasov equation with unstable initial conditions ($k = 0.6k_D$ and $\epsilon = 0.05$) was computed from $t = 0$ to $135(\omega_p)^{-1}$. In the linearized theory, k is unstable, but $2k$, $3k$, . . . are all stable. The $n = 1$ Fourier component of the electric field, E_1 , was observed to grow to its limiting amplitude at $t = 20(\omega_p)^{-1}$ and thereafter to undergo very slow variations in magnitude. The second Fourier component, E_2 , of the electric field was always smaller than E_1 by about a factor of 10, indicating rapid convergence of the Fourier series. By the time $t = 100$ to $135(\omega_p)^{-1}$, E_1 had become constant to within $\pm 10\%$, strongly suggesting that the asymptotic ($t \rightarrow \infty$) state of the unstable plasma is, in the absence of collisions, an inhomogeneous equilibrium of the Bernstein, Greene, and Kruskal⁽¹²⁾ type. Further investigation of the distribution function for long times $t \gtrsim 100(\omega_p)^{-1}$ shows it to satisfy approximately the time independent Vlasov equation throughout velocity space. These results reinforce an earlier speculation made by Armstrong^(7,8) that inhomogeneous equilibria may be approached as the limit of the two stream instability.

REFERENCES

1. Penrose, O.: Phys. Fluids, 3, 258-265, 1960.
2. Noerdlinger, P.: Phys. Rev., 118, 879-885, 1960.
3. Weissglas, P.: J. Nucl. Energy, C., 4, 329-336, 1962.
4. Engelman, F.; Feix, M.; Minardi, E.; and Oxenius, J.: Phys. Fluids, 6, 266-275, 1963.
5. Grant, F.; and Feix, M.: Preprint, 1966.
6. Grant, F.; and Feix, M.: Preprint, 1967.
7. Armstrong, T., Ph. D. Dissertation, Department of Physics and Astronomy, University of Iowa, 66-34, August 1966.
8. Armstrong, T., to be published in Phys. Fluids.
9. Backus, G., J. Math. Phys., 1, 178-191, 1960.
10. Knorr, G., Zeits. für Naturforsch., 18a, 1304-1315, 1963.
11. Kellogg, P., Phys. Fluids, 8, 102-110, 1965.
12. Bernstein, I., Greene, J., and Kruskal, M.: Phys. Rev., 108, 546-550, 1957.

ON SOME ASPECTS OF THE EIGENFUNCTION EXPANSION OF THE
SOLUTION OF THE NONLINEAR VLASOV EQUATION¹

By W. L. Sadowski

National Bureau of Standards

ABSTRACT

Solution of the nonlinear Vlasov equation was obtained for various values of nonlinearity parameters α and various values of the wave vector k .

An initial distribution function was assumed of the form:

$$\psi(x,v) = (1 + \alpha \cos kx) e^{-\frac{v^2}{2}}$$

The boundary conditions were assumed to be periodic. The distribution function was expanded into a set of polynomials in Fourier-Hermite space. The time behavior of the resultant matrix of coefficients gave the time behavior of the distribution function.

Truncation of the matrix both in Fourier and Hermite space was investigated. The solution of the equation was quite sensitive to this type of truncation error. When the truncation error exceeded certain limits, nonlinear damping was distorted to such an extent that a reappearance of damped harmonics was observed. This is a result also reported by Knorr but is believed by the author to be due to numerical errors.

A small damping term was included in the calculation to prevent an inordinate buildup of numerical errors. Nonlinear dispersion relations were obtained.

Nonlinear damping by each harmonic was calculated.

A film showing the solution will be presented.

¹The complete article prepared by the author was received after printing of this compilation was partly completed, and it is therefore placed at the end of the report (pages 433-440).

The author would like to thank Dr. Firor of HAO, Mr. S. Ruttenberg and the staff of the Computing Facility of NCAR for providing machine time and advice in a part of this work.

FOURIER-HERMITE EXPANSION OF THE VLASOV EQUATION

By Marc R. Feix*

NASA Langley Research Center

and the College of William and Mary

and Frederick C. Grant

NASA Langley Research Center

ABSTRACT

This different numerical attack on the one-dimensional, one-species Vlasov equation involves a double transform. Usually a box of length L with periodic boundary conditions is considered and a Fourier transform on space is introduced. This is adequate to study slightly nonlinear problems where the interaction between the different wave numbers is small. A Hermite series on velocity space, also used by Armstrong¹, is preferred to the Fourier integral expansion proposed by Knorr² for two different reasons.

1. The behavior of the long wavelengths is connected to moments of low order of the distribution function and consequently the small k should (and in fact is) described by a small amount of terms.

2. It is more practical to deal with a set of ordinary differential equations than to consider a set of partial differential equations in the λ space (λ being the Fourier conjugate of v).

Having delineated a $K \times N$ matrix, the game consists of watching how fast the neglected term propagates into the matrix and try to keep the associated error small. Two main propagations take place.

*NRC-NAS Senior Resident Research Associate on leave of absence from Euratom.

Along a given line (i.e., for a given k) the kinetic character of the problem introduces a cutoff error which already appears in the linear problem and which is due to the streaming term $v \partial f / \partial x$. This puts a limit \sqrt{N}/kD to the time of validity of the solution.

This problem has been taken care of by the introduction of a small but finite Fokker-Planck term characterized by a frequency ν where we let simultaneously $N \rightarrow \infty$ and $\nu \rightarrow 0$ with the product $N\nu > 1$. Different Fokker-Planck terms are discussed. A good insight into this problem is obtained by considering the linearized problem. A connection between the Van Kampen and the Landau treatment is established in this double limit.

The second cutoff error propagation is due to the nonlinear term. This problem is not too severe for small nonlinearity but no solution has yet been found for large nonlinearity. In such a case the wave concept (quasi-independent k components) is lost and we may have to use other representations.

Two series of results are finally presented: (1) Problem of long wavelengths. Characterized by $\alpha < kD < 0.1$: kD is the fundamental wave number and α the depth of the initial density modulation.

$$f(x, v, t = 0) = n(1 + \alpha \cos kx)(2\bar{u} v_T^2)^{-1/2} \exp -v^2/2 v_T^2$$

We recover in the limit $kD \rightarrow 0$ the results of the cold plasma case obtained by Kalman² but the limit is far from trivial. The fact that kD is not strictly zero obliges to use up to 30 Hermite polynomials. On the other hand, we can see how the thermal effect destroys the strict periodicity of the cold plasma solution and how harmonics in time appear. (2) Kinetic Regime - Small Nonlinearity $kD = 0.5$. High number of Hermite Polynomials (~250) small collision frequency ($\nu/\omega_p = 0.005$) and K up to 5 are used to study the nonlinear

Landau damping. It is found that for small α ($\alpha < 0.15$) the behavior of the harmonics is very difficult to obtain during long time but that the fundamental $f(k,v,t)$ and the space integrated velocity distribution $f(k = 0, v, t)$ are rather decoupled from the harmonics. The solution is consequently compared to a quasilinear theory (where only the fundamental and the $k = 0$ mode are kept) and agree very well with the full nonlinear theory. A discussion of the role of the harmonics is presented showing that although wave interaction is a priori an effect of the same order as the quasilinear one it seems reasonable to disregard it in the damping case in agreement with the numerical results.

REFERENCES

1. Amer. Phys. Soc., Div. of Plasma Physics, 8th Annual Meeting, Boston, Mass., November 2-5, 1966, Paper 7P4.
2. Knorr, G.: Z Naturforsch 18A 1304, 1963.

NUMERICAL SOLUTION OF THE VLASOV EQUATION
IN A FOUR-DIMENSIONAL PHASE SPACE*

John Killeen

Lawrence Radiation Laboratory, University of California
Livermore, California

ABSTRACT

In the Lawrence Radiation Laboratory's controlled-fusion experiment, Astron, relativistic electrons are injected into a cylindrical region containing an applied magnetic field. The object is to form an E-layer — a cylindrical layer of electrons — so that the self-field exceeds the applied field. The resulting configuration is intended to be axially symmetric with no azimuthal component of the magnetic field.

The mathematical model for the build-up of the electron layer and the self-field is the time-dependent Vlasov equation coupled with Maxwell's equations. Although transient radial and axial currents exist in this model, particularly in the early stages of formation and near the injection point, these are assumed to be small compared to the azimuthal current. Field components B_r and B_z can be derived from stream function $\psi(r, z, t)$. The canonical angular momentum, p_θ , is a constant of the motion, and we assume that all electrons are injected with the same value of p_θ . Hence, we can consider an electron-distribution function, f , defined in a four-dimensional

*Work performed under the auspices of the U. S. Atomic Energy Commission.

phase space (r, z, p_r, p_z) . We assume that the system is electrically neutral at every point. The ion distribution is not solved explicitly, but ions are assumed to be present, providing charge neutralization of the layer.

We specify the magnetic field by the single component of the vector potential, $A_\theta(r, z, t)$. The equation for A_θ is

$$\frac{1}{c^2} \frac{\partial^2 A_\theta}{\partial t^2} - \frac{\partial^2 A_\theta}{\partial z^2} - \frac{\partial}{\partial r} \left[\frac{1}{r} \frac{\partial}{\partial r} (r A_\theta) \right] = 4\pi j_\theta. \quad (1)$$

The canonical angular momentum may be expressed as $p_\theta = m_0 \gamma r v_\theta + (e r A_\theta / c)$, with $\gamma = [1 - (v/c)^2]^{-1/2}$. It is convenient to introduce the function $\psi(r, z, t)$, defined by

$$\psi = \gamma r v_\theta / c, \quad (2)$$

so that

$$\psi = \frac{p_\theta}{m_0 c} - \frac{e}{m_0 c^2} r A_\theta. \quad (3)$$

Since all the electrons have the same p_θ , we can use ψ in place of A_θ to determine the field. From Eqs. (1) and (3), we have

$$\frac{1}{c^2} \frac{\partial^2 \psi}{\partial t^2} - \frac{\partial^2 \psi}{\partial z^2} - r \frac{\partial}{\partial r} \left[\frac{1}{r} \frac{\partial \psi}{\partial r} \right] = - \frac{4\pi e}{m_0 c^2} r j_\theta \quad (4)$$

and

$$B_r = \frac{m_0 c^2}{e} \frac{1}{r} \frac{\partial \psi}{\partial z} \quad \text{and} \quad B_z = - \frac{m_0 c^2}{e} \frac{1}{r} \frac{\partial \psi}{\partial r}. \quad (5)$$

We introduce a dimensionless velocity, $u = \gamma v / c$, so that Eq. (2) becomes $r u_\theta = \psi$. In terms of u , we have $\gamma = (1 + u^2)^{1/2}$ or

$$\gamma = \left[1 + u_r^2 + u_z^2 + \left(\frac{\psi}{r} \right)^2 \right]^{1/2}. \quad (6)$$

Let $f(r, z, u_r, u_z, t)$ be the electron-distribution function in phase space, so that $f(r, z, u_r, u_z, t) dr dz du_r du_z$ is the number of electrons in the element $dr dz du_r du_z$ at the point (r, z, u_r, u_z) at time t . The dimensions of f are the number of electrons per square centimeter. The equation governing f is

$$\frac{\partial f}{\partial t} + \frac{\partial f}{\partial r} \frac{dr}{dt} + \frac{\partial f}{\partial z} \frac{dz}{dt} + \frac{\partial f}{\partial u_r} \frac{du_r}{dt} + \frac{\partial f}{\partial u_z} \frac{du_z}{dt} = S(r, z, u_r, u_z, t), \quad (7)$$

where S expresses the source of electrons injected into the phase space, and

$$\frac{dr}{dt} = \frac{cu_r}{\gamma} \text{ and } \frac{dz}{dt} = \frac{cu_z}{\gamma}. \quad (8)$$

We determine du_r/dt and du_z/dt from the relativistic equations of motion of the electrons. Using Eqs. (2), (5), and (8), we obtain

$$\frac{du_r}{dt} = -\frac{c}{\gamma} \frac{\partial}{\partial r} \left(\frac{\psi^2}{2r^2} \right) \quad (9a)$$

and

$$\frac{du_z}{dt} = -\frac{c}{\gamma} \frac{\partial}{\partial z} \left(\frac{\psi^2}{2r^2} \right). \quad (9b)$$

The equation for f can now be written

$$\frac{\gamma}{c} \frac{\partial f}{\partial t} + u_r \frac{\partial f}{\partial r} + u_z \frac{\partial f}{\partial z} - \frac{\partial}{\partial r} \left(\frac{\psi^2}{2r^2} \right) \frac{\partial f}{\partial u_r} - \frac{\partial}{\partial z} \left(\frac{\psi^2}{2r^2} \right) \frac{\partial f}{\partial u_z} = S \frac{\gamma}{c}. \quad (10)$$

The azimuthal current density, j_θ , may be written

$$j_\theta = \frac{e}{2\pi} \frac{\psi}{r^2} \int \frac{f}{\gamma} du_r du_z. \quad (11)$$

Equation (4) becomes

$$\frac{1}{c^2} \frac{\partial^2 \psi}{\partial t^2} - \frac{\partial^2 \psi}{\partial z^2} - r \frac{\partial}{\partial r} \left(\frac{1}{r} \frac{\partial \psi}{\partial r} \right) = -2\psi \frac{r e}{r} \iint \frac{f}{\gamma} du_r du_z, \quad (12)$$

where $r_e = e^2/m_0 c^2$ is the classical electron radius. Equations (6), (10), and (12) are the self-consistent set of equations that describe the formation of the E-layer.

It is useful in a numerical computation of this type to introduce dimensionless variables. In place of ψ we use the variable $\bar{\mu} \equiv m_0 c \psi / p_\theta$. In order to evaluate p_θ , we consider an equilibrium orbit in the vacuum field. At the midplane ($z = 0$) the end fields are assumed to be negligible, so that $A_\theta(r, 0) = B_0 r / 2$, where B_0 is a constant determined by the injection energy and radius and the desired pitch angle. We find $p_\theta = -(e B_0 r_0^2 / 2c)$, where r_0 is the radius of the equilibrium orbit at $z = 0$. From the definition of $\bar{\mu}$, it follows that

$$\bar{\mu} = -(2m_0 c^2 \psi / e B_0 r_0^2). \quad (13)$$

We introduce the following dimensionless quantities:

$$R = \frac{r}{r_0}, \quad Z = \frac{z}{r_0}, \quad \tau = \frac{ct}{r_0}, \quad \bar{a}_\theta = \frac{A_\theta}{B_0 r_0}, \quad \bar{b}_r = \frac{B_r}{B_0}, \quad \text{and} \quad \bar{b}_z = \frac{B_z}{B_0}.$$

From these definitions and from Eqs. (3), (5), and (13), it follows that

$$\bar{\mu} = 1 + 2R\bar{a}_\theta, \quad 2R\bar{b}_r = -\partial\bar{\mu}/\partial Z, \quad \text{and} \quad 2R\bar{b}_z = \partial\bar{\mu}/\partial R.$$

It is convenient to let $\bar{\mu} = \mu_c + \mu$, where μ_c represents the vacuum field and μ is the contribution from the electron layer. For the electron distribution function we use the dimensionless quantity $\rho = r_e r_0 f$, introduce the parameter $C_1 \equiv -(r_e r_0 B_0 / 2e) = -(2.93 \times 10^{-4}) B_0 r_0$, and define the function $P(R, Z, t)$ so that

$$P = C_1^2 \bar{\mu}^2 / 2R^2. \quad (14)$$

This is the potential function for the electron motion, and the equations of motion in these variables become $\gamma du_r / d\tau = -\partial P / \partial R$ and $\gamma du_z / d\tau = -\partial P / \partial Z$.

We can now give the complete set of equations in dimensionless form.

Equation (12) becomes

$$\frac{\partial^2 \mu}{\partial \tau^2} - \frac{\partial^2 \mu}{\partial Z^2} - R \frac{\partial}{\partial R} \left(\frac{1}{R} \frac{\partial \mu}{\partial R} \right) = - \frac{2\bar{\mu}}{R} \iint \frac{\rho}{\gamma} du_r du_z, \quad (15)$$

and Eq. (10) becomes

$$\frac{\partial \rho}{\partial \tau} + \frac{u_r}{\gamma} \frac{\partial \rho}{\partial R} + \frac{u_z}{\gamma} \frac{\partial \rho}{\partial Z} - \frac{P_r}{\gamma} \frac{\partial \rho}{\partial u_r} - \frac{P_z}{\gamma} \frac{\partial \rho}{\partial u_z} = \sigma, \quad (16)$$

where $\sigma = r_e^2 S/c$, $P_r = \partial P / \partial R$, $P_z = \partial P / \partial Z$, and $\gamma = (1 + u_r^2 + u_z^2 + 2P)^{1/2}$.

We shall now consider the solution of Eq. (16) by finite-difference methods. To illustrate the problem, consider the one-dimensional equation

$$\frac{\partial \rho}{\partial \tau} + u \frac{\partial \rho}{\partial x} = 0, \quad (17)$$

where u is a constant. The simplest two-level approximation would be

$$\rho_j^{n+1} = \rho_j^n - \frac{1}{2} \alpha (\rho_{j+1}^n - \rho_{j-1}^n),$$

where $\alpha = u \Delta \tau / \Delta x$. This scheme is unstable no matter how small $\Delta \tau$ is. The simplest alternative is

$$\rho_j^{n+1} = \rho_j^n - \alpha (\rho_j^n - \rho_{j-1}^n)$$

when $u \geq 0$, or

$$\rho_j^{n+1} = \rho_j^n - \alpha (\rho_{j+1}^n - \rho_j^n)$$

when $u < 0$. This scheme is stable so long as $|\alpha| \leq 1$. The generalization of this to Eq. (16) is straightforward and leads to the stability conditions

$$\left| \frac{kh^* \Delta \tau}{\gamma h} \right| \leq 1, \quad \left| \frac{\ell h^* \Delta \tau}{\gamma h} \right| \leq 1, \quad \left| \frac{P_z \Delta \tau}{\gamma h^*} \right| \leq 1, \quad \text{and} \quad \left| \frac{P_r \Delta \tau}{\gamma h^*} \right| \leq 1. \quad (18)$$

The first version of the LRL Layer computer code employed this scheme as well as an explicit approximation to Eq. (15). Unfortunately, the above scheme introduces an artificial diffusion that spoils the results after a short time.

We can consider a space- and time-centered three-level approximation to Eq. (17),

$$\rho_j^{n+1} = \rho_j^{n-1} - \alpha(\rho_{j+1}^n - \rho_{j-1}^n),$$

that is stable if $|\alpha| \leq 1$. The extension to more than one dimension is again immediate, leading to the stability conditions in Eq. (18). The second version of the Layer code used this scheme. Considerable computation has been done with this method and fairly satisfactory results have been obtained, but with the crude mesh employed in this problem it is still not accurate enough for extremely long running times. Furthermore, it has the disadvantage of being a three-level formula, and when the time step must be decreased for stability reasons, it is quite awkward.

The third version of Layer uses a three-point approximation to the advective term. For Eq. (17), this becomes

$$\rho_j^{n+1} = \rho_j^n - \frac{1}{2} \alpha (\rho_{j+1}^n - \rho_{j-1}^n) + \frac{1}{2} \alpha^2 (\rho_{j+1}^n - 2\rho_j^n + \rho_{j-1}^n).$$

This scheme is stable if $|\alpha| \leq 1$. It is accurate to the second order in the quantities $u\Delta\tau$ and Δx , and has the convenience of being a two-level formula. The extension to more than one dimension is not straightforward and can lead to an unstable method if it is not done correctly. We can write the above approximation in matrix form as $\rho^{n+1} = (I + A)\rho^n$. If we consider a two-dimensional equation and take the approximation given by the equation $\rho^{n+1} = (I + A + B)\rho^n$, where B is the advective difference operator in the other

direction, the scheme is unstable. However, if we use the operator equation $\rho^{n+1} = (I+A)(I+B)\rho^n$, the scheme is stable. This is the scheme that is used in the third version of Layer. The difference equation can be represented by

$$\rho^{n+1} = (I+A)(I+B)(I+C)(I+D)\rho^n.$$

The computational process involved in a single time step is divided into four cycles. In the first cycle we calculate advection in the z direction, then advection in the R direction using the results of the first cycle, then advection in the u_z direction using the results of the second cycle, and, finally, advection in the u_r direction using the results of the third cycle. The mesh currently being used for this problem is 51 in z , 8 in r , 19 in u_z , and 9 in u_r , or a total of 69,768 points. We solve Eq. (15) by an alternating direction-implicit method.

A program of this type is meant to be used for extensive parameter studies. In particular, the form and time behavior of the vacuum fields can be varied, as can the method of injection. There is a great variety of quantities that can be printed out or plotted at any given time step. Usually, we concentrate on dependent variables, such as the current density, that are functions of the spatial coordinates r and z . This, together with the magnetic field, describes the solution to the self-consistent field problem.

The boundary conditions, other computational details, and sample results are contained in a recently published paper.¹

¹J. Killeen and S. L. Rompel, J. Comp. Phys. 1, 29 (1966).

MAGNETOHYDRODYNAMICS AND PLASMA DEVICES

3 Magnetohydrodynamic Plasma Calculations

K.V.Roberts*

University of California, San Diego

ABSTRACT

Some of the problems which are encountered in simulating the behaviour of plasma devices on the computer are briefly outlined. Most of them only become serious when two- or three-dimensional calculations are attempted, and one of the critical problems lies in the treatment of the advective term. The paper describes how a conservative Eulerian difference scheme may be constructed. The MHD conservation laws can be given an integral, space-time representation, which is reflected in the mesh to be used, and in the definition of the variables to be stored in the machine. The advective term in each equation is handled by a fourth-order method².

*On leave of absence from Culham Laboratory, Abingdon, England

1. INTRODUCTION

One of the aims of MHD plasma calculations is to simulate the behaviour of an actual plasma machine by solving a set of partial differential equations on a computer, taking into account as many as possible of the basic physical phenomena that are expected to occur in the machine itself. This approach has been effective in several other fields of physics and engineering, for example in calculations on nuclear reactors and other devices, or on the global atmospheric circulation. It has worked rather well in 1-dimensional plasma calculations¹. But any real plasma apparatus which involves a magnetic field must be at least 2-dimensional, and so it is necessary to develop practical difference schemes² for solving the MHD equations in 2 and 3-dimensional geometry. This proves surprisingly difficult, and it raises a number of interesting problems in numerical analysis. I shall outline briefly what some of these problems are, and then work one of them out in detail by showing how to construct a conservative Eulerian difference scheme.

Mathematically, the problem is to solve a set of mixed hyperbolic and parabolic equations in a space-time region, bounded by the plane $t=0$ and by the walls and ends of the apparatus. Hyperbolic properties of the equations correspond to the propagation of various types of plasma wave, while parabolic features are related to diffusive processes such as field mixing and heat conduction.

By comparison with a typical large hydrodynamic calculation, one of the difficulties we find is that the dependent variables, coefficients and propagation velocities can change by several orders of magnitude from one part of the solution to another, often quite rapidly. The character of the equations

also changes; they may be hyperbolic in the main body of the plasma, and effectively elliptic in the outer regions near the wall where the density is low and the Alfvén propagation speed $(B^2/4\pi\rho)^{\frac{1}{2}}$ correspondingly high. (This difficulty does not occur in gaseous flow problems in hydrodynamics, since the sound speed is proportional to $T^{\frac{1}{2}}$ and is independent of density). The magnetic field also introduces a marked directional anisotropy in the electronic heat conduction, which may be 10^3 times larger along the field than across it. The usual difference formulation of the diffusion equation then breaks down, and it may be necessary to use the field lines themselves as coordinates for this term, even though their topology may be changing with time.

From the point of view of numerical analysis, the most difficult problem lies in the treatment of the advective term

$$\frac{\partial f}{\partial t} = -\underline{v} \cdot \nabla f + \dots$$

that occurs in each equation (Table 1). Physical variables tend to be advected by the plasma and only to diffuse slowly through it, but it is often this slow diffusion that is physically important, e.g. in determining the stability of the plasma, rather than the rapid bulk oscillations. Unless the advective term can be handled accurately, it may introduce errors that entirely mask the physics.

In one dimension the advective term can be transformed away altogether by choosing a Lagrangian mesh that moves with the plasma, and this is now usually done. If it is necessary to follow the behaviour of plasma which is being generated at the wall as the field lines move in¹, one can readily arrange to add new points, and to remove them as the plasma moves out and is absorbed. In two dimensions however, a Lagrangian mesh becomes distorted as the calculation proceeds. Apart from the loss of

accuracy which this entails, it leads to an awkward and inefficient program, so that purely Lagrangian methods are rarely used.

Two different approaches are being tried out by the writer at the present time. One is to use a 'rectangular' Eulerian scheme, which is kept as simple as possible in order to save machine time, storage space and programming effort. Accuracy is retained by using a 4th order treatment for the advective terms, (see §6). The other is to use an orthogonal curvilinear mesh, which is constantly adjusted to fit the moving plasma boundary and to be as Lagrangian as possible. It is hoped to make a critical comparison of the two methods for a range of MHD problems.

It is characteristic of plasmas that very sharp spatial variations can arise, for example at boundaries, shocks and current sheets. The temperature, density and magnetic field can vary across the plasma by several powers of ten. Therefore a uniform mesh is unlikely to use the available points in the most economical way, and in 1-dimensional calculations the mesh is automatically adjusted from time to time in order to give as good a representation as possible. It is difficult to see how to do this in two dimensions, because the regions where extra points are required are unlikely to conform to the global geometry and topology of the mesh. If some method of mesh optimization can be found, it may be best to carry this out by manual intervention at an on-line visual console, rather than to do it completely automatically.

The method of calculation may be implicit or explicit. An implicit method is required whenever the timestep Δt_e determined by explicit stability criteria would be too small, usually because of a high Alfvén speed, a small mesh spacing or a long time scale. An implicit method enables Δt to be

increased, but it runs several times slower and is more difficult to program. Since Δt_e is a rapidly-varying function of position and time, a versatile program ought to be able to determine automatically which type of method to select, independently for each region of space-time, by examining the solution itself. This ideal has not yet been attained, although such a program could undoubtedly save a factor ten in machine time. At present 1-dimensional programs are often made implicit so that they can be as general as possible, while 2-dimensional programs are made explicit to simplify the difference schemes.

The plasma energy is often only a small fraction, say 1 - 5%, of the total energy of the system, which resides mainly in the magnetic field, so that there is good reason to use conservative difference schemes in order to preserve accuracy. The conservation of linear quantities such as mass, momentum and magnetic flux can be given a precise physical interpretation which helps to determine the difference scheme, and which will be explored in detail in this paper. These laws can be represented by exact difference identities. For this purpose it is appropriate to replace the differential equations by integral conservation laws, (from which they are customarily derived!), and to interpret each variable in a manner that is guided by the physics. Thus, density is related to the mass inside a 3-dimensional box, while each component of the magnetic field is related to the flux through one of the faces, and the magnetic vector potential to line integrals along the edges. There appears to be no exact expression for the energy integral, and perhaps the conservation of energy is best left as a check on the accuracy of the calculation.

In order to have a well-defined problem it is necessary to impose initial and boundary conditions. These are often hard to determine experimentally. The initial conditions can be

found in principle by accurate measurement of the plasma density, temperature and degree of pre-ionization at $t=0$. In general there are no precise boundaries at all; the field lines simply leave the plasma at the ends, or through the walls, and expand into the space outside. Since it is impracticable to solve $\nabla^2 B=0$ in an infinite region, some form of cut-off is therefore required. Other processes which occur at the ends of a linear device such as a θ -pinch include escape of plasma, loss of heat and tying of field lines to the walls. Plasma and neutral gas may also be absorbed and emitted in unpredictable amounts at the walls.

Several versions of the MHD equations, of increasing complexity, can be and have been used. These include various physical effects such as ionization, radiation loss by impurities, Hall effect, finite Larmor radius and so on, and involve no new points of principle. There are, however, two places where the consistency of the MHD equations themselves may be questioned.

One occurs at the plasma boundary, where the MHD approximation breaks down, and leads formally to a singularity in the electron temperature. This is in fact usually suppressed accidentally, by numerical truncation errors, but it is preferable to make a physical modification in the differential equations, analogous to the artificial Von Neumann viscosity³ used for shocks.

The other place is at the shock front, where the solution becomes indeterminate because the Rankine-Hugoniot or de Hoffman-Teller relations do not give enough information to determine the proper division of energy between electron and ion heating. Strictly therefore, an exact set of equations should be integrated through the shock to give the physical conditions on the

downstream side, but this is not yet possible and some ad hoc assumption must be made. This contrasts with the situation in ordinary hydrodynamics, where any entropy-generating scheme that preserves energy, momentum and mass will give the correct solution outside the shock front, so that an enhanced artificial viscosity is commonly employed.

2. INTERLACED MESH LATTICES IN 2 AND 3 DIMENSIONS

It will now be shown how the Eulerian mesh can be determined, in a methodical way, from the requirements of exact mass, momentum and flux conservation, and second order accuracy. In this section the continuity equation is taken as an example. We shall find that conserved variables are to be defined as spatial averages, and that in p dimensions there are 2^p interlaced mesh lattices, each satisfying its own independent conservation law.

The basic differential equations of MHD are expressed in conservative form in Table 2. Associated with these are the integral conservation laws of Table 3. It is well known that either set of equations can be given a relativistic formulation, so that the continuity equation becomes

$$\frac{\partial}{\partial x^\mu}(\rho v^\mu) = 0, \quad (1)$$

or

$$\oint \rho v^\mu dS_\mu = 0. \quad (2)$$

Although the concept of relativistic invariance seems to play no obvious role in our difference schemes, it is advantageous to think of the Eulerian net as a space-time structure, rather like a crystal lattice, constructed out of 4-dimensional fundamental 'mesh boxes'. In the following discussion it will be assumed

for simplicity that an orthogonal Cartesian system is used. We obtain the difference scheme by applying integral formulae such as (2) to each box. This is illustrated in Fig.1 for the continuity equation in 1 and 2 dimensions. See also Fig.2.

In the 2-dimensional case (2) can be written as

$$M_2 - M_1 + F_N - F_S + F_E - F_W = 0, \quad (3)$$

where the 4 time-like faces of the box have been labelled (N,S,E,W) respectively, and the two space-like faces at t_1 and t_2 have been labelled (1,2). The individual terms of (3) represent 2-dimensional mass flow integrals over the various faces, e.g.

$$M_1 = \iint \rho(x,y,t_1) dx dy, \quad F_E = \iint \rho(x_E,y,t) v_x(x_E,y,t) dy dt \quad (4)$$

Equation (3) signifies that the total directed flux of the vector $\rho \mathbf{v}$ through the faces of any fundamental mesh box is zero.

Each face of the mesh belongs to 2 boxes, and the corresponding flux appears in (3) with a positive sign for one of these boxes and a negative sign for the other. Therefore, if precisely the same difference expression is used in each case, the conservation law (2) will be satisfied identically when applied to the surface of any space-time volume that is constructed out of complete mesh boxes. In particular

$$\iiint_{t_1} \rho dx dy dz = \iiint_{t_2} \rho dx dy dz \quad (5)$$

Mesh Points

It is convenient to associate each mass flux with the central point of the corresponding face, thus defining $(p+1)$ distinct types of mesh point. The coordinate system is now chosen so that a fundamental mesh box has sides $(2\Delta t, 2\Delta x, 2\Delta y, 2\Delta z)$, and unit basis vectors are denoted by $(\underline{e}_x, \underline{e}_y, \underline{e}_z, \underline{e}_t)$. Then mesh points are located at positions

$$P_{lmn}^{\Upsilon} = l\Delta x \underline{e}_x + m\Delta y \underline{e}_y + n\Delta z \underline{e}_z + \Upsilon \Delta t \underline{e}_t, \quad (6)$$

the various type being distinguished by whether the integers (l, m, n, Υ) are even or odd.

We shall start with Lattice 0, defined so that the points $(1, 2)$ have Υ even and $(1, m, \dots)$ odd. Then the space-like faces define p 'odd' lattices as indicated in Table 4. These are denoted by labels $(1, 3, \dots, 2p-1)$.

Definition of the Variables

The next step is to set up a relation between the fluxes, and the density and velocity variables to be used in the calculation. The usual mathematical convention is solving differential equations by numerical methods is to treat each variable value as a point function. We shall assume instead that each stored density value represents a spatial average, and denote it by $\tilde{\rho}_{lmn}^{\Upsilon}$. It is therefore defined as an integral over a space-like surface at a particular instant of time, the mass within a box of 3-volume $8\Delta x \Delta y \Delta z$ at time t_{Υ} being

$$M_{lmn}^{\Upsilon} = \tilde{\rho}_{lmn}^{\Upsilon} \cdot 8\Delta x \Delta y \Delta z = \int_{x^-}^{x^+} \int_{y^-}^{y^+} \int_{z^-}^{z^+} \rho(x, y, z, t_{\Upsilon}) dx dy dz \quad (7)$$

where $x_l^{\pm} = x_l \pm \Delta x$ etc. Velocity variables are defined in terms of momentum averages in a similar way (§3).

All the inaccuracy and complexity of the difference scheme is now to be attributed to the fact, that we also require mass fluxes (and other types of flux) across time-like faces, which correspond to averages $(\widehat{\rho v_i})_{lmn}^T \dots$ of a different type, e.g.

$$(\widehat{\rho v_x})_{lmn}^T \cdot 8\Delta x \Delta y \Delta z = \iiint \rho(x_l, y, z, t) v_x(x_l, y, z, t) dy dz dt \quad (8)$$

First Approximation

In the first approximation we treat the space-like averages $\tilde{\rho}, (\tilde{\rho v_i}), \dots$ as if they were point functions, and use them to construct the required time-like averages $(\widehat{\rho v_i}), (\widehat{\rho v_i v_j}), \dots$. But these \wedge -averages are needed at odd times, and in order to achieve second-order accuracy it is necessary to introduce \sim -averages which are centered at precisely the same points. We must in fact introduce p sets of 'odd' fundamental mesh boxes, each set having its space-like faces centered at the midpoints of one of the p sets of time-like faces of the original Lattice 0, i.e. at the points of Lattices 1, 3, ..., (2p-1).

The same process must now be repeated for each of the odd sets of boxes, so that these too have \sim -averages at the points where fluxes are required. In 2 dimensions this just brings in Lattice 2, whose points lie at the corners of the fundamental mesh box of Lattice 0, and the mesh is then complete. In 3 dimensions it brings in the midpoints of the spatial edges, and 1 further stage is needed to bring in the corners. Eventually we obtain 2^p sets of points, boxes and variables, one half

defined at even times and the other half at odd times. Each set satisfies an independent conservation law, and the basic difference equation represents a relation, such as equation (3), between $(p+1)$ distinct types of point.

Second Approximation

The essence of the second approximation, which has been described in a paper² with N.O.Weiss, is to get a more exact expression for time-like integrals such as (8), by making use of further space-like averages $\tilde{\rho}$, $(\tilde{\rho v}_i)$ which are available at neighbouring mesh points. The main incentive to do this comes from the need for a more accurate treatment of the advective term, and a brief discussion is given in §6.

3.EQUATIONS OF MOTION AND ENERGY

The analysis of §2 may be repeated for the equation of motion, and for the heat equation. Since momentum is a conserved quantity while velocity is not, it is preferable to solve the equation of motion in the form (2.2) or (3.2). However it is convenient to store the velocity in the machine, so we define

$$\tilde{v}_{lmn} = \frac{1}{8\Delta x \Delta y \Delta z \cdot \tilde{\rho}_{lmn}} \iiint \rho(x,y,z,t_\gamma) \underline{v}(x,y,z,t_\gamma) dx dy dz \quad (9)$$

Similarly for the temperature,

$$\tilde{T}_{lmn} = \frac{(\gamma-1)}{8\Delta x \Delta y \Delta z \cdot \tilde{\rho}_{lmn}} \iiint \frac{\rho(x,y,z,t_\gamma) T(x,y,z,t_\gamma) dx dy dz}{(\gamma-1)} \quad (10)$$

To solve the equation of motion, we require **average** fluxes of $\rho v_i v_j$ and of the total stress tensor P_{ij}^{tot} over the time-like faces of the fundamental mesh box. Some of the terms in the material stress tensor, (namely those concerned with viscosity and finite Larmor radius), depend on velocity derivatives. These require special treatment and are not dealt with in this section. All the remaining terms can be evaluated, in first approximation, by using the variables $\tilde{\rho}$, \tilde{v}_i , \tilde{T} which are already available at the midpoints of these faces, together with the magnetic field \tilde{B}_i to be discussed in § 4. Thus the correct centering of the field is determined from the equation of motion.

No very useful information is gained by examining the energy equation, so we now go on to discuss the magnetic field.

4. MAGNETIC FIELD AND VECTOR POTENTIAL

The basic differential conservation law to be satisfied by the magnetic field is

$$\text{div } \underline{B} = 0, \quad (11)$$

which holds at each instant of time. We can secure this automatically by writing

$$\underline{B} = \text{curl } \underline{A}, \quad (12)$$

where \underline{A} is the vector potential. In integral form (11) becomes

$$\iint \underline{B} \cdot d\underline{s} = \oint \underline{A} \cdot d\underline{l}. \quad (13)$$

Therefore each component of \tilde{B} is to be defined as a 2-dimensional average over a space-like region at an instant of time, e.g.

$$\tilde{B}_{x,lmn}^{\gamma} = \frac{1}{4\Delta y \Delta z} \iint B_x(x_l, y, z, t_{\gamma}) dy dz \quad (14)$$

while each component of $\tilde{\underline{A}}$ is a 1-dimensional space average, e.g.

$$\tilde{A}_{x,lmn}^{\gamma} = \frac{1}{2\Delta x} \int A_x(x, y_m, z_n, t_{\gamma}) dx \quad (15)$$

The relation (13) between $\tilde{\underline{B}}$ and $\tilde{\underline{A}}$, and the conservation law (3.4), are then exact difference identities (see Fig.3). It is convenient to choose $\tilde{\underline{A}}$ to be the basic variable to be stored in the machine, and to derive $\tilde{\underline{B}}$ by (for example)

$$\begin{aligned} \tilde{B}_{x,lmn}^{\gamma} = & \frac{(\tilde{A}_{z, \ell(m+1)n} - \tilde{A}_{z, \ell(m-1)n})}{2\Delta y} \\ & - \frac{(\tilde{A}_{y, \ell_m(n+1)} - \tilde{A}_{y, \ell_m(n-1)})}{2\Delta z} \end{aligned} \quad (16)$$

Since $\tilde{\underline{B}}$ is required at the existing mesh points in order to compute the stress tensor, equation (16) implies that $\tilde{\underline{A}}$ must be defined at 2^P new lattices of points, not used for any other variable, which are just the midpoints of the space-like edges of the fundamental mesh boxes.

We have now placed all the variables at their appropriate mesh points, and used the full set of $2^{(P+1)}$ lattices defined by (6) to do so.

The equation satisfied by \underline{A} is

$$\frac{\partial \underline{A}}{\partial t} = -\underline{E} + \text{grad } \phi \quad (17)$$

where ϕ is any scalar. Assuming that

$$\underline{E} + \underline{v}_x \underline{B} = \eta \underline{j} \quad (18)$$

for simplicity, where

$$\underline{j} = \text{curl } \underline{B} = \text{curl curl } \underline{A}, \quad (19)$$

and choosing the gauge so that

$$\phi = \eta \text{ div } \underline{A} \quad (20)$$

we obtain the equation

$$\frac{\partial \underline{A}}{\partial t} = \underline{v}_x \text{ curl } \underline{A} + \eta \nabla^2 \underline{A} + \text{div } \underline{A} \text{ grad } \eta. \quad (21)$$

The accuracy of the calculation depends mainly on the treatment of the first term, which is of advective type ($\S 6$). The diffusive term will be discussed in $\S 5$, while the third term is to be regarded as a small correction.

5. DIFFUSION TERMS AND LATTICE COUPLING

We have so far introduced 2^P independent lattices for each variable, and it is necessary to couple these together if unphysical computational modes are to be avoided. For most of the variables this can be achieved very conveniently, by a suitable difference representation of the physical diffusion terms that already exist, namely electrical resistivity, heat conduction and viscosity. Only the continuity equation has no term of this kind, and it may be necessary to perform a smoothing operation on the density from time to time in order to keep the various lattices in step with one another.

The simplest diffusion equation is

$$\frac{\partial \psi}{\partial t} = D \nabla^2 \psi \quad (22)$$

which does not lead to a conservation law if the diffusion coefficient is a function of position $D(x,y,z)$. This is actually the situation for the vector potential \underline{A} . Conservation of magnetic flux is guaranteed by (16), and is independent of the way in which (21) is solved. This is a principal reason for choosing the vector potential representation.

For momentum and energy we do require a conservation law, and (22) must be replaced by

$$\frac{\partial \psi}{\partial t} = \frac{\partial}{\partial x_i} \left(D \frac{\partial \psi}{\partial x_i} \right) \quad (23)$$

We use the Dufort-Frankel scheme³ for this equation; it is given in Fig.4. This is stable for all Δt , and couples together

(p+1) lattices for each fundamental mesh box. For equation (23) we represent the r.h.s. as the sum of 4p fluxes, defined at half-integral spacetime points as indicated in Fig.4. A typical example is

$$F_{(\ell+\frac{1}{2})mn}^{\gamma+\frac{1}{2}} = D_{(\ell+\frac{1}{2})mn}^{\gamma+\frac{1}{2}} \left(\frac{\psi_{(\ell+1)mn}^{\gamma+1} - \psi_{\ell mn}^{\gamma}}{\Delta x} \right) \Delta y \Delta z \Delta t \quad (24)$$

As in §2 each flux occurs twice with opposite signs, once in the diffusion equation for an even-time lattice, and once in the equation for an odd-time lattice, and this enables a formal conservation law to be set up.

Conservation Law

At present we have 2^p sets of overlapping boxes in space-time, with a separate conservation law for each. We now halve each space-like edge, so that the smaller boxes fit together exactly with no overlapping as indicated in Fig.5.

The best approximation to a complete space-like surface S_k is obtained by taking the set of p-dimensional space-like faces at time $t=2k\Delta t$, and the adjacent set at the slightly earlier time $t=(2k-1)\Delta t$, and then connecting these together by 'vertical' time-like faces, (Fig.5). It then follows from the basic difference equations that the total flux of a conserved quantity through any such S_k is the same. This may be seen by dividing the spacetime region between two such surfaces $S_k, S_{k'}$ into boxes and applying the conservative difference equations to each box in turn, when all contributions except those from $S_k, S_{k'}$ cancel one another in pairs.

6. FOURTH ORDER TREATMENT OF THE ADVECTIVE TERMS

It has been explained in §1 that some of the most serious errors in MHD computations may be expected to arise from inaccurate representation of the advective terms. In the conservative difference scheme that has been outlined in §§ 2-5, this corresponds to maltreatment of time averages such as

$$(\widehat{\rho v_i}), (\widehat{\rho v_i v_j}), (\widehat{\rho T v_i}), (\underline{v}_x \widehat{\text{curl } \underline{A}}) \quad (25)$$

The first approximation treats the space averages $\tilde{\rho}$, \tilde{v} , \tilde{T} , $\tilde{\underline{A}}$ as point functions, and then replaces the required time average by products of these functions.

It has been shown by Roberts and Weiss² that function values which are available at neighbouring mesh points may be used to obtain a better approximation to the advective terms without too much extra computation. They discussed only the cases of advection of a scalar ρ or vector \underline{B} by a time-independent velocity field in 2 dimensions, and further analysis is therefore needed.

It is not appropriate to attempt to get an exact expression for the complete time average, since there will be errors of similar order in other parts of the difference scheme which cannot be corrected in this way. The advective contribution is assumed to be dominant, and since this involves the velocity rather than its derivatives, we assume that \underline{v} can be taken out of the averages (25) wherever convenient. We therefore have to evaluate

$$(\widehat{\rho v_i}), (\widehat{\rho v_i}) v_j, (\widehat{\rho T}) v_i, \underline{v}_x (\widehat{\text{curl } \underline{A}}) \quad (26)$$

The treatment of the first three terms is now the same as in the earlier paper. For example, we require an \wedge -average $\iiint dydzdt$ centered on the point P_{lmn}^{γ} , and have available \sim -averages $\iiint dx dy dz$ at $P_{(\ell-1)mn}^{\gamma+1}$, P_{lmn}^{γ} , $P_{(\ell+1)mn}^{\gamma-1}$. In symbolic terms we write

$$\wedge P_{lmn}^{\gamma} = \frac{4}{3} \sim P_{lmn}^{\gamma} - \frac{1}{6} \sim P_{(\ell+1)mn}^{\gamma-1} - \frac{1}{6} \sim P_{(\ell-1)mn}^{\gamma+1} \quad (27)$$

which ensures 4th order accuracy in Δx . Treatment of the vector potential is essentially the same; for example we require to solve

$$\frac{\partial \underline{A}_x}{\partial t} = \underset{(xt)}{v_y} \underset{(xy)}{(\text{curl } \underline{A})_z} - \underset{(xz)}{v_z} (\text{curl } \underline{A})_y + \dots \quad (28)$$

with the 2-dimensional averages indicated in brackets. A y-averaging must be removed from the first term, and a z-averaging from the second, and this is done by formulae such as (27). Since each component of $\underline{A}(t_2)$ occurs in the equation for the other two components, a (3 X 3) matrix must be inverted, using Cramers rule.

7. CONCLUDING REMARKS

We have outlined in §§ 2 - 6 the logical steps by which a conservative Eulerian difference scheme may be constructed for the MHD equations. Each physical variable is defined in a precise way as a space average at a particular instant of time, the number of dimensions in the averaging integral depending on the variable concerned; 3 for the density ρ , momentum $\rho \underline{v}$ and

thermal energy $\rho T/(\gamma-1)$; 2 for the magnetic field \underline{B} ; and 1 for the vector potential \underline{A} . The physical conservation laws then appear as surface integrals over the boundaries of rectangular regions in space-time, (or in 3-dimensional space, for the equation $\text{div } \underline{B} = 0$), and are represented by exact difference identities. In order to maintain second order accuracy, it is necessary to introduce a mesh point at the center of each time-like face of each 'fundamental mesh box'. For a 3-dimensional set of equations this leads to 8 interlaced lattices for each variable, 4 at even times and 4 at odd times. It turns out that the variables ρ , \underline{v} , T , \underline{B} share a common set of lattices, while \underline{A} has a set of its own.

In the absence of diffusion, each of the 8 lattices has its own independent conservation law, so that computational modes may therefore arise. The lattices may be brought into line by using the Dufort-Frankel³ scheme for the physical diffusion terms, since this couples lattices together in groups. An exact conservation law still exists, and can be given a space-time interpretation, but it now applies to the entire mesh.

The energy equation has not been discussed in any detail, and it is not yet known whether an exact conservation law can be set up. The difficulty is that all the variables that occur in the energy integral

$$\iiint \left(\frac{B^2}{2} + \frac{\rho T}{\gamma-1} + \frac{\rho \underline{v}^2}{2} \right) dx dy dz \quad (29)$$

have been given a formal meaning, in terms of different types of averaging process, and it is not easy to give a similar meaning to their products. This applies for example to the first and third terms of (29), which one would like to interpret

as spatial averages. It also applies forcibly to cross terms representing energy exchange between kinetic, thermal, and magnetic forms, which must cancel in pairs by exact difference identities if conservation is to be achieved. It may therefore be best to regard conservation of energy as a measure of the numerical accuracy of the difference scheme.

The approach adopted throughout this paper has been Eulerian, and we have indicated in §6 how errors in the treatment of the advective terms, which may be quite serious in MHD, may be minimized by a 4th order treatment.

Stability conditions have not been touched on, although they have been discussed in some detail in an earlier paper². Since the scheme is explicit throughout, the Courant-Friedrichs-Lewy³ condition will apply (except for the diffusion terms).

In conclusion, what we have done is to explore, in depth, one possible approach to the solution of the MHD equations. In contrast to what one might term the 'mathematical' interpretation of a difference scheme, in which each stored variable is thought of as a point function, we have adopted a 'physical' point of view in which the status of each variable is deduced from its transformation properties, (scalar, vector, tensor etc.), and from the conservation law which it satisfies. By following this physical approach one is led naturally to a unique mesh, and to a particular difference representation of the equations.

The ultimate aim is to attain the most accurate solution possible for a given amount of resources, which will include machine time, storage space and programming effort. This implies that several different techniques should be developed in detail, and compared with one another both theoretically and empirically. the approach described in this paper is intended in this spirit;

it is certainly not the only scheme, and we have not proved yet that it is the best.

ACKNOWLEDGEMENTS

The 1-dimensional MHD computer program described in Ref. 1 was written at Harwell in 1959 by Dr.K.Hain, assisted by Mrs.G.Hain, Miss S.J.Roberts and the author. The Harwell-Culham version was subsequently developed by the author, and for several years past has been the responsibility of Mr.D.L.Fisher who has introduced many extensions and improvements. Other versions have been developed elsewhere, notably at Munich, Washington and Los Alamos.

A 2-dimensional program was written at Harwell in 1961 by Dr.F.Hertweck in collaboration with the author. This was an explicit version which described motion in the r-z plane of a θ -pinch.

Many of the techniques discussed in §§2 - 6 were worked out in collaboration with Dr.N.O.Weiss, and some of them have been described in Ref. 2.

REFERENCES

- 1.K.Hain, K.V.Roberts et.al., Zeits. für Naturf. 15a, 1039 (1960).
- 2.K.V.Roberts and N.O.Weiss, Math. Comp. 20, 272 (1966).
- 3.R.D.Richtmyer, "Difference Methods for Initial-Value Problems, Interscience, New York (1957).

TABLE 1.ADVECTIVE TERMS IN BASIC EQUATIONSCONTINUITY

$$\frac{\partial \rho}{\partial t} + \underline{v} \cdot \underline{\nabla} \rho = -\rho \operatorname{div} \underline{v} \quad (1.1)$$

VELOCITY

$$\frac{\partial v_i}{\partial t} + \underline{v} \cdot \underline{\nabla} v_i = -\frac{1}{\rho} \frac{\partial P_{ij}^{\text{tot}}}{\partial x_j} \quad (1.2)$$

ENERGY

$$\frac{\partial \mathcal{E}}{\partial t} + \underline{v} \cdot \underline{\nabla} \mathcal{E} = -\frac{5}{2} p^\circ \operatorname{div} \underline{v} + \dots \quad (1.3)$$

FIELD

$$\frac{\partial \underline{B}}{\partial t} + \underline{v} \cdot \underline{\nabla} \underline{B} = -\underline{B} \operatorname{div} \underline{v} + (\underline{B} \cdot \underline{\nabla}) \underline{v} + \dots \quad (1.4)$$

TABLE 2. BASIC EQUATIONS IN CONSERVATIVE FORM

MASS

$$\frac{\partial \rho}{\partial t} = - \frac{\partial}{\partial x_i} (\rho v_i) \quad (2.1)$$

MOMENTUM

$$\frac{\partial}{\partial t} (\rho v_j) = - \frac{\partial}{\partial x_i} (\rho v_i v_j + P_{ij}^{\text{tot}}) \quad (2.2)$$

HEAT
ENERGY

$$\frac{\partial \mathcal{E}}{\partial t} = - \frac{\partial}{\partial x_i} (\mathcal{E} v_i) + P_{ij}^{\text{nat}} \frac{\partial v_i}{\partial x_j} - \frac{\partial q_i}{\partial x_i} + \underline{j} \cdot (\underline{E} + \underline{v} \times \underline{B}) \quad (2.3)$$

FIELD

$$\frac{\partial \underline{B}}{\partial t} = - \text{Curl } \underline{E}, \quad \text{div } \underline{B} = 0 \quad (2.4)$$

FIELD
ENERGY

$$\frac{\partial}{\partial t} \left(\frac{\underline{B}^2}{2} \right) = - \text{div} (\underline{E} \times \underline{B}) + \frac{\partial P_{ij}^{\text{field}}}{\partial x_j} v_i - \underline{j} \cdot (\underline{E} + \underline{v} \times \underline{B}) \quad (2.5)$$

TABLE 3.INTEGRAL CONSERVATION LAWSMASS

$$\delta \iiint \rho d\tau = - \int dt \oint \rho v_i dS_i \quad (3.1)$$

MOMENTUM

$$\delta \iiint \rho v_i d\tau = - \int dt \oint (\rho v_i v_j + P_{ij}^{\text{tot}}) dS_j \quad (3.2)$$

HEAT
ENERGY

$$\delta \iiint \mathcal{E} d\tau = - \int dt \oint (\mathcal{E} v_i + q_i) \cdot dS_i + \iiint \left(\underline{j} \cdot (\underline{E} + \underline{v} \times \underline{B}) - P_{ij}^m \frac{\partial v_i}{\partial x_j} \right) dt d\tau \quad (3.3)$$

FIELD

$$\oint \underline{B} \cdot d\underline{S} = 0 \quad (3.4)$$

FIELD
ENERGY

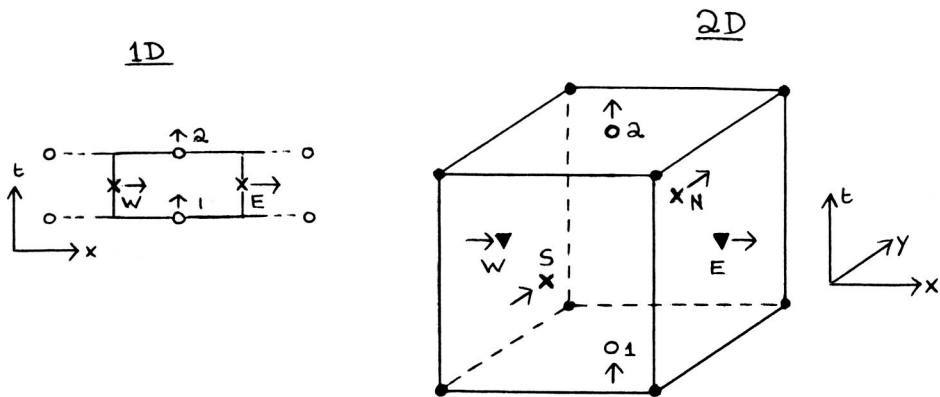
$$\delta \iiint \frac{B^2}{2} d\tau = - \int dt \oint (\underline{E} \times \underline{B}) \cdot d\underline{S} + \iiint \left(\frac{\partial P_{ij}^{\text{field}}}{\partial x_j} v_i - \underline{j} \cdot (\underline{E} + \underline{v} \times \underline{B}) \right) dt d\tau \quad (3.5)$$

TABLE 4. LATTICES FOR ALL VARIABLES EXCEPT A

<u>Lattice Number</u>	<u>Description</u>	<u>γ</u>	<u>l</u>	<u>m</u>	<u>n</u>
0	Center	E	0	0	0
1	yz-face	0	E	0	0
2	z-edge	E	E	E	0
3	zx-face	0	0	E	0
4	x-edge	E	0	E	E
5	xy-face	0	0	0	E
6	y-edge	E	E	0	E
7	Corner	0	E	E	E

Notes

1. E = 'even', 0 = 'odd'.
2. The parity product for all these lattices is 'odd'.
3. Change the parity of γ to get the lattices for A.



$$MASS_2 = MASS_1 - FLUX_N - FLUX_E + FLUX_S + FLUX_W$$

Figure 1.- Space-time conservation.

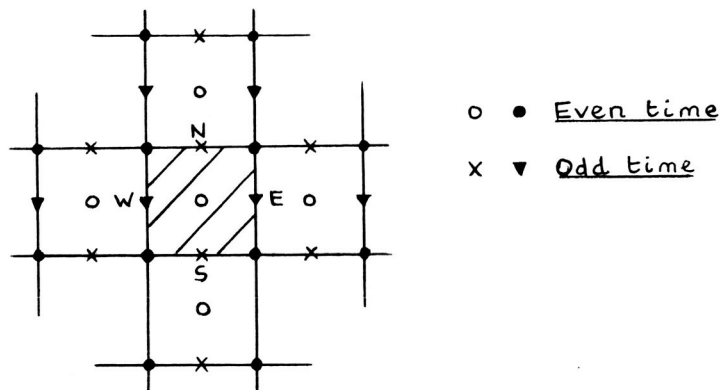


Figure 2.- Staggered 2D space mesh.

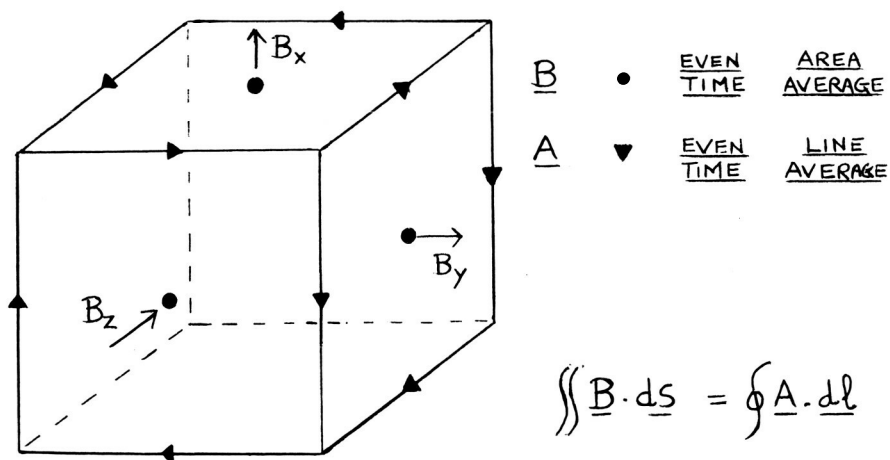
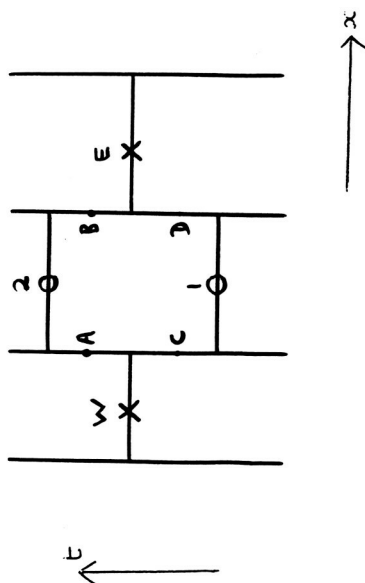


Figure 3.- Relation between B and A.

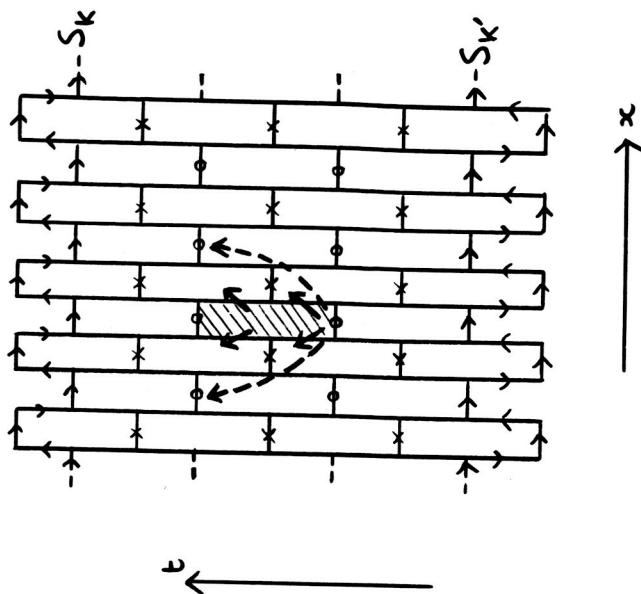


$$\frac{\partial \psi}{\partial t} = \frac{\partial}{\partial x_i} \left(D \frac{\partial \psi}{\partial x_i} \right)$$

$$F_A = -D(A) \frac{(\psi_2 - \psi_w)}{\Delta x} \quad (etc)$$

$$\psi_2 \Delta x - \psi_1 \Delta x = F_A + F_C - F_B - F_D$$

Figure 4.- Dufort-Frankel scheme in 1 dimension.



1. Main terms exchange ψ with points of same lattice (--->).
2. Diffusion terms exchange ψ with lattices of opposite parity, through walls of box (--->).
3. All contributions cancel in pairs, except those through S_k and $S_{k'}$.

Figure 5.- Conservation law, including diffusion term.

N67-37748

3 COMPUTER SIMULATION OF THE THETA PINCH

Thomas A. Oliphant
Los Alamos Scientific Laboratory
University of California

A basic numerical program for the computer simulation of the straight cylinder theta pinch has been written and is in operation. A good qualitative result has been obtained for the initial pinch compression and the early phase of end loss. Before making detailed comparisons with experiments some work will have to be done on improved parameterizations, finer meshing, and machine efficiency.

The geometry of the model is indicated schematically in figure 1. The plasma is initially confined within a specularly reflecting cylinder (a). A Scylla coil (b) which is a conducting cylinder carries the $\hat{\theta}$ -directed driving current. Coils (c) have been included to give a mirror effect to inhibit the end losses. To facilitate the mathematical handling of the boundary conditions we have introduced a periodicity of length $2L$. The region which corresponds to our actual physical system is located in the range $-L \leq z \leq L$.

The inertial motion of the plasma is dominated by the more massive ions. The motion of the ions is described by a Lagrangian transport theory. Each mass point carries some large number of ions, say 10^{12} . There will be about 10^3 Lagrangian mass points in the system.

The macroscopic current carrying properties of the system are dominated by the less massive electrons. We assume that the electron component moves as a fluid which on the average follows the ion component in such a way as to

maintain charge neutrality. The electromagnetic field penetration is assumed to take place in accordance with Spitzer's formula for electrical resistivity. This carries with it the assumption of electron equilibrium.

The electromagnetic fields are determined by the vector potential \vec{A} which satisfies the equation

$$-\nabla^2 \vec{A} = 4\pi \vec{j}. \quad (1)$$

The current density \vec{j} is made up of two parts,

$$\vec{j} = \vec{j}_c + \vec{j}_s \quad (2)$$

The current density \vec{j}_c is the contribution from the external coils (c). The current density \vec{j}_s is the shielding current which develops within the plasma. Equation (1) is solved in the entire space within the conducting coil (b).

The current density \vec{j}_s is given by

$$\vec{j}_s = \frac{\vec{E}'}{\eta} = \frac{\vec{E} + (\vec{u} \times \vec{B})}{\eta} \quad (3)$$

where \vec{E}' is the effective electric field in a frame of reference moving with the plasma and η is the electron resistivity. \vec{u} is the plasma velocity determined by the ion motion and \vec{E} and \vec{B} are the lab frame electromagnetic fields.

From the symmetry of the system we see that \vec{B} will have no $\hat{\theta}$ -component and that the fields will have no θ -dependence. Thus, (3) becomes

$$\vec{j} = \hat{\theta} \frac{1}{\eta} \left[-\frac{\partial A}{\partial t} - v \frac{\partial A}{\partial z} - \frac{u}{r} \frac{\partial(rA)}{\partial r} \right] \quad (4)$$

where

$$\vec{A} = \hat{\theta} A \quad (5)$$

The current density j_c is given by

$$\vec{j}_c = \hat{\theta} j_c \quad (6)$$

Thus, (1) becomes

$$-\nabla^2 \vec{A} = 4\pi \hat{\theta} \left[j_c - \frac{1}{\eta} \left(\frac{\partial A}{\partial t} + v \frac{\partial A}{\partial z} + \frac{u}{r} \frac{\partial (rA)}{\partial r} \right) \right] \quad (7)$$

Writing out the Laplacian and letting

$$\psi = rA \quad (8)$$

we obtain

$$\frac{\partial^2 \psi}{\partial r^2} - \frac{1}{r} \frac{\partial \psi}{\partial r} + \frac{\partial^2 \psi}{\partial z^2} + 4\pi r j_c - \xi \left(\frac{\partial \psi}{\partial t} + v \frac{\partial \psi}{\partial z} + u \frac{\partial \psi}{\partial r} \right) = 0 \quad (9)$$

where

$$\xi = \frac{4\pi}{\eta} \quad (10)$$

Here ξ is simply set equal to zero in the vacuum region. In terms of ψ the electromagnetic fields are given by

$$E_\theta = - \frac{1}{r} \frac{\partial \psi}{\partial t} \quad (11)$$

$$B_r = - \frac{1}{r} \frac{\partial \psi}{\partial z} \quad (12)$$

$$B_z = \frac{1}{r} \frac{\partial \psi}{\partial r} \quad (13)$$

The boundary conditions on ψ are as follows:

$$\frac{\partial \psi}{\partial t} = - \frac{V(t)}{2\pi} \quad (14)$$

on the outer conductor where $V(t)$ is an arbitrarily programmed emf on the Scylla coil. Since B_r will be zero on the symmetry planes at $z = 0$ and $z = L$ we there set

$$\frac{\partial \psi}{\partial z} = 0. \quad (15)$$

Since A must remain finite as $r \rightarrow 0$, we have on the axis,

$$\psi = 0. \quad (16)$$

The direct effect of the electromagnetic field on the ions comes through the Lorentz force. There will also be a $\mathbf{j} \times \mathbf{B}$ force acting on the current carrying electrons which in our model transfers itself directly to the ions by charge neutralization. The net acceleration per ion and hence per Lagrangian mass point is given by

$$\vec{a} = \frac{q}{m} [\vec{E} + \vec{v} \times \vec{B}] + \frac{1}{\rho} (\vec{j} \times \vec{B}) \quad (17)$$

Using Ampere's law on the second term we obtain

$$\vec{a} = \frac{q}{m} [\vec{E} + \vec{v} \times \vec{B}] + \frac{1}{4\pi\rho} (\nabla \times \vec{B}) \times \vec{B} \quad (18)$$

Writing out the components, we have

$$\begin{aligned}
\vec{a} = & \hat{r} \left[\frac{qv_{\theta} B_z}{m} + \frac{B_z}{4\pi\rho} \left(\frac{\partial B_r}{\partial z} - \frac{B_z}{\partial r} \right) \right] \\
& + \hat{\theta} \frac{q}{m} (E_{\theta} + v_z B_r - v_r B_z) \\
& + \hat{z} \left[-\frac{qv_{\theta} B_r}{m} - \frac{B_r}{4\pi\rho} \left(\frac{\partial B_r}{\partial z} - \frac{\partial B_z}{\partial r} \right) \right]
\end{aligned} \tag{19}$$

Although the Lagrangian mass points move in three dimensions, an average temperature and density are taken over θ for computing η so that the field dependences are two dimensional.

To get valid computations of electron and ion temperatures it will be necessary to include the effects of Joule heating and shock heating. To calculate shock heating it will be necessary to include ion-ion collision effects. To get a qualitative representation of collision effects we have included a Monte Carlo ion-ion collision mechanism. Preliminary calculations with this collision device in give good qualitative results although some refinement will be necessary before we can expect to get a good estimate of shock heating.

In particular we have run a calculation just past the first pinch compression in a plasma 8 cm long of initial radius 1 cm with and without a mirror coil. We used 500 Lagrangian mass points to represent a neutral plasma of ion density 10^{14} per cm^3 . Without the mirror coil we lost 99 of the 500 mass points and with the mirror coil we lost 76 out of the 500 mass points.

In summary, we feel that as it stands now our numerical program has all the essential elements in it and will be capable of good comparisons with experiment after some routine refinements.

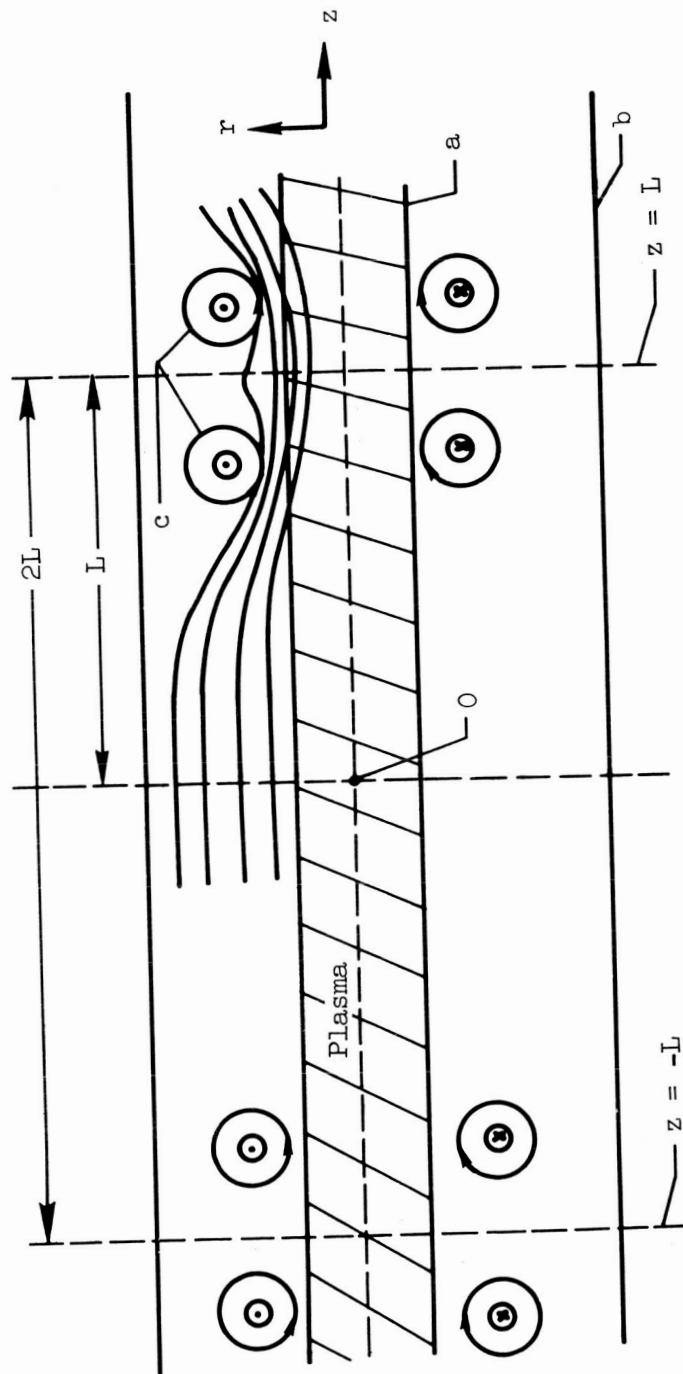


Figure 1.

Computer Simulation of Beam Bunching*

K. R. Crandall

Los Alamos Scientific Laboratory, Los Alamos, New Mexico

Before injecting a charged-particle beam into an accelerator it is desirable to longitudinally bunch the beam so that a larger percentage of the particles will be accelerated. This may be done by passing the beam through one or more buncher cavities that break a nearly monoenergetic, continuous beam into separate bunches of length L , where $L = u_0/f$, the velocity of the particles divided by the frequency at which the first buncher is operated. Efficient bunching can theoretically be achieved if the space-charge forces are negligible. If they are not negligible, then one would like to find out what effect they have on bunching. One means of studying space-charge effects is by numerical simulation.

For simplicity, the beam is assumed to be cylindrically symmetric and traveling in free space (the surrounding cylindrical conductor is ignored). A bunch is simulated by specifying initial values for r , z , r' , and z' for N particles, where N is typically 2000. r is the radial coordinate and z is the longitudinal coordinate relative to the trailing edge of the bunch. The prime denotes differentiation with respect to ξ , where ξ is the distance from the first cavity to the center of the bunch. As the center of the bunch moves a distance $\Delta\xi$ along the axis, the r , z , r' , and z' of each particle is modified, taking into account the radial and longitudinal space-charge electric fields as well as the impulses received by each particle as it passes a buncher cavity or a focusing lens.

A rectangular mesh is superimposed on the r - z space of the bunch. At each step in $\Delta\xi$, space-charge electric fields are computed at the mesh points. The field felt by a particle inside any rectangular box is obtained by a linear interpolation of the fields at the four surrounding mesh points.

The fields are computed directly from the charge distribution. The number of particles in a rectangular box determines the amount of charge that is in a toroid whose cross section is the box. This charge is assumed to be

concentrated in a uniformly charged circular ring located at the center of volume of the toroid. The electric field at a point produced by a ring of charge is a function of the ring radius and of the position of the point relative to the source ring. Since these remain fixed, the electric field components produced by a source ring containing $1/N$ th of the total charge in the bunch can be tabulated at every mesh point. Furthermore, it is necessary to construct these tables for only those boxes (source rings) along the trailing edge of the bunch; the contribution to the field at any mesh point produced by the charge in any box can then be obtained by multiplying the proper tabular value by the number of particles in the box.

The electric field produced by any number of neighboring bunches can easily be considered if these bunches are assumed to have the same charge distribution as the bunch being simulated. When the tables are constructed, the source is considered to be, instead of only one ring, a series of rings separated by a distance L . The only extra cost is the small additional computer time used in constructing the tables.

The amount of computer time used per step depends linearly on the number of particles and approximately on the square of the number of mesh points at which the fields are computed. Consequently, if a simple testing procedure is available, then the electric field should be computed at only those mesh points where there are one or more particles in a neighboring box.

* Work performed under the auspices of the U. S. Atomic Energy Commission.

3
NONLINEAR HIGH FREQUENCY-PLASMA INTERACTION
IN A MAGNETIC MIRROR

-:-:-:-:-

E. CANOBBIO* and R. COLLET

²Service d'Ionique Générale

Département de Physique du Plasma et de la Fusion Contrôlée

Centre d'Etudes Nucléaires de Saclay

B. P. n° 2 - 91 - Gif-sur-Yvette -

F r a n c e

-:-:-:-:-

Abstract. -

A large amplitude electromagnetic field accelerates the electrons of a beam injected in a mirror region.

The ion motion is produced by the self consistent axial space charge field.

When the electron velocity exceeds a critical value, steady electrostatic shock waves appear.

Analytical and numerical computations are presented.

* On leave of absence from EURATOM.

1. Some aspects of resonant wave-plasma interaction

The theory of the coupling between a magnetoplasma and an electromagnetic field at a frequency close to the gyrofrequency of one species of particle is well established only in the case of strictly uniform \vec{B}_0 field [1].

Actually, in most interesting cases the magnetic field is basically space dependent. For instance the high frequency axial plasma acceleration, injection and reflection in a mirror region is mainly due to the \vec{B}_0 gradient [2]. Since the gyroresonance is compatible with a large class of magnetic configurations, this wave-plasma interaction plays an important role in different fields like Fusion, Propulsion, Space- and Astrophysics.

In the following we present an analytical method to approximate particle trajectories, which is neither based on the adiabatical assumption nor on the time averaged Miller's force and we show a number of exact numerical tests in typical situations [3].

The analytical expressions we find allow a collective description of the plasma behaviour in a high frequency accelerating device [4].

The configuration we consider, in the simplest case, is the following (see fig. 1). A space independent electric field \vec{E}_\perp (approximation valid when the particle acceleration takes place in a volume which is small compared to λ^3) rotates around the symmetry axis of a mirror where the magnetic field is linearly dependent on space (expansion valid near the axis). A cold ion and electron beam is injected along z . The \vec{E}_\perp rotation frequency, ω , is equal to the electron-(ion) gyrofrequency on the plane $z = 0$, ω_{go} . The injected particle density is supposed to be so low that the oscillating part of the selfconsistent field is negligible as compared to \vec{E}_\perp [4]. On the contrary, the steady axial component of the space charge field is taken into

account, because it is responsible for the axial acceleration of the ions (electrons). The effect of the radial component is less important for our purposes [5].

Actually, when the external field is in resonance with the ions, we neglect the electrons throughout the calculations. As a consequence of the axial electrostatic field, the electrons follow closely the ions, $v_{ez} \approx v_{iz}$. In the opposite case ($\omega = \omega_{goe}$) a simplified approach has to be found, since the heavy particle acceleration by the electrons is a rather involved process. In this paper we first calculate the motion of a single electron either by neglecting the electrostatic interaction or by supposing that it is so strong that the electron and ion axial velocities are equal. In the last case a tensorial mass can be attributed to the electron ($m_{\perp} = m$, $m_{\parallel} = M$ [6]). Then we consider the Poisson equation for a steady onedimensional cold ion and electron beam and set an external term in the electron velocity to represent the action of the high frequency- and \vec{B}_0 field as calculated in the first part. We shall see that according to the density and injection velocity values, the solution of the Poisson equation is consistent with one or the other of the two limiting assumptions made in deriving the electron trajectories [7].

2. Particle trajectories

The main characteristics of the acceleration process appear in their simplest form when the electrons start with vanishing kinetic energy at the intersection on the magnetic axis with the resonance plane $z = 0$, where $\omega = \omega_{go} \equiv eB_0/mv$. We suppose that the electron mass in the axial motion is M and write the external fields in the form

$$\vec{B}_0 = B_0 \left(\frac{\delta\omega x}{2c}, \frac{\delta\omega y}{2c}, 1 - \delta Z \right), Z = \frac{\omega z}{c}, \vec{E}_1 \equiv E_x + iE_y = E \exp i\tau, \tau = \omega t.$$

It has been shown [3] that, if δZ , $\delta \dot{Z} \ll 1$ (as in all practical cases [2]) the nonrelativistic motion equation can be approximated to

$$\mu = g^2 |\Psi(\tau)|^2 \quad ; \quad d^2 Z / d\tau^2 = 1/2 \delta(m/M) \mu \quad (1)$$

where

$$\mu = (v_{\perp}/c)^2 (\omega_{g0}/\omega_g) \quad , \quad \omega_g = \omega_{g0}(1 - \delta Z) \quad , \quad g^2 = e^2 |E|^2 (mc\omega_{g0})^{-2}$$

and

$$\Psi(\tau) = \int_0^{\tau} d\tau' \exp i \left(\delta \int_0^{\tau'} d\tau'' Z(\tau'') \right) . \quad (2)$$

The results of the numerical integration of the exact equations indicate (fig. 2) that there are two distinct time intervals in which the acceleration process is basically different and correspond to the transit of the particle through a resonance region and an adiabatic region. In the first one, the magnetic moment μ , grows in time according to the simple law $\mu = g^2 \tau^2$ just as in the \vec{B}_0 uniform case. On the contrary, in the second region μ oscillated around the constant asymptotic value, μ_a , that μ would take if in this region $\vec{E}_{\perp} = 0$. These two intervals are separated by the transit time τ_T , obtained by setting $g^2 \tau_T^2 = \mu_a$.

According to eq. (1), the axial velocity is proportional to $\int_0^{\tau} \mu d\tau'$. It follows that in the resonance region (actually until the time $\tau_M > \tau_T$ where μ is maximum) the axial acceleration is not zero as in the $\delta = 0$ case, but it is equal to $1/2 \delta(m/M) g^2$. In the adiabatic region $\ddot{Z} = 1/2 \delta(m/M) \mu_a$. The expressions of μ_a , Z_a , τ_T and τ_M , within a constant factor of the order of unity are found analytically by putting either $\dot{Z} \sim \tau$ or $\dot{Z} \sim \tau^3$ in the expression of the phase angle between \vec{v}_{\perp} and \vec{E}_{\perp} (the argument of expi in eq. (2)) and calculating the asymptotic limit for $\tau \rightarrow \infty$. It is typical of the dependence of μ upon Z and τ that both preceding positions yield the same functional structure for μ_a . The constant factor can be found in a numerical example :

$$\mu_a = 5,8 \left(\frac{M}{m} \frac{g^3}{\delta^2} \right)^{2/5} ; \quad \tau_T = \frac{\tau_M}{1,29} = 2,4 \left(\frac{m}{M} \delta^2 g^2 \right)^{-1/5}.$$

The asymptotic value of the magnetic moment which is the main characteristics of the acceleration, does not depend very critically on the injection position of the particles before the resonance plane. The functions $\mu(\tau)$ and $\dot{Z}(\tau)$ are plotted for some values of the parameter $b = \omega_{g0}/\omega \geq 1$ in figs. (3) and (4). One sees that the maximum energy gain corresponds to $Z(t=0) \neq 0$. As b grows, before the resonance several oscillations appear produced by an alternating energy exchange between field and particle. If we plot $\mu_a(b)$ (fig. 5) we find a number of oscillations resulting from the variation of the phase between \vec{v}_\perp and \vec{E}_\perp at the resonance plane: the number of oscillations of $\mu_a(b)$ contained in the interval $(1, \alpha)$ are equal to the number of oscillations of $\mu(\tau)$ before the resonance in the case $b = \alpha$. We have shown analytically that the ratio $R \equiv \mu_a(b)/\mu_a(b=1)$ depends only on the quantity $Q^2 = 12 (M/m) (b-1)^5 (b \delta^2 g^2)^{-1}$, which is a function of $(b-1) \tau_R$. The resonance time τ_R is defined as the time at which the argument of $d\psi/d\tau$ is stationary.

The dependence of $R = f(Q)$ is tested in fig. 6, where the different points (\circ, \square, Δ) has been computed numerically. $R_{\max} \approx 1,2$ at $Z = 0,87 (m/M) (g^2/\delta^3)^{1/5}$ and the mean value \bar{R} is close to unity ($\bar{R} \approx 0,86$).

In all preceding cases, the relativistic effects have been neglected, even if they may actually be important also at low power regime, because they modify the phase between \vec{v}_\perp and \vec{E}_\perp , and the energy transfer from the field to the particle (see figs. (7) and (8)).

When $g \ll 1$ the equations (1) and (2) are still valid provided that the phase in eq. (2) is substituted by $1/2 \int_0^\tau (\vec{v}_\perp/c)^2 d\tau' + \delta \int_0^\tau \dot{Z} d\tau'$. It has been found [3] that the relativistic term predominates on the second

when

$$g \gtrsim g_c \approx 1/2 \left(\frac{m}{M} \delta^2 \right)^{3/4}.$$

This threshold separates the region where the functional dependence $1/2mv_{\perp}^2 \sim (g)^{6/5}$ is classic from the region where the kinetic energy has the relativistic form $m_0(g)^{2/3}$ (see fig. 9).

The results obtained in all the discussed cases hold even if the initial kinetic energy does not vanish, provided that the increase of axial velocity in the resonance region is much larger than the injection velocity (a similar condition on the perpendicular energy is always largely satisfied). However, the increase of axial velocity in the resonance region is in general a small quantity which can be smaller than the injection velocity.

When the axial electron velocity is roughly constant, we may set $m_{\parallel} = m$ for $\tau \leq \tau_M$, since the ion acceleration takes place mainly in the adiabatic region. In this case the analytical derivation of μ_a (and related quantities) is simple also for nonvanishing axial wave numbers: $\vec{E}_{\perp} = E \exp i(\tau - NZ)$ [3]. If $g \ll 1$ one has $\psi(\tau) = \int_0^{\tau} d\tau' \exp i \left\{ \int_0^{\tau'} d\tau'' \left(\frac{1}{2} \mu - \delta Z \right) - NZ \right\}$. One finds that μ_a is given in terms of Fresnel integrals. μ_a takes different forms according as the phase between \vec{v}_{\perp} and \vec{E}_{\perp} is determined by the effect of the mirror, by relativity or by the Doppler effect. Approximated expressions of μ_a and of the width of the resonance region in these three cases are given in the following table together with the validity conditions.

μ_a	$Z_T = \tau_T \frac{v_0}{c}$	Approximations	$\dot{Z}(\tau = \tau_T) \approx \frac{v}{c}(\tau = 0) \equiv \frac{v_0}{c}$
$\frac{\pi}{2} \frac{g^2 c}{\delta v_0}$	$\left(\frac{\pi v_0}{2 \delta c} \right)^{1/2}$	$\left \frac{\pi g^2 c}{2 \delta v_0} - N \frac{v_0}{c} \right \ll \left(\frac{\delta v_0}{c} \right)^{1/2}$	$\frac{\pi g^2}{4 \delta} \left(\frac{1}{3} \sqrt{\frac{\pi \delta}{2}} + N \sqrt{\frac{v_0}{c}} \right) \ll \left(\frac{v_0}{c} \right)^{5/2}$
$2 g^{2/3}$	$\frac{\sqrt{2} v_0}{g^{2/3} c}$	$g^{2/3} - N \frac{v_0}{c} \gg \left(\frac{\delta v_0}{c} \right)^{1/2}$	$\frac{\sqrt{2}}{3} \delta + N g^{2/3} \ll \frac{v_0}{c}$
$2\pi \frac{g^2 c}{\delta v_0}$	$\left(\frac{2\pi v_0}{\delta c} \right)^{1/2}$	$\frac{\pi g^2 c}{\delta v_0} - N \frac{v_0}{c} \ll - \left(\frac{\delta v_0}{c} \right)^{1/2}$	$\frac{\pi g^2}{\delta} \left(\frac{\sqrt{2\pi \delta}}{3} + N \sqrt{\frac{v_0}{c}} \right) \ll \left(\frac{v_0}{c} \right)^{5/2}$

The maximum energy transfer takes place when the Doppler shift of the external frequency is compensated by the relativistic shift of the electron gyrofrequency.

3. The electrostatic interaction

In this section we study the axial space charge field in the resonance region [7] (the corresponding problem for the adiabatic zone is considered in another paper [8]). Using the hypothesis of the tensorial electron mass we may define a potential $\phi(Z)$ representing the effect of the external field on the axial electron motion, in the case that $v_{ze}(\tau = \tau_M) \gg v_{ze}(\tau = 0)$ (we note that the effect of the high frequency field on the ions is negligible). If we suppose that the axial electron and ion flux is stationary, conservative and monokinetic, the Poisson equation can be written

$$4 d^2 \psi / dZ^2 = \alpha (1 + \alpha^2 \gamma \psi)^{-1/2} - (1 - \psi + \phi)^{-1/2} \quad (3)$$

where ψ is the electronic potential energy - eV normalized to the initial kinetic energy $1/2 m v_0^2$ and

$$(\psi)_0 = (d\psi/dZ)_0 = 0, \quad Z = \frac{z}{\lambda_D}, \quad \lambda_D = (v_{ze0}/\omega_{pe})_0 \cdot 2^{-3/2}, \quad \omega_{pe}^2 = 4\pi e^2 n_e / m,$$

$$\alpha = (v_{ze}/v_{ze0})_0, \quad \gamma = m/M, \quad \phi = AZ^{3/2} \equiv 0,69 \left\{ \frac{m_{\perp} \delta g^2 c (\omega/\omega_{pe0})^3}{m_{\parallel} v_{ze0}} \right\}^{1/2} \cdot Z^{3/2},$$

$$0 \leq Z \leq Z_m, \quad Z_m = 3,8 \frac{c}{\omega \lambda_D} \left(\frac{m_{\perp} g^2}{m_{\parallel} \delta^3} \right)^{1/5} \quad \text{if} \quad g < g_c \equiv \frac{1}{2} \left(\frac{m_{\perp}}{m_{\parallel}} \delta^2 \right)^{3/4}$$

$$Z_m = 0,17 \frac{c}{\omega \lambda_D} \frac{m_{\perp}}{m_{\parallel}} \delta g^{-2/3} \quad \text{if} \quad g > g_c.$$

The assumption $\phi = AZ^{3/2}$ for the external force requires that under the influence of both the external and the electrostatic field the electron motion is such that in almost all the resonance region at least the average of v_z^2 over a few oscillations is proportional to $Z^{3/2}$.

When the numerical integration of eq. (3) shows that for some A and Z_m values, the ions are not accelerated, we must set $m/m_{||} = 1$ in the expressions of A and Z_m , in order to make the problem self consistent.

In the case of large injection electron velocity, the result is consistent with the assumption $\phi = 0$ when v_{ze} averaged over a few oscillations is constant in the resonance region.

When one finds $\langle v_{ze}^2 \rangle \sim Z^\beta$ with $0 < \beta < 3/2$, only the order of magnitude of the potential is significant.

The results of the numerical integration for equal initial ion and electron velocities are plotted in figs. (10), (11) and (12).

The curves of fig. (10) are typical of low A values ($A \lesssim 0,3$). v_{ze} oscillates around v_{zi} and $|v_{ze} / v_{zi} - 1| \ll 1$. In this case the ion acceleration is optimum (proof of the validity of the tensorial mass-assumption). The oscillations are quasi-harmonic and $\lambda \approx (1 + 8A \times Z^{3/2})^{3/4}$. After a transition zone, where $Z \gg Z_a$, $v_{ze}^2 \approx v_{zi}^2 \sim Z^{3/2}$. At the point Z_a the total energy gained by the ions is equal to their initial energy: $\alpha^2 \gamma \psi \approx 1$, $\psi \approx \phi$, $Z_a \approx (\alpha^2 \gamma A)^{-2/3}$. The calculations are selfconsistent when $Z_m \gg Z_a$.

The case $A > 1$ is shown in fig. (11). The ions are not accelerated in the resonance region. The electrostatic reaction is negligible in comparison with the external field and $v_{ze}^2 \sim Z^{3/2}$. In the adiabatic region ($Z > Z_m$) v_{ze} vanishes abruptly. Since the electrostatic field is discontinuous one can speak of a (steady) shock wave.

When the coefficient A approaches unity, several shock fronts appear in the resonance region (fig. 12). If $Z_m < Z_a$, $\langle v_{ze}^2 \rangle$ is almost constant and there is self consistency at large injection velocity. If

$Z_m \gg Z_a$ there is selfconsistency in the opposite case. The discontinuous solutions become quasi-harmonic waves at large Z .

In the last figure (fig. 13) the effect of the ratio between electron and ion initial velocities is studied. The asymptotic values of v_{ze}^2 and v_{zi}^2 are roughly independent on α . When $\alpha \gg 1$, $\langle v_{ze}^2 \rangle$ presents a plateau on a region where the ions are strongly accelerated. When $\alpha \geq 2$ the electrostatic field is discontinuous as it happens in general when the axial accelerating force may be neglected [8].

We will point out explicitly that standard integration subroutines (e. g. the Runge-Kutta-Gill method) have been used throughout with the only exception of the case where the solution of eq. (3) has a discontinuous derivative. In this case an exact relation is found between the slope of ψ on the right of a discontinuity and that on the left. When the numerical calculation approaches such a point ($v_{ze}^2 \equiv 1 - \psi + \phi = 0$) the abscissa and the slope on the left are carefully determined to obtain the new initial conditions for the integration after the discontinuity.

Acknowledgement.

The authors are indebted to Dr. T. Consoli for many illuminating discussions. This paper is a theoretical proof of the validity of his ideas.

References.

1. C.S. Roberts and S.J. Buchsbaum : Phys. Rev. 135 A, (1964) 381 ;
R.F. Lutomirski and R.N. Sudan : Phys. Rev. 147 (1966) 156 ;
2. T. Consoli : Plasma Physics and Controlled Nuclear Fusion Research, IAEA, Vienna (1966) Vol. II, 483 .

3. E. Canobbio : Comptes Rendus Acad. Sc. Paris 262 (1966) 966 ;
E. Canobbio & R. Collet : loc. cit. 264 B (1967) 428 ; loc. cit. 264 B
(1967) ;
M. Brambilla, E. Canobbio & R. Collet : loc. cit. 264 B (1967) in press;
E. Canobbio : Physics Letters, in press.
4. M. Brambilla; Comptes Rendus Acad. Sc. Paris 264 B (1967) 514 ;
M. Brambilla; Internal Report DPh-PFC-IGn (in press) CEA, Saclay
5. E. Canobbio & U. Finzi; Rapport CEA-R 3103 (1966)
6. T. Consoli & R. B. Hall; Nuclear Fusion, 3 (1963) 237
7. E. Canobbio & R. Collet : Comptes Rendus Ac. Sc. Paris (1967) in press;
8. E. Canobbio & U. Finzi : Communication at the VIII International
Conference on Phenomena in Ionised Gases -
Vienna - 1967

-:-:-:-:-

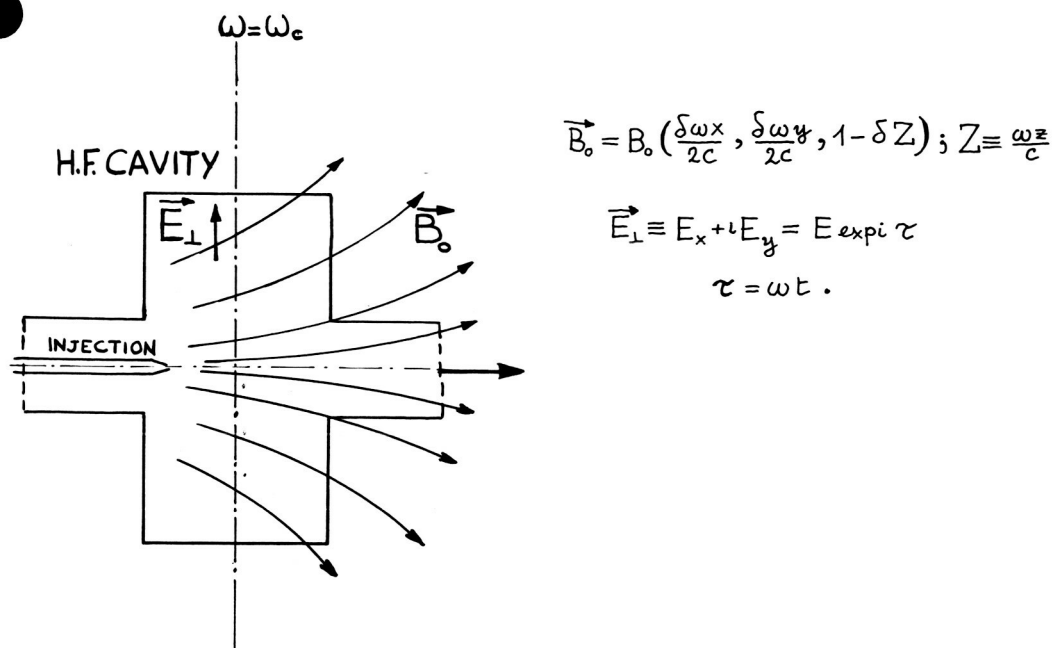


Figure 1.- A high frequency accelerating device.

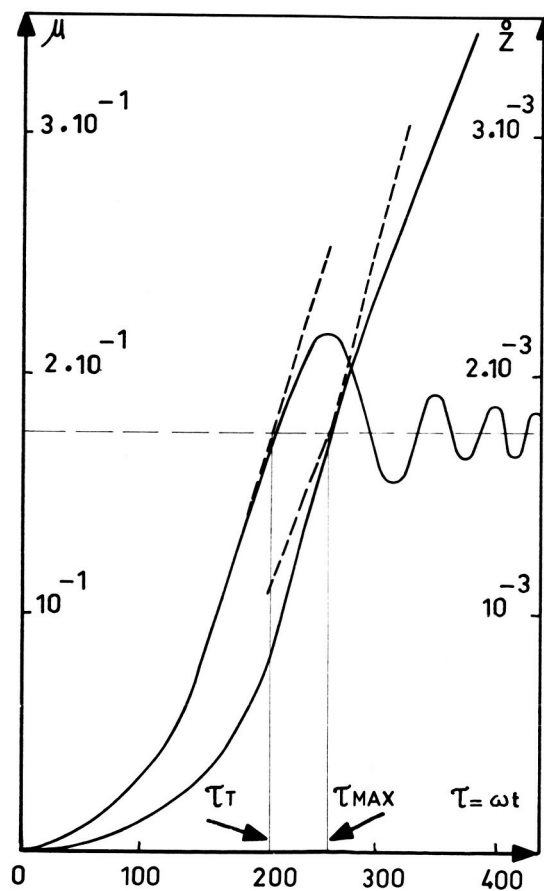


Figure 2.- The time evolution of the magnetic moment and axial velocity of a resonant particle.

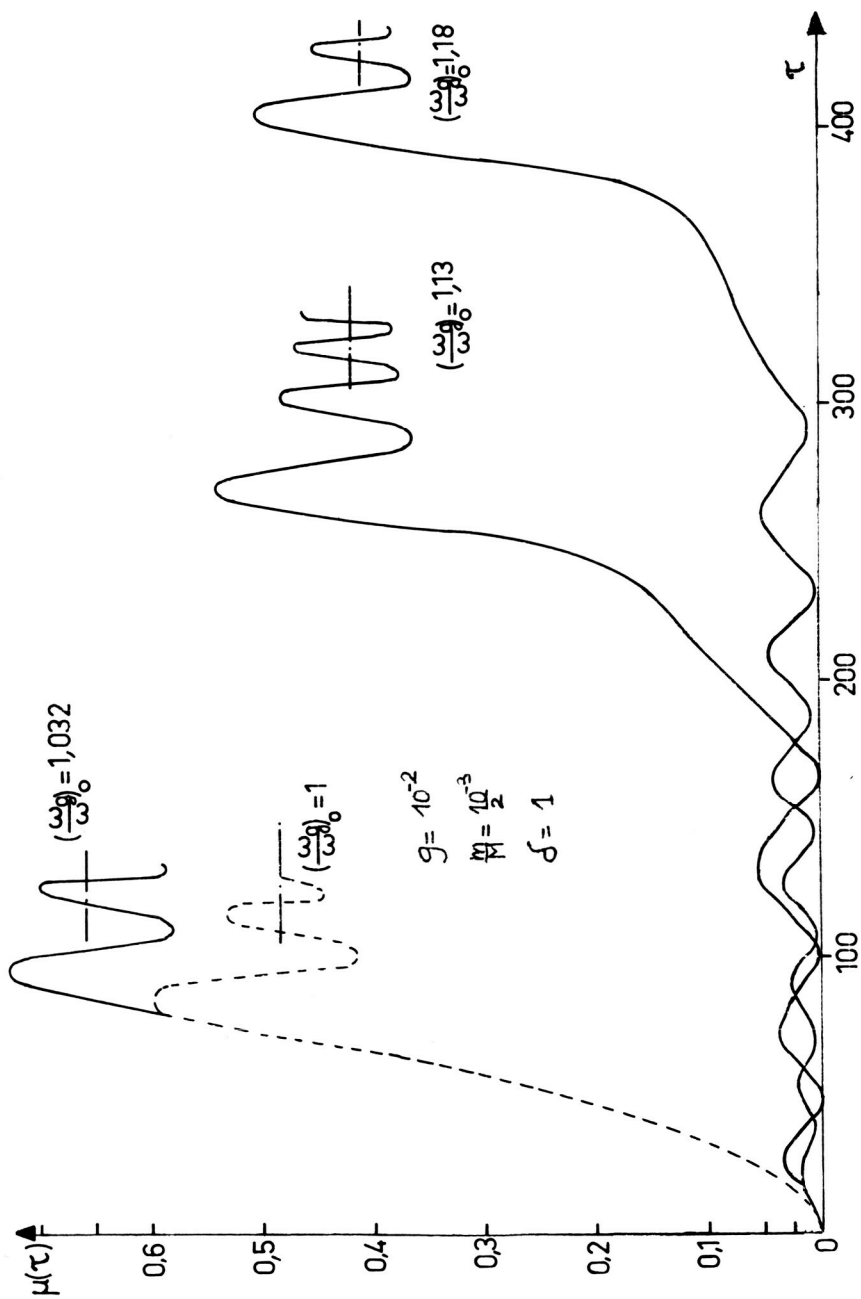


Figure 3.- The magnetic moment as a function of the injection position.

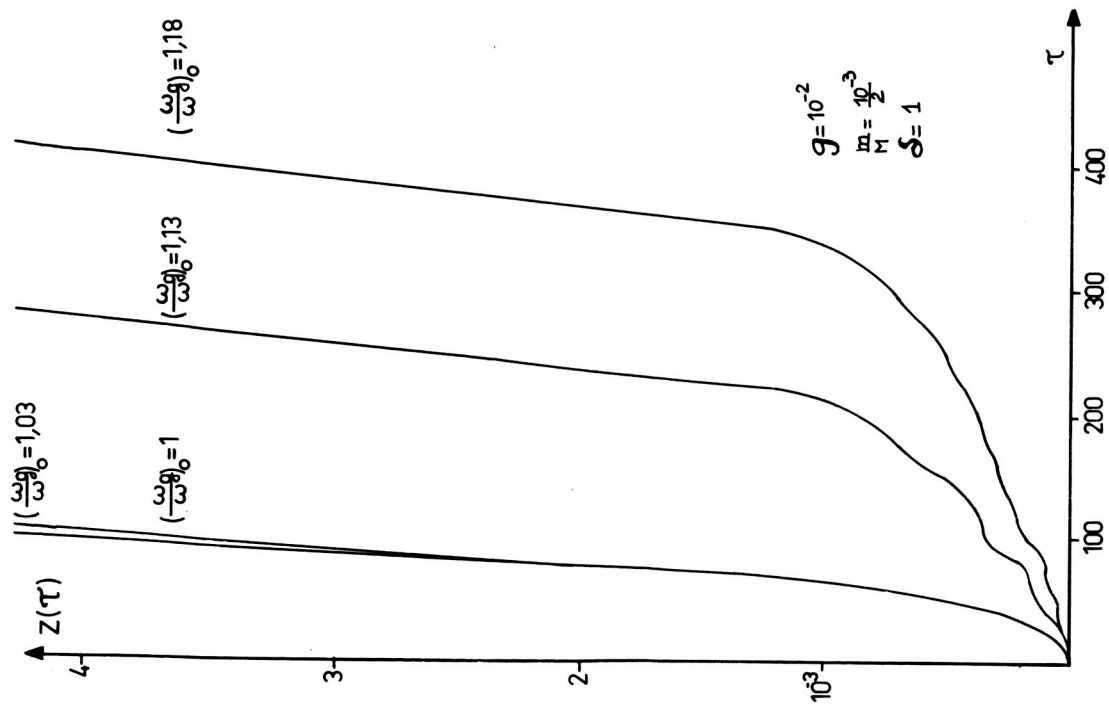


Figure 4.- The axial velocity as a function of the injection position.

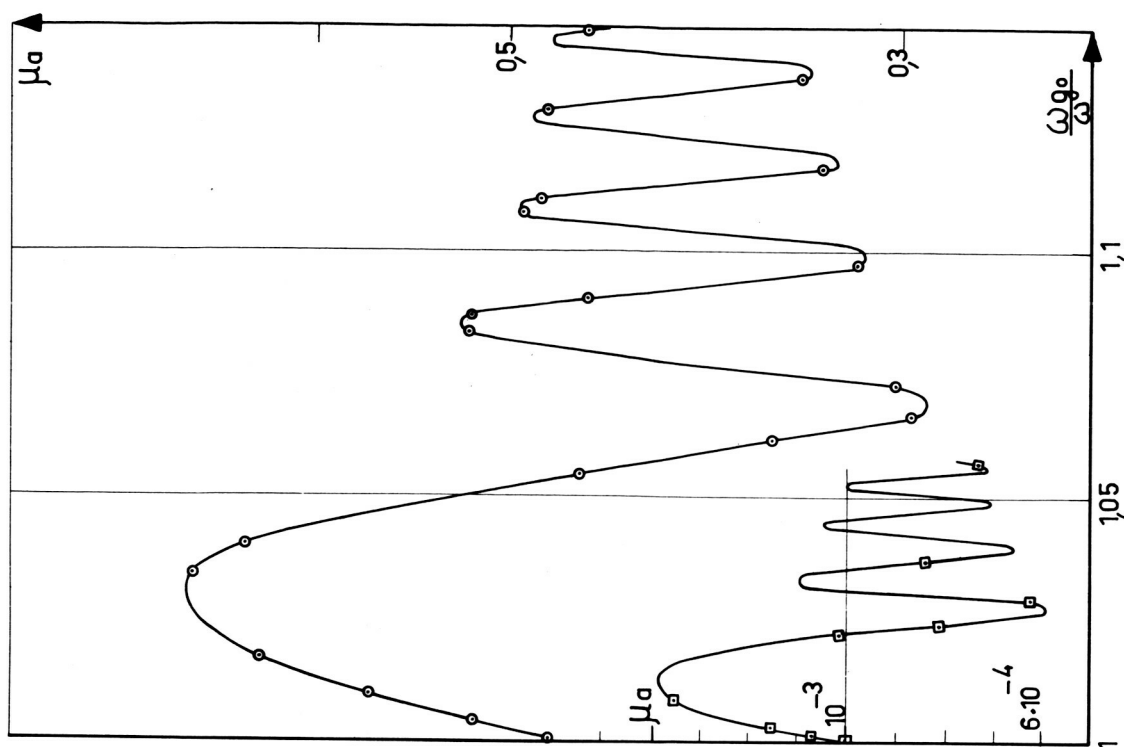


Figure 5.- The asymptotic value of the magnetic moment as a function of the injection position.

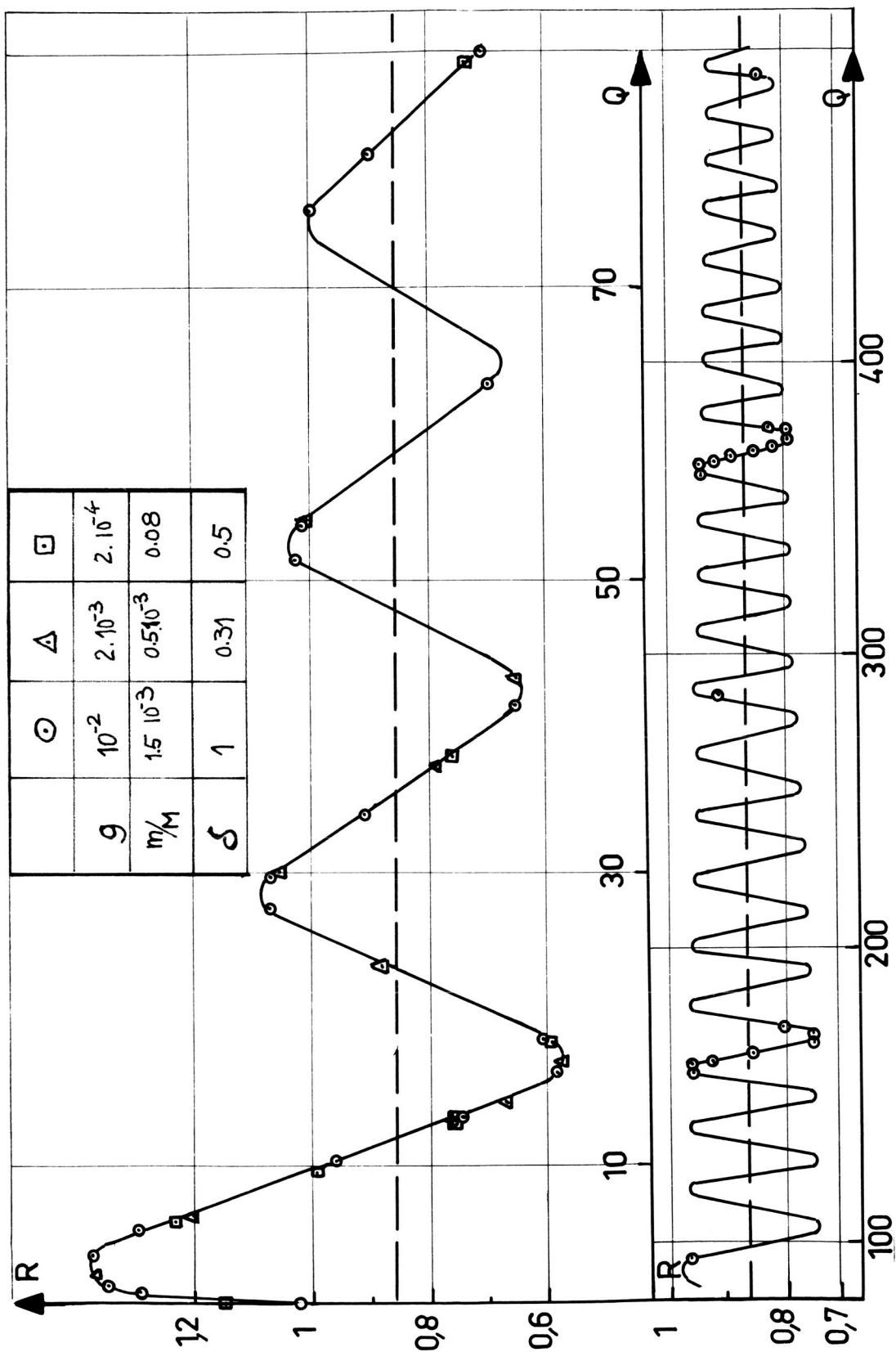


Figure 6.- The dependence of $R = \mu_a(b)/\mu_a(b=1)$ upon Q .

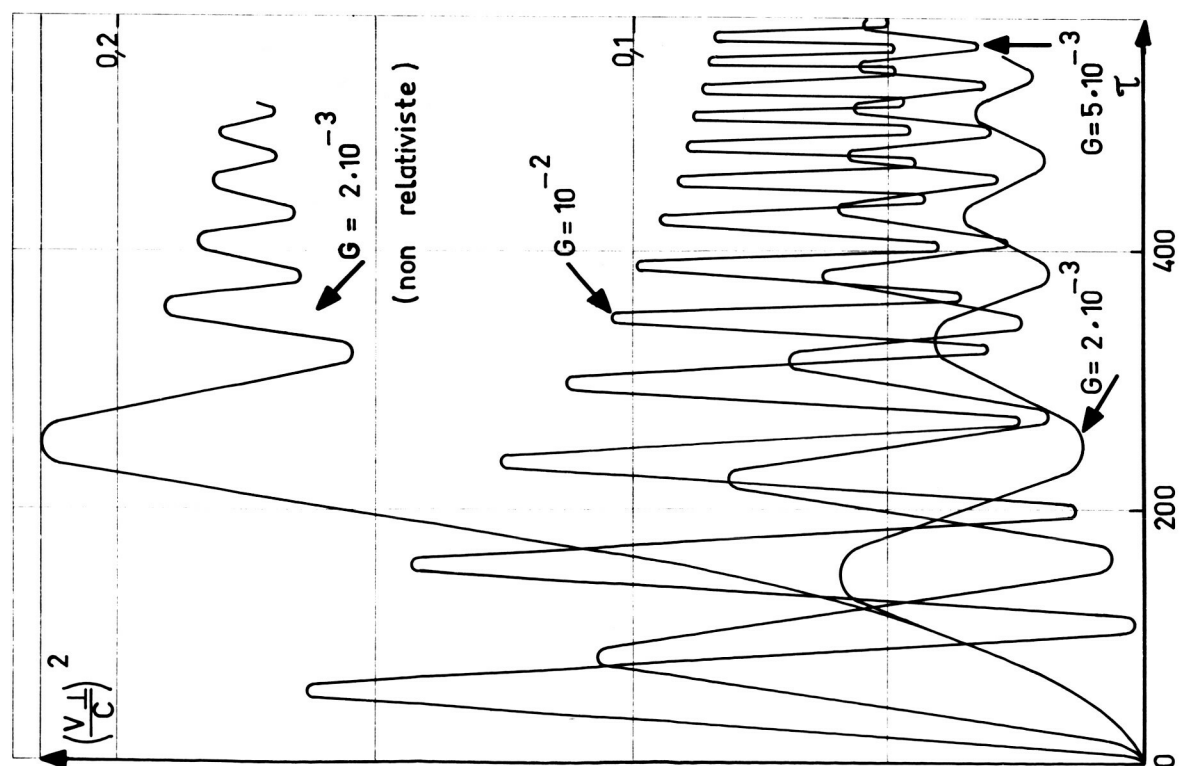


Figure 7.- Relativistic effects on the perpendicular velocity.

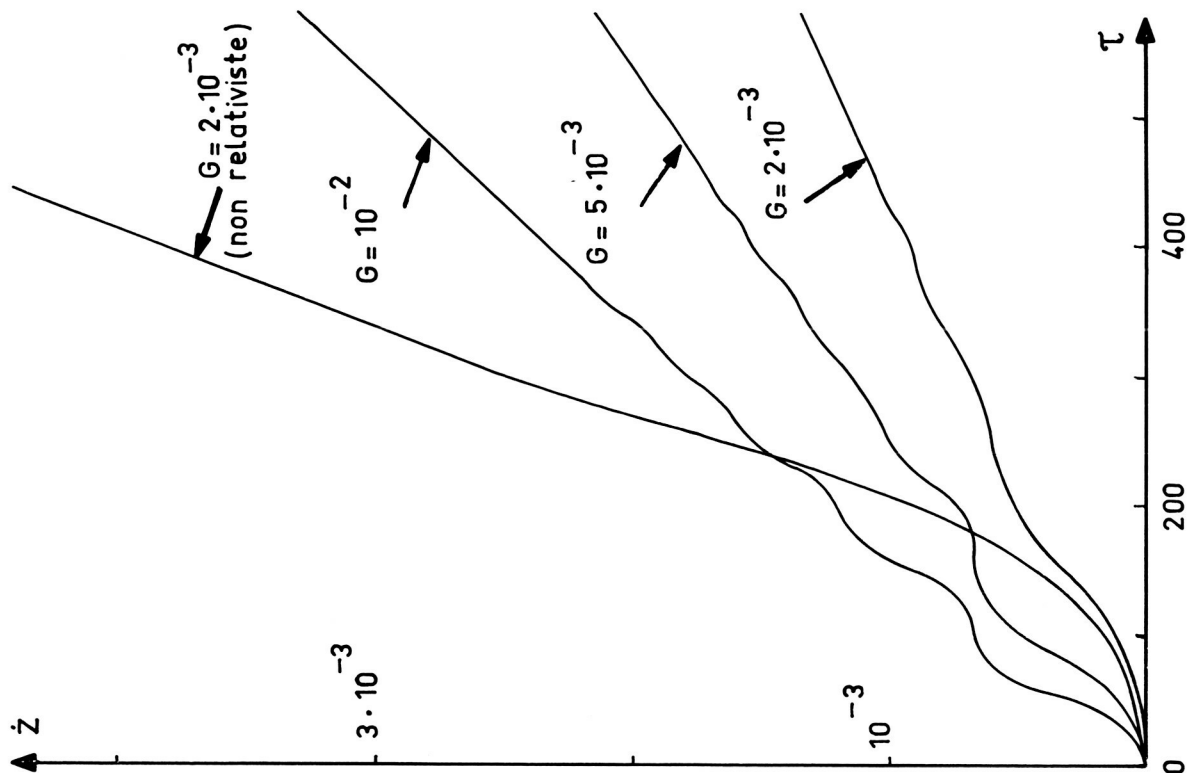


Figure 8.- Relativistic effects on the axial velocity.

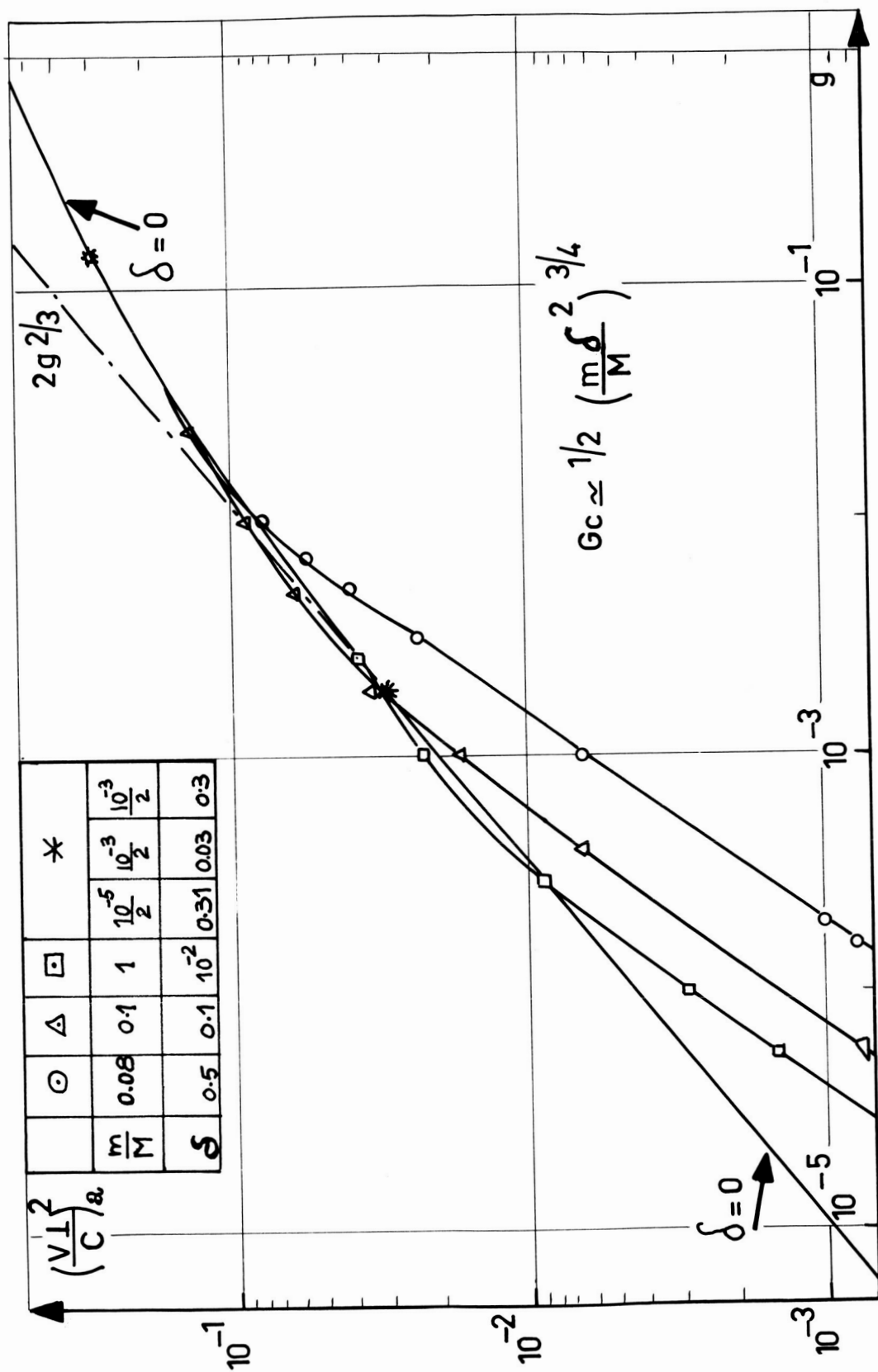


Figure 9.- Asymptotic values of $(v_{\perp}/c)^2$ versus g .

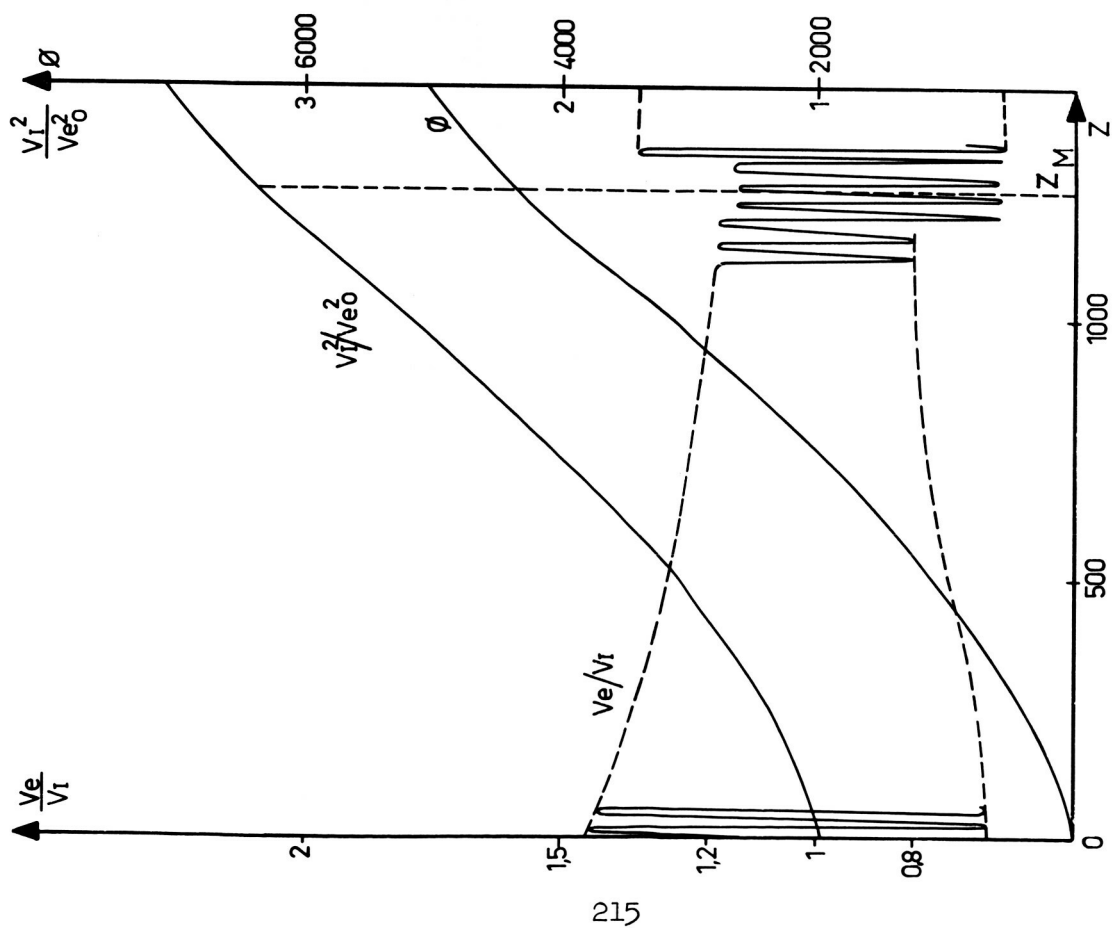


Figure 10.- Optimum ion acceleration in the resonance region.

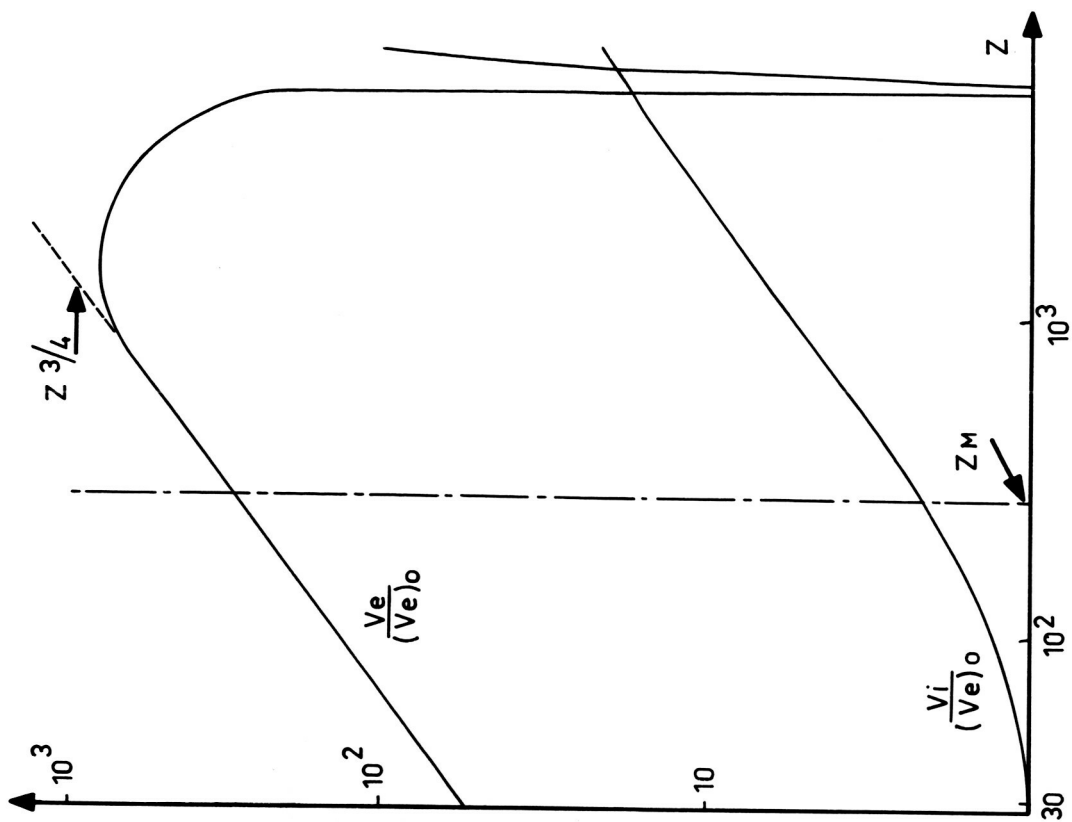


Figure 11.- Negligible electrostatic interaction in the resonance region.

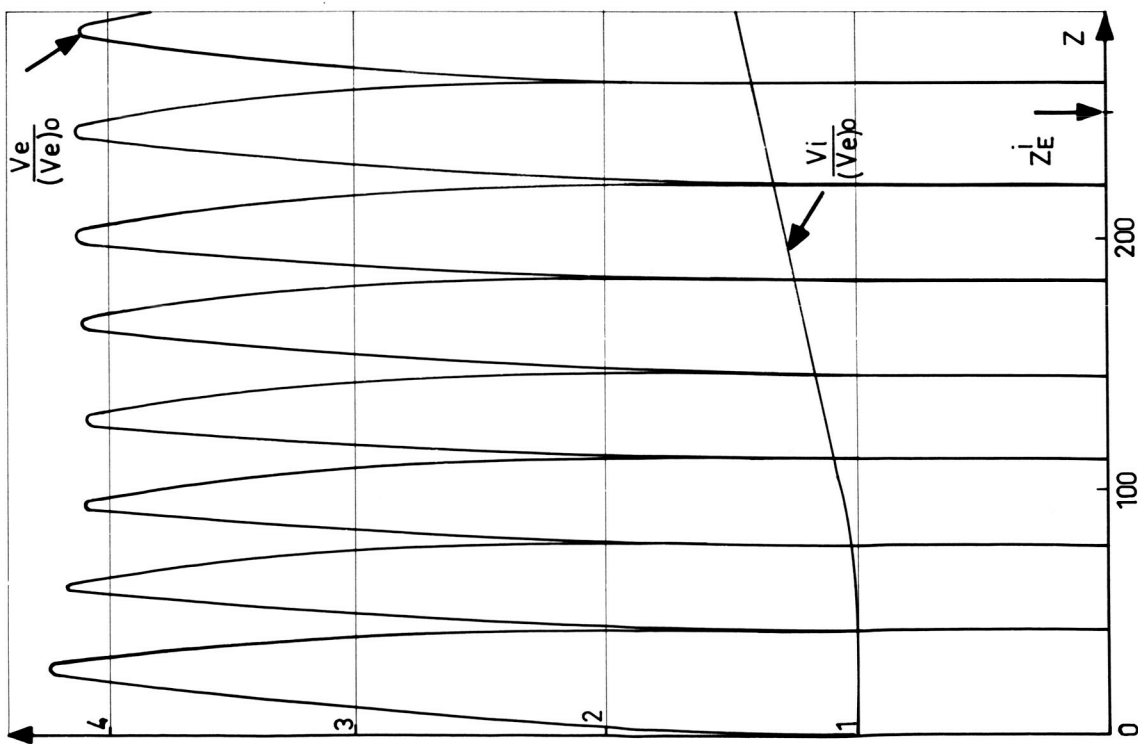


Figure 12.- The appearance of shock waves in the resonance region.

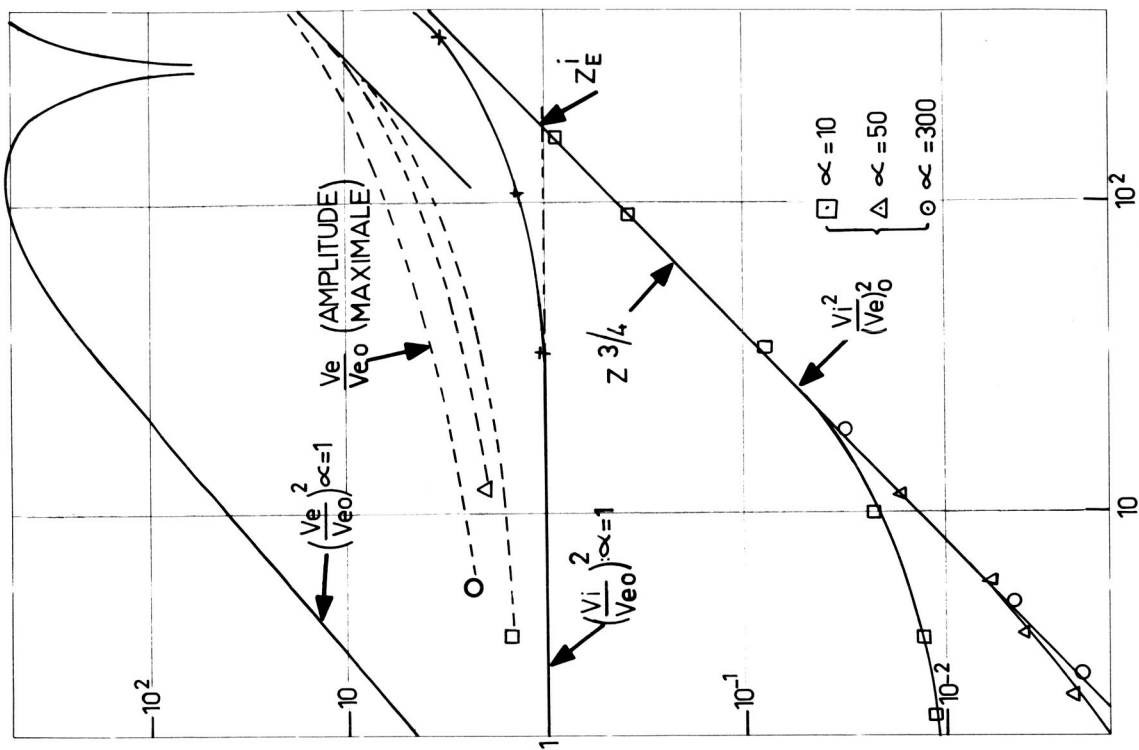


Figure 13.- The space charge field acceleration as a function of the initial electron and ion velocities.

Computer Simulation of the Beam-Plasma Interaction*

J. A. Davis and A. Bers

Department of Electrical Engineering and
Research Laboratory of Electronics
Massachusetts Institute of Technology
Cambridge, Massachusetts

ABSTRACT

We are studying the effects of longitudinal plasma density gradients on the steady-state nonlinear beam-plasma interaction, by computer modeling with a finite diameter beam in an infinite plasma. The gradients and finite beam diameter seem necessary to explain the relatively narrow collected beam velocity distribution observed experimentally. For a given plasma density profile and beam density, the interaction becomes less intense as the total plasma density increases.

*This work was supported by the National Science Foundation (Grant GK-1165).

INTRODUCTION

We are studying the steady-state nonlinear beam-plasma interaction. Our goal is to explain experimental measurements of the collected beam velocity distribution by computer modeling. The beam-plasma system is represented by an electron beam disk model injected into an infinite plasma whose response remains linear. Attempts to model the interaction with a homogeneous plasma produced much wider velocity spreads than observed. The introduction of longitudinal (i.e. along the beam flow direction) density gradients into the model has allowed considerably better agreement with experiment.

The experimental apparatus is described in Ref. 1. The Helmholtz coil generated magnetic field is mirror shaped with a mirror ratio of three. We typically use a pressure of 10^{-4} Torr of H_2 , which gives an electron-neutral collision frequency ν of about 10^6 /sec. The plasma is generated by the unmodulated electron beam.

The experimental parameters are:

$$\omega_p = 2\pi \times 1.5 \times 10^{10} \text{ rad/sec}$$

$$\omega_{pb} = 2\pi \times 1.25 \times 10^9 \text{ rad/sec}$$

$$\omega_c = 2\pi \times 1.4 \times 10^9 \text{ rad/sec}$$

$$V_B = 7 \text{ kV}$$

$$I_B = .6 \text{ amps}$$

$$T_- = 4 \text{ eV}$$

$$b = .125 \text{ cm}$$

$$L = 40 \text{ cm}$$

ω_p is the electron plasma frequency, ω_{pb} is the beam plasma frequency, ω_c the electron cyclotron frequency, V_B the beam voltage, I_B the beam current, T_- the plasma electron temperature, b the beam radius, and L the interaction length. By using the velocity analyzer shown in Fig. 1, we obtained the collected beam velocity distribution shown in Fig. 2.

HOMOGENEOUS PLASMA AND ONE-DIMENSIONAL BEAM

We first attempted to model the beam with sheets, but the plasma was assumed cold and linear, and hence was treated analytically. A sheet with charge per unit area Q moving through the plasma creates a wake given by

$$E(z, t) = \frac{-Q}{\epsilon_0} \sqrt{1 + \nu^2 / 4\omega_0^2} \exp \left[-\frac{\nu}{2}(t - t_1(z)) \right] \cos \left\{ \omega_0[t - t_1(z)] - \tan^{-1} \frac{\nu}{2\omega_0} \right\} u_{-1}[t - t_1(z)], \quad (1)$$

where u_{-1} is the unit step function, $\omega_0 = \omega_p \sqrt{1 - \nu^2 / 4\omega_p^2}$, ν = the electron-neutral collision frequency, and $t_1(z) =$

the time the sheet crosses the plane z . Since the plasma is assumed linear, the wakes can be superposed. The details of the model are given in Appendix II. The first computer experiments ignoring collisions showed unreasonably large beam-velocity spreads and fields for which the plasma oscillations were nonlinear. Introducing a large collision frequency ($\nu = .2 \omega_0$), reduced the magnitude of the electric fields. The results are shown in Fig. 3. Even under these conditions the fields (Fig. 3) are large enough to cause a beam velocity spread far exceeding the experimentally observed one. The beam was 2 % velocity modulated at ω_0 , at injection. A large charge bunch forms at the position (150) of initial beam overtaking that is synchronous with the traveling electric field in such a manner as to maximally decelerate the beam. Beyond overtaking two waves are clearly seen. One has a phase velocity about equal to that of the wave before overtaking. The other wave is synchronous with clumps of beam charge at low velocity, and is very effective at slowing these clumps until downstream the beam is highly dispersed in velocity.

If the plasma had a longitudinal plasma density gradient, the large beam charge bunch formed at the point of overtaking would drive the plasma at other than the local plasma frequency, i.e. off resonance. Hence the electric field there would be much less than in the uniform case. An inhomogeneous plasma would also be expected to disrupt the slow phase velocity wave that formed beyond overtaking and dispersed the beam in velocity. This wave

formed because the wakes of clumps of beam charge that pass a plane at times $2\pi/\omega_p$ apart add coherently. If ω_0 is a function of distance, this condition cannot be maintained over an appreciable distance, and the wave will be broken up.

ONE-DIMENSIONAL BEAM AND PLASMA WITH DENSITY GRADIENTS ALONG THE BEAM

We introduce a linear longitudinal plasma density gradient, described by

$$\omega_p^2(z) = \omega^2 + az. \quad (2)$$

The plasma is now assumed lossless ($\nu = 0$). "a" is chosen to be $\pi\omega_{p0}^2/L$, where ω_{p0} corresponds to the peak density of a sinusoidal density distribution in z . We assume a fixed frequency of excitation $\omega^2 = 0.15 \omega_{p0}^2$, corresponding to the plasma frequency at the position of beam injection.

The plasma is cold, lossless, linear and treated analytically. The beam is 0.1 % velocity modulated at ω . In the appendix we derive the linearized theory for a beam-plasma interaction with a gradient described by Eq. (2). We find the first order beam velocity grows as $I_0(Bz^{1/2})$, and the electric field is proportional to $I_1(Bz^{1/2})/z^{1/2}$, where I_0 and I_1 are modified Bessel functions, $B = 2a\omega_{pb}/v_0 a^{1/2}$ and v_0 is the beam velocity. This linear theory is well matched by the results of the computer experiments shown in Figs. 4 and 5, where the linear theory

results are shown by the curves labeled v_{bIII}/v_{ob} and qE_{III}/m . We note (see Appendix I) that for a positive density gradient the variables can only grow beyond the plane where $\omega = \omega_p(z)$. Hence by the time overtaking occurs, the beam finds itself in a region where $\omega < \omega_p(z)$. The large beam charge bunches formed at the plane of overtaking (Figs. 4 and 5 in the vicinity of 150 distance units) drive the plasma off resonance, so the response is quite finite.

In these results the electric fields remain quite finite, but the assumption of plasma linearity is only marginally satisfied ($v_p/v_o \approx .18$), and the beam velocity spread still exceeds that of the experiment.

FINITE DIAMETER BEAM AND ONE-DIMENSIONAL PLASMA WITH DENSITY GRADIENT

To obtain better quantitative agreement with experiment, we introduce disks to represent the beam. The fields generated by a disk moving through a plasma have been found^{2,3} for a uniform plasma and a constant velocity disk. There are two fields, a wake field and a nonoscillatory field. The acceleration on another disk due to the wake field is:

$$a(z,t) = \frac{-Q^2}{M\epsilon_o} [1 - 2I_1(\alpha) K_1(\alpha)] \cos \left[\omega_p \left(t - \frac{z}{v_o} \right) \right] u_{-1} \left(t - \frac{z}{v_o} \right), \quad (3)$$

where M is the disk surface mass (kg/m^2), $\alpha = \omega_p b/v_o$, and K_1 is the modified Bessel function of second kind. The acceleration on another disk due to the nonoscillatory field ahead of the disk is:

$$a(z,t) = \frac{Q^2}{M\epsilon_o} \int_0^\infty \frac{dx \, x \, J_1^2(x) \exp[-x\Delta z/b]}{x^2 + \alpha^2}, \quad (4)$$

where Δz is the disk separation. The nonoscillatory field behind the disk is the mirror image of the field ahead.

We want to allow for variations in $\omega_p(z)$ and disk velocity. We do this approximately as follows. To calculate the wake field at a plane z we use Eq. (3), with the local $\omega_p(z)$ and the velocity the disk has when it passes z . To calculate the nonoscillatory field at a plane z , we use the local $\omega_p(z)$ and the present velocity of the disk. The computer results are shown in Fig. 6.⁵ The beam is velocity modulated at $z = 0$ over a frequency band extending from $(.15)^{1/2} \omega_{po}$ to $.5 \omega_{po}$. This simulates the effects of plasma fluctuations of energy density $n\kappa T$. The plasma frequency in this case varies spatially as

$$\omega_p^2(z) = \omega_{po}^2 \sin(.15 + az). \quad (5)$$

The plasma remains quite linear ($v_p/v_o \approx \rho_p/\rho_{op} \approx 0.03$).

The velocity spread shown is comparable with experiment, but the interaction length shown is only 20 % that of the experiment.

DISCUSSION

We have found that the introduction of a longitudinal density gradient enables us to obtain the relatively narrow beam velocity spread observed experimentally, and allows us to justify the assumption of plasma linearity.

We can obtain estimates of the linearity conditions by manipulation of the one-dimensional equations in the appendix. Near overtaking,

$$(\rho_p/\rho_{op}) \approx (\omega_{pb}^2 \omega_p^2(z)/\omega^2 az)(\rho_b/\rho_{ob}) \quad (6)$$

$$(v_p/v_{ob}) \approx (\omega_{pb}^2/az)(\rho_b/\rho_{ob}) \quad (7)$$

$$(v_b/v_{ob}) \approx (\omega_{pb}/az)(\rho_b/\rho_{ob}) \quad (8)$$

$$\epsilon_0 |E|^2 / n_{ob} m v_{ob}^2 \approx [\omega^2 \omega_{pb}^2 / (az)^2] (\rho_b/\rho_{ob})^2 \quad (9)$$

Near overtaking, ρ_b/ρ_{ob} exceeds one. Then, for our parameters, ρ_p/ρ_{op} and v_p/v_{ob} are only a few per cent, and the beam velocity has a relatively small spread.

From Eq. (9), we note that as the plasma density increases, the electric field becomes weaker at the point of overtaking (ω^2 and "a" increase, but ω^2/a is

constant if the density profile is constant). Beyond overtaking, the beam nonlinearities seem to keep the electric field from growing appreciably (Fig. 6). In a beam generated plasma the ionization is done primarily by plasma electrons,⁴ which obtain their energy from the electric field. Hence, for a given beam density and confinement scheme, this weakening of the interaction may determine the final plasma density. These details of the beam generated plasma will require further study of the energy transfer mechanisms from the beam to the plasma electrons.

ACKNOWLEDGEMENT

This work was done in part at the M.I.T. Computation Center and in part using the facilities of Project MAC, at M.I.T. The assistance of the Computation Group of the Research Laboratory of Electronics at M.I.T. is also gratefully acknowledged.

APPENDIX I: LINEARIZED BEAM-PLASMA INTERACTION WITH A LINEAR PLASMA DENSITY GRADIENT

We consider a cold, lossless, one-dimensional plasma with no magnetic field, whose density is given by

$$\omega_p^2(z) = \omega^2 + az. \quad (A1)$$

We do a Fourier transform in time, but not in space, on the linearized force, conservation, and Poisson's equations, and obtain:

$$j\omega m v_p = qE \quad (A2)$$

$$j\omega m v_b + m v_o \frac{\partial v_b}{\partial z} = qE \quad (A3)$$

$$\frac{\partial}{\partial z} [\rho_{op}(z) v_p] = -j\omega \rho_p \quad (A4)$$

$$\frac{\partial}{\partial z} [\rho_{ob} v_b + \rho_b v_o] = -j\omega \rho_b \quad (A5)$$

$$\epsilon_o \frac{\partial E}{\partial z} = \rho_p + \rho_b. \quad (A6)$$

These equations can be combined to give a form of Bessel's equation,

$$\begin{aligned}
& az v_o \frac{\partial^2 v_b}{\partial z^2} + [av_o + j2\omega az] \frac{\partial v_b}{\partial z} \\
& + [j\omega a - (\omega^2/v_o)(az + \omega_{pb}^2)]v_b = 0.
\end{aligned} \tag{A7}$$

For $z < 0$

$$v_{bI} \sim \exp(-j\omega z/v_o) J_o[B(-z)^{1/2}] \tag{A8}$$

$$v_{bII} \sim \exp(-j\omega z/v_o) Y_o[B(-z)^{1/2}], \tag{A9}$$

and for $z > 0$

$$v_{bIII} \sim \exp(-j\omega z/v_o) I_o[Bz^{1/2}] \tag{A10}$$

$$v_{bIV} \sim \exp(-j\omega z/v_o) K_o[Bz^{1/2}], \tag{A11}$$

where

$$B = 2\omega\omega_{pb}/v_o a^{1/2}. \tag{A12}$$

If " a " < 0 (a decreasing density gradient) the solutions for $z > 0$ and $z < 0$ are interchanged. The remaining variables can be found from Eqs. (A2-A6). In particular

$$E_{III} \sim (B m v_o / 2qz^{1/2}) \exp(-j\omega z/v_o) I_1(Bz^{1/2}) \tag{A13}$$

The physical significance of mode II is unknown, since we have not been able to excite it in computer experiments. With the addition of collisions the resonance in ν_{bII} washes out as $\ln(\nu)$, but $E_{II}|_{z=0}$ varies only as $1/\nu$.

APPENDIX II: DETAILS OF THE COMPUTER MODEL

The wake due to a sheet moving through a cold plasma is given in Eq. (1). We note that the wake at any plane z is cosinusoidal in time, with a phase determined only by the time the sheet passed z . Since the wakes are all cosinusoidal at the same frequency, they can be combined into one cosine. We calculate the magnitude and phase of oscillations at discrete positions defined by cell points $0.2 v_0/\omega_{po}$ apart, which gives us about 30 cell points per wavelength. We interpolate with a second order polynomial the fields between three cell points at a time. In interpolation, we include only the fields of those sheets which have passed all three cell points. The fields due to sheets within the cell points are calculated separately, since the field discontinuities caused by the sheets would invalidate the interpolation. This involves keeping track of three separate sets of magnitudes and phases per cell point. One set includes the fields of all the sheets that have passed the cell point, another set includes the fields of only those sheets that have passed the cell point one beyond the considered cell point, and the third set includes only those fields due to sheets which have passed the second cell point beyond the considered cell point. Since we only need to know when the sheet passed a plane to determine the fields, we interpolate passing times from the sheet positions at the last three incrementation times.

We start calculating the trajectory of the sheet farthest from the gun first. When crossings occur, the

positions and velocities are corrected by approximating the cosine in the wake term as one, and estimating the crossing time from the uncorrected trajectories.

In the early runs we used the Milne method to calculate the trajectories and obtained energy conservation within 5 %. Later we used the Runge-Kutta method and obtained energy conservation within 0.5 %.

REFERENCES

1. H. Y. Hsieh, Ph.D. Thesis, Dept. of Electrical Engineering, M.I.T., (1964).
2. R. W. Gould and M. A. Allen, 5^e Congres International. Tubes pour Hyperfrequences, 445 (1964).
3. R. W. Gould, Microwave Associates, High Power Beam-Plasma Amplifier Rep. No. 2, p. 8 (1963).
4. W. D. Getty and L. D. Smullin, J.A.P., 34, 3421 (1963).
5. In this calculation we let the region $0 < z < 200$ approach a steady state, collecting sheets at $z = 200$, before letting sheets excite fields beyond $z = 200$. Then we allowed sheets to reach $z = 250$ before collecting. After a steady state was approached again, sheets were allowed to reach $z = 300$. This was done to avoid the large transient fields that would be excited downstream by initial beam overtaking, which occurs far downstream early in the transient buildup.

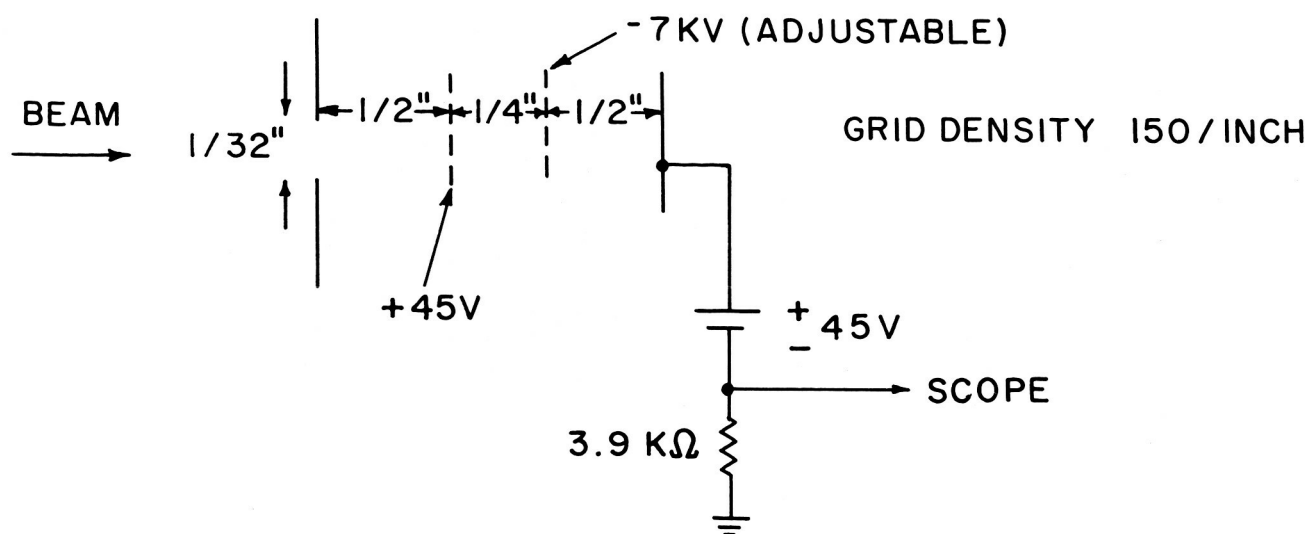


Figure 1.- Beam velocity analyzer.

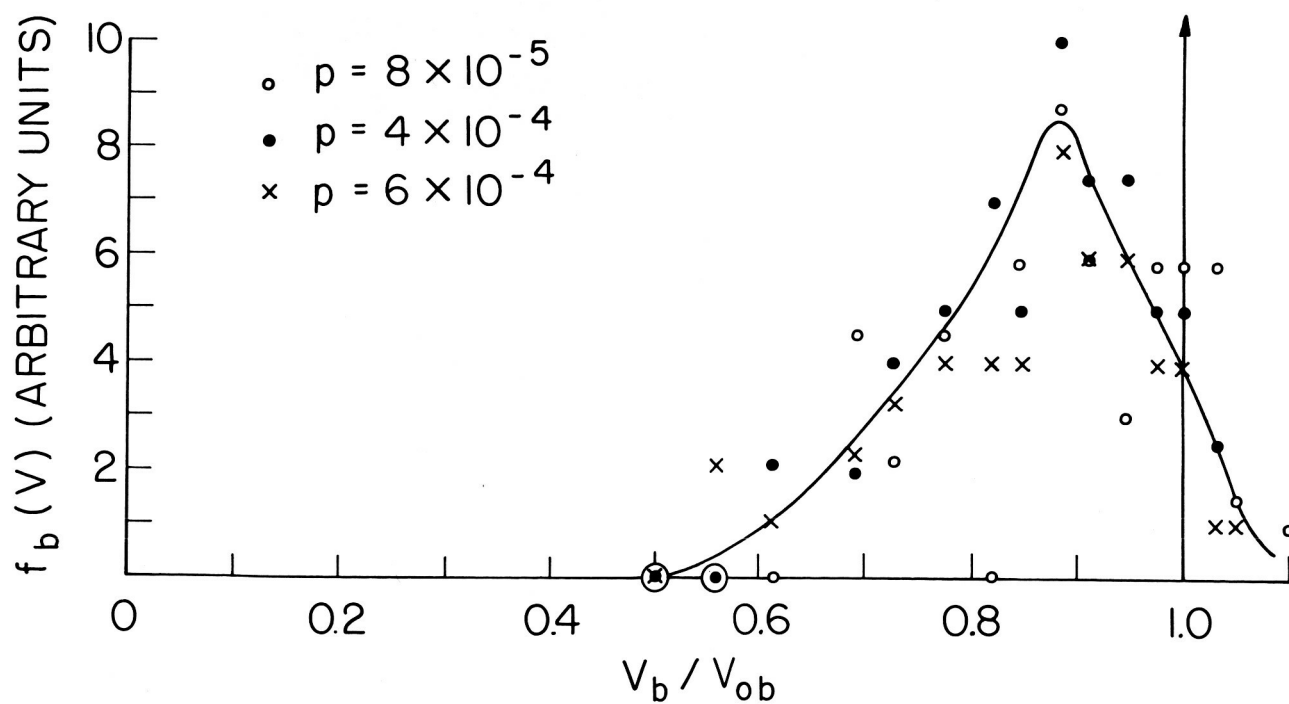


Figure 2.- Collected beam velocity distribution.

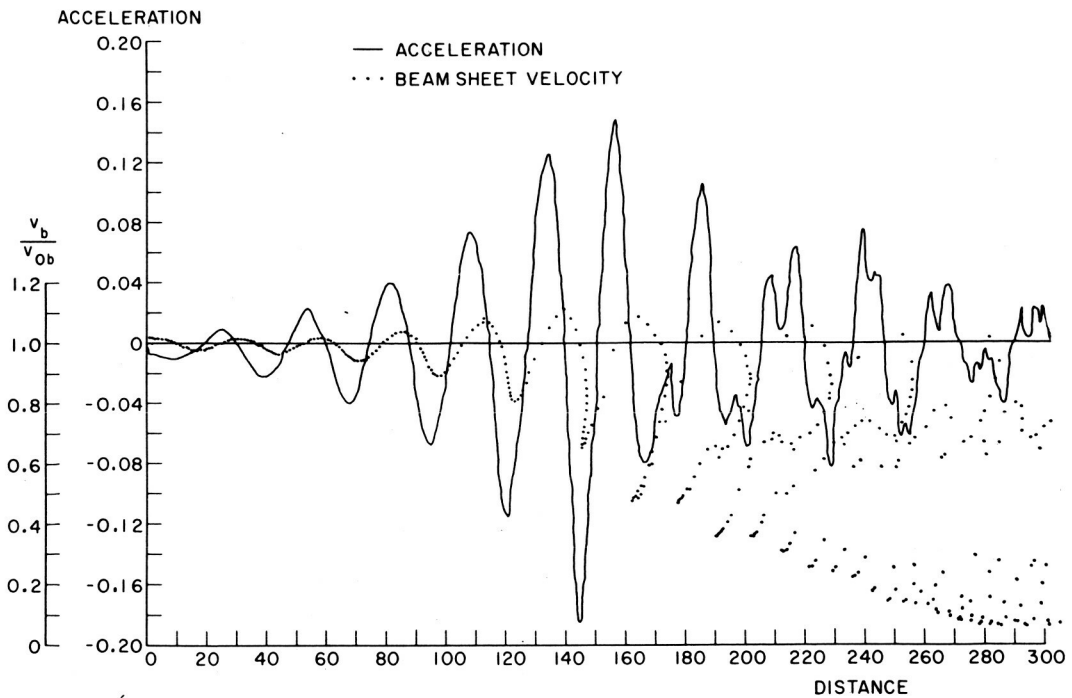


Figure 3.- Snapshot of sheet velocity and test particle acceleration vs. distance. Times are normalized to ω_0^{-1} , distances to $.2v_0\omega_0^{-1}$. This is a homogeneous plasma with $v = .2\omega_0$.

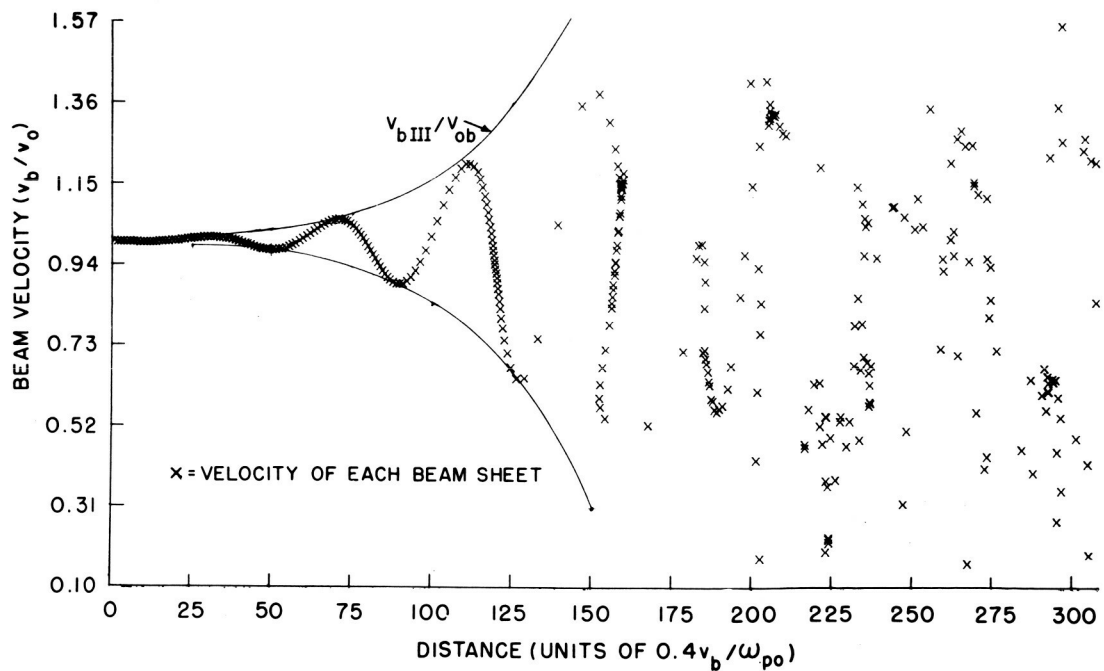


Figure 4.- Snapshot of beam sheet velocity with plasma density gradient $\omega_p^2 = .15 + .001z$. Times are normalized to ω_{p0}^{-1} , distances to $.4v_0\omega_{p0}^{-1}$.

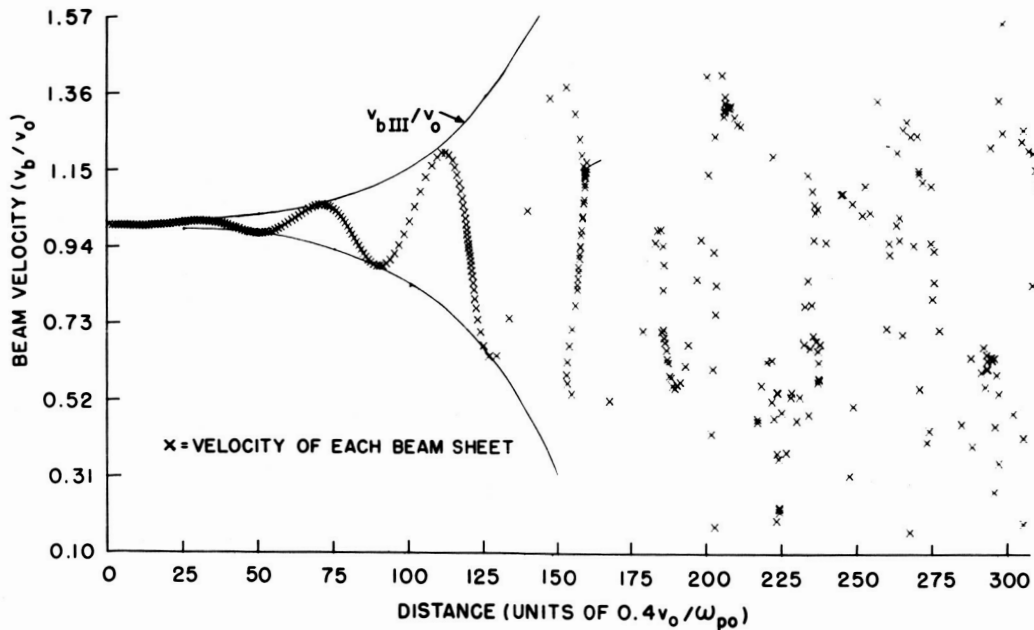


Figure 5.- Snapshot of test particle acceleration, with plasma density gradient.

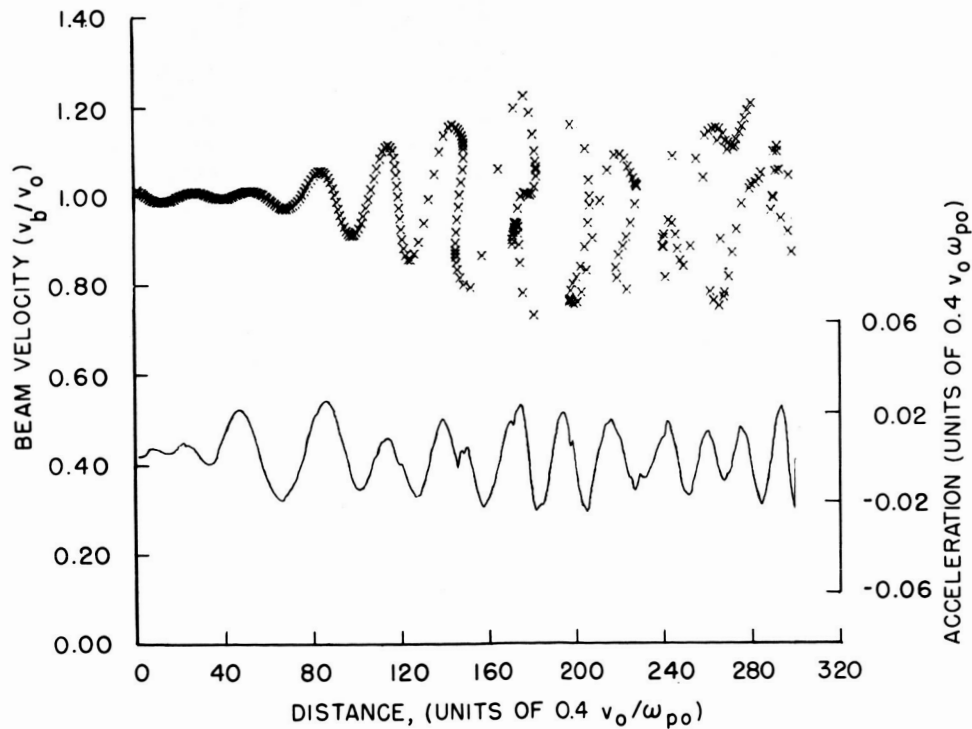


Figure 6.- Snapshot of beam disk velocity vs. distance and a snapshot of test disk acceleration vs. distance, with plasma density gradient. This is the same normalization as figure 4.

NUMERICAL SOLUTION FOR 1.5-DIMENSIONAL, TIME-DEPENDENT
MAGNETOHYDRODYNAMIC PROBLEMS

by

Klaus Hain

Laboratory for Theoretical Studies
NASA Goddard Space Flight Center
Greenbelt, Maryland

In some important problems such as θ -Pinches with parallel fields (after the first phases of implosion or solar flares), the overall structure is governed by a strong magnetic field. The Alfvén speed V_A across the field lines is so high that the transversal time $t = R/V_A$, where the radius R of the plasma is small compared with a characteristic time t_C of the system, so that a quasiequilibrium can be reached in the time interval t_C . The dimension perpendicular to the field is therefore counted as .5 dimension. In contrast, the full magnetohydrodynamic equations apply parallel to the field lines. In particular the behavior of shockwaves parallel to the magnetic field is studied here under various conditions.

The geometry is as follows: axial symmetry perpendicular to the field-lines with a boundary for $t = 0$ at R_0 . The initial conditions for $t = 0$ define an equilibrium. The time dependence is brought in by varying the magnetic field at the plasma boundary with time and as a function of z .

Two cases are studied here:

1. θ Pinch. A conducting wall is assumed at $R = R_C$. The magnetic is then compressed at one end with strength δB_B and a frequency ω . Also

a damping time τ is specified such that $B \sim e^{-t/\tau}$.

2. Simulation of the behavior of solar flares, which are assumed to have the structure of arcs consisting of magnetic fieldlines, produced by ring currents at the bottom. The following approximations are made: initially a constant magnetic field is assumed. The time dependent behavior is simulated by compressing the magnetic field. The fieldlines become weaker if one assumes that the flux containing walls to recede further as they are further away from the current carrying coils.

To give a good indication of how the plasma behaves under those conditions the results will be shown in movies.

The computations for the θ pinch show that no strong shock waves (Mach number < 2) are produced by compressing the field, unless the field becomes so strong as to confine the plasma very strongly or if the distance to the wall becomes very small.

As for the second case, the solar flares, it shows that a strong and long lasting field is required to achieve an appreciable amount of change in the geometry.

In a forthcoming paper the properties of injection of plasma and the eventual reaching of a steady state including gravity will be studied.

INTRODUCTION

In many problems the magnetic field determines the main structure of the plasma. Dynamics in these cases can be studied by assuming quasistationarity perpendicular to the magnetic field, or expressed in another way: the time $t_A = R/v_A$, where R is the extent of the plasma perpendicular to the field lines, and v_A , the Alfen velocity, is small compared to the transversal time t_C (or another characteristic time); i.e.

$$t_C = L/c \gg t_A$$

where L is the length of the cylinder and C the velocity of sound parallel to the magnetic field.

Here for the numerical computation axial symmetry is assumed. The magnetic field is initially parallel to the axis. The main advantage of the assumption of quasistationarity and axial symmetry is that one needs only relatively few space points in r - direction, so that the computation is reasonably fast, but the computer program can be extended to take into account any shape perpendicular to the field lines.

As the magnetic field is very strong, the field lines are taken as one set of (moving) coordinates. This excludes antiparallel field lines with points of zero magnetic fields.

In the following the magnetohydrodynamic equations are set up in a moving general coordinate system. Then the numeric scheme is discussed briefly. The results show how the strength of shock waves parallel to the magnetic field depends on the mirror ratio and the compression ratio. The results of the numerical computations are also represented in a movie to give an indication of the dynamical processes which may occur in a plasma.

MAGNETOHYDRODYNAMIC EQUATIONS IN A MOVING COORDINATE SYSTEM

The following assumptions are made here:

1. Assumption of quasistationarity across the field lines.

$$t_A = R/\sigma_A \ll t_c = L/\sigma_c \quad (1)$$

2. Infinite electrical conductivity is assumed, heat conductivity is neglected.

(But it would not be difficult to introduce heat conductivity parallel to the magnetic field).

3. Shocks parallel to the magnetic field are treated by the method of v. Neumann.

4. Axial symmetry perpendicular to the magnetic field lines, finite cylinder of length L.

5. $T_i = T_e$ The electron temperature is set equal to the ion temperature. This implies that the plasma is so dense that the temperature equalization time is short compared to t_c .

6. Coordinate system: Unit vectors \vec{e}_1, \vec{e}_2 for the coordinates η_1, η_2 such that

$$\vec{B} = \vec{e}_1 B \quad \text{and the line element} \quad ds^2 = h_1^2 d\eta_1^2 + h_2^2 d\eta_2^2 + r^2 d\varphi^2 \quad (2)$$

\vec{e}_1 is the unit vector along the magnetic field, \vec{e}_2 is the unit vector perpendicular to \vec{e}_1 . Coordinates are η_1 in field direction, η_2 perpendicular to it, with the corresponding distances h_1, h_2 .

The magnetohydrodynamical equations are then developed in covariant form, where $\vec{\nabla}$ is the covariant differential operator.

$$\frac{\partial \rho}{\partial t} + \vec{\nabla}(\rho \vec{\sigma}) = 0 \quad (3)$$

$$\rho \left(\frac{\partial \vec{\sigma}}{\partial t} + (\vec{\sigma} \vec{\nabla}) \vec{\sigma} \right) + \vec{B} \times \vec{j} + \vec{\nabla} p = 0 \quad (4)$$

$$\frac{\partial p}{\partial t} + (\vec{\sigma} \vec{\nabla}) p + \gamma p (\vec{\nabla} \vec{p}) = 0 \quad (5)$$

$$\frac{\partial \vec{B}}{\partial t} + \vec{\nabla} \times (\vec{B} \times \vec{\sigma}) = 0 \quad (6)$$

$$(\vec{\nabla} \vec{B}) = 0 \quad (7)$$

with

$$\vec{j} = \vec{\nabla} \times \vec{B} \quad (8)$$

$$\vec{\sigma} = \vec{e}_1 \sigma_1 + \vec{e}_2 \sigma_2 \quad (9)$$

where ρ is the density, \vec{v} the velocity, p the pressure and γ the ratio of the specific heats

$$\gamma = 1 + 2/f \quad (10)$$

where f is the number of degrees of freedom. $f = 3$ or $\gamma = 5/3$ is assumed here, which is consistent with the assumption (5) for a dense plasma.

For the coordinate system specified,

$$\vec{\nabla} \vec{B} = \frac{1}{r h_2 h_1} \frac{\partial}{\partial \eta_1} (h_2 r B) \quad (11)$$

Therefore, if one defines

$$h_2 = \frac{1}{rB} \quad (12)$$

the eq. (11) is automatically fulfilled. γ_2 is then the magnetic flux so that $\gamma_2 = \text{const.}$ characterizes the flux tubes.

Substituting $\vec{B} = \vec{e}_1 B$ into eq. (6) gives the two eqs.:

$$\frac{\partial \vec{B}}{\partial t} + \frac{1}{h_2 r} \frac{\partial}{\partial \gamma_2} (r B v_2) = 0 \quad (13)$$

for flux conservation, and

$$\frac{\partial \vec{e}_1}{\partial t} - \vec{e}_2 \frac{h_2}{h_1} \frac{\partial}{\partial \gamma_1} \left(\frac{v_2}{h_2} \right) = 0 \quad (14)$$

for the change of the direction of the magnetic field, which depends only on the change of v_2 in the direction \vec{e}_1 .

With the definition of the operator

$$\frac{\delta}{\delta t} = \frac{\partial}{\partial t} + v_2 \nabla_2 \quad (15)$$

(∇_2 is the covariant operator using eq. (12).) Eq. (13) can be rewritten in the form

$$\frac{\delta h_2}{\delta t} - \frac{1}{h_2} \frac{\partial v_2}{\partial \gamma_2} = 0 \quad (16)$$

and eq. (14) then becomes

$$\frac{\delta \vec{e}_1}{\delta t} - \vec{e}_2 \frac{1}{h_1} \frac{\partial v_2}{\partial \gamma_1} = 0 \quad (17)$$

With the definition (15) one obtains

$$\left(\frac{\delta}{\delta t} + \frac{v_1}{h_1} \frac{\partial}{\partial \eta_1} \right) \rho + \operatorname{div} \vec{v} \rho = 0 \quad (18)$$

$$\left(\frac{\delta}{\delta t} + \frac{v_1}{h_1} \frac{\partial}{\partial \eta_1} \right) p + f \operatorname{div} \vec{v} p = 0 \quad (19)$$

where

$$\operatorname{div} \vec{v} = \frac{1}{r h_2 h_1} \left(\frac{\partial}{\partial \eta_1} (h_2 r v_1) + \frac{\partial}{\partial \eta_2} (h_1 r v_2) \right) \quad (20)$$

Along the unit axes of the velocity vector, the time changes can be written as

$$\begin{aligned} \frac{\delta \vec{v}}{\delta t} = & \vec{e}_1 \left(\frac{\delta v_1}{\delta t} + \frac{v_1}{h_1} \frac{\partial v_1}{\partial \eta_1} + \frac{v_1 v_2}{h_1 h_2} \frac{\partial h_1}{\partial \eta_2} \right. \\ & \left. - \frac{v_2^2}{h_1 h_2} \frac{\partial h_2}{\partial \eta_1} - v_2 \frac{1}{h_2} \frac{\partial v_2}{\partial \eta_1} \right) \\ & + \vec{e}_2 \left(\frac{\delta v_2}{\delta t} + 2 v_1 \frac{v_1}{h_1} \frac{\partial v_2}{\partial \eta_1} + \frac{v_1 v_2}{h_1 h_2} \frac{\partial h_2}{\partial \eta_1} - \frac{v_1^2}{h_1 h_2} \frac{\partial h_1}{\partial \eta_2} \right) \end{aligned} \quad (21)$$

By neglecting small terms of order v_2 in the eq. for v_1 one finds for the momentum eq.

$$\begin{aligned}
& \oint \left(\frac{\delta \mathcal{L}}{\delta t} + \frac{v_1}{h_1} \frac{\partial}{\partial \eta_1} \right) v_1 + \frac{1}{h_1} \frac{\partial p}{\partial \eta_1} = 0 \\
& \oint \left[\frac{\delta}{\delta t} + 2 \frac{v_1}{h_1} \frac{\partial}{\partial \eta_1} \right] v_2 + \frac{v_1 v_2}{h_1 h_2} \frac{\partial h_2}{\partial \eta_1} - \frac{v_1^2}{h_1 h_2} \frac{\partial h_1}{\partial \eta_2} \\
& + \frac{1}{h_2} \frac{\partial p}{\partial \eta_2} + B \frac{1}{h_1 h_2} \frac{\partial}{\partial \eta_2} (h_1 B) = 0
\end{aligned} \tag{22}$$

BOUNDARY CONDITION AND INITIAL CONDITIONS

Initially a cylinder filled with plasma of the density ρ and with the temperature T is assumed to be in equilibrium, such that

$$\left[p + \frac{1}{2} B^2 \right]_{\text{inside}} = p_{\text{outside}} \tag{23}$$

Furthermore, reflection symmetry is assumed at $z = 0$, therefore

$$\vec{e}_1(z=0) = \begin{pmatrix} 0 \\ 0 \\ 1 \end{pmatrix} \quad \vec{e}_2(z=0) = \begin{pmatrix} 1 \\ 0 \\ 0 \end{pmatrix} \quad v_1(z=0) = 0 \tag{24}$$

and

$$\frac{\partial p}{\partial \eta_1} = \frac{\partial \mathcal{L}}{\partial \eta_1} = \frac{\partial B}{\partial \eta_1} = 0 \quad \text{at } z = 0$$

Two sets of boundary conditions whose parameters depend on time are taken. As the conductivity is infinite, a sharp boundary between plasma and vacuum can be defined. This moving boundary is determined by the condition

$$(p + \frac{1}{2} B^2)_i = p_o \tag{25}$$

where "i" designates inside and "o" outside (in η_2 direction).

One has to find the velocity $v_2(\eta_2 = b_2)$, because b_2 is η_2 at the boundary between plasma and vacuum.

One differentiates eq. (25) with respect to the time and finds

$$\left(\frac{\delta p}{\delta t} + B \frac{\delta B}{\delta t} \right)_{inside} = \frac{\delta p_r}{\delta t}$$

$\delta/\delta t$ is the differentiation in the moving coordinate system. Using eq. (18) and (16), this equation gives

$$\frac{1}{h_2 r} \frac{\partial}{\partial \gamma_2} (r v_2) = \left(-\frac{\delta p_r}{\delta t} + \gamma p \frac{1}{h_1 r} \frac{\partial}{\partial \gamma_1} (r v_1) + \frac{v_1}{h_1} \frac{\partial p}{\partial \gamma_1} \right) / (\gamma p + B^2) \quad \text{at } \gamma_2 = b_2(t) \quad (26)$$

as the boundary condition for v_2 .

Four different sets of boundary conditions have been used so far

1.
$$p_0 = p_0 e^{-t/\tau} + \frac{1}{2} B_1^2(\gamma_1, t) \quad (27)$$

with

$$B_1(\gamma_1, t) = \sin \omega t \cdot \begin{cases} \delta B_1 & \text{for } \gamma_1 \leq z_1 \\ \frac{\delta B_1 + \delta B_2}{2} + \sin \left(\frac{\pi}{2} \frac{\gamma_1 - (z_1 + z_2)/2}{z_2 - z_1} \right) \cdot \frac{\delta B_1 - \delta B_2}{2} & \text{for } \gamma_1 < z_1 < z_2 \\ \delta B_2 & \text{for } \gamma_1 \geq z_2 \end{cases}$$

2.
$$p_0 = p_0 e^{-t/\tau} + \frac{1}{2} B_1^2(\gamma_1, t) \quad (29)$$

Where B_1 has the same form as above with δB , or $\delta B_z = 0$. But it is assumed that a conducting wall is placed at $r = R_b$, so that the flux F

$$F = \frac{\pi}{2} (R_b^2 - R_e^2) \cdot B_0 (t=0) \quad (30)$$

is a constant, but $F = F_0 e^{-t/\tau}$

3. For $t = 0$ a homogeneous magnetic field $B_0 = \text{const.}$ is assumed.

The magnetic field of solar flares originates from ring currents. The magnetic fields from such ring currents (magnetic dipoles) fall off with d^3 ($d \gg a$). In order to simulate this behavior, a shape of the conducting wall is assumed to be of the following form.

$$R_b = R_{b0} + \delta R_b \left(z/z_{end} \right)^2 \quad (31)$$

with

$$F(z) = \frac{\pi}{2} (R_b^2 - R_e^2) B_0 (t=0) \quad (32)$$

where $F(z)$ is kept const. in time. The time variation is brought in by letting \bar{R}_b depend on time and keeping $F(t)$ const..

$$\bar{R}_b = R_b (1 + \delta R \sin \omega t) \quad (33)$$

where δR is the relative amplitude of the change.

4. As before, for $t = 0$, a homogeneous magnetic field $B = \text{const.}$ is assumed.

Expressed as a function of t and z , the outside pressure has the following form:

$$p_0 = p_0 \left[1 - (1 - e^{-t/\tau}) (1 - e^{-(z/t_0)^2}) \right]$$

and

$$p_0 = p_{int} + \delta p (1 - e^{-t/\tau_1})$$

This boundary condition is used to study the approach to a steady state.

OUTLINE OF THE COMPUTING TECHNIQUES.

The computation employed a mesh which usually had 10 points in the η_2 -direction and 50 points in η_1 -direction. The simplest method for interpolation for the convective terms in the η_1 -direction was used. To compute the shock parallel to the magnetic field, the von Neumann shock term with the constant $A_{SHOCK} = N_s^2$ was used, where N_s is the approximate number of mesh points, through which the shock is extended. As the coordinate system is moving, one has to compute the coordinates in every time step.

Let " \wedge " define the new quantities at the time $t + \delta t$, " K " the second index for η_2 (the direction perpendicular to the field lines), " j " the first index for η_1 parallel to the field. With help of these definitions the resulting difference equations may be written in the following way:

$$\begin{aligned} (div \sigma)_{j,K} = & \frac{1}{r_{j,K} h_{1,j,K} h_{2,j,K}} \left[\frac{1}{\Delta \eta_2} (\sigma_{2,j,K+1/2} r_{j,K+1/2} h_{1,j,K+1/2} \right. \\ & \left. - \sigma_{2,j,K-1/2} r_{j,K-1/2} h_{1,j,K-1/2}) \right. \\ & \left. + \frac{1}{\Delta \eta_1} (\sigma_{1,j+1/2,K} r_{j+1/2,K} h_{2,j+1/2,K} - \sigma_{1,j-1/2,K} r_{j-1/2,K} h_{2,j-1/2,K}) \right] \quad (34) \end{aligned}$$

The nonconvective change of new quantities " \sim " are given by

$$\tilde{s}_{j,K} = s_{j,K} \exp(-\delta t \cdot (div \sigma)_{j,K}) \quad (35)$$

$$\begin{aligned}
\tilde{p}_{j,k} &= p_{j,k} \cdot \exp(-f \cdot st(\text{div} \sigma)_{j,k}) \\
&\quad - Q_{j,k} (f-1) \cdot st \frac{1}{r_{j,k} h_{j,k} \Delta \eta} \\
&\quad \cdot (\sigma_{j+1/2,k} \tau_{j+1/2,k} - \sigma_{j-1/2,k} \tau_{j-1/2,k})
\end{aligned} \tag{36}$$

where $Q_{j,k}$ is the v. Neumann term

$$\begin{aligned}
Q_{j,k} &= 0 \quad \text{if} \quad \sigma_{j+1/2,k} - \sigma_{j-1/2,k} \geq 0 \\
&= A_{\text{SHOCK}} \cdot (\sigma_{j+1/2,k} - \sigma_{j-1/2,k})^2 \\
&\quad \text{if} \quad \sigma_{j+1/2,k} - \sigma_{j-1/2,k} < 0
\end{aligned} \tag{37}$$

Furthermore " \sim " quantities have to be corrected by the convection term to the " \wedge " quantities:

$$\begin{aligned}
\hat{\gamma}_{j,k} &= \tilde{\gamma}_{j,k} - \sigma_{j-1/2,k} \frac{st}{\Delta \eta, h_{j,k}} (\gamma_{j,k} - \gamma_{j-1,k}) \quad \text{if} \quad \sigma_{j+1/2,k} \geq 0 \\
&= \tilde{\gamma}_{j,k} - \sigma_{j+1/2,k} \frac{st}{\Delta \eta, h_{j+1,k}} (\gamma_{j+1,k} - \gamma_{j,k}) \quad \text{if} \quad \sigma_{j+1/2,k} < 0 \\
&= \tilde{\gamma}_{j,k} \quad \text{if} \quad \sigma_{j+1/2,k} \sigma_{j-1/2,k} \leq 0
\end{aligned} \tag{38}$$

The difference eqs. for σ are second order in time; i.e.:

$$\begin{aligned}\hat{\sigma}_{j+1/2,K}^{(r)} &= \sigma_{j+1/2,K} - \frac{\delta t}{2} (\sigma_{j+1/2,K}^2 - \sigma_{j-1/2,K}^2) \quad \text{if } \sigma_{j+1/2,K} \geq 0 \\ &\quad - \frac{\delta t}{2} (\sigma_{j+3/2,K}^2 - \sigma_{j+1/2,K}^2) \quad \text{if } \sigma_{j-1/2,K} < 0\end{aligned}$$

$$+ \frac{\delta t}{h_{j+1/2,K}} \Delta \eta_1 (P_{j+1,K} - P_{j,K}) / \rho_{j+1/2,K}$$

$$\begin{aligned}+ \frac{\delta t}{h_{j+1/2,K}} \Delta \eta_1 \left[q_{j+1,K}^{(r-1)} \rho_{j+1,K} (\hat{\sigma}_{j+3/2,K}^{(r)} - \hat{\sigma}_{j+1/2,K}^{(r)}) \right. \\ \left. - q_{j,K}^{(r-1)} \rho_{j,K} (\hat{\sigma}_{j+1/2,K}^{(r)} - \hat{\sigma}_{j-1/2,K}^{(r)}) \right] / \rho_{j+1/2,K}\end{aligned} \quad (39)$$

$$+ \frac{\delta t^2}{2 \cdot h_{j+1/2,K} \Delta \eta_1} P_{j,K} \left[(\text{div } \sigma)_{j+1,K} - (\text{div } \sigma)_{j,K} \right] / \rho_{j+1/2,K}$$

where

$$q^{(r)} = 0 \quad \text{if } \hat{\sigma}_{j+1/2,K}^{(r)} - \hat{\sigma}_{j-1/2,K}^{(r)} \geq 0$$

$$= -A_{\text{SHOCK}} \cdot (\hat{\sigma}_{j+1/2,K}^{(r)} - \sigma_{j-1/2,K}^{(r)})$$

$$\text{if } \hat{\sigma}_{j+1/2,K}^{(r)} - \hat{\sigma}_{j-1/2,K}^{(r)} < 0$$

Eq. (39) was solved implicitly. The subscript means the number of r the iterations for $r = 0$

$$\widehat{v}_{j+1/2, K}^{(0)} = v_{j+1/2, K}$$

Usually eq. (38) was iterated twice. The computations show this to be necessary; otherwise the results may become unstable, or else one has to use smaller time steps. Taking the last part of eq. (21) in difference form, the eq. for v_2 becomes

$$\begin{aligned} \widehat{v}_{j, K+1/2}^2 &= v_{j, K+1/2}^2 - \frac{2 \cdot \delta t}{h_{j, K+1/2} \Delta \eta_1} v_{j+1/2, K} (v_{j+1, K+1/2}^2 - v_{j, K+1/2}^2) \\ &\quad \text{if } v_{j+1/2, K} < 0 \\ &\quad - \frac{2 \cdot \delta t}{h_{j, K+1/2} \Delta \eta_1} v_{j-1/2, K} (v_{j, K+1/2}^2 - v_{j-1, K+1/2}^2) \\ &\quad \text{if } v_{j+1/2, K} \geq 0 \\ &\quad - \frac{\delta t}{h_{j, K+1/2} \Delta \eta_2} p_{j, K+1/2} \left[p_{j, K+1} - p_{j, K} + B_{j, K+1/2} \cdot \right. \\ &\quad \left. \cdot (h_{j, K+1} B_{j, K+1} - h_{j, K} B_{j, K}) \right] \\ &\quad + \frac{\delta t^2}{2} (\delta p_{j, K} + B_{j, K}^2) / p_{j, K} \left[\frac{1}{h_{j, K+1} h_{j, K+1} \Delta \eta_2 r_{j, K+1}} \cdot \right. \\ &\quad \cdot (h_{j, K+3/2} r_{j, K+3/2} \widehat{v}_{j, K+3/2}^2 - h_{j, K+1/2} r_{j, K+1/2} \widehat{v}_{j, K+1/2}^2) \\ &\quad - \frac{1}{h_{j, K} h_{j, K} r_{j, K} \Delta \eta_2} (h_{j, K+1/2} r_{j, K+1/2} \widehat{v}_{j, K+1/2}^2 - h_{j, K-1/2} r_{j, K-1/2} \widehat{v}_{j, K-1/2}^2) \\ &\quad + \frac{1}{h_{j, K+1} h_{j, K+1} r_{j, K+1} \Delta \eta_1} (h_{j+1/2, K+1} r_{j+1/2, K+1} v_{j+1/2, K+1}^2 - h_{j-1/2, K+1} r_{j-1/2, K+1} v_{j-1/2, K+1}^2) \\ &\quad \left. - \frac{1}{h_{j, K} h_{j, K} r_{j, K} \Delta \eta_1} (h_{j+1/2, K} r_{j+1/2, K} v_{j+1/2, K}^2 - h_{j-1/2, K} r_{j-1/2, K} v_{j-1/2, K}^2) \right] \\ &\quad - \frac{\delta t v_{j, K+1/2}}{h_{j, K+1/2} h_{j, K+1/2}} \left[v_{j, K+1/2}^2 \frac{1}{\Delta \eta_2} (h_{j, K+1} - h_{j, K}) - v_{j, K+1/2}^2 \frac{1}{\Delta \eta_1} (h_{j+1/2, K+1/2} - h_{j-1/2, K+1/2}) \right] \end{aligned} \quad (40)$$

The factor two in the first term comes from the fact that the coordinate system is also moving.

These eqs. were solved completely and implicitly, as indicated, to obtain stability. The coefficient in the last term is so big as to force the second derivative to become zero. This, together with the proper perpendicular boundary condition for v_z , gives an almost uniform contraction. The last term with v_z^2 is the centrifugal force.

The eq. for the mesh

$$\begin{aligned} \widehat{h}_z^{j,k} = h_z^{j,k} + \frac{\delta t}{r_{j,k} \Delta \eta_2} (r_{j,k+1/2} v_z^{j,k+1/2} - r_{j,k-1/2} v_z^{j,k-1/2}) \\ + \frac{\delta t^2}{2} \frac{B_{j,k}^3}{S_{j,k}} (\widehat{h}_z^{j,k+1} - 2 \widehat{h}_z^{j,k} + \widehat{h}_z^{j,k-1}) \end{aligned} \quad (41)$$

is again solved implicitly; then

$$\widehat{B}_{j,k} = 1 / (\widehat{r}_{j,k} \widehat{h}_z^{j,k}) \quad (42)$$

The mesh is computed in the following way. Let \widehat{e}_i be

$$\begin{aligned} \widehat{e}_i = \begin{pmatrix} \widehat{e}_z \\ \widehat{e}_r \end{pmatrix}_{j+1/2, k+1/2} \\ = e_i + \delta t \begin{pmatrix} -e_r \\ e_z \end{pmatrix} (v_z^{j+1, k+1/2} - v_z^{j, k+1/2}) \frac{1}{h_z^{j, k+1/2} \Delta \eta_1} \end{aligned} \quad (43)$$

Then

$$\begin{aligned}
 \hat{r}_{j, K+1/2} &= r_{j, K+1/2} + \delta t e z_{j, K+1/2} \hat{v}_2_{j, K+1/2} \\
 \hat{z}_{j+1/2, K} &= z_{j+1/2} - \delta t e r_{j+1/2, K} \hat{v}_2_{j, K+1/2} \\
 \left(h_{j, K} \Delta \eta_1 \right)^2 &= \left(z_{j+1/2, K} - z_{j-1/2, K} \right)^2 \\
 &\quad + \left(r_{j+1/2, K} - r_{j-1/2, K} \right)^2
 \end{aligned} \tag{44}$$

As eq. (31) requires flux conservation, an adjustment is made to eq. (44) to assure this. The correction factor

$$\hat{v}_2_{ccr} = (1 + \delta) \hat{v}_2$$

where δ is of the order 10^{-3} for each time step and is of variable sign.

Neglecting δ may lead to an error of the order 10%.

RESULTS

The results are given in dimensionless form. Let l_0 , t_0 , n_0 be the basic units for length, time, density. Then

$$\begin{aligned}v_0 &= l_0/t_0 \quad \text{cm sec}^{-1} \\ \rho_0 &= A \cdot 1.8 \cdot 10^{-24} n_0 \text{ g cm}^{-3} \\ B_0 &= \sqrt{4\pi \rho_0} v_0 \quad \text{r} \\ T_0 &= A \cdot 1.1 \cdot 10^{-12} v_0^2 \quad \text{eV}\end{aligned}$$

Let, for example,

$$l_0 = 1 \text{ cm}, t_0 = 1 \mu\text{s}, n_0 = 10^{16} \text{ cm}^{-3} \quad A = 2 \quad (\text{Deuterium})$$

Then

$$\begin{aligned}B_0 &= .75 \text{ kG} \\ T_0 &= 2.2 \text{ eV}\end{aligned}$$

As there are no dissipative processes in the present computation, all results are invariant under a length and time scale transformation.

All cases computed here have the same initial conditions for $t = 0$

$$\begin{aligned}B &= 4.0 & \rho &= 0.8 & T &= 1.5 \\ r_a &= 0.5 & z_e &= 10.0\end{aligned}$$

The frequency of change (eq. 27) $\omega = 1.0$

In the series of Fig. 1 to 4 the horizontal lines are the field lines. The vertical lines represent the density, so that the area between those two lines and field lines is inversely proportional to the density. The initial state is shown in Fig. 1.

Fig. 1 represents:	$\delta\left(\frac{B^2}{2}\right) = 40$	at $z = 10.0$	$r_e = 3.0$	$\tau = 5.0$
Fig. 2	"	$\delta\left(\frac{B^2}{2}\right) = 80$	at $z = 10.0$	$r_e = 0.75$
Fig. 3	"	$\delta\left(\frac{B^2}{2}\right) = 80$	at $z = 0.0$	$r_e = 0.75$
				$\tau = 10.0$

At the first maximum compression ($t = 1.5 \approx \frac{\pi}{2}/\omega$), the radius at the compression is roughly 0.3, and a weak SHOCK is developing at $z = 5.0$ in the density and temperature distribution. The higher compression for the cases (2) and (3) compared to (1) are largely compensated by higher stiffness of the field originating from the nearby coil.

At the time $t = 3.0 \approx \pi/\omega$, as the compression fields move through zero there is a shock moving toward $z = 0$ ($M \approx 1.3$), and the density has a minimum at $z = 7$. The Mach number is higher for case (3) where compression occurs at $z = 0.0$.

The last two graphs of cases (2) and (3) show the distribution at the time $t = 4.5 \approx \frac{3\pi}{2}/\omega$ and $t = 6.0 \approx 2\pi/\omega$. Whereas the Mach number in case (3) remains below 2, in case (4) the Mach number gets to be of the order of $M \approx 4$. For laboratory plasma the last case is not interesting, but in the dynamics at the sun surface these results may have some bearing.

The shape of the plasma surface as shown in Fig. 1d shortly after the reflection of the shock at $z = 0$ is quite typical; the shock wave is now approximately at $z = 3$, and at this higher pressure the plasma is pushed aside.

Other computer runs have shown that it has been not possible to get higher Mach numbers than approximately 1.5. The temperature increases approximately 2-3 times. The conclusion is that in medium β range ($\beta \approx 0.1$), one can not produce strong shock waves (in z -direction). With magnetic field changes whose frequency is comparable to transversal time of a sound wave along the field lines, one can increase the pressure by a factor of about 4. The next three graphs show the change in the geometry with the second set of boundary conditions.

For $\omega = 10.0$, as the frequency is very low, the changes are very slow. Nevertheless, the differences in pressure may be a factor, too. As it was proposed that the breaking up of solar flares may be due to resistive instabilities, it is planned to extend the calculation so to take into account the asymmetry around the axis, in order to see if a geometry develops which allows an instability.

Figs. 5a, 5b show an equilibrium situation, where a source is on the bottom, which ejects plasma. As a boundary condition at $z = z_e$, $v = v_c$ (sound speed) was assumed. These kinds of situations could occur in sun spots, if the field lines which form the boundary no longer come back to the sun. The pressure and density then follow approximately the adiabatic law, which means that the entropy is approximately a constant along the field lines. Different runs were made for varying r_a . The results are almost identical, except for a greater radius r_a , as indicated in Fig. 5a, there appears a hump in the magnetic field strength. In Fig. 5b, the deviations indicated, (near $z = 8.0$) show the influence of the boundary condition for $z = 10.0$. Before reaching this point the distributions are identical. At $z = 15.0$ the $v_{|| \text{ max}}$ is a bit higher than thermal speed.

ACKNOWLEDGEMENTS

The author would like to thank A. Jaggi for suggesting the equilibrium problem. Also he would like to thank the Culham Laboratories (U.K.A.E.A.), England, where part of the work was performed. Special thanks go to E. Monasterski of the Theoretical Division, GSFC, who did most of the programming.

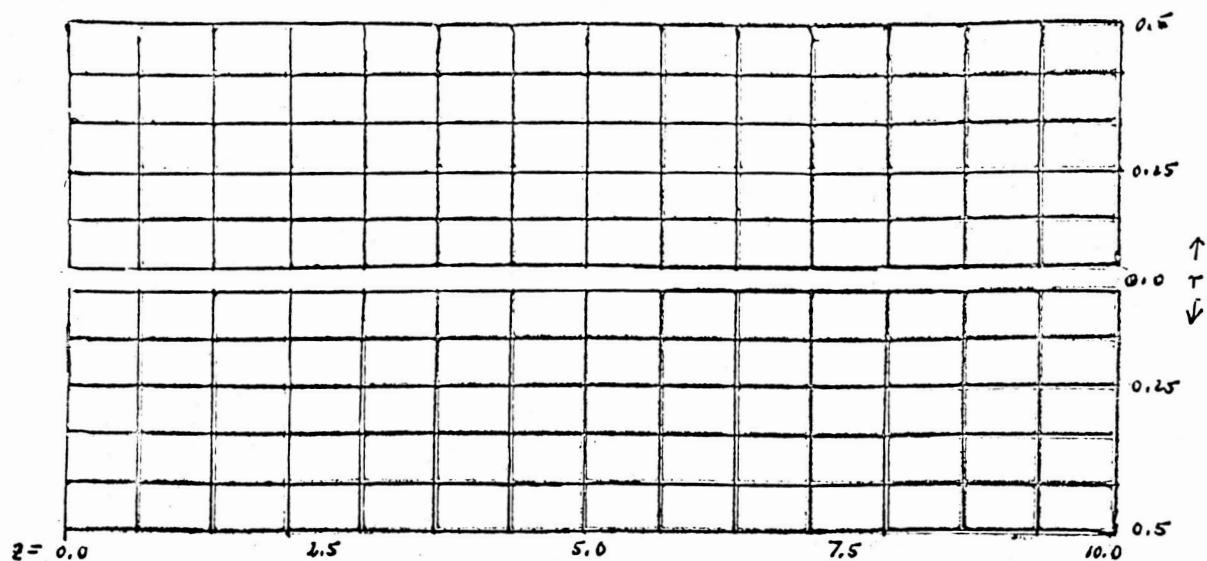


Figure 1.- $t = 0$.

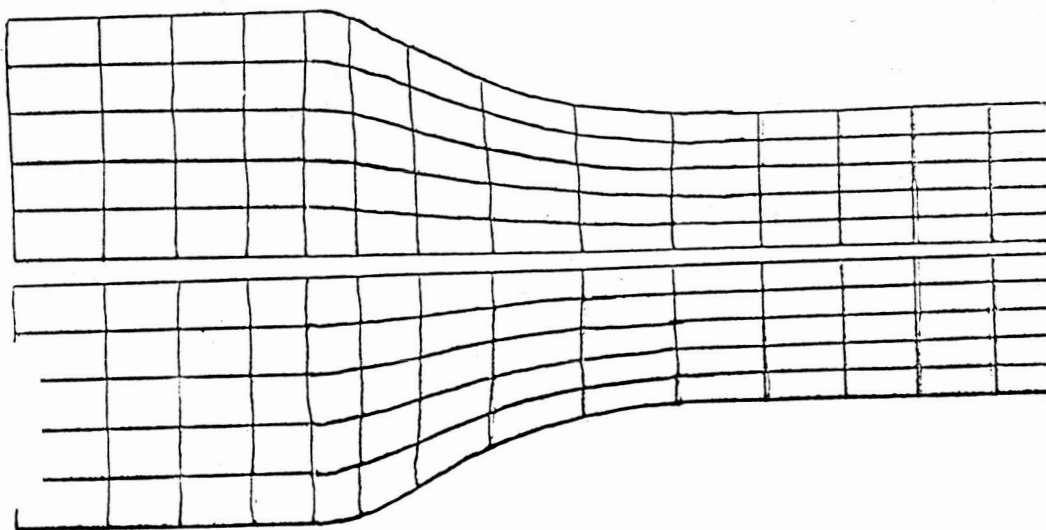


Figure 1a.- $\delta\left(\frac{B^2}{2}\right) = 40$ at $z = 10.0$, $t = 1.5$, coil $r_b = 3.0$.

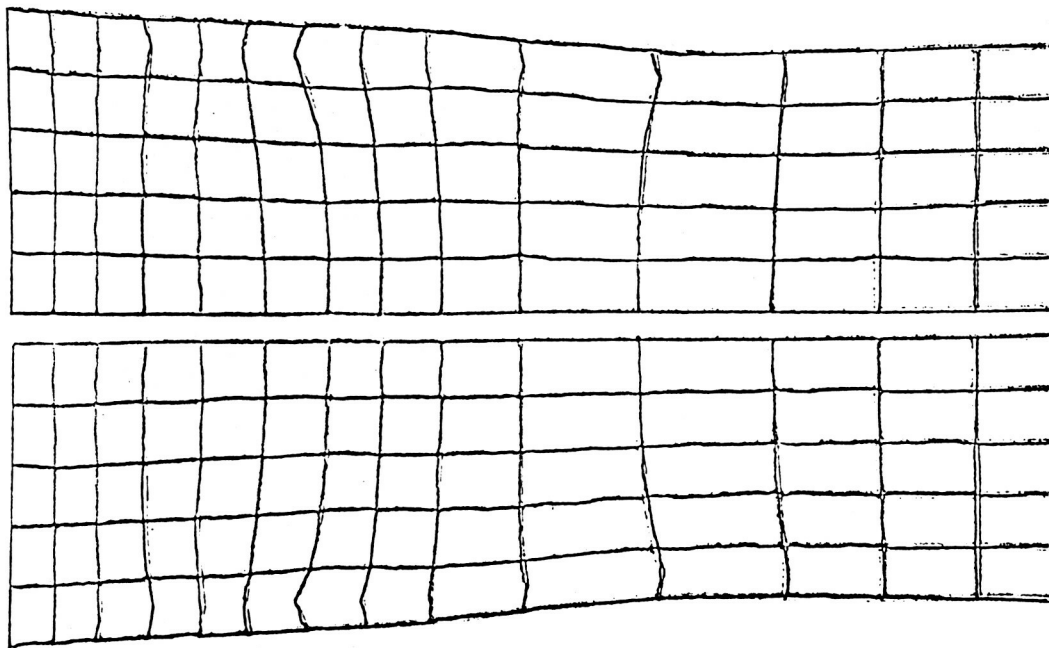


Figure 1b.- $\delta\left(\frac{B^2}{2}\right) = 40$ at $z = 10.0$, $t = 3.0$, coil $r_0 = 3.0$.

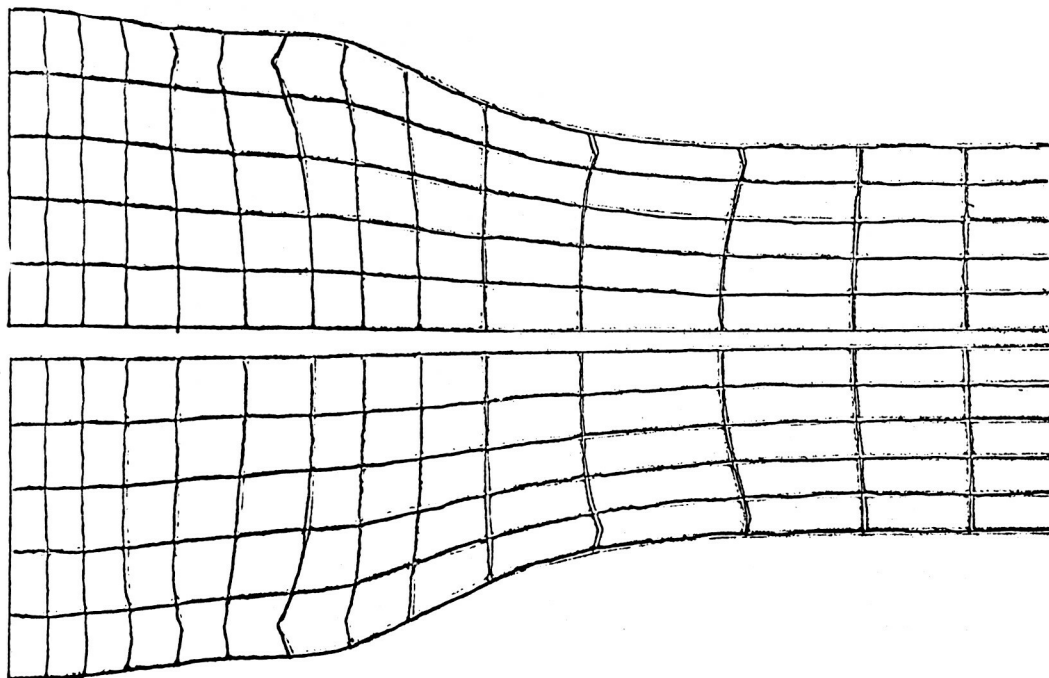
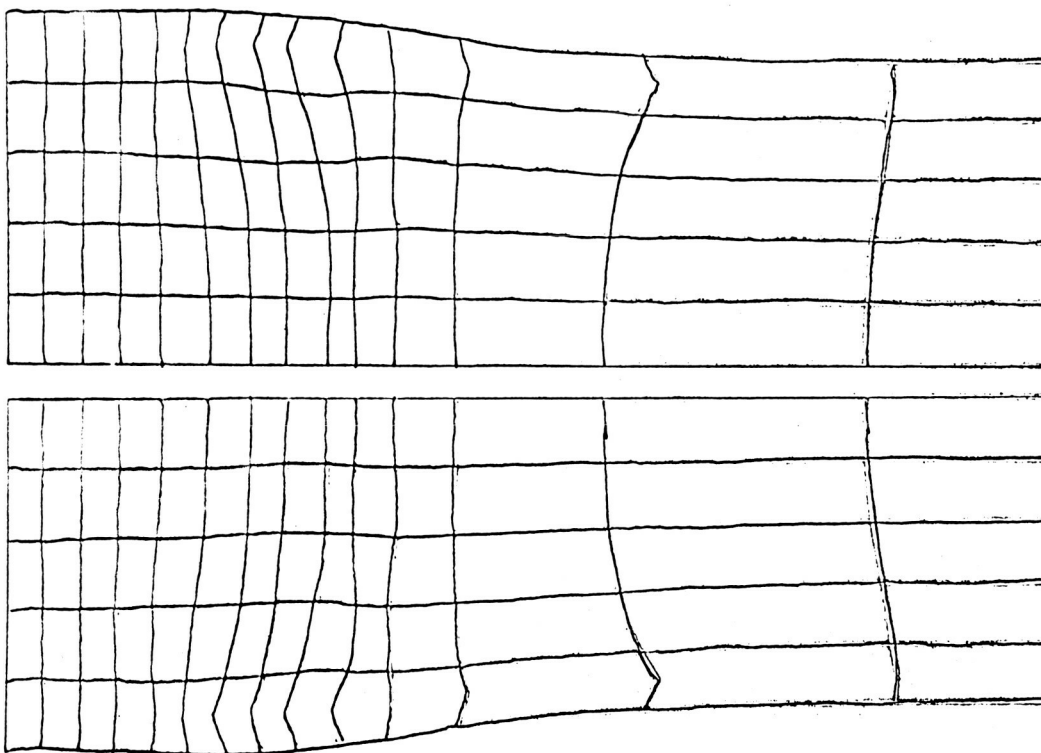
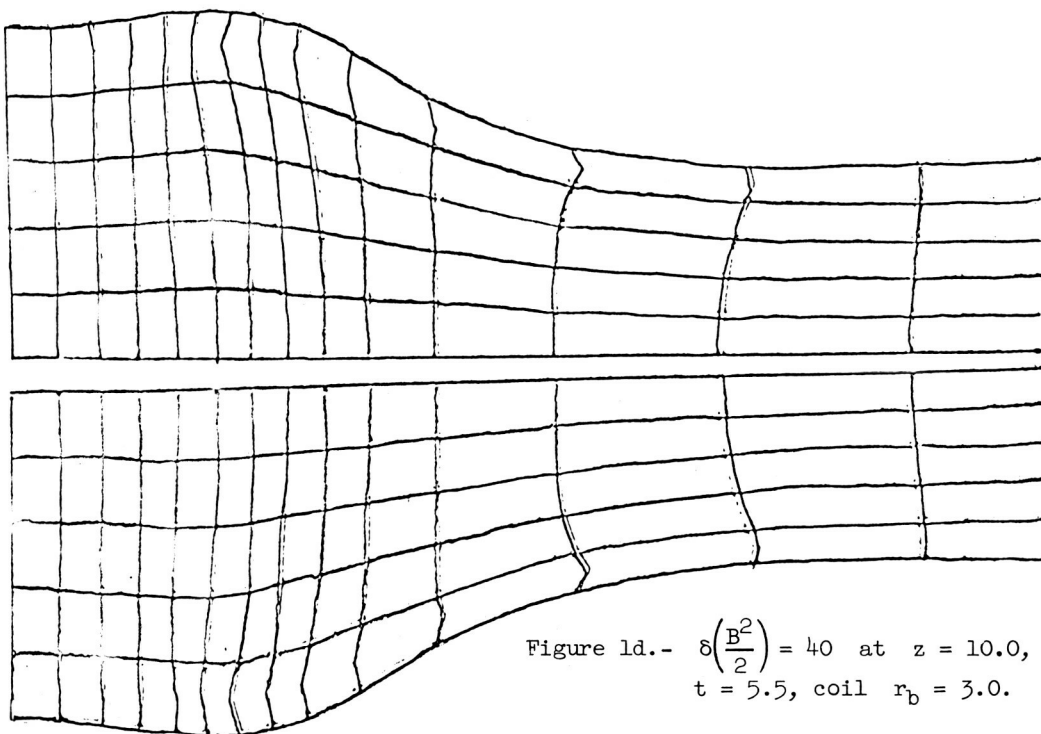


Figure 1c.- $\delta\left(\frac{B^2}{2}\right) = 40$ at $z = 10.0$, $t = 4.5$, coil $r_0 = 3.0$.



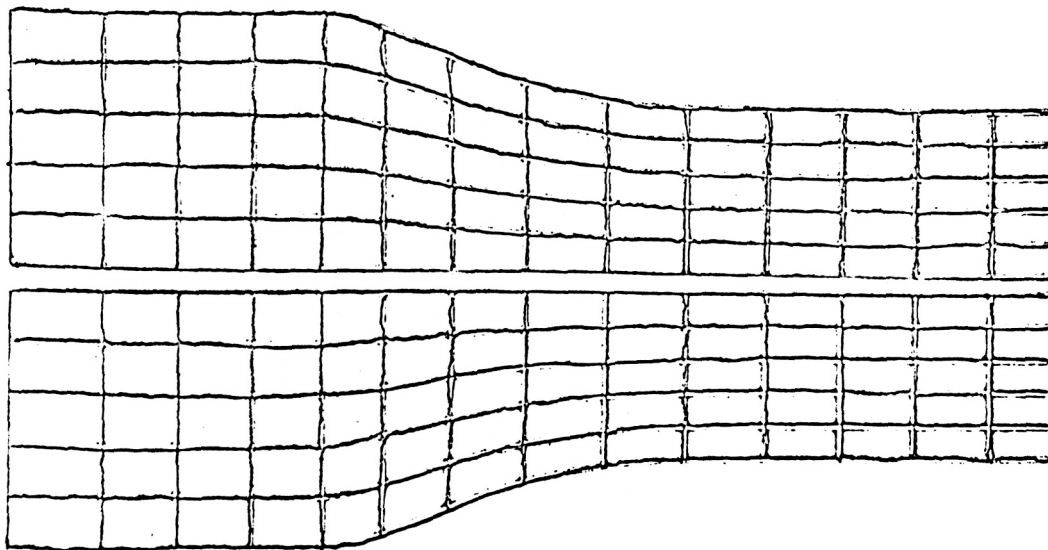


Figure 2a.- $\delta\left(\frac{B^2}{2}\right) = 80$ at $z = 10.0$, $t = 1.5$.

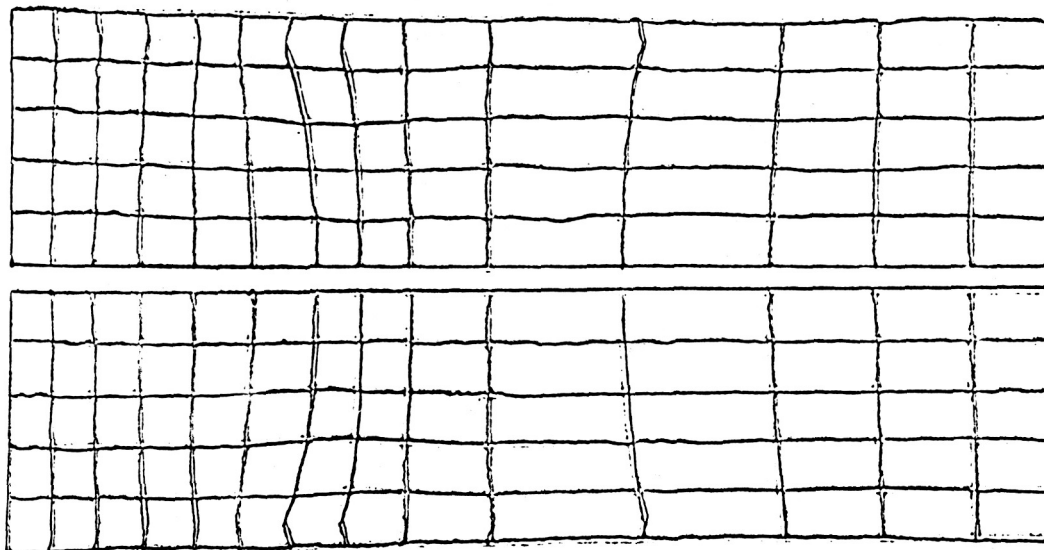
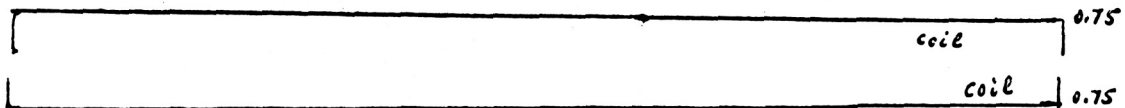
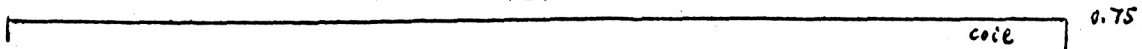


Figure 2b.- $\delta\left(\frac{B^2}{2}\right) = 80$, $t = 3.0$.



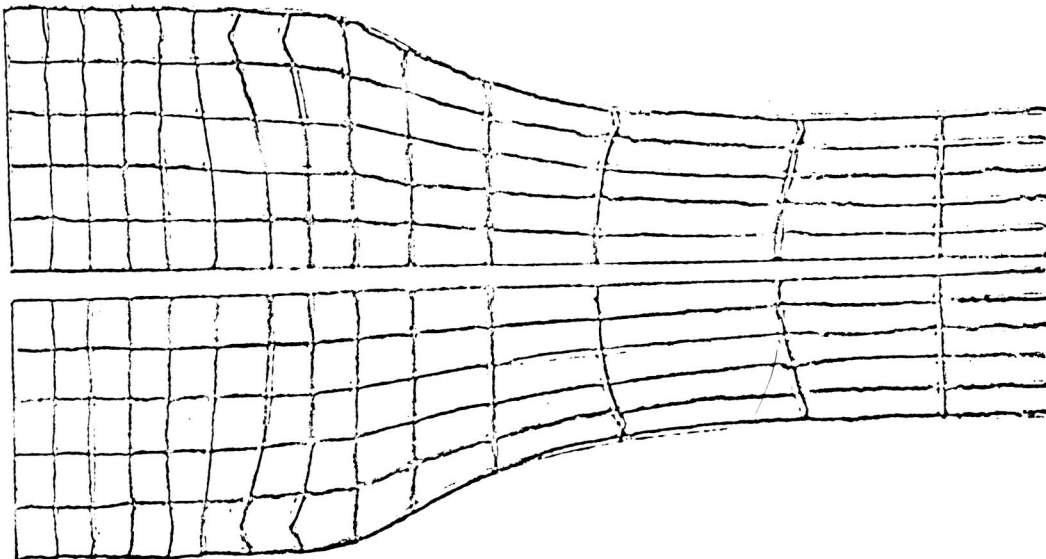


Figure 2c.- $\delta\left(\frac{B^2}{2}\right) = 80$ at $z = 10.0$, $t = 4.5$.

coil 0.75

coil 0.75

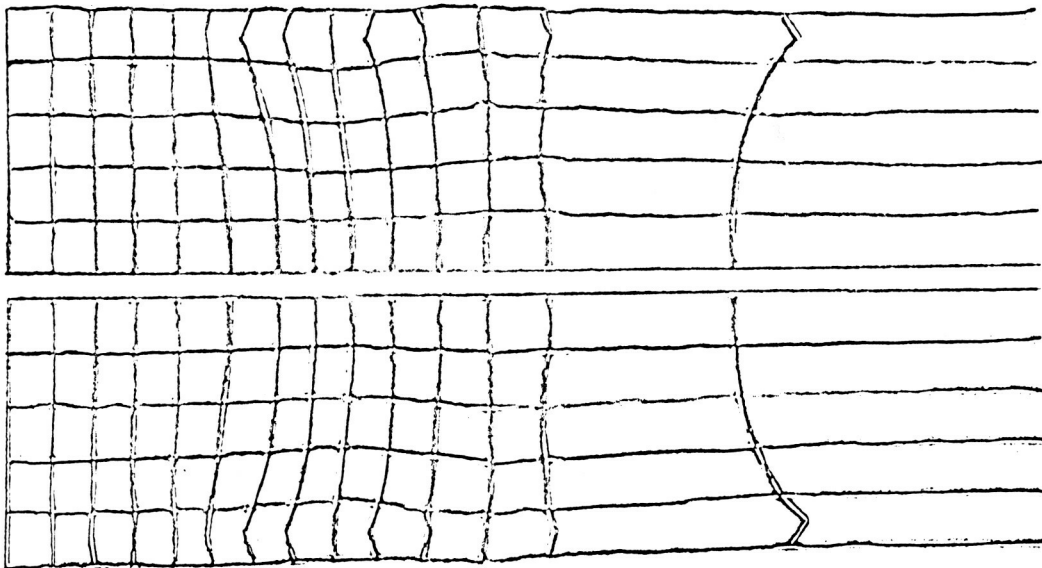


Figure 2d.- $\delta\left(\frac{B^2}{2}\right) = 80$ at $z = 10.0$, $t = 6.0$.

coil 0.75

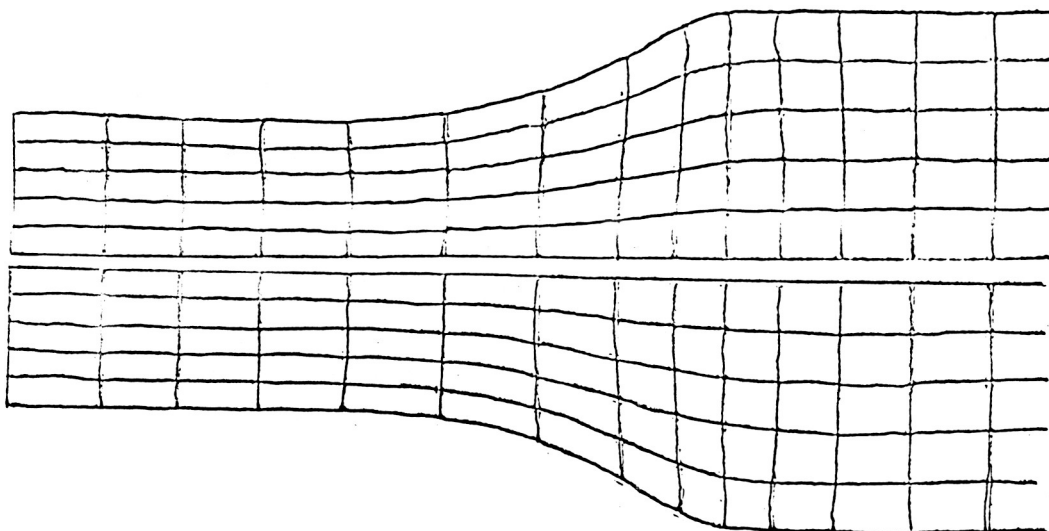


Figure 3a.- $\delta\left(\frac{B^2}{2}\right) = 80$ at $z = 0$, $t = 1.5$.

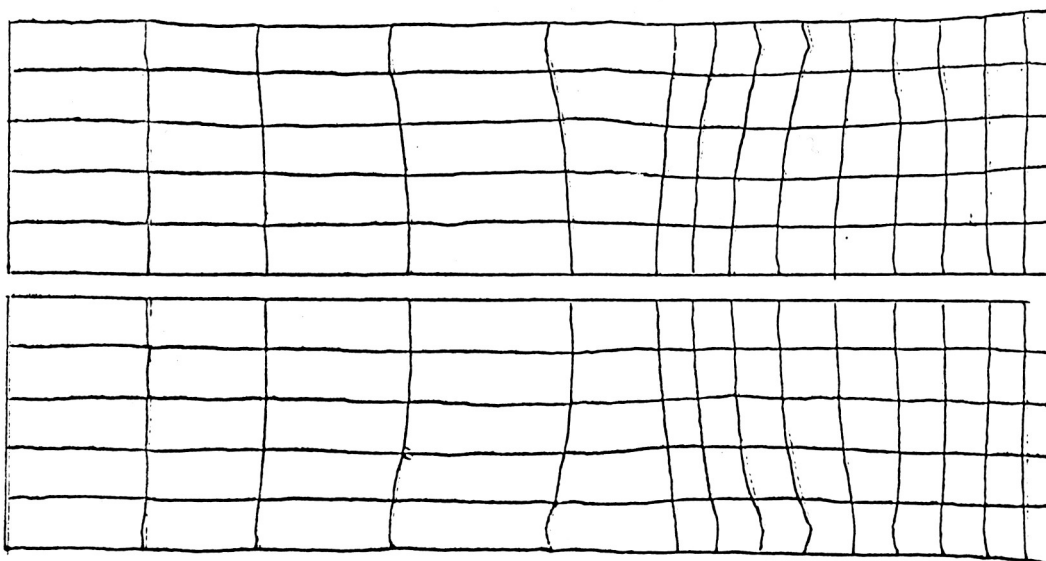
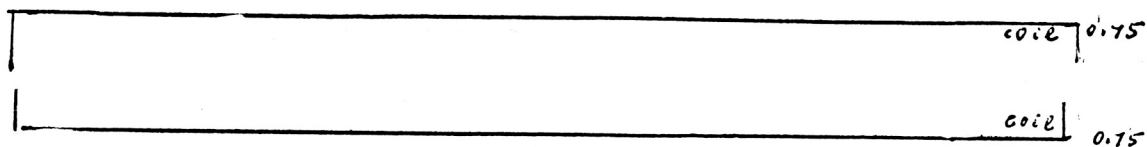
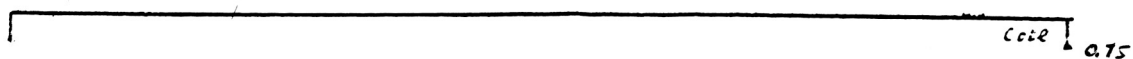


Figure 3b.- $\delta\left(\frac{B^2}{2}\right) = 80$ at $z = 0$, $t = 3.0$.



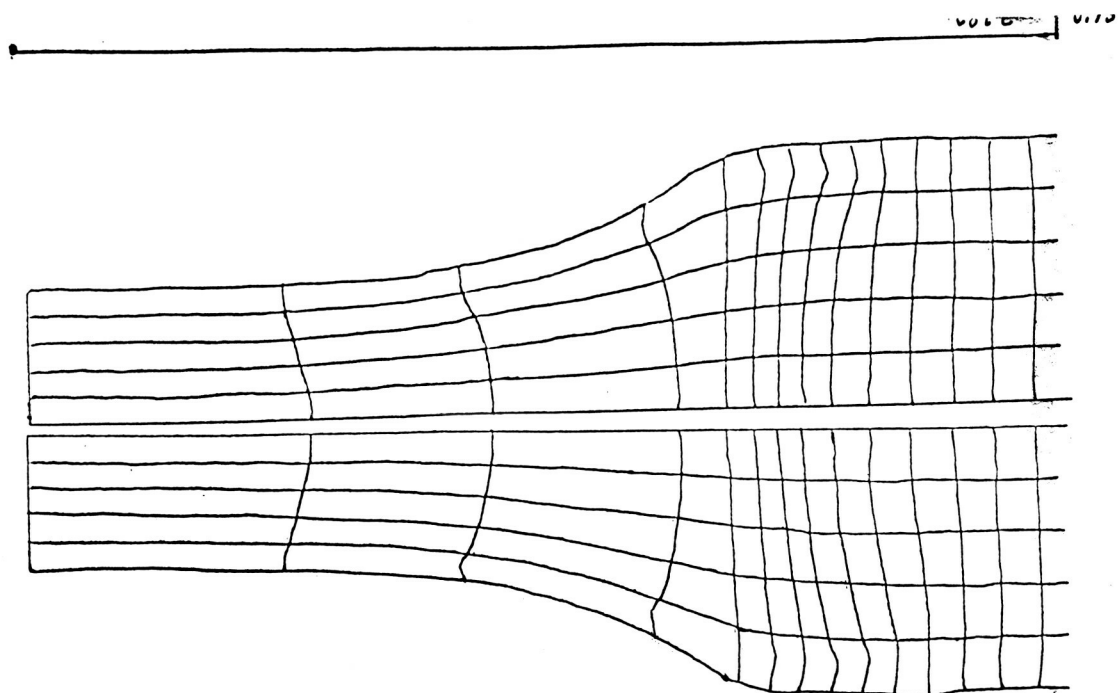


Figure 3c.- $\delta\left(\frac{B^2}{2}\right) = 80$ at $z = 0$, $t = 4.5$.

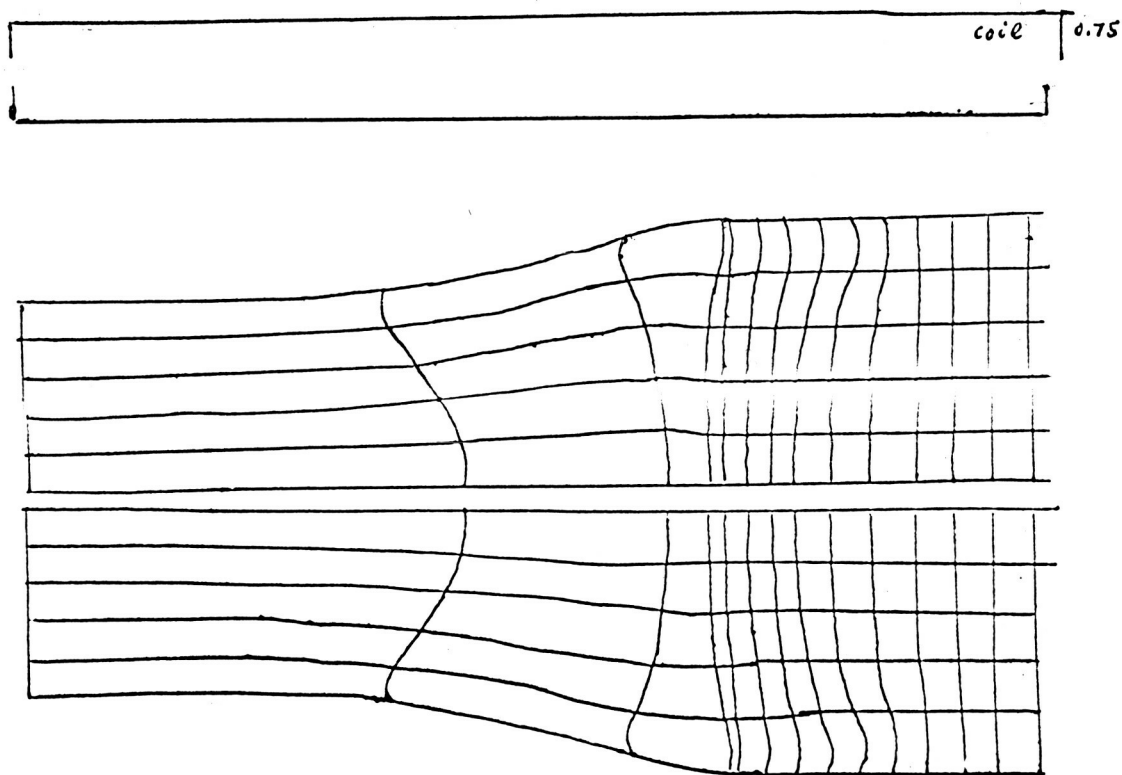


Figure 3d.- $\delta\left(\frac{B^2}{2}\right) = 80$ at $z = 0$, $t = 5.5$.

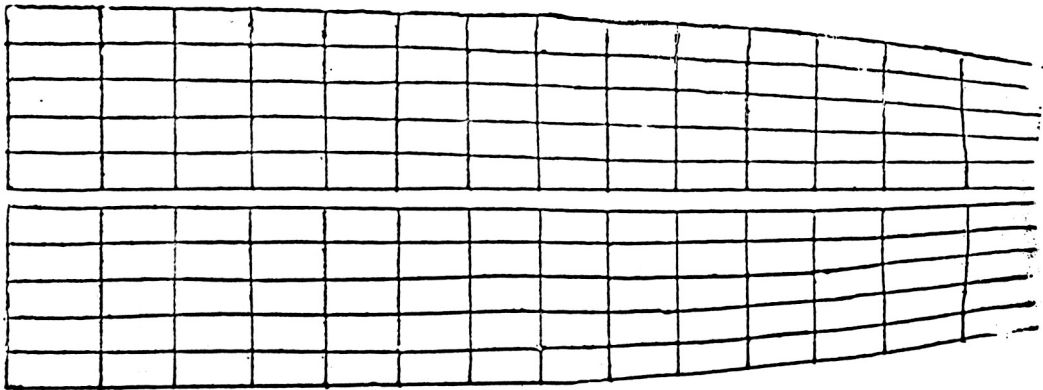


Figure 4a.- $\delta_r = .25$, $t = 1.5/\omega$.

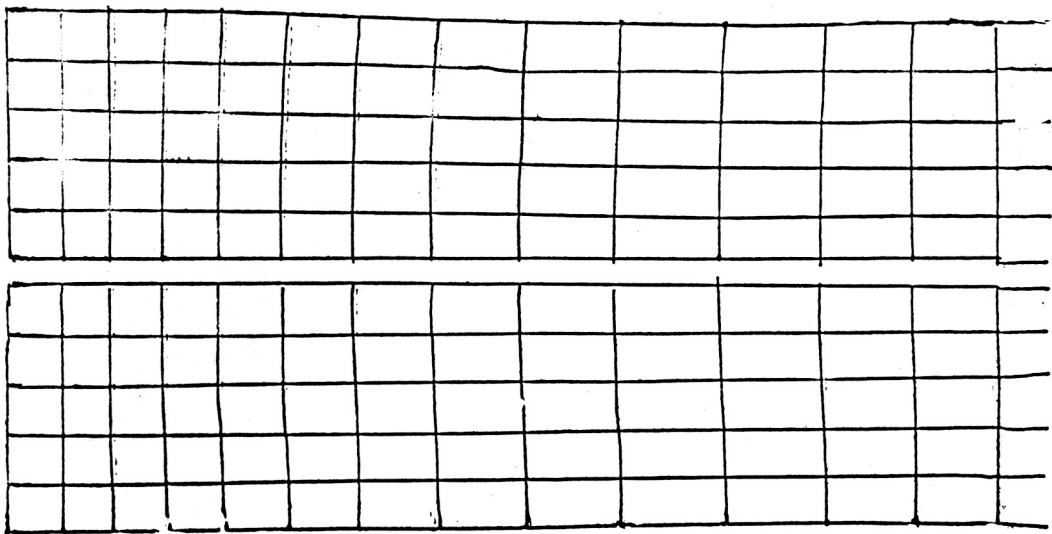


Figure 4b.- $\delta_r = .25$, $t = 3.0/\omega$.

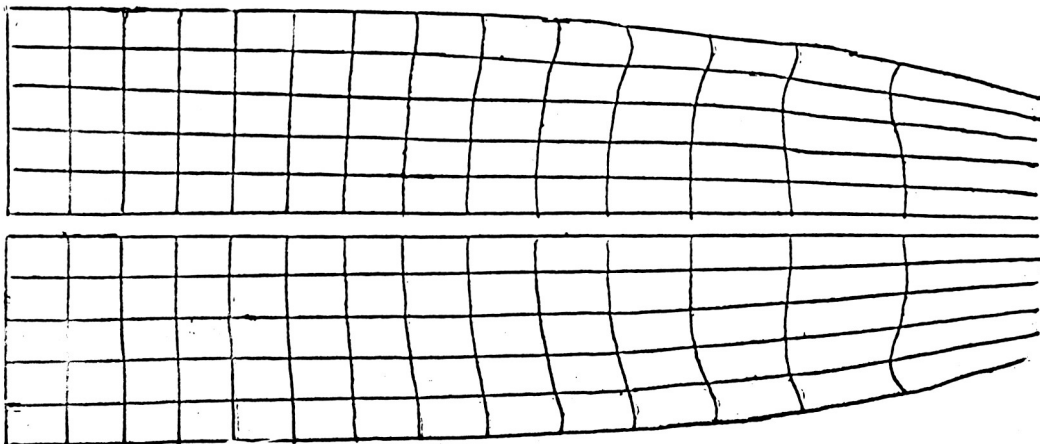
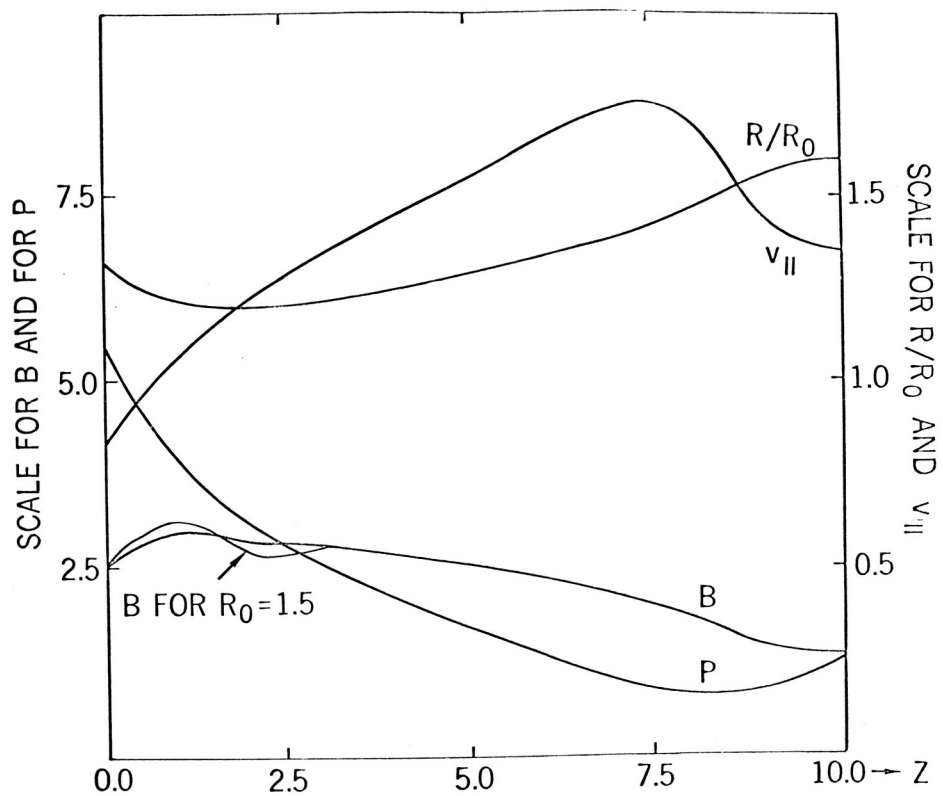
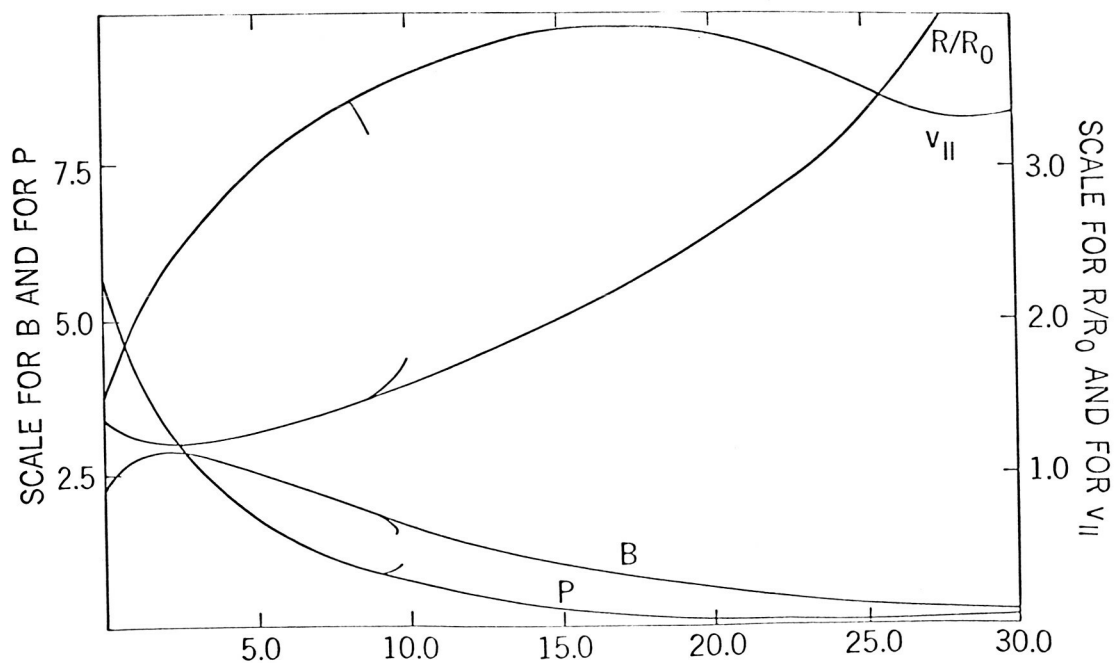


Figure 4c.- $\delta_r = .25$, $t = 4.5/\omega$.



STATIONARY DISTRIBUTION FOR $R = 1.0, Z = 10.0$

Figure 5a.



STATIONARY DISTRIBUTION FOR $R_0 = 1.0, Z = 30.0$

Figure 5b.

CALCULATION OF HIGHLY DISTORTED PLASMA INTERCHANGE MOTIONS
WITH A NONLINEAR TWO-DIMENSIONAL TWO-FLUID
COMPUTER MODEL*

J. A. Byers

Lawrence Radiation Laboratory, University of California
Livermore, California

ABSTRACT

Summary

The type of motions considered here are two dimensional low beta interchange motions perpendicular to a strong uniform magnetic field, B . A gravitational field g (perpendicular to B) is used to simulate effects of B field curvature. The model used is a fluid type model where the motion of a positively charged fluid and a negatively charged fluid is carried forward in time by a finite difference solution of the Eulerian equations of continuity. The fluid velocities are assumed to be given by the guiding center drift velocities. The electric field is obtained each time step by a finite difference solution of Poisson's equation. More details of the computational model are in Ref. 1.

It is clear that finite difference models are extremely limited for the purpose of observing highly distorted motions because such motion rapidly produces short wavelengths that the spatial grid cannot accurately represent. The validity of finite difference approaches to nonlinear flows which become severely distorted rests upon sometimes arbitrary criteria such as:

1. short time results - where one is satisfied with the answer obtained before the flow becomes too distorted.
2. long time results for the larger length scales - where one argues that one can put up with severe errors in the shorter length scales so long as such errors do not directly affect the longer length scales.

Several successful calculations with our model for various interchange modes have been reported earlier.^{2,3} The primary aim in these calculations was to follow the motions of unstable plasmas, excited initially at small amplitudes, for sufficiently long times in order to determine the final plasma state. Thus, as reported in Ref. 2, a gravity driven flute in the "one fluid" regime (mode A) was followed until the outward flux of the plasma was stopped by a confining wall. The plasma in this case reaches a physical barrier in a rapid direct path so that the "final state" is determined before extreme distortions of the fluid occur. The spatial differencing procedure thus encounters no difficulties.

Also as reported in Ref. 2, a Kelvin-Helmholtz or diocotron instability, with $g = 0$ and a slight charge imbalance to give an E/B velocity shear (mode B), was followed until the boundary layer deformed into large amplitude charge bunches or vortices. The vortices form well away from the confining wall and the growth has apparently stopped. The vortex formation involves extreme fluid distortion, but the long time behavior of the larger length scales seems adequately represented despite the certain misrepresentation of the smaller length scales. The validity of the long time results seems to rest upon the circumstance that there is no energy transformation process which depends on the short wavelengths.

Nonlinear stabilization of the type resulting from mode B is clearly due to the total disruption of the growth mechanism which for mode B is the localization in space of the net charge. In Ref. 3, another type of nonlinear stabilization was reported. In this case, (mode C) an unstable gravity driven flute in the "two fluid" regime, not too far away from a marginal stability point, reached a large amplitude stable state well away from a confining wall. The large amplitude stable wave which results does not involve extreme fluid distortions, and thus the spatial differencing encounters no serious difficulties. The stabilization seems to have occurred when nonlinear effects reduced the growth mechanism to a sufficient degree so that the originally weaker "two fluid" effects were able to effectively compete with the growth and stabilize the system. It is clear that this

nonlinear stabilization process does not require total disruption of the growth mechanism. It is plausible that this type of nonlinear stabilization is a fairly general one; i.e., whenever conditions are not too far from a marginal stability point, nonlinear effects might be expected to reduce the growth mechanism sufficiently so that the competing processes can stabilize the system at large amplitudes. It was the aim of the present calculations to test this concept on a different mode.

The particular interchange mode here (mode D) is combination of mode A and mode B described above. Conditions are chosen such that if $g = 0$ the velocity shear mode (mode B) is stable. The magnitude of g is chosen sufficiently large such that the combination of unstable mode A and stable mode B is unstable although not far from the marginal stability condition predictable from linear theory. The ensuing motion for this case becomes highly distorted after a relatively short time. This is a direct result of the velocity shear and severely limits the finite difference approach. In contrast to the calculations for mode B where similar fluid distortions occurred, there is here an energy transformation process (due to the g field) which is directly dependent on the short wavelengths, and thus the calculation will break down when a significant amount of the energy appears in the short wavelengths. The net effect is that with the present spatial resolution only short time results have been obtained, and the question of whether or not the gravity driven flute coupled with velocity shear has a large amplitude stable state is not yet answered. Indications are that the fluting motion can, so to speak, break through the shearing notion and continue its growth, but this is only tentative.

Examples of the computer output for mode D will be shown, and different methods of differencing compared. It will be seen that calculations can be decidedly improved when differencing scheme has some means for imposing control on the errors in the short wavelengths ($\lesssim 4 \Delta x$). In particular, in one example, it is seen preferable to use a lower order scheme which includes short wavelength control rather than a higher order scheme which includes no short wavelength control.

The time decay of a certain class of perturbations of a stable shearing layer is also of interest. Case⁴ has shown, for particular stable shear flows, that small amplitude perturbations corresponding to the continua singular normal modes will damp with an asymptotic time variation proportional to $1/t$. The time decay of such perturbations can also be followed with the computer model. The computer model is of course applicable to large as well as small amplitude perturbations. The shearing motion of stable flow, despite the fact that the amplitude of the motion does not grow, can also cause extreme distortion and thus severely limit the finite difference model. In fact, observing a stable shearing layer for too long a time can produce a false return of a damped perturbation. This effect is due entirely to exceeding the limitations of the spatial finite difference grid. Also, the time which one must wait for the validity of the asymptotic limit is relatively long, and a relatively fine spatial resolution would be required in order for the damped motion to be observed for such times. The initial time decay, however, can easily be followed on a relatively coarse grid. The results obtained here indicate that most of the energy of the perturbation decays during this initial transient time, and thus the relatively slow asymptotic decay would appear to have little physical significance.

* Work performed under the auspices of the U.S. Atomic Energy Commission.

¹J. A. Byers, Journal of Computational Physics, (to be published).

²J. A. Byers, Phys. Fluids 9, 1038 (1966).

³J. A. Byers, Large Amplitude Stabilization of Flute Growth Due to a Nonlinear Effect of the Ion Precessional Drifts, Presented at November 1966 meeting of Plasma Physics Division of American Physical Society, Boston, Massachusetts.

⁴K. M. Case, Phys. Fluids 3, 143 (1960).

To be presented at the Symposium on Computer Simulation of Plasmas and Many-Body Problems, College of William and Mary, Williamsburg, Va., April 19-21, 1967.

N67-37752

THETA-PINCH SHOCK IMPLOSION CALCULATIONS
BY MODEL SIMULATION OF COLLISIONLESS ION VLASOV EQUATION

R. W. Kilb

General Electric Research and Development Center
Schenectady, New York

ABSTRACT

Computations describing the implosion phase of high voltage low density theta-pinches are carried out by using the collisionless Vlasov equation for the ions, and using the fluid equation for adiabatic electrons. The calculations are on a time scale long compared to the electron cyclotron time, but short compared to the ion cyclotron time. The equations are reduced to a set of equivalent cylindrical plasma sheets. The calculations show that the non-adiabatic ion heating in very low bias, negative bias, and positive bias theta pinches results from ion interaction with rapidly fluctuating electric and magnetic fields inside the plasma, and with the rapidly converging outside surface of the plasma. The mean ion energy was 1 keV at two microseconds for very low bias and negative 1.5 kG bias, while it was only 0.6 keV for positive 1.5 kG. For very low bias the ion pressure is non-isotropic with $P_{rr} \gg P_{\theta\theta}$, and the density tends to peak on the axis. These effects do not occur for +1.5 kG and -1.5 kG bias. All three cases show plasma mass rotation, with the outside portion counter-rotating with respect to the inner portion in order to conserve over-all zero angular momentum. This rotation appears to be related to finite Larmor effects. Comparisons are made with experimental results.

1. Introduction

The purpose of these calculations was to describe the non-adiabatic implosion phase of low density, high voltage theta₁ pinches. In the first two microseconds of the GE theta-pinch¹ ions are heated to ~ 1 keV and the electrons to ~ 0.15 keV when no initial bias fields are applied. Thus the ions are found to be much more non-adiabatic than the electrons during the implosion phase. A physical basis for expecting the electrons to behave more adiabatically than the ions is that for an initial bias magnetic field of a few hundred gauss the electron cyclotron time is approximately a nanosecond, whereas the ion cyclotron time is roughly a microsecond. The possibility of high frequency instabilities is ignored here. Since the implosion front travels transverse to the magnetic

field, one expects Adlam-Allen magnetic waves,² which have a time scale of $1/\sqrt{n_i n_e}$ and a length scale of c/ω_{pe} .

We therefore propose to study in detail the non-adiabatic ion motion in low density, high voltage theta-pinchs by use of the collisionless Vlasov equation for the ions, but use an adiabatic fluid description for the electrons. This allows the numerical integration to be carried out on the time scale of $1/\sqrt{n_i n_e}$. If the Vlasov equation were used for the electrons also, it would be necessary to compute on the time scale of $1/\omega_{pe}$, which then requires extremely long computer runs to find the motion corresponding to the first two microseconds of the experiments.

The model described below is an adaptation to cylindrical coordinates of our previous work^{3,4} on planar collision-free plasma shock waves. Using an extension of our codes, W. P. Jones and V. J. Rossow⁵ have taken into account initial thermal ion motions. Rossow⁶ has done computations employing the Vlasov model for the electrons, and found no major change in the ion behavior for the plasma parameters of interest here. Rossow⁷ has also considered oblique planar shock waves.

Extensive MHD calculations have been carried out for cylindrical theta pinches, especially in the high density regime. These calculations generally assumed isotropic ion and electron pressures, and used a Richtmyer-von Neuman⁸ artificial shock dissipative mechanism when necessary. Heat conduction and resistivity were taken into account. The pioneering work was done by Hain, Roberts, and Koppendorfer.⁹ Further studies were made by Hain and Kolb,¹⁰ and Niblett and Fisher.¹¹ Lagrangian coordinates were employed by Oliphant.¹² The effect of initial partial ionization was studied by Duchs.^{13,14} The effect of high-Z impurities and radiation loss was considered by Kolb and McWhirter.¹⁵ Duchs and Griem¹⁶ made a detailed study of ionization and radiation effects using a three-fluid model.

In the work reported here, the Vlasov equation is used to study the non-adiabatic ion motion, which is simulated in the previous MHD studies⁹⁻¹⁶ by the Richtmyer-von Neuman approximation. For low or zero initial magnetic field bias, we find that the plasma-vacuum boundary is involved in the ion thermalization, and that the ion pressure is not isotropic ($P_{rr} > P_{\theta\theta}$). Finite Larmor effects are also important for the ions. Our model does not include resistivity, heat conduction, radiation, or neutral gas effects. The finite electron mass is taken into account.

2. Ion Equations of Motion

We consider an infinitely long and cylindrically symmetric theta-pinch. Thus all fields and velocities depend only on the radial coordinate and time. The electric field has the components $\underline{E} = (E_r, E_\theta, 0)$, and the magnetic field has $\underline{B} = (0, 0, B_z)$. Velocities in the z -direction are therefore invariant and will be ignored. The ion Vlasov equation is reduced to a cylindrical sheet model by replacing the distribution function by a sum of N δ -functions:

$$f_i = \sum_k n_s(r, t) \delta(r - r_k^+(t)) \delta(v_r - v_{rk}^+(t)) \delta(v_\theta - v_{\theta k}^+(t)) \quad (1)$$

Let dV be the volume element in the ion phase space. Then by Liouville's theorem $f_i dV$ is constant along the phase space path. Since we may ignore z and v_z coordinates, the volume element is $r dr d\theta dv_r dv_\theta$. Integrating Eq.(1) over a region enclosing one ion sheet, we obtain by Liouville's theorem $2\pi r_k n_s(r_k, t) = 2\pi r_k^0 n_s(r_k^0, 0)$. The latter quantity is simply the total number of ions per unit z -length of the ion cylindrical sheet, which is $\pi R_0^2 n_0 / N$, where R_0 is the original plasma radius and n_0 is the original ion volume density. Therefore the instantaneous surface density of ions on sheet k is given by:

$$n_s(r_k, t) = R_0^2 n_0 / 2N r_k \quad (2)$$

The equations of motion along the ion phase space path may be derived from the Hamiltonian in cylindrical coordinates:

$$H = \frac{1}{2M} p_r^2 + \frac{1}{2Mr^2} \left[p_\theta - \frac{e}{c} r A(r, t) \right]^2 + e\Phi(r, t) \quad (3)$$

where $A(r, t)$ is the θ -component of the magnetic vector potential, and $\Phi(r, t)$ the electric potential.

Essentially, we are sampling segments of the ion distribution, and computing how these segments move about in phase space. If the sampling is sufficiently dense, a good description of the Vlasov equation is obtained.

Because of the assumed cylindrical symmetry it follows from the Hamiltonian that the theta-momentum p_θ is a constant of the motion p_k^+ for each ion sheet:

$$P_k^+ = M r_k v_{\theta k}^+ + \frac{e}{c} r_k A(r_k, t) \quad (4)$$

This expresses $v_{\theta k}^+(r_k, t)$ in terms of the magnetic field $B(r_k, t)$ and the constant P_k^+ , which is set by the initial θ -velocity and fields $B(r, 0)$. Here we make use of the definition:

$$r_k A(r_k, t) = \int_0^{r_k} r B(r, t) dr \quad (5)$$

The radial equation of motion also follows from the Hamiltonian:

$$M \ddot{r}_k^+ = e E_r(r_k, t) + \frac{e}{c} v_{\theta k}^+ B(r_k, t) + M (v_{\theta k}^+)^2 / r_k \quad (6)$$

Equations (4) and (6) are, of course, simply the equation of motion of an ion in given axisymmetric fields $E(r, t)$ and $B_z(r, t)$. The central problem is to eliminate $E_r(r, t)$ and obtain a difference equation for $B_z(r, t)$. This is accomplished by using the fluid equations for the electrons, and Maxwell's equations.

3. Electron Equations of Motion

The fluid equation of motion for the electrons is given in Eulerian coordinates by

$$mn \left[\frac{\partial \underline{v}^-}{\partial t} + \underline{v}^- \cdot \nabla \underline{v}^- \right] = -ne \left[\underline{E} + \underline{v}^- \times \underline{B}/c \right] - \nabla p_e \quad (7)$$

We convert this equation to Lagrangian fluid coordinates. The θ -component of Eq.(7) may be integrated once if we observe that the full time derivative of $rA(r, t)$ along the Lagrangian fluid coordinate is given by:

$$\begin{aligned} \frac{\partial(rA)}{\partial t} + v_r \frac{\partial(rA)}{\partial r} &= \int_0^r r \frac{\partial B}{\partial t} dr + v_r \frac{\partial}{\partial r} \left[\int_0^r r B dr \right] \\ &= -r c E_\theta + r v_r B_z \end{aligned} \quad (8)$$

Using Eq.(8) in the θ -component of Eq.(7) yields:

$$m \frac{d}{dt}(rv_{\theta}^{-}) = \frac{e}{c} \frac{d}{dt}(rA) \quad (9)$$

which integrates to:

$$P^{-}(r^0, 0) = mr v_{\theta}^{-} - \frac{e}{c} r A(r, t) \quad (10)$$

where $P^{-}(r^0, 0)$ is the integration constant determined by the initial electron fluid velocity and initial magnetic fields. It is clear that Eqs.(4) and (10) are quite analogous, but it is important to remember that Eq.(3) applies to an ion sheet in phase space, whereas Eq.(7) applies along the Lagrangian coordinate of the electron fluid. This distinction is the basis for allowing ion sheets to "orbit cross", while the electron sheets are required to remain in their original sequence. M. N. Rosenbluth first pointed out to us the need for not allowing the electrons to orbit cross.

Note that the finite mass of the electron is retained in Eq.(9), which means that the electron fluid does not conserve local magnetic flux. This is to be contrasted with the usual MHD equations for perfectly conducting fluids which generally neglect the electron mass.

The radial component of Eq.(7) is reduced by assuming that the electron pressure varies adiabatically, $p_e = p_0 B^2/B_0^2$. Using $\text{curl } \underline{B} = 4\pi \underline{J}/c$, one finds from Eq.(7):

$$m\dot{r}^{-} = -eE_r(r, t) - \frac{e}{c} v_{\theta}^{-} B(r, t) + \frac{e}{c}(v_{\theta}^{+} - v_{\theta}^{-}) \beta_e B(r, t) + \frac{m}{r}(v_{\theta}^{-})^2 \quad (11)$$

where $\beta_e \equiv 8\pi p_0/B_0^2$. We now observe that the electron fluid is tied very closely to the ion charge density, because the Debye length of non-relativistic electrons, $\langle v_{th}^{-} \rangle/\omega_{pe}$, is small compared to our field scale length c/ω_{pe} . Thus the electron fluid may be split into N sheets corresponding to the N ion phase space sheets, and the electron and ion sheets may be assumed to move together in their radial motions.

4. Cylindrical Sheet Equations

The electric field $E_r(r, t)$ is eliminated by adding Eqs.(6) and (11) and assuming $r_k^{-} = r_k^{+}$:

$$(M+m) \dot{r}_k = \frac{M}{r_k} \left(v_{\theta k}^+ \right)^2 + \frac{m}{r_k} \left(v_{\theta k}^- \right)^2 + \frac{e}{c} (1+\beta_e) \left(v_{\theta k}^+ - v_{\theta k}^- \right) B(r_k, t) \quad (12)$$

We also add Eqs.(4) and (10) to eliminate $A(r, t)$:

$$Mr_k v_{\theta k}^+ + mr_k v_{\theta k}^- = P_k^+ - P_k^- \quad (13)$$

where P_k^+ and P_k^- are the constant canonical momenta determined by the initial conditions. The plasma has now been represented by a set of N cylindrical sheets. The θ -currents flow in these idealized thin sheets, resulting in a step increase of the magnetic field as one crosses the plasma sheet, and the magnetic field is constant in the space between adjacent sheets. As shown in Fig. 1, the field just outside cylindrical sheet k is labeled B_k , and the field just inside by B_{k-1} . The surface ion density on sheet k is $n_s(r_k, t)$ given by Eq.(2). By integrating $\text{curl } \underline{B} = 4\pi \underline{J}/c$ across plasma sheet k , one finds:

$$B_{k-1} - B_k = \alpha (v_{\theta k}^+ - v_{\theta k}^-) / r_k \quad (14)$$

where $\alpha \equiv 4\pi e n_0 R_0^2 / 2Nc$. We solve for $v_{\theta k}^+$ and $v_{\theta k}^-$ by Eqs.(13) and (14):

$$r_k v_{\theta k}^+ = \frac{m r_k}{\alpha(M+m)} [B_{k-1} - B_k] + \frac{P_k^+ - P_k^-}{M+m} \quad (15)$$

$$r_k v_{\theta k}^- = - \frac{M r_k}{\alpha(M+m)} [B_{k-1} - B_k] + \frac{P_k^+ - P_k^-}{M+m} \quad (16)$$

These equations may be used to eliminate $v_{\theta k}^+$ and $v_{\theta k}^-$ in the radial equation of motion.

To obtain a recursion formula for the magnetic field, substitute Eqs.(4) and (10) into Eq.(14):

$$r_k^2 (B_{k-1} - B_k) = \frac{\alpha}{M} \left[P_k^+ - \frac{e}{c} r_k A(r_k, t) \right] - \frac{\alpha}{m} \left[P_k^- + \frac{e}{c} r_k A(r_k, t) \right] \quad (17)$$

Set the index $k \rightarrow k-1$ and subtract the resulting equation from Eq. (17). Observing that

$$r_k A(r_k, t) - r_{k-1} A(r_{k-1}, t) = \frac{1}{2} (r_k^2 - r_{k-1}^2) B_{k-1} \quad (18)$$

we find the basic recursion relation for $N \geq k \geq 3$:

$$\begin{aligned} -r_{k-1}^2 B_{k-2} + \left[r_k^2 + r_{k-1}^2 + \frac{e\alpha(m+M)}{2cmM} (r_k^2 - r_{k-1}^2) \right] B_{k-1} - r_k^2 B_k = \\ = \frac{\alpha}{M} (P_k^+ - P_{k-1}^+) - \frac{\alpha}{m} (P_k^- - P_{k-1}^-) \end{aligned} \quad (19)$$

For $k = 2$, we find from Eq.(17):

$$\left[r_2^2 + \frac{e\alpha(m+M)}{2cmM} r_2^2 \right] B_1 - r_2^2 B_2 = \frac{\alpha}{M} P_2^+ - \frac{\alpha}{m} P_2^- \quad (20)$$

For $k = N+1$, we must allow for an electron pressure current sheath, which reduces the effective field just outside the r_{N+1} sheet to $B_{N+1}/\sqrt{1+\beta_e}$. Therefore for $k = N+1$ we use Eq.(19) with B_{N+1} replaced by $B_{N+1}/\sqrt{1+\beta_e}$.

The final equation for $k = N+2$ links the magnetic field to the rate of increase of magnetic flux in the coil which is the time integral of the voltage applied to the coil. Observing that:

$$\begin{aligned} r_{N+1} A_{N+1} + \frac{1}{2} (r_{N+2}^2 - r_{N+1}^2) B_{N+1} = r_{N+2} A_{N+2} \\ = \frac{c}{2\pi} \int_0^t V(t') dt' + r_{N+2} A(r_{N+2}, 0) \end{aligned} \quad (21)$$

we substitute Eq.(21) into Eq.(17) to find for $k = N+2$:

$$\begin{aligned} r_{N+1}^2 B_N - \left[\frac{r_{N+1}^2}{\sqrt{1+\beta_e}} + \frac{e\alpha(m+M)}{2cmN} (r_{N+2}^2 - r_{N+1}^2) \right] B_{N+1} = \frac{\alpha}{M} P_{N+1}^+ - \frac{\alpha}{m} P_{N+1}^- \\ - \frac{e\alpha(m+M)}{cmM} \left[r_{N+2} A(r_{N+2}, 0) + \frac{c}{2\pi} \int_0^t V(t') dt' \right] \end{aligned} \quad (22)$$

The coil voltage $V(t)$ is determined by the circuit parameters in conjunction with the coil current. Let ℓ be the effective coil length. Then the coil current and voltage is:

$$I = \frac{\ell c}{4\pi} \left[B_{N+1}(t) - B_{N+1}(0) \right] \quad (23)$$

$$V(t) = V(0) - L \frac{dI}{dt} - \frac{1}{C} \int_0^t I dt - IR - K|I|^{0.25} \quad (24)$$

where $V(0)$ is the initial capacitor bank voltage, and the other terms are the voltage drops because of the bank leads, the capacitor discharge, the bank resistance, and Thyrite damping. The $V(t)$ is roughly constant during the initial implosion phase.

Equations (19), (20), and (22) are $(N+1)$ linear equations for the unknown B_k . The form of the $(N+1) \times (N+1)$ matrix is tri-diagonal, and thus the B_k can be found by continued fractions.¹⁷ Using the B_k found from Eqs.(19-22), one may then integrate forward the radial sheet motion by Eq.(12).

Equation (12) and the field matrix Eqs.(19-22) are considered to be the fundamental equations of our sheet model. One may derive from them rigorous energy and momentum conservation laws which serve as a check on the accuracy of the numerical calculations even when the sheet spacing is not small. A discussion of the relation of this sheet model to the difference equations representing the Vlasov equation is given in Reference 4.

In the results reported below 320 plasma sheets were used, and the ion-electron mass ratio was taken as 100 to reduce the computation time. The integration step was 0.34 nanoseconds. The bank parameters were $V(0) = 50$ kV, $C = 220$ μ F, $L = 27.6$ nH, $R = 1.1$ m Ω , $K = 8$ kV at one megamp, and $\ell = 55.3$ cm. The coil radius r_{N+2} was 9.84 cm, the initial D_2 density was 10 mTorr and had an initial radius of 7.2 cm, and the initial T_e^0 was about 1 eV. The energy check on the computations agreed to better than 5 parts in 1000 throughout the computations.

5. Results for Very Low Bias Fields

Using +0.2 kG initial bias and $\beta_e = 0.2$, the plasma motion was computed corresponding to the first 2 μ sec of the theta-pinch.

Experimentally, it is found that the plasma with zero initial bias is quite similar to that with +0.2 kG initial bias. True zero bias calculations were not carried out because the ion motion is then essentially radial, and the electrons cannot be expected to undergo cyclotron motion. It seems possible that a small amount of magnetic field leaks into the plasma in the zero bias experiment, thus justifying the use of our electron fluid model.

Figure 2 shows the time variation of the plasma radius and the mean ion random energy. Qualitatively these agree with experiment and MHD calculations, but the amplitude of the radius fluctuations is perhaps larger than observed. Experimentally, we found a mean ion energy¹ of 1.4 - 1.85 keV at 2 μ sec which is somewhat higher than the computed value of 1 keV. This deviation may reflect the large particle loss occurring in the experiment¹, which under some conditions can lead to further compression and ion heating.¹⁸ Relaxation of the ion distribution from 2-dimensions to 3-dimensions would also lead to further compression and heating.

Figure 3 shows the radial variation of the magnetic field at successive times from 0 to 2 μ sec. For this low bias case, a single magnetic pulse is launched into the plasma. After the first microsecond, the field profile is quasi-static and shows a peaking toward the axis. This peaking is associated with the density peak near the axis (discussed below), and indicates a tendency toward local flux conservation despite the use of the finite electron mass in Eq.(9).

Figure 4 shows the plasma density profile at successive times. Note the correlation of the density wave with the magnetic wave in Fig. 3 during the first 0.6 μ sec. again showing approximate flux conservation. After the first microsecond, the density shows a peaking near the axis. This can be understood by the following very simple model. Consider a true zero bias pinch with a sharp plasma-vacuum boundary. Then the ions are accelerated only by the sheath radial electric field and therefore have a purely radial motion. Thus the only non-zero component of the pressure tensor is P_{rr} . In the quasi-steady state occurring after the first microsecond one then must have zero divergence of the pressure tensor:¹⁹

$$\frac{1}{r} \frac{\partial}{\partial r} \left(r P_{rr} \right) = 0 \quad (25)$$

Therefore $r P_{rr}$ is a constant, and since $P_{rr} = 2n \langle v_r^2 \rangle$ with $\langle v_r^2 \rangle$ roughly independent of radius, one then obtains $n \propto 1/r$. For low bias calculations we expect a similar density variation if the ion

Larmor radius in the internal magnetic field is larger than the plasma diameter, which occurs in our case. The essential conditions are that $P_{rr} > P_{\theta\theta}$ and $P_{rr} > B^2/8\pi$ in the plasma. The peaking of density near the axis has been observed in zero bias pinches by the Garching,²⁰ Culham,²¹ and Los Alamos²² theta pinch groups. An alternative explanation of this peaking has been given by Morse,²³ which involves the collapse of the radial electric field.

Figure 5 shows the mass θ -velocity profiles at successive times. The outside rotates in the same direction as an ion in cyclotron motion, and the inside counter-rotates to conserve momentum. Total canonical momentum is strictly conserved throughout the computations because of the use of Eqs.(4) and (10). This type of counter-rotation cannot occur in the usual MHD calculations, and appears to be related to finite Larmor effects. Spatially resolved plasma rotation experiments for low bias conditions have not been reported, but it is known that distortions on the outside surface of the plasma rotate in the ion cyclotron direction with velocities $\sim 10^7$ cm/sec. Morse's theory²³ also yields plasma rotation, but involves non-conservation of angular momentum.

Figures 6 and 7 show an end view of the transverse motion of five ions. Note the predominantly radial motion which is reflected in $P_{rr} > P_{\theta\theta}$. Ions 321 and 240 clearly have cyclotron radii much greater than the plasma radius, and are contained by the sheath E_r . Ions 80 and 2 have cyclotron radii somewhat smaller than the plasma radius, but their cyclotron motion is very distorted because of the electric field and field gradients.

Figures 8 and 9 give ion phase space projections onto the planes v_r - r , v_θ - r , and v_θ - v_r . The velocities and radial positions of the 320 ion sheets are plotted at successive times. From 0 to 0.5 μ sec the distributions remain locally continuous. During this time we believe the sheet model represents the Vlasov equation quite accurately, and it indicates that the ion distribution function is an extremely ridge-like, tortuous function, with knobby growths, discontinuities and bifurcations.⁴ After 0.6 μ sec (i.e., following the first radial contraction), the ion phase space loses its detailed structure, and takes on a "thermalized" distribution. Previous experience with planar shock calculations⁴ lead us to believe that the rather random appearance of the distribution at 1.05 μ sec results in part from the finite number of sheets used in the calculations, and therefore the exact Vlasov equation is not well-represented at late times, unless many more plasma sheets are employed. However, the gross properties are still well-represented, since total energy and momentum are conserved. Thus we believe the

sheet calculations after the first microsecond, have about the same validity as MHD calculations employing the Richtmyer-Von Neuman viscosity.⁸ Note that at 1.05 μsec , the v_θ - v_r projection at the bottom of Fig. 9 is very elliptical. This ellipticity persists out to 2 μsec , and shows that $P_{rr} > P_{\theta\theta}$ in the low bias calculations.

6. Results for Positive Bias Fields

A computer run with +1.5 kG bias, $\beta_e = 0.02$, and 320 sheets was made corresponding to the first 1.5 μsec of the experiment. Figure 2 shows that the plasma radius contracts slightly faster than in the low bias case. Because of the trapped field, the mean radius is somewhat larger than for low bias. The mean ion random energy is definitely lower for positive bias, in agreement with MHD calculations¹² and experiment.¹

Figure 10 shows the radial variation of the magnetic field. A sequence of Adlam-Allen waves is launched into the plasma at 0.2 - 0.3 μsec . These waves are analogous to those we found in low Alfvén Mach number planar shocks.³ The spacing of the waves shown in Fig. 10 at 0.3 μsec is artificially large because we used $M/m = 100$. Since the spacing should be roughly $10 c/\omega_{pe}$, a true deuteron-electron plasma would have a wave density six times greater than that shown at 0.3 μsec . The sharp spatial field fluctuations after 1 μsec may result in part from the finite number of plasma sheets used. The field tends to become uniform in the plasma at late times, and does not exhibit the axial peaking occurring in the low bias case. The density profiles also are quite flat after the first microsecond.

Figures 11 and 12 show an end view of the transverse motion of five ions. The cyclotron radii are clearly smaller than the plasma diameter. The ions show distorted cyclotron motions plus circumferential drift arising from the inward E_r field. Ion 321 at the top of Fig. 12 shows a curious similarity to Spitzer's wall reflected particle.²⁴ In our case the "wall" is the strong E_r of the plasma-vacuum sheath.

Figure 13 shows the ion phase space distribution of the 320 ion sheets. At 0.2 - 0.4 μsec one can see the organized ion motion associated with the Adlam-Allen waves. This organized motion breaks up because of the cylindrical convergence and disappears after the first plasma pinch. At times later than 1 μsec , the v_θ - v_r distribution becomes quite symmetrical, showing that $P_{rr} \approx P_{\theta\theta}$ for high bias. This is also reflected in the nearly uniform density inside the plasma after the first microsecond.

7. Results for Negative Bias Fields

A computer run was made with -1.5 kG bias, $\beta_e=0.02$, and 320 sheets. Figure 2 shows that the first plasma contraction is delayed because of an initial outward motion as the driving field reverses. This is in agreement with MHD calculations and experiment. The mean ion random energy is approximately the same as for very low bias. The greater ion energy for reverse bias as contrasted with positive bias appears to be associated with the large E_r occurring at the magnetic field reversal point. The field reversal point is located very near the plasma-vacuum boundary since plasma resistivity is not included in our model. Experiments¹ generally show that reverse bias gives higher energies than even zero bias. Possibly this is a result of additional heating from axial contraction not included in our model.

Figure 14 shows radial profiles of the magnetic field at successive times. Note that the magnetic waves launched into the plasma at 0.4 and 0.5 μsec are much broader than the Adlam-Allen type waves in the positive bias case. The magnetic field shows no quasi-static tendency to peak near the axis. The peaks at 0.6 and 1.5 μsec are of the dynamic type. The sharp spatial fluctuations after 1 μsec may result in part from the finite number of plasma sheets. The density distribution is quite flat after the first 0.5 μsec . This is in agreement with density profiles of Sawyer, et al., who found²² the profile to be significantly flatter with negative bias than with zero bias.

Figure 15 shows the mass θ -velocity profiles at successive times. Note that for negative bias the inside and outside rotation is just the opposite from that occurring in the low bias case (Fig. 5). This is because the rotation is controlled by the trapped magnetic field, which here is in the negative direction (i.e., into the paper). Keilhacker, et al., have carried out experiments²⁵ with reversed bias fields from which they conclude that a counter-rotating plasma is unlikely, although not completely ruled out.

Figures 16 and 17 show the transverse motion of five ions. The ions show distorted cyclotron motions plus circumferential drift. Note that this drift is in the opposite direction from that in Figs. 11 and 12, since the internal magnetic field is into paper here. Ion 321 again shows the Spitzer-type bouncing.²⁴

Figure 18 shows the ion phase distribution of the 320 ion sheets. No Adlam-Allen type organized motion is seen, and the distribution shows marked bifurcations and discontinuities as early

as 0.3 μsec . These distortions are associated with the spatial field reversal. After 1 μsec the $v_\theta-v_r$ distribution becomes quite symmetrical, which is reflected in $P_{rr} \approx P_{\theta\theta}$ and a nearly uniform density profile.

8. Conclusions

Our Vlasov equation calculations show that one should not generally assume that the ion pressure tensor has $P_{rr} = P_{\theta\theta}$ during the initial implosion of low density, high voltage theta pinches. The low bias, positive bias, and negative bias cases all showed $P_{rr} > P_{\theta\theta}$ during the first and second plasma contraction (Figs. 8, 13 and 18). After the second contraction (i.e., after 1 μsec), the positive and negative bias cases do have $P_{rr} \approx P_{\theta\theta}$ because the ion cyclotron radius in the plasma is small compared to the plasma diameter. However, in the low bias case, P_{rr} remained significantly larger than $P_{\theta\theta}$ throughout the first two microseconds (seven plasma contractions). Of course, one may invoke instabilities or collisions to obtain $P_{rr} \approx P_{\theta\theta}$, but the experimentally observed^{20,21,22} peaking of the plasma density near the axis may be interpreted as evidence for $P_{rr} > P_{\theta\theta}$ in zero bias pinches.

Our calculations also predict counter-rotating plasmas. The usual MHD calculations do not show this phenomena because it is implicitly assumed that the ion cyclotron radius is extremely small compared to the plasma radius. This is clearly untrue in high power theta pinches. We speculate that the inclusion of finite Larmor terms in the MHD equations^{26,27} would yield counter-rotating plasmas.

We also found Adlam-Allen magnetic waves before the first contraction in the positive bias case. These are not seen in the MHD calculations because the electron inertia is omitted in the usual generalized Ohm's law (the inertia term is the left side of Eq. 2-12 in Spitzer²⁴). It is also noteworthy that we find the initial magnetic waves in the reverse bias case to be much broader than Adlam-Allen waves.

Our model does not include resistivity or electron heat conductivity which may be important in actual experimental conditions. It might be possible to include these effects in our model by using more general Lagrangian fluid equations¹² for the electron fluid. The difference form of these equations is essentially a sheet representation, which could be combined with our Vlasov ion sheets.

ACKNOWLEDGMENTS

The author is indebted to Drs. H. Hurwitz, Jr., and L. M. Goldman for many valuable discussions and insights concerning these computations.

REFERENCES

1. R. L. Bingham, L. M. Goldman, R. W. Kilb, "Plasma Physics and Controlled Nuclear Fusion Research," Vol. I, pp.301-313, I.A.E.A. Vienna (1966), Culham Conf. Paper CN-21/87.
2. J. H. Adlam and J. E. Allen, Phil. Mag. 3, 448-455 (1958).
3. P. L. Auer, H. Hurwitz, Jr., and R. W. Kilb, Phys. Fluids 4, 1105-1121 (1961).
4. P. L. Auer, H. Hurwitz, Jr., and R. W. Kilb, Phys. Fluids 5, 298-316 (1962).
5. W. P. Jones and V. J. Rossow, NASA TN D-2536 (1965).
6. V. J. Rossow, Phys. Fluids 8, 358-366, (1965).
7. V. J. Rossow, Phys. Fluids 10, to be published.
8. R. D. Richtmyer, "Difference Methods for Initial Value Problems," Interscience Pub., N. Y. (1957), p.208.
9. K. Hain, G. Hain, K. V. Roberts, S. J. Roberts, W. Koppendorfer, Z. f. Naturforsch. 15a, 1039-1050 (1960). Also see K. Hain, AERE Report R3383 (1961).
10. K. Hain and A. C. Kolb, Nucl. Fusion Supplement, Part 2, 561-569 (1962).
11. G. B. F. Niblett and Fisher, CLM-R-19 (1962), Culham.
12. T. A. Oliphant, Jr., LAMS-2944 (1963), Los Alamos.
13. D. Duchs, IPP 1/14 and IPP 6/10 (1963), Garching.
14. D. Duchs, Proc. 6th Int. Conf. on Ion Phen. in Gasses, Paris (1963), Vol. II, p.567.
15. A. C. Kolb and R. W. P. McWhirter, Phys. of Fluids 7, 519-531 (1964).
16. D. Duchs and H. R. Griem, Phys. of Fluids 9, 1099-1109 (1966).
17. E. L. Wachspress, Chapter 10, PP.122-123 in "Mathematical Methods for Digital Computers," Edited by A. Ralston and H. S. Wilf, Wiley Inc., New York (1960).

References (continued)

18. A.C. Kolb, Rev. Mod. Phys. 32, 748-757 (1960).
19. C. L. Longmire, "Elementary Plasma Physics," Interscience Pub., N. Y. (1963), - Eqs.(1-21) and (1-39).
20. C. Andelfinger, G. Decker, E. Funfer, A. Heiss, M. Keilhacker, J. Sommer, M. Ulrich, "Plasma Physics and Controlled Fusion Research," Vol. I, pp.249-260, Int. Atomic Energy Agency, Vienna (1966).
21. H. A. B. Bodin, T. S. Green, A. A. Newton, G. B. F. Niblett, J. A. Reynolds, *ibid.* pp.193-221.
22. G. A. Sawyer, V. A. Finlayson, F. C. Jahoda, K. S. Thomas, Phys. of Fluids 10, to be published (1967).
23. R. L. Morse, Phys. of Fluids 10, to be published (1967).
24. L. Spitzer, Jr., "Physics of Fully-Ionized Gases," 2nd edition, Interscience Pub., N. Y. (1962), Fig. 2.1.
25. M. Keilhacker, H. Herold, J. Cooper, D. E. Roberts, "Plasma Physics and Controlled Fusion Research," Vol. I, pp.315-330, I.A.E.A. (1966).

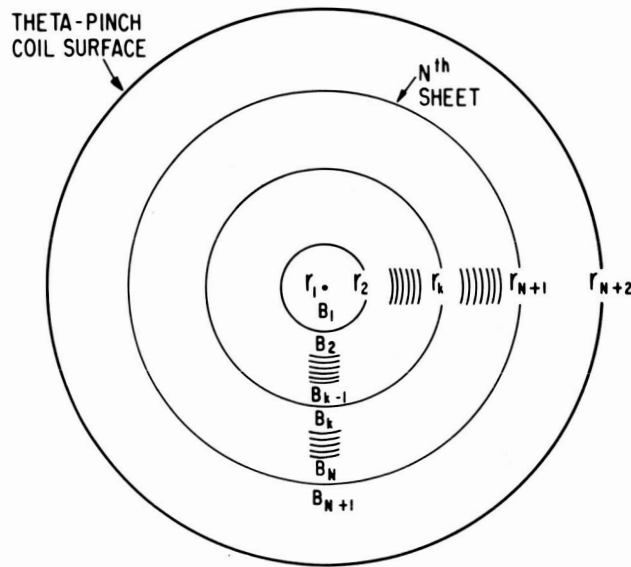


Figure 1.- Sheet and field labeling scheme. Note the axis is labeled r_1 , the first sheet r_2 , the N th sheet r_{N+1} , and the fixed coil surface r_{N+2} .

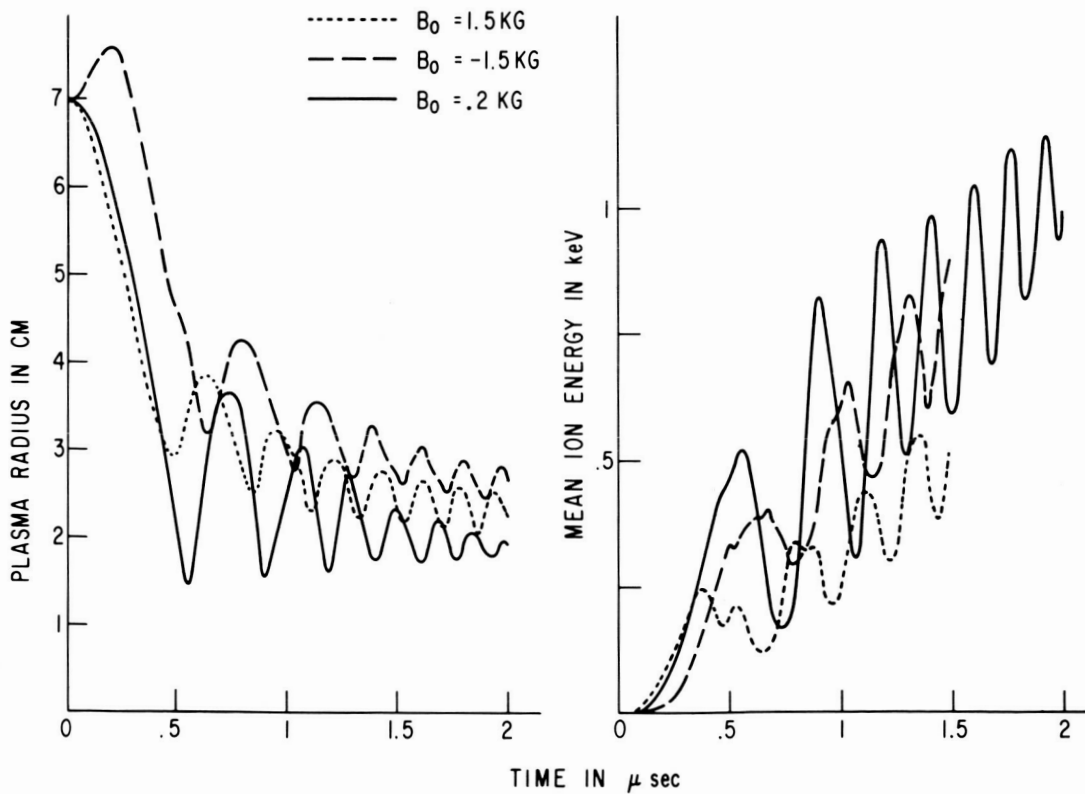


Figure 2.- Plasma radius and mean ion random energy versus time for positive bias, negative bias, and low bias.

FIELD PROFILES

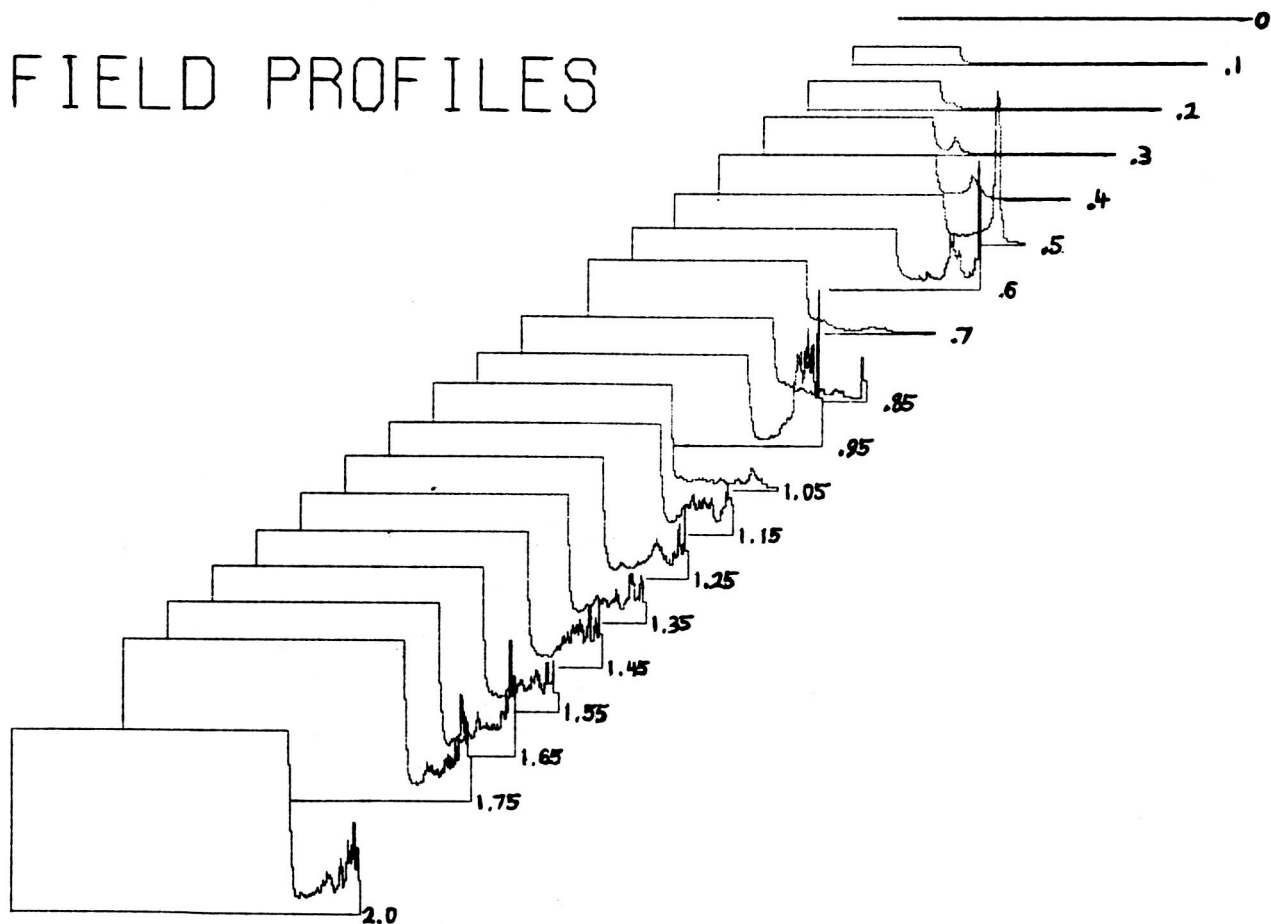


Figure 3.- Magnetic field profiles from axis to coil surface at successive times from 0 to 2 μ sec. Initial bias magnetic field of 0.2 kG. The plasma-vacuum boundary occurs at the radius where the field rises sharply.

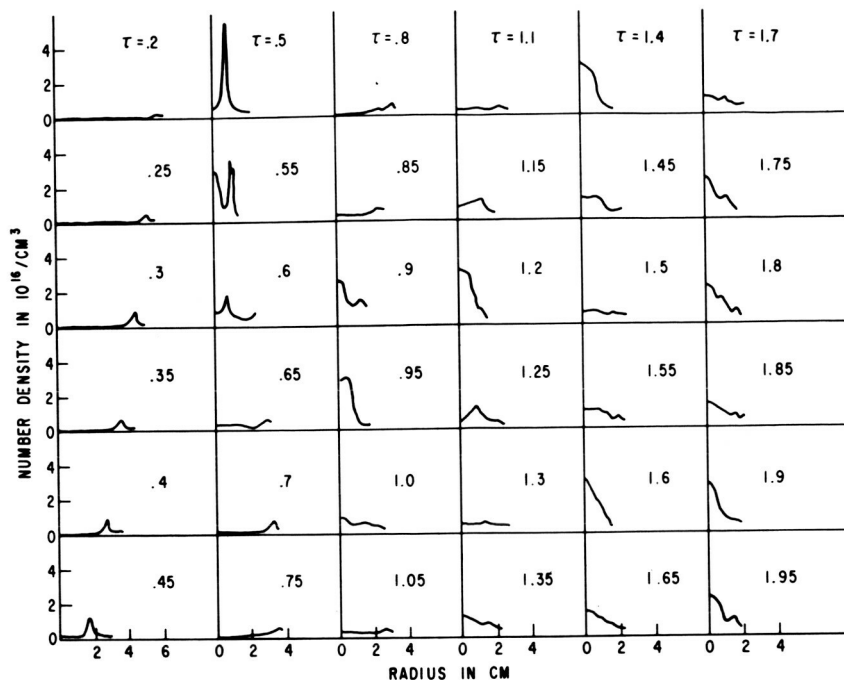


Figure 4.- Plasma density profiles for initial bias of 0.2 kG.

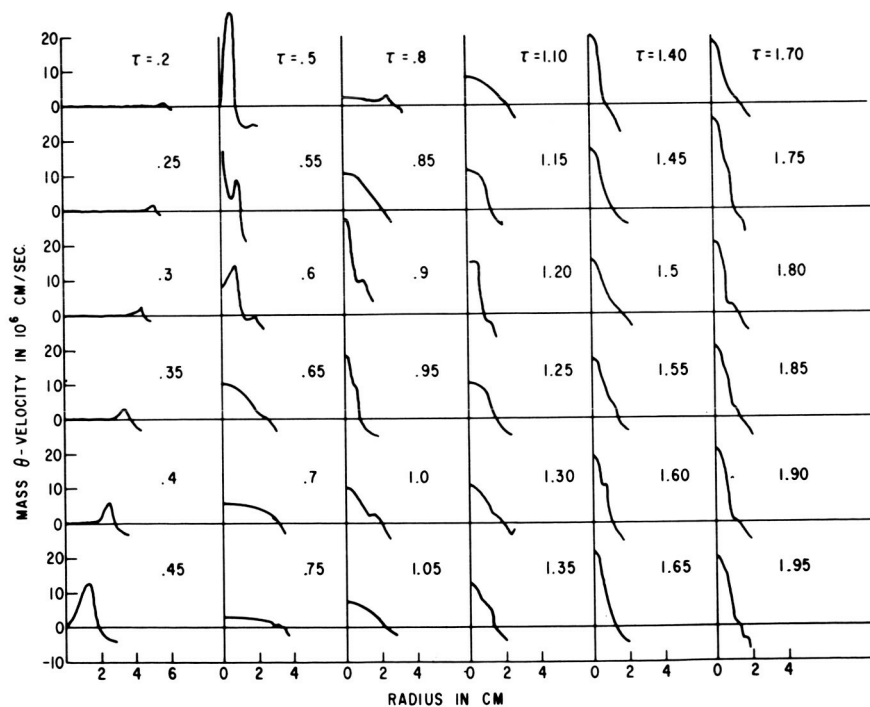


Figure 5.- Mass θ -velocity profiles for initial bias of 0.2 kG. The outside portion rotates in the same direction as an ion, and the inside counter-rotates to conserve overall momentum.

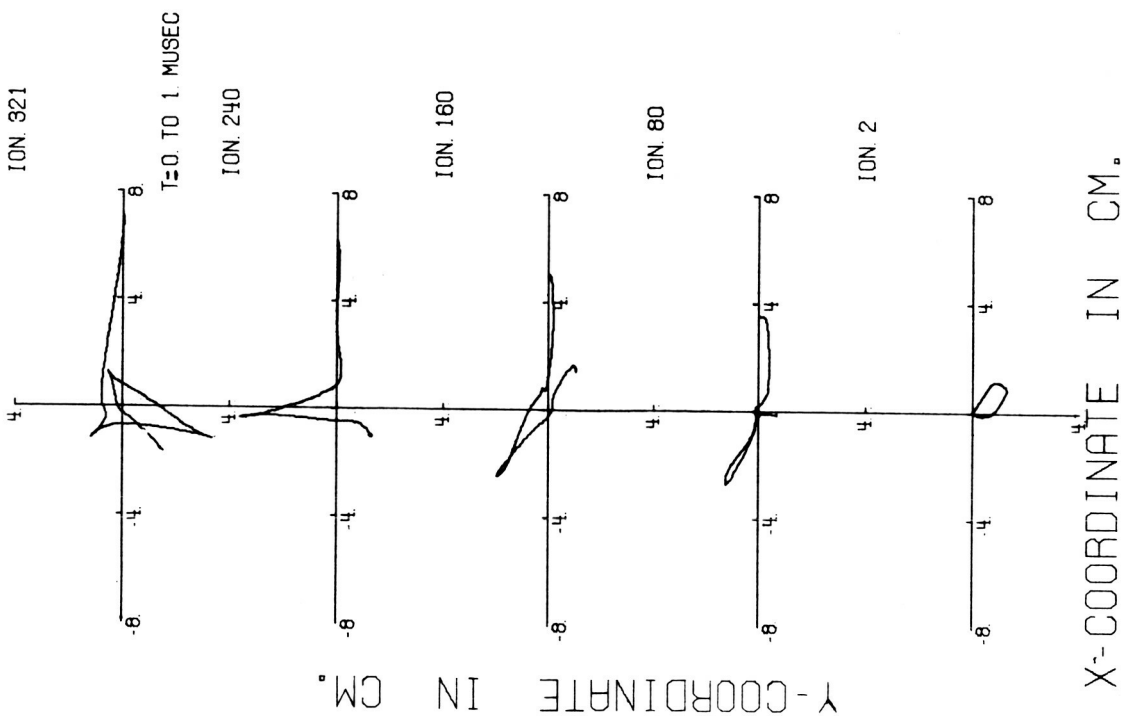


Figure 6.- End view of transverse motion for five ions during the first microsecond. The magnetic field is upward, and the initial bias was 0.2 kG.

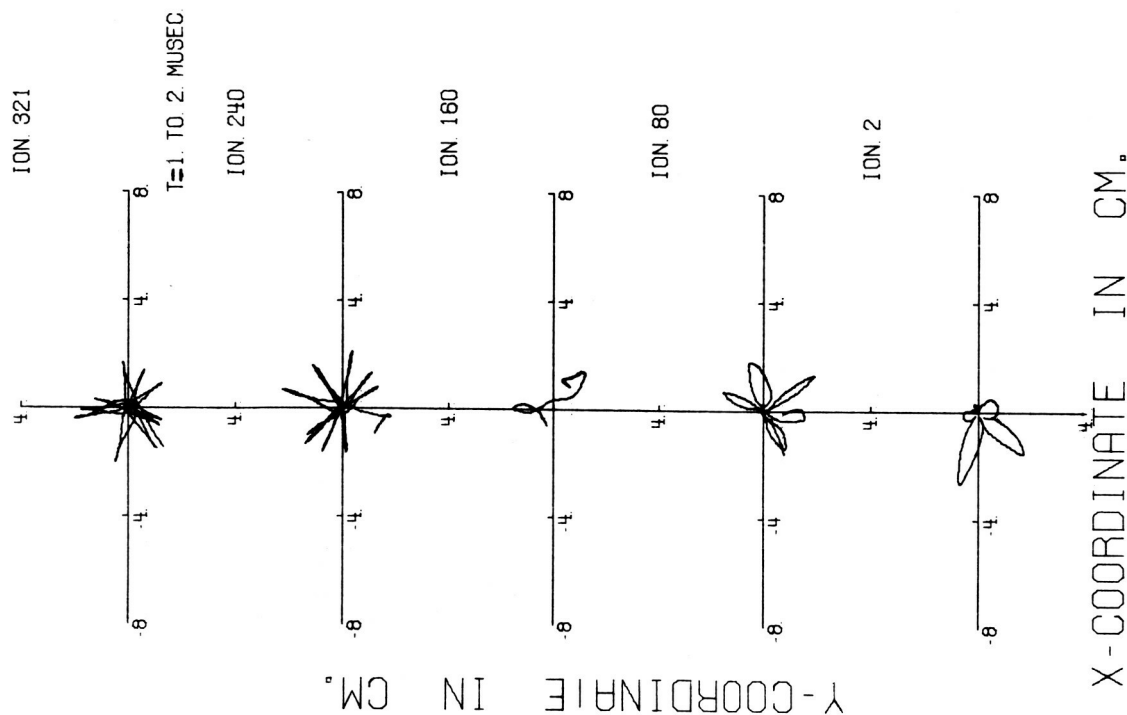


Figure 7.- Transverse ion motion during the second microsecond.

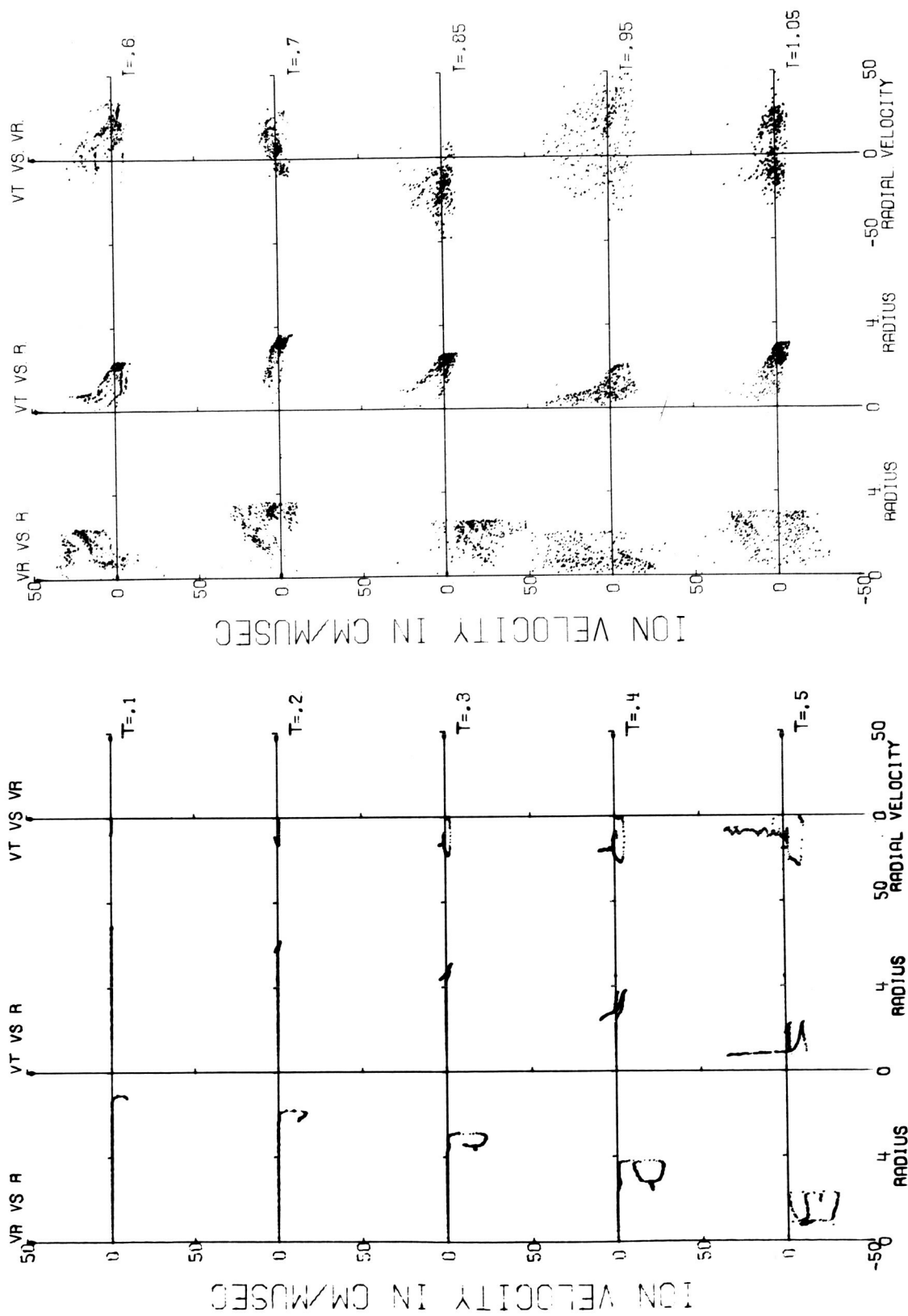


Figure 8.- Ion phase space distribution during $0 - 0.5 \mu\text{sec}$, projected onto the planes $v_r - r$, $v_\theta - r$, and $v_\theta - v_r$. Initial bias of 0.2 kG .

Figure 9.- Ion phase space distribution during $0.6 - 1.05 \mu\text{sec}$.

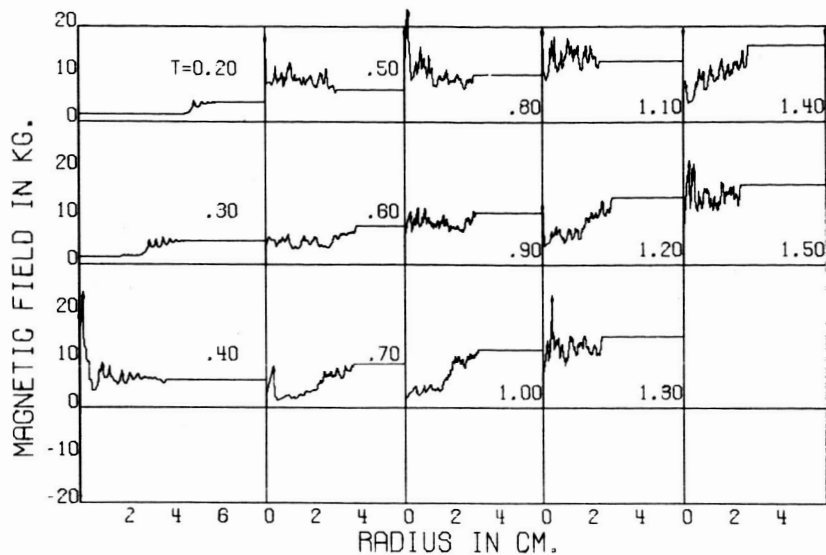


Figure 10.- Magnetic field profiles at successive times. Initial bias field of +1.5 kG.

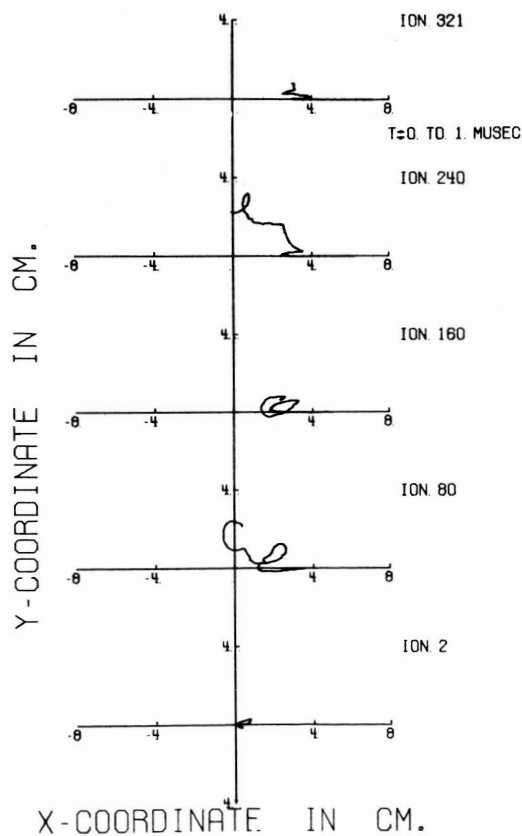


Figure 11.- End view of transverse motion for five ions during the first microsecond. The magnetic field is upward, and the initial bias was +1.5 kG.

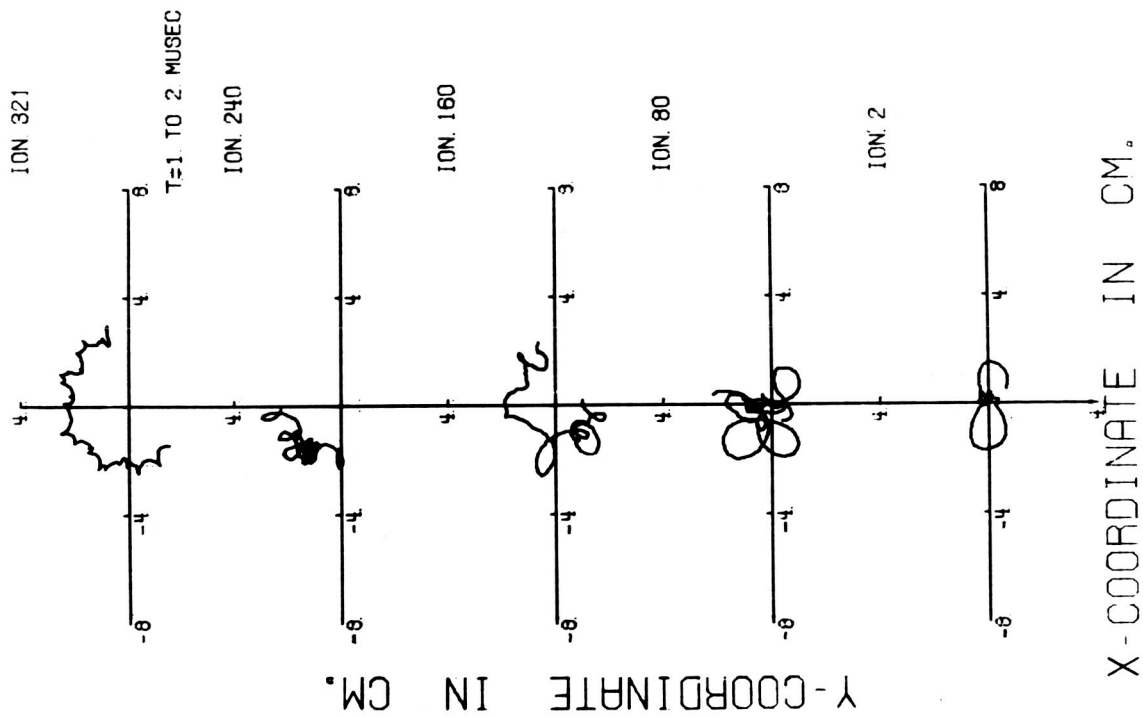


Figure 12.- Transverse ion motion during the second microsecond.

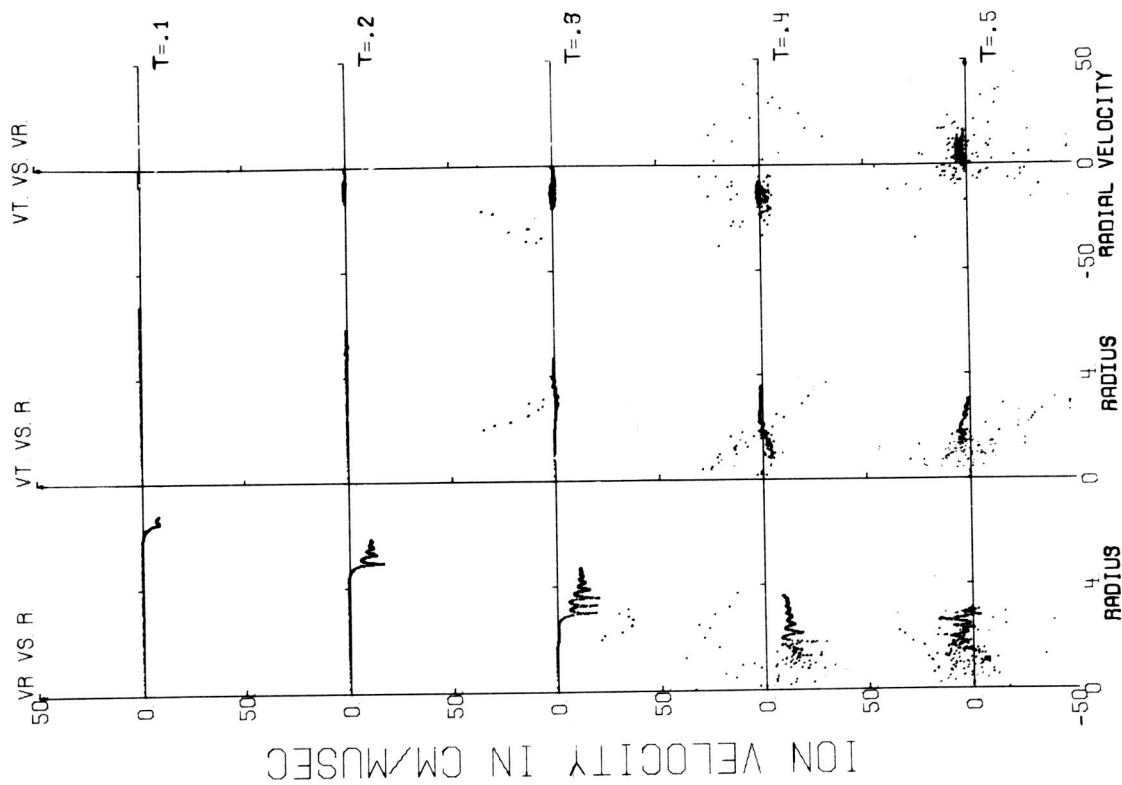


Figure 13.- Ion phase-space distribution during 0 - 0.5 μ sec, projected onto the planes $V_r - r$, $V_\theta - r$, and $V_\theta - V_r$. Initial bias of +1.5 kG.

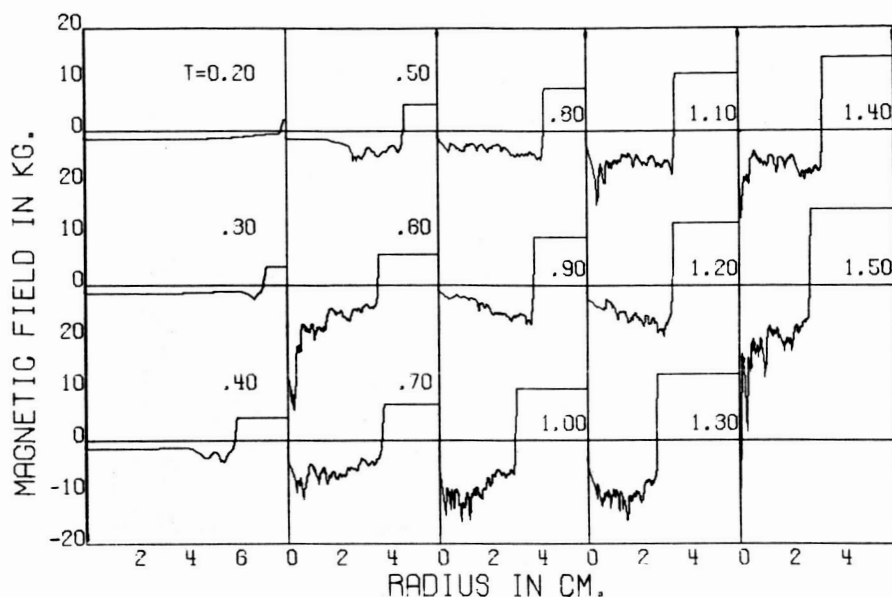


Figure 14.- Magnetic field profiles at successive times. Initial bias fields of -1.5 kG.

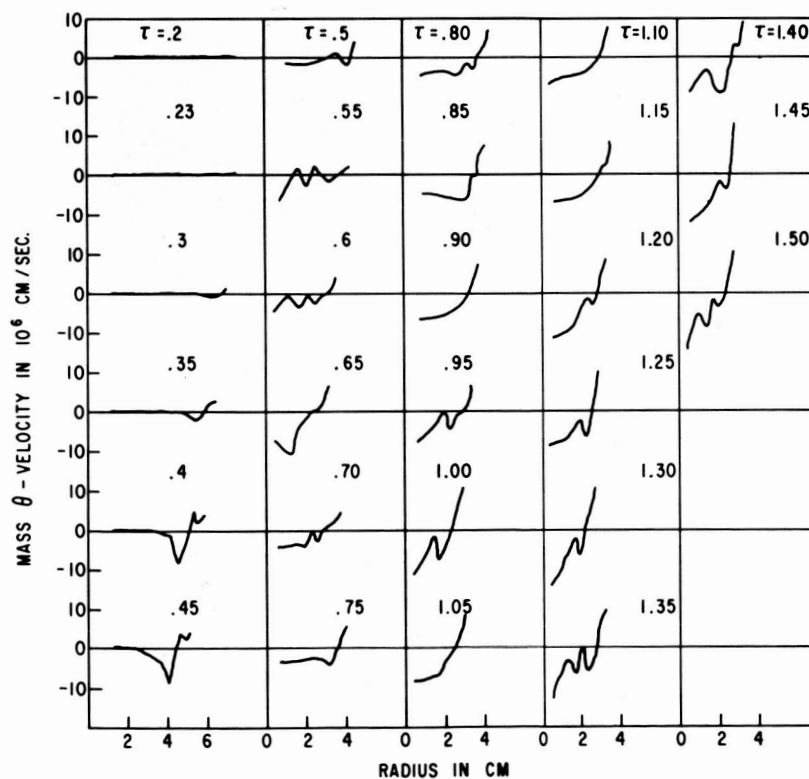


Figure 15.- Mass θ -velocity profiles for initial bias field of -1.5 kG. The outside portion rotates in the same direction as an ion in the internal field (which is into the paper), and the inside counter-rotates to conserve overall momentum.

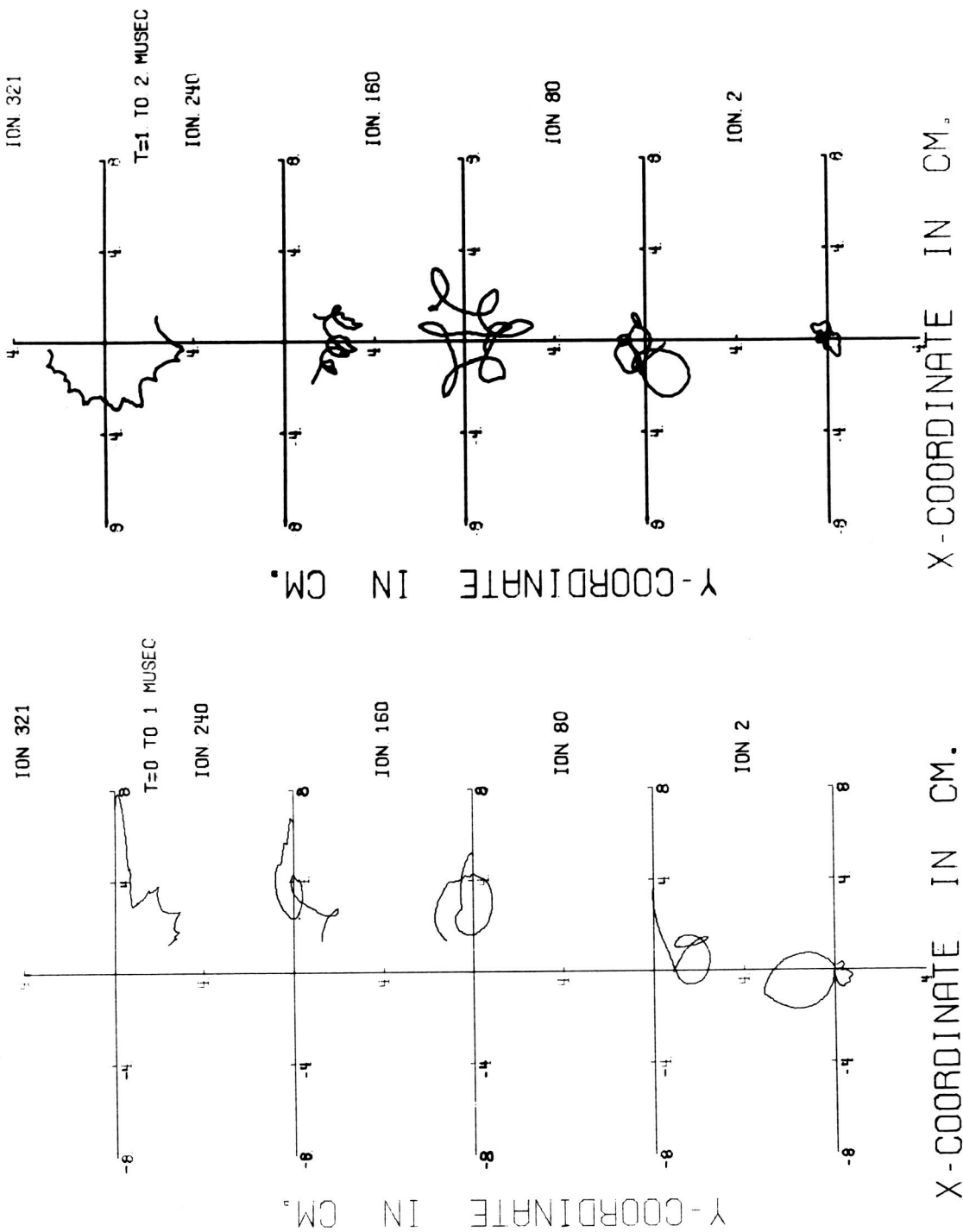


Figure 16.- End view of transverse motion for five ions during the first microsecond. The internal magnetic field is inward, and the external field is upward. Initial bias field of -1.5 kG.

Figure 17.- Transverse motion of ions during second microsecond.

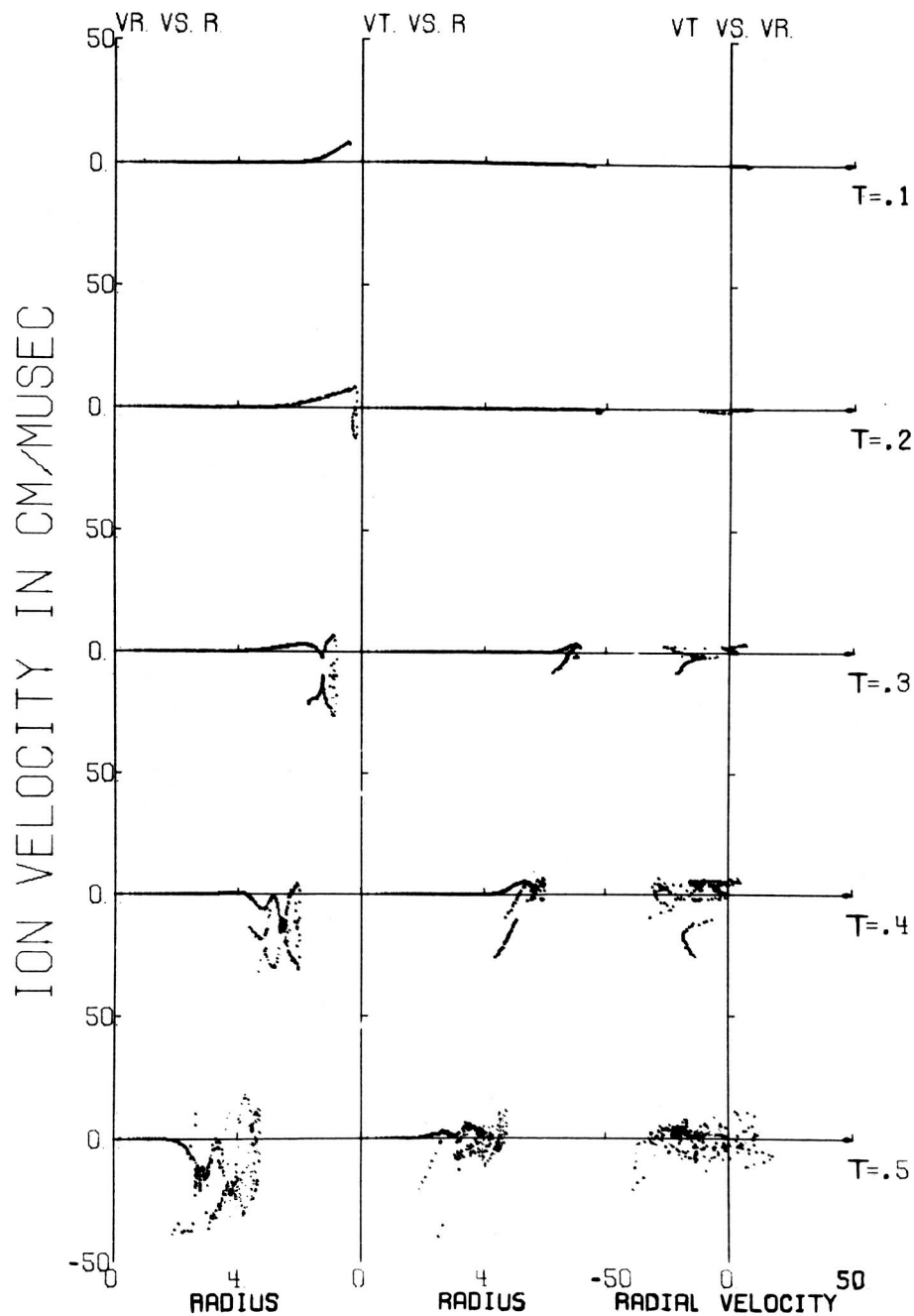


Figure 18.- Ion phase-space distribution during 0 - 0.5 μ sec, projected onto the planes $v_r - r$, $v_\theta - r$, and $v_\theta - v_r$. Initial bias of -1.5 kG.

ASTROPHYSICS

MONTE CARLO METHODS IN STELLAR DYNAMICS

Michel Hénon

C.N.R.S., Institut d'Astrophysique, Paris

There are two fundamental time scales in a stellar system. The first time scale is associated with collective motions and is often called the "crossing time" t_c because it is roughly the time a star takes to cross the system from side to side. (The corresponding time in a plasma is the plasma period.) The second time scale is the "relaxation time" t_r which is associated with the effect of binary interactions. It can be shown (Chandrasekhar, 1942) that:

$$\frac{t_r}{t_c} \approx \frac{1}{40} \frac{N}{\ln N}$$

where N is the total number of stars in the system. For most actual systems the relation $t_r \gg t_c$ holds. Thus, there are two quite different phases in the evolution of the system: first, a comparatively short mixing phase, associated with t_c , and characterized by violent collective motions which presumably die out after some time (this corresponds to Landau damping in a plasma); and a second, much longer relaxation phase, associated with t_r , in which there is a slow change of the structure of the system under the effect of binary encounters. (In plasma physics this is sometimes called "diffusion" or "thermalization.")

This first paper will be devoted to the second phase, or relaxation phase. Thus it is assumed that collective motions have already died out and that the system is now in a quasi-steady state, changing only under the effect of encounters. The evolution of such a system has been studied, until now, by two quite different methods. The first one is the method of pure numerical

experiments: one computes exactly the motions of all stars in the three-dimensional space. This approach is very attractive because it is simple in principle and it does not involve any arbitrary assumption. But unfortunately the computing time grows as $N^{7/2}$ approximately. Thus there is a practical upper limit for N , which is presently about $N = 100$. This is unsatisfactory, because for this value of N , t_r and t_c are of the same order (see formula above), so that the two phases are not separated and there is at the same time mixing and relaxation. Thus the physical situation is not the same as in a actual clusters or galaxies. We would like to have $N = 1000$ at least to be on the safe side. Perhaps this will be possible in the future.

The second classical method is the statistical approach. In this approach the system is represented by a distribution function, which in general is a function of eight arguments: $f(x,y,z,u,v,w,m,t)$, where x,y,z are the coordinates of position, u,v,w are the coordinates of velocity, m is the mass of a star, and t is the time. The change of f with time is given by a Fokker-Planck equation, which can be written in principle (Rosenbluth, MacDonald, and Judd, 1957), but which cannot be solved in practice, except in very particular cases, because it is much too complicated. In order to reduce the Fokker-Planck equation to a manageable form, one has to make a number of more or less arbitrary simplifying assumptions.

We present here a third approach, based on the Monte Carlo technique, which seems to offer some advantages. The basic idea is that during one time step, one does not compute all the interactions between the stars, but only one of them, chosen at random. This approach has been tested in the case of a system homogeneous and infinite in space, with various starting conditions:

1. Initial velocities having all the same modulus, and isotropically distributed. This case has been numerically solved by MacDonald, Rosenbluth, and Wong Chuck (1957), using the Fokker-Planck equation. Their results are exactly reproduced with the Monte Carlo method, and the need of an analytical approximation for the initial phase is eliminated.

2. Velocities initially in a plane. Diffusion in the perpendicular direction is then observed: the distribution tends towards isotropy. A new relaxation time, associated with this process, can be defined, and is found to be of the same order as the usual relaxation time.

3. Velocities initially parallel to a given direction. There is then diffusion in the two perpendicular directions.

4. Stars of different masses (range 1 to 100) and initial velocities not correlated with masses. The system tends towards equipartition of energy and lighter stars are accelerated at the expense of heavier ones.

The advantages of the Monte Carlo method are discussed. It is very fast. The computing time is proportional to N only, and systems of several thousand stars can easily be considered. Also it does not presuppose any restriction on the shape of the distribution function. On the other hand, it rests, as the Fokker-Planck equation itself, on the assumption that the system is adequately described by the one-particle distribution function; this excludes all effects involving correlations between stars, such as the formation of binaries or multiple subsystems. In that respect the Monte Carlo approach cannot supersede the exact N -body computations.

The Monte Carlo method can also be applied to the more realistic case of a finite and inhomogeneous stellar system (Hénon, 1966). Some trial computations have been made for this case and are discussed briefly.

(The full text of this paper will appear in: Bulletin Astronomique, 1967, 3e série, vol. 2, pp. 91-105.)

REFERENCES

- CHANDRASEKHAR, S., 1942, Principles of stellar dynamics (Dover, New York).
HENON, M., 1966, Comptes Rendus Acad. Sci. Paris, 262, 666.
MACDONALD, W. M., ROSENBLUTH, M. N., WONG CHUCK, 1957, Phys. Rev. 107, 350.
ROSENBLUTH, M. N., MACDONALD, W. M., JUDD, D. L., 1957, Phys. Rev. 107, 1.

RELAXATION OF A ONE-DIMENSIONAL SELF-GRAVITATING GAS

Myron Lecar

N67-37753

Smithsonian Astrophysical Observatory
Harvard College Observatory

Leon Cohen

Hunter College of the City University of New York
Smithsonian Astrophysical Observatory

On a suggestion by Prendergast, one of us (Lecar, 1964) began exploiting the one-dimensional ("sheet") model to study the relaxation of a self-gravitating gas. This model describes with fair accuracy ($\sim 1\%$) the motions of stars in the solar neighborhood in a direction perpendicular to the plane of the Galaxy.

To establish a common language, let us point out that in analogy with the plasma frequency $\omega_p^2 \sim n(e^2/m)$, the frequency of the free oscillation of a self-gravitating gas is $\omega^2 \sim n(Gm)$, where G is the gravitational constant and, in one dimension, m is the mass per unit area. Likewise, in analogy with the Debye length $\lambda_D^2 \sim mc^2/n(e^2)$, the radius of a self-gravitating system is $\lambda^2 \sim mc^2/n(Gm^2)$, where c is the thermal velocity. In contrast to a plasma, stable self-gravitating systems have strong density and pressure gradients. Also, the total extent of the system is λ .

Eldridge and Feix (1963) and Dawson (1964) have shown that for a one-dimensional plasma consisting of N sheets, two-particle "encounters" (i.e., correlations) can be neglected for times $< N^2 \omega_p^{-1}$. One of us (Lecar, 1966) obtained similar results for the one-dimensional self-gravitating gas. In fact, we suspect (see appendix) that two-particle correlations can be neglected for times $< N^3 \omega^{-1}$. For galaxies where $N \sim 10^{11}$, two-particle correlations

are negligible for times \gg the lifetime of the universe, and we are led to ask what form $f(x,v,t)$ will be driven to by collective interactions. The most immediate question is: Does f go to a function of the energy or are there additional (collective) integrals? For example, Ford (1961; Ford and Waters, 1963; Waters and Ford, 1966), in his investigation of nonlinearly coupled oscillators, found that the normal modes were essentially integrals of the motion.

Since the energy is symmetric in x and v , the most obvious experiment is to start with an asymmetric distribution and to see if it becomes symmetric. A 1000-sheet model was integrated with the initial conditions

$$\rho(x) = 0.225, \quad 0 \leq x \leq 8/3$$

$$\rho(x) = 0.100, \quad -4 \leq x \leq 0$$

The velocity distribution was Gaussian, with $\langle v^2 \rangle \approx 1$ for all x . Initially, twice the kinetic energy divided by the potential energy was 0.9. This quantity (2 K.E./P.E.) is plotted versus time in Figure 1. The ratio

$$\frac{\int_0^{\infty} \rho(x) dx - \int_{-\infty}^0 \rho(x) dx}{\int_{-\infty}^{+\infty} \rho(x) dx} = \frac{N_{\text{right}} - N_{\text{left}}}{N}$$

is plotted versus time in Figure 2.

A more accurate measure of the asymmetry is the quantity

$$\alpha = \frac{\int_0^{\infty} dx |\rho(x) - \rho(-x)|}{\int_{-\infty}^{+\infty} dx \rho(x)}$$

Values of α at three different times are shown below:

$t\omega^{-1}$	α
0	0.47
12	0.003
24	0.002

A measure of the constancy of ρ is

$$\int_{-\infty}^{+\infty} dx |\rho(x,t) - \rho(x,t + \tau)| = \beta(t,\tau)$$

at $t = 12\omega^{-1}$, $\tau = 12\omega^{-1}$, $\beta = 0.01$. As is shown in Figures 3 and 4, the distribution of energies, $N(\epsilon)$ = Number of sheets with $\epsilon < \epsilon' < \epsilon + 0.2$, also goes to a steady state (the time labels 5000, etc., are in units of $1/208\omega$; $5000 \approx 24\omega^{-1}$). We were surprised by the valley in $N(\epsilon)$ and wondered if $f(x)$ had gone to $f(\epsilon)$. We checked this point in the following way:

1. The statistical weight (phase space volume) of an "energy state" is

$$g(\epsilon) = A(\epsilon + \Delta\epsilon) - A(\epsilon)$$

$$A(\epsilon) = \int_0^\epsilon dx dv = 2 \int_0^{\psi(x)=\epsilon} dx \sqrt{2[\epsilon - \psi(x)]}$$

2. $f(\epsilon)g(\epsilon) = N(\epsilon)$.

3. If ρ is generated by an f that is a function of ϵ only, then

$$\rho[x(\psi)] = 2 \int_0^\infty f(\epsilon) dv = 2 \int_\psi^\infty \frac{f(\epsilon) d\epsilon}{\sqrt{2(\epsilon - \psi)}}$$

The ρ obtained from equation 3 is compared with the experimental value of ρ in Figure 5.

Alternatively, equation 3 considered as an integral equation for $f(\epsilon)$, can be inverted to give

$$f(\epsilon) = -\frac{1}{\pi} \int_{\epsilon}^{\infty} \frac{\frac{d\rho}{d\psi} d\psi}{\sqrt{2(\psi - \epsilon)}}$$

From the experimental values of ρ , an f is generated that is compared with the experimental values of f in Figure 6.

There seems to be little doubt that the system has settled down to an $f(\epsilon)$. But it is an $f(\epsilon)$ that no current statistical theory (e.g., that of Lynden-Bell) would predict. It is clear that any statistical theory will predict an $f(\epsilon)$ monotonically decreasing with ϵ . Our next step must be to investigate a wide class of initial conditions to see if such cases are typical or pathological.

APPENDIX

RELAXATION TIME

If the system is continuous ($N \rightarrow \infty$), the acceleration is

$$a(x) = -4\pi G \int_0^x \rho(y) dy$$

where for simplicity we have assumed $\rho(x) = \rho(-x)$. Hence,

$$a(x' \leq x \leq x' + \Delta x) \approx a(x') - 4\pi G \rho(x')(x - x')$$

On the other hand, if the system is discrete, the acceleration is constant between sheets. So, if there is no sheet between x' and $x' + \Delta x$, then

$$a(x' \leq x \leq x' + \Delta x) = a(x')$$

Thus,

$$\Delta a \approx 4\pi G \rho \Delta x = \frac{\Delta v}{\Delta t}$$

Since $\Delta t \sim (\Delta x/v)$,

$$\frac{\Delta v}{v} \sim \frac{4\pi G \rho (\Delta x)^2}{v^2}$$

From the Virial Theorem ($2 \text{ K.E.} = \text{P.E.}$) we can estimate that

$$v^2 \approx 4\pi G \rho l^2$$

where l is the length of the system. Thus,

$$\left(\frac{\Delta v}{v}\right)^2_{\text{per "collision"}} \sim \left(\frac{\Delta x}{l}\right)^4 \sim \frac{\Delta \epsilon}{\epsilon}$$

Since the number of "collisions" per period $\sim l/\Delta x$,

$$\left(\frac{\Delta \epsilon}{\epsilon}\right)_{\text{per period}} \sim \left(\frac{\Delta x}{l}\right)^3 \sim \frac{1}{N^3}$$

and

$$\tau \sim N^3 \omega^{-1}$$

This gives the second-order effect of two-particle correlations. Dawson (1964) found that $\tau \sim N^2 \omega^{-1}$, which he attributed to three-particle correlations.

REFERENCES

DAWSON, J. M.

1964, Phys. Fluids, vol. 7, 419.

ELDRIDGE, D. C., AND FEIX, M.

1963. Phys. Fluids, vol. 6, 398.

FORD, J.

1961. Journ. Math. Physics, vol. 2, 387.

FORD, J., AND WATERS, J.

1963. Journ. Math. Physics, vol. 4, 1293.

LECAR, M.

1964. IAU Symposium No. 25, Thessaloniki, Greece, August. (See
Proceedings published by Academic Press, New York, 1966, p. 46.)

1966. Fourteenth International Astrophysical Symposium, Cointe-Sclessin,
Belgium, June.

WATERS, J., AND FORD, J.

1966. Journ. Math. Physics, vol. 7, 399.

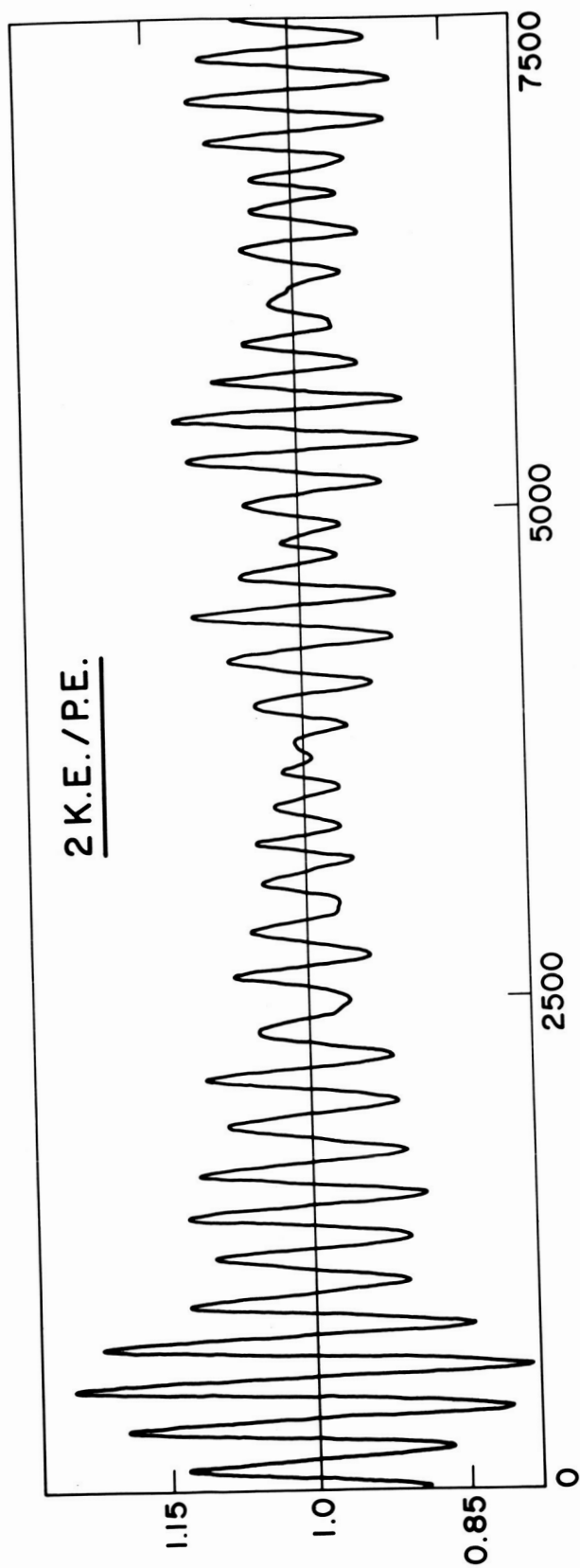


Figure 1.

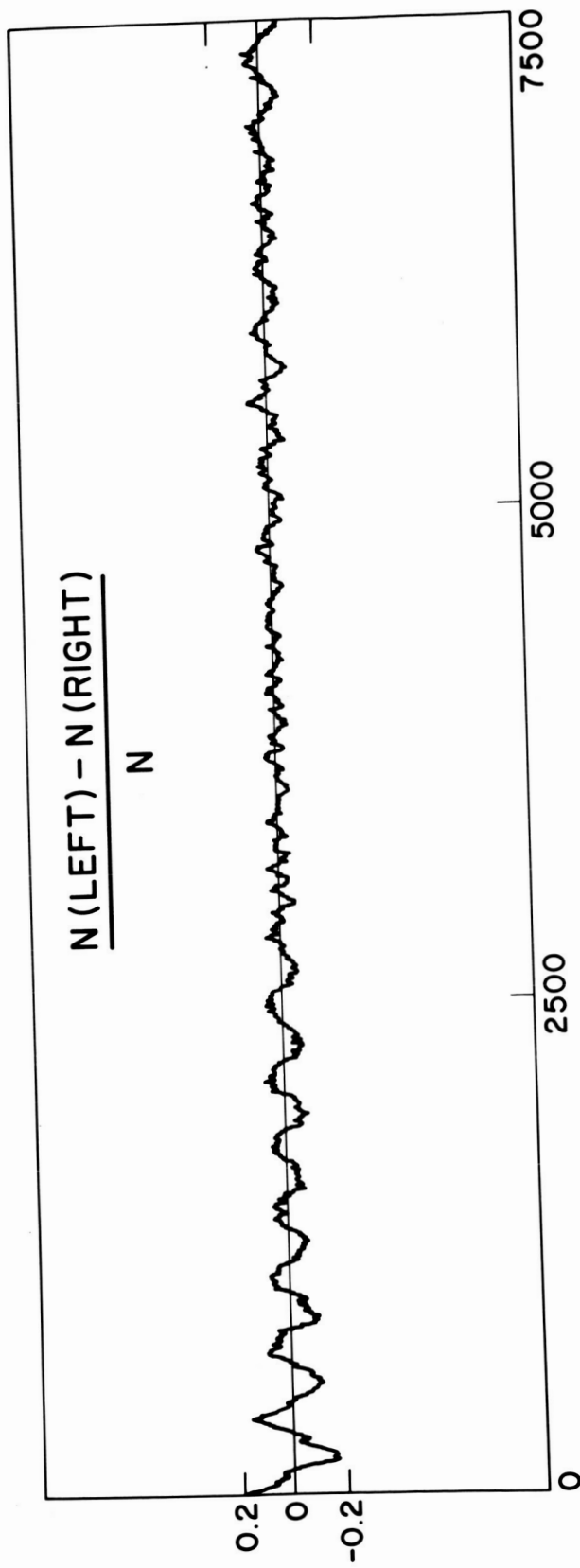


Figure 2.

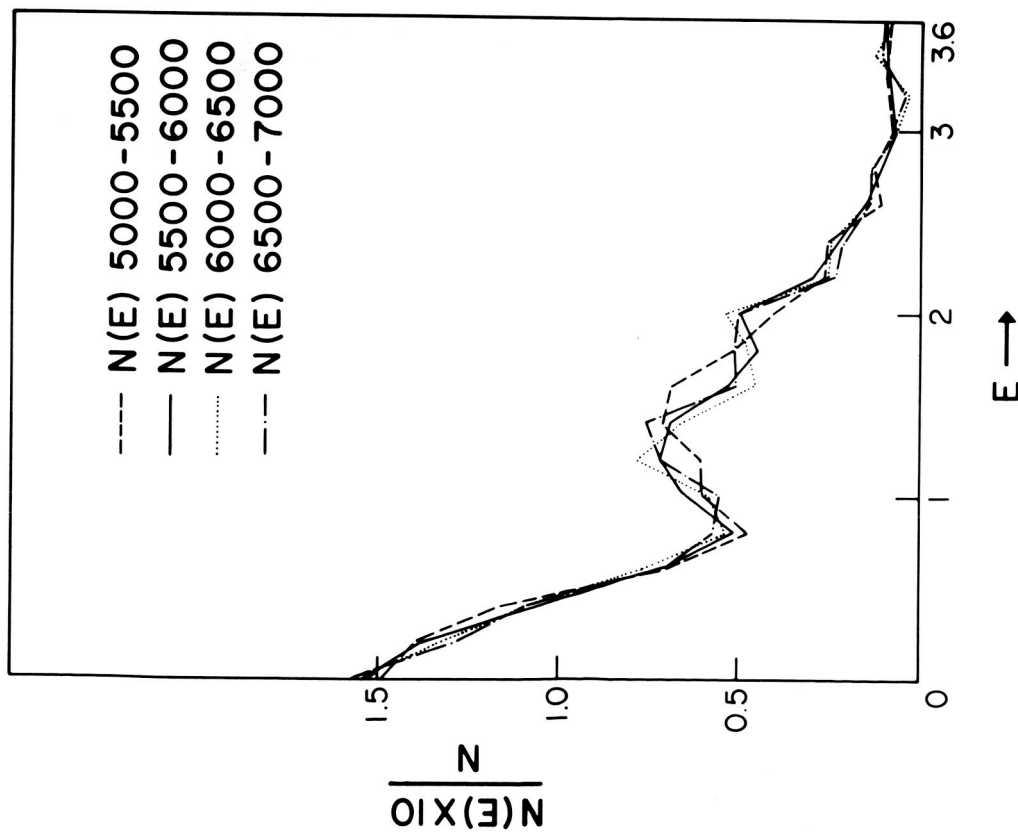


Figure 3.

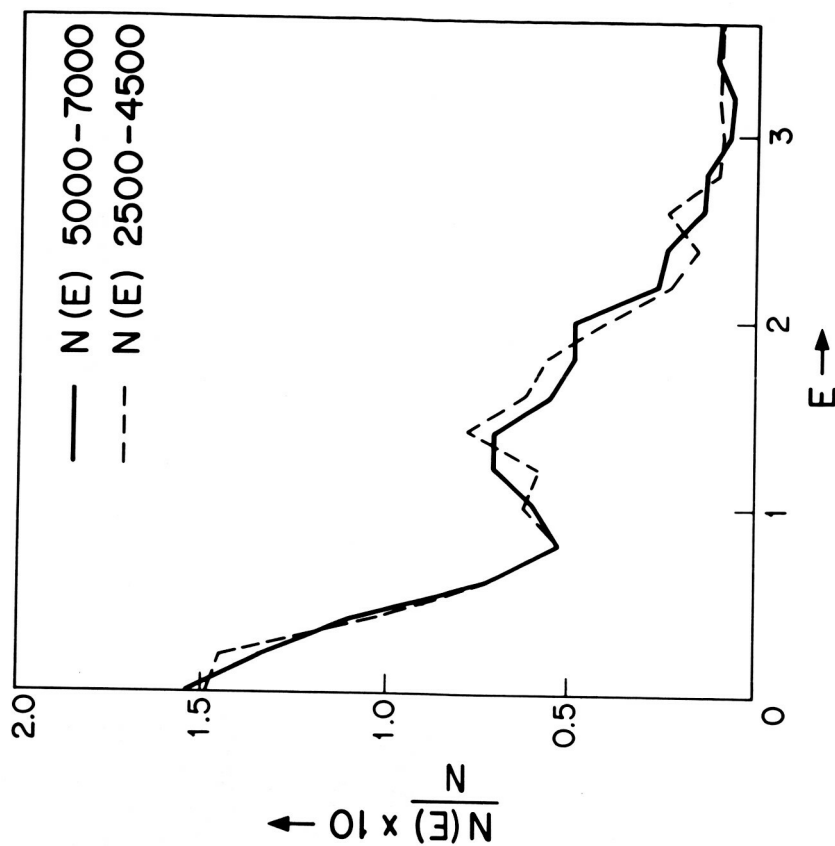


Figure 4.

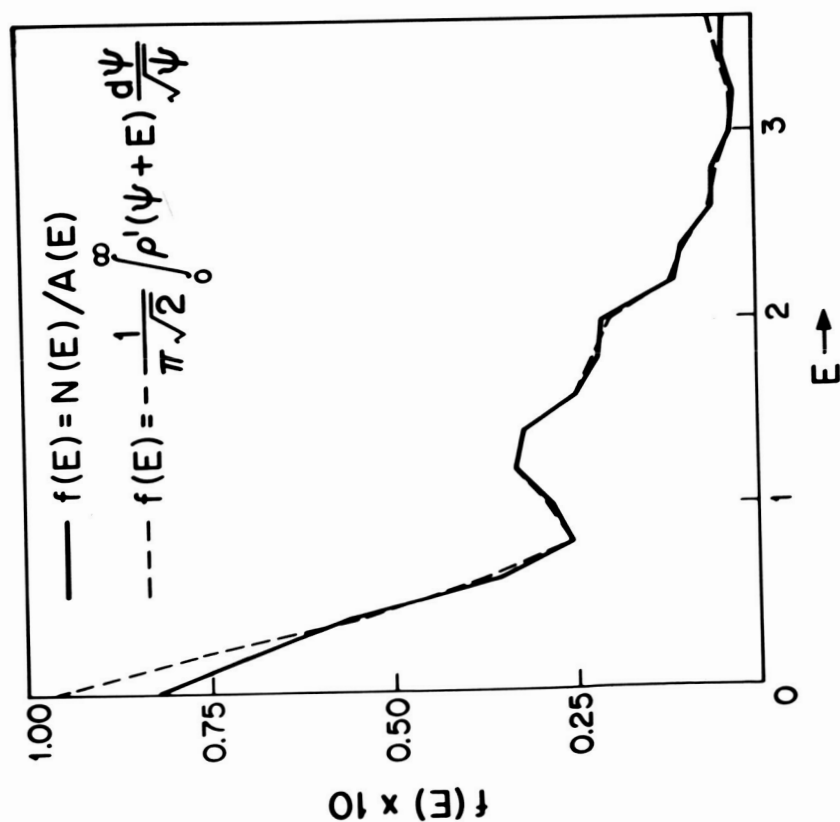


Figure 5.

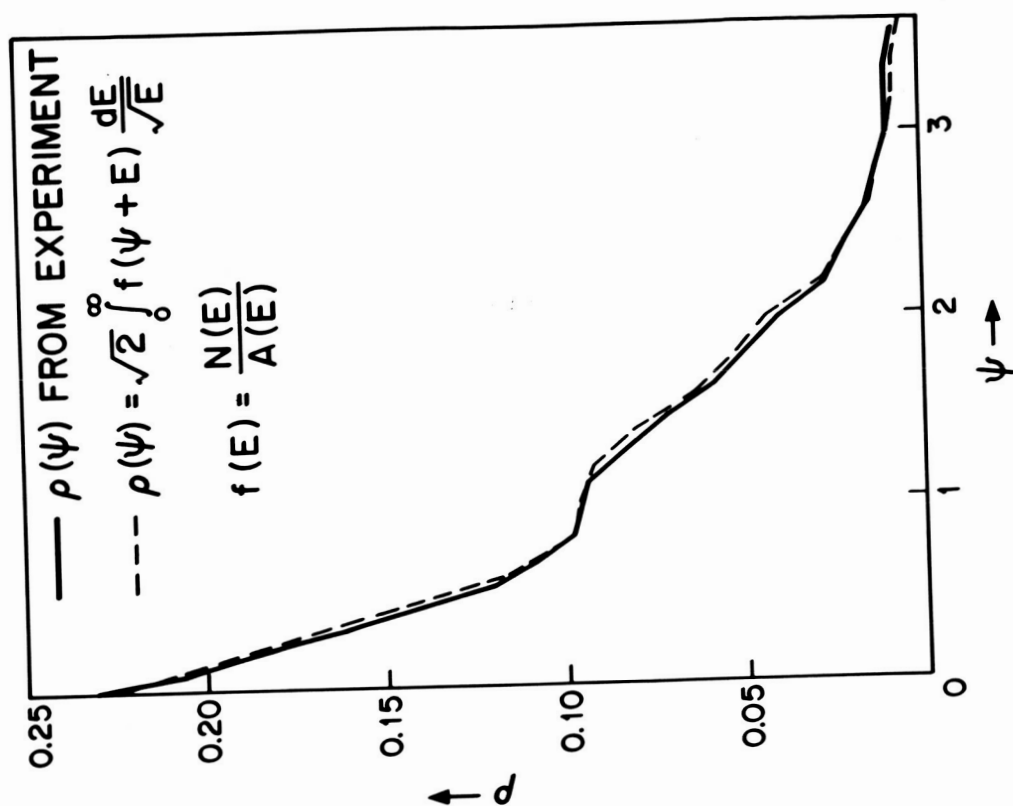


Figure 6.

RELAXATION OF A TWO-COMPONENT
SELF-GRAVITATING GAS

Leon Cohen

Hunter College of the City University of New York
Smithsonian Astrophysical Observatory

Myron Lecar

Smithsonian Astrophysical Observatory
Harvard College Observatory

For self-gravitating systems, the Vlasov equation predicts that the distribution function evolves independent of mass. Hence one can check whether the use of the Vlasov equation is valid by observing certain quantities that would normally be mass dependent. In particular, equipartition of energy among the lighter and heavier masses should not hold.

A numerical experiment was performed on the one-dimensional "sheet" model to verify the above. A system of 1000 particles, 500 of unit mass and 500 of mass 10, was integrated for about 20 dynamical periods. Figures 1 and 2 show the number density for each mass at the beginning and after 20 periods. Figure 3 shows the evolution of the total number density. The time coordinate is so chosen that 1.5 units of time correspond to one period. The words "low" and "high" refer to the lighter and heavier masses, respectively. It is clear that there is no tendency for the higher mass particles to concentrate near the center as would be the case if relaxation by collisions were dominant. Figures 4 and 5, which show the evolution of the total mass density, illustrate the same effect — that the steady state approached is independent of mass.

That equipartition of energy is not obeyed is clearly seen when one follows the time development of the energies possessed by the lighter and heavier masses. Figure 6 shows the time evolution of the average velocity

squared, i.e., kinetic energy per unit mass. The initial conditions were chosen so that the heavy-mass system had considerably more kinetic energy per unit mass than the light-mass system. But as the system evolves, the kinetic energies per unit mass for both subsystems tend to approach the same value. The same result should, of course, hold for the total energy per unit mass. This is illustrated in Figure 7.

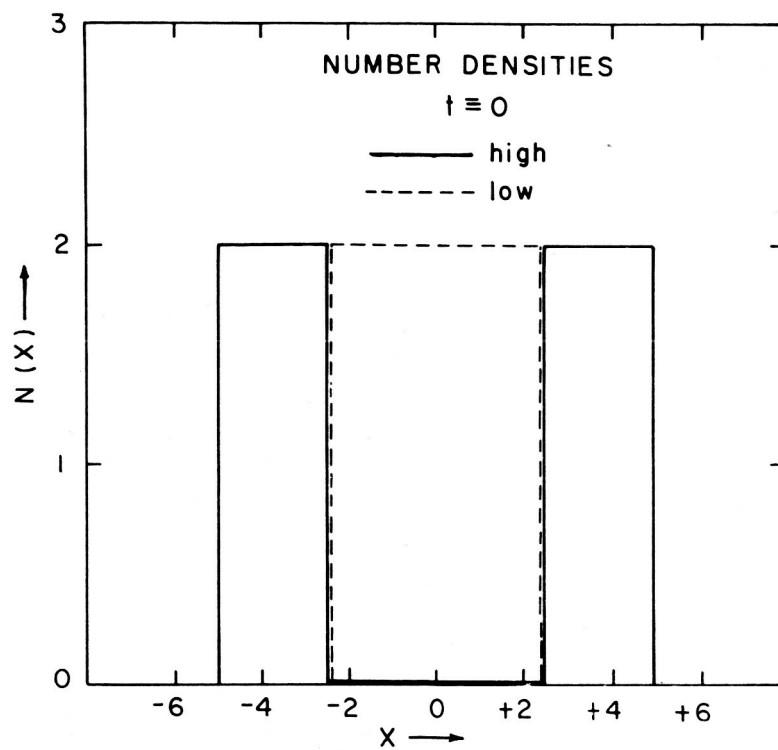


Figure 1.

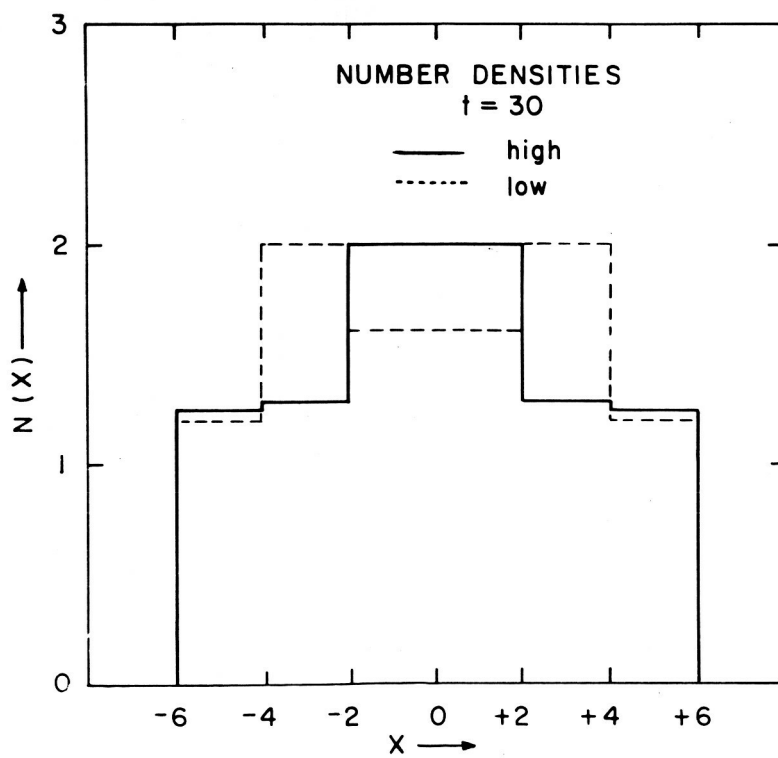


Figure 2.

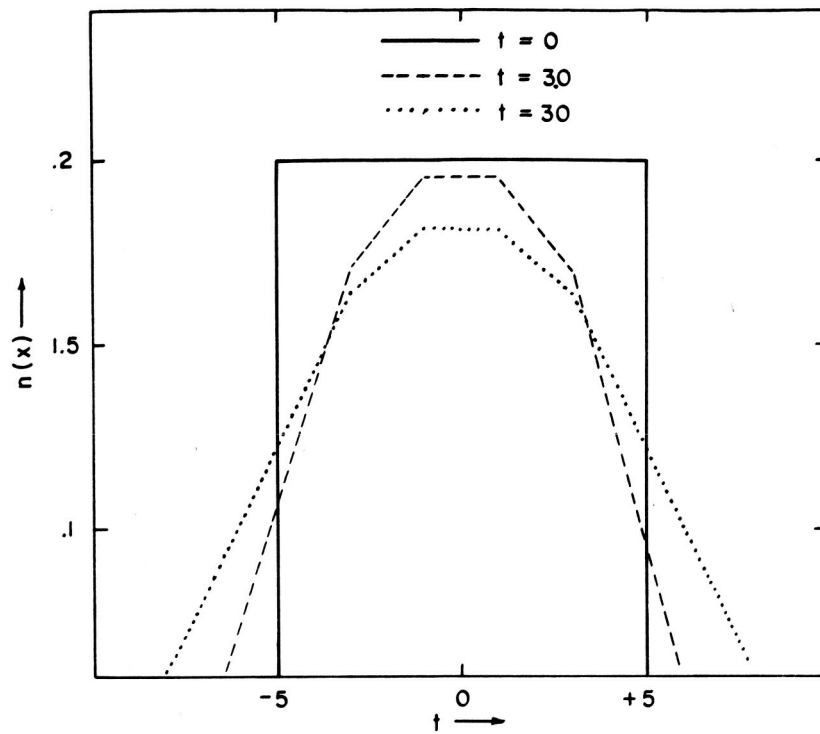


Figure 3.

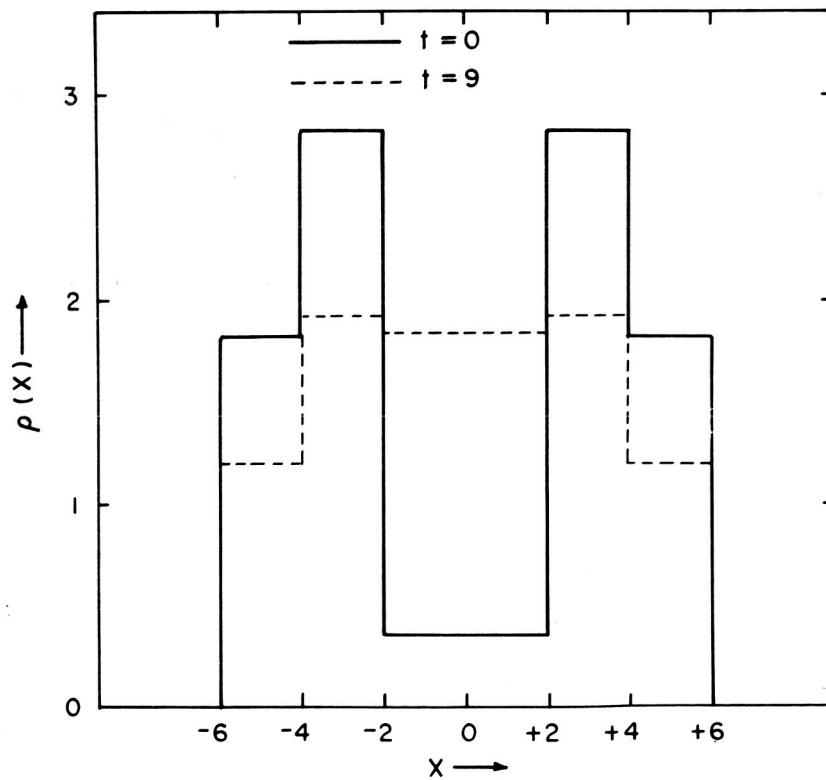


Figure 4.

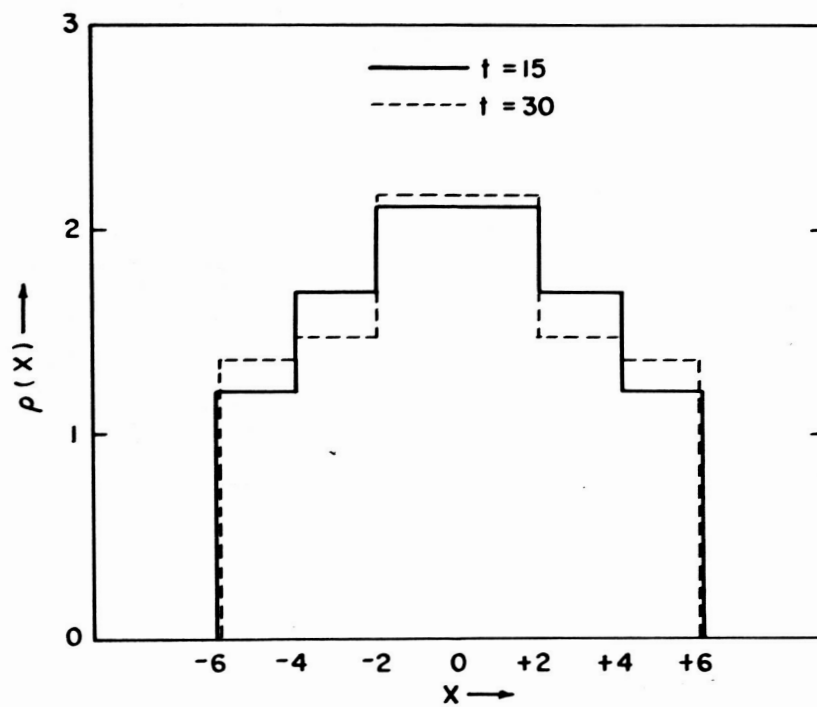


Figure 5.

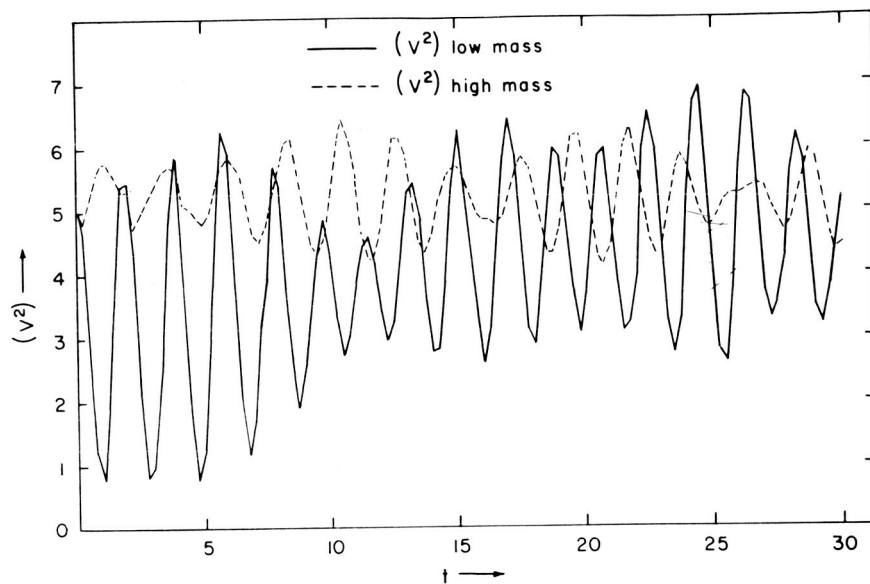


Figure 6.

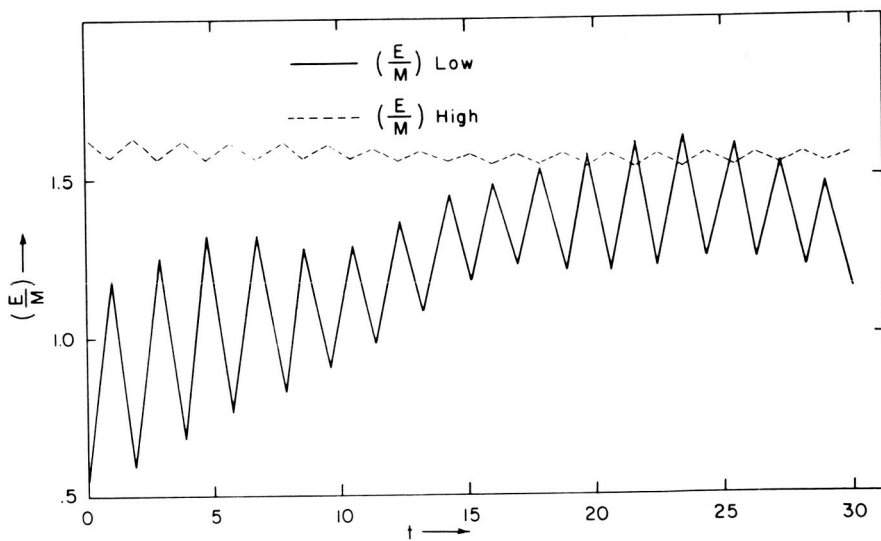


Figure 7.

3
THE N-BODY GRAVITATIONAL PROBLEM
AND THE SIMULATION OF GALACTIC CLUSTERS

By A. HAYLI
Institut d'Astrophysique, and Faculté des Sciences
PARIS 3

SUMMARY

We shall review rapidly the results obtained by different authors in the integration of the N-body problem both in the absence and in the presence of an external field. The problem of simulating galactic clusters will then be discussed and the equations of motion and the first integrals written down. The principle of a new method for integrating the problem is introduced. Finally some results will be given obtained for clusters with 25, 31, 32 and 48 stars with and without a galactic field.

INTRODUCTION

The numerical investigation of the N-body problem in the absence of an external field was first investigated by Von Hoerner [1], [2] and continued by Aarseth [3], [4] and Wielen [5]. The experimental relaxation times agree with Chandrasekhar's formula [6]. A density peak is observed at the center of the systems; binaries are not formed at a very high rate but they are stable especially when they involve massive stars. The velocity distribution is not Maxwellian and shows an excess, for low velocities due to high energy stars close to their apocenter, and for high velocities due to close binaries and stars of the dense central nucleus. The escape rate depends on the mass distribution; it is relatively small in the case of equal masses and the desintegration of such systems due to internal energy exchanges is slow.

The author [7] has studied systems with 15 stars of equal and unequal masses evolving in the galactic field near the galactic plane. Here also the formation of binaries is observed. The escape rate was greater when the stars involved had unequal masses and when a galactic field was present; the escapes took place in directions which made a small angle with the galactic plane.

SYMBOLS

N : number of stars.

m_i : mass of the i -th star.

x_i, y_i, z_i : coordinates of the i -th star in the Ωxyz frame.

$\dot{x}_i, \dot{y}_i, \dot{z}_i$: components of the i -th star velocity.

$\ddot{x}_i, \ddot{y}_i, \ddot{z}_i$: components of the i -th star acceleration.

r_{ij} : $r_{ij}^2 = (x_j - x_i)^2 + (y_j - y_i)^2 + (z_j - z_i)^2$ is the distance between the i -th and j -th stars.

v_i^2 : $v_i^2 = \dot{x}_i^2 + \dot{y}_i^2 + \dot{z}_i^2$

r_i^2 : $r_i^2 = x_i^2 + y_i^2$

R_0 : Sun's distance from the galactic center. $R_0 = 10$ pc.

V_0 : rotational velocity of the Galaxy in the galactic plane at distance R_0 from the center. $V_0 = 250$ km/sec.

ω : $\omega = \frac{V_0}{R_0} \approx 25 \times 10^{-3}$ km/sec.pc.

k_z^2 : component of the force perpendicular to the galactic plane in the vicinity of the Sun at the distance z from the galactic plane.
 $k^2 \approx 8.5 \times 10^{-3}$ km²/sec².pc².

A, B : Oort constants
 $A = 15$ km/sec.kpc ; $B = -10$ km/sec.kpc.

G : Gravitational constant.

λ : $\lambda = -2\omega (A + B + \omega)$.

STATEMENT OF THE PROBLEM

The artificial clusters were placed on a circular orbit (C) of radius R in the galactic plane, R being the Sun's distance from the galactic center. The galactic potential was chosen to have both axial symmetry and symmetry with respect to the galactic plane. Since the stars do not go very far from the circumference of the radius R , we will use a Taylor development of the potential in the vicinity of the latter; the galactic potential in the Sun's neighborhood is determined by the Oort constants and the component of the force perpendicular to the galactic plane.

The stars will be referred to a rotating frame whose origin Ω describes the circumference (C) with the constant angular velocity ω . Fig. 1

THE EQUATIONS OF MOTION AND THE FIRST INTEGRALS.

In the Ωxyz frame the equations of motion of the i -th star can be written

$$m_i (\ddot{x}_i - 2\omega \dot{y}_i + \lambda x_i) = \sum_{\substack{j=1 \\ j \neq i}}^N G \frac{m_i m_j}{r_{ij}^3} (x_j - x_i)$$

$$m_i (\ddot{y}_i + 2\omega \dot{x}_i) = \sum_{\substack{j=1 \\ j \neq i}}^N G \frac{m_i m_j}{r_{ij}^3} (y_j - y_i)$$

$$m_i (\ddot{z}_i + k^2 z_i) = \sum_{\substack{j=1 \\ j \neq i}}^N G \frac{m_i m_j}{r_{ij}^3} (z_j - z_i)$$

In order to know at each instant the positions and the velocities of all the stars, we thus have to integrate a system of $6N$ differential equations of the first order.

It can be shown that the center of mass of the stellar system remains at rest in the Ωxyz frame if its velocity was zero at $t = 0$.

On the other hand a first integral similar to the Jacobi integral in the three-body problem can be found, which, in the absence of an external field, reduces to the energy integral. This first integral can be written

$$\frac{1}{2} \sum_{i=1}^N m_i (v_i^2 - \omega^2 r_i^2) + \frac{1}{2} \sum_{i=1}^N m_i \left[(\lambda + \omega) x^2 + \omega^2 y^2 + k^2 z^2 \right] - \sum_{i=1}^N \sum_{j=1}^{i-1} G \frac{m_i m_j}{r_{ij}} = \text{Const.}$$

We thus have seven quantities which should remain constant in the course of time and which allow us to control the integration. However the "energy" integral is by far the most sensitive to errors in the integration and thus defines the precision.

THE METHOD OF INTEGRATION

In general, the integration of this kind of problem is very long and the use of an individual and variable step becomes indispensable.

Computing time can further be saved by calculating at each integration step not all the forces which act on a star but only those which have varied appreciably. We are thus led to introduce for each force a time scale which is the time after which this force is recalculated.

In order to achieve this, we "quantify" the time by deciding that the time scales pertaining to the different calculated forces may not have any value but only certain determined values which form a geometrical progression

$$\frac{t_0}{b}, \frac{t_0}{b^2}, \frac{t_0}{b^3}, \dots, \frac{t_0}{b^m}, \dots$$

where t_0 is a unit time and b an integer greater than 1; $\frac{t_0}{b}$ must be of

the order of the largest possible time scale.

In this manner, the forces are arranged in a certain number of categories with each category t having a determined time scale; the category corresponding to the time scale $\frac{t_0}{b^m}$ will be called category m .

The stars themselves are grouped in categories; the category order to

which a star belongs is that of the highest category to which one or more of the forces acting on the star under consideration belong.

As far as the stars are concerned, this classification in categories of increasing order corresponds roughly to a decreasing distance from the central region; however, this localization is only approximative as the two components of a close binary situated far from the central region will belong to a high order category.

Physically, we will thus have a small central nucleus in the cluster whose stars belong to the highest appearing category and in which the forces will very often be recalculated; we then have a larger nucleus containing the stars of the two highest categories and in which the forces will be recalculated b times less, and so on.

Thus at any given moment we integrate the equations of motion considering only the stars of one nucleus. The effect on the nucleus of the external stars is represented by a time polynomial which is reajusted at the end of the integration step.

Finally, it is obvious that a star will not always belong to the same category. Each time that it is reconsidered in the integration process, it may be able to pass to a different category depending on its situation relative to the other stars. Thus categories can appear which have an order higher than the ones used at the beginning of the calculation. However a limit is fixed for the highest order which can appear. The method is described with more details in [7].

This integration method has proved to be useful from the viewpoint of saving calculation time. Till now only integration formulae of the first order have been used. However the utilization of higher order formulae will probably increase the precision without an exaggerated increase of computing time, i.e., the efficiency of the method will be increased.

THE INITIAL CONDITIONS

Similar initial conditions were used in all cases, viz, a constant density stellar distribution within a sphere of 1 pc radius and an isotropic and uniform velocity distribution; at $t=0$ a suitable transformation is applied to the velocity magnitudes such that the virial theorem is satisfied and the center of mass remains at rest at the origin.

For $N=25, 32$ and 48 , the stars all have masses equal to $1 M_{\odot}$. In the cases $N=31$ there is 1 star of $16 M_{\odot}$, 8 stars of $2 M_{\odot}$ and so on yielding a total mass of $80 M_{\odot}$.

RESULTS

The investigation of systems with 25, 31, 32 and 48 stars during a time interval varying from 30×10^6 years to 90×10^6 years leads to the following general results.

1) The central density increases in spite of significant fluctuations whether the cluster is isolated or evolves in the galactic field or whether it contains stars of different masses or not. For the examples calculated, the density attains mean values greater than $2500 M_{\odot} / \text{pc}^3$ in the central nucleus. The number of stars making up the central peak diminishes with time. It is relatively small when the cluster contains stars of different masses; in this case it is the more massive stars which contribute to the central density peak.

2) The escape rate depends largely on the mass distribution whether the cluster is isolated or not; it is much higher when the cluster contains stars of different masses; in the examples here considered the rate does not seem to increase in the presence of a galactic field.

3) A formation of close binaries is observed in the small central nucleus. Their number is not big and they are more stable when they contain one very massive star. In the case of clusters with stars of equal masses, it may happen that one member of the binary changes its companion star, the new companion always already belonging to the central nucleus.

4) As we may expect on account of the reasons discussed in the introduction, the velocity distribution shows a significant deviation from the Maxwellian distribution.

5) Finally, the result which specifically applies to clusters evolving in the vicinity of the galactic plane is their flattening. This flattening is not due to stars which have escaped; in fact, it is found that the clusters left behind are still significantly flattened in a direction normal to the galactic plane. Due to this reason the remaining clusters have a large extension in the galactic plane. This fact might be important from the observational viewpoint; hence, when a galactic cluster is observed, it is possible that its central region - which is larger than the small central dense nucleus - is taken to be the whole cluster, the stars which are farer away being held for field stars. The fact that the calculations show in which direction the flattening occurs and give an idea of its magnitude could help in looking for stars which belong to a galactic cluster but are far from the central region.

FUTURE RESEARCH

We intend to continue the simulation of galactic clusters with N of the order of 100, using a more powerful computer than the one used for the preceding investigations (IBM 7040).

The central regions of clusters should be investigated more carefully during larger physical times. In particular, it would be interesting to know the rate of formation of binaries with more precision and to compare with observations. This rate might lead to a dynamical determination of the ages of clusters if the existence of original binaries is excluded, i.e., of binaries existing since the birth of the clusters and issuing from a condensation of the gas into two very close stars. On the same plan, the evolution of such

binaries in an artificial cluster could also be investigated.

The execution of these projects necessitates a higher precision in the integration method. This also is a point which will be developed.

REFERENCES

- | | | |
|---------------------|------|---------------------------------|
| [1] VON HOERNER, S. | 1960 | Zs.f.Ap. <u>50</u> , 184. |
| [2] " | 1963 | Zs.f.Ap. <u>57</u> , 47. |
| [3] AARSETH, S.J. | 1963 | M.N.R.A.S. <u>126</u> , 223. |
| [4] " | 1966 | M.N.R.A.S. <u>132</u> , 35. |
| [5] WIELEN, R. | 1965 | Thesis, Heidelberg. |
| [6] CHANDRASEKHAR | | Principles of stellar dynamics. |
| [7] HAYLI, A. | 1967 | Bull. Astr. Tome 2, Fasc.1. |

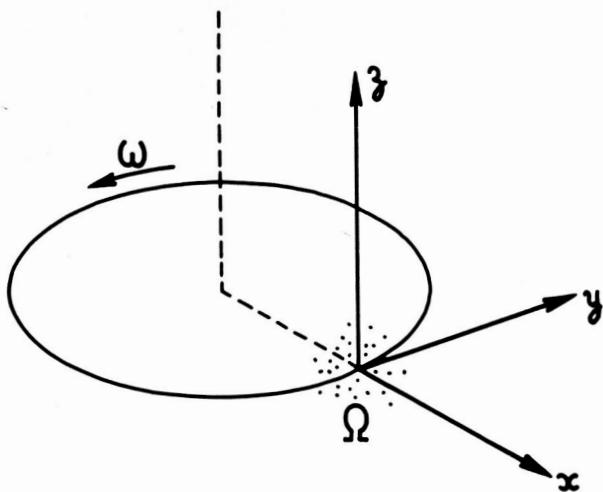


Figure 1.

N67-37756

ONE- AND TWO-DIMENSIONAL MODELS TO STUDY

THE EVOLUTION OF STELLAR SYSTEMS

by Frank Hohl

Langley Research Center

A variational principle has been applied to one-dimensional stellar systems to show that stationary distribution functions which are always decreasing in going outward from the center of the system are stable. Other stationary distributions may be unstable as is illustrated by means of computer experiments.

Numerical experiments with a simple two-dimensional rod model show that the spiral structure and other filamentary structure of galaxies may result from purely gravitational effects.

It will now be shown that the minimum energy property which has been obtained by Hohl and Feix (ref. 1) for a special distribution can be extended to arbitrary distribution functions. The water-bag model illustrated in figure 1 is used in the analysis. The contours $v_+^{(k)}(x,t)$ and $v_-^{(k)}(x,t)$ describe surfaces of constant distribution function $f = f_k$. According to the Liouville theorem the phase space bounded by the contours is incompressible so that the area bounded by the contours is conserved. In the limit of a very large number of contours the water-bag model can be used to construct arbitrary distribution functions.

To simplify the equations we assume symmetric contours $v_+^{(k)} = v_-^{(k)} = v^{(k)}$. It is easily shown (ref. 2) that the equations which stationary contours $v^{(k)}$

must satisfy are

$$v^{(k)} \frac{dv^{(k)}}{dx} - E = 0. \quad (1)$$

E is given by

$$E(x) = 4\pi Gm \left(\frac{N}{2} - 2 \sum_k A_k \theta^{(k)}(x) \right) \quad (2)$$

where G is the gravitational constant, N is the number of mass sheets, each of mass m per unit area, in the system.

A_k is defined by the distribution function

$$f = \sum A_k [\delta_{-1}(v-v_-^{(k)}) - \delta_{-1}(v-v_+^{(k)})]$$

with $\delta_{-1}(z) = \int_{-\infty}^z \delta(\zeta) d\zeta$. The variable $\theta^{(k)}$ used in equation (2) is

$$\theta^{(k)} = \int_{-x_s^{(k)}}^x v^{(k)}(\zeta) d\zeta \quad (3)$$

where $x_s^{(k)}$ is the end point of the contour k. The total energy of the system is

$$\begin{aligned} W &= \sum_k \int_{-x_s^{(k)}}^{x_s^{(k)}} g dx \\ &= \sum_k \int_{-x_s^{(k)}}^{x_s^{(k)}} \left\{ \frac{1}{3} m A_k v^{(k)3} - 2 m x A_k \left[4\pi Gm \left(\frac{N}{2} - 2 \sum_k A_k \theta^{(k)} \right) \right] \right\}. \quad (4) \end{aligned}$$

Extremizing the integral for W requires that g satisfy the Euler-Lagrange equation

$$\frac{\partial g}{\partial \theta^{(k)}} - \frac{d}{dx} \left(\frac{\partial g}{\partial v^{(k)}} \right) = 0 \quad (5)$$

or

$$v^{(k)} \frac{dv^{(k)}}{dx} - E = 0 \quad (6)$$

which are the equations for the stationary contours.

If equations (6) are to represent a minimum energy configuration then Legendre's criterion of the second variation of g must be satisfied. That is, the quadratic form whose coefficient matrix has the elements

$$a_{ij} = \frac{\partial^2 g}{\partial v^{(i)} \partial v^{(j)}} \quad (7)$$

must not be negative. Since only the diagonal elements

$$a_{kk} = 2m A_k v^{(k)} \quad (8)$$

are nonzero, the Legendre condition requires that

$$A_k > 0 \quad (9)$$

for all k . Equation (9) is equivalent to stating that the distribution function must always decrease in going outward from the center of the system where $f = f_1$ must be the largest. If equation (9) is satisfied the system is a minimum energy configuration and is always stable. However, if $A_k > 0$ is not satisfied for all k the system is not a minimum energy configuration. The system may then be unstable since the contours $v^{(k)}$ can now be deformed while keeping the total system energy constant. Numerical experiments with a one-dimensional model have been performed for two contour systems to illustrate the interchange instability which destroys the stationary state. For the

two systems investigated $A_1 = -A_2$. Figure 2 shows the normalized stationary contours for four values of u , the ratio of the minimum to maximum star energy. The results of the computer experiments are shown in figures 3 and 4. In the first case shown in figure 3 the ratio of the minimum to maximum star energy is 0.4. The figure shows that the stationary contours of the 2000 star system are quickly distorted while the heavier outer water bag tries to displace the inner bag. Figure 4 shows the results for a 2000 star system with a ratio of minimum to maximum star energy equal to 0.25. The growth of the instability is now much slower because the central water bag or hole is much smaller.

Results of additional computer experiments have shown that certain distribution functions, $F(U)$, that are not always decreasing with increasing energy, U , remain stable over many periods, $2\pi/\sqrt{4\pi G\rho}$, where ρ is the mass density of the sheets per unit area. For such distribution functions the bulk of the "stars" are in a region where $F(U)$ is monotonically decreasing but $F(U)$ has a high energy bump corresponding to particles in the spiral arm that develop in the two-dimensional phase space (ref. 2).

The evolution of two-dimensional stellar systems made up of mass rods that are of infinite extent in the z -direction has also been investigated for 400 and 500 rod systems. The force acting on a particular mass rod is obtained by summing directly over the $1/r$ force from each mass rod. This is a time-consuming process and the application of fast methods of solving the Poisson equation would speed up the calculations. The relatively large grid size which would be required by the method of solving the Poisson equation will smooth the force due to the near neighbors of the particles and will

affect the evolution of the system. The effect of the near neighbors is included if the force acting on a mass rod is obtained by summing directly the $1/r$ force from each particle in the system. It would be more desirable to study the evolution of a system of mass points moving in a plane. This can also be done by simply summing the $1/r^2$ force from each mass point. However, the more rapid divergence of the $1/r^2$ force for near neighbors now requires that a much smaller time step be used in the computations resulting in a considerable increase in computer time.

The system is advanced in time in the following manner. First, the force acting on all particles is computed by summing the $1/r$ force for all particles. Second, the system is advanced for a small time step Δt and the process is repeated. The results of the calculations are displayed in x - y coordinate space. During the calculations the total energy and angular momentum is computed to check on the accuracy of the computations. The normalizations $4\pi G = 1$ and $m = 1$ have been used for all the calculations.

Figure 5 shows the time development of a system of 400 mass rods which has an initially rectangular distribution of uniform density in x - y space. The system has an initial thermal energy equal to $1/5$ of the initial potential energy plus an initial solid body rotation equal to nearly twice that required to oppose the gravitational force towards the center of the system. It can be seen from figure 5 that the system quickly develops into a barred spiral. However, at a later time the spiral structure has almost completely disappeared and the system approaches a configuration similar to an elliptical galaxy. The time has been normalized to ω_r^{-1} , the inverse of the frequency of rotation.

The remaining two-dimensional calculations were performed for 500 particle systems which have an initially uniform circular distribution in x - y space and zero thermal velocity. The evolution of such systems is then studied for various values of initial solid body rotation. The initial positions are obtained by using a random number generator which gives a nearly uniform distribution over a circular region of the x - y plane.

We now present the results for the case where the frequency of rotation, ω_r , equals ω_g , the frequency required such that the centrifugal force balances the gravitational force. Thus,

$$\omega_r = \omega_g = \sqrt{2\pi G\rho} \quad (10)$$

where ρ is the mass density of the rods per unit length. The resulting evolution of the system is shown in figure 6. The time has been normalized to ω_g^{-1} . Figure 6 shows that the system is relatively stable. At $t = 6.32\omega_g^{-1}$ there appear four irregular spiral arms. However, at a later time the spiral arms almost completely disappear and the system takes an appearance reminiscent of an elliptical galaxy.

The results for the case of zero initial rotation are presented next. Figure 7 shows that after an initial implosion the system expands again and presents some highly irregular filamentary structure. After a second implosion the temperature of the system increases due to the randomness of the initial positions. The pressure due to the temperature then tends to reduce the oscillations and the system again takes a form similar to an elliptical galaxy.

For $\omega_r = \frac{1}{2} \omega_g$ the system again contracts initially and then expands again. The results are shown in figure 8. An irregular structure appears

initially which tends to disappear at a later time. Also at time $t = 4.20\omega_g^{-1}$ the system is clustered into two aggregates which combined again at a later time.

In figure 9 the results for the case $\omega_r = 1.3 \omega_g$ are shown. The system pulsates and shows some irregular structure. The general behavior is very similar to that of the previous case for $\omega_r = \frac{1}{2} \omega_g$.

The simple two-dimensional model for a stellar system showed that spiral and other filamentary structure can result from purely gravitational effects. Since the spiral structure and other filamentary structure tend to disappear in time one would conclude that the spiral galaxies are young galaxies which later develop into elliptical galaxies. However, these results should be confirmed with a computer model using point masses that are confined to move in a plane.

REFERENCES:

1. Hohl, F., and Feix, M. R. 1967, *Astrophys. J.*, vol. 147, no. 3, March 1967, pp. 1164-1180.
2. Hohl, F., Ph.D. Thesis, 1967, College of William and Mary, Williamsburg, Virginia.

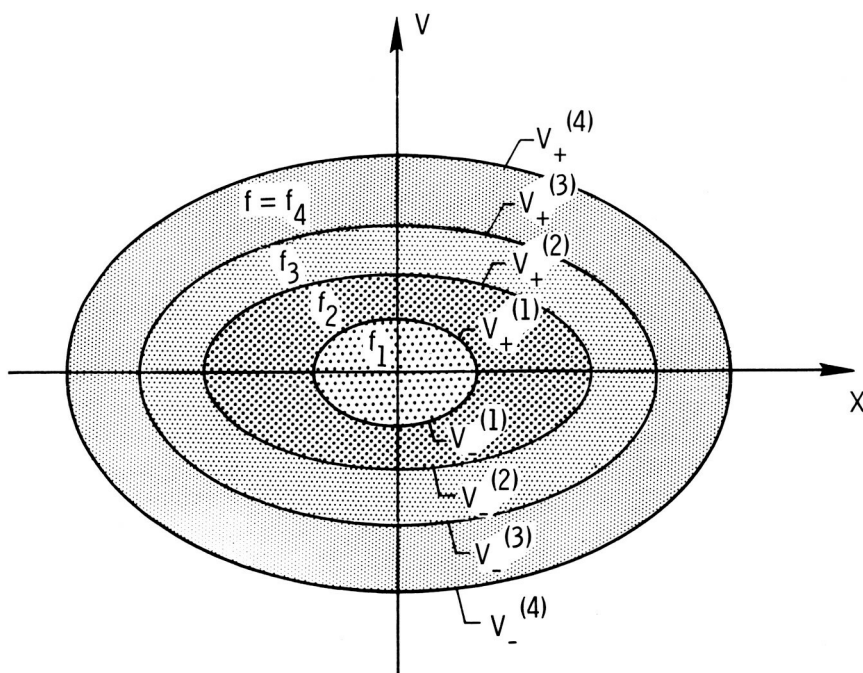


Figure 1.- Illustration of a multiple contour water-bag distribution.

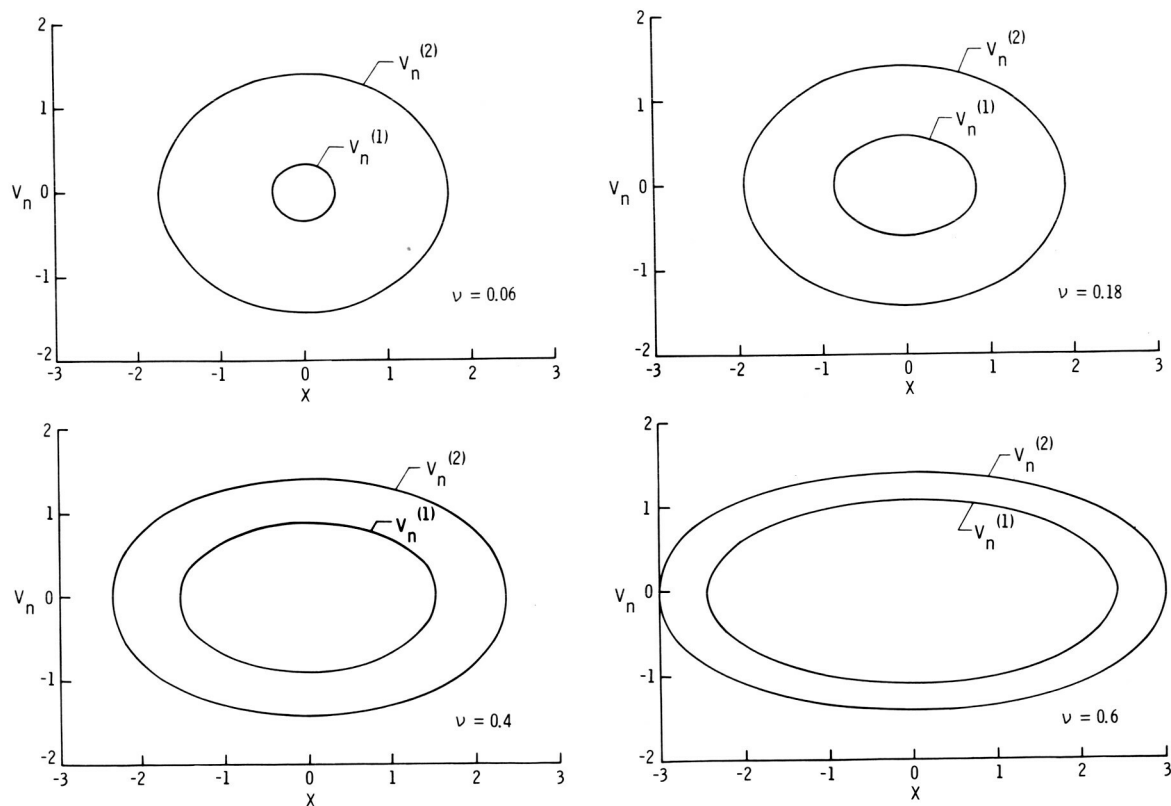


Figure 2.- Stationary contours for two-contour water-bag distributions.

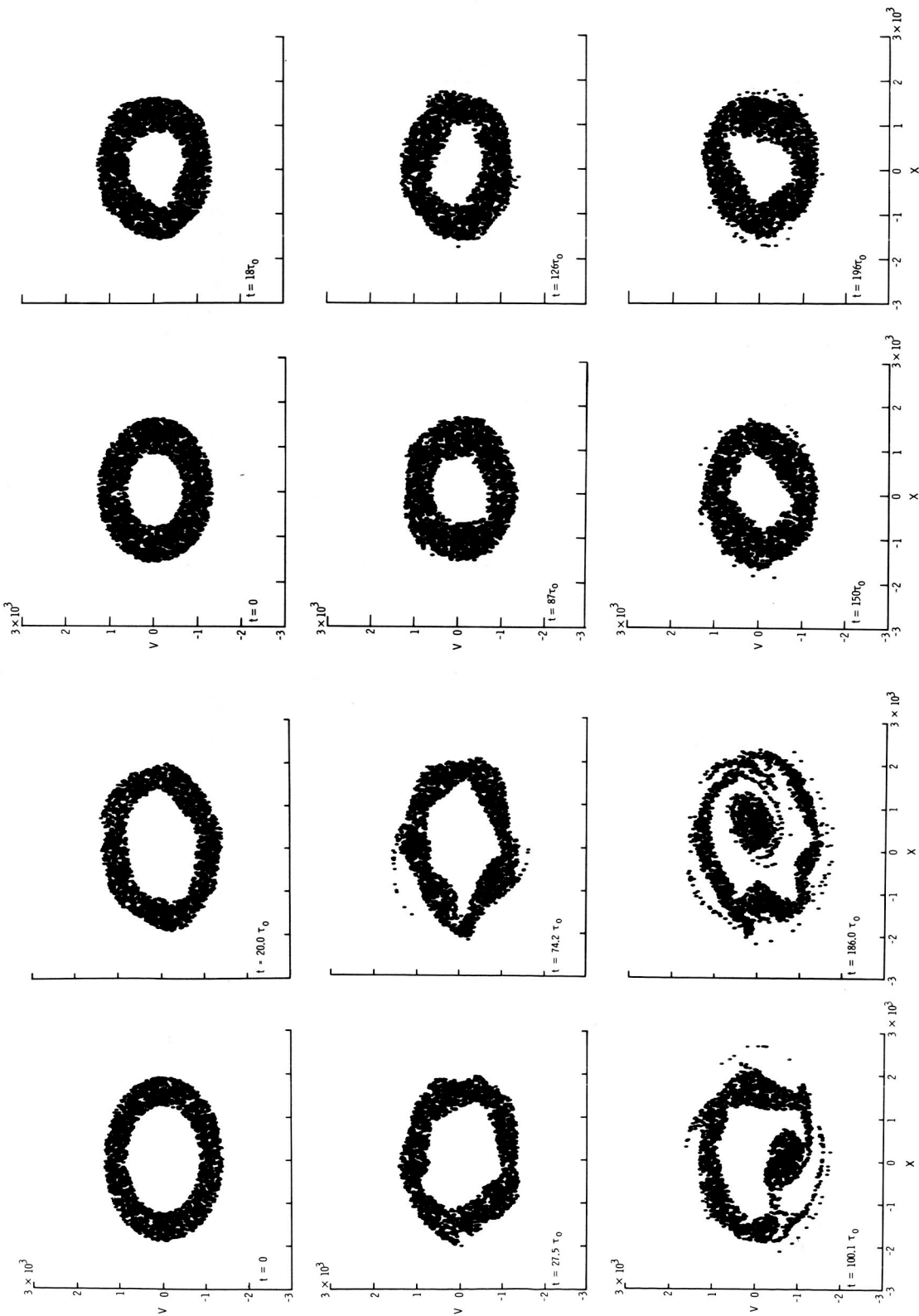
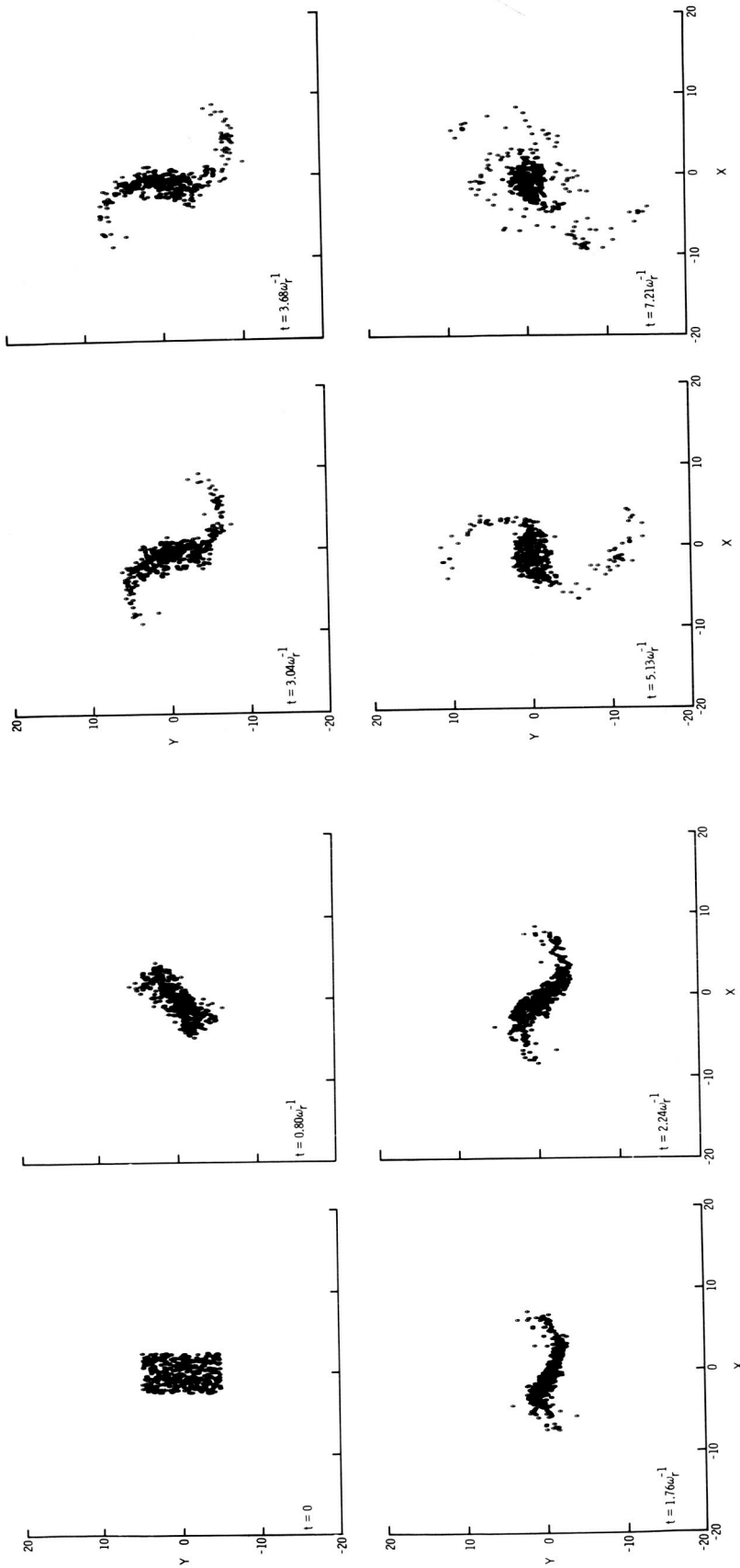


Figure 3.- Illustration of the time development of an unstable two-contour system with $\nu = 0.4$.

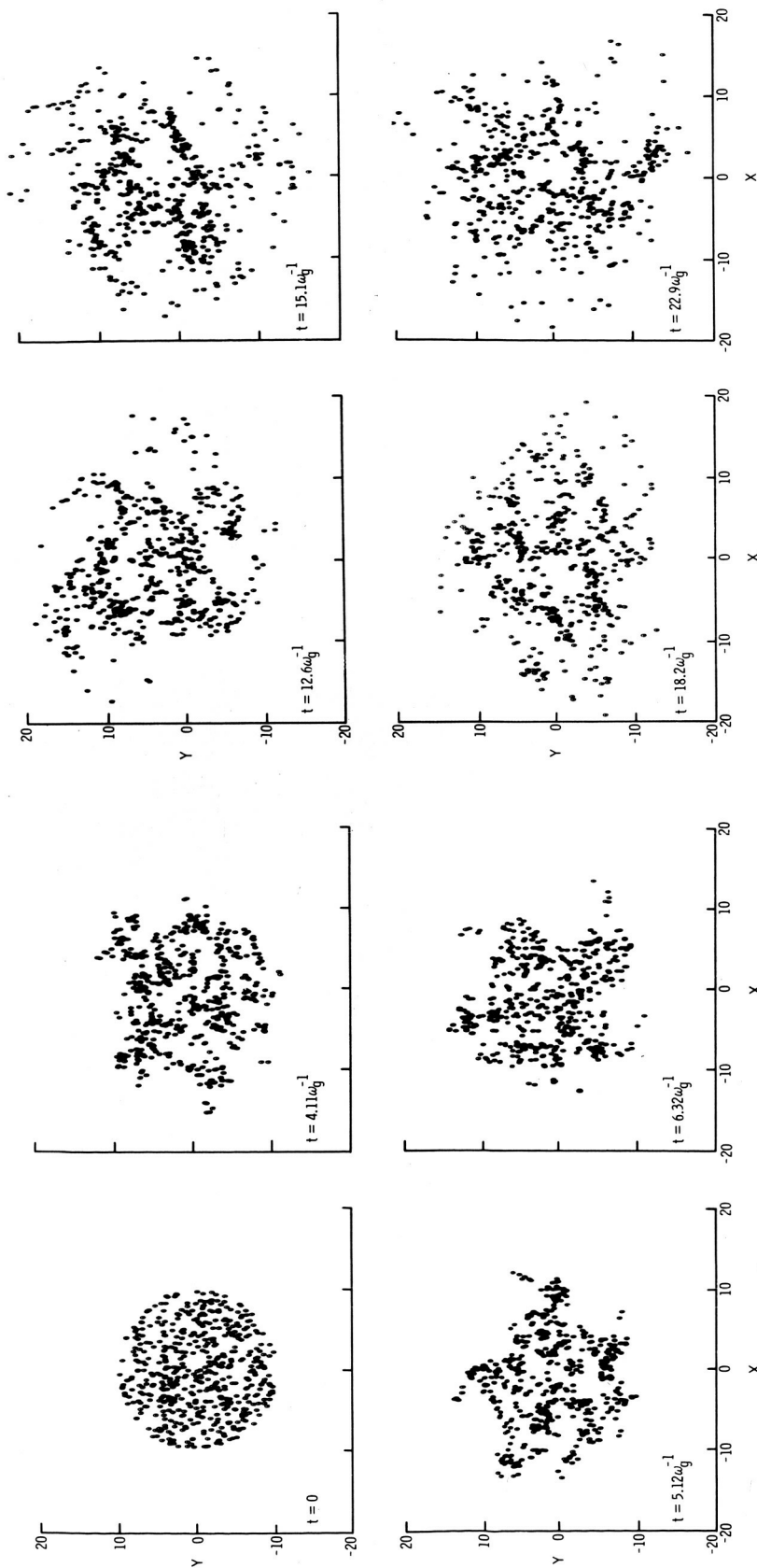
Figure 4.- Illustration of the time development of an unstable two-contour system with $\nu = 0.25$.



(a) Time development up to $t = 2.24\omega_r^{-1}$.

(b) Time development up to $t = 7.21\omega_r^{-1}$.

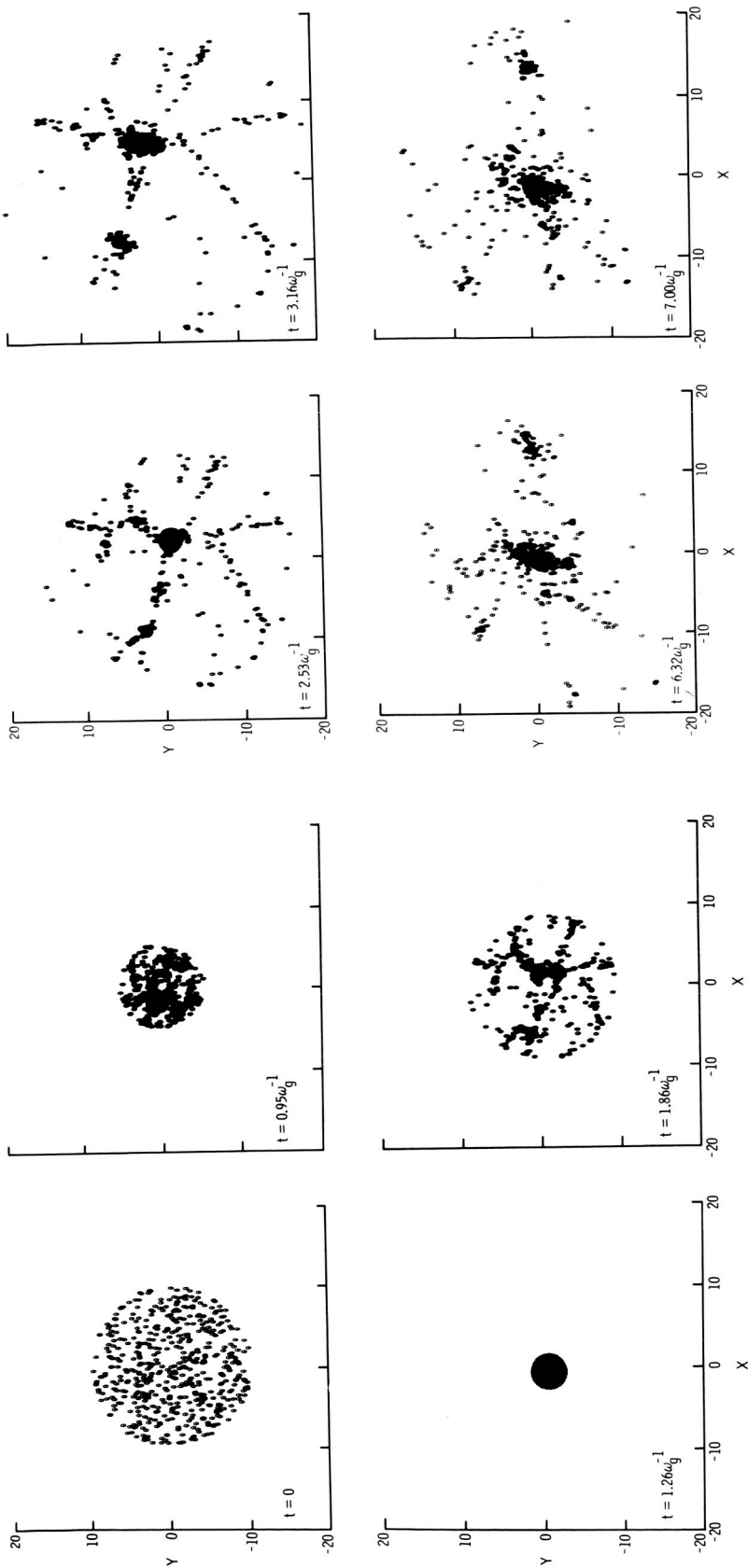
Figure 5.- Time development of a stellar system of 400 mass rods.



(a) Time development up to $t = 6.32\omega_g^{-1}$.

(b) Time development up to $t = 22.9\omega_g^{-1}$.

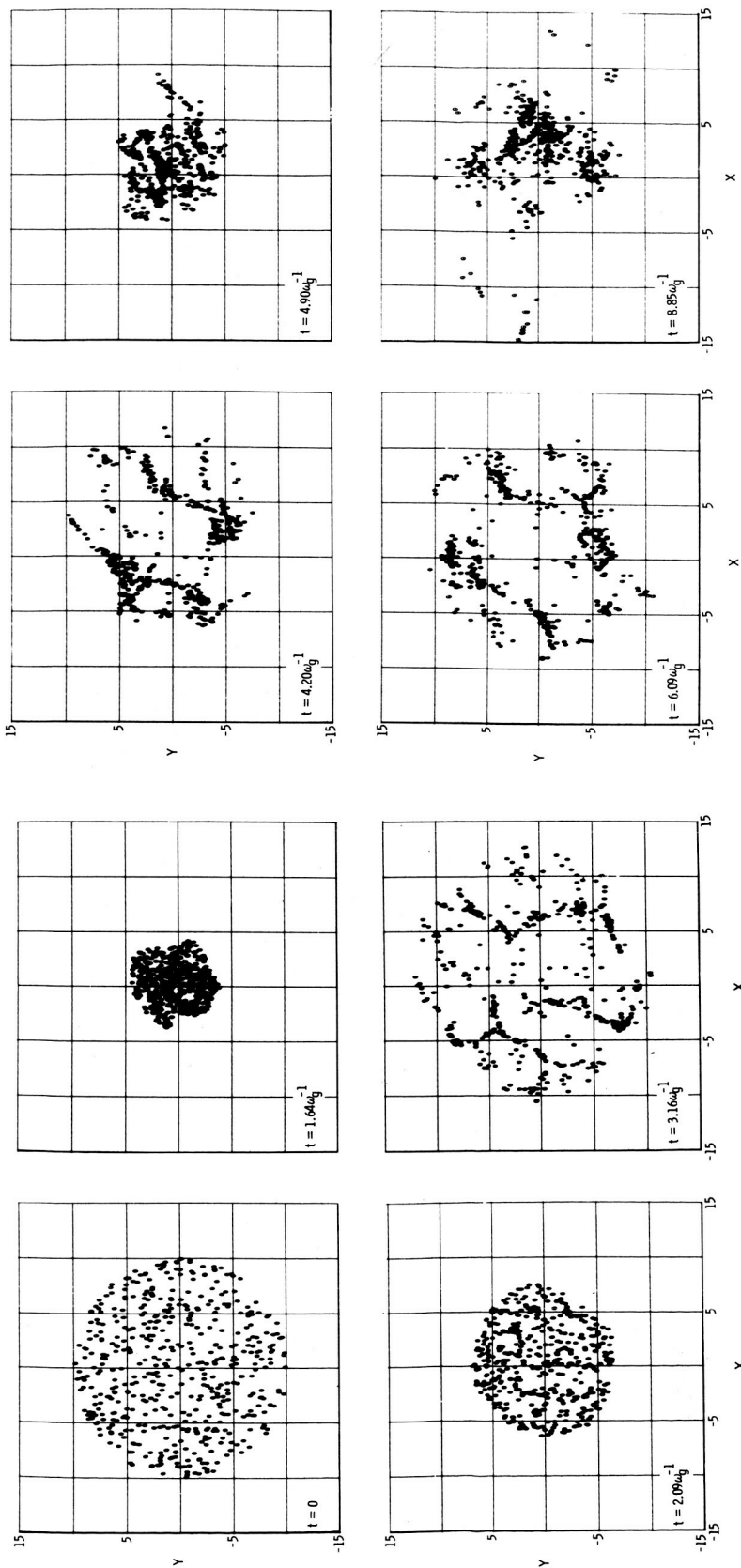
Figure 6.- Evolution of a cylindrical stellar system with $\omega_r = \omega_g$.



(a) Time development up to $t = 1.86\omega_g^{-1}$.

(b) Time development up to $t = 7.00\omega_g^{-1}$.

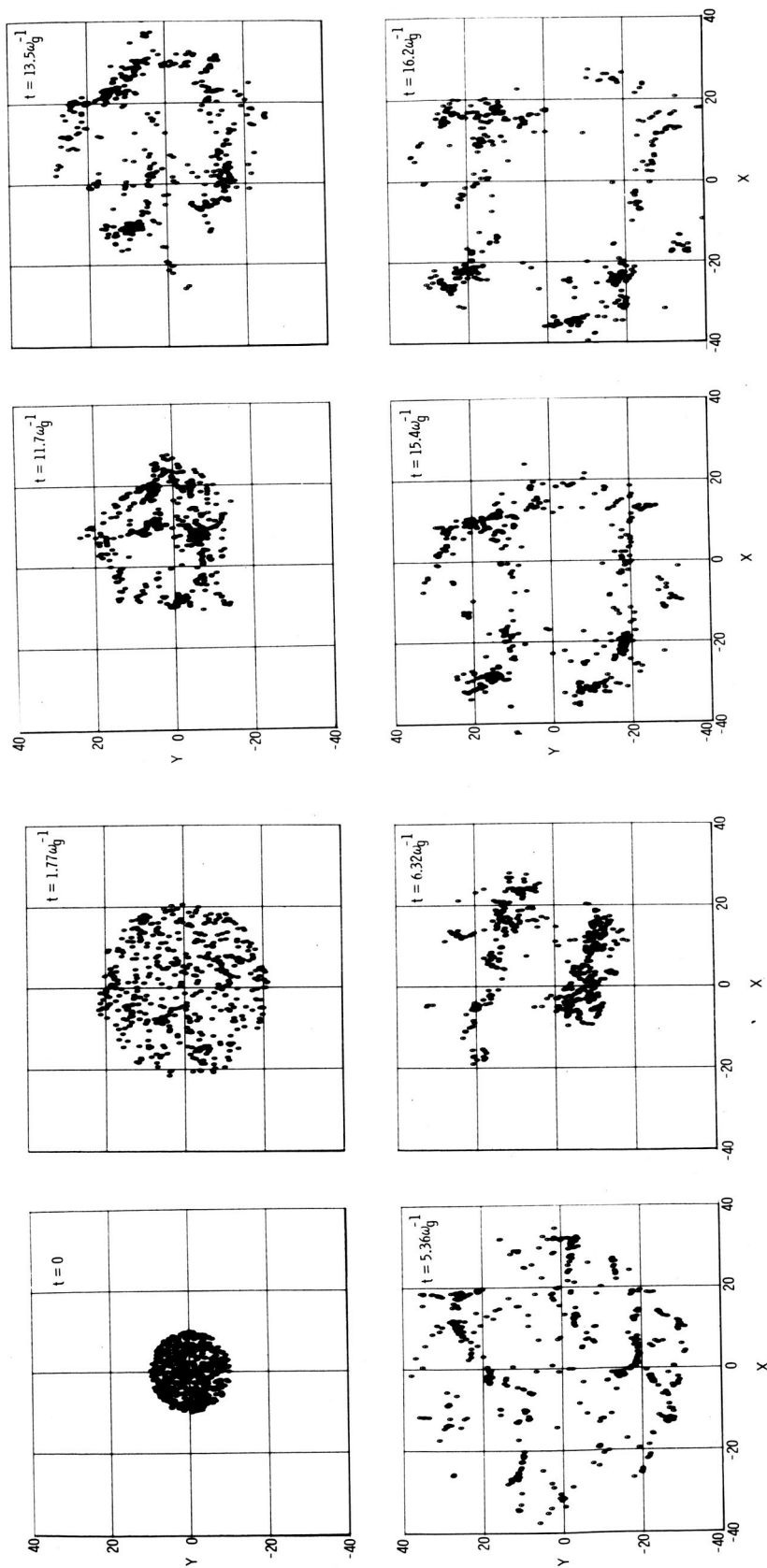
Figure 7.- Evolution of a cylindrical stellar system with $\omega_r = 0$.



(a) Time development up to $t = 3.16\omega_g^{-1}$.

(b) Time development up to $t = 8.85\omega_g^{-1}$.

Figure 8.- Evolution of a cylindrical stellar system with $\omega_r = 0.5\omega_g$.



(a) Time development up to $t = 6.32\omega_g^{-1}$.
 (b) Time development up to $t = 16.2\omega_g^{-1}$.

Figure 9.- Evolution of a cylindrical stellar system with $\omega_r = 1.3\omega_g$.

Gravitational Experiments with a
Cylindrical Galaxy[†]

N67-37757

by

R. W. Hockney
Institute for Plasma Research, Stanford University

A computer model is used to perform gravitational experiments on the evolution of a two-dimensional galaxy. The motion of 2000 rod-stars is computed step-wise in time as they move according to Newton's law of motion in their mutual gravitational field.

The effect of collisions between stars may be estimated from the formula*

$$\frac{\tau_{\text{rot}}}{\tau_{\text{coll}}} = \frac{1}{N} \log_e \left(\frac{L}{H} \right)$$

where

- τ_{coll} - the collision time
- τ_{rot} - the rotation time of the galaxy
- N - total number of stars in the galaxy
- L - diameter of galaxy
- H - mesh spacing used in solution of Poisson's equation.

In the cases described below $\tau_{\text{coll}} = 630 \tau_{\text{rot}}$. We are studying below phenomena over a time span between 1 and 10 galactic rotations and for these intervals the computer model does represent a collisionless star system, and is thus a good model of a real galaxy.

A. THE STABILITY OF A BALANCED ROTATING CYLINDER

Figure 1 shows the time development of a rotating cylindrical galaxy of stars in which the initial rotation is such as to balance the gravitational attraction. For the case of constant density, this

[†]The full paper will appear in the Astrophysical Journal.

*See the earlier paper in this symposium "Preliminary Measurements of Noise in a Two-dimensional Rod Model of a Plasma"

condition is satisfied if the cylinder is given a solid-body rotation with angular frequency:

$$\omega_{\text{rot}}^* = (2\pi G\rho)^{1/2},$$

where ρ is the constant mass density of the cylinder. A characteristic time of the problem is then the rotation period:

$$\tau_{\text{rot}}^* = 2\pi/\omega_{\text{rot}}^* = (2\pi/G\rho)^{1/2},$$

which is used as the unit for time measurements. The time-step is taken to be approximately one hundredth of this period. In the initial condition ($t = 0$) mass rods are distributed at random within a circle and given an angular rotation of ω_{rot}^* . The small deviations from a constant density, due to the random distribution of discrete rods, provide small initial disturbances to a perfectly balanced state from which instabilities may grow. Between $t = 0$ and $t = 0.8$ surface waves grow, leading to a distinctly fluted shape at $t = 0.8$. If we describe the surface perturbation in radial coordinates as $\propto \cos k\theta$, where θ is the azimuthal angle, then these flutes correspond to a wave number k , of four or five. After $t = 1.0$ the wave number $k = 2$ begins to dominate the disturbance. The cylinder now resembles an egg rotating at ω_{rot}^* . The amplitude of the $k = 2$ mode varies periodically, resulting in the galaxy having maximum eccentricity at $t \simeq 3.0$ and $t \simeq 7.0$, and becoming almost circular again at $t \simeq 5.0$ and $t = 9.0$.

Measurements are made of the amplitude and phase of the first 4 harmonics of potential. The $k = 1$ harmonic remains at constant amplitude since this follows from the absence of linear momentum in

the initial condition. Harmonic $k = 2$ appears as a standing wave with respect to a frame rotating with angular velocity ω_{rot}^* . Similarly harmonics $k = 3$ and 4 behave as standing waves with respect to frames rotating at $2\omega_{\text{rot}}^*$ and $3\omega_{\text{rot}}^*$ respectively. The frequencies of the standing waves are such that they can be represented approximately by the dispersion relationship

$$(\omega - k(k-1)\omega_{\text{rot}}^*)^2 \approx \frac{\omega_{\text{rot}}^{*2}}{400} k^2$$

The balanced rotating cylinder is thus unstable, but non-linear effects limit the amplitudes of the disturbances to about a fifth of the initial radius. There is no evidence (at least over the time scale of 10 rotations) of any tendency for the cylinder to fission and divide into two lumps. This confirms, in two-dimensions, the findings of Lyttleton (1953) who concludes that such a fission process will not occur in a rotating gravitating fluid and therefore cannot be the origin of double stars, as was proposed by Jeans (1919, Page 102) and others.

B. THE CASE OF ZERO ROTATION

Figure 2 shows the time development of the collapse of a cylindrical galaxy of stars with no initial angular momentum. Between $t = 0$ and $t = 0.2$ there is a radially directed implosion. The collisionless nature of the model however allows the stars to pass through each other and expand again to about the initial radius, during which time condensation occurs. At $t = 0.4$ five distinct condensations are visible which after a further implosion and expansion have, at $t = 0.8$, become concentrated into three globular lumps. By $t = 2.0$ these three

lumps have become fused into a single condensation which represents a steady state. This state is one in which the gravitational attraction is balanced by the temperature (or random motion of the stars about the center). In the movie one can distinguish two classes of stars. The vast majority of the stars are describing oscillatory motion with a short period in the main mass of the condensation, or nucleus. Some 50, which might be described as the halo stars, have a higher energy and describe oscillatory motion out to about four or five times the radius of the nucleus. The period of oscillation of the halo stars is some 10 times that of the stars in the nucleus. The separation of the stars into two classes is clearly seen even as early as $t = 0.6$, when the majority of stars have imploded for the second time into a small radius whilst the halo stars are left scattered out as far as twice the radius of the initial cylinder.

C. TOO LITTLE ROTATION

Figure 3 shows the collapse of a cylindrical galaxy which has initially half the angular velocity necessary to balance gravitational attraction. In the time development we see a mixture of the effects noted in IIIA and IIIB. There is now a tendency for the cylinder to pulsate between a maximum and minimum radius as seen at $t = 0.4$ and $t = 0.8$ respectively. The tendency to condense into smaller pieces is most pronounced when the maximum radius is reached and the velocities are small. These subsidiary condensations as seen at $t = 0.6$ and $t = 1.0$ are filamentary in shape rather than the globular condensations seen in the absence of rotation. Between $t = 1.4$ and $t = 1.8$ barred spiral structures are evident but these seem to be shortlived and from

$t = 2.0$ to $t = 4.4$ there is no evidence of spiral structure and a steady state seems to have been set up which is roughly circular and is the two-dimensional analogue of an elliptical galaxy.

In order to show the structures in more detail we have performed the case of half the necessary rotation with twice the resolution in space (there are now 32 space cells across the cylinder as compared with 16 previously) and with half the time-step. This is shown in Fig. 4. The motion is followed from $t = 0.0$ to $t = 2.4$ and follows the same general development as that of Fig. 3 but the greater space resolution enables more subsidiary condensations to occur; about 10 at $t = 0.6$ and the spiral structures are more pronounced. This is because the model divides the square region into a 48×48 mesh or 2304 space-cells and is such that the force between mass-rods vanishes if both rods are in the same space-cell. Thus no condensation can be held together that is smaller than three or four cells in diameter which is about the size of the smaller condensations at $t = 0.6$. The filamentary nature of these condensations appears to indicate the presence of significant rotation and is reminiscent of the condensations seen in red-light photographs of the Crab Nebula, NGC1952. Filamentary condensations are also seen in some peculiar galaxies, for example compare Fig. 4 at $t = 1.1$ or Fig. 3 at $t = 1.0$ with the galaxy NGC1741 (Arp 1966 number 259 plate 44).

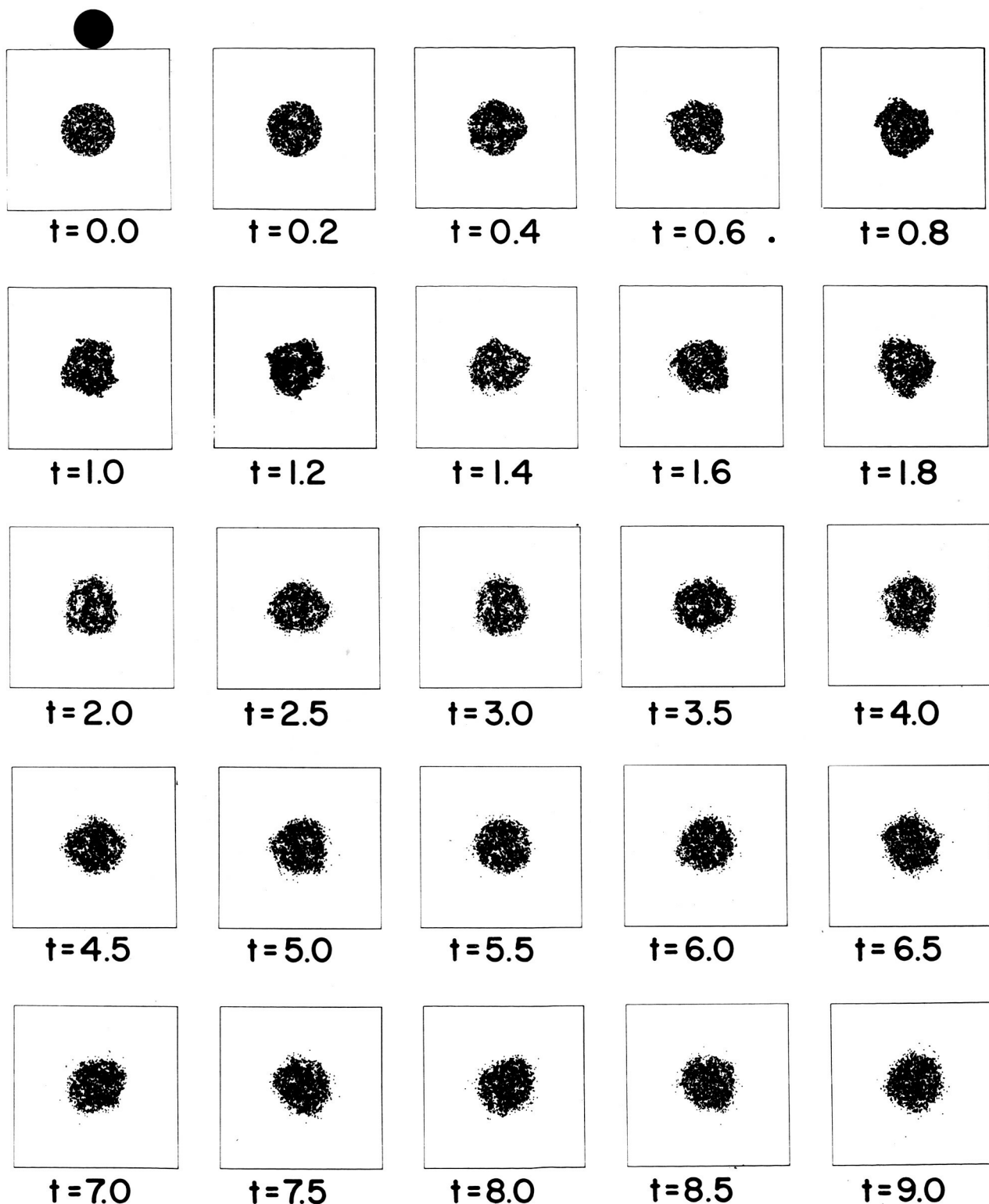
Between $t = 2.0$ and $t = 2.2$ one can see the evolution of a spiral structure into a barred structure by purely gravitational effects. The structure at $t = 2.0$ resembles for example the Sc galaxy NGC5457 (M101, Sandage 1961 plate 27) and that at $t = 2.2$ the SBb

galaxy NGC5850 (frontispiece of Chandrasekhar 1942, plate II Hubble 1936). Examination of the movie shows that the motion of the stars in the spiral arms at $t = 2.0$ is predominately longitudinally along the arm, from the outside inwards. Thus the arm is roughly the orbit of the stars which compose the arm. One can also distinguish a 'halo of stars' which execute eccentric orbits with a long period. These orbits pass close to the center of the nucleus and reach out to the edge of the square region. The majority of the stars move in much more circular orbits in the nucleus of the condensation.

D. TOO MUCH ROTATION

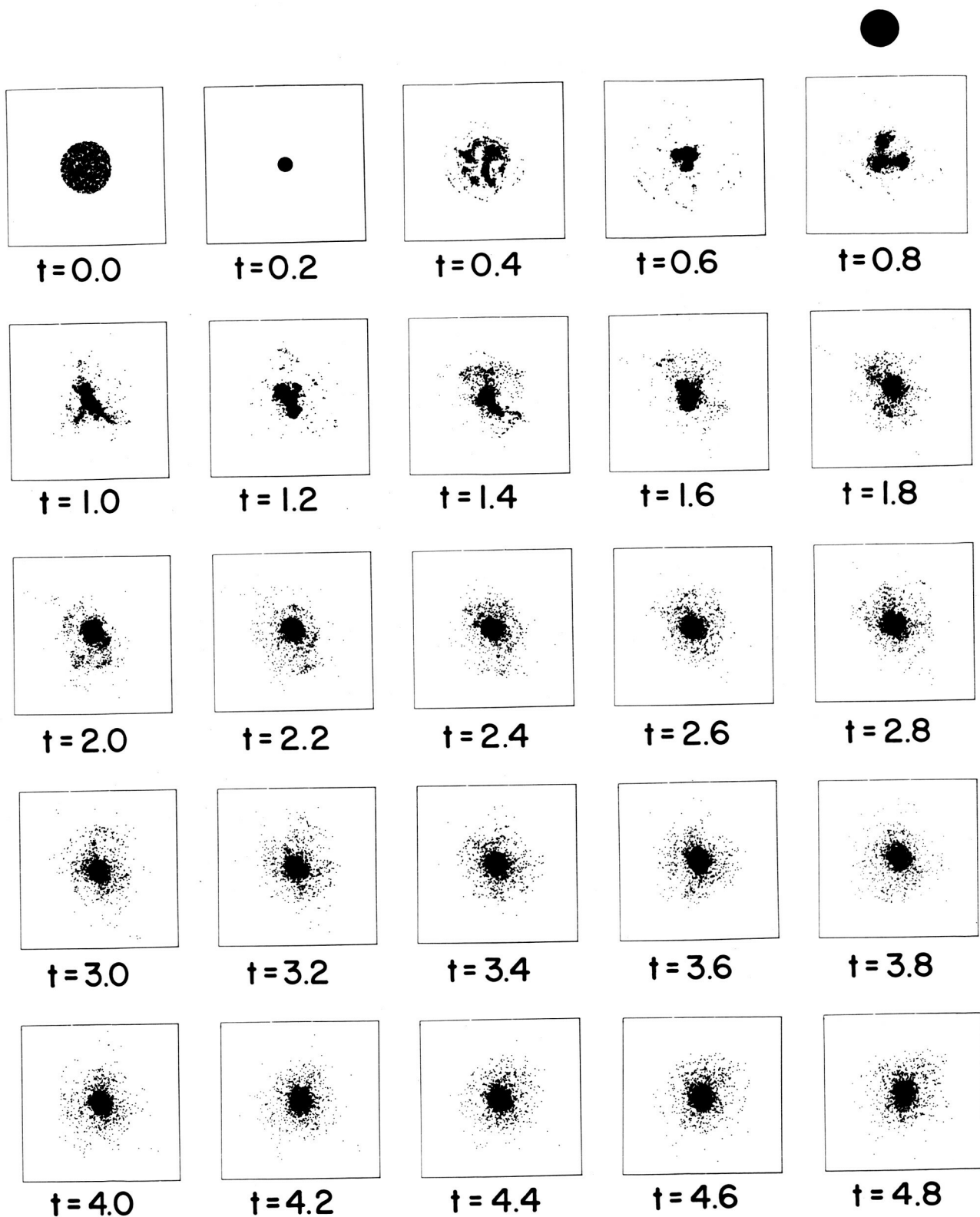
Figure 5 shows the case of a small cylinder which is given initially 1.5 times the angular velocity necessary to balance gravity. This is similar to the case of Fig. 3 if we take $t = 0.2$ as the origin of time, and shows the same general evolution from filamentary condensations, through spirals and barred spirals to an elliptical steady state. One can see a resemblance between the S shaped condensation at $t = 4.8$ and the SBc galaxy NGC7479 (Chandrasekhar frontispiece, Hubble plate II) or NGC3359 (Sandage 1961, plate 49). This form is also seen in Fig. 3 at $t = 1.4$.

The normalized time measurements change rapidly in this case due to the higher density in the initial state, and the resulting small unit of time.



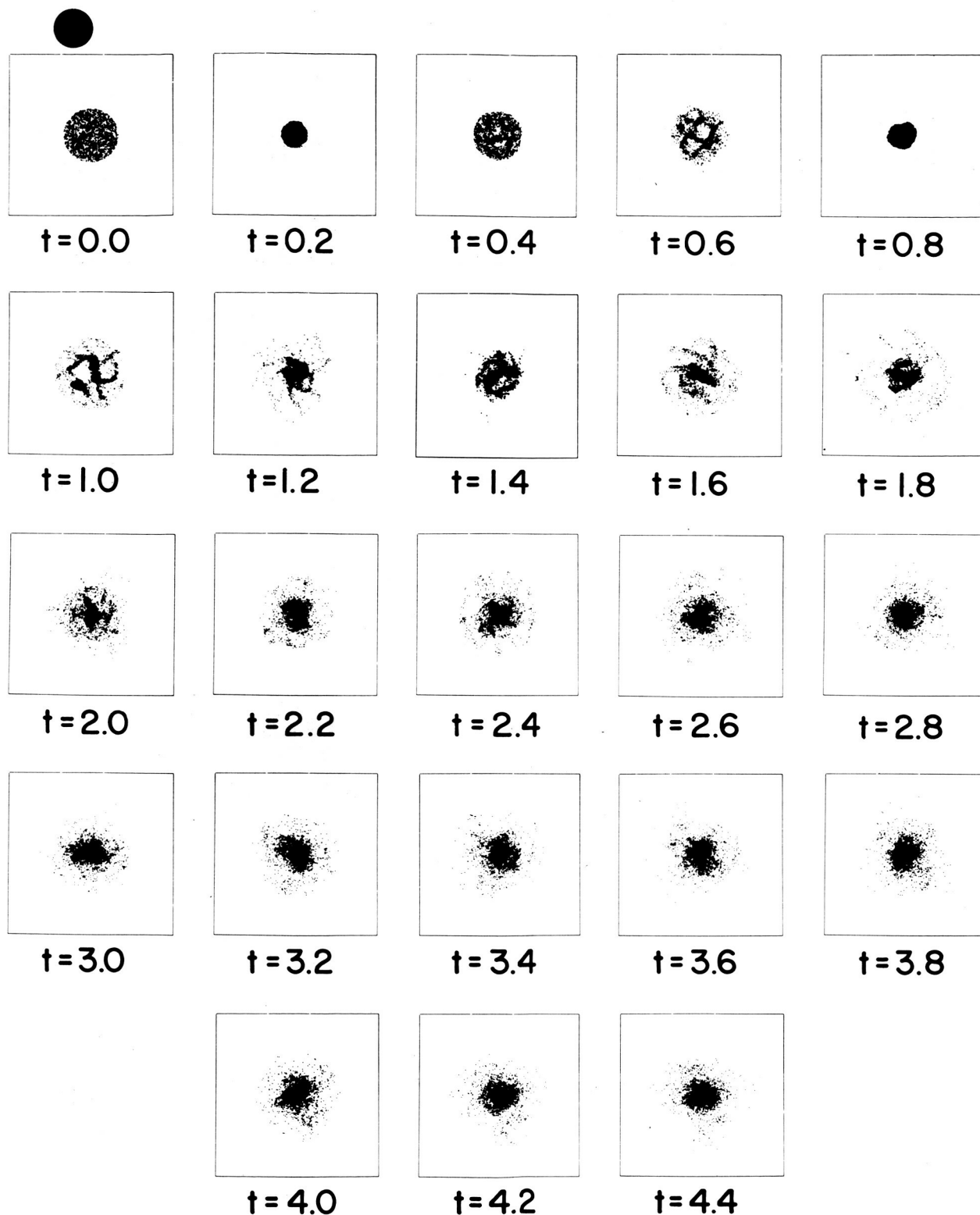
THE STABILITY OF A ROTATING CYLINDER IN WHICH CENTRIFUGAL FORCE AND GRAVITATIONAL ATTRACTION ARE INITIALLY IN BALANCE. TIME IN UNITS OF $1.04 \tau_{\text{rot}}^*$. $\tau_{\text{rot}}^* = (2\pi/G\rho_0)^{1/2}$ IS THE ROTATION PERIOD FOR BALANCE. ρ_0 IS THE INITIAL DENSITY.

Figure 1.



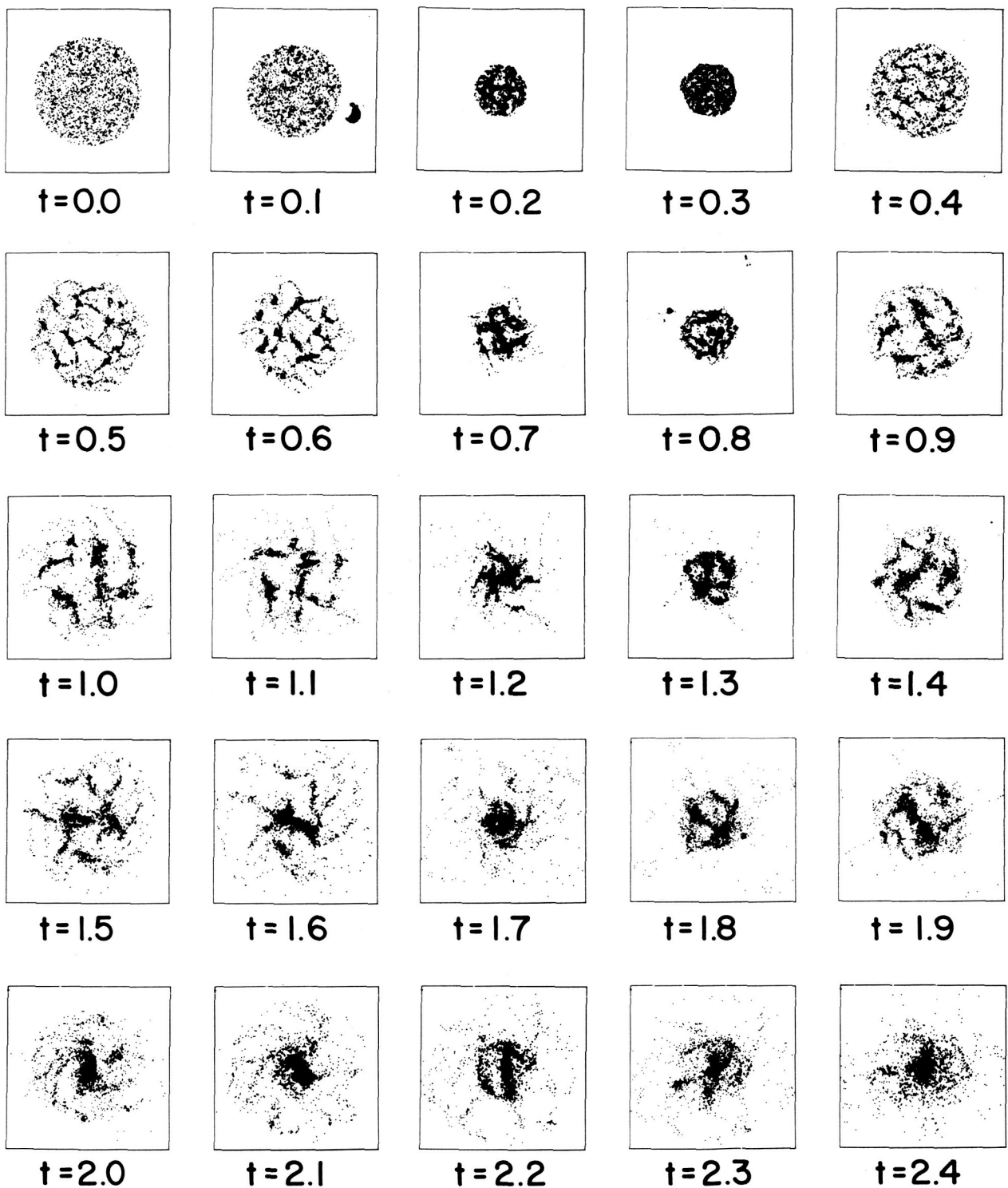
THE COLLAPSE OF A GRAVITATING CYLINDER IN THE ABSENCE OF ROTATION. TIME, t , IN UNITS OF $1.04 (2\pi/G\rho_0)^{1/2}$ SECS. ρ_0 IS THE INITIAL DENSITY.

Figure 2.



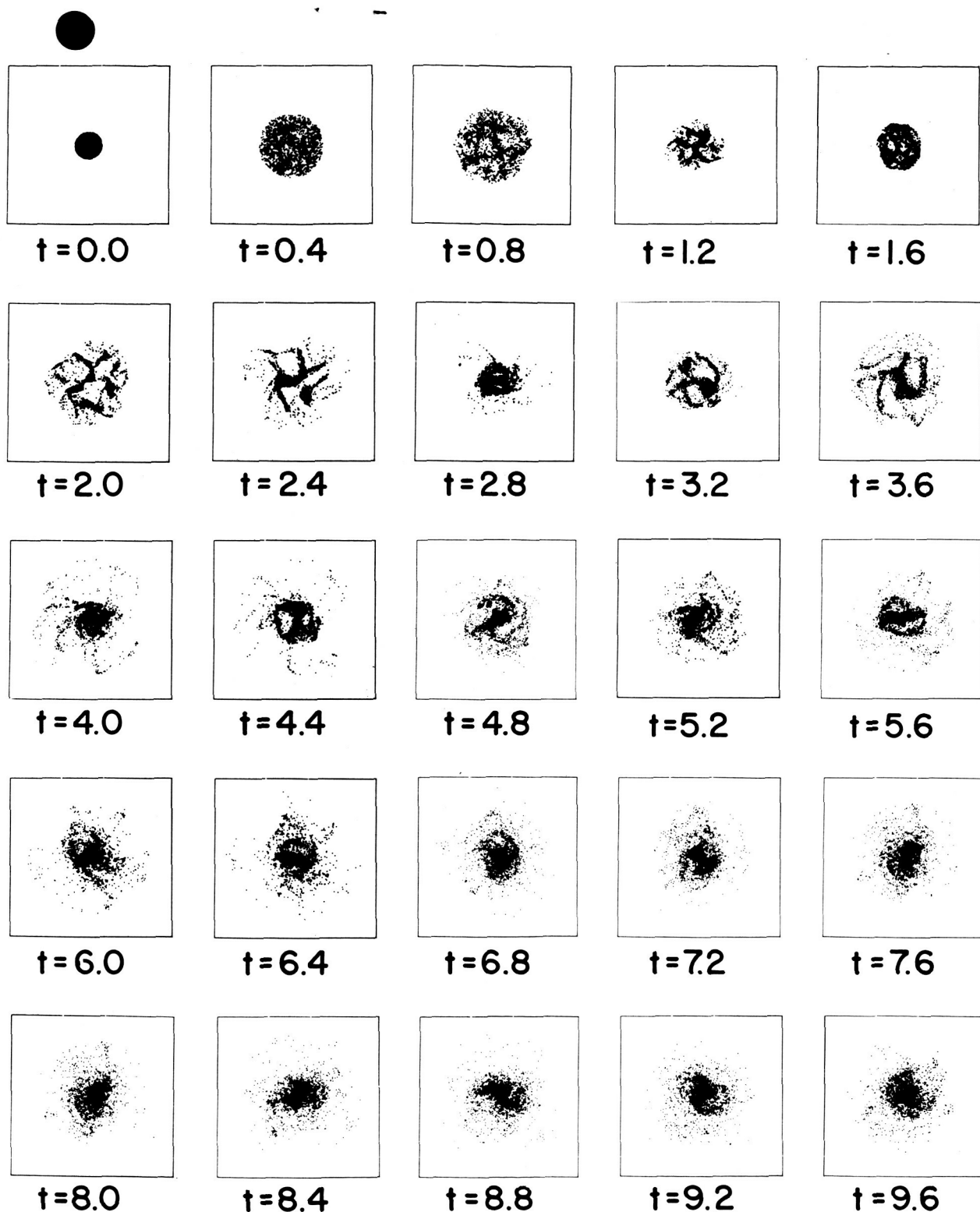
THE COLLAPSE OF A CYLINDER WITH HALF THE ROTATION NECESSARY TO BALANCE GRAVITY. TIME, t , IN UNITS OF $1.04 (2\pi/G\rho_0)^{1/2}$ SEC. ρ_0 IS THE INITIAL DENSITY.

Figure 3.



THE EARLY DEVELOPMENT OF A COLLAPSING CYLINDER WITH HALF THE ROTATION NECESSARY TO BALANCE GRAVITY. TIME, t , IN UNITS OF $1.04 (2\pi/G\rho_0)^{1/2}$. ρ_0 IS THE INITIAL DENSITY.

Figure 4.



THE EXPANSION OF A CYLINDER WITH 1.5 TIMES THE ROTATION NECESSARY TO BALANCE GRAVITY. TIME, t , IN UNITS OF $1.04 (2\pi/G\rho_0)^{1/2}$ SEC. ρ_0 IS THE INITIAL DENSITY.

Figure 5.

COLLECTIVE MOTIONS IN A SPHERICAL STAR CLUSTER

Michel Hénon

C.N.R.S., Institut d'Astrophysique, Paris

In contrast to my previous paper (see above: "Monte Carlo methods in stellar dynamics"), I shall consider here the first phase of evolution of a stellar system, i.e., the mixing phase. The associated time scale is the crossing time t_c , which is short compared to the relaxation time t_r , so that the effect of encounters can be neglected. The mechanism of the evolution is then completely different, and also the numerical technique used will be completely different.

Let us consider the usual picture of the formation of a star cluster. We consider a gas cloud in hydrostatic equilibrium and we assume that at a given time, for some reason, this cloud condenses into a number of stars. We shall not be interested here in the mechanism of star formation, but in what happens just after the stars are formed. For each piece of gas there was a balance between the gravitational force, directed inwards, and the pressure force, directed outwards. When the stars are formed, the pressure force suddenly vanishes, and the stars fall towards the center. Thus the dynamical evolution of the star cluster will begin with a general inward motion.

On the other hand, as soon as the cluster is condensed into stars, the total energy: $E = T + \Omega$, becomes constant. T is the kinetic energy, and Ω is the potential energy. Thus we can expect that the collapse will be followed by an expansion: each star will pass near the center, and will continue its motion on the other side. After some time, the expansion will stop and there will be a new contraction, and so on. We have thus a collective oscillation of the cluster. Now what will happen in the end? Will these oscillations

continue indefinitely, or will they be damped, so that the system will reach a steady state? This is of course a very important question in relation to actual clusters.

A first possible numerical approach to this problem is the exact n-body computation. But then, as we have seen (see first paper) n is of the order of 100 only and the two phases of evolution are not separated. One can therefore not distinguish between the effects of mixing and the effects of encounters.

Another possible approach is the representation of the system by a distribution function f . One must then solve the Liouville-Boltzmann equation (also called Vlasov equation in plasma physics), without the collision term, since the effect of encounters can be neglected. This is much simpler than the full Fokker-Planck equation, but it is still a partial differential equation with seven independent variables in the general case. If we assume spherical symmetry, the number of independent variables can be reduced to four: time, t ; distance to the center, r ; and radial and tangential components of the velocity, u and v . This is still a very difficult problem for a numerical treatment.

We shall use here a third method, which was first described by Campbell (1962, 1966). It is specially adapted to the problem, and it turns out to work quite well. From now on, we shall assume that the cluster has spherical symmetry. Then a star is subject only to a central force, and its angular momentum with respect to the center of the cluster is a constant:

$$rv = A = \text{Constant}$$

and we have the equations of motion:

$$\dot{r} = u$$

and

$$\dot{u} = \frac{v^2}{r} - \frac{GM(r)}{r^2}$$

where $M(r)$ is the mass contained inside the sphere of radius r . These equations show that the variation in time of the three quantities r , u , and v is completely determined if we know the initial values of these quantities. It is not necessary to know the three other coordinates which would determine completely the position and the velocity of the star in space. This is a consequence of the spherical symmetry.

In order to take advantage of this fact, we shall collect together all the stars which have the same values of r , u , and v . These stars form a spherical shell of radius r . This shell expands or contracts with the radial velocity u . The shell is not rigid. The stars which make up the shells are moving on the surface of the shells, with velocity v , in all directions.

The cluster is thus made of a number of concentric shells, whose radii are changing with time. The shells can of course cross each other, since they consist of stars. Each shell is characterized by a constant value of A .

This model is very similar to the "sheet model" which has been used by Lecar and Cohen and by Hohl (see communications in the present volume) for gravitational stratified systems, and which is also widely used in plasma models. Only the geometry of the problem is different: instead of parallel plane sheets, we have here concentric spherical shells. Also there are three variables instead of two.

A first advantage of this method as compared to the exact n -body integration, is that the number of bodies to be considered has been very much reduced since many stars have been grouped in one shell. A second advantage is that

the computation of the forces is very easy. Thus, one can easily consider systems of 1000 shells, which will be equivalent to physical systems with much more than 1000 stars. The two time scales t_c and t_r are then well separated, and the effect of encounters is negligible.

In a first computation, a homogeneous spherical cluster with a Maxwellian distribution of velocities was taken for the initial state. The quantity $\alpha = -2T/\Omega$, which according to the virial theorem should be equal to 1 for the steady state, was initially equal to 0.5, so that the velocities are too small for equilibrium and the cluster starts contracting. Units were normalized by taking: $G = 1$, $M = 1$ (total mass), and $R = 2$ (initial radius). The number of shells was 1000. Figure 1 represents the evolution of the space structure of the cluster with time. The curves represent the radii of the spheres which contain $1/10$, $2/10$, . . . of the total mass, plotted against time. The initial collapse of the cluster and the subsequent expansion are apparent on the left of the diagram. After that the oscillations are strongly damped and the cluster reaches a steady state quite rapidly. The curves then become horizontal lines. The small irregular waves which subsist are just statistical fluctuations ("noise"): This has been checked by varying the number of shells. The final structure is very different from the initial structure. The sphere which contains $1/10$ of the total mass is now much smaller, indicating a much greater central density. Also the sphere which contains $9/10$ of the mass is greater, indicating the formation of a halo.

The damping of the oscillations is due to the different periods of the stars. This is illustrated in figure 2, which shows the radii of two particular shells as functions of time. (This is taken from a computation with 50 shells.) There is obviously a great difference of period. In general, shells with a

greater amplitude in r have a longer period. For great amplitudes, Kepler's law is approximately obeyed and the period is proportional to $r^{3/2}$. This spread of periods explains the fast damping.

Figure 3 represents the final structure in a different way with the space density plotted against radius. The rectangular curve represents the initial state, and the inclined curve represents the final steady state. Both scales are logarithmic.

Figure 4 shows the distribution of velocities in the final state: The mean square of the tangential velocity, and twice the mean square of the radial velocity, are plotted against radius. In the initial state, these two quantities would have been represented by the same horizontal line, because the initial cluster was isothermal. The final state is far from isothermal and the velocities decrease outwards. Also the velocity distribution is flattened near the center, and elongated in the radial direction in the outer regions.

The astronomical implications of these results have been discussed elsewhere (Hénon, 1964, 1966).

Other experiments have been made with the purpose, not so much of gaining detailed information about actual stellar systems, but rather of understanding collective motions in a general way. Lynden-Bell (1966, 1967) has recently given a theory of the mixing phase, which uses the methods of statistical mechanics and predicts a definite form for the distribution function \bar{f} of the final steady state. In the simple case where the initial distribution function f is equal to a constant value η in some region of the phase space and to 0 outside, the final distribution function \bar{f} should be:

$$\bar{f} = \eta \frac{e^{-\beta(\epsilon-\mu)}}{1 + e^{-\beta(\epsilon-\mu)}} \quad (1)$$

where $\epsilon = U + \frac{u^2 + v^2}{2}$ is the total energy of a star. U is the gravitational potential, and β and μ are two constants, determined by the conditions that the total mass and the total energy of the system must be conserved. This is formally identical with the classical Fermi-Dirac distribution. In the general case where f is arbitrary, \bar{f} is given by a more complicated expression.

In order to test this theory with the shell model, it is necessary first to assume that all shells have the same angular momentum A . Then each shell is completely defined by a point in a (r, u) plane, and we have in fact a one-dimensional problem in r . Figure 5 shows, for one of the computed examples, the evolution of the system in the phase plane (r, u) . Initially (a), the density of the points is constant inside the rectangle $1 < r < 2$, $-0.5 < u < 0.5$, and the constant A is equal to 0.4. As evolution proceeds, the rectangle is distorted (b); but it still has a well-defined boundary, with a constant density inside, in accordance with the property of conservation of density in phase space along the motion. A spiral pattern develops (c), because the period of oscillation of a shell is shorter for small amplitudes. Some local instabilities appear and tend to break the regular pattern (d). The spiral becomes more and more tightly wound (e). Finally a state is reached where the arms cannot be distinguished any more (f). This corresponds to the establishment of a steady state. In principle, if the number of points was much greater and if we looked at figure 5(f) on a sufficiently small scale, we would still see very thin spiral arms, with a density equal to η inside the arms and to 0 between them. But in practice we observe a smoothed-out density \bar{f} . Since it results from the mixing of pieces of phase space with densities η and 0, \bar{f} can only have values in the interval $0 \leq \bar{f} \leq \eta$; this is in agreement with the theoretical equation (1). \bar{f} is not constant in the plane, but decreases

continuously from a value close to η in the central region (fig. 5(f)) to very small values outside.

In order to obtain a quantitative check on the theoretical formula, the phase plane was divided into a number of cells. A number of diagrams such as figure 5(f), corresponding to different times, were superimposed in order to increase the accuracy. Then in each cell the number of points and the mean energy ϵ were computed. Figure 6 shows the result. Each point corresponds to one cell. The abscissa is the energy ϵ . The ordinate is the quantity $y = \ln \frac{\bar{f}}{\eta - \bar{f}}$. If the theoretical relation (1) holds, there should be a linear relation: $y = -\beta(\epsilon - \mu)$. This is quite well verified in the left upper part of the diagram, corresponding to low energies. The dotted line represents an approximate linear relationship, which is obeyed by 75 percent of the mass of the cluster. In the right lower part, this relationship is no longer obeyed. Lynden-Bell (1967) suggests the explanation that stars with great amplitudes and long periods go far out of the cluster and when they come back, the main body of the cluster has already settled into a steady state, so that there is no longer an opportunity for the operation of the mixing mechanism.

In order to avoid this effect, a reflecting sphere was introduced around the cluster, with a radius $R = 3$. Stars are supposed to bounce elastically on this sphere. The period of a shell then increases with the amplitude until it hits the sphere, and decreases afterwards. Figure 7 shows the resulting evolution of the cluster. The meaning of the curves is the same as for figure 1. Unexpectedly, instead of the usual fast damping of the oscillations, we observe a large collective oscillation which does not seem to damp at all. Its amplitude is an order of magnitude too great to be explained by statistical fluctuations.

This phenomenon can be explained, in fact, by a curious phase-locking mechanism. Consider a shell which participates in the collective oscillation and which has, at some time, a period T somewhat greater than the collective period T_0 . It will soon lag with respect to the general oscillation. Then its energy will increase, because when it moves inwards the mass inside it and the force acting upon it are greater than when it moves outwards. But, assuming that the shell hits the reflecting sphere, an increase of energy means a decrease of period. Thus the shell will again catch up with the others and is automatically kept in phase with the general motion.

Two conditions are necessary for the existence of this mechanism. First, the collective oscillation must be started; this was provided by the initial collapse of the cluster. Second, the period must be, at least in some range, a decreasing function of the energy; this was provided by the introduction of a reflecting sphere.

Finally, another experiment was made, without a reflecting sphere, and with very small initial radial velocities: $-0.005 < u < 0.005$. Figure 8 shows that a very strong collective oscillation results, in which most shells participate. The mechanism cannot be the same as in the previous case. In fact, it is simply an effect of gravitational instability. Initially the shells have very small relative velocities, and under the effect of their mutual attraction they fall towards one another, as can be seen on the left of figure 8. They form then a tight clump which oscillates just as one large shell.

These various results indicate that the general theory of collective motions in a gravitational system may be rather complex. In particular, no definite conclusion can be drawn regarding the final state of the system. There are mechanisms which can prevent the establishment of a steady state and lead

instead to permanent oscillations. Of course the models considered here were rather artificial; but we cannot be sure that similar mechanisms do not operate in actual clusters. Apparently much work remains to be done before these problems are clarified.

REFERENCES

CAMPBELL, P. M., 1962, Proc. Nat. Acad. Sci. U.S.A., 48, 1993.

CAMPBELL, P. M., 1966, Proc. Nat. Acad. Sci. U.S.A., 55, 1.

HÉNON, M., 1964, Ann. Astrophys., 27, 83.

HÉNON, M., 1966, Paper presented at the 14th International Astrophysical Symposium, University of Liège, Belgium, June 1966.

LYNDEN-BELL, D., 1966, Paper presented at the 14th International Astrophysical Symposium, University of Liège, Belgium, June 1966.

LYNDEN-BELL, D., 1967, Bull. Astron., 3e série, vol. 2, p. 163.

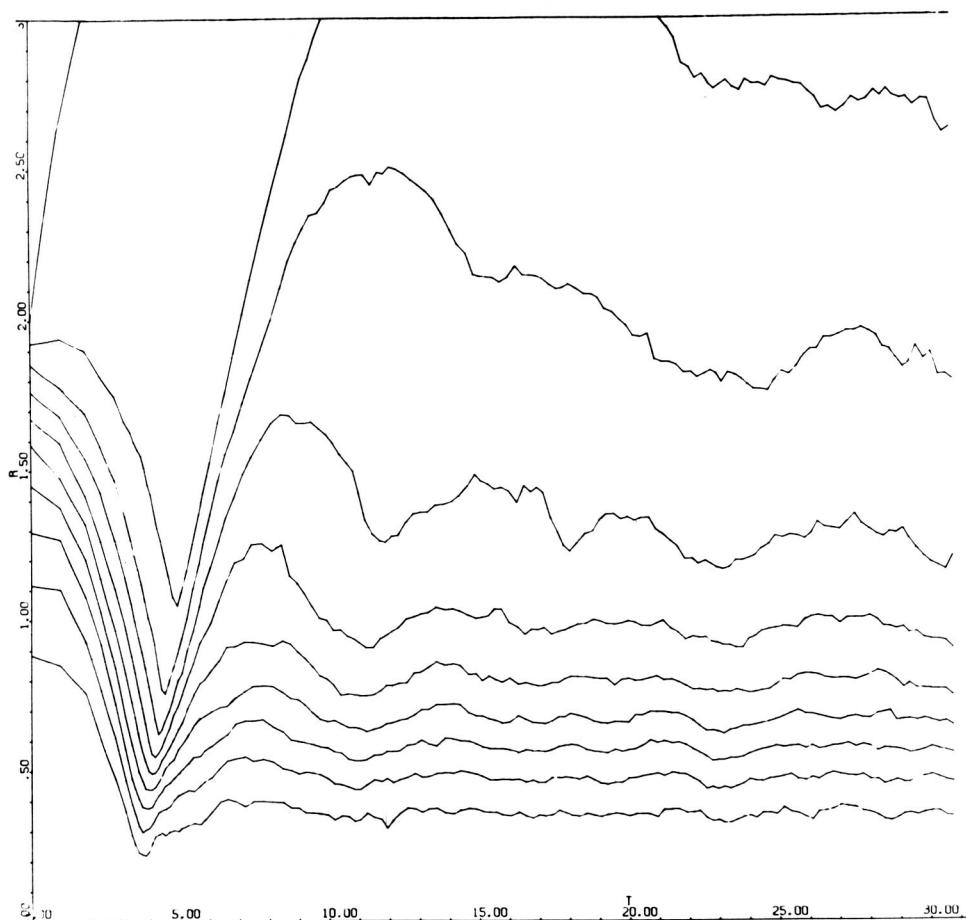


Figure 1.- Structure of the cluster, as a function of time. The curves represent the radii of the spheres which contain $1/10$, $2/10$, $3/10$... of the total mass.

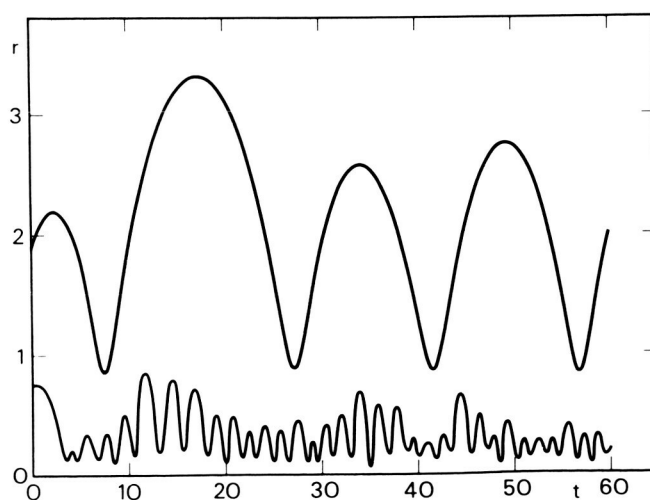


Figure 2.- Motion of two particular shells.

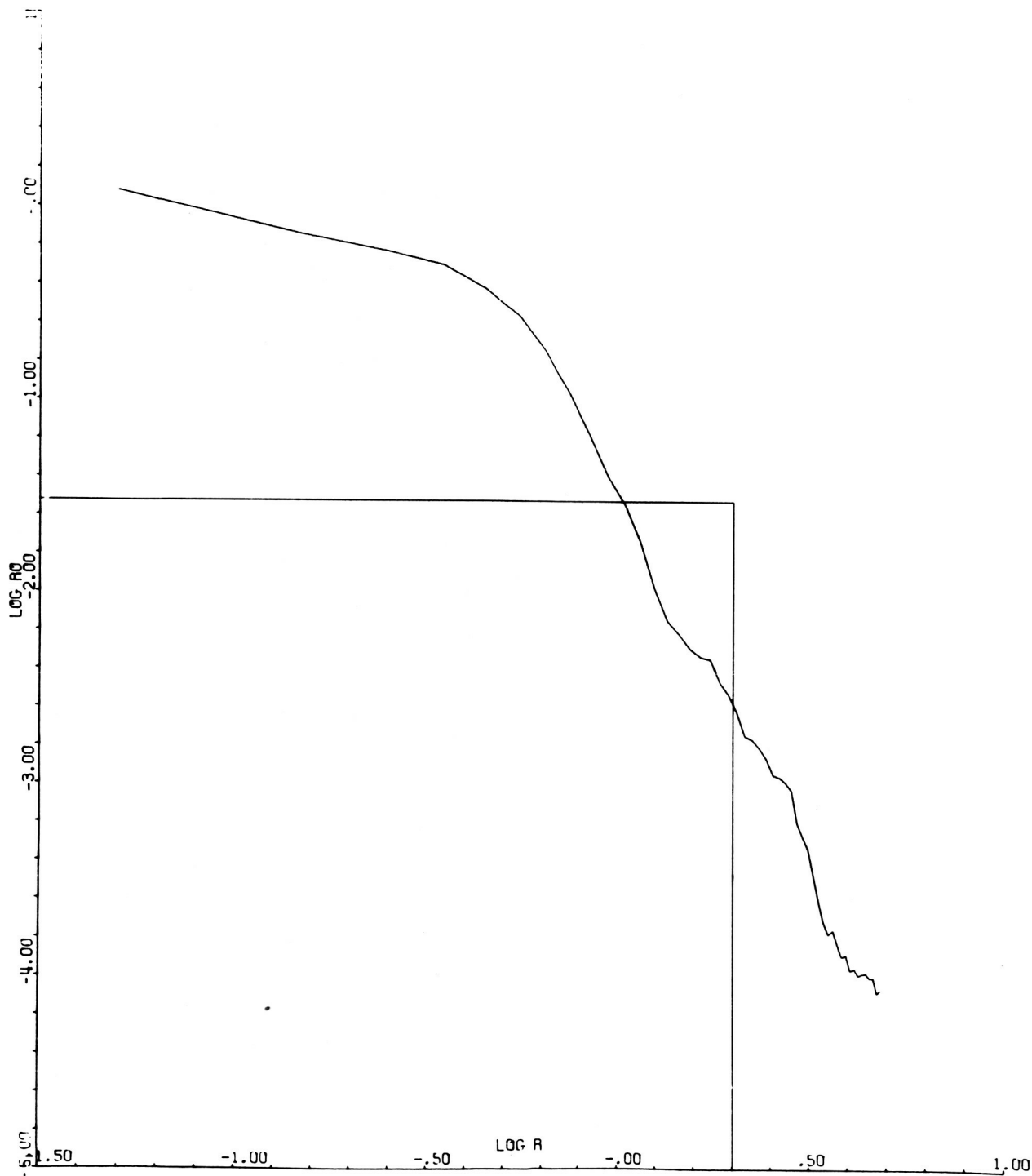


Figure 3.- Spatial density of the cluster, as a function of distance to centre.
 Rectangular curve: initial state. Inclined curve: final state.

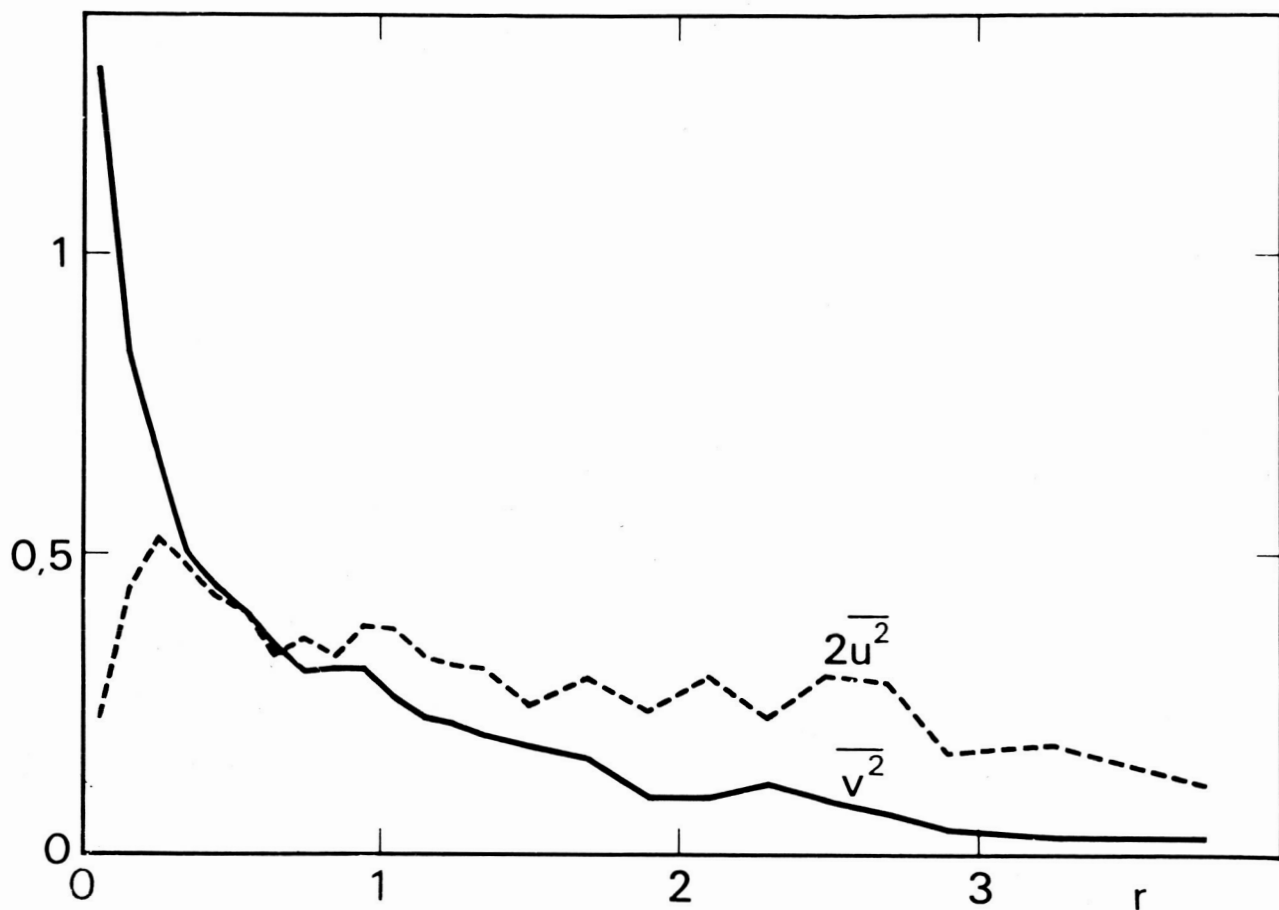


Figure 4.- Radial and tangential velocity dispersions, as a function of distance to centre, in the final state. .

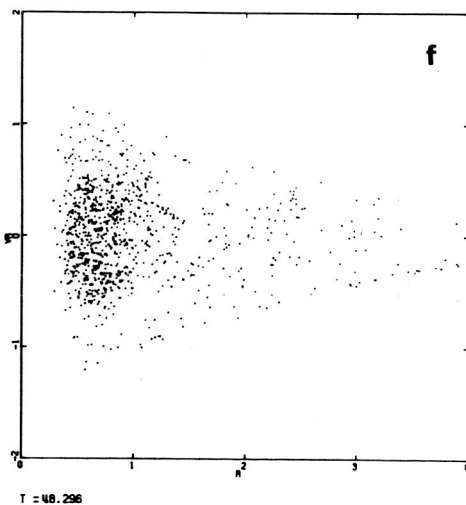
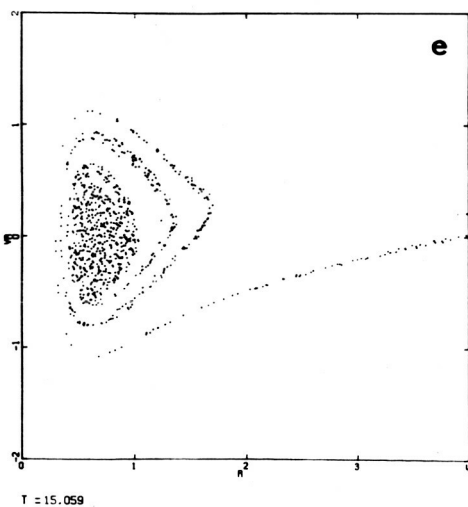
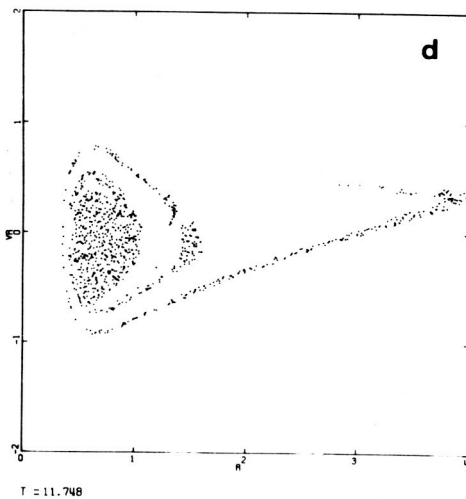
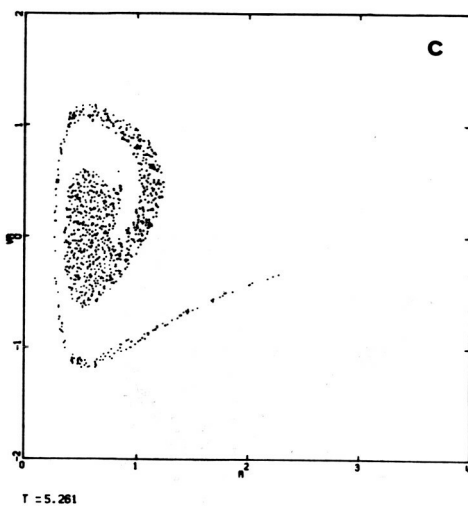
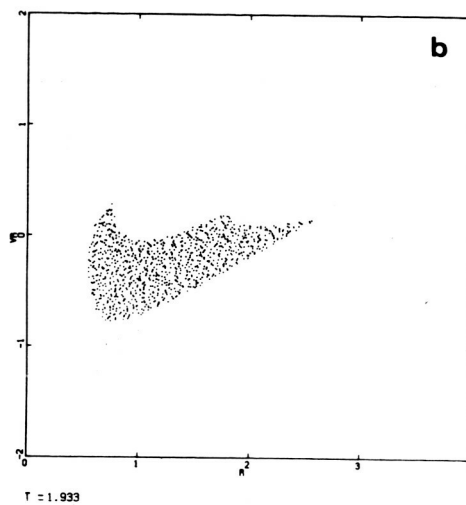
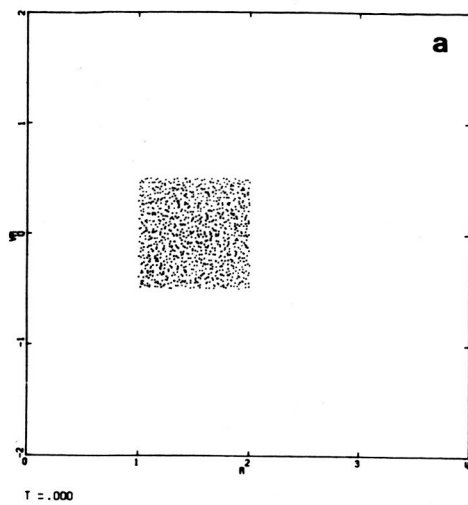


Figure 5.- Evolution of the system in the (r, u) phase plane.

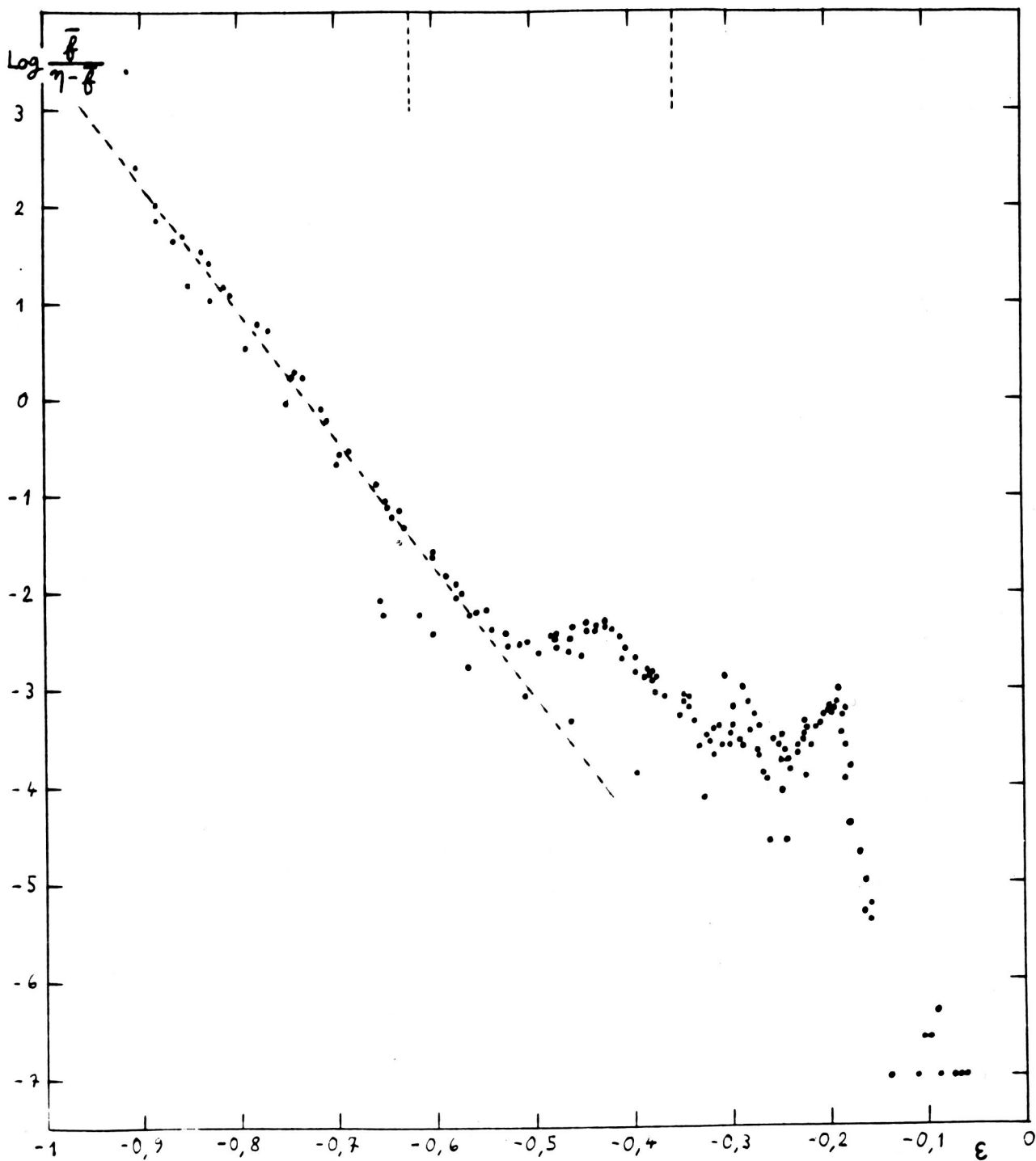


Figure 6.- Plot of $\ln \frac{\bar{f}}{\eta - \bar{f}}$ against energy ϵ .

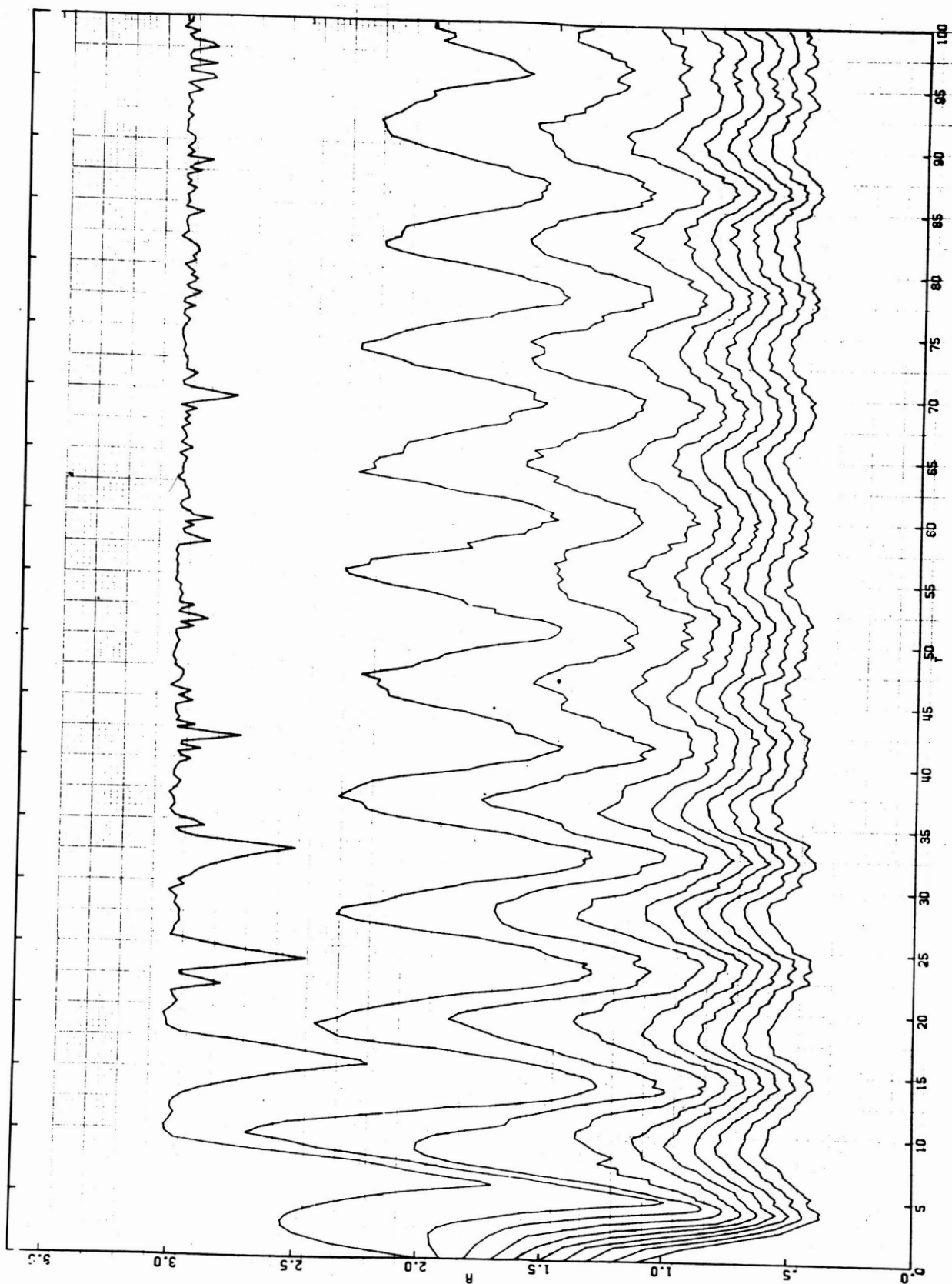


Figure 7.- Structure as a function of time when a reflecting sphere is present. The curves have the same meaning as on figure 1.

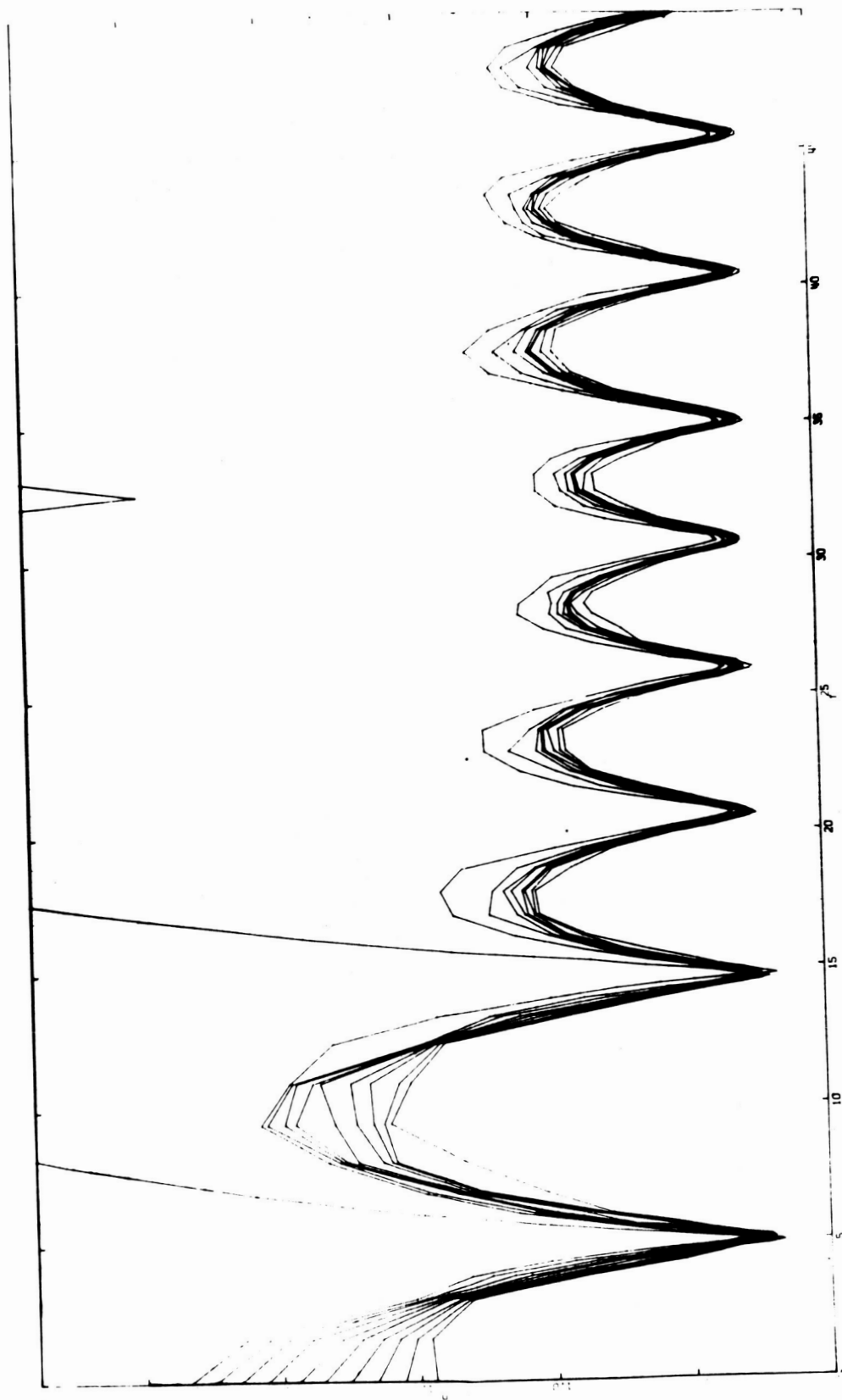


Figure 8.- Structure as a function of time for small initial radial velocities. The curves have the same meaning as on figure 1.

STABILITY OF NUMERICAL INTEGRATION AND REGULARIZATION

IN THE N-BODY PROBLEM

By V. G. Szebehely, E. M. Standish,

and C. Frederick Peters

Yale University

ABSTRACT

It is known that the microscopic reversibility of the gravitational n-body problem cannot be produced numerically because of the macroscopic irreversibility of such a system. Numerical studies of this dynamical effect are performed on a computer, and the analyses of individual particle behaviors indicate that this effect through caused primarily by two-body encounters, is amplified by cooperative phenomena. Gross quantities, such as density distribution, moment of inertia, etc., as opposed to the microscopic motions of single particles, are seen to be well produced when integrated in the forward sense of evolutionary time. These same quantities, however, are less accurately represented when the integration goes from a later stage of evolution backward toward some set of arbitrary initial conditions. Implications concerning the reliability of n-body calculations are discussed.

Regularization of isolated binary collisions in the planar n-body problem can be treated in a manner similar to that used by Levi-Civita for the restricted problem. For three-dimensional motion the generalization of the Levi-Civita transformation by Kustaanheimo and Stiefel may be used. Numerical results are presented for the planar three-body problem.

NEUTRAL GASES

VELOCITY AUTOCORRELATIONS FOR HARD SPHERES*

B. J. Alder and T. E. Wainwright

Lawrence Radiation Laboratory, University of California
Livermore, California

A study of the velocity autocorrelation function for hard spheres over the entire fluid density region has shown that deviations from exponential behavior are small. At very low density a small positive deviation is found which is accounted for in the Boltzmann theory of the self-diffusion coefficient by the Sonine polynomial corrections. The first-order density dependent correction to the diffusion coefficient is given numerically. At higher densities the principle non-Markovian process is identified with the surprisingly long persistence of velocity currents. At still higher densities, near solidification, the anticorrelating backscattering events predominate.

*Published in Physical Review Letters, vol. 18, no. 23, June 1967, pp. 988-990; work performed under the auspices of the U.S. Atomic Energy Commission.

NUMERICAL EXPERIMENTS ON THE NONLINEAR KROOK MODEL
OF THE BOLTZMANN EQUATION*

C. K. Chu

N67-37759

Department of Mechanical Engineering
Columbia University

The Krook model of the Boltzmann equation (ref. 1) replaces the collision integral in the Boltzmann equation with the difference between the local Maxwellian distribution $F = F(x, v, t)$ and the actual distribution function $f = f(x, v, t)$ multiplied by a collision frequency ν , thus:

$$\frac{\partial f}{\partial t} + v_x \frac{\partial f}{\partial x} = \nu(F - f)$$

The collision frequency may depend on density, temperature, etc., in an arbitrary manner, and in more refined versions of the model it can also depend on particle velocity. This model greatly simplifies the form of the Boltzmann equation, yet it maintains the essential nonlinear features of the Boltzmann equation.

In recent years, the Krook equation has been studied numerically by a number of investigators, and considerable experience has been accumulated that would be applicable to solving more realistic kinetic equations (Boltzmann, Fokker-Planck, etc.). This paper surveys a number of attacks that have proved interesting in one-space-dimensional time-dependent problems in neutral gases, in which shock waves occur.

The first attempt to study shock waves by the Krook model was made by Liepmann, Narasimha, and Chahine in 1962 (ref. 2). They obtained the steady

*Work supported by AFOSR under contract AF 49 (638) - 1634.

structure of a shock wave by first replacing the steady (time-independent) Krook equation by an integral equation, and solving the integral equation by iterations. The Navier-Stokes solution is taken as a first iterate, and the macroscopic variables (moments of the distribution function) are obtained at each point in space by numerical integration over the velocity space. Convergence was rather slow, and many modifications were subsequently employed to improve the accuracy. The final results (ref. 3) were very satisfactory and agree with experimental measurements. A similar approach using Gauss-Hermite integration and Chebyshev integration, instead of straightforward trapezoidal or Simpson's rule, was made by Anderson in 1965. This vastly increased the speed of convergence, and gave high accuracy (refs. 4 and 5). In both approaches, because of the singularity in the time-independent differential operator at $v_x = 0$, special procedures were required to treat the kernel of the integral equation near this point.

A considerable effort is going on in obtaining shock wave structure by evaluating the collision integral (in most cases, the actual Boltzmann collision integral) by Monte-Carlo methods. Early attempts by Bird and Havilland (ref. 6) resulted in a shock profile which was not smooth and had large spacewise oscillations. A systematic approach has been made over the past several years by Hicks, Nordsieck, Yen, etc., at the University of Illinois, and they have reported on the "pseudo-shock" problem (spacewise uniform distribution with discontinuity in velocity space), with careful estimates of errors (ref. 7); thus far, however, no accurate structure of an actual shock wave has yet been reported.

A fruitful line of attack using the so-called discrete ordinate method has been initiated by Broadwell (ref. 8), Hamel and Wachman (ref. 9), and

Huang and Giddens (ref. 10). The method is applicable to unsteady problems as well as to steady problems. Essentially, the integrations in velocity space of the moments of f are replaced by sums involving the values f_i of f at certain discrete points v_i as determined by, say, Gauss-Hermite integration, and the Krook equation is replaced by a system of differential equations for the f_i , which are in turn solved numerically. For linear problems, the method works very well. For nonlinear problems involving shock waves, no results (except again the pseudo-shock (ref. 9)) have been reported yet, although preliminary indications are encouraging (ref. 11).

The author has successfully employed a direct numerical method for the Krook equation in one-dimensional unsteady problems. The Krook equation (ref. 1) for the distribution function $f(x, v, t)$ is first replaced by two or three (depending on the concrete problem) simultaneous Krook equations, each for a function of x , v_x , and t . This reduction, resulting from integrating out the velocity components in the ignorable directions, permits us to deal with two or three functions of three arguments, rather than one function of five arguments, thus rendering feasible computing storage. The left-hand side of the Krook equation is then interpreted as a directional derivative along the particle path, and regarding v_x as a parameter, the equation is integrated along each characteristic corresponding to the value of v_x . The integration in velocity space is carried out numerically by trapezoidal or Simpson's rule. This method has been employed to treat the formation of a shock in a conventional shock tube (ref. 12), and also to study the flow with shock induced by the shearing motion of a flat plate (ref. 13). In reference 12, the structure of a steady shock wave was also obtained merely by resolving an initial discontinuity. In this case, no special treatment was needed for $v_x = 0$, since

there is no singularity corresponding to this point in the time-dependent operator. The results are in excellent agreement with those of Chahine.

These different approaches have given valuable experience and insight to the numerical treatment of kinetic equations, and have paved the way to numerical solution of the actual Boltzmann equation for shock problems. Some preliminary attempts have been reported already (e.g., ref. 14).

REFERENCES

1. Bhatnagar, P. L., Gross, E. P., Krook, M., Phys. Rev. 94, 511 (1954).
2. Liepmann, H. W., Narasimha, R., Chahine, M., Phys. Fluids 5, 1313 (1962).
3. Chahine, M. T., Narasimha, R., Rarefied Gas Dynamics, 4th Symp. (Toronto 1964), Academic Press 1965, p. 140.
4. Anderson, D. G., Macomber, H. K., in Rarefied Gas Dynamics, 4th Symp. (Toronto 1964), Academic Press 1965, p. 96.
5. Anderson, D. G., J. Fluid Mech., 25, 271 (1966).
6. Bird, G. A., in Rarefied Gas Dynamics, 4th Symp. (Toronto 1964), Academic Press 1965, p. 216.
Havilland, J. K., in Rarefied Gas Dynamics, 3rd Symp. (Paris 1962), Academic Press 1963, p. 274.
7. Nordsieck, A., Hicks, B. L., in Rarefied Gas Dynamics, 5th Symp. (Oxford 1966), Academic Press 1967, p. 695.
Yen, S. M., Hicks, B. L., in Rarefied Gas Dynamics, 5th Symp. (Oxford 1966), Academic Press 1967, p. 785.
8. Broadwell, J. E., Phys. Fluids 7, 1243 (1964); J. Fluid Mech., 19, 401 (1964).
9. Hamel, B., Wachman, M., in Rarefied Gas Dynamics, 4th Symp. (Toronto 1964), Academic Press 1965, p. 370; 5th Symp. (Oxford 1966), Academic Press 1967, p. 675.
10. Huang, A. B., Giddens, D. P., in Rarefied Gas Dynamics, 5th Symp. (Oxford 1966), Academic Press 1967, p. 481; Phys. Fluids, 10, 498 (1967).
11. Huang, A. B., private communication.
12. Chu, C. K., Phys. Fluids 8, 12 (1965); Phys. Fluids 8, 1450 (1965).

13. Chu, C. K., in *Rarefied Gas Dynamics*, 5th Symp. (Oxford 1966), Academic Press 1967, p. 589.
14. Chahine, M. T., in *Rarefied Gas Dynamics*, 5th Symp. (Oxford 1966), Academic Press 1967, p. 711.

BIBLIOGRAPHY AND CLASSIFICATION

ERRATA

NASA SP-153

SYMPOSIUM ON COMPUTER SIMULATION OF
PLASMA AND MANY-BODY PROBLEMSWilliamsburg, Virginia
April 19-21, 1967

It has been brought to the attention of the Symposium Organizing Committee that the contribution of Charles K. Birdsall included on pages 375 to 406 was not the correct copy submitted at the time of the meetings but an earlier uncorrected report, incomplete, and with some parts never intended for publication. Attached hereto is the correct copy of Birdsall's contribution to replace the material included on these pages in NASA SP-153.

THIS ERRATA REPLACES PAGES 375 - 406

JMW 11/6/67

Symposium on Computer Simulation of Plasma and Many Body Problems,
NASA, College of William and Mary, April 1967

COMPUTER EXPERIMENTS IN ELECTRONICS

Charles K. Birdsall

Department of Electrical Engineering and Computer Sciences
and Electronics Research Laboratory
University of California, Berkeley, California 94720

ABSTRACT

Nonlinear and many-body problems in electron and ion stream devices have been studied using computers for about 20 years. Particle-in-cell and continuous fluid models have been used in initial-boundary value problems to obtain large amplitude response, or noise output spectrum, or instability final state and so on. Particle models have included sheet, block, disk, ring, rod, shell, point, with and without self fields. The distinguishing features from plasma problems are: concern with only one species generally; interaction with applied dc or ac fields from nearby electrodes or wave circuits. The answers obtained have ranged from verification of theory (e. g., shot noise from space charge limited emitter) to device design, to yes-no answers in stabilization studies.

'Tis clear that there is a great deal in common in methods and models.

The research reported herein was supported in part by Atomic Energy Commission under Contract AT(11-1)-34, Project 128.

Computer Experiments of Electronics

I. Introduction

The need for knowledge of noise properties and of large amplitude response long ago led engineers into use of computer experiments. Noise is unwanted random fluctuations about a mean voltage or current, usually relatively small, due to either the particle nature of electron or ion streams (shot noise) or thermal fluctuations (velocity noise). The large amplitude or large signal response is simply the device output when driven hard, such as saturation of an amplifier or limiting amplitude of an oscillator. The noise properties are many body in nature, and not necessarily nonlinear; the large amplitude behavior is nonlinear, but not necessarily many body. These two areas exist at the two ends of the power spectrum, one at microwatts, the other at megawatts.

The third area of interest is in instabilities, as at critical changes of state, or where there are no wholly time-independent states. Instabilities, of course, affect device behavior and must be understood so as to effect cures or adaptations. This area of use of computer experiments has much in common with plasmas.

Charge motion in electronic devices differs from that in plasmas in some rather obvious ways. Devices use streams, usually electrons only, with no collisions, with strong interaction between particles and grids or cylinders or wave circuits, with stream injected at a definite place, collected at another. There generally are applied dc and ac electric and magnetic fields. The time or frequency response at device terminals is generally more interesting than spatial behavior.

II. Classification of Computer Experiments in Electronics by Application

Magnetron:	Yu, Looyers and Buneman (1965) Hull and Kooyers (1960)
Traveling-wave tube:	Nordsieck (1953) Tien, Walker and Woluntis (1955) Tien (1956) Poulter (1954) Rowe (1965 a) Sauseng (1964) Hess (1961) Webber (1960)

Double stream amplifier:	Mihran (1966)
Diode noise:	Tien and Moshman (1956) Wadhwa and Rowe (1963) Dayem (1960) Pollack (1962) Lambert (1960)
Diode stability:	Bridges and Birdsall (1960, 1961, 1962, 1963, 1966) Lomax (1960) Hartree (1950)
Triode stability:	Twombly and Lauer (1960, 1966)
Thermionic converter:	Burger (1964 a, b, 1965 a, b) Cutler and Burger (1966) Lomax (1966) Goldstein (1965) Goldstein and Goldstein (1965)
Plasma probe resonance:	Hellberg (1965)
Ion propulsion:	Dunn and Ho (1963 a, c) Wadhwa and Brauch (1965) Buneman and Kooyers (1963) Wadhwa, Buneman and Brauch (1965) Brauch, Buneman and Wadhwa (1963, 1966) Wadhwa and Kooyers (1964)
Electron stream with velocity distribution:	Yu and Mihran (1963(2))
Beam-plasma interaction:	Rowe (1964, 1965 b)
Beam generated plasma:	Dunn and Ho (1963 b) Halsted (1965)
Klystron:	Webber (1958 a, b, 1959) Mihran (1959 a, b, 1965)
Drift tube stability:	Twombly (1963, 1966)
Centrifugal-electrostatic flow stability:	Lundgren (1965)

III. Classification of Computer Experiments by Charged Particle Model

Superparticles, with the same charge-to-mass ratio as electrons or ions but zero thickness, are self-evident choices for particle models. Sheets, disks, blocks, rings and rods have all been used as superparticles in computer experiments, with and without applied electric and magnetic fields, with and without collisions. Cylindrical and spherical shells are additional candidates.

In most models, each particle is identified by numbered and followed exactly, using the Lorentz equation of motion, through the interaction space, from creation to annihilation; no equation of continuity is needed. In a few models, the self fields are obtained by counting particles in a cell, an averaging process. In most, changes of forces at crossovers are ignored by either making the number of crossovers per step small or by using correction terms; in a few, exact crossing times are calculated, producing exact trajectories.

Hence, the hydrodynamic equations of motion are generally Lagrangian and the fields are generally calculated exactly. There are few if any serious problems in numerical methods having to do with accuracy or stability.

Incidentally, the idea of sheets dates back at least to the 1920's and was widely used in the 1930's for electrons in planar devices, primarily in linear analysis.

The listing here includes electronics and plasmas.

Electron Sheets electric forces, motion and fields in one dimension (1D)

Hartree (1950)
Tien and Moshman (1956)
Dayem (1960)
Lambert (1960)
Bridges and Birdsall (1960, 1961, 1962, 1963, 1966)
Lomax (1960)
Twombly and Lauer (1960)
Twombly and Cerviera (1966)
Pollack (1962)

Electron and Ion Sheets electric forces, motion and field in 1D

Buneman (1959, 1961)
Hartman, Colgate and Kellogg (1961)
Dunn and Ho (1963 a, b, c, 1965)
Smith and Dawson (1963)
Burger (1964 a, b, c, 1965)
Halsted (1965) (includes ionization)
Buneman and Kooyers (1963)
Cutler and Burger (1966)

Electron Sheets in an Ion Sea electric forces, motion and fields in 1D

Dawson (1960, 1962 a, b, 1964)
Eldridge and Feix (1962 a, b, 1963)
Hellberg (1965)
Shanny, Dawson and Greene (1966)

Electron Disks electric forces, motion in 1D, fields in 2D (r, z), no shear in z

Tien, Walker and Woluntis (1955)
Tien (1956)
Hess (1961)
Bridges and Birdsall (1962, 1963)
Webber (1958 a, b, 1959, 1960)
Yu and Mihran (1963 a, b)
Mihran (1966, 1959 a, b)
Sauseng (1964)

Electron Blocks Hess (1961)

Electron Rings electric forces, motion in 1D, fields in 2D (r, z), allows shear along z
Rowe (1965 a)
Sauseng (1964)

Electron Sheets in Crossed E, B Fields electric and magnetic forces, motion in 2D, fields in 1D, sheets shear
Wadwha and Rowe (1963)
Pollack (1962)

Ion Sheets with Transverse Motion also (Current), in an Electron Sea in dc Magnetic Field magnetic and electric forces, motion in 3D (circular + translation), fields in 1D

Auer, Hurwitz and Kilb (1961, 1962)
Hasegawa and Birdsall (1964)
Hasegawa and Kamimura (1965)
Tsuda and Obayashi (1965)
Kilb (1962)
Jones and Rossow (1965)
Rossow (1965)

Electron Rods in dc Electric Fields, electric forces, motion in 2D, fields in 2D
Lundgren (1965) (r, θ)

Electron and Ion Rods, electric forces, motion in 2D (x, y), fields in 2D (x, y)
Wadwha, Buneman and Brauch (1965)
Wadwha and Kooyers (1964)
Brauch, Buneman and Wadwha (1965)
Wadwha and Brauch (1965)

Electron Rods in dc Electric and Magnetic Fields electric and magnetic forces, fields in 2D (x, y), motion in 2D (x, y)
Hull and Kooyers (1960)
Yu, Kooyers and Buneman (1965)
Hockney (1966 a, b) (x, y)

Electron Rods electric forces, motion in 2D, fields in 2D
Twombly (in x, y) (1963, 1966)

IV. Some Milestones

Confronted with these lists, you may be confused or bored, but hopefully impressed that engineers have been active with computer experiments. Hence, let's jump to looking at a few of the more significant milestones, at least as recalled by this observer.

Nordsieck (in 1947, published in 1953) chased electrons through a slow wave circuit in order to predict traveling wave tube efficiency (also signal distortion, harmonic generation). His electrons had no self field; his integration of the continuity equation used the klystron trick (Webster, 1939) of

avoiding multivalued departure times (for a given arrival time) by switching to integration over entrance times. Tien et al (1955) added the self fields of the electrons by approximating the stream as a set of disks, with axial field decaying exponentially from the disks; the e-folding length (range) was directly related the effective plasma frequency of a cylindrical stream partially filling a conducting cylinder. The results showed break-up of bunches due to large repulsive self fields. Tien next (1956) included stronger coupling to the circuit fields. Tien's calculations used 24 disks per wavelength, on an IBM 701.

The check between computer and laboratory experiments was not exactly outstanding initially. However, at present, several traveling wave tube manufacturers use computer experiments fed by laboratory measurements to aid in new device development and improvement; for example, see Hughes programs at end of biography.

Noise in a space-charge limited, short circuited diode was obtained by Tien (1956). He used electron sheets emitted randomly in time with a Maxwellian velocity distribution, $kT_c = 0.1\text{eV}$. The average number of sheets in the diode was 363, with 165 between cathode and potential minimum (virtual cathode) a distance of about a Debye length (as referenced to the density at the minimum). About 8 sheets are emitted each Δt , created in space short distances in front of the emitter to appear as if emitted at different times during Δt . $f_p \Delta t = 0.0076$. An average-velocity sheet goes cathode-to-minimum in $20 \Delta t$, and crosses the whole diode in $142 \Delta t$.

The computation was done on Univac I with 1000 word memory. One Δt took 25 to 40 seconds of computing and 3000 Δt were run, or about 24 plasma cycles taking 25 hours of computing. For the first 120 Δt , the actual fields were used; the next step was $t = 0$ for the noise studies.

The results showed space charge smoothing of shot noise up to about $\omega = 0.8\omega_p$ minimum with a peak above pure shot noise at $\omega \cong \omega_{pm}$, then return to full shot noise at larger ω . The detailed shape predicted has not been seen experimentally. Dayem (1960) and Lambert (1960) continued the simulation for open-circuited models, with somewhat different results.

The time averaged results check very well with the Langmuir (1923) time-independent theory, a pleasant comfort. However, perhaps more sheets could have been used, as the mean square fluctuations in current are not small compared with the average current squared, due to use of a small number of sheets.

Instabilities in diodes have become quite well known in a variety of ways. Lomax (1960) and ourselves [Bridges and Birdsall (1960)] discovered that beyond the well known diode limiting current, the virtual cathode solution was never reached and instead an oscillating state at about plasma frequency was set up. This was then predicted for plasma diodes and later seen both in computer and laboratory experiments [Cutler and Burger (1966)] at electron and ion plasma frequencies. As a further result a plasma diode, with steady creation of electron-ion pairs, but no collisions, is shown [Burger et al (1965)] also to have no wholly dc state, with rf fluctuations randomizing the electron velocities (acting as elastic collisions) and producing the high energy particles known as the "Langmuir paradox." None of these electrostatic type fluctuations is a two-stream instability.

Two dimensional instabilities which are self stabilizing at large amplitude have been found in our group, with accompanying satisfaction that some small amplitude growths still allow confined plasmas. The first was by Lundgren (1965) for a hollow cylindrical electron stream, focused by the balance between radial E with centrifugal acceleration. A bunching perturbation sets up an S shaped deformation which then becomes a spiral (or vortex) and then radial growth stops; the final result is a shearing stream. Byers (1966) with a plasma with an excess charge larger has seen the same general effect, but with a final state of vortices; Hockney and Levy (1966) also showed the same result for an e-layer focused by crossed \underline{E} (self) and \underline{B} (applied) fields. Thus, we see that thin charge layers, focused by B fields or centrifugal acceleration, tend toward a thicker stable state with velocity shear or vortices.

My listing covers only part of the milestones in electron and ion devices. The klystron should be put in, as well as electron-ion propulsion devices, and certainly the Gunn oscillator in solid state. However, as computer experiments with charged particles publications increase (by my count) as $\exp(1/3)$ (T-1956), covering everything is hopeless.

V. Bibliography of Computer Experiments

The listing given here applies primarily to the motion of charged particles and charged fluids, both in self and applied electric and magnetic fields. Single particle or trajectory calculations are not listed, nor are time-independent boundary value solutions. The ordering is simply by year.

Journal articles and reports are listed. Obviously the list is incomplete but not intentionally so. The author welcomes additions and corrections.

- 1950 Hartree, D. R., Some calculations of transients in an electronic valve Appl. Sci. Res., B1, 379-390.
- 1953 Nordsieck, A., Theory of large signal behavior of traveling-wave amplifiers, Proc. IRE, 41, pp. 630-637, May (work done in 1947).
- 1954 Poulter, H., Large signal theory of the traveling wave tube (including the effects of loss, space charge, finite C), T.R. No. 73, E.R.L., Stanford Univ., January.
- 1955 Tien, P. K., Walker, L. R., and Woluntis, V. M., A large signal theory of traveling-wave amplifiers, Proc., IRE, 43, 269-277.
- 1956 Tien, P. K., A large signal theory of the traveling-wave amplifier including the effects of space charge and finite coupling between the beam and the circuit, B.S.T.J. 35, pp. 349-374.
Tien, P. K. and Moshman, J., Monte Carlo calculation of noise near the potential minimum of high-frequency diode, J. Appl. Phys., 27, 1067-1078, September.
- 1958 (a) Webber, S. E., Ballistic analysis of a two-cavity finite beam klystron IRE Trans. Electron Devices ED-5, pp. 98-108, April.

(b)....., Large signal analysis of the multicavity klystron, same jour., 306-315, October.

- 1959 , Large signal bunching of electron beams by standing-wave and traveling wave systems, IRE Trans. Electron Devices, ED-6, pp. 365-372, October.
- Buneman, O., Dissipation of currents in ionized media, Phys. Rev. 115, 503-517.
- (a) Mihran, T. G., The effect of space charge on bunching in a two cavity klystron, IRE Trans. Electron Devices, ED-6, pp. 54-64, January.
- (b)....., Harmonic current growth in velocity-modulated electron beams, Jour. Appl. Phys., 30, pp. 1346-1350, September.
- 1960 Hull, J. F., and Kooyers, G. P., Experimental and theoretical characteristics of injected beam type forward-wave amplifiers, Proc. Intl. Congr. on Microwave Tubes, pp. 151-158.
- Dayem, A. H., Monte Carlo calculation of diode noise in the multivelocitv region, Bell Tel. Labs., MM-60-124-32. (theory)
- Lambert, C. A., Monte Carlo calculation of noise propagation in two open-circuit diodes (computations)., Bell Tel. Labs., MM-60-124-38.
- Dayem, A. H., Monte Carlo calculation of diode noise in the multivelocitv region (results and discussion)., Bell Tel. Labs., MM-60-124-41.
- Webber, S. E., Some calculations on the large signal energy exchange mechanisms in linear beam tubes, IRE Trans. Electron Devices, ED-7, 154-162, July.
- Bridges, W. B. and Birdsall, C. K., Transient behavior of an electron stream at and beyond limiting current, Rept. 60-303, E.R.L., Univ. of Calif., Berkeley, August 2.
- Lomax, R. J., Transient space-charge flow, J. Elec. and Cont., 9, 127-140, August.
- Twombly, J. C. and Lauer, J. E., A study of self-actuated transients in high-perveance planar electron tubes, Tech. Rept. No. 2, Contract Nonr-1147 (06), Univ. of Colo., Engr. Exp. Sta., Boulder, December 1.
- Dawson, J. M., The breaking of large amplitude plasma oscillations, MAT-31, P.P.L., Princeton Univ., Princeton, N. J., February.
- Killeen, J. and Colgate, S. A., Boundary-Layer formation in the pinch, Phys. Fl., 3, pp. 387-394, May-June.
- Hain, K., Hain, G., Roberts, K. V., Roberts, S. J., and Köppendörfer, W., Fully ionized pinch collapse, Zec't, fur Natur. 15a, pp. 1039-1050.
- 1961 Auer, P. L., Hurwitz, H. Jr., and Kilb, R. W., Low Mach number magnetic compression waves in a collision-free plasma, Phys. Fl., 4, 1105-1121, September.
- Birdsall, C. K. and Bridges, W. B., Space charge instabilities in electron diodes and plasma converters, J. Appl. Phys., 32, 2611-2618, December.
- Hess, R. L., Large-signal traveling-wave tube operation; concepts and analysis, Tech. Rept. No. 60-361, E.R.L., Univ. of Calif., Berkeley, July.
- Hartman, C. W., Colgate, S. A., and Kellogg, P. J., (counter-streaming plasmas), Bull. Am. Phys. Soc., 6, p. 299.
- Buneman, O., Maintenance of equilibrium by instabilities, J. Nucl.

Energy, Part C, 2, 119-134.

Ashby, D. E. T. F., Roberts, K. V. and Roberts, S. J., Experimental and theoretical observations on a fast linear pinch, J. Nucl. Energy, Part C: Plasma Physics, 3, pp. 162-166.

1962

Bridges, W. B. and Birdsall, C. K. An electron stream instability, Tech. Rept. No. 60-443, E.R.L., Univ. of Calif. Berkeley, March 23.

Fisher, D. L., Green, T. S. and Niblett, G. B. F., An experimental and numerical study of radial hydromagnetic oscillations, Plasma Physics, Jour. Nucl. Energy, Part C, 4, pp. 181-184, June.

Killeen, J. Heckrotte, W. and Boer, G., Energy transfer from hot ions to cold electrons in a plasma, Nuclear Fusion, 1962 Supplement, Part 1, pp. 183-191.

Niblett, G. B. F., Fisher, D. L., Numerical calculations on reversed field heating in the latron, Tech. Rept. CIM-R 19, Culham Lab., Culham, Abingdon, Berks., England, March.

Pollack, M. A., Noise transport in the crossed field diode, Tech. Rept. No. 60-485, E.R.L., Univ. of Calif., Berkeley, October. (See also Pollack, M. A. and Whinnery, J. R., *ibid.*, I.E.E.E. Trans. Electron Devices, ED-11, 81-89, March 1964.)

Auer, P. L., Hurwitz, H., Jr., and Kilb, R. W., Large amplitude magnetic compression of a collision-free plasma, Development of a thermalized plasma, Phys. Fl. 5, pp. 298-316, March.

(a) Dawson, J., One-dimensional plasma model, Phys. Fl. 5, pp. 445-458, Kilb, R. W., Plasma magnetic shock waves with initial temperature, Gen. Elec. Co., Report No. 62-RL-3169 E, (See Jones and Rossow, 1965).

(a) Eldridge, O. C. and Feix, M., One-dimensional plasma model at thermodynamic equilibrium, Phys. Fl. 5, pp. 1076-1080, September.

(b).....Fokker-Planck coefficients for a one-dimensional plasma (letter, addition to Dawson (above, 1962)). Phys. Fl. 5, pp. 1307-1308, October.

(b) Dawson, J. M., Investigation of the double stream instability, Nucl. Fusion, 1962 Supplement, Part 3, pp. 1033-1043, 1107. (This was also MATT-63, P.P.L., Princeton Univ., 1961)

1963

Bridges, W. B. and Birdsall, C. K., Space-charge instabilities in electron diodes, J. Appl. Phys., 34, pp. 2946-2955, October.

(a) Dunn, D. A. and Ho, I. T., Longitudinal instabilities in an electrostatic propulsion beam with injected current neutrality, A.I.A.A., Preprint 63-041, March.

(b)....., Computer model of a beam generated plasma, Stanford, Elec. Labs. Rept. 0309-2, December.

(c) Dunn, D. A. and Ho, I. T., Computer experiments on ion beam neutralization with initially cold electrons, A.I.A.A.J., 1, pp. 2770-2777, December.

Buneman, O., and Kooyers, G. P., Computer simulation of the electron mixing mechanism in ion propulsion, A.I.A.A.J., 1, pp. 2525-2528.

Yu, S. P., and Mihran, T. G., Nonlinear rf behavior of electron beams with velocity distribution, I. General Analysis, J. Appl. Phys., 34, pp. 2972-2975, October.

Mihran, T. G. and Yu, S. P., Nonlinear rf behavior of electron beams with velocity distribution, Application to rectangular velocity distribution, J. Appl. Phys., 34, pp. 2976-2983, October.

- Eldridge, O. C., and Feix, M., Numerical experiments with a plasma model, Phys. Fl., 6, pp. 398- , March.
- Fried, B. D., and Culler, G. J., Plasma oscillations in an external electric field, Phys. Fl., 6, pp. 1128-1138. (This is a computer solution as contrasted with a computer experiment.)
- Smith, C., and Dawson, J. M., Some computer experiments with a one-dimensional plasma model, Rept. MATT-151, P.P.L., Princeton Univ., Princeton, N. J., January.
- Wadhwa, R. P. and Rowe, J. E., Monte Carlo calculation of noise transport in electric and magnetic fields, IEEE Trans. ED-10, pp. 378-388, November.
- Burger, P., The complete dc theory of an opposite stream diode, TR. No. 0833-1, Stanford Elec. Lab. S., Stanford, California, July.
- Twombly, J. C., Dynamic behavior of a long thin electron beam beyond critical perveance, Univ. of Colo. TR. No. 3, Contract Nonr-1147 (06), December.
- Hockney, R. W., A fast direction solution of poissons equation using Fourier analysis, A.C.M. meeting Denver, Colorado, August.
- Hockney, R. W., Computer simulation of a plasma in two dimensions, paper M8, 5th Annual Meeting, A.P.S. Plasma Physics Division, San Diego November 6-9.
- Roberts, K. V., Hertweck, F., Roberts, S. J., Thetatron, A two dimensional magnetohydrodynamic computer programme, Part 1, General discussion, CIM-R29 Tech. Rept. CIM-R, Culham Lab., Culham, Abingdon, Berks., England, June.
- 1964 Dawson, J. M., Thermal relaxation in a one-species, one-dimensional plasma, Phys. Fl., 7, pp. 419-425, March. (also MATT 213, P.P.L., Princeton Univ., July 1963.)
- (b) Burger, P., Nonexistence of dc states in low pressure thermonic converters, J. Appl. Phys., 35, pp. 3048-3049, October.
- Hasegawa, A. and Birdsall, C. K., Sheet-current plasma model for ion-cyclotron waves, Phys. Fl., 7, pp. 1590-1600, October. (See also Rept. 64-5, E.R.L., Univ. of Calif., Berkeley, 1964.)
- Sauseng, O. G., Applied Research on efficiency improvements in O-type traveling-wave tubes, series of reports, Contr. AE 33(615)-1951, thru 1966. (See attached listings from Hughes Microwave Tube Div. for their programs.)
- (a) Burger, P., The opposite stream plasma diode, Stanford Elec. Lab., TR. 0254-1, April.
- (c) , Computer simulation technique for the one-dimensional low-pressure thermionic converter, Therm. Conv. Specialist Conf., Cleveland, October.
- Dolph, C. L., and Lomax, R. J., The solution of nonlinear boundary value transport problems in electron and plasma devices, Univ. of Mich., TDR. No. RADC-TDR-64-393, October. (See also Dolph and Lomax, 1966)
- Rowe, J. E., Nonlinear beam-plasma interactions, TR. No. 69, Elec. Phys. Lab., Univ. of Mich., March.
- Wadhwa, R. P., and Kooyers, G. P., Analysis of electron-ion mixing in ion engines, Litton Industries, Rept. on Contract No. NAS 3-2503, March.

PANEL DISCUSSIONS AND CONCLUSIONS

COMPUTER PROGRAMS IN USE AT HUGHES MTD

<u>PURPOSE</u>	<u>DESCRIPTION</u>	<u>FEATURES</u>	<u>LANGUAGE</u>
Electron trajectories (gun design and beam focusing)	Paraxial rays with space charge and arbitrary magnetic field on axis	Laminar flow and thermal motion	FORTRAN
Boundary value	Electron trajectories with space charge and arbitrary magnetic field on axis	Translaminar electron motion, no thermals	BALGOL and FORTRAN
Small signal gain of TW Tubes	TWT small signal theory	Circuit cold test data can be used directly	FORTRAN
Large Signal Theory of TW Tubes (Efficiency)	Beam disc model, confined flow	Fundamental and harmonic frequency interaction	FORTRAN
Initial value	Ring disc model (three layers) of beam, confined flow	Fundamental and harmonic frequency interaction	FORTRAN

Information kindly supplied by Dr. Otto Sauseng,
Hughes Microwave Tube Division, 11105 S. La Cienaga Blvd.,
Los Angeles, California, 90045

- Birdsall, C. K. and Kamimura, T., Plasma computer experiments in three dimensions: Development of a code for guiding center fluids, Inst. of Plasma Physics, Nagoya, IPPJ 55.
- Killeen, J. and Rompel, S. I., A computation for studying the formation of the relativistic electron layer in Astron, Jour. Comp. Phys., 1, pp. 29-50, July.
- Hockney, R. W., Levy, R. H., Computer experiments on the containment of crossed-field electron beams, paper 1P-12, 8th Annual Meeting A.P.S. Plasma Physics Division, Boston, November 1966.
- (b) Hockney, R. W., A computer experiment of anomalous diffusion, Phys. Fl. 9, pp. 1826-1835.

Tsuda, T., and Obayashi, T., Computer experiment on thermal conduction in a collision-free plasma across a magnetic field, Ionosphere Res. Lab., Inst. of Elec. Kyoto Univ. Int. Doc. No. 1, November.

Kellogg, P. J., Some properties of the two-stream instability at large amplitudes, Phys. Fl. 8, 102- , January.

Goldstein, C. M., Monte Carlo method for the calculation of transport properties of a low-density ionized gas, Lewis Res. Centr., Cleve., NASA TN D-2959.

Goldstein, C. M. and Goldstein, A. W., A single-collision model for electron beam currents between plane electrodes, Lewis Res. Centr., Cleve., NASA TN D-3058. (Note: the Goldstein papers are computer solutions.)

1966

Sato, T., Tsuda, T. and Maeda, K., Computer study of nonlinear cross field instability process in a weakly ionized plasma, Ionosphere Res. Lab., Inst. of Elec., Kyoto Univ. Int. Doc., No. 2, March.

Tajima, T., Tsuda, T., and Maeda, K., Recent results of computer calculations on electron mobility in the ionosphere, IRL, IE, Kyoto, ID. No.

Matsumoto, H., Computer experiments on the motion of trapped electrons in the magnetosphere, IRL, IE, Kyoto.

Cutler, W. H. and Burger, P., Oscillations in the thermal cesium plasma diode, Jour. Appl. Phys., 37, pp. 2867-2873, June.

Dolph, C. L. and Lomax, R. J., The solution of nonlinear boundary-value transport problems in electron and plasma devices, Jour. Math. Anal., Appl., 13, pp. 361-403, March.

Lomax, R. J., Time dependent nonlinear solution of the Landau-Vlasov equations for an electron-ion diode, Elec. Phys. Lab., Univ. of Mich., Contr. No. DA-36-039 AMC-02269 (E).

Shanny, R. A., Dawson, J. M., Greene, J. M., Numerical experiments in plasma physics, P.P.L., Princeton Univ., MATT-441, March.

Twombly, J. C., Dynamic behavior of a long thin electron beam, IEEE Trans. Electron Devices, ED-13, pp. .

Twombly, J. C. and Cerviera, A. G., The effect of injection systems dynamics on the limiting current behavior of an ideal planar diode, Univ. of Colo., TR. No. 4, Contract Nonr-1147 (06), May.

Brauch, D. F., Buneman, O., and Wadwha, R. P., Computer studies of plasma boundaries and lens effects created by immersed and withdrawn neutralizers, A.I.A.A.J., 4, pp. 651-653, April.

(a) Hockney, R. W., Computer simulation of anomalous plasma diffusion and numerical solution of Poisson's equation, Stanford Univ., SUIPR No. 53, May.

(c) , Minimum multiplication Fourier analysis, submitted to Numerische Mathematik.

Mihran, T. G., Nonlinear limiting of the double stream instability, J. Appl. Phys., 37, pp. 624-630, February.

Byers, J. A., Confined and nonconfined interchange instabilities obtained from nonlinear computer models, Phys. Fl. 9, pp. 1038-1040, May.

Birdsall, C. K. and Bridges, W. B., Electron Dynamics of Diode Regions, Academic Press, N. Y. (See Chap. 3, Stability of flow; nonlinear solution of multiparticle model.)

Gould, R. W., Allen, M. A., Large signal theory of beam-plasma amplifiers, Proc. 5^e Congress International Tubes Hyperfrequencies, Paris, pp. 445-450.

- 1965
- Hasegawa, A. and Kamimura, T., Computer experiments on ion cyclotron heating, J. Phys. Soc., Japan, 20, p. 1525.
- Wadhwa, R. P., Buneman, O., and Brauch, D. F., Two-dimensional computer experiments on ion-beam neutralization, A.I.A.A.J., 3, pp. 1076-1081, June.
- Hockney, R. W., A fast direct solution of Poisson's equation using Fourier analysis, J. A.C.M., 12, pp. 95-113, January. (See also Tech. Rept. No. 0255-1 E.D.L., S.E.L., Stanford Univ., Stanford, Calif., May, 1964)
- Yu, S. P., Kooyers, G. P. and Buneman, O., A time dependent computer analysis of electron-wave interaction in crossed-fields, J. Appl. Phys., 36, pp. 2550-2559, August.
- Brauch, D. F., Buneman, O., and Wadhwa, R. P., Computer studies of plasma boundaries and lens effects created by immersed and withdrawn neutralizers, paper presented A.I.A.A., San Francisco, July, 1965.
- Lundgren, R. E., The instability of centrifugal-electrostatic-focused flow, Tech. Rept. pp. 65-22, E.R.L. Univ. of Calif., Berkeley, Calif., August.
- Hellberg, M. A., A theoretical investigation of the resonance probe, Tech. Rept. CLM-M49, Culham Lab., Abingdon, Berks., England.
- Wadhwa, R. P., and Brauch, D. F., Analysis of electron-ion mixing in ion engines, Litton Industries final report on Contract NAS 3-5757, July.
- (a) Burger, P. Theory of large amplitude oscillations in the one-dimensional low-pressure cesium thermionic converter, J. Appl. Phys., 36, pp. 1938-1943, June.
- Burger, P., Dunn, D. A., and Halsted, A. S., Computer experiments on the randomization of electrons in a collisionless plasma, Phys. Fl., 8, pp. 2263-2272, December.
- Buneman, O. and Dunn, D. A., Computer experiments in plasma physics, Tech. Rept. SU-0254-2, I.P.R., Stanford Univ., Stanford, Calif., January. (A review, 58 pages.) Shortened version to appear in Science Journal, London.
- (a) Rowe, J. E., Nonlinear Electron Wave Interaction Phenomena, Academic Press, N. Y.
- (b), Collision effects in nonlinear beam-plasma interactions, Proc. Intl. Conf. on the Micr. Behavior of Ferrimagnetics and Plasmas, London, 80-1 to 80-3, September.
- (b) Burger, Peter, Computer simulation methods for plasma diodes with collisions, Therm. Conv. Specialist Conf., San Diego, November.
- Mihran, T. G., Phase shift in velocity modulated beams of finite diameter, Gen. Elec. Co., Rept. 65-RL-3879E, March.
- Jones, W. P. and Rossow, V. J., Graphical results for large amplitude unsteady one dimensional waves in magnetized collision-free plasmas with discrete structure, (Ames. Lab.) NASA Rept. TND-2536.
- Rossow, V. J., Magnetic compression of collision-free plasma with charge separation, Phys. Fl., 8, pp. 358- .
- Halsted, A. S., Equilibrium conditions and beam focusing effects in a beam-generated plasma, Stanford Univ., SUIPR No. 10, Chap. 4, 5, June.

Panel Discussion On:

METHODOLOGY IN THE N-BODY PROBLEM:
LAGRANGE VERSUS EULER APPROACH

FIRST PANEL:

Oscar Buneman
 John M. Dawson
 Marc R. Feix (Moderator)
 Roger W. Hockney
 Craig G. Smith

Feix: One of the difficulties with most panel discussions is that each of the panel members stands up and gives a 10 minute talk with no audience participation. I hope that this won't be the case here. I would first like to have all the panel members give their philosophy about the computer experiments.

Let me start with a remark which is half serious and half joking and show you a slide which has been brought to my attention by Macon Ellis:

"I think we may have more difficulty in exploring the full limits of the computer than we have had with earlier gadgets. I think there may be more danger in the period of trial and error than there has been with earlier devices. These earlier devices - looms, engines, generators - resisted at critical points human ignorance and stupidity. Overloaded, abused, they stopped work, stalled, broke down, blew up, and there was the end of it. Thus they set clear limits to man's ineptitudes. For the computer the limits, I believe, are not so obvious. Used in ignorance or stupidity, asked a foolish question, it does not collapse, it goes on to answer a fool according to his folly. And the questioner being a fool will go on to act on the reply."¹

I think there is a lot of truth in this little paragraph, but let us go back to the main discussion!

Oscar Buneman has already given his opinion in his introductory address and I think John Dawson disagrees with this philosophy.

Dawson: I feel that the computer is a very powerful new tool and we are really just beginning to learn how to use it. We must develop new techniques and we must learn what the computer can do and what answers we can get from it. Generally, we get so many answers that we don't know what to do with them so we have to learn how to ask the right questions. I think a computer is suited for two types of use - one is a practical use where we try to simulate real plasma devices and let the computer tell us what they are going to do.

The second use is really to look at fundamental problems, such as the statistical mechanics problem Marc mentioned yesterday, and then we try our

¹E. E. Morison in "Men, Machines and Modern Times," M. I. T. Press, Cambridge, 1966, p. 91.

theories out and see if they explain what the computer tells us. For this kind of study, we just can't go at it blindly and say, "Well, turn the thing loose and see what it turns out." As in any experiment, we must have some ideas as to the direction in which we want to go. We should, however, be prepared to find unexpected answers or unexpected results so we should look at the answers with a rather open mind. When we see something happen we should always ask: "Why didn't my theory predict that? What have I left out?" Of course, if the theory does predict the results, we are very happy, but as Marc mentioned yesterday there are some calculations which don't agree with the theory; we should now go back and ask: "Why did the theory fail?"

My own interest in computers lies in this second line of investigating fundamental problems and trying to deepen our understanding of the dynamics involved in them. I think that both the theory and the experiment have to be worked together and we have to realize that we are not going to understand everything, but at least the computer gives us clues and, hopefully, will help to expand our theories.

Feix: I see that we already have a dangerous split between the theoretical computer experimenter and the experimental computer experimenter. Roger, what do you think about that, on the experimental side?

Hockney: The advantage of computer experiments is that one has in a sense a perfect experiment. One has, for example, control over the initial condition and time; one can stop the experiment and examine it in great detail. Also one can put in measuring instruments without disturbing the experiment, which is what one would like to do in a real experiment.

On the other hand, of course, the computer experiment brings along its own errors of numerical and mathematical instability which are of no relation to the physical problem and which can quite easily occur if you do the wrong thing. So one has to watch out on this course as well. Also one has to watch the numbers of particles in the particle-like models. We obviously cannot treat as many particles as we have in nature and as a consequence we usually exaggerate the noise. Provided one can convince himself to believe what the model does, I think one has, in a sense, the perfect experiment.

Feix: Craig, would you like to comment about your own philosophy?

Smith: In general I agree with Roger, but I sometimes have my doubts as to the standard *raison d'être* for doing computer experiments. I think we should be more cavalier with the computer aspects of the problem and put more plasma simulation into the model. I would like to see more honest-to-goodness model making, rather than just deciding how many dimensions we are going to work in and deciding whether we should use sheets or rods and what not. Along with studying some very basic questions regarding the kinetic theory and relaxation processes, we should also help those people with real experiments who are trying to understand effects of boundary conditions.

Feix: Oscar, do you want to answer some of these comments?

Buneman: I want to ask John what happens if we haven't got a theory and we have the situation which we discussed this morning, where we have a lot of evidence from the computer but nobody is happy about the theory; people were quite rude to each other about this Fermi-Pasta-Ulam experiment. What do you do in that case? Do you throw the experiment away?

Dawson: You try to get a theory. I think that is what Norm [Zabusky] was trying to do. You have these very interesting results. Of course, it's like nature - we don't understand them completely but we still keep looking and we try to fit them into a theory. The only way one learns to trust the computer is to start out from a known situation where you know the answers and computers give reasonable answers and then you extend its use to a known situation.

Smith: There are two levels of trust: there's the level where you question the computational accuracy and there's the second level where you question the ability of your model to describe the given situation.

Buneman: I like the idea of the control experiment - one where you know the answer if the computer performs properly - and then I would trust the computer in other cases!

Feix: One of the big advantages of computer experiments is that we have in one man both the theoretician and the experimentalist which is the best situation. Now, perhaps we can go ahead and ask ourselves what is a perfect experiment. We will now discuss more special topics, for example, how perfect are the experiments? How much can we trust them? We can discuss two models - the field models (Vlasov equation, water bag), and the particle models or sheet models. Put it in another way, we have two points of view: the Eulerian and the Lagrangian. I'd like to ask the panel if they believe that we can have a very good experiment when we want long-time simulation of systems which have very large numbers of particles, and where there are several very different time scales, such as, the different electron, ion, plasma or cyclotron frequencies found for plasmas. How long can we go with the discrete sheet model, for example?

Hockney: If you have a certain number of rods or particles that you move around, that will give you a certain number per Debye square and this determines a certain time that you can go along in a collisionless situation. Now there are two things you can do: you can either analyze this noise, and on the basis of that find out how long you can go before it becomes important, or you can try to theorize on it to get the limit. But it's the very nature of the problem, I think, that gives you confidence that you know what noise you have and how long you can go before it's going to dominate.

Feix: Do you think we can perform numerical experiments with the discrete model where we can be confident that we simulate correctly over 100 to 1000 plasma oscillations or star rotations?

Hockney: We can have 100 rotations before collisions become important.

Feix: Do you think we can do it in one, two, and three dimensions?

Hockney: If given enough superparticles we should be able to do it. Surely something like 100,000 superparticles should be satisfactory.

Dawson: I think there are two possibilities. First of all, in the discrete model we can try and soften the potential for short distances, as Roger did, so as to minimize collisions or fluctuations. Also we can try to understand exactly what these collisions do and how they affect our results. Finally, in a discrete model we can start out with slightly different initial conditions, and then to see how much the effect that we are interested in depends on the different initial conditions. If the deviation is small then we can have some confidence that the discreteness is not really affecting our results seriously.

Buneman: I'd like to say something on this point of having to trace the system for a very long period. It seems to me that if anything takes more than a thousand basic periods then there are likely to be facts that we have not fed into the computer; typically there may be an ionization going on which is very rarely put into the computer (you would have to do a lot more hard work), and therefore anything that shows up only after a thousand basic periods is under suspicion. If we want to compare long time with short time scales on the computer without too much expense, we reduce the masses as is often done to mass ratios of 64 or 16.

Feix: But in phenomena like stellar systems or problems like those treated by Dr. Zabusky this morning we have to go to very long times.

Buneman: In practice there will be a random process going on which will spoil the third or fourth term in Dr. Zabusky's series. This will be a naturally occurring process. The Zabusky problem is a nice exercise in nonlinear analysis.

Feix: I'd like to introduce now the topic of microreversibility and accuracy. Are there any comments?

Birdsall: Could the question be put this way: how does each member of the panel make his results believable to the audience? Does he use conservation of energy, angular momentum? What do you do?

Buneman: I say I do all these things but I never really do.

Dawson: Well, I think there is a certain amount of faith, too. I have used reversibility. I used it once, and now I believe it.

Buneman: I believe John.

Dawson: We've written new codes and modified old codes but we haven't checked every time. Also I think the energy is one good thing to keep track of and if that's being conserved, you can be pretty sure things are going all right. Certainly you can conceive of many things that could go wrong and the energy wouldn't change, but I think over a long time if the energy is not changing things are all right, at least for the discrete models.

Feix: We have a question from the audience.

Sadowski: Concerning Fourier-Hermite expansion of the Vlasov equation, you can get senseless negative kinetic energy and yet conserve total energy to one part in 10^7 .

Dawson: That's right. The energy is only one number and you have 2,000 numbers in the computer so you can certainly shuffle them around and get anything you want, but to think that your code and machine will do this every time is rather unbelievable to me - again, I am thinking of discrete sheet models.

Roberts: Let me make one point: there are certain codes, certain techniques you can use to guarantee exact conservation. I shall be talking about one tomorrow. Now, is it a good idea when you can guarantee exact conservation to get it and say it's bound to improve the calculation, or not to get it and then use this numerical conservation to check on your accuracy? In the case of magnetohydrodynamics, you can get exact conservation of mass and momentum and magnetic flux. You can't so easily get exact conservation of energy and therefore we just use energy as a check on the calculation. But should you give away all these exact conservation laws, you get accurate physical checks on your solution.

Hockney: In the case of the star gas I can check angular momentum and energy, but in the diffusion problem I am on less firm ground because the number of particles varies and energy is not conserved.

Smith: I agree that if it doesn't cost anything you can use energy or any other constant as a check, but I can envision going into more complicated problems where you can reduce the running time greatly by making use of the constants of the motion. But I'd be willing to give up this independent check and make it believable by overall physical self-consistency.

Dawson: When one does these numerical experiments, the person who is most difficult to convince should be the man who is doing it himself. He should be skeptical of all his results until he obtains reasonable checks of them; of course, you can't be absolutely sure and you will force yourself into a straight jacket if you have to be absolutely sure. We have had examples of codes that ran for a long time until a rare event occurred that the code would not take into account correctly. I think you can never really prove that this won't happen.

Feix: Maybe we'll pose the same question again - the question of the credibility gap. I'd like to propose a little paradox based on the language. Inaccuracy means uncertainty, uncertainty means lack of information, lack of information means increase of entropy, increase of entropy means irreversibility. Now we hear Dr. Buneman say that we can sacrifice accuracy and get reversibility. Now I think that this appears to be a paradox. Can somebody comment on this?

Hockney: By using a lower order truncation approximation to a derivative, the program is therefore less accurate because the truncation error is larger; however, it's symmetric and therefore reversible.

Buneman: I think I ran through an example of this yesterday. You may, for example, find that using a numerical code will produce an instability. You can then change your numerical code because you feel that this instability is due to numerics, and you can put in a strong damping term in the form of a first derivative or in the form of a reference back to the previous time step; in so doing you are in fact killing the instability and have made the system irreversible and therefore I would immediately doubt whether that was the right way of insuring your accuracy. I prefer a system which is reversible, though maybe inaccurate.

Hockney: For some problems you may prefer accuracy instead of reversibility; in other cases it may be the other way around.

Feix: We can put it this way: Is reversibility absolutely necessary? As a matter of fact nature is irreversible.

Buneman: It is not necessary, but I have often had to convince people that irreversibility is the result of some physical process and not the result of some finite difference equation. This is why I'm a bit biased in that direction, particularly when people want to explain how entropy is created in the collisionless shock. Then you are really up against it. You start with completely reversible equations. If you want to do anything to convince people, you've got to make sure that in your shock calculations you do not make anything irreversible.

Roberts: I think that you ought to have a number of tools in your armory which you could use in a controlled way and one of these is a reversible code. I think reversible codes are probably not normally necessary and they take longer to run, but if you find something which looks irreversible it is nice to have a reversible code which can convince you that indeed the irreversible behavior is not due to the numerical code but to the physics. After that you may use an irreversible - but faster - code to pursue your problem.

Sadowski: There are certain very simple differential equations which have two solutions: a positive exponential and a negative exponential. Of course, the negative exponential will damp out. Now if you insist on going out in time and coming back, you will never come back on the same curve for obvious reasons, because the sign of the exponential has been reversed. Even though you achieved reversibility with a twist or a different formulation, the fact remains that there are legitimate exact solutions which are irreversible. In fact, in any kind of computer program there are all kinds of extraneous solutions.

Hockney: Perhaps you won't get an extraneous solution if you take the right order of polynomial approximation. If you use a second order differential equation you should only use a second order difference equation; if you use a third or fourth order difference equation you may introduce spurious solutions.

Buneman: If I solve these equations, I go forward and then reverse, and then I come back to the original point except for the rounding off error in the third or fourth digit. Otherwise I come back to the original point. This could be vital if one is faced with a situation where the truncation error is extremely important.

Feix: We can close this discussion with a comment made by Dr. Roberts: "We should have two codes - one to convince the people of reversibility and one to do the job." I'd like to move to another topic - the question of dimensions. How much progress can we make and how rapidly can we move in two and three dimensions?

Buneman: I see great future in one dimension, particularly the extended one-dimension idea that is the one and a half dimension, where one keeps certain effects of two dimensions but x and v are the only independent variables; that is an area which I shall certainly develop immediately at great speed. One thing I will try out there is to use a Fourier analysis in the other two dimensions and pick up this idea of the conductivity kernel that we heard about, except instead of Fourier analysis in time as was done there, with an ω label on the kernel, I shall put a k label for the other two dimensions. The nice thing about that approach is that you can treat each Fourier component separately - work out the conductivity kernel as if you had a one-dimensional program - except that you are now working a two- or three-dimensional problem.

Feix: But Dr. Leavens talked about a linear system.

Buneman: It would only apply to the studies of perturbation of systems which are uniform in two out of three dimensions but which are nonuniform in one, and this dimension I am giving up is the idea of Fourier analysis.

Feix: The linearized problem that Dr. Leavens has been talking about is a problem where the velocity field has been eliminated. We don't have to compute the perturbed trajectories, only the unperturbed trajectories. Still the problem is very difficult.

Hockney: I think that whether it is difficult to go to one, two or three dimensions depends on how well you formulate the method of solution. If you do it by summing up the influences of all the particles you couldn't care less whether you sum up cosines or other forces. The problem with the calculations is that the amount of work increases as the square of the number of particles involved, and as a consequence it is limited to a few hundred particles - let us say 500. On the other hand if you go via Poisson's equation, which is my own route, then the time to find the field is proportional to the number of mesh points times the logarithm of that number, which you can more or less neglect. Therefore, the time goes linearly with the number of mesh points. And again the amount of time to move through the loop, which is of course the number of particles, is proportional to the number of particles, and I can treat up to 2000 particles. And I don't think it would be much more difficult to do this sort of field calculation in two or three dimensions, so the number of dimensions doesn't seem to matter. What we have to decide now is if you can use only 1000 "particles." Does it make sense to spread them in two or three dimensions?

Feix: The next topic is a discussion of the Vlasov or field-type equations. These equations describe a system like a galaxy or hot plasma much better than the discrete model. We should treat 10^{11} particles, but with the discrete model we study typically 10^3 particles. If we now go to the limit of an infinite number of particles, we have the Vlasov equation to describe the system. This field-type limit is much more interesting than the superparticle model but may be more difficult to treat. What can we say about a direct attack on the Vlasov equation? Would somebody comment about the merit of x-v space attack and the use of different transforms.

Buneman: As many as 10^{11} particles in six-dimensional phase space means 60 or 70 in each dimension which looks more discrete than continuous to me. I feel that the Lagrangian approach has the edge on the other method.

Dawson: Obviously all computers are finite and they can handle only so much information. Particles have a natural way of keeping the amount of information finite. If you start working with a Vlasov equation or the water-bag or any other field-type model, sooner or later you are going to have to start to throw away information. It is a question of how far you can go and when you start to throw away information. Which method throws away more information, or applies best to the situation under investigation, depends on the individual problem. This also applies whether you use transforms or work in x-v space.

Smith: The most immediate virtue of the Lagrangian approach is conservation of particles so that the total charge is conserved. One thing I always worry about in the computer experiments is that any departure from it could lead to a build-up of spurious electric fields. There is one problem that doesn't come under this topic but has to do with scaling; the fact that we always have rather large Debye lengths, but in most physical applications that we are interested in, they are small, which says that we should be setting the species density equal and dropping Poisson's equation and getting the field some other way. If we want to be sure, we should use a fluid description and a generalized Ohm's Law. That would be my motivation for pushing the Eulerian point of view.

Armstrong: I have several comments. It is possible to use integral representation to preserve charge neutrality exactly. That doesn't change the problem except in representation on an x-v grid where you don't have identical conservation to start with. Also by using a transform representation you can reduce the problem of the Vlasov equation to a first-order ordinary matrix differential equation, which is much more suitable for computer analysis. I feel rather strongly about the usefulness of the transform representation.

Feix: I would like to stand in favor of Euler for the following reason. In problems with the Vlasov equation when the nonlinearity is small, we can take advantage of the smallness of the wave-wave interactions and use a small number of waves, and the space Fourier transform is certainly useful. In problems of strong nonlinearity such as turbulence I am not so sure.

Sadowski: It's not so much a question of nonlinearity as a question of looking at the truncation of your expansion which has a physical meaning. The whole formulation is much more transparent physically. When you throw away high k , that is the higher harmonics in Fourier or Hermite representations, you know what you are doing much better than if you introduce a grid of $\Delta x = 0.2$, etc.

Montgomery: In connection with the Fourier-Hermite program you have two checks. For two cases you have analytical solutions and you can compare them. One is a free-streaming problem where you turn off all the particles' interactions altogether and is, by the way, quite hard to do on a computer; nonetheless, it can be compared with your results by putting the charge equal to zero. The second is the linearized problem where you have the Landau analysis to compare with and only a very small change between the two programs is necessary to both the linear and nonlinear problems. These are very good checks on the accuracy.

Feix: Unfortunately, these two cases are linearized cases and you have to be prudent when you extrapolate the credibility to the nonlinear problem. Our experience, for example, is that even if you very incorrectly represent the wave-wave interaction for linear or quasi-linear problems the convergence is pretty good. Now I think Dr. Berk wants to comment about the water-bag model.

Berk: This is a model which is a compromise between a Eulerian and a Lagrangian point of view, the point being that we're not limited by the discretization. On the other hand, we have to consider simpler problems. We think that we have essentially extracted the essence of the two-stream instability. We see the evolution of the Bernstein-Greene-Kruskal mode as Armstrong sees it and now we have an idea of the formation of these solitary modes.

Buneman: I'm glad to find that the water bag is so successful as we heard this morning. I was most impressed with that and I really want to try it out myself on some problems, but don't kid yourself - you are in fact discretizing, first of all the distribution function, and also, whenever you come to the field, you probably cut up at least the x -plane, although maybe not the v -plane.

Roberts: We tried cutting up the x -plane with 32 points and 64 points; at each major instant of time when we print out, we Fourier analyze the field, but the higher harmonics are incredibly small. You really don't get a very inaccurate representation of the electric field. As I say, these runs are very short - five minutes.

Feix: First a remark: It seems to me that the real problem is how we are going to handle the information. Can we get some idea or help from the information theorists? It seems to me that they have looked at this problem. Another question is whether we can get help from quantum statistics. The first point is whether we recover the Linden-Bell theory. The second point is that classically we have an x - v problem, but in quantum mechanics we can use either x - or k -space. Of course, the amount of information is always the same but maybe it would be simpler to store it on only one form - for example, the Fourier component $\psi(k)$ of the wave function.

uneman: You raised the question this morning concerning whether there is a Heisenberg principle and I tried to see what happens in $x-v$ space. I can see why there is exclusion. You are not in a strictly classical regime when you divide your chessboard up into squares and thereby quantize, because you are not allowed to pile two castles on top of each other as you move them about in $x-v$ space. That is not possible classically if you integrate accurately because if you integrate accurately, two particles will never run across each other in $x-v$ space. If they did, they must have run parallel for all times before and therefore in $x-v$ there is an exclusion principle that there can be no particles in the same place simultaneously. I think this is the answer to the controversy which started this morning.

ecar: I think that is wrong. It is true that one can quantize in the Linden-Bell theory any fixed distance - let's call it h in phase space - at an initial time. But unfortunately as time goes on, the quantum effect goes to zero. If you wait long enough all of the degeneracy in the Linden-Bell problem disappears.

eix: I think we have run out of time. Let me just say we have not solved all the problems. We, of course, like to keep some of the problems for the future. I'm quite sure that tomorrow the second panel will also solve many of the practical problems. I am happy to thank the panel members and the audience for their participation.

Panel Discussion On:

APPLICATIONS AND ORGANIZATION OF THE NEW FIELD
OF COMPUTATIONAL PHYSICS

SECOND PANEL:

Bernard J. Alder
Charles K. Birdsall (Moderator)
Michel Henon
Ralph W. Kilb
Keith V. Roberts

Birdsall: The general theme for this afternoon is somewhat in contrast to that for yesterday; in effect we would like to talk about applications and then take a look into the crystal ball in order to see what things we would like to do in the future and some of the things we think we should be able to do. The panel does not have all of the available information, so we would like to draw also on the audience. Ralph [Kilb] will start off talking about fusion.

Kilb: In general, we are in fairly good shape for low-density problems where we can use the single-particle picture. The principles are fairly straightforward, and it is just a matter of running the computer. We are also in reasonably good shape for high-pressure problems such as in high-density theta pinches where we can use the MHD equations. There are still difficulties with boundary conditions, but people have approached reality within a factor of 2 or 3, at least in plasma turbulence. I think a factor of 2 is a reasonable criterion. So I am fairly happy about the extreme ends (low density or high density), but in the intermediate range, in the stellarator regime, I feel there are still problems in choosing a plasma model. In the low-density theta pinch, it appears that we have a situation where we cannot use the MHD equations for the ions; we also have a problem on how many dimensions must be included in the plasma model. We still don't quite know what the rules are that we have to follow in order to really decide what's happening in the experiment. I think we are making some progress in that direction, and I hope the next conference is going to see some real results in this intermediate regime. I hope there will be more thoughts on the effects of magnetic fields, because I think this is the main area where experimentalists are working and we need more numerical work on that sort of problem.

Birdsall: Craig [Smith], would you like to comment on the Princeton work?

Smith: The stellarator is a nonaxisymmetric machine. There are problems not with the plasma behavior but with the field behavior; that is, the topology of the field. There are several programs under way - one from the fluid point of views, the other from the plasma point of view.

Feix: I have a question. I wonder if we are in such good shape in the low-density limit, and in particular, I would like to ask about the high energy accelerator where the single particle picture is certainly valid. In these

accelerators, the particles turn 10^8 or 10^9 times. Can we follow, on the computer, the one particle motion (with no collective effects) for such a long time? Can somebody comment on this?

Birdsall: John [Killeen], the question was asked about the particles turning many times around in the machines. You have done some of this.

Killeen: Well, I think we are talking about two different things. As far as I know, no one has taken anything around a toroidal device. Orbital trajectories in the baseball magnets and in the mirror machine have been calculated and some of these cases have been followed for a long time.

Feix: What about the big accelerators?

Killeen: I'm not familiar with them at all. The other thing I thought perhaps that you were talking about is that we calculate field-line trajectories many times around the torus on an accelerator-type configuration. When you follow the field line there you solve an ordinary set of differential equations forming a smooth surface. We follow the trajectories around at least a hundred times without any problems. The differential equations are, in fact, more sensitive than the equations of motion of particles.

Hess [R. V.]: How does the collisionless shock fit into your discussions?

Some solutions have been obtained for simple geometries. Could you comment on this?

Kilb: Well, I think we are all right in a simple geometry, but the question is, does a simple geometry correspond to reality. For instance, it appears to me that the earth's bow shock (the three-dimensional nature of it) is not understood in detail. I don't think we yet have a convincing example of an experiment with a true collisionless shock.

Hess: Lots of experiments claim to have collisionless shocks.

Kilb: You are going to see more experiments that touch on collisionless shocks. There are still complications on how to treat the electrons theoretically. Apparently, the electrons do not behave in an adiabatic manner, as I would like to believe myself. Therefore, it appears that there are streaming instabilities or some other mechanisms which involve more than one dimension which are disturbing the electron behavior. Compared with what one would want to believe on simple terms, the multidimensional problem is with us and we will have to face up to it.

Birdsall: Who would like to comment on the fusion problem?

Roberts: I would like to comment on a practical point. A calculation in which you simulate an actual experiment is much harder than one in which you just do an abstract theoretical problem. It is probably worthwhile to do a large number of calculations of the second kind, and relatively few in which you try to simulate the detailed conditions of an actual experimental device. In two-dimensional magnetohydrodynamics for example, most of the difficulties

are associated with the unknown boundary conditions at the end of the apparatus, and with the changing shape of the curved plasma boundary. It is possible to calculate most of the phenomena which occur in a real device, such as the behavior of shocks, by doing a much simpler calculation with a fixed rectangular mesh and rigid, perfectly conducting walls.

Alder: I agree that we should use the computer to keep the theoretician honest. They can work a problem for some idealized situation where it is possible to check their approximations on a computer.

Kilb: I'd like to make a final point. There seems to be a great need for us to suggest experiments which the experimentalist can perform. These experiments would allow a check against our computations. The Princeton stellarator is too complex to be studied on a computer and, therefore, I suppose it's up to us to come up with reasonable experiments which the experimentalist can carry out and which we can compute accurately.

Birdsall: I'd like to make one comment concerning the simple diode instability that has come up a couple of times. The oscillations following the instability had never really been seen experimentally, so after we did the computer experiments we went to the laboratory and tried to see them in an electron diode. However, the oscillations were not seen clearly until experiments were done on the plasma diode. In the plasma diode, the oscillations were then seen. The high-frequency oscillations (ω_{pe}) had been postulated by the electron diode instability. The point is that a computer experiment, and not a very complicated one, first predicted them. More firsts of this kind are beginning to occur.

Keith Roberts has volunteered to provide guidelines of two kinds. I'm afraid that if he's not careful he's going to make himself sort of president of a data bank, so if we will excuse him from this, he is going to tell us how we can do various things that he thinks are very necessary.

Roberts: I would like to discuss how we can understand one another's programs, exchange useful programs and subroutines, and run them without difficulty on different machines. This is a problem which we have encountered at Culham, because we have had a number of people working at the laboratory for a time to write programs for us, and then going elsewhere. We have had a series of different machines ourselves, and from time to time people at other installations have asked us whether they could have copies of our programs. This has usually been quite embarrassing. We have either had not to reply, or to say no, or something equivalent - the conversion problems have been much too great.

We have therefore been looking at the problem from an operational point of view. What actually makes a program unintelligible, and what makes it difficult to run on other machines? A related question which can be examined at the same time is what makes a mathematical paper intelligible, and how do we bring some of the intelligibility of a mathematical or scientific paper into a computer program?

Well, there are many things. It is very easy to make a program intelligible if you deliberately set out to do so, and this approach will also help to get it written more quickly and will minimize mistakes. The listing should be well laid out, like a page in a printed text-book. One of the most important things is to put in enough comments; these correspond to the text in mathematics, with the executable instructions corresponding to the formulas. A good distribution is about two or three times as many comment characters as actual instruction characters - much as in mathematics. The comments should start in a different column from the code, to make them more distinguishable to the eye, and it is useful to introduce various types of section heading, again using different columns. I place various symbols on the far right-hand side to indicate boundary conditions, inner loops (which must be coded efficiently), and so on. A useful dodge is to keep a large stock of "blank" comment cards - just "C" in column 1 - which can be used as spacers to emphasize the various "paragraphs" of the program, just as in a book. Cards with a dash or asterisk punched right across are used to separate major sections.

In mathematics, one can often guess the meaning of a symbol from its appearance, and quite elaborate conventions are used. In a similar way, one can use standard conventions for the initial letters of COMMON variables, internal variables, loop indices, logical variables, and formal parameters, so that the reader can tell at a glance what the status of a variable is. Another convention in mathematics is always to define the meaning of a variable before using it. This can easily be achieved by setting up an alphabetic index for all COMMON variables in the program, and one for the internal variables of each subroutine. It is almost no work to do all these things as you are writing the program. Another entirely obvious thing is to have all the statement numbers in numerical order, or some sensible decimal scheme, so that if the program says "GO TO 6" the reader knows where "6" is; whether to look up or down the page, and roughly how far. What would any of us think of a man who published a paper with all the equation numbers in random order? It would never get past the referee, and if it did, it would certainly never get past the editor.

So, there are lots of elementary things one can do to make a program more intelligible, but we have gone a bit beyond that. Joyce Staples and Klaus Hain, who are here, have both written automatic flowcharting programs which take other programs and make them as intelligible as possible. David Fisher and I wrote an automatic documenter, which did much the same thing for a large systems program written in machine code.

The next question is how to write programs so that they will run on many different types of machine. This again is not difficult, if it is deliberately planned from the start. The various versions of Fortran do not differ very much, but they differ in annoying ways, for example input-output. So if you know the inconsistencies between the different versions you can choose to write your programs in such a way that most of the subroutines will run fairly universally, and segregate input-output statements in just a few special subroutines, which are clearly marked. I keep a stock of cards marked "WARNING", "INPUT", "OUTPUT", "NOTE n", etc. on the right-hand side, which can be

inserted in the deck to draw the user's attention to possible conversion difficulties. It is important to signal library subroutines, which the program makes use of but which may not be available in other installations, and to include a note explaining exactly what these do. It is not usually difficult to re-create them, provided their function is known. People have written programs which automatically alter other programs to run on different machines, and these programs can also alter themselves, just as flowcharters can flowchart themselves.

With all these techniques it is really quite easy, if you think about it from the outset, to write programs that you can give to your colleagues, and that will run on their machines with very little trouble. It is also very much quicker to write a program in the first place, and to get it running, if this policy is adopted. The water-bag program which I talked about earlier actually worked the first time, and this is because I wrote it quite rigorously and gave it to Herb Berk to referee for correctness and intelligibility before we put it on the machine. I think that we had one comma and one bracket wrong by the time that we started to compile.

When an institution publishes a scientific paper, or even a report, the division head or professor won't let it go out without its being checked by colleagues and refereed by himself. So equally, I would advocate that we should write programs and subroutines that we are not afraid to give to other people. We should try to make each program as readable as a mathematical textbook, and should try to adopt the principle that all important programs are published. If a program is never published and if it is not intelligible, how are we to know that the results are right? In a few years, some of these programs may produce a great amount of data and some very interesting physical results, which are analogous to astronomic observations or to records of careful scientific measurements - say on the earth's magnetic field. If this data is based on programs of quite unknown validity, nobody can check the results and I think that the scientific literature may get corrupted. So I feel that we should actually publish all our programs in an intelligible form, and set very high standards comparable to those of the rest of science.

Birdsall: I think one point you didn't make clear is what was meant by "publish."

Roberts: By "publish" I mean publish the code, possibly as a report, possibly as microfilm. As long as the results exist in the literature it must be possible to get at the program from which they were computed, but there needn't be many copies of it. There must be archives, for example in some AEC laboratory or the National Bureau of Standards or a library, so that you can get hold of the program to find out precisely what the results mean. I think that in other fields of knowledge this principle of "documentation of sources" is accepted.

Birdsall: I think one of the problems in distributing programs and communicating with other programmers is the language. You are talking about Fortran. Apparently there is a movement afoot in the mathematical journals, the numerical mathematical journals, to use Algol. If you are going to make a recommendation you might want to think about which language to use.

Roberts: I think each program has to be communicated in the language in which it is written. Algol, of course, is more readable than Fortran. I would say that a program is intended to be read at least as much by people as by the machines. It's actually read more by people, especially by the initial programmer, and by those who try to modify it. If you have left out all the comments it's like publishing a mathematical paper with all the English left out.

Once programs and subroutines have been made intelligible and reliable, and reasonably efficient and universal, it will become sensible to talk of setting up an international library. At present we are trying this out at Culham on a national scale, in collaboration with a number of universities and with organizations such as the National Physical Laboratory. The library at present includes a variety of mathematical subroutines, a number of standard programs of interest in plasma physics, and several display packages. There is a project underway to set up a compatible Fortran-Algol system, so that the library can accept routines written in either language.

Birdsall: I would just like to say a few words about the display. We have many different types of display. I think display in these big programs is just as important as diagnostics are to an experimentalist. If you do a calculation and don't explain the results at all, that's just like making a pinch collapse experimentally but not actually looking at it - it's not very useful. We really ought to concentrate on display. Perhaps what we should do is to throw the discussion open to what sort of display people find useful. I think we find movies useful; graphs of all kinds, of course; color ought to help - it gives us an extra dimension; how about stereoscopic display and on-line display? Is it possible that there is a calculation you can do with an on-line display which you couldn't do any other way?

Killeen: You mentioned stereoscopic displays. With regard to particle trajectories in the baseball geometry, this has been done. Perhaps some of you have seen the film; you can actually follow the trajectories in complicated geometries and see them in three dimensions. These movies have actually predicted difficulties in the experiment and enabled the experimenter to modify the baseball coils to take care of some things that the computations showed should happen. In other words, they predicted some problems and then they modified the coils, so that when they turned on the modified coils the difficulties didn't appear.

Birdsall: With many particles having a variety of initial conditions, one obtains a collection of orbits, which is more meaningful than a single orbit, but it only tells you that something's running. I would advise looking at the trajectories only as a first step. For example, we once found almost indistinguishable trajectories for two different runs but with the harmonic content of the potential quite different: one with a strong fundamental, the next with a strong third harmonic. My point is that other quantities, especially integrated or averaged (energy, etc.) should be followed as well.

Alder: I once gave a talk on melting with a lot of theory and numerical analysis. At the end I showed one slide generated by the computer which

showed the trajectories of particles in a system where there were regions of crystal and regions of liquid. That convinced more people - more than all the talking about the theory of melting.

Kilb: I think that's all right to convince an audience, but if you want to do things that can be measured experimentally, you can't measure trajectories, so you've got to specify gross macroscopic quantities in units that can be understood.

Dawson: Besides the question of how to display, there's also the question of what to display because the computer generates a tremendous pile of numbers. Some of these tell you something, others don't. For particle orbits, we can take short time averages which smooth out things that look quite erratic and help make sense of the data.

Henon: This problem of display will be more and more serious as the computer is used to study problems of more dimensions. There's certainly a limit to the number of dimensions we can display, even in color. Suppose I give you a number of points in four-dimensional space, and I want to know if these fill a region of the four-dimensional phase space or, for example, a three-dimensional subspace. At the moment, I don't see any practical means of answering this question.

Roberts: One thing we haven't done is build three-dimensional displays. People studying nuclear reactions do this - for example, a flat table with rods projecting out of it, which can be pushed in and out. We built a three-dimensional model of a minimum-B magnetic mirror device, and it took 5 man-days to do it. It was immensely useful and we really didn't understand the device until we built the display. We just built it in cardboard, from a set of two-dimensional contours drawn on a graph plotter. I think the ideal thing is to have a visual console, which may or may not be 3-D, and to have all your information stored on the disks and to interact with your information in various ways on-line. If you have a model you can put a ruler inside it, but if you have a movie film you can't, so you really want to be able to get into your display and change it.

Tuck: There's a very sophisticated display at MIT for looking at organic molecules associated with DNA, in which you can put a molecule on the screen and, by turning a knob, turn the molecule over.

Birdsall: I think we can cut off this discussion and go to another topic. The most interesting thing to many of us here is the cross-fertilization among the different fields that are represented here.

Henon: I must say that I am very much impressed by the variety of techniques that have been developed in plasma physics. Certainly in astronomy we do not have such variety of techniques. We should try to borrow them and see how well they can be used for astronomical problems. Not all of them can be used because of differences in the two problems, but it is still worthwhile to try them. For example, these techniques for fast solution of the Poisson equation have not been used in astronomy before Hockney (Roger Hockney). Also of interest are approaches to the direct attack on the Vlasov equation. For

example, the Fourier-Hermite expansions and the water-bag model. The only things which have been done previously are computation or analytical theory.

Also, in astronomy we cannot make experiments, and the observations are not very good. We cannot extract from the systems as much information as we'd like - for example, the masses of the stars are very difficult to determine from observation. Thus, we have to rely very much on theory and numerical experiments. I think it would be very helpful for us to develop numerical techniques, and if the same techniques are used with plasma problems, then we can have more confidence in them.

Tuck: There is another very intriguing field - that is biology. There is a particular problem that is tremendously important. In the cell we have the code in the nucleus from the DNA which sends out messages on RNA. The RNA takes something from the code and goes out for processing. How does it do this? Many people are now actually beginning to get the very mechanistic view that these little fellows actually go out and look. A more intelligent view is that it's diffusion. I think we could settle this by means of a computer experiment.

Birdsall: The physical experiment of Glaser involves setting up little Petri dishes, scanning them with a computer and watching for changes. You keep those that change and discard those that do not.

Tuck: This establishes that they go, but the question I'm asking is what will the computer tell us? Remember that diffusion on the microscale is very fast; remember that a molecule can scan the interior of a cell very rapidly, and I am convinced that it's a random process. I think that he can establish that they are going there, but how?

Birdsall: There are some good questions to be asked about where we are going from here. Most of our machines have 32K memory, so that we are forced to make a trade-off between the number of mesh points we use and the number of particles or the number of fluid elements. Now suppose that we have unlimited computer development. We could go to bigger problems, and should re-do old problems more precisely as well. We have always been pushing the computer as far as it can go into new problems, and we have not been doing the latter. I have asked Bernie Alder to comment on the upcoming generations of computers.

Alder: First of all, I shall say I'm not an expert on this topic. I do know of two computers which are coming along beyond the 6600. One which has been called the CDC 6800 and is now called the CDC 7600 will come along in about a year. It will be four times faster than 6600 and have about 500K memory as opposed to the present 6600 which has 128K. Beyond that there are two competitive designs of which one is sponsored by Livermore, about which, unfortunately, I know very little; the other one is sponsored by Illinois. The University of Illinois is building Illiac IV. I visited there a couple of months ago and learned about this machine. First of all, my impression is that it is designed by computer people instead of by users. My impression of that machine is that it will be exceedingly difficult to program for. In fact, I think that they have started to worry themselves. The machine is

beautiful, but it is not clear how the user would get maximum use of it. The basic concept of this machine is to have in parallel 256 machines which are slightly faster than the 7094 - each of these 7094's will have a 2K memory. The difficulty in using this machine is that these 256 machines are supposed to be used in four independent banks. That is, you can only do four different operations in parallel. So 64 machines are tied together and have to perform the same operation at the same time. Now I will explain our experience with the 6600 at Livermore which has some parallel processing features to it. Most Fortran schemes are serially designed. Most people think things in series of operations and Fortran on the 6600 is consequently inefficient. So that already for the 6600, which has a number of parallel operations, one should in fact, do hand coding to take maximum advantage of two features of that machine. The first is the parallel aspect and the second is the very fast, small memory of 32 words. However, if you can use parallel coding in your numerical scheme, the Illiac IV may offer advantages. We spent a whole afternoon trying to code my specific problem on the Illiac and we were completely unsuccessful in taking good advantage of the parallel features.

Roberts: I would like to remark that in many programs, the relative frequency with which different parts are executed can vary by an enormous factor, even up to 10^9 . So it might well be that you could make use of a complicated machine with parallel operations by writing the critical parts in machine code, and the less frequently used parts in Fortran. It often happens that these critical portions are quite short, so that the penalty of writing in machine code is not serious. This is particularly true of a Vlasov program, where the critical parts are concerned with the motion of the particles. By writing in machine code, one can use several times as many particles for the same amount of computer time. So I should imagine that the new machines would help here.

Sadowski: I should think that any explicit scheme such as your sodium crystal finite difference scheme could be coded so that it could run two of the half-time steps in parallel.

Roberts: I should like to ask other people if it is possible to write critical parts of their programs in machine code, and all the rest in inefficient Fortran?

Alder: You can go in and out of Fortran and write the heart of our program in machine code.

Hockney: In superparticle calculations we do exactly the same thing for all of the 2000 particles. If we could do 250 at a time we would gain a factor of 250 in computing speed. Also in the Poisson solution where we Fourier analyze on a line at a time, one can do 250 lines in parallel. The ordinary differential equation you get for each harmonic is independent and can be solved in parallel. The whole thing is very powerful, and it's really up to the compilers, if they can help us to code properly.

Birdsall: Well, we've gone over our hour, so all those who have not made comments are welcome to make comments. We have scheduled for last, the panel's view on Williamsburg meeting. Do we have any last minute comments?

Zabusky: May I ask you a question? What do you think of outputting data on tape and storing it in archives?

Roberts: I don't think it would be relevant to do it now. I don't think we have good enough information yet to store in public archives, but it's something that might be done in the future, just as the astronomers keep their plates. When our calculations get respectable, particularly the weather calculations, they will be stored. I think at the moment it's something to be done on a personal basis.

Henon: The question as to what kind of computer we would like to have. I think for the pure N-body problems the ideal computer would be a parallel one where each small unit would be in charge of just one particle and would follow it at all times. Then it would be close to the ideal system but it would be almost an analog computer and it would have to be specially designed for the problem.

Roberts: Well, the Illiac could have each computer take care of ten particles.

Feix: What about analog computers in computer simulation problems?

Kilb: I tried to use one but it wasn't very satisfactory.

Smith: I might say that I once heard a paper by someone who was solving diffusion equations and had to invert a matrix. He sent that part out to a network. The network inverted the matrix and sent it back to the machine. He claimed a substantial improvement in machine time.

Birdsall: There are electron gun calculations which have been done quite elegantly by setting up two electrolytic tanks. One tank solves Poisson's equation and the other tank solves for the magnetic field. There are two little pickups that run in parallel that pick up both potentials. These go off to the analog computer which moves the pickup and will calculate in parallel both the electric and magnetic field. The device runs only one trajectory at a time, but makes a first guess as to what the charge density is and reinserts this through sources that are in the tank. The scheme converges rapidly after about three trials and is very useful in shaping electrodes, etc. However, these are time-independent problems so one can afford to iterate them. For time-dependent problems I think such approaches would be very time consuming if not impossible.

Sadowski: I think the analog computer would be very suitable for a display system. If you have a complicated harmonic analysis to do where the functions are not really periodic (i.e., the amplitudes change with time) you might reproduce the output wave on an analog computer rather than do a complicated harmonic analysis.

Birdsall: We have now run out of time. I think that it is very clear that there has been very fine organization behind the symposium for which we are all most grateful and that the symposium has more than accomplished all that it set out to do.

REGISTRATION

ATTENDEES

SYMPOSIUM ON COMPUTER SIMULATION
OF PLASMA AND MANY-BODY PROBLEMS

*Alder, B. J.	Lawrence Radiation Laboratory, University of California
*Armstrong, T. P.	University of Iowa
Baker, D. A.	Los Alamos Scientific Laboratory, University of California
*Barnes, C. W.	Stanford University
*Berk, H. L.	University of California, San Diego
*Bers, A.	Massachusetts Institute of Technology
*Birdsall, C. K.	University of California, Berkeley
*Buneman, O.	Stanford University
*Byers, J. A.	Lawrence Radiation Laboratory, University of California
*Canobbio, E.	Commissariat à l'Énergie Atomique, Centre d'Etudes Nucléaires de Saclay
Chang, T. S.	North Carolina State University
*Chu, C. K.	Columbia University
*Cohen, L.	Hunter College and Smithsonian Astrophysical Observatory
*Crandall, K. R.	Los Alamos Scientific Laboratory, University of California
Crownfield, F. R.	William and Mary College
*Davis, J. A.	Massachusetts Institute of Technology
*Dawson, J. M.	Princeton, Plasma Physics Laboratory
Deem, G. S.	Bell Telephone Laboratories (Whippany, N. J.)

*Presented a paper.

DePackh, D. C.	Naval Research Laboratory
Dolique, J.	Université de Grenoble
*Dunn, D. A.	Stanford University
Ellis, M. C.	NASA Langley Research Center
*Feix, M. R.	NASA Langley Research Center and College of William and Mary
Flores, L. M.	Lockheed Electronics Company (Houston)
Freidberg, J.	New York University
Frenkiel, F. N.	Applied Mathematics Laboratory, David Taylor Model Basin
Fu, Jerry H. M.	University of Michigan
Grossmann, W., Jr.	New York University
*Hain, K.	NASA Goddard Space Flight Center
*Hayli, A.	Institut d'Astrophysique and Faculté des Sciences (Paris)
*Henon, H.	Institut d'Astrophysique (Paris)
Hess, R. V.	NASA Langley Research Center
*Hockney, R. W.	Institute for Plasma Research, Stanford University
*Hohl, F.	NASA Langley Research Center
*Kilb, R. W.	General Electric Research and Development Center
*Killeen, J.	University of California, Lawrence Radiation Lab.
Lamborn, B.	Florida Atlantic University
*Langdon, B. A.	Plasma Physics Laboratory, Princeton University
*Leavens, W. M.	Environmental Science Services Administration
*Lecar, M.	Smithsonian Astrophysical Observatory and Harvard College Observatory
*Leith, C. E.	Lawrence Radiation Laboratory, University of California

*Presented a paper.

*Lomax, R. J.	University of Michigan
Mann, L. W.	Los Alamos Scientific Laboratory, University of California
*Massel, G. A.	NASA Langley Research Center
Montgomery, D. C.	University of Iowa
Nielson, C.	Swarthmore College, Swarthmore, Pa.
Norwood, J.	NASA Langley Research Center
Oliphant, T. A.	Los Alamos Scientific Lab., University of California
*Parker, L. W.	Mount Auburn Research Association, Cambridge
*Peters, F.	Yale University Observatory
*Roberts, K. V.	University of California, San Diego
*Sadowski, W. L.	National Bureau of Standards
*Schneider, H. M.	Massachusetts Institute of Technology
Shanny, R.	Princeton University
Shoosmith, J. N.	NASA Langley Research Center
Sinz, K.	Texas A. & M. University
*Smith, C. G.	Princeton University
Southworth, R.	William and Mary College
*Standish, E. M.	Yale University
Staples, J.	New York University
Staton, L. D.	NASA Langley Research Center
*Szebehely, V. G.	Yale University
Tuck, J. L.	Los Alamos Scientific Lab.
Walton, W. C., Jr.	NASA Langley Research Center
*Weinstein, R. H.	NASA Langley Research Center

*Presented a paper.

Whitney, J.

Columbia University

Winter, R.

William and Mary College

*Zabusky, N. J.

Bell Telephone Lab.

*Presented a paper.

ON SOME ASPECTS OF THE EIGENFUNCTION EXPANSION OF THE SOLUTION OF THE NONLINEAR VLASOV EQUATION

By W. L. Sadowski
National Bureau of Standards

Numerical difficulties encountered by the author in the solution of the non-linear Vlasov equation by finite difference methods* led to a development of a different technique of dealing with the problem. A similar technique was developed independently by M. Feix and F. Grant¹ as well as by T. Armstrong and D. Montgomery².

The model used is a one-dimensional periodic electron plasma with a fixed neutralizing ion background. The distribution function at the time $t = 0$ is given by the expression

$$f(x, v, t = 0) = (1 + \alpha \sum_n A_n \cos nkx) e^{-\frac{v^2}{2}} \quad \text{Eq. 1}$$

where α is the nonlinearity parameter.

In dimensionless form the Vlasov equation is

$$\frac{\partial f}{\partial t} + v \frac{\partial f}{\partial x} + E \frac{\partial f}{\partial v} = 0 \quad \text{Eq. 2}$$

The solution of this equation is expanded in a set of eigenfunctions of the differential space and velocity operators.

The space dependence is expressed by Fourier series while the velocity dependence is expressed in terms of Hermite polynomials.

Thus one obtains

$$f(x, v, t) = \sum_{\ell, n} a_{\ell n}(t) e^{i n k x} H_{\ell}(v) e^{-\frac{v^2}{2}} \quad \text{Eq. 3}$$

With the aid of the recursive relations on Hermite polynomials the partial differential equation (Vlasov equation) is reduced to an ordinary differential equation in time on the matrix of the Fourier - Hermite expansion coefficients.

* To be published.

1. M. Feix NASA report entitled "Mathematical Models of Plasmas", 1966.
2. T. Armstrong, Ph.D. Dissertation, Dept. of Phys. & Astron., Iowa University, 1966.

This permits the use of Range - Kutta techniques to obtain a small truncation error in the integration of the equation with respect to time.

The nonlinear term $E \frac{\partial f}{\partial v}$ becomes a convolution of Fourier components.

$$\sum_{k'} E_{k-k'} \frac{\partial f_{k'}}{\partial v}$$

This sum can be represented as a sum of two matrices which contain the sum and the difference of k' and k'' respectively. The program, written to solve the non-linear Vlasov equation, executes the convolution sum diagonal by diagonal in the two matrices. Thus it is possible to control the physical processes treated by the program and check the results against the full numerical treatment.

For instance if only the $k'' - k' = 0$ diagonal is included in the calculation, the potential energy of the electric field is allowed to be converted to kinetic energy only, with no harmonic decaying into a lower harmonic. Taking the first horizontal row in the $k'' + k'$ matrix in conjunction with above gives the quasilinear treatment. If the diagonals $k'' - k' = 0$ and $k'' - k' = 1$ are used, the neighboring harmonics are allowed to decay into the fundamental, etc. One thus controls mode-mode coupling by setting up various cascade processes.

The quasilinear solution represents the fundamental Fourier component rather well for a few plasma periods. The higher harmonics begin to deviate from their true values in a short time.

The calculation was performed on a $M \times N$ coefficient matrix, with M being the number of Fourier harmonics and N being the number of Hermite polynomials used in the expansion. Values of M and N ranged between 6 and 13 and 35 and 75, respectively. As discussed by T. Armstrong² if one requires that the solution of the non-linear Vlasov equation represent "at least" the free-streaming solution, one obtains an estimate of the number of Hermite polynomials required to represent the solution. Thus we solve the equation

$$\frac{\partial f_n}{\partial t} + inkvf_n = 0 \quad \text{Eq. 4}$$

The solution is

$$f_n = a_n e^{-inkx} e^{inkvt} g(v)$$

where $g(v)$ is an arbitrary function of velocity.

This can be expressed in terms of Hermite polynomials with the aid of the generating function. If $g(v)$ is defined as $e^{-\frac{v^2}{2}}$, then

$$e^{-x^2 - \frac{1}{2}} = \sum_{m=0}^{\infty} \frac{H_m(x) 1^m}{m!} \quad \text{Eq. 5}$$

Multiplying the solution by $\exp\left(-\frac{(inkt)^2}{2} + \frac{(inkt)^2}{2}\right)$

we obtain:

$$f_n = a_n e^{-inkx} \sum \frac{H_m(v) (inkt)^m}{m!} \quad \text{Eq. 6}$$

This can be written as

$$f_{nm} = z_{nm} e^{-inkx} H_m(v) \quad \text{Eq. 7}$$

where

$$z_{nm} = a_n \frac{(inkt)^m}{2\pi\sqrt{m!}} e^{-\frac{(nkt)^2}{2}} \quad \text{Eq. 8}$$

where the normalization $\frac{1}{\sqrt{m!}}$ has been absorbed by the m -th Hermite polynomial. One can now determine the time at which z_{nm} will reach its maximum value.

This time is given by

$$T_{mn} = \frac{m}{nk} \quad \text{Eq. 9}$$

This means that with a given number of harmonics in the Fourier expansion for a given k and a given time over which the equation is to be integrated, the highest polynomial in the expansion is determined by Eq. 9.

Whether this estimate can be extended to the non-linear or even the linearized equation is not clear, since the electric field based on the free-streaming solution has the form

$$E_n \sim e^{-\frac{(nkt)^2}{2}} \quad \text{Eq. 10}$$

while Landau damping is proportional to the first power of time in the exponent. The first two orders of a perturbation expansion of the linearized Vlasov equation in terms of the free-streaming solution show the same damping characteristics as in Eq. 8.

Since both the convolution term and the $v \frac{\partial f}{\partial x}$ term of the Vlasov equation generate higher terms in the double expansion, working with a finite matrix results in truncation errors being propagated from the ends of the finite

matrix into the interior. These may be amplified and will result in a numerically unstable solution^{*}. One of the methods of stabilizing the solution is the introduction of the Fokker-Planck term. It is easy to show that

$$\left(\frac{\partial f}{\partial t} \right)_{\text{coll}} = v_c \left(\frac{\partial(vf)}{\partial v} + \frac{\partial^2 f}{\partial v^2} \right) \quad \text{Eq. 11}$$

is expressed in terms of the Hermite polynomials as

$$\left(\frac{\partial f}{\partial t} \right)_{\text{coll}} = \gamma_c \sum_n n H_u e^{\frac{v^2}{2}} \quad \text{Eq. 12}$$

Here γ is the collision frequency and its universe is the time necessary to thermalize the plasma.

Figures 1 through 3 show the behavior of the first three harmonics for $\epsilon = .5$, and $\alpha = .1$ while Fig. 4 shows the velocity distribution function. The damping frequency had the value $\gamma = 10^{-3}$ and was applied from the 13th polynomial on. As we can see no levelling off of the damping is observed and the shoulder due to the trapping of electrons by the electric field in the velocity space is washed out. Landau damping and dispersion relations were obtained from such graphs, but not the details pertaining to trapping.

Fig. 5 shows a comparison of the velocity distribution functions with no damping and damping beginning at $M = 99$, M being the order of the Hermite polynomial. As can be seen from Fig. 4, 13 polynomials are not sufficient to properly describe the velocity distribution function and the damping smooths out the shoulder. In the other case the shoulder persists with time and a levelling off of the Landau damping is observed (see Fig. 6).

Thus it seems unnecessary to include as many as 1200 terms in the Hermite expansion of velocity space, provided proper cut off is assured with the aid of the Fokker-Planck term.

* The discussion of numerical difficulties encountered by the author in this formulation of the problem is to be published.

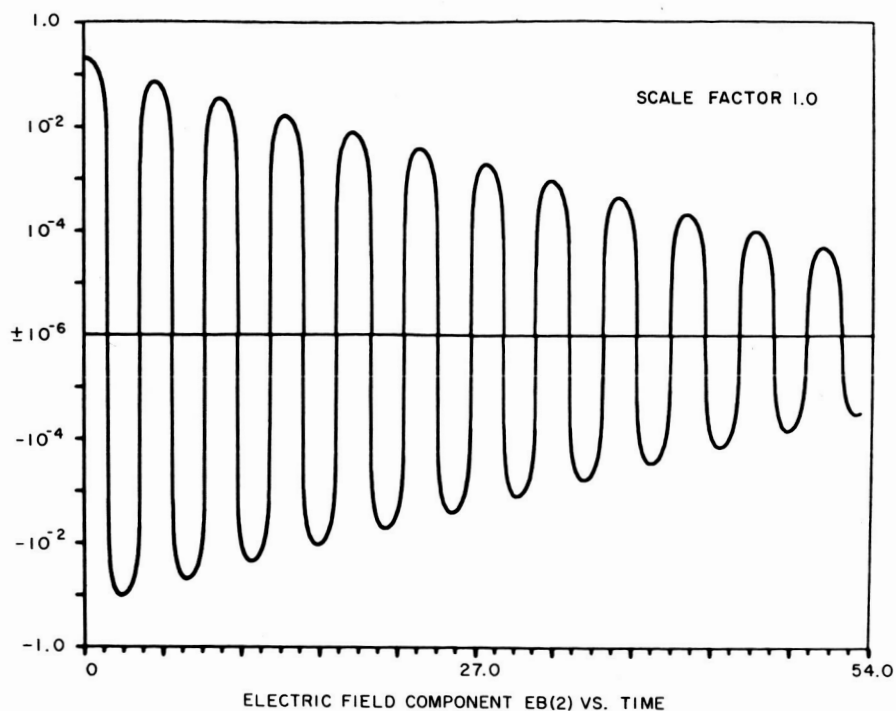


Fig. 1. First harmonic of the electric field vs time for $k = 0.5$ semilog scale.

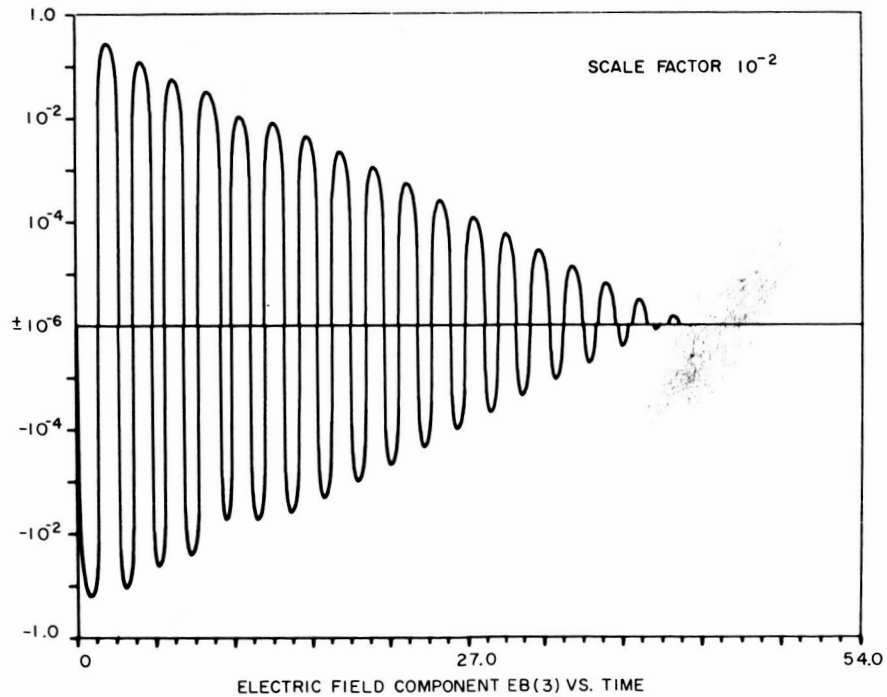


Fig. 2. Second harmonic of the electric field vs time for $k = 0.5$ semilog scale.

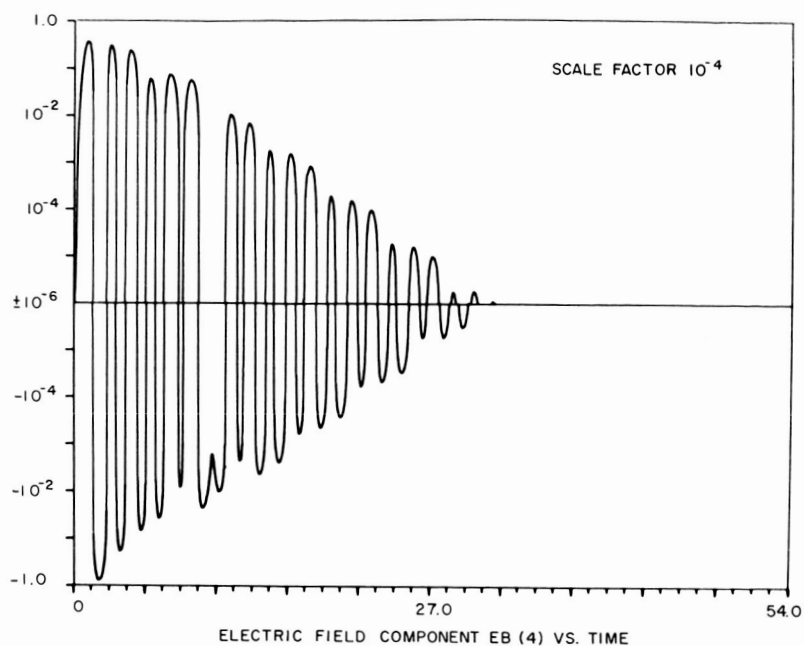


Fig. 3. Third harmonic of the electric field vs time for $k = 0.5$ semilog scale.

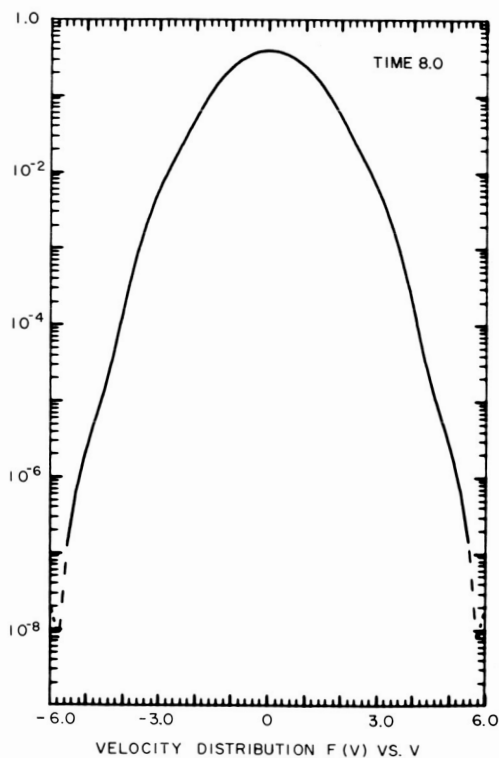


Fig. 4. Velocity distribution function $f(v)$ vs velocity at the time $t = 8.0$.

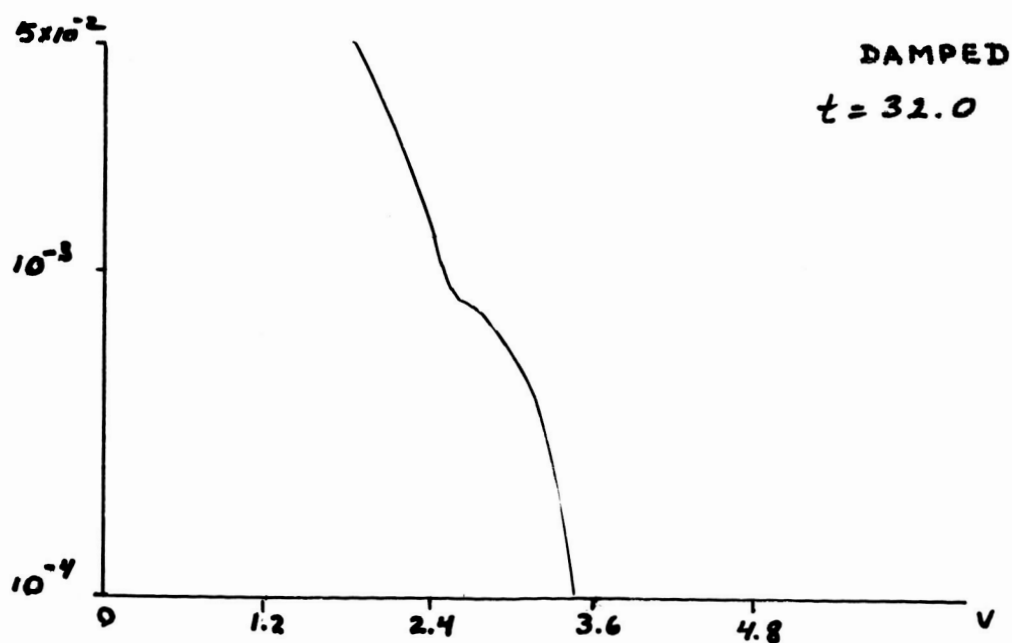
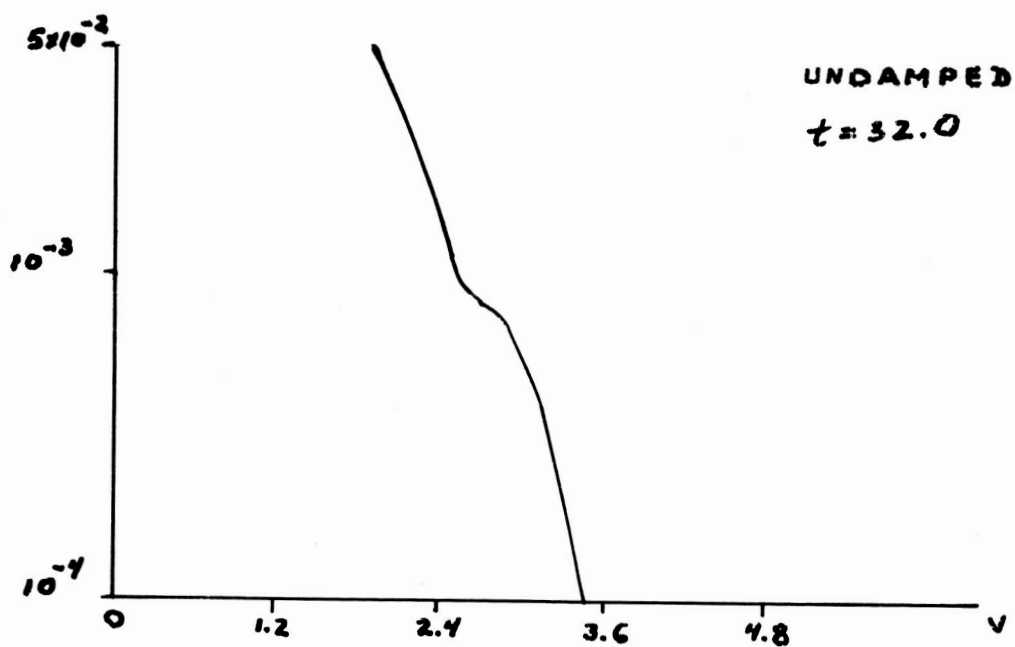


Fig. 5. Comparison of $f(v)$ vs velocity for a run where damping was used with the run where damping was absent. The time vs $t = 32.0$.

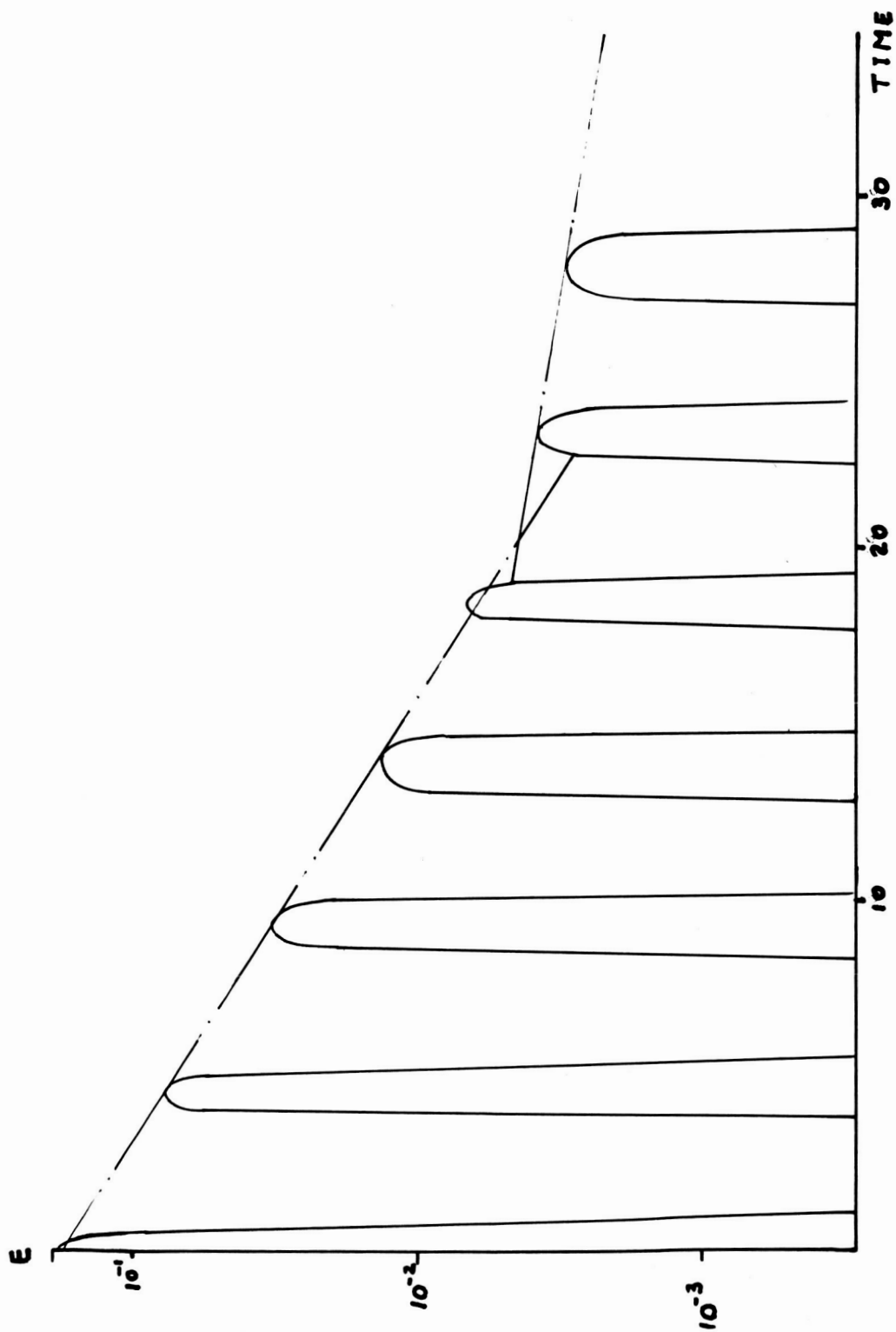


Fig. 6. Plot of the first harmonic of the electric field with damping applied at the 99th polynomial.